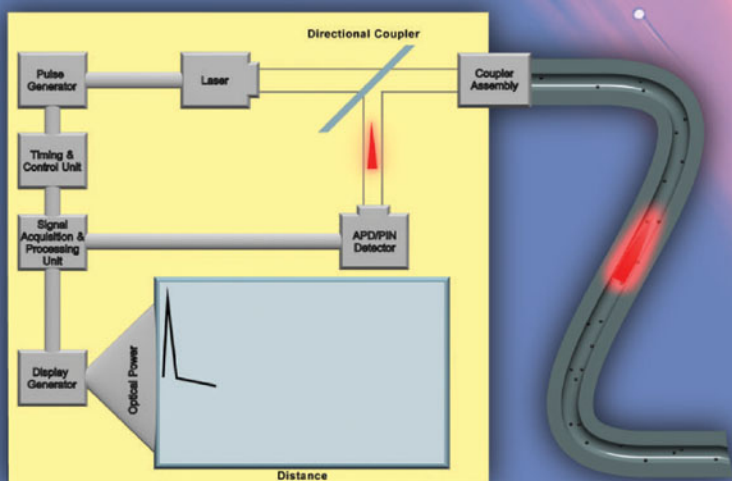




Troubleshooting Optical-Fiber Networks

Understanding and Using Your
Optical Time-Domain Reflectometer

SECOND EDITION



Duwayne R. Anderson
Larry Johnson
Florian G. Bell



INCLUDES OTDR
TRAINING CD-ROM



Troubleshooting Optical-Fiber Networks

Second Edition

Troubleshooting Optical-Fiber Networks

Understanding and Using Your
Optical Time-Domain Reflectometer

Second Edition

Duwayne R. Anderson
Principal Engineer

Larry Johnson
President, The Light Brigade, Inc.


Florian G. Bell, Ph.D.
Production Manager, MiniMitter, Inc.



ELSEVIER
ACADEMIC
PRESS

Amsterdam Boston Heidelberg London New York Oxford
Paris San Diego San Francisco Singapore Sydney Tokyo

Elsevier Academic Press
525 B Street, Suite 1900, San Diego, California 92101-4495, USA
84 Theobald's Road, London WC1X 8RR, UK

This book is printed on acid-free paper. 

Copyright 2004, Elsevier, Inc. All rights reserved.

No part of this publication may be reproduced or transmitted in any form or by any means, electronic or mechanical, including photocopy, recording, or any information storage and retrieval system, without permission in writing from the publisher.

Permissions may be sought directly from Elsevier's Science & Technology Rights Department in Oxford, UK: phone: (+44) 1865 843830, fax: (+44) 1865 853333, e-mail: permissions@elsevier.com.uk. You may also complete your request on-line via the Elsevier Science homepage (<http://elsevier.com>), by selecting "Customer Support" and then "Obtaining Permissions."

Library of Congress Cataloging-in-Publication Data

British Library Cataloguing in Publication Data

A catalogue record for this book is available from the British Library.

ISBN: 0-12-0586614

For all information on all Academic Press publications
visit our website at www.academicpress.com

Printed in the United States of America

04 05 06 07 08 9 8 7 6 5 4 3 2 1

To our families

Contents

Foreword	xiii
Chapter 1 Early developments	1
1.0 Introduction	1
1.1 The birth of the OTDR.....	2
1.2 Features, functions, and performance improvements	4
1.3 Summary.....	9
Suggested reading	11
Chapter 2 Fundamentals of fiber optics	13
2.0 Introduction	13
2.1 Total internal reflection	13
2.2 Fiber attenuation.....	19
2.3 Numerical aperture.....	23
2.4 Multipath (modal) dispersion	24
2.5 Chromatic dispersion	28
2.6 Wavelength-division-multiplexed systems	35
2.7 V-parameter, cut-off wavelength, and spot profile.....	36
2.8 Splices and connectors.....	42
2.9 Bending loss	48
2.10 Coherence	52
2.11 Summary.....	55
Suggested reading	57
Problems.....	57
Chapter 3 Fundamentals of OTDR operation	59
3.0 Introduction	59
3.1 OTDR design	62
3.2 A typical OTDR waveform	63
3.3 Multiple-wavelength OTDRs.....	65
3.4 Optical masking.....	67
3.5 Evolution of the OTDR	69
3.6 Rayleigh backscatter	72
3.7 Dynamic range	74
3.8 Differences between multimode and single-mode OTDRs ...	78
3.8.1 Physical differences	81
3.8.2 Reflectivity differences between single-mode and multimode fiber connectors	81
3.8.3 Differences in backscatter levels	82
3.8.4 Optical-power differences	83

3.8.5	Pulse-width differences	83
3.8.6	Operating-wavelength differences	84
3.9	Echoes and ghosts.....	87
3.10	Other types of OTDR configurations.....	91
3.10.1	Standard OTDR with an EDFA.....	91
3.10.2	Coherent-detection OTDR	93
3.10.3	Correlation OTDR.....	95
3.10.4	Short-coherence-length coherent OTDRs (multimode)....	96
3.10.5	Photon-counting OTDRs.....	98
3.11	Summary.....	99
	Suggested reading	100
	Problems.....	101
Chapter 4	Performance characteristics of OTDRs.....	103
4.0	Introduction	103
4.1	Figures of merit	103
4.2	Historical figures of merit.....	105
4.3	Detailed figures of merit	107
4.3.1	Reflective dynamic range	108
4.3.2	Scattering dynamic range	109
4.3.3	Derivation of the noise floor	115
4.3.4	Dynamic-range margin	121
4.3.5	Usable dynamic range	123
4.3.6	Measurement range	124
4.3.7	How offset errors affect dynamic-range and measurement-range calculations.....	125
4.3.8	Event resolution.....	135
4.3.9	Loss-measurement resolution	137
4.3.10	Return loss	139
4.3.11	Linearity	140
4.3.12	Data resolution.....	141
4.3.13	Clock accuracy.....	143
4.3.14	Cursor resolution	144
4.3.15	Refractive-index uncertainty	144
4.3.16	Speed of measurement	146
4.3.16.1	Fiber length.....	146
4.3.16.2	Interleaving.....	147
4.3.16.3	Data-processing speed	147
4.3.16.4	Display speed.....	148
4.3.17	Event-detection accuracy	148
4.4	Standards	149
4.5	Summary.....	150
	Suggested reading	151
	Problems.....	151

Chapter 5	Measuring nonreflective events	153
5.0	Introduction	153
5.1	Sources of nonreflective events.....	153
5.2	Cursor placement for manual loss and distance measurements	156
5.3	Distance-measurement errors of nonreflective events	158
5.3.1	Distance-measurement errors caused by waveform noise	158
5.3.2	Distance-measurement errors caused by filtering	167
5.3.3	Other contributions to distance-measurement errors	170
5.4	Summary	176
	Suggested reading	177
	Problems.....	178
Chapter 6	Loss-measurement error	179
6.0	Introduction	179
6.1	Loss-measurement errors caused by waveform noise	179
6.2	Loss-measurement errors due to mismatch of single-mode fibers.....	185
6.3	Loss-measurement errors on multimode fiber	190
6.4	Bending loss and stress loss in single-mode fibers.....	196
6.5	Wavelength-dependent loss in fusion splices and connectors between single-mode fibers	198
6.6	Intrinsic loss in single-mode fusion splices.....	200
6.7	Summary.....	205
	Suggested reading	206
	Problems.....	206
Chapter 7	Measuring reflective events.....	209
7.0	Introduction	209
7.1	Background	209
7.2	Causes of reflection.....	212
7.2.1	Reflections from angled cleaves	212
7.2.2	Reflections from connectors	214
7.2.3	Reflections from mechanical splices.....	220
7.3	Measuring reflective events using an OTDR.....	221
7.4	Effects that can reduce the accuracy of reflectivity measurements	226
7.5	Calibrating the OTDR's backscatter coefficient	229
7.5.1	Calculating the backscatter coefficient	230
7.5.2	Measuring the backscatter coefficient.....	233
7.5.2.1	Measuring the backscatter coefficient with a calibrated reflector	233

7.5.2.2	Measuring the backscatter coefficient using a CWR	235
7.5.2.3	Measuring the backscatter coefficient using an OTDR.....	237
7.6	Integrated return loss.....	240
7.7	Summary.....	245
	Suggested reading	247
	Problems.....	247
Chapter 8	Complications caused by reflective events.....	249
8.0	Introduction	249
8.1	Reflections and the dead zone.....	249
8.2	Improving the dead zone by optical masking.....	252
8.3	Impact of reflections on transmitters and receivers	257
8.4	Dead zone box.....	263
8.5	Summary.....	265
	Suggested reading	265
	Problems.....	265
Chapter 9	Measuring the numerical aperture and mode-field diameter of single-mode fiber.....	267
9.0	Introduction	267
9.1	The far-field scanning method of determining numerical aperture	268
9.2	Measuring the numerical aperture of single-mode fiber using an OTDR.....	272
9.3	Measuring the cut-off wavelength of a single-mode fiber using an OTDR.....	275
9.4	Summary.....	277
	Suggested reading	277
	Problems.....	278
Chapter 10	Analyzing passive networks containing splitters and couplers	279
10.0	Introduction	279
10.1	Determining the locations of breaks in systems containing splitters	284
10.2	OTDR requirements for testing networks with splitters	287
	Suggested reading	289
	Problems.....	290
Chapter 11	Automatic event-marking algorithms and calibration	291
11.0	Introduction	291
11.1	Types of event markings	291

11.2	Functionality of different types of event markings.....	293
11.3	Optimizing acquisition parameters.....	298
11.4	Measuring individual events.....	304
11.5	Testing event-marking software	312
11.5.1	Test-fiber calibration.....	312
11.5.2	Repeatability testing	314
11.5.3	Summary of testing event-marking software.....	317
11.6	Event-marking features.....	317
11.7	Remote OTDRs for monitoring networks.....	321
11.8	Summary.....	325
	Suggested reading	326
	Problems.....	327
Chapter 12	Test fixtures.....	329
12.0	Introduction	329
12.1	Dead zone fixture	329
12.2	Fiber circulator.....	330
12.3	External-source test fixture	337
12.4	Loss calibration with fiber standard.....	338
12.5	Summary.....	340
	Suggested reading	341
	Problems.....	342
Chapter 13	Polarization mode dispersion	343
13.0	Introduction	343
13.1	Measurement techniques	346
13.2	PMD model of optical fiber.....	349
13.3	Mathematical model of a polarization OTDR.....	353
13.4	Summary.....	357
	Problems.....	358
Chapter 14	Dispersion in optical fibers	359
14.0	Introduction	359
14.1	Intermodal dispersion.....	361
14.2	Intramodal dispersion	364
14.2.1	Material dispersion	364
14.2.2	Waveguide dispersion.....	366
14.3	Dispersion reduction in optical fibers.....	368
14.4	Measuring dispersion using an OTDR	369
14.5	Measuring chromatic dispersion using multiple-wavelength OTDRs.....	372
14.6	Summary.....	375
	Suggested reading	376
	Problems.....	377

Chapter 15	Considerations when selecting an OTDR	379
15.0	Introduction	379
15.1	Durability	380
15.2	Display and controls	382
15.3	Human interface	386
15.4	Optical port	387
15.5	Accessories, options, and features	394
15.6	Safety.....	396
15.7	Performing a fiber-acceptance test	399
15.7.1	Sequential steps of an acceptance test.....	400
15.8	Measuring the splice attenuation.....	402
15.8.1	Corrective actions	403
15.9	When should OTDR traces be taken?	404
15.10	Span measurements.....	405
15.10.1	What measurements are required?	405
15.11	Field technician's top-ten list	406
15.12	Summary.....	407
	Problems.....	407
	Glossary of Terms.....	409
	Mathematical Glossary	425
	Answers to Problems	431
	Index.....	433

Foreword

Two of us (Anderson and Bell) wrote the first edition of this book, titled *Optical Time-Domain Reflectometry*, published in 1997. At the time we were engineers at Tektronix, in the company's Cable and Network Analysis Division. In 1997, Tektronix was a major producer of optical time-domain reflectometers (OTDRs), and our book was the first single-source handbook describing OTDRs. Tektronix sponsored our work in writing the book, and they published it and distributed it worldwide.

At the time, worldwide investment in fiber-optic networks was expanding at double-digit rates, and Tektronix was one of the top manufacturers of OTDRs, responsible for both their early innovation and the development of several key technologies. Neither of us could have anticipated the dramatic changes that would take place in the next six years. While fiber optics proceeded at a steady and respectable pace during most of the 1990s, the industry exploded in irrational exuberance near the turn of the century as part of the telecom bubble, only to be followed by a deep depression that would see many companies, including Tektronix, abandon key business sectors devoted to optical telecom by the end of 2003.

Through these tumultuous times, the OTDR continued its remarkable evolution, resulting in today's machines, which are considerably smaller, faster, more capable, and less expensive than their predecessors. This evolution has been driven largely by the widespread use and deployment of optical fiber and the need to put high-powered test capability into the hands of the optical technicians that engage daily in installing, maintaining, and repairing these networks. The days when optical engineers do field tests with bulky \$35,000 OTDRs are gone forever.

It is because of the dramatic changes in the markets and the science of OTDRs that this second edition is needed. Furthermore, the widespread use of OTDRs necessitates publishing and distributing the book in a manner that makes it more widely available to field technicians as well as engineers. These changes also demand a new title, one that reflects a broader theme and goes beyond simply testing with OTDRs to address additional issues surrounding fiber-optic networks in general and how to keep them working properly.

Because OTDRs have evolved from difficult-to-use, specialized equipment to ubiquitous mainstay status, we found the book required contributions from a third author. The obvious choice was Larry Johnson, owner and founder of The Light Brigade. Larry's company is a leading training organization with nearly two decades of experience teaching technicians how to use OTDRs in the field to install, maintain, and repair fiber-optic networks. He has an intimate knowledge of the challenges and needs of the technician that are unmatched in the industry, as well as a high degree of familiarity with different OTDR manufacturers, their products, and related fiber-optic standards.

As with the first edition, our objective in writing this book is to go beyond a simple handbook that discusses operational procedures such as cursor placement and waveform interpretation. While we do cover these topics, we also explain more esoteric subjects and offer insight into the technical nuances of OTDRs that enable nontraditional OTDR measurements, such as mode-field diameter, cut-off wavelength, and polarization mode dispersion. We also give considerable attention to measurement errors and how to estimate them. This, especially, is a subject with which all OTDR users should be quantitatively familiar. As a part of this, we have devoted an entire chapter (11) to event-marking software, which was the key innovation that resulted in OTDRs being readily used by field technicians.

Our target audience comprises practicing engineers, system technicians, and field technicians. We have constructed each chapter so that, for the most part, simpler concepts and ideas are discussed first, followed by concepts of increasing difficulty as the chapter progresses. The level of difficulty varies. When this happens, we try to warn the reader that the level of difficulty may rise for a while but subside in succeeding sections. We have also added a short quiz at the end of each chapter so that the book can be used in the classroom as a text or for self-study.

We make no apologies for equations and mathematical detail, which are used liberally throughout. These are intended to provide quantitative support for many of the book's central points. Though we use them unabashedly, most of the equations are summaries, with few derivations, and involve only algebra or elementary calculus. Where appropriate, we use diagrams and text that illustrate ideas embedded within the equations so that full command of the mathematics is not necessary to obtain an intuitive feel for the subject being discussed.

For the most part, the book can be read and the key points understood without having to understand the mathematical equations. For those who want to delve a little deeper, however, the mathematics opens the door to understanding OTDRs at a level of detail that should appeal to design engineers.

We hope this book serves as a useful desk reference and provides value even if not read cover to cover. Toward this end, we have included a detailed table of contents, a glossary of terms, a mathematical glossary, and a detailed index.

One of the most difficult aspects of writing this book was researching the appropriate references. OTDRs are a relatively new type of test instrument, and references abound regarding their early development and use. The difficulty has primarily been in searching vast databases in an attempt to determine first usage. Additionally, the proprietary nature of much of the information makes it difficult to assign credit to the originators. Although we have made a concerted effort to do so, there are undoubtedly instances where we have failed to reference the original author. In such cases, we offer our apologies, and we welcome suggestions and comments that might be included in future editions of this book.

Too many people have helped us write this book to name them all here, but some have made contributions for which particular thanks and recognition is warranted. We are especially grateful for the technical reviews provided by Mark Lund, William Trent, Mark Marineau, Mehrdad Givehchi, Raza Ahmed, Ronald Larrick, Kenneth Ditto, Matthew Harcourt, Morris Anderson, Brandon DuRette, Robert Cook, Robert Jahn, Peter Schweiger, and Peter Lovely. Without the technical advice and excellence of the engineering staff at Tektronix, CNA, this book would not have been possible. Thanks especially to those who spent endless hours in technical conversation about the details of OTDR operation: Richard Lane, Frank Borden, Glenn Bateman, Kevin McDonald, Bob McMahon, Doug Rasmussen, and Ken Coulson. As with any book, responsibility for technical accuracy lies with the authors. Without the association of these very talented scientists and engineers, however, this task would have been unapproachable. In addition, special thanks to Dr. Mel Holzman, Dave Bartlett, and the late Ellis Dupuy for opening many doors with their mentoring and early work in fiber optics. Special thanks also to Harvey Jauvtis, who provided much of the material for chapter 10, and to Matthew Diessner, who has added to our insight regarding

customer applications, and Gina Lynd, who organized and coordinated the content of the book for editing.

Finally, we thank our publisher and especially Charles Glaser for his help, encouragement, and professional demeanor in bringing this project to fruition.

Duwayne Anderson

Larry Johnson

Florian Bell

Chapter 1

Early developments

1.0 Introduction

The development of optical fiber has enabled a revolution in modern telecommunications. In the 35 years since optical fiber was first suggested, the effective speed at which information can be transmitted has increased from kilohertz rates to multigigabit rates. State-of-the-art long-distance transmission systems transmit digital pulses of light at OC-192 (10.0 gigabits per second (Gb/s)) and greater, at a single wavelength. With dense wavelength division multiplexing (DWDM), system bandwidth can easily approach several hundred gigabits per second, while best-in-class demonstrations have delivered 1.6 Tb/s over 10,000 kilometers¹; several manufacturers have demonstrated 5 Tb/s for use in metropolitan-area networks (MANs). It is not inconceivable that modern high-speed transmission systems may soon reach the effective bandwidth of single-mode optical fiber itself, about 25 THz. Along with these increased transmission speeds comes the requirement to test the optical medium through which the signals are passed. This book is devoted to describing one instrument used to perform tests on optical fibers: the *optical time-domain reflectometer*, generally referred to as an OTDR.

To verify that fibers are able to transmit light reliably, a variety of commercial instruments have been developed for certification, maintenance, and restoration of fiber systems. For example, loss test sets, consisting of a stabilized light source and power meter combination, are used for testing the end-to-end loss of an optical fiber. Optical return-loss (ORL) test sets measure the amount of light reflected back toward a transmitter.* Visible fault locators inject light from a visible laser or LED into a fiber. Where a break or sharp bend occurs, they allow the operator to “see” the location of the fault by virtue of light coupled out of the waveguide at the break. Each of these instruments has its own benefits and attributes, and each can be used to test a limited subset of the complete fiber performance characteristics.

In the past, only the transmission loss of fiber cables was routinely measured. However, today’s ever-increasing demand for higher speed has led to the requirement that fiber cable systems be tested and certified for operation at higher bit rates. Even though single-mode fibers have

*ORLs are also called continuous-wave reflectometers (CWRs).

essentially unlimited transmission bandwidth, actual installed fiber cable systems can contain reflective connections and losses that may limit the speed at which light can be reliably transmitted. Test instruments have been developed that can assist in determining the speed limitations of installed fiber systems. For example, bit-error-rate testers (BERT sets) introduce a pseudo-random code into one end of a fiber system and measure the fraction of bits that are incorrectly transmitted at the receiving end. In this way, the effective noise floor and, therefore, the dynamic range of the system can be determined.

Light sources, power meters, ORL testers, and the BERT sets can determine the loss of a fiber or noise-floor penalty of a transmission system, but they cannot determine the location of a problem within the fiber itself. The OTDR is an instrument used to test the light-transmission ability of an optical telecommunications fiber or cable, and it can also determine the location of a problem. The OTDR has become the most widely used and versatile instrument for testing optical fibers during installation, maintenance, and restoration. The OTDR can determine the length of a fiber and its end-to-end loss as well as the amount of reflected light and loss from various discrete components within the fiber. Modern OTDRs can locate and evaluate the losses of fusion splices and connectors and can even report whether each location and loss is within certain specification tolerances. Among all electronic test instruments, the OTDR is truly unique in its combination of extremely high dynamic range, rapid acquisition capabilities, and high resolution. No other instrument used for any test application can boast over 200 dB of electrical dynamic range together with nearly 1 GHz of bandwidth and a 10-MHz sampling rate, all in the same package. In this book, we explore some of the performance attributes, applications, measurement techniques, and evaluation criteria of modern OTDRs. In doing so, we hope that those who use and evaluate OTDRs can benefit from the information we present. We hope that the reader will not only gain a better appreciation of the tremendous capabilities of the instrument, but also improve the efficiency of the work that can be accomplished with this instrument.

1.1 The birth of the OTDR

The underlying principle of the OTDR is the detection and analysis of light scattered from tiny imperfections and impurities in the optical fiber. Rayleigh scattering in optical fibers has been understood for many years.² The earliest publications reporting measurements of backscatter

in optical fibers using a time-domain method appeared in early 1976.³ This technique, which is much the same as the principle used in modern OTDRs, involved introducing a short pulse of light into one end of an optical fiber (see figure 1.1). When the light traveled to the opposite end of the fiber, a small portion would reflect from the far end and travel back to the near end. Through the use of a beam splitter, in the form of a tapered fiber, the outgoing pulse could be introduced into the near end and the reflected pulse could be collected from the near end as well. The reflected pulse was directed into a photomultiplier, where it was amplified and converted to a current pulse. The current pulses from both the incident pulse and the reflected pulse could then be viewed simultaneously on an oscilloscope. The length of the fiber was determined by multiplying a constant with the time difference of the incident and reflected pulses. The experimental setup could also be used to measure Rayleigh backscatter.

Time-domain backscatter methods for assurance testing of optical communications fibers appear to have been developed independently in the mid-1970s by two different research groups: Barnoski and Jensen at Hughes Research Laboratories and Personick at Bell Telephone Laboratories. The results of Barnoski and Jensen's work were originally published in Ref. 3; those of Personick appear in Ref. 4. We shall take a moment to describe the early work of Personick, since this work was applied directly to actual installed fiber-telecommunication links.

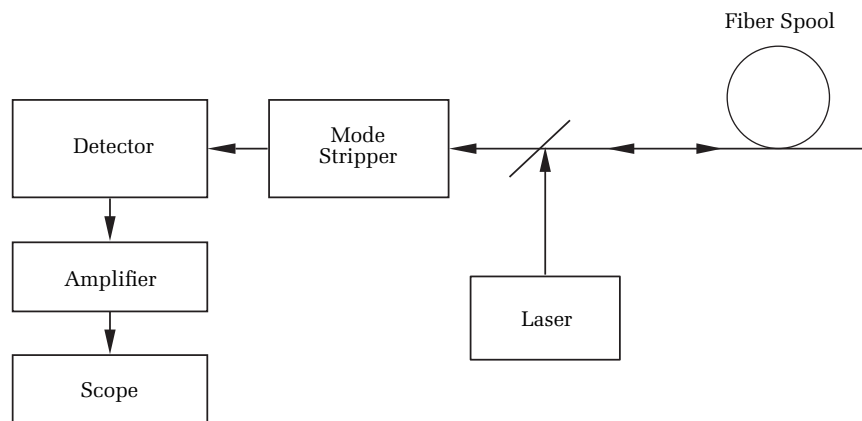


Figure 1.1. Original experimental arrangement used to detect Rayleigh scattering in multimode fibers. Based on a diagram in Ref. 3.

In early 1976, Stewart Personick, then working at Bell Telephone Laboratories, was pursuing a means to test the lengths and losses of optical fibers using a time-of-flight method. Personick was experimenting with ways to reduce optical-detector overload in the laboratory. Using a back-reflection method similar to that illustrated in figure 1.1, Personick noticed an exponentially decaying signal immediately following the incident reflection on the oscilloscope. Personick recognized that the exponential signal was, in fact, due to Rayleigh scattering from microscopic imperfections in the fiber itself. Reasoning that a logarithmic amplifier would “straighten out” the exponential signal, Personick employed such a log system.* This improvement to the linear-amplifier method enabled the straightforward measurement of the fiber scattering (and thus fusion-splice losses and connector losses) based on the change in backscatter signals before and after the events.†

Additional improvements to this primitive OTDR were quick to follow, including the use of an avalanche photodiode (APD) for improvements in sensitivity and the collection of various system components together into a self-contained instrument, similar to modern monolithic instruments. Following these important improvements, Personick and colleagues began using their OTDR successfully to measure the losses of splices and connectors in a research field trial of multimode fiber, then being installed under the streets in an area of Chicago.

1.2 Features, functions, and performance improvements

Personick’s early work resulted in a landmark paper published in 1977 in the *Bell System Technical Journal* entitled “Photon probe—an optical time-domain reflectometer.”⁴ This publication was followed by a number of pioneering works on the technique of OTDRs.^{5,6,7}

In addition to the investigative work by the research community, several groups in the United States and Europe began designing commercial instruments to test optical-fiber length and loss. In those days, all fiber systems were of the multimode type, using LEDs as transmission sources at 850 nm and 1300 nm. Due to the ready availability of silicon APDs and fast analog oscilloscopes, basic analog

*The logarithmic method is also illustrated by Barnoski and Jensen in Ref. 2.

†In former times, splice loss was estimated by manually evaluating, at the location of the event, the difference in the extrapolated backscatter before and after the event. In modern OTDRs, more sophisticated algorithms, such as pattern-matching algorithms, provide a higher level of accuracy. These newer methods are described in chapter 11.

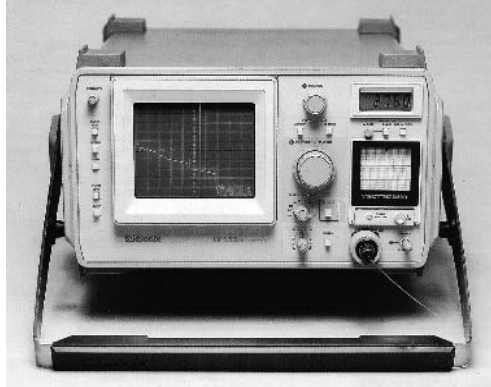


Figure 1.2. The Tektronix OF 150 was the first commercially successful OTDR, in 1981. [Credit: Tektronix.]

OTDRs were relatively straightforward to design. Therefore, the first commercial manufacturers of OTDRs were quick to provide instruments to the emerging optical-fiber-test market (see figure 1.2). They were able to offer updates and improvements to existing instruments on a regular basis. Thus, competition and innovation among the two or three initial suppliers led to rapid advances in the technology of OTDRs. These early improvements included the development of sensitive preamplifiers based primarily on Personick's work in telecommunications receiver design. Other improvements included dedicated oscilloscope designs, more efficient data-acquisition systems, chart recorders to improve interpretation and documentation of test results, adoption of improved fiber-connector types, and the use of display measurement tools such as movable cursors. By 1985, there were at least five commercial suppliers of OTDRs whose instruments were designed for testing multimode fiber systems.

There have been essentially four phases in the history of OTDR development. The first was the invention and early development of the OTDR. The second phase consisted of the years in which OTDRs were brought from the laboratory into commercial development and gradually refined. The third phase was the period in which the OTDR was transformed from basically a refined oscilloscope to a monolithic instrument designed specifically for testing optical fiber and capable not only of measuring the fiber waveform data but also of interpreting them. The latest phase has been the reduction of the OTDR into a form factor that is small and portable, capable of running off batteries, and complete with software that produces automatic waveform analysis as well as test reporting. Several manufacturers have further enhanced the utility of

their test solutions by building the OTDR as one module designed to operate on a field-portable platform that accepts additional test modules, such as optical power meters and optical spectrum analyzers.

The 1980s saw the formative, refinement phase for OTDRs. Their development for multimode testing was a direct result of the introduction of multimode fiber into the telecommunications industry. In addition, the first half of the 1980s saw the emerging use of systems based on single-mode fiber.^{8,9} These systems offered the possibility of transmitting information over longer distances at greater speeds. With the introduction of single-mode systems, multimode fibers were gradually transitioned to local-area networks (LANs), where shorter distances tolerated the greater loss and larger dispersion of multimode fiber. Also, cost sensitivity was a driving force to use the lower-cost components available for transmission at 850 nm and 1300 nm, which are the operating wavelengths of standard multimode fiber. Due to this change in emphasis in the early 1980s, multimode OTDR development in the late 1980s was de-emphasized relative to the development of instruments used for testing single-mode fibers. It is fair to say that few significant performance improvements have been made to multimode OTDRs since 1991 (though operational, ergonomic, and analysis performance has improved dramatically). Meanwhile, single-mode OTDRs have realized regular and significant improvements in performance up to the present time.

The development of single-mode transmission systems led to improvements in the transmission quality of optical fibers, in the power of transmitters, and in the sensitivity of receivers. Because of these improvements, designers were able to increase the length of single-mode fiber cables. This led to requirements for OTDRs that were capable of testing fibers of ever-increasing length. To provide the instrument dynamic range that is required to test these fibers, several technologies were investigated. These technologies included techniques to improve the overall sensitivity of the instrument, such as photon counting, photomultiplier detectors, and coherent detection. The literature contains several reviews of these alternative technologies.^{10,11,12,13} In addition, reflective frequency-sweep techniques have been proposed, but these are only able to detect the positions of discrete reflective events in fiber and integrated optic systems.^{14,15,16}

Curiously, few of these exotic techniques led to practical performance improvements for the OTDR. In retrospect, it was primarily simple and incremental changes that gradually provided the performance improvements required for testing single-mode

fibers.^{17,18,19} We have already mentioned silicon APDs for use in the multimode OTDR preamplifier. For single-mode testing, germanium and InGaAs APDs were developed that provided improved sensitivity within the longer wavelength windows located at 1310 nm and 1550 nm. OTDR preamplifiers with improved noise, bandwidth, and sensitivity characteristics were developed. Noise reduction and resolution were improved by using high-speed acquisition systems. OTDR laser sources enjoyed regular increases in peak-power capabilities. One of the most significant enhancements to traditional OTDRs arrived with the introduction of digital acquisition systems that replaced the “real-time” analog displays. This led to improvements in speed, accuracy, sensitivity, and averaging capabilities as well as the ability to further improve noise characteristics using sophisticated digital signal processing of the OTDR waveform.

As a result of these changes, the dynamic range of single-mode OTDRs increased over the years, though as figure 1.3 shows, this trend has stabilized in recent years as device limits have come into play. Two

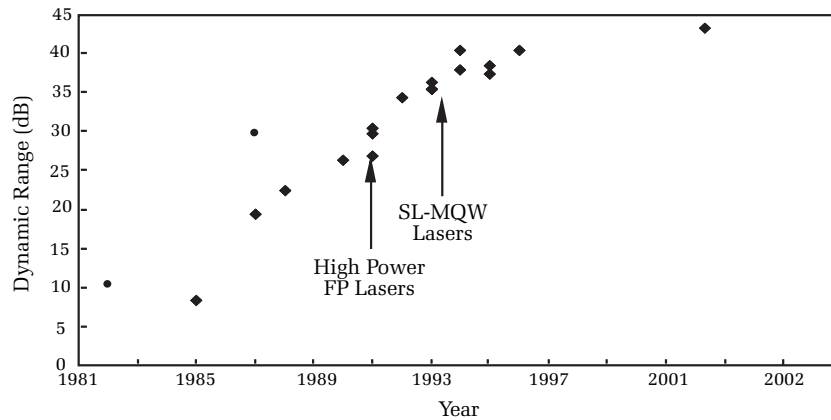


Figure 1.3. The dynamic range (SNR = 1) of commercial, long-range 1550-nm OTDRs, by year of release. Where available, values have been reported with a 10- μ sec (1-km) pulse width. Earlier years’ data have been normalized to a 10- μ sec pulse. Chart includes data from suppliers (♦) who advertised a long-range test module as well as laboratory research results (•). As time progressed, more suppliers entered the market with a wider variety of performance, creating the increase in scatter among product performance. Notice that dynamic range has effectively stabilized as the OTDR’s front-end noise has become dominated by the APD detectors and as laser output powers have stabilized at several hundred milliwatts, maximum.

important improvements to long-range OTDRs were enabled with the introduction of high-power Fabry–Perot lasers in 1992 and with the new generation of strained-layer multi-quantum-well (SL-MQW) lasers in 1994. Essentially all instrument lasers are now of the SL-MQW type. It is also interesting to point out that laboratory developments have preceded commercial improvements by about three years.

In the past, OTDRs were designed and used primarily as tools for measuring basic transmission characteristics of the fiber, such as length, loss, and back-reflection. With these traditional instruments, the OTDR operator had to set up the measurement parameters, wait for the data to be acquired, and then set about interpreting the waveform features to determine the loss characteristics of the fiber. In those times, the OTDR user was likely a technician or engineer who was highly trained in the use of the instrument and the interpretation of the data in terms of how various waveform features would affect the transmission system.

By the second half of the 1990s, OTDR development had entered an evolutionary phase that may be called the *expert system* phase. Several important driving factors have led to the new expert-systems requirements. During the 1990s, OTDRs became increasingly used in a wider variety of test situations, including not only installation, but also maintenance and restoration. Along with this increase in the variety of test applications, OTDRs became used by a wider variety of people. Maintenance testing has shifted from the optical-transmission technician or engineer to technicians who may have responsibility for other testing functions, such as metallic cable and LAN maintenance. Consequently, maintenance and restoration of the existing fiber system may occupy a small portion of their workday activities. As in installation, time is often of the essence in restoration testing. When these technicians need to use an OTDR, they prefer instruments that have the ability to perform “one-button testing.” These technicians require rapid information about the location of a fiber problem, rather than raw waveform information that they would have to analyze to get the same results.

The requirements for one-button testing and expert systems have led to modern OTDRs capable not only of acquiring data but also of analyzing the waveform data to determine the location and severity of each trouble point in the fiber cable. Those who use the instruments for installation and restoration find these expert solutions to be tremendous time- and money-saving features. Early instruments that had these new features enjoyed remarkable success in the optical-test market. The chart in figure 1.4 shows the growth in the number of OTDR suppliers

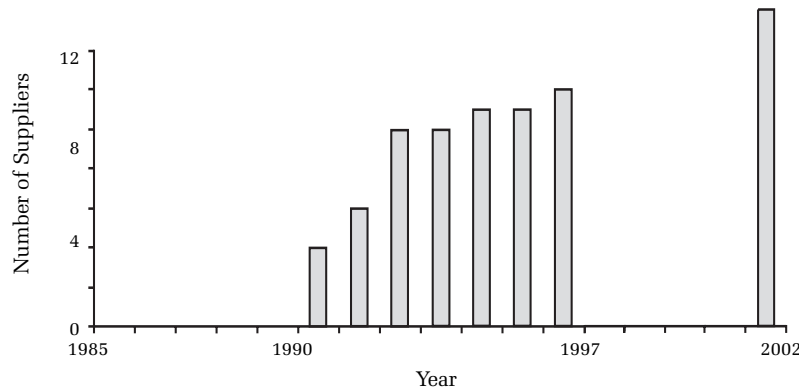


Figure 1.4. Growth in the number of suppliers whose OTDRs have automatic event detection. This feature of modern OTDRs is one aspect of the expert-systems approach to waveform analysis. In this approach, not only does the OTDR acquire the waveform data, but it also interprets the data and evaluates the location and severity of each fault within the fiber cable. The number of suppliers has fallen somewhat since 2002, primarily as a result of the steep recession that hit the fiber-optic industry and led several suppliers to leave the market.

whose instruments have one aspect of expert systems, automatic event detection. Today, virtually all OTDRs have automatic test features that calculate the location, loss, and reflectivity of the connectors, splices, bends, and breaks on optical fibers. Some features also include automatic merging and calculation of bidirectional measurements, as well as other unique and useful measurements. We expect that OTDR designers will continue to make improvements in the instrument's ability to interpret waveform data.

1.3 Summary

The history of OTDR is still being written, so all of it cannot be told here. We can, however, bring the reader up to date on the current status of OTDR developments. In the remaining chapters of this book, we cover certain key aspects of OTDR design, use, and characterization. In chapter 2 we begin with a summary of the fundamentals of fiber optics; we follow this with a discussion of OTDR fundamentals in chapter 3. Chapter 4 is an extensive description of the many performance characteristics of OTDRs: how to interpret performance and how to compare performance among instruments from different manufacturers.

We devote two chapters to discussions of the measurement of event loss. Much of the material in these two chapters is original work developed by the authors to evaluate the performance of automatic event-detection algorithms. Chapter 5 is a discourse on the measurement of nonreflective events. Since there are no sharp edges associated with nonreflective events, reliably evaluating the distance location of this type of event requires special algorithms. In addition, the measurement accuracy associated with locating nonreflective events is strongly influenced by noise. We felt it essential to devote considerable discussion to this topic, since it is such an important aspect of modern OTDR performance. We follow with a general description of loss-measurement error in chapter 6.

Two chapters are focused on the measurement of reflective events within fiber systems. In chapter 7 we describe the causes and effects of reflections within fibers as well as some techniques for measurement of backscatter coefficients of fibers. Chapter 8 is a brief discussion of the effects of reflective events on the evaluation of waveform data.

Several chapters are dedicated to the use of OTDRs for performing nontraditional measurements. Chapter 9 describes some basic principles of measuring the numerical apertures (NAs) and cut-off wavelengths of single-mode fibers using OTDRs. In chapter 10 we cover some interesting aspects of interpreting OTDR waveforms that have been obtained from passive splitter networks. Again, much of the material in that chapter is original work done by several investigators at Tektronix.* Chapter 11 is a discussion of the relative advantages and disadvantages of various types of event-marking algorithms. In order to illustrate some of the preferred methods of testing OTDRs, we have dedicated chapter 12 to a discussion of OTDR test fixtures. Chapter 13 is a basic primer on polarization mode dispersion (PMD) in single-mode fibers and how one might use a polarization OTDR to probe PMD. Chapter 14 is an attempt to assemble and summarize some of the information available in the literature on dispersion in optical fibers; chapter 15 provides some practical information about features and functions as well as on safety.

We have written this book from a technical perspective. Where necessary, we provide a first-level demonstration of the mathematical basis for various OTDR principles. In addition, chapter 15 includes useful information on how to select an appropriate OTDR for a particular

*Our gratitude goes to Harvey Jauvtis of Tektronix and Dan Hayes of FICO for considerable time spent in exploring this technique.

test application. Those considering the purchase of an OTDR may find this chapter useful in evaluating the many different types of OTDRs that are currently on the market. This chapter, like others in the book, can be read as a stand-alone reference. Some of the material in this chapter has already appeared in the industry literature.

Suggested reading

- Barnoski, M. K., editor, *Fundamentals of Optical Fiber Communications* (Orlando: Academic Press, 1981).
- Miller, S. E., and Chynoweth, A. G., editors, *Optical Fiber Telecommunications* (Orlando: Academic Press, 1979).
- Miller, S. E., and Kaminow, I. P., editors, *Optical Fiber Telecommunications II* (San Diego: Academic Press, 1988).
- Chaffee, C. D., *The Rewiring of America* (Orlando: Academic Press, 1988).

-
- ¹ Liu, Fenghai, postdeadline paper presented at *Optical Fiber Conference*, Atlanta, Georgia, March 2003. Liu reported 40 channels operating at 40 Gb/s over 10,000 km without electrical regeneration.
- ² Kapron, F. P., Maurer, R. D., and Teter, M. P., "Theory of backscattering effects in waveguides," *Applied Optics*, Vol. 11, No. 6 (1972), pp. 1352–1356.
- ³ Barnoski, M. K., and Jensen, S. M., "Fiber waveguides: a novel technique for investigating attenuation characteristics," *Applied Optics*, Vol. 15, No. 9 (1976), pp. 2112–2115.
- ⁴ Personick, S. D., "Photon probe—an optical time-domain reflectometer," *Bell System Technical Journal*, Vol. 56 (1977), p. 355.
- ⁵ Barnoski, M. K., Rourke, M. D., Jensen, S. M., and Melville, R. T., "An optical time-domain reflectometer," *Applied Optics*, Vol. 16, No. 9 (1977), p. 2375.
- ⁶ Barnoski, M. K., and Personick, S. D., "Measurements in fiber optics," *Proceedings of the IEEE*, Vol. 66, No. 4 (April 1978), pp. 429–441.
- ⁷ Neumann, E.-G., "Optical time-domain reflectometer: comment," *Applied Optics*, Vol. 17, No. 11 (June 1978), p. 1675.
- ⁸ Chaffee, C. David, *The Rewiring of America, the Fiber Optics Revolution* (Orlando: Academic Press, 1988).
- ⁹ Garrett, I., and Todd, C. J., "Components and systems for long-wavelength monomode fiber transmission," *Optical and Quantum Electronics*, Vol. 14 (1982), pp. 95–143.
- ¹⁰ Cermak, O., and Jasenek, J., "On increasing the performance parameters of an optical time-domain reflectometer," *Elektrotechn. Cas.*, Vol. 43, No. 7 (1992), pp. 220–224.
- ¹¹ Newton, S. A., "Novel approaches to optical reflectometry," *Proceedings of IMTC '90* (invited paper B-2, San Jose, CA, 1990), pp. 329–333.
- ¹² Healey, P., "Optical time-domain reflectometry—a performance comparison of the analogue and photon-counting techniques," *Optical and Quantum Electronics*, Vol. 16 (1984), pp. 267–276.
- ¹³ Healey, P., "Review of long-wavelength single-mode optical-fiber reflectometry techniques," *Journal of Lightwave Technology*, Vol. LT-3, No. 4 (1985), pp. 876–886.
- ¹⁴ Shadaram, M., and Kuriger, W. L., "Using the optical frequency-domain technique for the analysis of discrete and distributed reflections in an optical fiber," *Applied Optics*, Vol. 23, No. 7 (1984), pp. 1092–1095.

- ¹⁵ Uttam, D., and Culshaw, B., "Precision time-domain reflectometry in optical fiber systems using a frequency-modulated continuous-wave ranging technique," *Journal of Lightwave Technology*, Vol. LT-3, No. 5 (1985), pp. 971–977.
- ¹⁶ Kingsley, S. A., and Davies, D. E. N., "OTDR diagnostics for fiber and integrated-optic systems," *Electronics Letters*, Vol. 21, No. 10 (1985), pp. 434–435.
- ¹⁷ Healey, P., and Smith, D. R., "OTDR in single-mode fiber at 1.55 μm using a semiconductor laser and PINFET receiver," *Electronics Letters*, Vol. 18, No. 22 (1982), pp. 959–961.
- ¹⁸ Gold, M. P., and Hartog, A. H., "Ultra-long-range OTDR in single-mode fibres at 1.3 μm ," *Electronics Letters*, Vol. 19, No. 13 (1983), pp. 463–464.
- ¹⁹ Namihira, Y., et al., "OTDR in a 147-km single-mode fiber in 1.55- μm -wavelength region using an LD and GaInAs/InP APD at room temperature," *Electronics Letters*, Vol. 23, No. 23 (1987), pp. 1219–1221.

Chapter 2

Fundamentals of fiber optics

2.0 Introduction

Since OTDRs are used almost exclusively to test optical fibers, it will be useful to review some of the basics of fiber optics before we begin discussing the details of OTDRs.* There are many fine texts on the subject of fiber optics, but this chapter concentrates on those fundamental elements of fiber optics that are likely to be important when testing optical fibers using OTDRs.† We begin by illustrating some of the problems that must be overcome to transmit information using light. Then we introduce the concepts of internal reflection, Rayleigh scattering, absorption, numerical aperture, modal properties of fiber, dispersion, and coherence. We have attempted to summarize the material in an understandable fashion, with working equations that are adequately referenced for those readers wishing a more detailed and rigorous development of the subject. Later chapters treat some of these subjects, such as chromatic dispersion, in greater detail as they relate to specialized tests that you might perform with an OTDR.

2.1 Total internal reflection

Imagine you want to transmit information from one point to another at a very high data rate. How would you accomplish this? One approach might be somehow to modulate a lightwave carrier. Light seems an obvious candidate for high-speed, high-data-rate transmissions since it has a very high bandwidth (in the terahertz range) and travels faster than anything in the universe. In your attempt to use light to transmit information, you might collimate a laser beam, modulate it, and point it at an optical receiver. This seems like an obvious solution, as long as no light-blocking or light-scattering objects (such as dust, water moisture, or solid objects) come between the transmitter and receiver.

Besides the obvious problems of scattering and blocking, free-space transmission with collimated laser beams has other limitations.

*Certain high-resolution OTDRs are used to test discrete optical components, such as connectors, pigtailed, and waveguides. This book, however, is devoted to OTDRs that test only optical fiber, and are used primarily by the telecommunications industry. In chapter 3 we give a brief description of some OTDRs that can be used to test discrete optical components.

†Readers wishing a more complete treatment of the subject are referred to the Suggested reading section at the end of this chapter.

Since light behaves as a wave phenomenon, free-space transmission is subject to diffraction effects. Diffraction is a phenomenon of all waves, including light, and causes the waves to spread out as they propagate. As a result of diffraction, the farther away you place the receiver, the wider the laser beam will be. As the distance between transmitter and receiver increases, this increasingly wide laser beam greatly overlaps the optical receiver, dropping the amount of power on the receiver and reducing the signal-to-noise ratio (SNR). Increasing the size of the optical receiver does not help, because this invariably reduces the receiver's bandwidth. Thus, with free-space transmission, we face some fundamental limits on SNR, bandwidth, and interference from objects that block or scatter the light beam.

Another problem with free-space transmission is the requirement for precise pointing accuracy. For the receiver to detect the signal, the laser source must be accurately pointed at the receiver. The difficulty in achieving the required pointing accuracy increases as the distance to the receiver grows larger. Because of these problems, free-space transmission is often not a good solution for terrestrial applications. It is sometimes a good solution for communication between orbiting satellites, especially if the communication needs to be relatively safe from eavesdropping. Other uses include point-to-point communication between buildings that are part of a local-area network. For terrestrial telecommunication applications, however, free-space transmission is relatively rare.*

To get around some of the problems with free-space transmission, we might decide to try containing the light in some way. For instance, suppose we design a hollow tube with highly polished and highly reflective inside walls (see figure 2.1). We could launch a modulated beam into the tube. The light would reflect off the inside of the tube until it reached the opposite end, where it could be detected by an optical receiver. For this method to work, however, the inside of the hollow tube must be extremely reflective. To understand just how reflective it must be, let's consider a hypothetical example. Suppose we design our hollow tube to be about a millimeter in diameter. We transmit using a near-infrared laser and select polished gold as the interior reflecting material. At 800 nm, gold has a reflectivity of about 95%. This may sound high, but consider an example. Suppose the light that travels down the pipe

*A notable exception is microwave transmission. Microwave stations, aimed at each other over long distances, have been used for many years in telephony. Microwave transmission is limited mostly to line of sight and is far more tolerant of atmospheric conditions (such as rain and dust) than visible light.

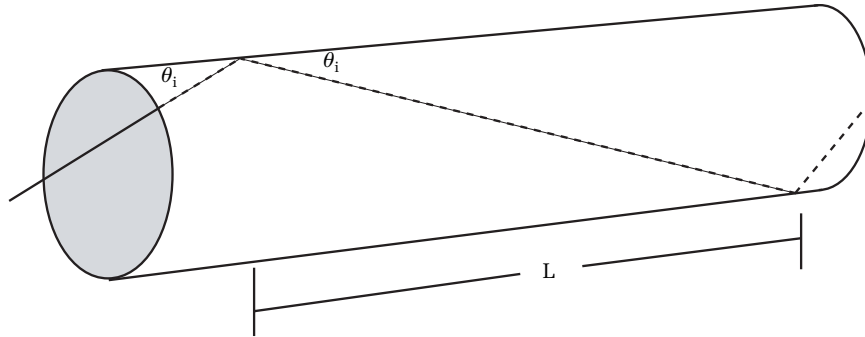


Figure 2.1. A possible design for a hollow light pipe. The inside of the pipe is coated with a very reflective material. Light injected into one end of the light pipe reflects from the inside surface as it propagates from the transmitter to the receiver. The inside of the pipe must be very reflective, or even short lengths will have unacceptable end-to-end loss.

reflects, on average, once every centimeter. After 1 meter, the light has reflected 100 times, and those reflections have attenuated it by about 22 dB. Clearly, to be practical over long distances, our light pipe must have interior walls that are far more reflective than gold.

We might try improving the attenuation of our light pipe by using a multilayer dielectric coating on the inside instead of gold. Some multilayer dielectric coatings are capable of reflectivities as high as 99.99%. However, even if we coat the inside of our light pipe with a coating as efficient as 99.99%, the attenuation is still 0.043 dB per meter, or 43 dB per km (assuming 100 reflections per meter). For comparison, high-quality metallic coaxial cable has an attenuation of between 20 and 80 dB per km at 100 MHz. So even with highly reflective dielectric coatings, we will have a difficult time building a light pipe that performs much better than coaxial cable at frequencies below 100 MHz.*

Even if we coated the inside of our light pipe with an efficient multilayer dielectric coating, many other problems would remain to be solved. First, highly reflective dielectric coatings usually require many coatings — sometimes as many as a dozen or more individual layers.¹ Applying these coatings uniformly to the inside of the light pipe would be very difficult. Another difficulty in designing such coatings is that they must work at large angles of incidence (many of the light rays will be almost parallel to the walls of the light pipe). Under such conditions,

*This comparison is based solely on attenuation. The hollow light pipe will also have dispersive effects that make it even less likely to perform as well as metallic coaxial cable.

however, dielectric coatings can be sensitive to the state of polarization, so our light pipe may suffer from polarization-dependent attenuation.² Finally, this design is subject to dispersive effects. We discuss dispersion later, but for now it is sufficient to note that the hollow light pipe tends to spread out pulses of light. At high data rates this spreading causes adjacent pulses to overlap, limiting the maximum data rate that the light pipe can transmit. Thus, even if it is possible to solve the attenuation and polarization problems, coating the inside of a light pipe does not seem the best way to transmit information-carrying light waves.

These examples illustrate the nontrivial problems associated with transmitting information via light waves. Now let's look at a third possibility. Suppose we have a thin slab of very pure optical material into which we direct a collimated laser beam at an angle (see figure 2.2).

Because of the index discontinuity between air and glass, about 4% of the incident laser beam is reflected at the slab's end face, and the

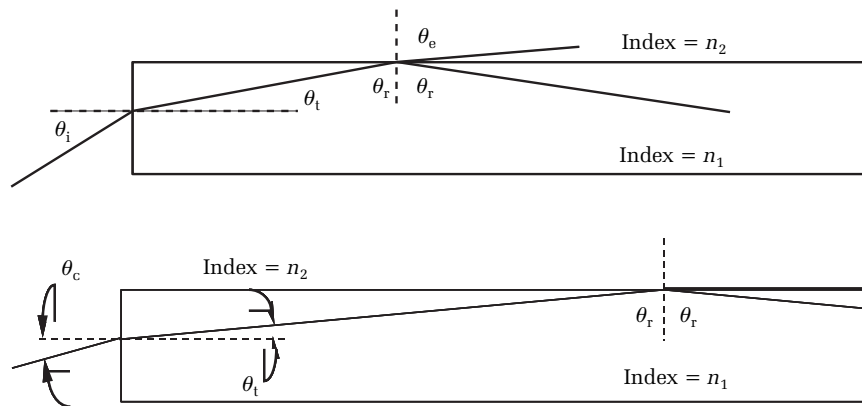


Figure 2.2. A light guide made from a slab of transmissive material. The index of the core material is n_1 and the index of the cladding (material around the core) is n_2 . The core index is greater than the cladding index. When the input angle (θ_i) is large, the transmitted light is both reflected and transmitted when it strikes the top surface of the slab (see top figure). As the input angle is reduced, the transmitted ray bends toward the surface of the slab. If the input angle is reduced enough, the transmitted ray is parallel to the surface of the slab. For input angles less than this critical angle, the light is totally reflected at the boundary between the cladding and the core (see bottom of figure). When this happens, we say the light is contained by total internal reflection. If we make the boundary between the cladding and core very smooth (so there is no surface scattering) then the light propagating along the slab has zero loss (except for absorption and scattering within the bulk material).

rest is transmitted into the slab.* Once inside the slab, the beam strikes the sides at an angle that depends on the beam's input angle and the slab's index of refraction. When the beam strikes the side of the slab, part of the light transmits and part is reflected. The reflected light travels downward and strikes the opposite side of the slab, where, again, part of it is transmitted and part of it is reflected. This looks very much like the light pipe, except we seem to lose more light. What could be the advantage in this?

Suppose we gradually reduce the angle of the input laser beam so that it is more nearly parallel to the axis of the slab. As we reduce the angle of the input beam, the transmitted light emerging from the upper surface of the slab moves closer to being parallel to the slab's surface (see figure 2.2). If we keep making the input angle smaller, we eventually reach an angle where the transmitted beam emerges exactly parallel to the surface of the slab. If we make the entry angle smaller than this critical angle, the transmitted beam disappears altogether, and we achieve 100% reflectivity at the slab's boundary. The difference between 100% internal reflection and 99.99% reflection may not seem significant, but when multiplied over hundreds of thousands of reflections, the difference adds up to a very significant improvement in overall transmission loss. With total internal reflection, transmission through the slab becomes efficient because the only contributions to optical attenuation are absorption and scattering in the slab's material.

Our slab is thin but of infinite width. Consequently, as the light propagates along the slab, its width continues to diverge. To solve this problem and fully contain the beam, we simply use a cylindrical rod instead of the slab. A very thin rod, with a polished cylindrical surface, seems like a good candidate for transmitting light. To optimize our design, we might add a cladding material around the rod to prevent the outer surface of the glass core from being marred or otherwise damaged. Protecting this surface is important because scratches or other damage scatter light out of the core, increasing the attenuation. To maintain the waveguide properties of the core (so that total internal reflection is still possible), the cladding needs to have a lower index of refraction than the core.

Finally, to use our light guide for practical purposes, we need it to be flexible so we can build it into a cable. Glass, however, is very brittle and tends to break when you bend it. If you bend a glass fiber so the surface

*Chapter 7 explains how to calculate this 4% figure.

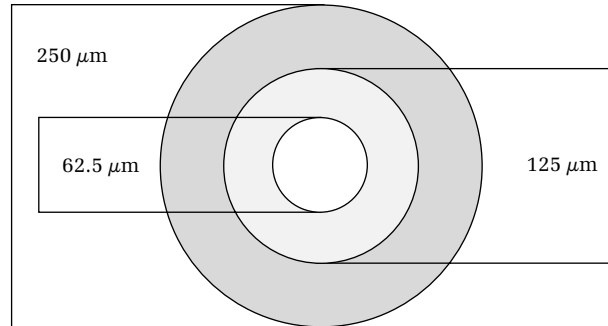


Figure 2.3. Multimode 62.5- μm /125- μm cable schematic. [Credit: The Light Brigade.]

strain exceeds about 0.2%, significant stress cracking is likely over the lifetime of the fiber.³ The surface stress in a bent rod is proportional to the fiber radius divided by the bend radius. Thus, one way to make the fiber more flexible is to make it very thin and then to encase it in a buffer material that prevents easy bending below a safe radius. To achieve good flexibility, we might choose an outer cladding diameter of about 125 μm , with a core diameter of 62.5 μm (see figure 2.3). We could then surround this with a pliable acrylate buffer about 250 μm in diameter.

What we have “invented” in this little scenario is a modern multimode optical fiber that is both optically functional and of a physical size for handling, splicing, and connectorization. In practice, of course, optical fiber is far more complicated than the simple model we just described. In the remaining sections of this chapter we discuss some of the more specialized aspects of optical fiber.

If we look back in the history of fiber optics, we find that the first demonstration of total internal reflection for guiding light was first scientifically demonstrated by Daniel Colladon at the University of Geneva in 1841. His experiment involved collecting sunlight and piping it through a tube to his lecture table. A lens focused the light through a water tank and out along a water jet escaping from a small hole in the opposite side of the tank. Total internal reflection trapped light rays in the water stream, bouncing along the curving arc of water until the jet broke up.

Jacques Babinet, a French optics specialist, made similar demonstrations in Paris. He also noticed that the experiment worked with glass rods bent into various shapes. Because glass fibers are actually very thin glass rods, Babinet was the first to anticipate fiber optics.

But Babinet also knew the glass of his time was not very clear, so light could not travel very far within the material. Look into the edge of modern window glass, and you can see the same green color that Babinet saw a century and a half ago. This led him to conclude that light guiding was merely a parlor trick, and he turned his attentions elsewhere.

But the pioneers of fiber optics did not credit the discovery of total internal reflection to Daniel Colladon or even to Jacques Babinet, but to John Tyndall, who demonstrated it a full thirteen years after Colladon. Tyndall incorporated the demonstration in his lectures.

When later physicists looked back for the origins of light guiding, they came upon Tyndall's account. By then Colladon's papers were buried in scholarly libraries, unreferenced and forgotten. Even today, the Tyndall award provided by the Optical Society of America is incorrectly named.

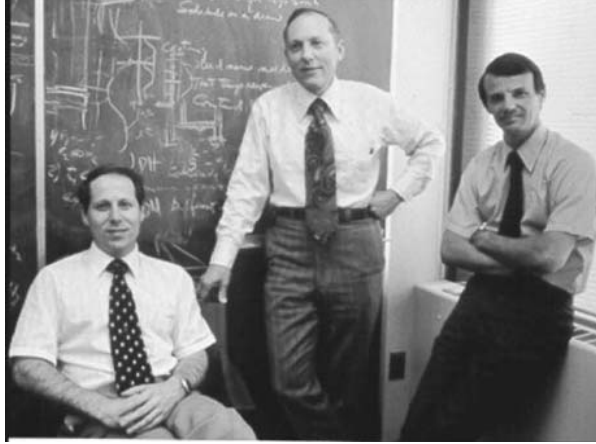
2.2 Fiber attenuation

Total internal reflection allows us to transmit light through an optical fiber with great efficiency, provided attenuation and scattering from the glass are sufficiently low. Toward that goal, tremendous improvements have been made in the attenuation characteristics of optical fibers since their earliest inception. As recently as 1960, the best optical glass had an attenuation of about 1000 dB/km. In November 1965 Charles Kao (see figure 2.4) and Charles Hockham, working with Standard Telecommunications Laboratories in Harlow, England, wrote a paper titled "Dielectric-fiber surface waveguides for optical frequencies," which was published as part of the IEEE proceedings in 1966. The paper identified the requirements of an optical fiber for use in communication systems including the structure of the optical fiber, the causes of



Figure 2.4. Dr. Charles Kao, whose 1966 paper set the requirements for fiber-optic communications. [Credit: The Light Brigade.]

Figure 2.5. The Corning team of Donald Keck, Robert Mauer, and Peter Schultz, who manufactured the first optical fiber to meet Charles Kao's performance requirements. [Credit: Corning.]



attenuation in optical glass (such as absorption and scattering), the present state of optical glasses, mode characteristics, bending losses, dispersion, physical aspects, and experimental investigations.

A team at Corning Glass led by Robert Mauer, Donald Keck, and Peter Schultz (see figure 2.5) were able by 1970 to reduce this attenuation to 2 dB/km by eliminating absorbing impurities. Today, high-quality single-mode fibers have an attenuation of only a few tenths of a decibel per kilometer.⁴

To appreciate just how clear modern optical fibers are, consider this: If the ocean were made of glass having 1000 dB of attenuation per kilometer, the bottom of the ocean would be completely black; so black, in fact, that out of 10^{805} photons (an unimaginably large number) striking the surface of the ocean, only one would reach the bottom.* If the ocean were made of glass having 2 dB of attenuation per kilometer, the bottom of the ocean would still appear black. At this attenuation, roughly one of 41 photons striking the ocean surface would get to the bottom. However, at 0.35 dB of attenuation per kilometer, the bottom of the ocean is easily visible, with slightly more than half of the photons that strike the surface reaching the bottom of the ocean.

Optical attenuation within the fiber results from absorption and scattering. Absorption is a material property of the fiber and results when light excites resonances at the molecular level, which are then followed by nonradiative relaxation processes. Stained glass is an example of absorption. With absorption, the photons are lost when

*Assuming an ocean depth of five miles.

they are absorbed, and their energy is converted into heat.* Scattering is also a material property; it results when imperfections within the fiber redirect, or scatter, some of the light into rays that are no longer guided by the fiber.† For instance, we saw that when light strikes the sides of the waveguide at angles steeper than the critical angle, it is partially reflected and partially transmitted. When an impurity or index discontinuity within the fiber scatters light, it scatters in all directions. Some of the light is scattered at angles outside the fiber's critical angle, where it is quickly lost.

To reduce absorption, the optical fiber must be free of impurities that have electronic or atomic resonance near the transmission wavelength. Much of the work devoted to reducing the amount of absorption in optical fibers has been directed toward the development of ultrapure silica glass. The impurities of most concern are water vapor and the first row of transition metals (vanadium, chromium, magnesium, iron, cobalt, and nickel). As a general rule, concentrations of these impurities must be kept below about one part in 10^9 , or their contribution to absorption exceeds 1 dB/km at wavelengths near $1\ \mu\text{m}$.

The problem with water contamination arises from the O–H bond, which has a fundamental frequency near the optical wavelength of $2.73\ \mu\text{m}$ and harmonics near wavelengths used in modern telecommunications systems. The two harmonics of most concern in telecommunications systems are roughly $1.39\ \mu\text{m}$ and $1.24\ \mu\text{m}$. The harmonic at $1.39\ \mu\text{m}$ results in attenuation of 65 dB/km when O–H exists in concentrations of only one part per million. The harmonic at $1.24\ \mu\text{m}$ results in attenuation of 2.3 dB/km at the same concentration.⁵ Clearly, to manufacture low-loss optical fiber, virtually all water must be removed from the glass preform from which the optical fiber is drawn.

Scattering can result from the presence of microscopic bubbles or contaminants. Sunsets are a common example of the phenomenon of scattering. They appear red because the atmosphere scatters the blue light more than the red, leaving a predominance of red light in the transmission path to the eye. In the ultrapure glass used to manufacture

*The absorbed photons are converted in the glass to phonons (lattice vibrations). These lattice vibrations warm the glass, and the warm surface of the glass emits photons of very long wavelength in the infrared portion of the electromagnetic spectrum.

†So far we have treated light as consisting of rays that travel in straight lines. This simplistic view, although technically incorrect, is sufficient for understanding many aspects of light. Later in this chapter we will discuss the wave nature of light and introduce the concept of modes. A more technical description of loss due to scattering is that the light is scattered into unguided modes.

optical fiber, the dominant source of scattering is the presence of microscopic inhomogeneities. Unlike minerals such as diamond and quartz, glass does not have a crystalline structure, so it is by nature somewhat disordered. In this disordered structure, there are variations in material density that fluctuate around a mean. These variations result in microscopic changes in the material's index of refraction; when light encounters these discontinuities, it scatters. When light is scattered from objects much smaller than the wavelength of light, as it is in optical fiber, we call it *Rayleigh scattering*. In modern telecommunications fiber, Rayleigh scattering is the primary source of attenuation. Fiber manufacturers try to minimize the amount of light lost to Rayleigh scattering by reducing the size of the microscopic discontinuities. One way to do this is to cool the fiber slowly and in a carefully controlled manner.

A fundamental characteristic of Rayleigh scattering is that it is inversely proportional to the fourth power of the wavelength. Because of this wavelength sensitivity, shorter wavelengths of light are scattered more strongly than longer ones. Since Rayleigh scattering is so dependent upon wavelength, one way to reduce the scattering loss in an optical fiber is to increase the transmission wavelength. For example, since $(1550/1310)^4 \cong 2$, the scattering loss at 1310 nm is about twice what it is at 1550 nm. This is the principal reason that many long-range transmission systems operate at 1550 nm instead of 1310 nm.

Although troublesome because of its attenuation aspects, Rayleigh-scattered light is advantageous for testing optical fibers. When light travels along an optical fiber, the light scatters in all directions. Most of this scattered light is outside the critical angle for total internal reflection and is thus lost from the waveguide. Some of the light scatters in the forward direction and travels along the fiber with the original pulse. Some of the light scatters in the backward direction, away from the traveling pulse, and returns to the transmitter. This backscattered light forms the basis of operation for OTDRs. OTDRs launch pulses of light into the fiber and then measure the intensity of the backscattered light as a function of time. Using this methodology, OTDRs can measure such properties as the fiber's total loss, loss per kilometer, and the individual losses of splices and connectors that are distributed along the fiber.

Optical attenuation has been greatly reduced since the first practical fibers were developed roughly 20 years ago. Today, modern single-mode telecommunications fibers have attenuation less than 0.35 dB/km at 1310 nm, and less than 0.25 dB/km at 1550 nm. Multimode fibers have

slightly higher loss. Typical loss for multimode fibers is 0.5 dB/km at 1300 nm and 2.4 dB/km at 850 nm. (We discuss the differences between multimode and single-mode fibers in sections 2.4 and 2.6.) These dramatic improvements have been achieved by reducing absorption due to contaminants (primarily O–H ions) and by carefully controlling the fabrication process to reduce inhomogeneities that cause scattering.

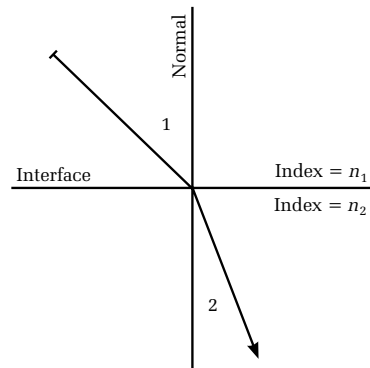
2.3 Numerical aperture

Total internal reflection is the mechanism that makes optical-fiber communications possible. It is only through total internal reflection, which reflects light with 100% efficiency, that the attenuation in optical fibers can be reduced to practical levels. Recall our earlier discussion of the critical angle for which a slab of glass achieves total internal reflection. In this section we shall see that this critical angle is related to the fiber's numerical aperture, which is one of the most fundamental characteristics of an optical fiber.

When light encounters a discontinuity in the index of refraction, it diffracts (or bends) according to Snell's law. You can see this bending when you hold a stick partly submerged in water. The stick appears to bend at the water's surface because the light reflected from the submerged part of the stick diffracts as it leaves the water. Now imagine an interface between two materials that have different indices of refraction, with an imaginary line drawn perpendicular to the interface (see figure 2.6).

Suppose we shine a laser beam at the interface. We call the imaginary line the normal, and we reference the angle of our laser beam between the normal and the path followed by the light. The index of refraction on the incident side of the interface is n_1 and the index on the transmission side of the interface is n_2 . If the angle between the incident

Figure 2.6. Snell's law of refraction. When light encounters a discontinuity in the index of refraction, it bends. The light bends toward the normal when transmitting into a higher index. When transmitting into a lower index, it bends away from the normal. Equation [2.1] describes the transmission angle as a function of the incident angle and the index of refraction of the two materials.



light and the normal is θ_1 , then according to Snell's law the angle between the normal and the transmitted light is

$$\theta_2 = \sin^{-1}\left(\frac{n_1}{n_2} \sin(\theta_1)\right) \quad [2.1]$$

Using equation [2.1] it is possible to trace the rays in figure 2.6 and show that total internal reflection occurs when the incident angle at the endface of the fiber is less than critical angle, defined as

$$\theta_c = \sin^{-1}\left(\sqrt{n_1^2 - n_2^2}\right) \quad [2.2]$$

Equation [2.2] gives the fiber's critical angle when n_1 is the core index and n_2 is the cladding index. Rays that enter the fiber within a cone defined by this angle are trapped in the fiber through internal reflection. They become guided rays. Rays that enter the fiber outside this cone are quickly attenuated by partial transmissions and lost from the fiber. The sine of this critical angle defines the fiber's numerical aperture. We see later in this chapter that the numerical aperture is one of the most important parameters used to describe an optical fiber. For practical communications fibers, the difference between the index of the cladding and of the core is usually very small, so we can approximate the numerical aperture as

$$\text{NA} = \sqrt{n_1^2 - n_2^2} = n_1 \sqrt{2\Delta} \approx n_1 \sqrt{2\delta} \quad [2.3]$$

where $\Delta = \frac{(n_1^2 - n_2^2)}{2n_1^2} \approx \delta = \frac{(n_1 - n_2)}{n_1}$, which is the *refractive index contrast*.

2.4 Multipath (modal) dispersion

Understanding the sources of attenuation and solving them are the first steps toward designing practical optical fibers for high-speed telecommunications networks. Besides attenuation, however, the engineer must be careful in designing the more esoteric parameters, or the fiber will exhibit unacceptable levels of dispersion. *Dispersion* refers to the tendency of pulses of light to broaden (in the time domain) as they propagate along the fiber. Left unchecked, dispersion can easily limit the bandwidth of an optical-fiber network. In this section we describe some

of the causes of dispersion and how engineers and scientists design their products to minimize its effects.

In section 2.3 we saw that all the light rays that enter a fiber within the cone of the numerical aperture are captured by the fiber. These rays propagate along the fiber and (after being attenuated by absorption and scattering) emerge from the opposite end. When optical fiber is used in communications systems, a light source (typically a laser) launches a series of short pulses into the fiber. These pulses of light consist of many different rays, each of which makes a slightly different angle with the fiber's axis. Because of these different angles, each of the rays travels a slightly different distance as it propagates along the fiber. Rays that are almost parallel to the fiber's axis travel the shortest distance, while rays that are at the critical angle travel the farthest. The difference in distance traveled by the various rays can be enough to add a measurable time delay among the family of rays that constitute the pulse. The result of this time delay is that the pulse energy spreads out, or disperses, and adjoining pulses begin to overlap each other. When this happens, the signal's modulation depth decreases, and transmission errors begin to occur. We can estimate the effects this dispersion has on the system bandwidth by examining the time delay between the axial rays and those that are at the critical angle. This time delay is

$$\Delta t = \frac{Ln_1^2}{cn_2} \delta \quad [2.4]$$

In equation [2.4], L is the fiber's length and c is the speed of light in a vacuum ($c = 299,792,458$ m/sec). From this equation you can see that the time delay between the axial and maximal rays increases with the numerical aperture and fiber length.

As an example, suppose we have a fiber with a core index of 1.5 and a cladding index of 1.49. Accordingly, the difference in index is 0.01, the numerical aperture is 0.173, and the acceptance angle is about 10° . Using equation [2.4] we see that the time delay for this type of fiber is about 34 ns/km. For many purposes, you can approximate the fiber's bandwidth as a function of the time delay by using the equation

$$B \approx \frac{1}{2\pi \Delta t} \quad [2.5]$$

For our example, the fiber's bandwidth is about 4.7 MHz·km. Notice that we have normalized the bandwidth to 1 km. This is a convenient

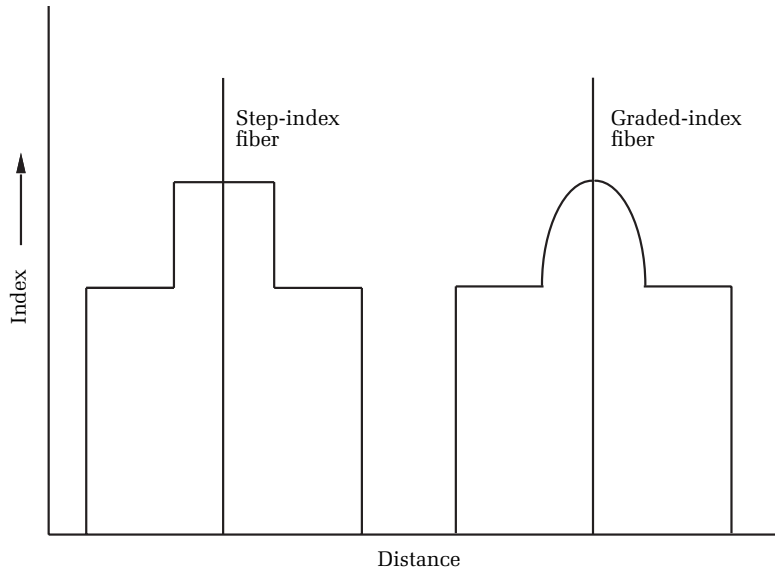


Figure 2.7. Step-index and graded-index fiber. Step-index fiber has high multipath dispersion because maximal rays propagate along the fiber more slowly than axial rays. In graded-index fiber the maximal rays still travel further than the axial rays. Because of the graded-index profile, however, the maximal rays travel mostly through lower-index material, so they travel faster. The increase in speed compensates for the increase in distance, so the maximal and axial rays arrive at nearly the same time, and multipath dispersion is greatly reduced.

way of expressing the bandwidth, since the time delay increases as the fiber gets longer. The dispersion-limited bandwidth of a step-index multimode fiber is much less than the inherent bandwidth limitation imposed by using a carrier wave at optical frequencies.* This means that multipath dispersion is wasteful and significantly reduces the fiber's potential for carrying high-speed data. One way to reduce multipath dispersion is to change the fiber's index profile. So far, we have assumed that the fiber has a sharp demarcation between the cladding and the core (see figure 2.7). Inside the core the index is n_1 and outside the core the index is n_2 . The maximal rays propagate more slowly along the fiber than the axial rays because they travel farther. Suppose, however, that we change the index profile so that the index near the core-cladding boundary is lower than it is near the core's center.

*We address single-mode fibers later in this chapter. For now, you can think of a multimode fiber as one that supports different "rays," as in our simplistic derivation of the time delay in equation [2.4].

If we adjust the index profile just right, we can compensate for the extra distance that the maximal rays travel by making them travel faster through lower-index material near the edges of the core. With the proper radial variation in the index, it is possible to design graded-index fiber such that the maximal and axial rays arrive at almost the same time. Using an ideal profile, multipath dispersion can be reduced below 0.1 ns/km. In manufactured fibers, multipath dispersion is usually less than 1 ns/km. Common graded-index fibers have cores with a parabolic profile, described by the equation

$$n(r) = n_1 \left(1 - \delta \cdot \left(\frac{r}{a} \right)^2 \right) \quad [2.6]$$

In equation [2.6], n_1 is the index on axis, r is the radial distance from the axis, a is the core radius, and $\delta = (n_1 - n_2)/n_1$.

Another way to reduce dispersion is to keep the step-index core profile but to reduce the core size until only the axial “ray” is transmitted. When we do this, however, we must stop thinking of light as defined rays. The ray approximation for light is sometimes acceptable as long as the physical dimensions of the fiber are large compared with the wavelength of light. This is often the case for multimode fibers, where core sizes are relatively large. Typical multimode fibers, for example, have a core diameter of 50 or 62.5 μm . Telecommunications fibers carry information at wavelengths between 1300 and 1600 nm, so the core of a multimode fiber is roughly between 30 and 50 times as large as the wavelength of light. Consequently, in some instances (but not all) the ray model is sufficient for multimode fibers.

If we reduce the core size to about 10 μm , the ray model no longer suffices for our analysis. In this realm, we must model the fiber’s transmission characteristics by treating it as a waveguide and solving Maxwell’s equations with the appropriate boundary conditions.* Doing this, we discover that when the core diameter and numerical aperture are reduced to certain limits, the fiber supports only one mode, and this effectively eliminates multipath dispersion.†

*James Clerk Maxwell (1831–1879) showed theoretically that the electromagnetic field could propagate as transverse waves. His equations show that these waves travel at the speed of light, which is a function of the electric and magnetic properties of the medium through which the wave propagates. His equations are reproduced in equation [2.21].

†Some multipath dispersion may remain, since single-mode fibers have degenerate polarization modes that may exhibit modal dispersion in the presence of birefringence. We discuss this at greater length in chapter 13. Single-mode fibers also exhibit chromatic dispersion, which is the subject of the next section.

2.5 Chromatic dispersion

Dispersion, or the spreading out of optical pulses over time, comes from several possible sources. In section 2.4 we saw that multipath dispersion can be significant for multimode fibers and that graded-index fibers are an effective way of reducing this type of dispersion. Even if all the modes travel the same speed, however, chromatic dispersion may still limit the fiber's bandwidth capability. Chromatic dispersion (CD) is the wavelength dependence of the speed of light when traveling through a medium other than a vacuum, such as a glass fiber. We refer to such media, where the index of the material changes with wavelength, as dispersive. In a vacuum, light travels with the constant velocity c . When traveling through a dielectric material such as glass, however, the speed of light decreases. The ratio of the speed of light in a vacuum to its phase velocity in the medium (v_p) is the material's index of refraction, n .*

$$n \equiv \frac{c}{v_p} \quad [2.7]$$

In bulk optics, the word dispersion normally refers to the change in index divided by the change in wavelength, or $dn/d\lambda$. This ratio determines, for instance, the amount of color spreading when you pass white light through a prism. When you shine white light through a prism, the prism's dispersive glass and angles cause the frequency components in white light to fan out into the familiar colors of the rainbow. In optical-fiber communications our concern is with the tendency for pulses to spread out and overlap as they propagate along the optical fiber. This spreading out, or dispersing, of pulses is a function of the second derivative of the refractive index with respect to wavelength, not the first derivative.

Since CD results only when different wavelengths of light are present, it seems reasonable to solve this problem by simply requiring the optical transmitter to operate at a single frequency. Using ultranarrow optical sources is, indeed, one way to reduce the negative effects of CD. However, in the real world, perfectly monochromatic light sources are not possible. Even if a perfectly monochromatic source were available, it would not be monochromatic when used to transmit information in a fiber-optic system. This is because transmission of information

*Phase velocity is the speed at which wavefronts of constant phase travel. In a dispersive medium, this is different from the velocity that a pulse of light travels. The speed with which the pulse travels is called the group velocity. We discuss group velocity in greater detail later in this section.

requires the source to be modulated in either amplitude or phase, and it is a fundamental property of physics that all modulated carriers have a finite bandwidth.* Laser sources used in telecommunications networks have spectral widths that are much smaller than those of incandescent lights or light from the sun. Although the spectral bandwidth is small, however, the different wavelengths travel at slightly different velocities due to the fiber's chromatic dispersion. Consequently, after traveling a sufficiently long distance, the pulses broaden. If the pulses broaden enough that they begin to interfere with each other, the bit-error rate (BER) of the telecommunications system starts to increase. This increase in the BER is the primary reason for wanting to minimize dispersion.

With single-mode fibers, the group velocity changes with wavelength for two reasons. First, there is chromatic dispersion in the bulk material. This bulk dispersion results from the wavelength dependence of the fiber's refractive index. Second, there is waveguide dispersion. Waveguide dispersion results from the wavelength dependence of the fiber's mode-field diameter (MFD). To understand this phenomenon, consider figure 2.8, which shows the relative distribution

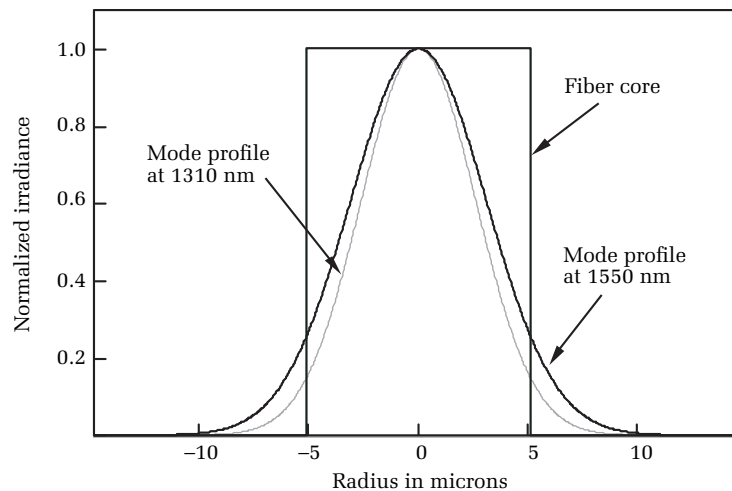


Figure 2.8. Variation in mode size with wavelength. As the wavelength increases, more of the mode is carried by the cladding. The core's index of refraction is higher than the cladding's, and the effective index seen by the mode is a function of both. When the mode extends further into the cladding, the effective index seen by the mode decreases. This variation in effective index would occur even if the material in the cladding and the core were not dispersive.

*All optical sources with finite bandwidth are composed of more than one wavelength.

of light in the fundamental mode at 1310 and 1550 nm, along with the fiber core of a standard single-mode fiber. From this figure, you can see that the light in a single-mode fiber extends well into the cladding and that the mode is slightly wider at longer wavelengths than at shorter ones. Since the mode extends into the cladding, the effective index that it experiences is a function of both the core and the cladding indexes. Mathematically, the expression for this effective index is^{6,7,8}

$$n_{\text{eff}} = n_2 + b(\lambda)(n_1 - n_2) \quad [2.8]$$

$b(\lambda)$ is a function that depends on wavelength. Since the shape of the mode depends on the wavelength of light, the effective index seen by the mode also depends on the wavelength of light, even if there is no material dispersion. In other words, because of the fiber's construction and the profile of the mode, chromatic dispersion in single-mode fibers occurs even if there is no bulk chromatic dispersion in the material from which the fiber is manufactured.

A third source of dispersion is profile dispersion. This results from the different wavelength dependencies of the refractive indices of the core and the cladding and is an important design parameter for high-performance graded-index (multimode) fibers. In single-mode fibers, profile dispersion often is treated as part of the waveguide dispersion.

Manufacturers specify chromatic dispersion as the number of picoseconds of pulse broadening per kilometer of fiber length, per nanometer of source bandwidth (typically specified in ps/(km-nm)). Mathematically, we express the dispersion of fiber-optic systems as

$$D_\lambda = \frac{1}{L} \frac{d\tau}{d\lambda} \quad [2.9]$$

To estimate the amount of pulse broadening for a given fiber and transmitter, multiply the length of the fiber (in km) by the source spectral bandwidth (in nm) and by the manufacturer's specified chromatic-dispersion number. As a general rule, you want to keep the pulse broadening less than about 10% of the width of one bit of data. To improve the dispersion characteristics of the system, you can either use fiber with less chromatic dispersion, operate at a wavelength where the dispersion is smaller, reduce the fiber's length, or use an optical transmitter with a narrower spectral source.*

*Consider a chromatic-dispersion compensator. These are special devices with built-in dispersion that is equal in magnitude and opposite in sign to the system dispersion. Chromatic-dispersion compensators must be chosen individually for each system.

If you plot the total chromatic dispersion versus wavelength for a step-index single-mode fiber, you find the dispersion is negative for shorter wavelengths and positive for longer ones.* At one wavelength, called the *zero-dispersion wavelength*, the chromatic dispersion is zero. For standard single-mode fibers defined by the International Telecommunications Union (ITU) ITU-T G.652 recommendation, the zero-dispersion wavelength is about 1310 nm, so operating at 1310 nm is a natural way of reducing dispersion in standard single-mode fibers. Another way to reduce chromatic dispersion is to use a distributed-feedback (DFB) laser with external modulation, because these lasers typically have narrow spectral widths.

For long fibers it may not be practical to transmit at 1310 nm because of the relatively high fiber attenuation at this wavelength due to Rayleigh scattering. In this case, the designer may choose to transmit at 1550 nm, where fiber attenuation is lowest. To overcome dispersion, the designer may then choose to use a specially designed fiber in which the waveguide dispersion balances the effects of material dispersion at a specific wavelength (1550 nm, in this case). Are we talking about dispersion-compensating fiber here or a DS fiber? Using waveguide dispersion to offset chromatic dispersion has the effect of shifting the zero-dispersion point away from 1310 nm, earning these fibers the name dispersion-shifted (DS) fibers, which are defined by the ITU-T G.653 recommendation.† Additionally, the designer may also choose to use a 1550-nm DFB laser, with a very narrow linewidth, to ensure that the fiber system can support the highest possible bit rate.

So far, we have qualitatively examined some of the issues related to chromatic dispersion. Now let's examine the issue in more quantitative detail. As we mentioned earlier, the phase velocity is the speed with which wavefronts of equal phase travel. In equation [2.7], v_p is the phase velocity of light. This is not, however, the speed at which laser pulses travel. Signals superimposed or modulated onto a light beam do not travel at the phase velocity; instead, they move at the group velocity. The phase velocity, given in equation [2.7] can also be expressed as

$$v_p = \frac{\omega}{\beta} \quad [2.10]$$

*The total dispersion includes the chromatic dispersion of the bulk material as well as waveguide dispersion.

†Some fibers are designed to have nearly zero total dispersion over a wide range of wavelengths; these fibers are called *dispersion-flattened*.

where $\omega = 2\pi c/\lambda$ and $\beta = 2\pi n/\lambda$. The group velocity, as a function of ω and β , is⁹

$$v_g = \frac{d\omega}{d\beta} = \frac{1}{d\beta/d\omega} \quad [2.11]$$

In a nondispersive medium, the phase velocity is independent of the optical frequency. In a nondispersive medium, therefore, the group and phase velocities are equal:

$$\beta = \frac{\omega}{v_p}, \quad v_g = \frac{1}{d\beta/d\omega} = v_p \quad [2.12]$$

In a dispersive medium, however, the phase velocity differs from the group velocity. When light travels in a dispersive medium the group velocity is

$$v_g = \frac{1}{d\beta/d\omega} = \frac{v_p}{(1 - \omega/v_p)(dv_p/d\omega)} \quad [2.13]$$

We can simplify equation [2.13] by noting, from equations [2.7] and [2.10], that

$$\begin{aligned} \frac{\omega}{v_p} &= \frac{2\pi n}{\lambda} \\ \frac{dv_p}{d\omega} &= \frac{dv_p}{dn} \cdot \frac{dn}{d\lambda} \cdot \frac{d\lambda}{d\omega} = \left(-\frac{c}{n^2}\right) \left(\frac{dn}{d\lambda}\right) \left(\frac{1}{-2\pi c/\lambda^2}\right) \end{aligned} \quad [2.14]$$

Substituting equation [2.14] into equation [2.13] and simplifying, we have

$$v_g = \frac{c}{n - \lambda \frac{dn}{d\lambda}} \quad [2.15]$$

A good approximation for the index of refraction in bulk glass, over the wavelength range from 365 to 2300 nm, is¹⁰

$$n = \left(\frac{B_1 \lambda^2}{\lambda^2 - C_1} + \frac{B_2 \lambda^2}{\lambda^2 - C_2} + \frac{B_3 \lambda^2}{\lambda^2 - C_3} + 1 \right)^{0.5} \quad [2.16]$$

In equation [2.16], λ is the wavelength of light (in μm) and the constants B_1 through C_3 (usually supplied by the manufacturer) depend on the specific glass. Table 2.1 lists these constants for a few common bulk glasses and for fused quartz.^{11,12}

	BK7 Glass	SF11 Glass	F2 Glass	Fused Quartz
B_1	1.03961212	1.73848403	1.34533359	0.6961663
B_2	0.231792344	0.311168974	0.209073176	0.4079426
B_3	1.01046945	1.17490871	0.937357162	0.8974794
C_1	$6.00069867 \cdot 10^{-3}$	$13.6068604 \cdot 10^{-3}$	$9.97743871 \cdot 10^{-3}$	$4.679148 \cdot 10^{-3}$
C_2	$2.00179144 \cdot 10^{-2}$	$6.15960463 \cdot 10^{-2}$	$4.70450767 \cdot 10^{-2}$	$1.351206 \cdot 10^{-2}$
C_3	$1.03560653 \cdot 10^2$	$1.21922711 \cdot 10^2$	$1.11886764 \cdot 10^2$	$9.896161 \cdot 10^1$

Table 2.1. Dispersion constants for some common types of glass.

Figure 2.9 shows how the index of refraction changes with wavelength for fused quartz, which is the basic material used to manufacture optical fibers.

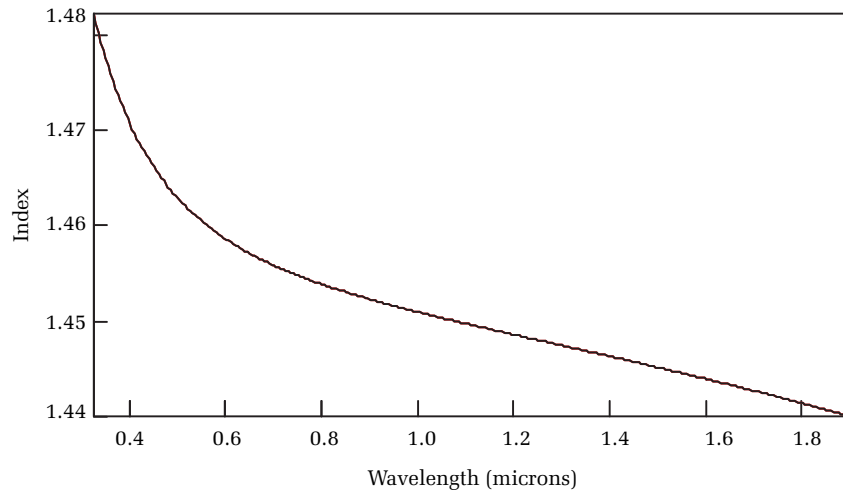


Figure 2.9. Wavelength dependence of the index of refraction of fused quartz.

For a pulse traveling along an optical fiber, the propagation time, τ , equals the length of the optical fiber divided by the group velocity

$$\tau = \frac{L}{v_g} \quad [2.17]$$

Substituting equation [2.15] into equation [2.17] and then into equation [2.9] we have

$$D_\lambda = -\left(\frac{\lambda}{c}\right) \frac{d^2 n}{d\lambda^2} \quad [2.18]$$

Equation [2.18] shows that the dispersion is proportional to the second derivative of the effective index of refraction with wavelength.

Taking the second derivative of equation [2.8] and substituting this into equation [2.18] we have

$$D_\lambda = -\frac{\lambda}{c} \left(\frac{d^2 n_2}{d\lambda^2} + \delta n_1 \frac{d^2 b(\lambda)}{d\lambda^2} + 2 \frac{db(\lambda)}{d\lambda} \frac{d(\delta n_1)}{d\lambda} + b(\lambda) \frac{d^2(\delta n_1)}{d\lambda^2} \right) \quad [2.19]$$

where $\delta n_1 = (n_1 - n_2)$.

For most fibers, the core and the cladding are made of the same material, with small amounts of dopants in the core that increase its index slightly to form a waveguide. Thus, for most applications we can consider δn_1 to be independent of wavelength. Making this assumption, we simplify equation [2.19] and have

$$D_\lambda = -\frac{\lambda}{c} \left(\frac{d^2 n_2}{d\lambda^2} + \delta n_1 \frac{d^2 b(\lambda)}{d\lambda^2} \right) \quad [2.20]$$

The first term of equation [2.20] represents the bulk chromatic dispersion of the material. The second term represents the waveguide dispersion. In non-dispersion-shifted fibers, the zero-dispersion point of equation [2.20] is around 1310 nm. Thus, for non-dispersion-shifted fibers there is a strong impetus to transmit at 1310 nm in order to have the highest optical bandwidth available. The minimum attenuation of optical fibers, however, occurs at wavelengths between 1550 and 1625 nm, where the dispersion is relatively high. To transmit at 1550 nm without excessive pulse broadening, the dispersion properties of the fiber must be adjusted to shift the zero-dispersion point from 1310 nm to the 1550 nm window.

One way to accomplish this shift is to modify the index profile of the fiber's core so that waveguide dispersion balances material dispersion at the desired transmission wavelength. One way to shift

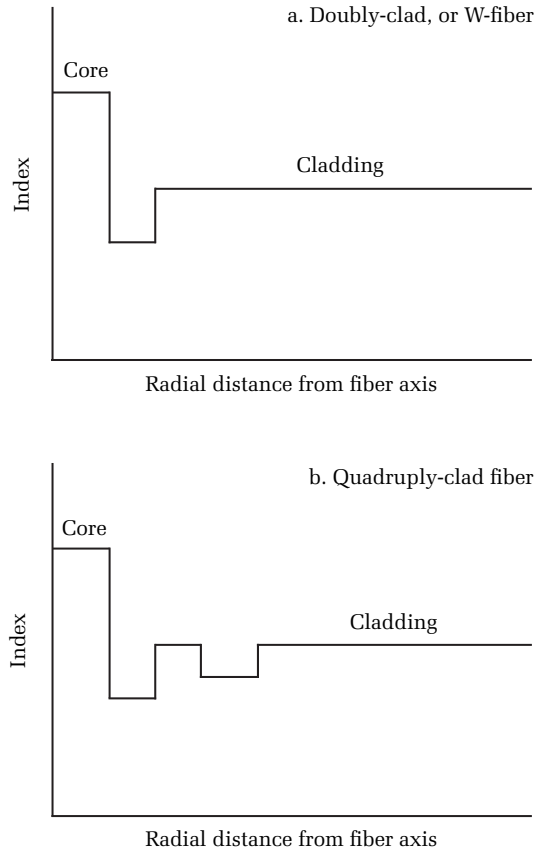


Figure 2.10. Index profiles that could be used for dispersion-shifted and nonzero-dispersion-shifted fibers. In dispersion-shifted fibers the core index profile is modified to increase the amount of waveguide dispersion. This increase in waveguide dispersion compensates for CD and shifts the zero-dispersion point to the desired wavelength (usually 1550 nm).

the zero-dispersion point is to doubly clad the core. Another way is to quadruply clad the core. Figure 2.10 illustrates the core profiles of doubly clad and quadruply clad fibers. With these designs the waveguide dispersion counteracts the material dispersion near 1550 nm, resulting in a flatter dispersion curve, with the zero-dispersion point near 1550 nm.

2.6 Wavelength-division-multiplexed systems

Since CD broadens optical pulses, you might think that optimally designed fiber-optic systems have zero CD. As long as the optical

network transmits only one wavelength, this is usually true. But with wavelength-division multiplexing (WDM), where many different channels at different wavelengths are present, too little chromatic dispersion can actually be a detriment because of nonlinear effects within the optical fiber.

Ordinarily, a material's index of refraction is independent of the intensity of the light. But if the intensity is increased to very high levels, the intensity of the light can modify the index of refraction. When this happens we say the fiber is operating in the nonlinear regime, and this can introduce a new set of phenomena that have the potential for greatly affecting the optical networks.

One of these phenomena is called *four-wave mixing* (FWM), which involves energy in adjacent channels mixing and converting some of their energy to a difference frequency. This has the effect of depleting energy out of the affected channels and (when channels are evenly spaced) introducing noise into adjacent channels. The net effect of FWM is to increase the BER.

One of the ways to mitigate the consequences of nonlinear effects such as FWM is to introduce a small amount of CD so that the digital pulses in adjacent channels are not phase locked. This reduces greatly the interaction length over which the pulses can interfere. So with WDM systems, there is a "sweet" spot for chromatic dispersion, where it is small enough to prevent excessive pulse distortion but large enough to avoid problems with nonlinear effects.

With the advent of WDM, the wavelengths of optical systems have been partitioned into standard wavelength bands, which are summarized in table 2.2.

Bands		Wavelength Range
Original	O	1260–1360
Extended	E	1360–1460
Short	S	1460–1530
Conventional	C	1530–1565
Long	L	1565–1625
Ultra Long	U	1625–1675

Table 2.2. Optical bands for single-mode optical fiber.

2.7 V-parameter, cut-off wavelength, and spot profile

We began this chapter treating light as if it consisted of "rays." The ray approximation for light is justifiably used in some circumstances where

the wavelength of light is small compared with the physical size of the objects it encounters. The ray approximation is useful because it is an intuitive model that is easy to understand and because it lends itself to relatively simple mathematical treatment. Light, however, does not really consist of rays. To describe more fully the behavior of light in very small confines, we need to use Maxwell's classical equations, which describe light as an electromagnetic wave.* Maxwell's equations (in nonabsorptive, gainless media) are:

$$\begin{aligned} \text{curl } \vec{E} &= -\frac{\partial \vec{B}}{\partial t} & \text{curl } \vec{H} &= \frac{\partial \vec{D}}{\partial t} \\ \text{div } \vec{D} &= 0 & \text{div } \vec{B} &= 0 \end{aligned} \quad [2.21]$$

Assuming a weakly guiding fiber (core and cladding index nearly the same), the solutions to equations [2.21] are traveling waves with cross-sectional fields described by Bessel functions within the fiber core and by modified Hankel functions in the cladding. We also find an infinite number of solutions to equations [2.21], called *modes*. In multimode fibers, many modes are guided, whereas single-mode fibers support only one.

Before continuing, let's discuss what we mean by the word *mode*. Imagine a string that is stretched between a solid support and a harmonic oscillator (see figure 2.11). We start the oscillator and gradually increase its frequency. At first, the string bounces and wiggles in an apparently chaotic way. Then when we reach a certain critical frequency, the string suddenly stabilizes in a regular pattern like that shown at the top of figure 2.11. Here the string's vibrations are in phase with the oscillator. As we continue to increase the oscillator's frequency, the string's motion again becomes chaotic. Then at a second (higher) frequency, the string's vibrations again become synchronous with the oscillator. This time the standing waves look like the center pattern in figure 2.11. As we continue increasing the frequency, we find a third point where the string and oscillator vibrate in phase. Here the standing wave looks like the pattern in the lower part of figure 2.11.

We could continue this experiment indefinitely. As it turns out, there is an infinite number of solutions that describe the motion of a tight string vibrating in phase with the oscillator. Each of these mathematical

*In still other applications we find that the wave approximation of light is also incorrect. There, we must treat light as quanta, called *photons*, and use quantum electrodynamics to describe completely the behavior of light under all circumstances.

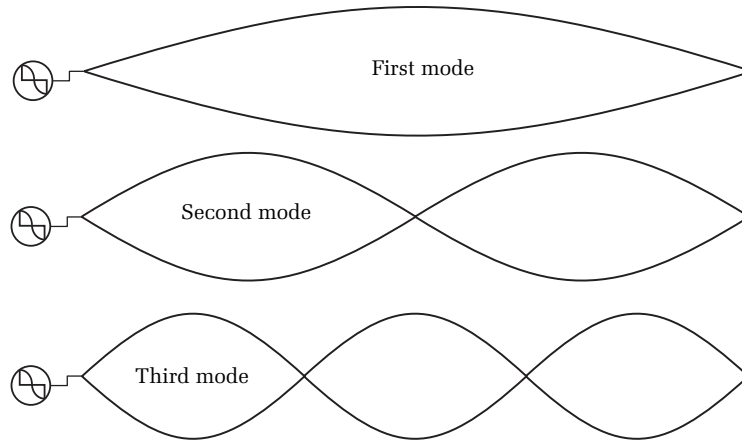


Figure 2.11. Modes on a vibrating string. The string supports only specific modes because of the requirement that integral numbers of half-waves fit between the supports. Fractional modes quickly decay and are not supported by the steady-state solutions.

solutions differs from its neighbor by an integer. We call these integral solutions modes, and we can assign integral numbers to each one based on the number of half wavelengths that each mode supports on the string. For example, we might call a vibration with a single maximum mode 1. A vibration with two maxima would be mode 2, and so on.

Vibrational modes occur all around us. When your car goes over a bumpy railroad track, vibrational modes in the suspension make the car bounce up and down. Automobile manufacturers use shock absorbers to dampen these vibrations. When a spacecraft lifts off the launch pad there are hundreds of vibrational modes that bend and twist it. Designers must be particularly aware of these vibrational modes, or they can grow to dangerous proportions and tear the spacecraft apart.

When we speak of modes in optical fibers, we are dealing with the same underlying physical processes that occur in strings, automobiles, and spacecraft.* Some distributions of light within the core result in a resonance between the light and the core-cladding boundary conditions. We call these resonances modes. To be contained within the optical fiber, light must travel in one of these guided modes. Light that does not travel in a guided mode is coupled into the cladding and lost.

*The modes in optical fibers are transverse, or perpendicular to the optical axis.

When the core diameter and numerical aperture are large, the fiber can support many different modes. If we reduce the core diameter, however, the number of modes the fiber supports gets smaller. Eventually, if we continue reducing the core diameter and numerical aperture, the number of modes the fiber supports reaches 1. One particular parameter helps us determine how many modes the fiber will support. This parameter is called the *normalized spatial frequency*, or *V-parameter*:

$$V = \frac{2\pi a}{\lambda} \sqrt{(n_1^2 - n_2^2)}$$

$$V = \frac{2\pi a}{\lambda} \text{NA} \quad [2.22]$$

If the normalized frequency is less than 2.405, the fiber supports only one mode. This lowest, or fundamental, mode is called the LP₀₁ mode.* As *V* increases, the fiber supports more and more modes. If *V* is less than 3.832, the fiber supports the LP₀₁ and LP₁₁ modes. If *V* is less than 5.136, the fiber supports the LP₀₁, LP₀₂, LP₁₁, and LP₂₁ modes. As *V* continues to increase and the number of modes becomes very large, the number of modes supported by the fiber is given approximately by†

$$M \approx \frac{V^2}{2} \quad (V \gg 10) \quad [2.23]$$

From equation [2.22] we see that the *V*-parameter depends on wavelength and that *V* gets larger as the wavelength gets smaller. This has important implications for single-mode fibers because it means that below a certain wavelength the fiber transitions from being single mode to being multimode. This transitional wavelength is called the *cut-off wavelength*. The cut-off wavelength is important in single-mode fiber systems because operation below this wavelength is in the multimode region, where we can expect modal dispersion and reduced bandwidth. Consequently, with single-mode fiber it is important to be sure that the system is operating above the cut-off wavelength. The cut-off wavelength occurs when we reduce λ to the point that $V = 2.405$. Thus, the critical wavelength is given by

$$\lambda_c = \frac{2\pi a}{2.405} \text{NA} \approx 2.613(a \cdot \text{NA}) \quad [2.24]$$

*LP stands for linear polarization. The subscript refers to the mode numbers of the mathematical solutions.

†Assuming degenerate polarization.

Now that we have examined the V -parameter and the cut-off wavelength, let's consider the mode or spot profile of a single-mode fiber. Suppose we inject light into one end of a single-mode fiber and then cleave the fiber's other end and examine it with a high-power microscope. What distribution of the light do we see? If we assume that the core and cladding indexes are nearly the same, then we can solve equations [2.21] for step-index fiber. When we do, we find that the field distribution for a single-mode fiber* is given by^{13,14,15}

$$A(r) = J_0\left(\frac{u \cdot r}{a}\right) \quad \text{for } r < a$$

$$A(r) = \frac{J_0(u)}{K_0(w)} K_0\left(\frac{w \cdot r}{a}\right) \quad \text{for } r \geq a$$
[2.25]

In equation [2.25], $J_0(r)$ is the zero-order Bessel function and $K_0(r)$ is the modified Hankel function. The radius of the core is a , and the radial

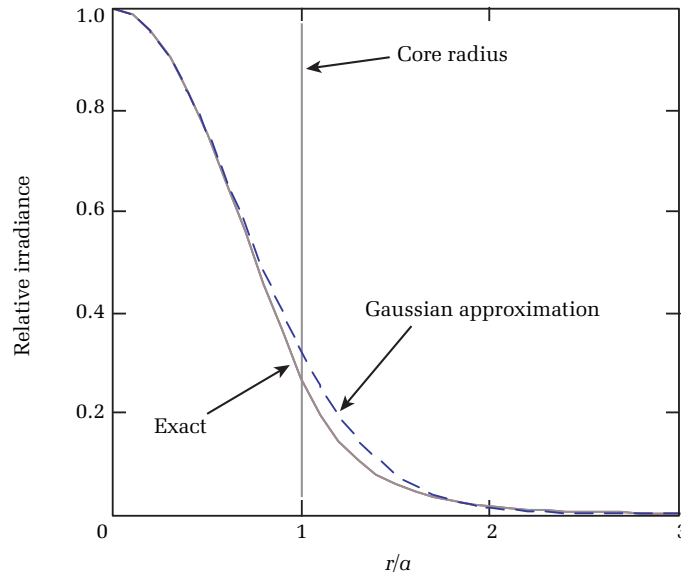


Figure 2.12. Normalized radial distribution of irradiance in the fundamental (LP_{01}) mode. Notice that the mode is roughly Gaussian and that much of the light is carried by the core ($V = 1.9$).

*The distribution we see in the microscope is the irradiance distribution (optical power per unit area). The irradiance distribution is proportional to the square of the field distribution.

coordinate is r . The constants u and w must be solved numerically. For purposes of calculating the spot profile (as opposed to derivatives), w is approximately linearly proportional to V . In such cases you can use the approximation

$$w \approx 1.1261 \cdot V - 0.958714 \quad [2.26]$$

From equation [2.26] you can calculate u from the expression

$$V^2 = u^2 + w^2 \quad [2.27]$$

Figure 2.12 shows the radial irradiance distribution for a single-mode fiber with $V = 1.9$. The mode distribution is nearly Gaussian. Notice that the mode is considerably wider than the fiber's core. For the case $V = 1.9$, roughly 29% of the mode's power is carried in the cladding. Figure 2.13 shows how the amount of power carried in the cladding changes with V . At the cut-off wavelength, the amount of power carried in the core is about 17%. As V increases (the wavelength decreases), the amount of power carried by the cladding decreases. As the wavelength increases, the amount of power carried in the cladding increases. Suppose, for example, that we have a fiber for which $V = 2.2$ at 1550

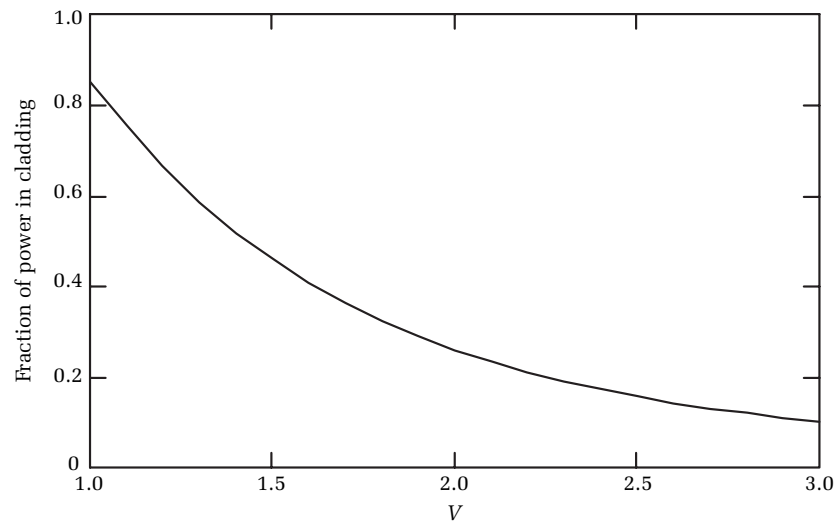


Figure 2.13. Relative amount of power in the LP_{01} mode carried by the cladding. As the core increases in size and becomes multimode, the amount of power in the cladding decreases. For single-mode fibers, as the wavelength increases and V decreases, the amount of power in the cladding increases.

nm. Accordingly, the cladding carries about 21% of the light. At 1310 nm, the same fiber has a V -parameter of 2.6 (see equation [2.22]) and the cladding carries slightly more than 14%, or roughly 67% as much power as it did at 1550 nm.*

Equation [2.25] is not amenable for use with hand calculators. Fortunately, for quick calculations you can often approximate the fundamental mode as a Gaussian distribution. For the Gaussian approximation, the ratio of the $1/e^2$ irradiance point to the core radius is given approximately by¹⁶

$$\frac{\omega_0}{a} \approx \left(0.65 + \frac{1.619}{V^{1.5}} + \frac{2.879}{V^6} \right) \quad [2.28]$$

2.8 Splices and connectors

To build a network with optical fibers, you must eventually connect one fiber to the next. This presents a unique problem for fiber-optic networks. The physical dimensions of metallic conductors, such as twisted-pair wires and coaxial cable, are large enough to see with the unaided eye. Optical fibers, on the other hand, have microscopic dimensions.

The mode-field diameter of typical single-mode fiber, for example, is roughly $10 \mu\text{m}$, and the core diameter is slightly smaller. Multimode fibers are much larger, with typical core diameters of either 50 or $62.5 \mu\text{m}$ (other multimode fibers are also used, but these are the two most common sizes). Multimode and single-mode fibers both have cladding diameters of $125 \mu\text{m}$. The cladding is usually sheathed in a pliable outer material made of acrylyte, called the *buffer coating*, which is $250 \mu\text{m}$ or $900 \mu\text{m}$ in diameter, depending on the cable application.

Several mechanisms exist for connecting optical fibers. One method is the fusion splice. When fusing optical fibers, any cable or jacketing material is first cut back to expose several inches of buffered fiber. The buffer coating is carefully removed using special stripping tools that clamp around the fiber and cut the buffer (almost, but not quite) to the fiber. The buffer is removed, usually by pulling the tool. After removing the buffer, the technician wipes the cladding with a clean cloth soaked in a solvent such as isopropyl alcohol to remove any residual buffer material.

*We assume here that the numerical aperture is approximately independent of wavelength.

With the buffer removed and the cladding clean, the technician cleaves the fiber using a precision carbide or diamond tool. This tool is specially designed to scribe the glass and apply stress to propagate the crack across the diameter of the fiber. One of the most important requirements of the cleaving tool is that it cleave the fiber so the endface is square to the fiber's axis. Additionally, the cleaving tool must leave the fiber's end-face smooth and flat, with no hackles or burrs.

After preparing both fiber ends, the technician places the fibers into the fusion splicer. Fusion splicers come in many different varieties (see figure 2.14). Some fusion splicers have nonadjustable, prealigned V-grooves that hold and align the fibers in abutment to each other. Although adequate for many purposes, these are generally less expensive and less accurate than other fusion-splicing machines that use active alignment to optimally position the cores. However they accomplish it, the first main objective of the fusion splicer is to align the fibers so their cores are coaxial and parallel, with the cleaved ends just a few microns apart.

With the fibers aligned, the fusion splicer applies an arc of electric current between two electrodes on opposite sides of the fibers. The hot electric arc melts the fibers, while micropositioners in the fusion splicer push the fibers toward each other. When the arc is turned off, the fibers have been fused (thus the name fusion welder) together into a continuous piece of fiber. If everything is done perfectly, the fiber cores and cladding of the two fibers are aligned exactly, forming one continuous waveguide.



Figure 2.14. Example of profile alignment system and local injection and detection fusion splicers. [Credit: Aurora Instruments.]

Of course, things never come out perfectly. Although many fusion splicers do an exceptional job of aligning and fusing the fibers, there are always residual misalignments. These alignment flaws result in loss at the splice point. Besides these alignment errors, the fibers have slightly different cladding and mode-field diameters and fiber tolerances. Differences in mode-field diameter result from slightly different core diameters or slight differences in the fibers' numerical apertures. Mismatched mode-field diameters, which always occur to some extent but are usually small, result in intrinsic splice loss.

You face similar situations with mechanical splices and connectors. Unlike profile alignment systems (PASs) and local injection and detection (LID) techniques used by fusion splicers to align the fiber's core, mechanical splices and connectors must provide the alignment based on the outside diameter of the optical fiber. These tolerances with multimode fibers are $125 \pm 2 \mu\text{m}$ and with single-mode fibers are $125 \pm 1 \mu\text{m}$. Mechanical splices require the fiber's coating to be stripped of its buffer coating, cleaned, and then cleaved to a length determined by the splice manufacturer for optimum alignment of the fiber in the mechanical splice. The fibers are then clamped into alignment, with the fiber ends in contact with index matching fluid or gel used to reduce the Fresnel reflections.

As with splices, connectors are limited by mechanical tolerances and statistical processes. If the ferrules are not both the same size or are slightly elliptical (instead of being perfectly cylindrical), they do not align perfectly. Alignment errors also happen if the holes in the ferrules are not exactly coaxial with the ferrule axis. To meet acceptable loss budgets, the tolerances on the fiber and the parts that make up the connector are often less than $1 \mu\text{m}$. Similar design concerns apply to mechanical splices that, like connectors, hold the fiber by mechanical means. Mechanical splices use epoxies, mechanical cams, or other means to lock the fibers into place after they have been aligned in V-grooves or capillary tubes.

Most optical connectors use ceramic ferrules with precision holes approximately $126\text{--}127 \mu\text{m}$ in diameter for single-mode plugs and slightly larger for multimode connectors. The fiber connection depends on tight tolerances of the fiber's outside diameter (O.D.) and the inside diameter of the ferrule. Additional tolerance includes the ferrule's O.D. and the mating receptacles inside diameter of the ceramic c-clip. The precision of the fiber and connector tolerances allow for accurate physical mating and contact of the ferrules and fibers. Standard attenuation values are 0.5 dB for single-mode and 0.75 dB for multimode connections.

The connectorization process starts with the removal of the fiber's buffer coating, cleaning the cladding of any coating residue, and inserting the fiber into the ferrule, along with an epoxy used to bond the optical fiber to the ferrule. After the epoxy is cured, the fiber is hand scribed and the end of the fiber polished in gradual steps. This polish can vary depending on the system requirement. To minimize reflections, physical contact (PC) polishes done with automated polishing equipment are used. Common polishes for single-mode use are the PC, UPC (ultraphysical contact), and the APC (angled physical contact). Most multimode polishes are flat and have the highest reflective or optical return loss (ORL) values. The strain relief boot is then added to the plug, which provides the strain relief using the aramid yarn in the optical-fiber cordage.

Whether the fibers are joined via a fusion splice, a connector, or a mechanical splice, they must be aligned properly or optical loss results. Misalignments can happen in three ways: The fibers can be laterally misaligned, longitudinally misaligned, or angularly misaligned (see figures 2.15 through 2.18). Of these three, lateral misalignment is usually the most critical, followed by angular misalignment. Longitudinal misalignment is typically the least sensitive.

Loss between multimode fibers can be very difficult to calculate accurately, because the loss depends a great deal on the mode distribution. The mode distribution describes which modes carry light and which modes are empty. If low-order modes (whose light distribution is weighted more toward the fiber's center) carry most of the

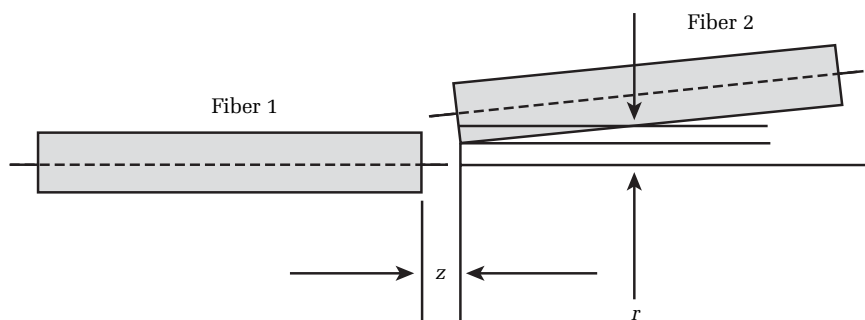


Figure 2.15. Misalignment between two single-mode fibers. Loss is least sensitive to the longitudinal misalignment, z , and most sensitive to the lateral misalignment, r .

light, then the effective core of the fiber looks smaller than if the higher-order modes carried the light. In this case the connector's loss might be less than if most of the light was carried in higher-order modes.

In contrast to multimode fibers, the loss between two single-mode fibers is relatively easy to predict accurately. The equation for loss in a single-mode splice is based on coupling theory between Gaussian beams. Recall from section 2.8 that the fundamental mode in a single-mode fiber is nearly Gaussian. For two Gaussian beams, the coupling loss (in decibels) is^{17,18}

$$\text{Loss} = -10 \log \left\{ \left(\frac{16n_1^2 n_0^2}{(n_1 + n_0)^4} \right) \frac{\sigma}{q} \exp \left(\frac{-\rho U}{q} \right) \right\} \quad [2.29]$$

where

$$\rho = (k\omega_1)^2/2$$

$$q = G^2 + (\sigma + 1)^2/4$$

$$U = (\sigma + 1)F^2 + 2\sigma FG \sin(\theta) \cos(\gamma) + \sigma \left(G^2 + \frac{\sigma + 1}{4} \right) \sin^2(\theta)$$

$$F = \frac{r}{k\omega_1^2}$$

$$G = \frac{z}{k\omega_1^2}$$

$$\sigma = \left(\frac{\omega_2}{\omega_1} \right)^2$$

$$k = \frac{2\pi n_0}{\lambda}$$

n_1 = refractive index of fiber core

n_0 = refractive index of medium between fibers

λ = wavelength of light

r = lateral offset

z = longitudinal offset

θ = angular misalignment

ω_1 = $1/e^2$ mode-field radius in first fiber

ω_2 = $1/e^2$ mode-field radius in second fiber

The angle between the direction of tilt and the plane containing the transverse offset and the fiber axis is γ . The cosine term was not included in the original expression. Figures 2.16, 2.17, and 2.18 illustrate the alignment sensitivity for a typical single-mode fiber with a $4.5\text{-}\mu\text{m}$ mode-field radius at 1310 nm . From these figures, you see that alignment tolerances of fractions of a micron must be observed for the very low splice losses required in today's fiber-optic installations.

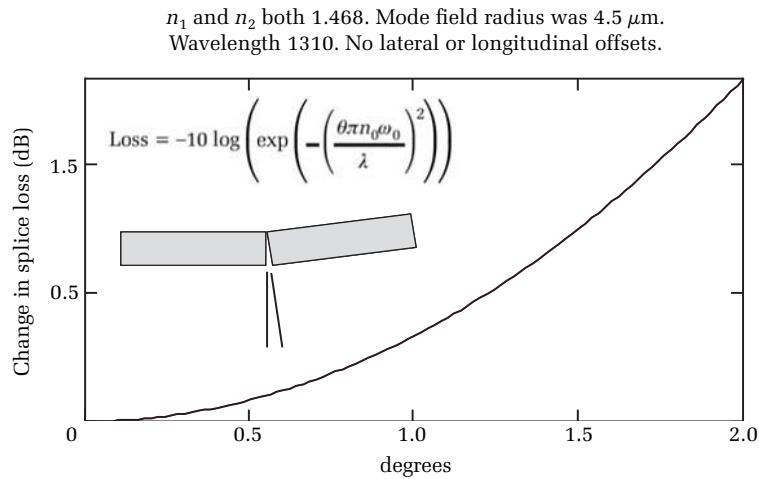


Figure 2.16. Coupling loss in single-mode fiber as a function of tilt misalignment. The mode-field diameter for both fibers is $4.5\ \mu\text{m}$, and the core index is 1.468. Here, n_0 is the index of the fiber's core.

Some fusion-splicing machines use estimated splice loss (ESL) after the fibers are fused together. Some fusion splicers image the cores and estimate the splice loss by measuring the amount of core misalignment. LID fusion splicers locally inject light into one of the fibers through a macrobend and measure the light coupled through the splice and into the other fiber, where the light is detected through a second macrobend. The greater the amount of received light, the better the alignment of the fibers. Although sometimes accurate, the ESL values given by fusion splicers are not always appropriate for installation. Imaging the misalignment, for example, cannot measure the intrinsic loss from mode-field mismatch, while LID techniques suffer from measurement uncertainties. The most accurate way to measure and document splice loss at the system's operating wavelength is to use an OTDR. OTDRs are also preferred because they provide clear documentation of all the splices along the entire length of the fiber.

longitudinal misalignment, air index = 1, fiber = 1.468, 4.5 μm mode field radius

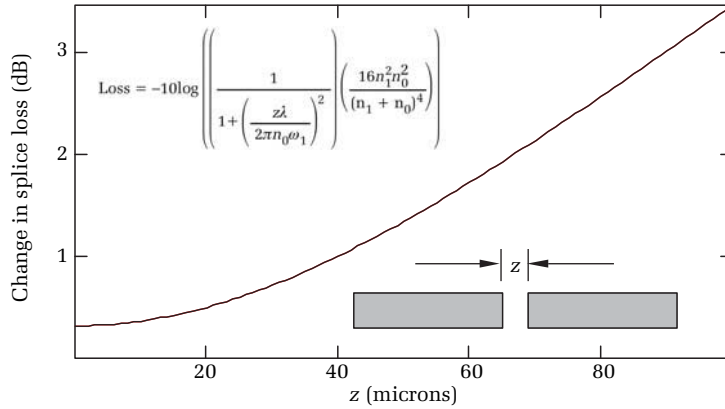


Figure 2.17. Coupling loss in single-mode fiber as a function of longitudinal misalignment. The mode-field diameter for both fibers is 4.5 μm, and the core index is 1.468. The index of air is 1. Nonzero loss at 0-μm misalignment is caused by surface reflections (interference effects are not included).

Mode field radius 4.5 μm in each fiber. Both fibers, core index 1.468.

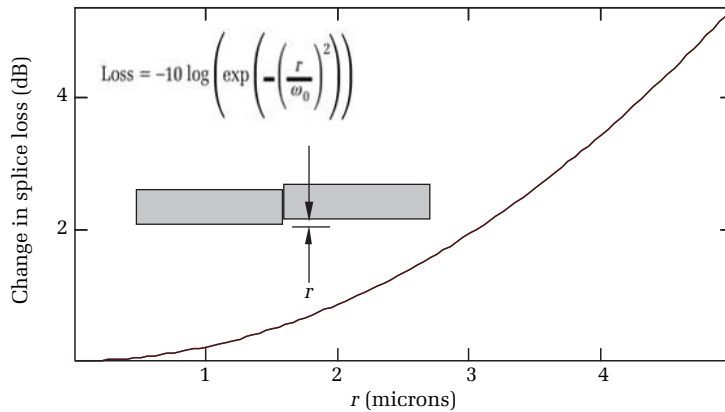


Figure 2.18. Coupling loss in single-mode fiber as a function of lateral misalignment. The mode-field diameter for both fibers is 4.5 μm.

2.9 Bending loss

At the beginning of this chapter we described the light-guiding properties of optical fibers as resulting from total internal reflection. Total internal reflection results when light traveling in a high-index material encounters a boundary with a lower-index material at a sufficiently shallow angle

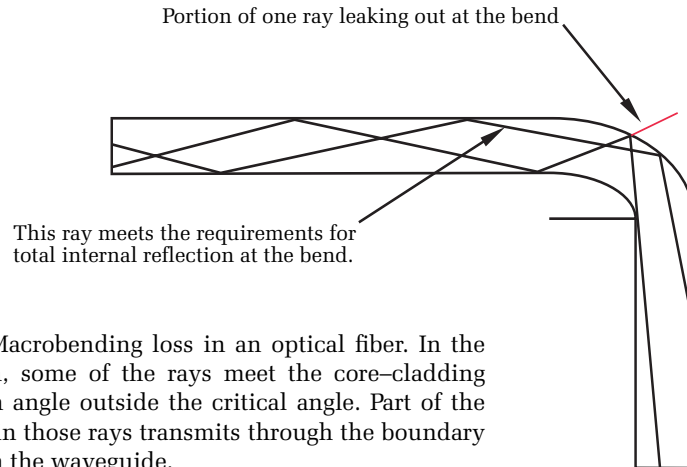


Figure 2.19. Macrobending loss in an optical fiber. In the bending region, some of the rays meet the core-cladding boundary at an angle outside the critical angle. Part of the optical energy in those rays transmits through the boundary and is lost from the waveguide.

(see figure 2.2). With this understanding, consider what happens when we bend the fiber as shown in figure 2.19. Using the ray approximation, we see that when some rays encounter the bend, they are still within the critical angle, so they undergo total internal reflection.* Other rays, however, encounter the bent fiber at an angle outside the critical angle, so a portion of the optical power in those rays is lost.

You can see that the tighter the fiber bend, the greater the number of rays that fail to be within the critical angle along the entire length of the bend. Rays that strike the fiber walls outside the critical angle are partially transmitted and partially reflected and are thus attenuated from the power traveling within the optical fiber. From this simple examination, we expect optical loss to occur at bends, and we expect the amount of loss to increase as the bend radius decreases.

As with coupling loss, analysis of bending loss in multimode fibers is much more difficult than it is with single-mode fibers. The reason is the vast number of modes that exist in multimode fiber. To analyze the bending loss in multimode fiber properly, you must derive the bending-loss equations for each mode and know what percentage of the optical power is carried in each of them. With single-mode fibers the problem is much more tractable. Approximating the radial field distribution by a Gaussian function, the pure bending loss in a single-mode fiber is¹⁹

*Since this explanation is based on the ray approximation, it is not rigorously true. For example, this explanation does not predict wavelength sensitivity for bending loss.

$$\alpha'_b = \frac{1}{2} \left(\frac{\pi}{4aRw^3} \right)^{0.5} \left(\frac{u}{VK_1(w)} \right)^2 \exp \left(-\frac{1}{6\pi^2} \frac{w^3 \lambda^2 R}{a^3 n_2^2} \right) \quad [2.30]$$

In equation [2.30], α'_b is the bend's attenuation in Nepers/km. To convert from Nepers/km to dB/km, multiply by 8.686. The radius of the bent fiber is R , $V^2 = u^2 + w^2$ (refer to equations [2.26] and [2.27]), and $K_1(w)$ is the modified Hankel function.

Figure 2.20 shows how the bending attenuation in a single-mode fiber changes with different bend radii at 1310 nm and 1550 nm. Observe the same general trend at both wavelengths.

There is essentially no bending loss until a certain critical radius is reached, whereupon the bending loss increases dramatically. Notice also that the critical bend radius is dramatically different for the two wavelengths. At 1310 nm, the critical bend radius is about 1.5 cm; at 1550 nm it is about 2.5 cm (these critical bend radii change, depending on the fiber's numerical aperture and core radius). For optical systems operating at 1625 nm, the sensitivity to macro- and microbending loss is greater still. Microbends are stress related and not bend related. Common types of microbends are intrinsic imperfections on the core/cladding boundaries of optical fibers, but they are most commonly caused by the

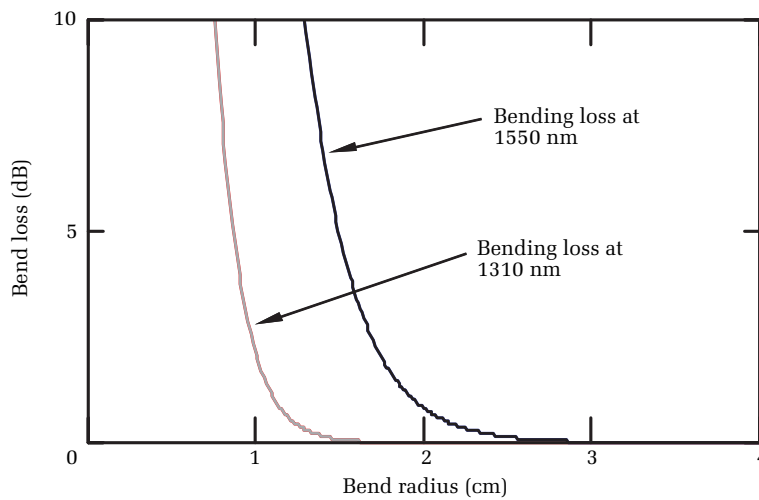


Figure 2.20. Bending loss as a function of bend radius (180° bend) using equation [2.30]. Loss at 1550 nm is considerably greater than it is at 1310 nm.

improper use of tie wraps by installers. Other notable causes are crushed buffer tubes and direct stresses placed on the optical cable stressing the internal fibers. For practical purposes in this book, both macrobends and microbends are addressed as bending losses.

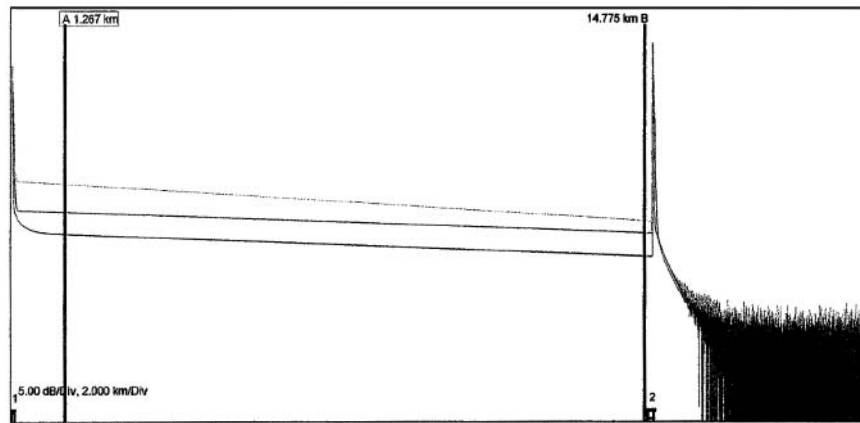


Figure 2.21. OTDR screen showing 1310-nm, 1550-nm, and 1625-nm traces overlaid. [Credit: The Light Brigade.]

On the OTDR display, fusion splices and bends look identical. Both show a drop in the backscatter, with no reflection. Figure 2.21, however, suggests an interesting way to determine whether a nonreflective event is a bend or a splice by using a dual-wavelength OTDR. Measure the loss at 1310 nm, and at 1550 nm or 1625 nm: if the loss is less at either of the longer wavelengths than it is at 1310 nm, then the event is a fusion splice, with essentially no bending loss. If no bending is present, then the loss is due to lateral misalignment. Loss due to lateral misalignment is less severe with large mode-field diameters than it is with small modal diameters. Since the modal diameter is larger at 1550 nm than it is at 1310 nm, the loss resulting from a given lateral misalignment is slightly less at 1550 nm than it is at 1310 nm. However, if the fiber is bent, the loss due to bending is much greater at 1550 nm than it is at 1310 nm. If you test the fiber at 1550 nm and find the event loss is greater than when you measure it at 1310 nm, then you know that the primary cause of the loss is bending. If the location is documented as being at a splice location, the cause is a microbend or macrobend stress on the optical cable and fibers at the splice closure.

2.10 Coherence

We end this chapter with a brief discussion of coherence. Although coherence is a property of light and not optical fiber, it plays an important part in many fiber-optic communications systems, so its mention here is warranted.

When we talk of coherence in a beam of light, we mean the degree with which individual photons in the beam of light are in phase with each other. Often, when trying to simplify our analysis, we approximate real light sources (such as lasers) as perfectly monochromatic point sources. A perfectly monochromatic source of photons, however, is an idealization. In reality, such sources are not possible, for several reasons. First, the simple fact that the source is on for a finite amount of time means that its spectral width is finite, so it cannot be perfectly monochromatic.* Second, real sources generate photons from electrons that change energy states. These electrons are never fully coherent,

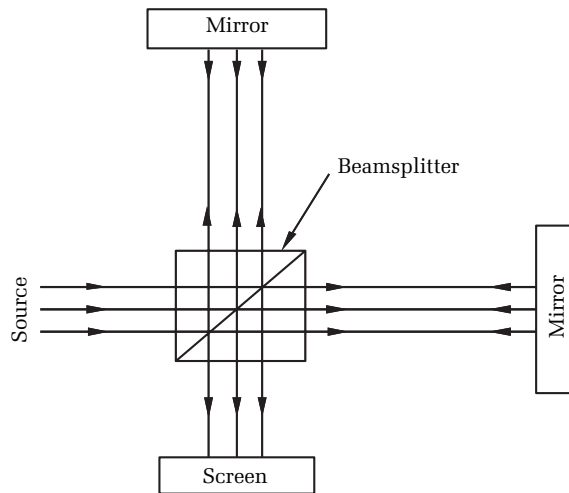


Figure 2.22. Michelson interferometer. The Michelson interferometer splits an incoming optical beam into two paths. The light in each path travels to a mirror, where it is reflected back to the beam splitter, recombined, and projected onto a viewing screen. If the difference in path length between the two mirrors and the beam splitter is less than the coherence length, a diffraction pattern is visible on the screen. If the recombining beams are not quite parallel, then the diffraction pattern is a series of light and dark bands.

*This results from the Fourier transform theory.



Figure 2.23. Interference pattern seen in a Michelson interferometer. The dark and light bands result from destructive and constructive interference. In this example, the mirror in one leg of the interferometer was tilted very slightly so that the recombining beams were not quite parallel and the difference in the path lengths of the two beams was much less than the coherence length. By increasing the difference in the two path lengths, the contrast between the dark and bright bands would be reduced. If the difference were much greater than the coherence length, the screen would be uniformly bright, without any interference fringes.

however, so the photons they emit are never perfectly in phase with each other. In a laser, for example, the radiation consists of stimulated photons as well as spontaneous photons. Photons radiated by stimulated emission are in phase with each other, but photons radiated by spontaneous emission are not.

The degree of coherence in an optical beam affects physical phenomena that we can observe in experiments. For example, consider a simple Michelson interferometer (figure 2.22). In the Michelson interferometer a beam of light is split in two and each beam is reflected off a mirror and then recombined. If the optical components are perfectly flat, the distances in each of the interferometer's arms are exactly the same, and the recombining beams are not quite parallel, then you see a series of bright interference fringes (see figure 2.23). Now imagine that one of the mirrors is mounted on a very precise translation stage. Moving the mirror so the distances in the interferometer's arms are no longer exactly the same results in less contrast between the dark and bright bands in the interference pattern. As you continue to move the mirror, the contrast becomes increasingly weak, until you reach a point where no interference fringes are discernible at all.

What we have seen in this experiment with the Michelson interferometer is an effect resulting from the coherence length of the light beam. The coherence length is the distance over which photons in the beam remain coherent with each other. If you use a source that is very coherent (such as a single-frequency laser), you may still see interference fringes even when the difference in the path lengths of the Michelson interferometer are a meter or more. If you use a source with very little coherence (such as an LED), then the two paths must be almost exactly equal, or interference fringes are not visible.* Mathematically, the coherence length of a light source is related to its coherence time, which is related to the spectral bandwidth. Light sources with narrower spectral widths are more coherent than sources with wider spectral widths.

If the RMS linewidth of the spectral distribution of a light source is σ_λ , then the coherence length is

$$L_c = \frac{\lambda^2}{\pi \cdot \sigma_\lambda} = t_c \cdot c \quad [2.31]$$

In equation [2.31], L_c is the coherence length and t_c is the coherence time. Table 2.3 illustrates the coherence length of some typical light sources ($\lambda = 1.3 \mu\text{m}$) that might be used in a fiber-optic communications system.

Source	σ_λ	t_c	L_c
LED	42 nm	43 fs	13 μm
Multimode LD	2.1 nm	0.87 ps	0.26 mm
Single-frequency LD	$2.4 \cdot 10^{-4}$ nm	7.3 ns	2.2 m

Table 2.3. Spectral width, coherence time, and coherence length for some common light sources.

The significance of coherence length for fiber-optic systems applies mostly to reflective components. In chapter 6 we shall see that the total reflection from a mated connector can be reduced dramatically by designing it so the light reflecting from the two ferrules adds

*It is important to note here that the distance we speak of is the optical path length. This is the integral of index times physical path length traveled along each arm in the interferometer.

destructively by coherently canceling out. If the connector is damaged or contaminated with dirt, the end faces of the ferrules might be slightly separated. When this happens, the light reflecting from the ferrule end faces may add constructively. If this occurs, the resulting reflection can be very large. Coherent effects, therefore, play an important role in the reflective characteristics of fiber-optic systems that use connectors. When sources with very high coherence are used, coherent effects can also result in signal fading and coherent mixing noise at the receiver. These effects can increase the system's BER.

2.11 Summary

Before ending this chapter, let's pause briefly and review the material we have covered. We began with the problem of finding some practical way of transmitting information from point to point by amplitude modulating a beam of light. Free-space transmission is possible, but it has some significant problems that make it difficult to use in many terrestrial applications. Using a hollow waveguide to carry the light turned out to be no less a problem because of the high attenuation we encountered when the light reflected off the waveguide's inside walls. Even with the waveguide coated with a highly reflective multilayer coating, the attenuation was many tens of decibels per kilometers.

After examining some of the difficulties associated with alternative designs, we found a solution to the problem of high attenuation in the principle of total internal reflection. With total internal reflection, light reflects from the core-cladding boundary with 100% efficiency. Since total internal reflection is lossless, the attenuation in the waveguide depends only on the scattering and absorption properties of the optical glass from which the waveguide is fabricated.

Using total internal reflection, it is possible to consider the possibility of building low-loss optical fiber, if sufficiently pure glass can be fabricated with low absorption. Rayleigh scattering is the result of microscopic inhomogeneities in the fiber's index of refraction. Scientists reduce Rayleigh scattering by transmitting information with longer-wavelength light and by cooling the fiber slowly during manufacture to minimize the size of the inhomogeneities. Attenuation is reduced by using ultrapure fiber and by doping the fiber with ions that have resonances far from the operating wavelength. By using total internal reflection, and glass with low-scattering and low-absorption properties, scientists have built practical low-loss fibers that allow repeaterless transmission over lengths exceeding 100 km.

Low-loss fiber is the first step toward realizing the capability of high-speed data transmission over optical fiber. Even with low-loss fiber, other problems remained to be solved. After discussing optical attenuation and seeing how it was reduced to practical levels, we turned our attention to the problem of dispersion. Dispersion in optical fibers is the tendency for optical pulses to broaden as they travel along the fiber. If dispersion is excessive, adjacent pulses can broaden so much they begin to overlap. When this happens, the system BER increases. To reduce multipath dispersion in multimode fibers, scientists changed the core design. Instead of a simple step-index profile, they use a graded-index profile that equalizes the time it takes for the maximal rays and the axial rays to travel along the length of the fiber.

Another way to reduce the dispersion in an optical fiber is to reduce the core diameter until the fiber supports only one mode. We introduced the concept of guided modes. When light is modeled as a wave phenomenon and Maxwell's equations are solved for light traveling along an optical fiber, only certain quantized solutions are possible. These are modes, and they are similar in their mathematical nature to the modes on a vibrating string. To estimate the number of modes on an optical fiber, we introduced the V -parameter, or normalized frequency. Single-mode fibers do not have modal dispersion, but they do have CD. CD is the tendency for pulses to spread out when the pulses are made of light that has a band of wavelengths. To reduce CD, fiber-optic systems are designed to operate at the fiber's zero-dispersion wavelength, and they use optical transmitters with very narrow spectral bandwidths.

Single-mode fibers have very small dimensions. Core diameters are only about $10\ \mu\text{m}$. The microscopic dimensions of optical fiber dictate how two fibers are connected together. Because of the small dimensions of the fundamental mode, splices and connectors on single-mode fibers have very demanding tolerances. To make a proper connection between two optical fibers requires precise optical connectors or fusion splices. OTDRs are useful because they allow the fiber installer to test the losses of these splices and connectors and verify that they fall within specified tolerances.

We ended this chapter with a brief introduction to the concept of coherence. Unlike the other topics covered, coherence is a property of the light in the fiber and not of the fiber itself. We introduced the concept of coherence length and showed that one way to measure the coherence length is to use a Michelson interferometer. When the light is highly coherent, the difference in path lengths between the two legs

of the interferometer can be large, and an interference pattern may still be visible. When the coherence length is small, the difference in path lengths must also be small, or no coherence pattern is visible. Although coherence seems somewhat unrelated to the other topics we have discussed, its importance will become obvious in later chapters.

The remainder of this book is devoted to the application of OTDRs in testing optical fiber. We refer to this chapter frequently as we describe how the design of optical fiber affects the design of OTDRs and as we describe how to measure some of the parameters of the optical fiber with an OTDR. Those readers needing further information on the principles of fiber optics are referred to the Suggested reading section at the end of this chapter.

Suggested reading

- Saleh, B. E. A., and Teich, M. C., *Fundamentals of Photonics* (New York: Wiley, 1991).
- Hentschel, C., *Fiber Optics Handbook* (Germany: Hewlett Packard, 1988).
- Hecht, E., and Zajac, A., *Optics* (Reading, MA: Addison-Wesley, 1974).
- Basch, E. E., *Optical-Fiber Transmission* (Indianapolis: Howard W. Sams, 1987).
- Neumann, E. G., *Single-Mode Fibers* (Berlin: Springer-Verlag, 1988).
- Gowar, J., *Optical Communication Systems* (Englewood Cliffs, NJ: Prentice-Hall, 1984).
- Rancourt, J. D., *Optical Thin Films User's Handbook* (New York: Macmillan, 1987).
- Kashima, N., *Passive Optical Components for Optical Fiber Transmission* (Norwood, MA: Artech House, 1995).
- Miller, S. E., and Kaminow, I. P., *Optical Fiber Telecommunications II* (San Diego: Academic Press, 1988).

Problems

1. If a fiber is bent enough to cause measurable loss, is the bending loss greater at longer wavelengths than it is at shorter wavelengths?
2. For WDM systems, should the chromatic dispersion be designed to be zero?
3. For standard single-mode fibers there is a certain wavelength, and below this wavelength the fiber is actually multimode. What do we call this wavelength?
4. What is the primary cause of attenuation in modern optical fibers?
5. What are the basic types of dispersion in optical fibers?

6. What type of index profile is used in multimode fibers to reduce modal dispersion?
7. True or false: The spread of light rays leaving an optical fiber depends on the numerical aperture.
8. True or false: The numerical aperture depends primarily on the difference between the index of refraction of the core and cladding.
9. True or false: Optical fibers have greater attenuation at 1550 nm than they do at 1310 nm.
10. True or false: Multimode fibers have smaller core diameters than do single-mode fibers.

¹ Rancourt, J. D., *Optical Thin Films* (New York: Macmillan, 1987), chapter 4.

² *Ibid*, p. 3.

³ Gowar, J., *Optical Communication Systems* (Englewood Cliffs, NJ: Prentice-Hall, 1984), p. 79.

⁴ *Ibid*, p. 4.

⁵ *Ibid*, p. 74.

⁶ Stewart, W. J., "Simplified parameter-based analysis of single-mode optical guides," *Electronics Letters*, Vol. 16, pp. 380–382.

⁷ Neumann, E. G., *Single-Mode Fibers* (Berlin: Springer-Verlag, 1988).

⁸ Hentschel, C., *Fiber Optic Handbook* (Germany: Hewlett Packard, 1988).

⁹ Hecht, E., and Zajac, A., *Optics* (Reading, MA: Addison-Wesley, 1974), equation (7.37).

¹⁰ *Handbook for Optics* (Irvine, CA: Melles Griot, 1995/1996), pp. 4–5.

¹¹ *Ibid*, pp. 4–8.

¹² Gowar, J., *Optical Communication Systems* (Englewood Cliffs, NJ: Prentice-Hall, 1984), p. 44.

¹³ Gloge, D., "Weakly guiding fibers," *Applied Optics*, Vol. 10, pp. 2252–2258.

¹⁴ Neumann, E. G., *Single-Mode Fibers* (Berlin: Springer-Verlag, 1988), chapter 5.

¹⁵ Marcuse, D., "Loss analysis of single-mode fiber splices," *Bell Systems Technical Journal*, Vol. 56 (1977), pp. 703–717.

¹⁶ *Ibid*, pp. 703–718.

¹⁷ *Ibid*, pp. 703–717.

¹⁸ Nemoto, S., and Makimoto, T., "Analysis of splice loss in single-mode fibers using a Gaussian field approximation," *Optical Quantum Electronics*, Vol. 11 (1979), p. 447.

¹⁹ Marcuse, D., "Curvature loss formula for optical fibers," *Journal of Optical Society of America*, Vol. 66 (1976), pp. 216–220.

Chapter 3

Fundamentals of OTDR operation

3.0 Introduction

In chapter 2 we saw that practical optical fibers used in telecommunications have microscopically small cores. There are two reasons for this. The first relates to a fiber's need to be flexible so that it can be used in cables. To be flexible, the glass fiber must be very thin. The second reason relates to the need for the fiber to be able to carry vast amounts of information. Recall from chapter 2 that intramodal dispersion limits a fiber's information-carrying capacity. To increase this capacity, manufacturers design the fiber with graded-index profiles, or they reduce the core to such a small size that it supports only one mode. For single-mode operation in the range of 1300–1625 nm, the fiber core must be about 10 μm in diameter.

These microscopically thin fibers pose a problem when you want to connect two fibers together. In chapter 2 we saw that, for single-mode fibers, the alignment tolerances are roughly a micron or less. When a fiber-optic system is deployed, the question naturally arises as to the quality of the splices and connectors used to assemble the different sections of fiber. If any of these sections are connected via splices or connectors that do not hold the necessary tolerances, excessive system loss occurs.

It is not difficult to test the final fiber-optic physical plant for excess loss. One way to do this is to attach a stabilized light source to one end of the system and to measure the amount of light emanating from the other end using a calibrated optical power meter. This gives a good measure of the overall system loss, assuming you have a low-loss connection between the light source and the fiber you are testing. Suppose the system loss you measure this way is excessive. What can you do? The excess loss could result from a dirty connector, a bad splice, a bend in the fiber, or a damaged cable. The light source and power meter allow you to detect excessive system loss, but they provide no information as to where the problem originates.

Now consider another scenario. Suppose you install the fiber-optic system, test its end-to-end loss with an optical source and power meter, and find that it meets the installation requirements. Two weeks later you find that the system bit-error rate has increased dramatically

so you measure the end-to-end loss again. This time you find the loss has increased dramatically, and no longer meets the installation requirements. What can you do? You could clean and remate each connector. If this does not solve the problem, you could redo each fusion splice. Suppose this still does not solve the problem. You could walk the line, looking for damage, but this might be impossible if the fiber is underground or in conduit where you cannot make a visual inspection. It is not too hard to imagine yourself running out of options. Obviously, the repair scenario could be very involved.

Although power meters and light sources are useful for quick checks and final system qualification, they do not allow you to measure the location or nature of a problem on the fiber.* Ideally, what you want is a piece of test equipment that can measure the fiber loss, splice loss, connector attenuation, and the optical return loss (ORL). Additionally, you would like it to provide you with a report that describes the condition of each optical component and where it is located. Furthermore, you would like this test equipment to make these measurements without destroying the fiber, and you would like to make the measurements from just one end of the fiber (unlike end-to-end loss measurements with a source and power meter, which require simultaneous access to both ends of the fiber). Fortunately, this is not as impossible as it sounds.

Consider a 75-km spool of microscopically thin, ultrapure silica glass. The outer diameter of this glass is only 125 μm , and the inner core that guides the light is only about 10 μm in diameter. This spool of fiber is composed of three shorter spools that have been connected together. Each section is roughly 25 km long. The sections were connected very precisely by aligning the fiber cores and fusing the fibers together with a hot electric arc. The splicing machine, however, was not perfect. It slightly misaligned the fibers at each joint. At the first joint, the fibers are offset by 1.1 μm ; at the second splice, the fibers are offset by 0.8 μm . The result of these slight offsets is an optical loss of 0.24 dB at the first splice and 0.13 dB at the second splice. Although the fiber is a masterpiece of modern science and engineering, it is not quite perfect. All fibers have a variety of fiber tolerances, which will create losses when connected or spliced together. The mode profiles of the light distributions in all three sections are nearly the same, but there are some slight differences. The

*Like all rules, this one has its exceptions. You can measure the insertion loss at 1310 nm and 1550 nm; if the loss is higher at 1550 nm than it is at 1310 nm, then the probable cause is fiber bending or stress. This, however, is about the extent of diagnostic work you can perform using just a light source and a power meter.

diameters of the modal profiles in the first two sections are different by $0.6\ \mu\text{m}$, and the diameters of the modal profiles in the second and third sections are different by $0.8\ \mu\text{m}$.

We can measure these small losses, offsets, and mode-field diameter variations using an optical time-domain reflectometer, or OTDR. This instrument makes these remarkable measurements by probing the optical fiber with intense short pulses of laser radiation. To say OTDRs are versatile is probably an understatement. Using an OTDR, you can:

1. Measure the distance to a fusion splice, mechanical splice, connector, or significant bend in the fiber.
2. Measure the loss across a fusion splice, mechanical splice, connector, or significant bend in the fiber.
3. Measure the intrinsic loss due to mode-field diameter variations between two pieces of single-mode optical fiber connected by a splice or connector.
4. Determine the relative amount of offset and bending loss at a splice or connector joining two single-mode fibers.
5. Determine the physical offset at a splice or connector joining two pieces of single-mode fiber, when bending loss is insignificant.
6. Measure the optical return loss of discrete components, such as mechanical splices and connectors.
7. Measure the integrated return loss of a complete fiber-optic system.
8. Measure a fiber's linearity, monitoring for such things as local mode-field pinch-off.
9. Measure the fiber slope, or fiber attenuation (typically expressed in dB/km).
10. Measure the link loss, or end-to-end loss of the fiber network.
11. Measure the relative numerical apertures of two fibers.
12. Make rudimentary measurements of a fiber's chromatic dispersion.
13. Measure polarization mode dispersion.
14. Estimate the impact of reflections on transmitters and receivers in a fiber-optic system.
15. Provide active monitoring on live fiber-optic systems.
16. Compare previously installed waveforms to current traces.

3.1 OTDR design

Clearly, OTDRs are versatile instruments for testing optical fiber. Figure 3.1 illustrates the principal optical components in a simple standard OTDR. A laser is pigtailed to a connector on the OTDR (commonly called the front panel) through a 3-dB optical coupler. This coupler is typically a fused bidirectional device but may also be made of bulk optics. The laser fires short, intense bursts of light that are directed through the coupler and then out through the front-panel connector and into the fiber under test.* As the pulse travels along the fiber, some of the light is lost via absorption and Rayleigh scattering. The pulse is also attenuated at discrete locations, such as splices, connectors, and bends, where local abrupt changes in the waveguide geometry couples light out of the core and into the cladding. When the pulse encounters discontinuities in the index of refraction (such as those found in connectors or the cleaved end of a fiber), part of the pulse's optical energy is reflected back toward the OTDR.

We saw in chapter 2 that scattered light radiates in all directions, and some of it is scattered in the direction opposite the pulse and returns to the OTDR. Connectors, mechanical splices, and unterminated fiber ends are all causes of Fresnel reflections that return light back to the

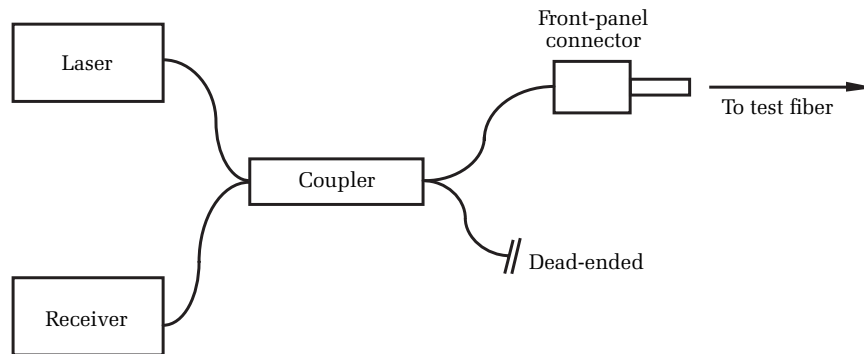


Figure 3.1. Principal optical components in a standard OTDR.

*Actually, the coupler splits the light. Because of this, only half of the laser pulse is directed to the OTDR's output port. The other half of the light is wasted. This waste can be avoided if a circulator is used. Circulators are made of bulk optical components and are directional devices that send all the outgoing light to the front panel while directing all the reflected/scattered light to the detector. Circulators are used to maximize the OTDR's dynamic range, but they cost several hundred dollars more than simple couplers, making high-dynamic-range OTDRs more expensive.

OTDR. When this backscattered and back-reflected light reaches the OTDR, the coupler directs it to the optical receiver.* This receiver typically is an avalanche photodiode (APD), but in some designs it may be a p-type-intrinsic-n-type (PIN) detector or even a photomultiplier tube. Whatever device is used in the optical receiver, the receiver's function is to convert the optical power into an electric current, which is then amplified, sampled, digitized, and displayed to the operator.

3.2 A typical OTDR waveform

Figure 3.2 shows a typical OTDR signal trace, commonly referred to as a *waveform*. The broad, sloping regions of the waveform result from Rayleigh backscattering, and the sharp spikes result from discrete points of reflection on the fiber. The spike near the beginning of the waveform, on the left side, is a reflection from the OTDR's front-panel connector. If you look closely, you can see a second spike shortly after the first. This second spike was caused by the connector on the jumper connected at the

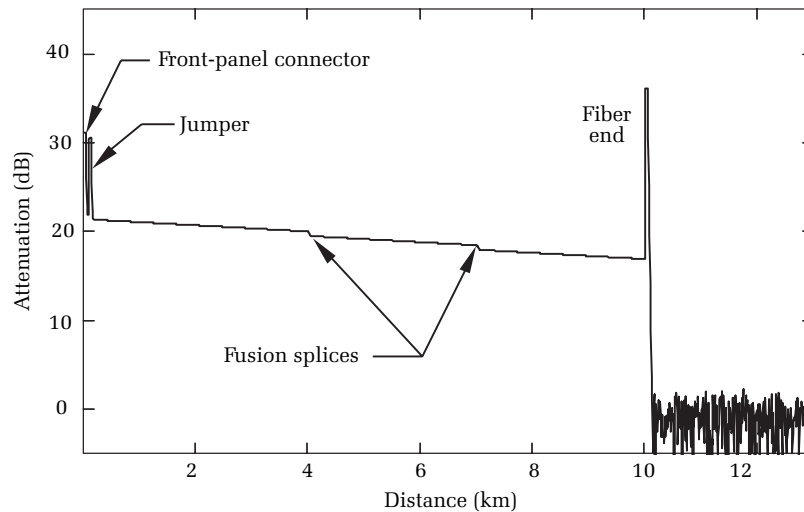


Figure 3.2. A typical OTDR waveform. The two spikes near the beginning of the waveform are from the reflective connectors at the instrument's front panel and from a jumper used to connect the instrument to the OTDR. The two dips in the waveform result from nonreflective fusion splices. The large reflection at the end of the waveform is caused by a reflection from the unterminated end of the fiber. The "grass" after the end of the fiber results from the OTDR's system noise. [Credit: The Light Brigade.]

*The coupler splits the light. Consequently, only half of the scattered and reflected light is directed to the receiver.



Figure 3.3.
Typical
mini-OTDR linked
to a fiber-optic
patch panel.
[Credit: The Light
Brigade.]

patch panel (see figure 3.3), which terminates the outside plant cable for cable management and access for cross-connecting the communications equipment. Along the broad, sloping portion of the waveform you can see two points where the Rayleigh scattering level drops abruptly. These two drops in the backscatter result from a pair of nonreflective fusion splices. The large spike at the end of the waveform is caused by reflected light off the patch panel's connector located at the opposite end. These connections tend to be highly reflective due to the glass-to-air surface when not cross-connected to a patch cord or when connected to the optical receiver.

When troubleshooting or documenting an optical fiber, you want to know what the losses of splices and connectors are in decibels, and the distances to events, in meters or feet. Accordingly, notice that the vertical scale of the OTDR's waveform is marked in decibels, and that the horizontal scale is marked in distance units (see figure 3.2). To provide measurements in decibels and meters, the OTDR must make internal conversions because its receiver measures the linear optical power (not decibels) as a function of time (not distance). To display the events as functions of distance, the OTDR divides the time base by 2 (since the light must travel out and back, thus going twice the distance) and multiplies this time by the group velocity of light in the fiber.*

Ordinarily, when you calculate power attenuation in decibels you use the equation $10 \cdot \log(P_0/P_1)$. The OTDR needs to display the attenuation that you would see if you were (for example) measuring the loss with an optical power meter. To do this, however, the OTDR uses the

*The group velocity is the speed of light in a vacuum divided by the group index (see chapter 2), and it is specified as the index of refraction (I.R.).

equation $5 \log(P_0/P_1)$, where P_0 is the strength of the Rayleigh scattering just before the event and P_1 is the strength of the Rayleigh scattering just after the event. The OTDR uses $5 \log$ instead of $10 \log$ because light that returns to the OTDR has traveled down the fiber and back, thus being attenuated twice by the fiber and its components.

3.3 Multiple-wavelength OTDRs

OTDR configurations can be much more complicated than the simple one shown in figure 3.1. For example, many OTDRs can test the optical fiber at two or more different wavelengths. Testing at several wavelengths can be important since fiber attenuation and the losses of some discrete events are functions of wavelength. In single-mode applications this might involve testing at 1310, 1550, and 1625 nm. For multimode applications the wavelengths are usually 850 nm and 1300 nm. In either case, to test at two wavelengths the OTDR uses two lasers and a device called a *wavelength-division multiplexer*, or WDM. The WDM is specially constructed to multiplex, or combine, two different wavelengths of light onto one fiber.* Figure 3.4 illustrates a dual-wavelength single-mode OTDR, and figure 3.5 illustrates a dual-wavelength multimode OTDR.

Notice the difference between the multimode and single-mode OTDRs. Since a dual-wavelength single-mode OTDR tests at 1310 and 1550 nm, it can use a single optical detector, usually a germanium or indium-gallium-arsenic (InGaAs) APD. A dual-wavelength multimode OTDR, however, tests at 850 nm and 1300 nm. No inexpensive, readily available optical detector has the proper performance for operation at both of these wavelengths. Consequently, dual-wavelength multimode OTDRs must use two detectors. The receiver for 850-nm operation is generally a silicon APD, and the receiver for operation at 1300 nm is usually made of germanium or InGaAs. In either case, the operator typically selects the test wavelength from a user menu and the OTDR tests at that wavelength by firing only the appropriate laser.

Notice in figure 3.2 that the loss of the fusion splices can be measured, but not the loss of the front-panel connector. This is because there is no backscatter signature before the first connector. Rayleigh backscatter is the OTDR's reference for loss measurements. Without this backscatter the loss of the front-panel connector cannot be measured. To

*Unlike the directional coupler, WDMs do not lose half of the light in this combining operation. While directional couplers lose slightly more than 3 dB, WDMs typically lose only about 0.5 dB. For this reason, dual-wavelength OTDRs usually have slightly less dynamic range than single-wavelength OTDRs built of the same optical components.

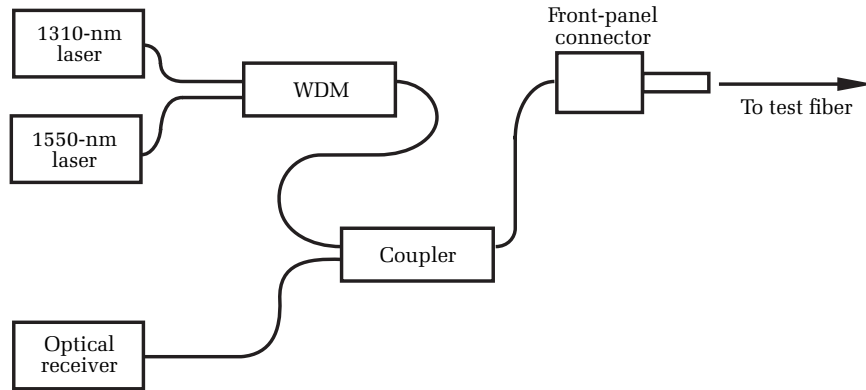


Figure 3.4. Principal optical components in a dual-wavelength, single-mode OTDR. Some OTDRs use WDMs that allow testing at 1310, 1550, and 1625 nm.

overcome this problem, many operators use a long jumper, sometimes called a *pulse suppressor* or *dead zone fiber*, to connect the OTDR to the fiber being tested. Pulse suppressors provide the necessary backscatter signature in front of the fiber's first connector so that the loss may be measured. To make operation more convenient, some OTDRs have this fiber built into the instrument, saving the operator the necessity of carrying around the pulse suppressor.

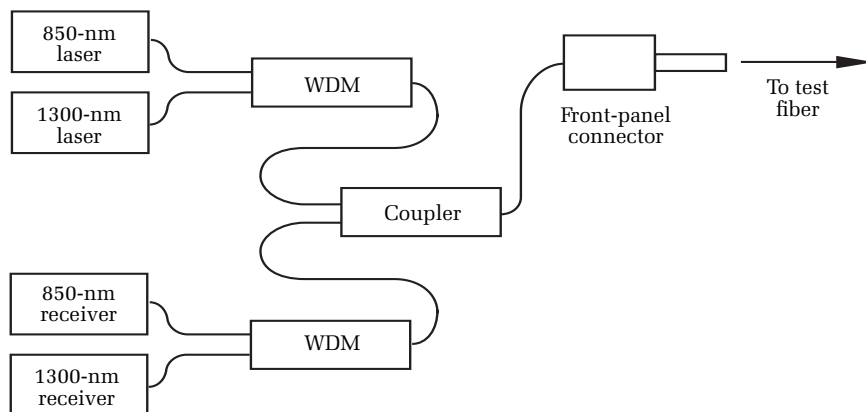


Figure 3.5. Principal optical components in a dual-wavelength, multimode OTDR. Notice that this instrument, unlike its single-mode counterpart, has two optical receivers and two WDMs (in some instruments, some of the multiplexing operations are done with couplers instead of WDMs).

If the OTDR used for testing does not include a pulse suppressor, the Fresnel reflection from the front-panel connector on the OTDR will also prevent an accurate measurement of the patch panel's connector. The use of a dead zone fiber (or box) is recommended in TIA/EIA 455 fiber-optic test procedures (FOTP) 59A "Measurement of fiber point discontinuities using an OTDR" and FOTP 61A "Measurement of fiber or cable attenuation using an OTDR." Both FOTPs reference that the fiber length may be up to 20 times the pulse length. The dead zone box also allows for an accurate ORL measurement of the patch panel connection to be made by the OTDR.

3.4 Optical masking

In chapter 7 we discuss some of the difficulties associated with measuring the losses of events near large reflections. Large reflections make the OTDR incapable of measuring events after the reflection until the OTDR has recovered from the reflection's bright light. This "dead zone" after a reflection is detrimental, and OTDR designers work hard to reduce its impact on the instrument user. Part of the problem is in the amplifier recovery time, and part of the problem results from carriers in the APD that slowly diffuse out of the active region. One way to reduce the dead zone is to increase the OTDR's bandwidth. The amount of noise in any electrical receiver increases with the bandwidth, however, so increasing the OTDR's bandwidth reduces the dead zone but also reduces the instrument's dynamic range.* To improve their instruments' performance with reflections, some manufacturers incorporate in their mainframe OTDRs a feature called *optical masking*. Optical masking reduces some of the negative effects of large reflections. The essential element in optical masking is an optical switch that will momentarily deflect the bright light of reflections away from the OTDR's sensitive receiver (see figure 3.6). Notice that the optical switch replaces the optical coupler. Earlier in the development of OTDR, optical masking was the preferred method used in high-end OTDRs to reduce the effects of large reflections and improve the dead zone. More recent approaches have emphasized improved receiver design and improvements in optical detectors that minimize the number of diffuse carriers. These approaches have proven to have a better cost/performance ratio, so most modern OTDRs do not require optical switching to achieve acceptable dead zone performance. Although optical masking is not currently offered on most

*We run across this design trade-off repeatedly in this book. Dynamic range and dead zone drive the OTDR's design and acquisition parameters in opposite directions.

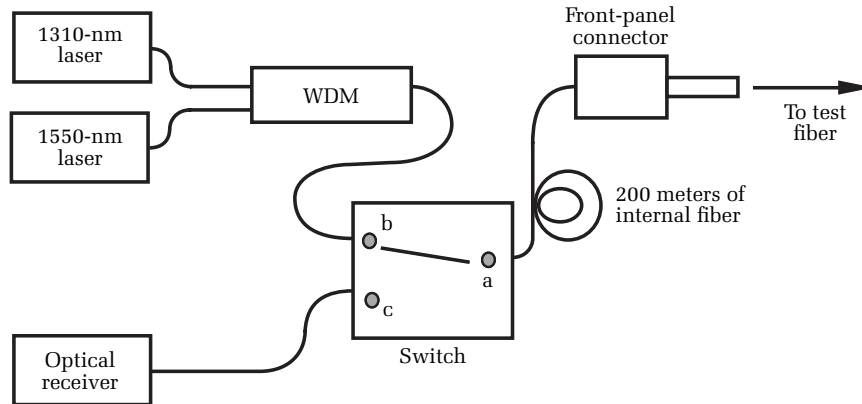


Figure 3.6. Principal optical components in an advanced OTDR with dual-wavelength capability, optical switch, and internal fiber for measuring the front-panel connector loss. The switch is connected from a to b when launching the laser pulse into the test fiber. It is connected from a to c when receiving the scattered and reflected light. It is connected (for only a few tens of nanoseconds) from a to b when blocking bright reflections that might saturate the APD receiver or amplifier.

modern OTDRs, there is a large installed base of these instruments that were purchased in the 1990s.

When used in an OTDR for optical masking, the switch accomplishes three important functions. First, the switch launches the outgoing laser pulse into the fiber under test. Second, the switch couples the return light to the receiver. Third, the switch masks the receiver from bright reflections, thus improving the OTDR's dead zone. Depending on its implementation, optical masking can provide the additional benefit of reduced optical loss within the instrument. Standard OTDRs with optical couplers suffer a 3-dB loss in the outgoing light and another 3-dB loss in the return light. If the OTDR uses an efficient optical switch, however, the roundtrip optical loss can be much less than the coupler's 6 dB. Consequently, an OTDR with an efficient optical switch not only benefits from the masking function of the switch, but it also achieves greater dynamic range (though the same benefit in dynamic range can be achieved with an optical circulator, at significantly lower cost and complexity).

Implementation of optical masking varies between OTDR manufacturers. Most OTDRs that offer masking require the operator to acquire a normal waveform, place masking cursors around the reflections, and then acquire another waveform with the masking

function engaged. Some OTDRs automatically find the reflective events and mask them for the user. In chapter 7 we discuss optical masking in more detail and explain some of the features that differentiate OTDRs that offer this capability.

3.5 Evolution of the OTDR

In chapter 1 we saw that the first OTDRs consisted of discrete instruments that launched the laser pulses, measured the backscattered and back-reflected light, and displayed a linear signal on an oscilloscope. The first commercial instruments were dedicated to performing OTDR functions and contained all these elements internally. They also added such features as a digital waveform, averaging, a distance scale (instead of time), and a log display. These were the early mainframe instruments. Mainframe OTDRs grew to include dual wavelengths, optical switching, high-resolution CRT displays, and internal printers. They also had internal and floppy-disk memory for storing and retrieving waveforms. Mainframe OTDRs stressed performance and were often expensive, with typical prices around \$30,000 U.S. or higher.

In the early 1990s, smaller instruments began to appear. These instruments were battery powered, had LCD displays instead of CRT, were much smaller, generally had less dynamic range than mainframe OTDRs, and were considerably less expensive. Their smaller size and restricted performance earned them the name *mini-OTDR*. Battery operation, more than size, limited early mini-OTDRs. Their limited power budget essentially prevented them from using cooled lasers or detectors. Cooling (typically with thermoelectric devices) allows lasers to operate at higher optical power and results in receivers that operate with less noise. Cooling was important in mainframe OTDRs for achieving high dynamic range and more stable wavelength.* Battery operation and selling price also precluded mini-OTDRs from using optical switching.

Developments in critical components led the way in improving OTDR performance. Laser power steadily increased, with present-day uncooled lasers delivering more than 200 mW of coupled output power. Meanwhile, components used in optical networks improved so that reflections at connectors became smaller. Reduced reflections and better APDs reduced the dead zone after reflective events, which led to

*The operating wavelength of laser diodes is a function of temperature. By cooling their lasers to a constant temperature, mainframe OTDRs can maintain a more constant wavelength. This results in more constant (repeatable) measurements of event and fiber loss.

competitive performance without the use of optical masking or detector cooling. Integrated receiver designs reduced power requirements further and led to improved instrument dynamic range.

With these developments, both mini-OTDRs and mainframes evolved through the 1990s, and mini-OTDRs soon began to rival mainframes in some areas of performance (see figure 3.7). To compete, mainframe OTDRs became less expensive and smaller. This evolution continued through the end of the 20th century, and by 2001 the mini-OTDR and mainframe had converged into a workhorse OTDR that was a battery-powered instrument the size of earlier mini instruments but with even more performance than mainframes of the 1990s. Meanwhile a new class of mini-OTDR, called a *fault locator* or *fault finder*, had emerged. The fault finder is much smaller than earlier mini OTDRs, is designed with the look and feel of a multimeter, and is targeted at premises installation and restoration. Though they work on the principle of OTDR, fault locators often lack the analog display, with some models simply displaying a numeric readout with the distance to the end of the fiber or break.

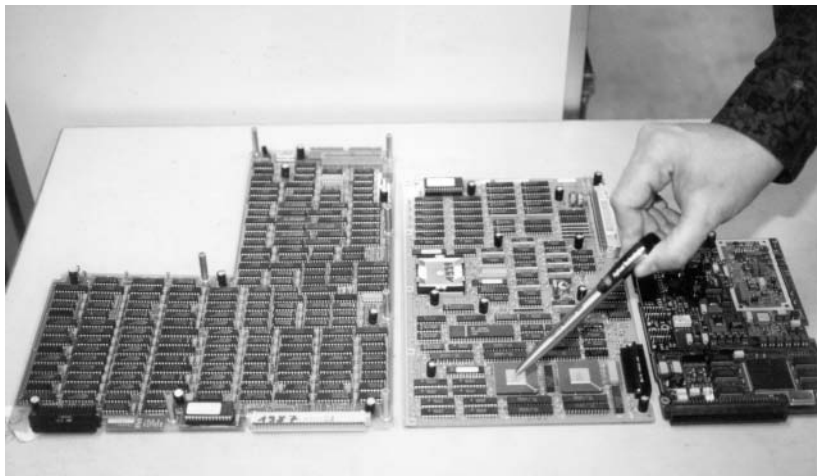


Figure 3.7. Evolution of digital circuit boards in OTDRs. Left: typical digital circuit board from 1987, showing many 74 series TTL integrated circuits (ICs). Middle: 1991, increasing use of MSI and LSI ICs, gate arrays, and digital signal processors delivers complex functionality. Right: 1995, high-performance digital signal processing is achieved by combination of a complex ASIC, an FPGA, and a powerful DSP. [Credit: The Light Brigade.]

Another extremely useful type of instrument is called the *visual fault locator* or *visual fault finder*. This is simply a red laser diode that can inject about a milliwatt of optical power into an optical fiber. Since the laser operates in the visible part of the spectrum, if there is a break in the fiber, it can be seen as a consequence of the visible laser light being scattered at the dislocation. Visible fault locators come as accessories to OTDRs as well as stand-alone instruments, some as compact as a pen. For those situations where the fiber is broken in the connector or within a few meters of the connector, the visual fault locator offers an almost unsurpassed solution for finding the break. The combination of the OTDR and the visual laser provide the fiber technician the best combination for locating fiber faults.

Recall that the optical components in an OTDR include a laser and a detector. These are also key optical components for two other important optical-test instruments, the light source and the optical power meter. To increase the utility of the OTDR, some manufacturers have added software features that stabilize the OTDR's internal laser for use as a light source. Additionally, the OTDR's receiver can be used as the receiver in an integral optical power meter. Other manufacturers migrated their OTDRs toward a platform topology, with the OTDR becoming one of many possible modules for the platform, along with specialized modules for other test applications.

OTDR evolution continues in the 21st century, with workhorse OTDRs that have the size and portability of early mini-OTDRs and outstanding performance in a battery-powered multiple-use instrument, at a price that is typically less than \$20,000 U.S. The most versatile instruments incorporate an OTDR as one of many possible modules that can be used with a field-portable platform (see figure 3.8). In addition



Figure 3.8. Example of a “platform” OTDR.
[Credit: Agilent Technologies.]

to OTDR modules of various varieties (single-mode, multimode, multiwavelength, etc.) other modules available for use with these photonic tool chests include:

1. Chromatic dispersion tester
2. Polarization mode dispersion tester
3. Optical power meter
4. Microscopic viewer for inspecting connector surfaces
5. Stabilized laser light source
6. Fiber identifier (nonintrusive probe for measuring optical power and direction of traffic)
7. Visual fault locator
8. Optical switch

3.6 Rayleigh backscatter

Rayleigh backscattering is fundamental to OTDR operation and is the method by which OTDRs measure the end-to-end loss of a fiber-optic line as well as the discrete losses of splices and connectors. Recall from chapter 2 that Rayleigh scattering occurs when light is scattered by the microscopic index fluctuations in the fiber and that it is the primary contributor to fiber attenuation in modern telecommunications-grade fiber.

Standard OTDRs launch repetitive laser pulses (these are typically rectangular) into the test fiber.* Suppose that at time $t = 0$, an OTDR launches an infinitesimally narrow pulse into a fiber with duration $dz = dt \cdot v_g$ (v_g is the group velocity of the laser pulse) and peak power P_0 . Ignoring multiple backscattering, the total backscatter power near the OTDR's front-panel connector is^{1,2}

$$dP_{bs} = 0.5 \cdot P_0 \cdot \alpha_S \cdot S \cdot dz \quad [3.1]$$

In equation [3.1], S is the backscatter factor, α_S is the attenuation (1/km) due to Rayleigh scattering, P_0 is the pulse power, and dz is the physical length of a differential pulse section. The total backscatter near the OTDR's front panel from a wide pulse is thus

$$P_{bs} = 0.5 \cdot P_0 \cdot \alpha_S \cdot S \int_0^D \exp(-z \cdot \alpha) dz \quad [3.2]$$

*The pulse appears rectangular when its power as a function of time is plotted. In other words, the pulse power is constant during the pulse duration.

In equation [3.2], α is the total attenuation constant (1/km) for the fiber and D is the physical pulse width (twice the displayed pulse width).^{*} In modern telecommunications fiber, α and α_S are nearly the same.

Solving equation [3.2] we have

$$P_{bs} = 0.5 \cdot P_0 \cdot \alpha_S \cdot S \left(\frac{1 - \exp(-D \cdot \alpha)}{\alpha} \right) \quad [3.3]$$

Expanding the exponent term in equation [3.3] and keeping only the first- and second-order terms, we have

$$P_{bs} = P_0 \cdot \alpha_S \cdot S \cdot W(1 - W \cdot \alpha) \quad [3.4]$$

In equation [3.4], W is the displayed pulse width (km) and is half the physical length of the pulse on the fiber, D . If the length of the laser pulse is small compared with the fiber's attenuation constant, then the quantity $(1 - W\alpha)$ is approximately 1, and we have

$$P_{bs} = P_0 \cdot \alpha_S \cdot S \cdot W \quad [3.5]$$

The backscatter coefficient, S , depends on the type of fiber being tested, and is proportional to the square of the ratio of the fiber's numerical aperture to its core index:^{3,4,5,6}

$$\begin{array}{ll} S = (\text{NA}/n)^2/4 & \text{graded index multimode fiber} \\ & /4.55 \quad \text{step-index single-mode fiber} \quad [3.6] \\ & /2.67 \quad \text{step-index multimode fiber} \end{array}$$

From equation [3.5], we see that the backscatter level is directly proportional to the scattering coefficient, pulse width, laser power, and S . Recall from chapter 2 that the scattering coefficient (α_S) is a strong function of wavelength and is proportional to $1/\lambda^4$. This explains why OTDRs typically have less dynamic range when operating at longer wavelengths. For example, at 1310 nm the backscatter coefficient is nearly twice as large as it is at 1550 nm, since $(1550/1310)^4 \approx 2$. This results in an inherent dynamic range benefit of about 1.5 dB, because $5 \log(2) \approx 1.5$.

^{*}The displayed pulse width is half the actual pulse width because of the factor of 2 used in arriving at the OTDR's distance scale (see section 3.0).

From equation [3.6] we also see that the backscatter level is proportional to the square of the numerical aperture. This is the reason the backscatter level (when testing single-mode fibers) rises at some splice points. Suppose, for example, that the fiber on one side of a splice is standard single mode, with a numerical aperture of 0.13, and the fiber on the other side of the splice is dispersion-shifted single mode, with a numerical aperture of 0.17. The difference in backscatter level for these two fibers is about 1.2 dB. Consequently, as long as the fusion splice has less than about 0.6 dB of loss, the backscatter level increases across the splice.* This gives the mistaken impression that the splice is a point of power amplification (we discuss this in much greater detail in chapter 6) and is sometimes referred to as a *gain splice*. Table 3.1 lists some typical backscatter levels for different types of fiber, at different wavelengths.†

Wavelength (nm)	Fiber type	Numerical aperture	Scattering coefficient (dB/km)*	Pulse width (km)	Backscatter level (dB)§
1310	Standard single-mode	0.130	0.40	0.020	-55.0
1550	Standard single-mode	0.130	0.20	0.020	-58.0
1300	Multimode	0.275	0.50	0.020	-47.0
850	Multimode	0.275	2.10	0.020	-40.7

Table 3.1. Backscatter level for some typical fibers, using typical acquisition settings.

3.7 Dynamic range

As we shall see in chapter 4, one of the most important specifications for an OTDR is dynamic range. The industry uses several different definitions for dynamic range, all essentially related ways of specifying the strength of the backscatter signal to the noise level. Consequently,

*The splice loss is half the backscatter difference because the backscatter light originating on the far side of the splice is attenuated twice by the splice. The pulse is attenuated once as it passes through the splice on its way down the fiber. The scattered light is attenuated again when it passes through the splice on its way back to the OTDR.

†The multimode fiber is assumed to be graded index, and the single-mode fiber is assumed to be step index. Core index in both is assumed to be about 1.468.

*To convert from dB/km to 1/km, multiply by 0.23.

§Measured in 10 log, relative to the launch pulse power.

to increase an OTDR's dynamic range, the designers must increase the backscatter level, decrease the system noise, or do both.

In chapter 2 we saw that attenuation in an optical fiber results from absorption and scattering. In a telecommunications system, high optical attenuation results in lower system SNR, lower system performance, and higher system cost. Consequently, it is not surprising that fiber manufacturers have expended considerable effort in reducing the attenuation properties of their products. As a result, typical attenuation values for modern telecommunications-grade fiber are only about 0.35 dB/km at 1310 nm and about 0.25 dB/km at 1550 nm. Although much of the effort has been directed toward ultrapure glass with very low absorption, effort has also been directed toward making the glass very homogenous to reduce the amount of scattering. Since little light is scattered by the fiber, OTDRs must work with extremely small signal levels and so must have optical receivers with demanding performance specifications for bandwidth and noise.

Even using low-noise receivers, an OTDR waveform is unacceptably noisy unless the instrument acquires many different waveforms and averages the results. Averaging is a common way of reducing noise in many systems, and OTDRs make exceptionally good use of this technique. Suppose a single waveform acquisition is superimposed with Gaussian noise having a standard deviation of σ . If we take two such waveforms and average them, then the standard deviation is $\sigma/\sqrt{2}$. If we average three such waveforms, the resulting standard deviation is $\sigma/\sqrt{3}$. In general, if we average n such waveforms the resulting standard deviation is σ/\sqrt{n} .*

Because of the nature of the square-root function, this method of averaging waveforms provides impressive gains in dynamic range at first, with diminishing returns as the number of averages increases. For example, suppose the SNR is 10:1 (5 dB) for a single waveform acquisition without averaging. By acquiring 100 such waveforms and averaging them, we can extend the SNR to 100:1 (10 dB). In this example, the first 100 averages increase the dynamic range by 5 dB. However, if we average another 100 times (200 averages altogether), the dynamic range increases by only another 0.8 dB. To achieve another 5-dB improvement after we have already averaged 100 times, we must take a total of 10,000 averages (this brings the total dynamic range to 15 dB). To increase the dynamic range from 15 dB to 20 dB requires 1,000,000 averages, and so forth.

*This holds true for random noise that is uncorrelated to the waveform. Noise that is synchronous to the waveform is not reduced by averaging.

The amount of averaging an OTDR can perform in a given amount of time depends on the length of the fiber. Longer fibers require more time for a given amount of averaging because it takes longer for each pulse to travel the length of the fiber.* Typically, an OTDR manufacturer specifies its instrument's dynamic range at a given pulse width and for a given amount of averaging time (usually three minutes). Be careful when comparing the dynamic ranges of two instruments. Since dynamic range depends strongly on the amount of averaging, you should not compare the dynamic ranges of two OTDRs unless they are both specified for the same amount of averaging on fibers of similar length.†

From equation [3.5], we see that if you want to increase the backscatter level, you can increase the OTDR's pulse width or laser power. To decrease the noise level, you reduce the receiver's bandwidth, increase the amount of averaging, or digitally filter the OTDR waveform.‡ Each of these actions involves trade-offs against other key parameters. Although larger pulse widths increase the dynamic range, they also reduce the OTDR's ability to measure closely spaced events, limiting the instrument's two-event resolution. Similarly, reducing the receiver bandwidth reduces the noise floor but also makes the OTDR more sluggish in responding to changes in signal. This, in turn, increases the minimum distance between two events that can be independently identified and measured. Digital filtering is often a good way to increase dynamic range. However, as we shall see in chapter 5, digital filtering can sometimes introduce distance-measurement errors. Increasing the laser power does not limit the OTDR's performance in other ways, but power increases have limits because of safety concerns and nonlinear effects that arise in the fiber.⁷ It takes time to reduce the noise floor by increased averaging, which means more time to analyze the fiber fully.

In chapter 4 we discuss these issues in much greater detail. Until then, remember that it is important to keep all these factors in mind when comparing OTDR data sheets. A good practice is to specify the dynamic range for specific averaging times and pulse widths. If a given manufacturer does not offer the exact pulse width and averaging time at

*Sending out pulses that are spaced closer together than the fiber's length results in ghosting. This is a waveform artifact to be avoided. We discuss ghosting later in this chapter and in subsequent chapters.

†The basis of comparison should be averaging time, not the number of averages, since time is the variable of interest for the OTDR operator.

‡These are things you would do apart from careful circuit design rules aimed at reducing the inherent noise in discrete components, or noise coupled into the receiver from outside sources.

which you are comparing the dynamic ranges of various instruments, you can still make the comparison by using the equation*

$$DR_2 = 5 \log \left(\sqrt{\frac{T_2}{T_1}} \cdot \left(\frac{W_2}{W_1} \right) \right) + DR_1 \quad [3.7a]$$

In equation [3.7a], DR_2 is the dynamic range with averaging time T_2 and pulse width W_2 and DR_1 is the dynamic range with averaging time T_1 and pulse width W_1 . When using equation [3.7a], be especially cautious of extrapolating the averaging time too far, because the equation applies only for Gaussian noise. If the OTDR suffers from synchronous noise, then additional averaging will not improve its dynamic range as much as predicted by equation [3.7a].[†]

To see how to use equation [3.7a], consider the following example. Suppose you want to compare two OTDRs whose dynamic-range specifications are not given for exactly the same conditions. OTDR A, for example, might specify a dynamic range of 32 dB with a 400-meter pulse and three minutes of averaging. OTDR B might specify a dynamic range of 34 dB with a 500-meter pulse and 20 minutes of averaging. Which OTDR has the best dynamic-range specifications? To find out, we can normalize the two OTDRs by calculating the dynamic range of each of them at some intermediate conditions. Suppose we pick for our intermediate conditions a pulse width of 450 meters and an averaging time of 5 minutes. Under these intermediate conditions, using equation [3.7a], we see that OTDR A has a dynamic range of

$$DR_2 = 5 \log \left(\sqrt{\frac{5}{3}} \cdot \left(\frac{450}{400} \right) \right) + 32 = 32.8 \text{ dB} \quad [3.7b]$$

and OTDR B has a dynamic range of

$$DR_2 = 5 \log \left(\sqrt{\frac{5}{20}} \cdot \left(\frac{450}{500} \right) \right) + 34 = 32.3 \text{ dB} \quad [3.7c]$$

*This only applies if all manufacturers use the same definition of dynamic range. As we shall see in chapter 4, several different definitions exist.

[†]Also, be careful about extrapolating the results of equation [3.7a] too far, because bandwidth changes frequently accompany changes in pulse width. Equation [3.7a] assumes that system noise and bandwidth remain constant between W_1 and W_2 .

In this example we see that although OTDR B specifies a dynamic range that is 2 dB larger than OTDR A, in reality the two instruments have essentially the same dynamic range when compared at the same operating conditions. OTDR B has a larger specification because its manufacturer chose to specify it with a longer pulse and more averaging than OTDR A.

In the previous example we saw that, for purposes of comparing dynamic range, you can use equation [3.7a] to extrapolate the instrument's performance. Equation [3.7a] allows you to go from the specified operating conditions of T_1 and W_1 to the desired operating conditions of T_2 and W_2 . In doing this, you must be sure that the specified operating conditions are sufficiently close to the desired operation conditions so that the instrument is still usable.* Use care in extrapolating too far, since some manufacturers change their OTDR's receiver bandwidth when the pulse width is changed, and this results in a changing noise floor that may invalidate some comparisons. The key point to remember when comparing the dynamic range of one OTDR with that of another is that dynamic range is a complicated quantity that depends on many different parameters. To make a useful comparison, you must compare the dynamic ranges of different OTDRs under the same conditions of pulse width and averaging.

3.8 Differences between multimode and single-mode OTDRs

How an OTDR works, the components it uses, and its performance specifications depend intimately on the type of fiber the instrument is designed to test. Although multimode and single-mode OTDRs are built in the same basic configuration (see figure 3.1), there are some significant differences between them. Some of these differences result from the differences in operating wavelength between single-mode and multimode systems, while others result from differences between single-mode and multimode fiber. In this section we discuss some of those differences. Since fiber parameters are key to the differences between single-mode and multimode OTDRs, we will begin with a review of the differences between single-mode and multimode fiber.

*For example, suppose you are comparing the dynamic ranges of several instruments at a 400-meter pulse width and 3 minutes of averaging. Suppose, however, that one of the OTDRs does not use a 400-meter pulse, but instead uses a 500-meter pulse. You might use the instrument's 500-meter pulse specifications and extrapolate back to 400 meters using equation [3.7a].

In chapter 2 we described optical fibers as conduits that transmit light “rays” by containing them within the fiber core through total internal reflection. We also saw that this picture of light propagating through optical fibers by reflecting back and forth from the core–cladding boundary is adequate for some purposes in optical communication systems that use multimode fibers. We learned, however, that we must remember that light is an electromagnetic wave phenomenon and that we really should be thinking of modes of guided wave propagation, instead of rays.

In chapter 2 we showed that a quantitative description of the modes supported by an optical fiber is possible if you solve Maxwell’s equations for a dielectric waveguide while using the appropriate boundary conditions. For the general solution, you must solve the equations numerically. The problem becomes tractable, however, by assuming that the core is circularly symmetric and that the difference between the core index and the cladding index is small.* With these approximations, Bessel functions describe the modal energy in the core, and modified Hankel functions describe the modal energy in the cladding. Recall that an interesting result of the waveguide solutions is that the field strength in the cladding is finite, dying away exponentially at large radial distances from the core.

We saw in chapter 2 (equation [2.22]) that the normalized frequency parameter, or V -parameter, for an optical fiber is

$$V = \frac{2\pi a (n_1^2 - n_2^2)^{1/2}}{\lambda} = \frac{2\pi a}{\lambda} NA \quad [3.8]$$

In equation [3.8], λ is the wavelength, a is the core radius, n_1 is the core index, n_2 is the cladding index, and NA is the fiber’s numerical aperture. Recall that the condition for single-mode operation is that $V < 2.405$. If $V > 2.405$, then the fiber can support multiple modes. For multimode fibers, the number of modes is approximately

$$\begin{aligned} N &\approx V^2/2 && \text{for step-index fiber} \\ N &\approx V^2/4 && \text{for graded-index fiber with parabolic profile} \end{aligned} \quad [3.9]$$

As an example, a typical multimode fiber has a core radius of 31 μm and a numerical aperture of 0.275 and operates at a wavelength of either 850 nm or 1310 nm. Thus, at 850 nm the number of modes is roughly 1000 and at 1310 nm it is about 400.† As you can see, there are

*In this case, the solution applies to what we call a weakly guided wave.

†We have assumed here that the fiber core has a parabolic profile.

Manufacturer	Fiber size (microns)	Index of refraction		Attenuation (dB/km)		Bandwidth (MHz•km)	
		850	1300	850	1300	850	1300
Standard multimode fibers (overfilled launch condition)							
Alcatel	50/125	1.482	1.480	≤2.4	≤0.6	600	1200
	62.5/125	1.497	1.492	≤2.8	≤0.8	250	800
Corning	50/125	1.490	1.486	≤2.5	≤0.8	500	500
	62.5/125	1.496	1.487	≤3.0	≤0.7	160	500
Draka/Plasma	50/125	1.482	1.477	≤2.5	≤0.7	1000	1500
	62.5/125	1.496	1.491	≤3.0	≤0.7	300	1000
OFS	50/125	1.483	1.479	≤2.4	≤0.7	500	500
	62.5/125	1.496	1.491	≤2.9	≤0.7	200	500

Manufacturer	Fiber size (microns)	Index of refraction		Attenuation (dB/km)		Max distance (meters)	
		850	1300	850	1300	850	1300
Laser enhanced multimode fibers							
Alcatel Glight	62.5/125	1.497	1.492	≤2.9	≤0.8	—	—
Avaya	LazrSpeed 150	50/125	1.483	1.478	≤3.5	≤1.5	600
	LazrSpeed 300	50/125	1.483	1.478	≤3.5	≤1.5	600
	OptiSpeed Plus	62.5/125	1.496	1.491	≤3.5	≤1.5	300
Corning	Infinicor 600	50/125	1.490	1.486	≤2.5	≤0.8	600
	Infinicor 300	62.5/125	1.496	1.487	≤3.0	≤0.7	300
Draka/Plasma	Max-Cap	50/125	1.482	1.477	≤2.5	≤0.7	600
	Hi-Cap	62.5/125	1.496	1.491	≤3.0	≤0.7	500
OFS Gigaguide XL	Gigaguide XL	50/125	1.483	1.479	≤2.4	≤0.7	600
	Gigaguide XL	62.5/125	1.496	1.491	≤2.9	≤0.7	500

Manufacturer	Fiber size (microns)	Index of refraction			Attenuation	
		1310	1550	1625	1310	1550
ITU-T G.652 single-mode fibers						
Corning	8.2	1.467	1.468	N/A	.35 dB/km	.22 dB/km
OFS (Lucent)	8.3	1.466	1.467	1.467	.34 dB/km	.195 dB/km
Alcatel	8.8	1.464	1.465	N/A	.35 dB/km	.25 dB/km
Plasma/Draka	9.3	1.467	1.467	N/A	.38 dB/km	.23 dB/km
ITU-T G.653 dispersion-shifted single-mode fibers						
Corning SMF-DS	8.2	1.471	1.471		.38 dB/km	.25 dB/km

Manufacturer	Fiber size (microns)	Index of refraction			Attenuation	
		1310	1550	1625	1550	1625
ITU-T G.655 nonzero dispersion-shifted single-mode fibers						
Corning Leaf MetroCor	9.2	1.468	1.468	1.469	.22 dB/km	.24 dB/km.
	8.6	1.469	1.470		.25 dB/km	.25 dB/km
OFS TrueWave RST™	8.4	1.471	1.470	1.470	.39 dB/km	.20 dB/km
Alcatel Teralight™	9.2	1.469	1.469		.38 dB/km	.25 dB/km

Table 3.2. Physical and optical properties of common multimode and single-mode fibers.

hundreds of modes in multimode fiber, and the number is greater for short wavelengths than for longer ones.

3.8.1 Physical differences

Table 3.2 shows some of the differences in the physical and optical parameters of multimode and single-mode fibers. Typically, multimode fibers have larger numerical apertures, larger core diameters, and slightly higher attenuation coefficients.⁸

Standard single-mode fibers have a simple step-index profile. That is, the core index is slightly higher than the cladding index, and there is a sharp demarcation at the core–cladding boundary. Multimode fibers, in contrast, typically have a parabolic-index profile, with the index being highest on the fiber’s core and decreasing as a parabolic function to the cladding index at the core–cladding boundary. Recall from chapter 2 that fiber manufacturers use this parabolic profile to minimize modal dispersion. Multimode fibers are also usually designed to operate at 850 nm or 1300 nm, whereas single-mode fibers usually operate at 1310 and 1550 nm and sometimes as high as 1625 nm.*

3.8.2 Reflectivity differences between single-mode and multimode fiber connectors

Multimode connectors typically have higher reflectivity than single-mode connectors. This is because the larger core diameters make it more difficult to achieve physical contact over the full width of the fiber’s core.[†] The relevance of multimode connector reflectivity to the OTDR designer is threefold. First, multimode systems that use connectors typically have larger reflections than similar single-mode systems. Consequently, the event- and attenuation-dead-zone specifications for the OTDR should correspond to reflections that are larger than those for single-mode OTDRs.[‡] Second, since reflections are frequently not as important in multimode systems due to the use of light-emitting diodes (LEDs) and vertical cavity surface emitting lasers (VCSELs), it is

*Most single-mode fibers become bimodal below their single-mode cut-off wavelength of about 1200 nm.

[†]We see in chapter 6 that one way to achieve low reflectivity in connectors is to polish them with a hemisphere such that the cores of the two fibers are in intimate contact. These are called physical-contact connectors.

[‡]*Event dead zone* is the distance after a reflective event before another reflective event can be identified (but its loss not measured). *Loss, or attenuation, dead zone* is the distance after a reflective event before another event can be identified and its loss measured. Event and loss dead zones are discussed in more detail in the next chapter.

sometimes possible to reduce the accuracy specifications for measuring those reflections. Third, to measure reflections accurately on multimode systems, the upper range of the OTDR's dynamic range must be extended to avoid saturation.

3.8.3 Differences in backscatter levels

The differences between multimode and single-mode fibers combine to give higher backscatter levels for multimode OTDRs. Using equations [3.5] and [3.6], we can express the optical power that is scattered back to the OTDR as:

$$P_{bs} = S\alpha_s W \cdot P$$

$$S = \left(\frac{NA}{n}\right)^2 \frac{1}{q} \quad [3.10]$$

In equation [3.10], q equals 4 for graded-index multimode fibers and 4.55 for single-mode fibers. The scattering coefficient (1/km) is α_s , P is the (local) power of the laser pulse, W is the displayed fiber length, and n is the axial core index.

From equation [3.10] you can see that the primary reason backscatter is higher for multimode than for single-mode fiber is the increase in numerical aperture. Additionally, the q factor for multimode is slightly smaller for graded-index multimode fibers than it is for single-mode fibers. Combining these two factors results in a backscatter level for Corning 62.5/125 CPC3 that is inherently about 3.5 dB higher than it is for SMF-28 single-mode fiber (at a given wavelength and pulse width).*

Another factor that contributes to differences in backscatter between single-mode and multimode OTDRs is operating wavelength. Single-mode OTDRs rarely operate at 850 nm; multimode OTDRs frequently do. Rayleigh backscatter is inversely proportional to the fourth power of the wavelength of light, so at 850 nm the backscatter level is inherently 3.7 dB higher than it is at 1310 nm. This gives the multimode 850-nm OTDR an even greater advantage in terms of high backscatter level.

Another reason multimode OTDRs have higher dynamic range is that they use more powerful laser pulses. They achieve more powerful laser pulses because laser coupling to large-core multimode fibers is

*This is 3.5 dB higher on the OTDR display, which, as we have seen, is calculated using 5 log, not 10 log.

very efficient and because multimode lasers typically have more optical power than single-mode lasers. It is not uncommon to have laser pulses of 1500 or even 2000 mW in a multimode OTDR. Single-mode OTDRs, in contrast, rarely have laser pulses with more than about 200 mW.*

3.8.4 Optical-power differences

Even if single-mode lasers were significantly more powerful, there are upper limits to the amount of optical power that a single-mode fiber can carry compared with a multimode fiber. First, because of their larger core size, multimode fibers can carry more optical power than single-mode fiber before nonlinear effects start to become important.† Second, as we shall see in chapter 15, multimode fibers can carry more optical power than single-mode fibers while remaining within the most stringent laser safety classification. One of the considerations in evaluating laser safety is the amount of divergence in the light source. Generally, more divergent sources are inherently safer and may be more powerful than less divergent sources. Since multimode fibers have large numerical apertures, the light from the end of the fiber is highly divergent. Single-mode fibers have lower numerical apertures, so the light from the end of the fiber is less divergent. Thus, it is possible for a multimode OTDR to use more powerful laser pulses without exceeding laser safety standards. The extra optical power used by multimode OTDRs can add about 6 dB to their backscatter advantage.

3.8.5 Pulse-width differences

The inherently greater backscatter level of multimode OTDRs may not be obviously expressed in the instrument's dynamic range specification. Single-mode OTDRs are designed to analyze fibers that might be over 100 km long. To accomplish this, the single-mode OTDR uses relatively long pulse widths that are as much as one or two kilometers or longer. Multimode OTDRs, on the other hand, usually test relatively short fibers that are typically less than 2 km and often just a few hundred meters long. Consequently, the multimode OTDR uses a much smaller maximum pulse width than the single-mode OTDR. For the multimode OTDR, the pulse width is typically between 1 and 50 meters long.

*This limit applies to standard OTDRs using laser diodes. Exceptions might be OTDRs with YAG lasers and power optical amplifiers.

†This is because nonlinear effects are a function of power density. The core area of a typical multimode fiber is about 35 times greater than that of a typical single-mode fiber, so it can carry roughly 35 times more optical power before nonlinear effects become important.

OTDR manufacturers often specify the instrument's dynamic range at the instrument's longest pulse width. Comparing just the longest pulse widths, we see that $5 \log(1000/50) = 6.5$ dB. The multimode OTDR gives up (on the data sheet) a large part of the specified dynamic range it gained because of numerical aperture, wavelength, coupling efficiency, and laser power.

3.8.6 Operating-wavelength differences

As we mentioned before, a major difference between single-mode and multimode installations is that single-mode fiber is almost never used at 850 nm, while multimode fiber sometimes is. An option on many multimode OTDRs is an optical front end that operates at 850 nm. OTDRs operating at 850 nm have additional advantages, including the use of silicon APDs, very high-power (many watts) multimode lasers, and more Rayleigh backscattering because of the inverse fourth power Rayleigh scattering law. Being able to use silicon APDs is an especially great advantage over germanium or InGaAs APDs because silicon devices have greater gain and lower noise. Table 3.3 compares some of the performance parameters for silicon, germanium, and InGaAs APDs.

Characteristic	Silicon ⁹	Germanium ¹⁰	InGaAs ¹¹
Reverse breakdown voltage (V)	300 max.	48 max.	100 max.
Dark current (nA)*	1.0 max.	500 max.	50 max.
Quantum efficiency (%) [†]	70 typ.	80 typ.	77 typ.
Useable wavelength range (nm)	400–1100	800–1500	1000–1800
Current multiplication factor [‡]	150 typ.	40 typ.	40 typ.
Excess noise factor [§]	0.30 max.	0.95	0.7

Table 3.3. Comparison of key performance parameters for silicon, germanium, and InGaAs APDs.

Earlier in this chapter, we described the OTDR's detector and said that it could be a PIN detector, APD, or even a photomultiplier

*At 2V below the breakdown voltage for silicon, 90% of breakdown for germanium and InGaAs.

[†]At 850 nm for silicon, 1300 nm and $M = 1$ for germanium and InGaAs.

[‡]At 2V below the breakdown voltage for silicon, at a reverse current that gives 10 μ A dark current for germanium, and 1 μ A dark current for InGaAs.

[§]At 850 nm for silicon, gain of 100, at 1300 nm and $M = 10$ for germanium and InGaAs.

tube. Generally, APDs are used, but PIN detectors are acceptable in some circumstances, such as coherent-detection OTDRs.* In PIN-type photodiodes, at most one electron hole pair is generated for each photon absorbed. PIN detectors, therefore, have no gain mechanism. In APDs, however, this is not the case. APDs have a sufficiently wide depletion region and sufficiently high reverse bias that the field within the region produces avalanche multiplication. In this case, electron hole pairs (EHPs) traverse the depletion region with sufficient kinetic energy to produce additional EHPs through collisions. This process results in more than one EHP for each photon absorbed, giving APDs gains greater than 1. The multiplication factor for an APD is†

$$M_e = \frac{I}{I_{op}} = \frac{(1 - k_a)}{\exp\{-(1 - k_a)\alpha_e w_d\} - k_a} \quad [3.11]$$

where

- w_d = width of the depletion layer
- I = total amplified current
- I_{op} = photocurrent
- k_a = α_h/α_e
- α_h = hole ionization coefficient
- α_e = electron ionization coefficient

If electrons and holes both have roughly the same ionization constant, then $k \approx 1$. When this happens, the holes moving in one direction create electrons moving in the other, and additional holes are generated. This feedback process increases the APD's gain but is generally undesirable because it reduces the device bandwidth, increases the device noise, is unstable, and can result in device breakdown. The optimum condition is for k to be either very large or very small so that only one type of carrier (either electrons or holes) affects the ionization process. APDs with values of k as low as 0.006 have been fabricated from silicon, providing excellent performance. In germanium, $k \approx 1$, so germanium APDs are noisier than silicon devices.

From table 3.3 we see that the current multiplication factor is typically much higher for silicon APDs than it is for germanium or InGaAs. Reverse bias is also typically much higher. Because of their greater multiplication factor and lower excess noise factor, silicon APDs

*We discuss coherent OTDRs and other types of nonstandard configurations at the end of this chapter.

†The ionization coefficients are defined such that their reciprocals give the average distance between ionizing collisions.

have a dynamic-range advantage over InGaAs of about 4.7 dB. This helps give multimode OTDRs operating at 850 nm an even greater inherent dynamic-range advantage over their single-mode counterparts (for a given pulse width and averaging).

To summarize, there are a number of significant differences between multimode and single-mode OTDRs. As expected, many of these differences arise from the differences between single-mode and multimode fibers. Multimode fibers have larger numerical apertures and larger cores. This makes it much easier to couple high power into the fibers and to collect the Rayleigh scattered light detected by the OTDR. Some multimode OTDRs also operate at 850 nm, where the Rayleigh scatter coefficient is much higher than it is at 1310 or 1550 nm and where silicon APDs may be used. This gives multimode OTDRs an inherently higher dynamic range (for given acquisition settings), although the specified dynamic range might not reflect this because multimode OTDRs use shorter pulse widths. Table 3.4 summarizes some of these design considerations.

Design criterion	Multimode OTDR	Single-mode OTDR
Pulse width	Generally uses shorter pulse widths. This reduces dynamic range but gives better two-point resolution.	Generally uses longer pulse widths. This increases dynamic range but gives poorer two-point resolution.
Detector	Can sometimes use silicon APD [highest performance, low cost]. For 1300 nm use either germanium APD [medium cost, lowest performance] or InGaAs APD [higher cost, medium performance].	Must use either germanium APDs [low cost, lower performance] or InGaAs APDs [higher cost, better performance than germanium, but not as good performance as silicon].
Laser	Easier coupling. Can use high-power multimode lasers at either 850 or 1300 nm. Higher threshold for nonlinear effects.	Single-mode laser coupling is more difficult. SM laser output about 10 times less than for multimode lasers. Lower threshold for nonlinear effects.
Fiber	Multimode fiber has high NA, so collects a much larger percentage of backscatter than single-mode fiber. Multimode fiber has high attenuation, so range is typically short.	Single-mode fiber has low attenuation, so range is typically large. Fiber has small numerical aperture, so collects relatively small amount of backscatter radiation.

Table 3.4. Summary of dynamic-range concerns for single-mode and multimode OTDRs.

3.9 Echoes and ghosts

As we have seen, an OTDR displays a waveform that is generated by reflections and Rayleigh backscatter. Without reflections and scattered light, the OTDR would have no waveform and provide no information about the fiber. Although the instrument depends on reflections, unwanted multiple reflections are a source of annoyance and confusion to the operator. In optical systems with many reflections, portions of the laser pulse can easily reflect more than once before returning to the OTDR. When this happens, those portions of the laser pulse that reflect more than once result in waveform artifacts called *echoes*. Echoes are just like any other reflection and look like real events. However, because they have been reflected more than once, their locations are falsely portrayed on the OTDR waveform. Because of this, echoes appear (except for coincidences) where no real events exist.

Figure 3.9 illustrates how echoes form and multiply. The horizontal axis in the right-hand figure represents distance along the fiber, and the

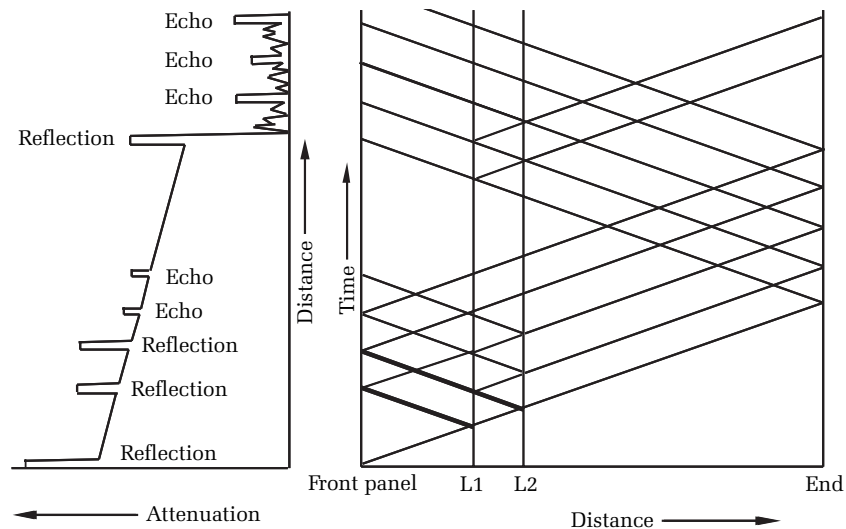


Figure 3.9. How echoes can multiply in a system with reflective events. Echoes occur whenever light returns to the OTDR after reflecting more than once. The number of echoes grows exponentially. Fortunately, in most systems the echoes become far too attenuated to see after being reflected more than three times. In this figure the primary pulse and reflections are shown with a heavy line, and the echoes are shown with a lighter line. This figure shows only a small number of the infinite number of possible echoes.

vertical axis represents time. At time 0, the OTDR emits a laser pulse. This pulse (represented by the heavy line originating at the intersection of the horizontal and vertical axes) encounters a reflective event (a connector, for example) at L1. At L1, part of the light in the laser pulse is reflected, and the rest of the pulse is transmitted. The transmitted light encounters a second reflective event at L2, where (again) some of the light is reflected and some is transmitted. The laser pulse continues to the end of the fiber, where the transmitted light is lost and the reflected light returns to the OTDR. So far in this description, everything is as we expect it. Real events reflect light that is detected by the OTDR and accurately displayed to reveal the locations of the fiber end and two connectors.

Now the description begins to become complicated. Notice that the light reflecting from L1 does not all return to the OTDR's receiver. Some of it reflects again at the front panel and travels back down the fiber. Meanwhile, the light from L2 also does not all return to the OTDR's receiver. On its way back to the OTDR, some of the light that was reflected at L2 is reflected again at L1. When the reflected light from L2 reaches L1, some of the light continues to the OTDR, and the rest is directed back toward L2. In the figure, the initial pulse and its first reflections are shown as dark lines. The multiple reflections, which are echoes, are shown as lighter lines. Each time one of the sloping lines (representing the laser pulses or one of its reflections) encounters a vertical line (representing a reflective component), the sloping line divides in two. One of the sloping lines continues through the vertical line, and the other reflects. Thus, echoes increase and multiply exponentially (only a few of the infinite number of echoes are shown in figure 3.9).

Echoes are most likely to appear in OTDR traces when the instrument has high dynamic range and is used to test optical fibers where there are multiple highly reflective events. Because multimode OTDRs tend to have higher dynamic range and are tested on shorter fibers with more reflective connectors, echoes tend to be more of a problem for multimode OTDRs than they are for single-mode instruments. Echoes can be very confusing because they often appear to be real events. Besides discrete echoes, it is also possible to see echoed backscatter. You might, for instance, see echoed backscatter beyond a fiber's reflective end. Although possible, echoed backscatter is far less common than discrete echoes.

Echoes cannot be eliminated from the waveform, but they can be identified and marked to help the operator avoid confusion. The first

two reflective events in any waveform are never echoes. The reason for this is that at least two reflective events are required before any laser pulse can reflect more than once back to the OTDR. Another identifying feature of echoes is that they seldom have loss associated with them (the exception is when echoed backscatter is present), as shown in figure 3.10. Beyond these two traits, to identify an echo we must show that its location is consistent with the calculated position of echoes from known reflective events. This means tracing out the possible echo positions, as shown in the example in figure 3.9. Of course the total number of possible echoes is infinite, so in practice you only look for reflective events that match the position of first- or second-order echoes. Even with this simplifying assumption, however, for most systems it is impractical for OTDR operators to identify possible echoes manually. The only truly practical solution is to purchase an OTDR with automatic event-marking algorithms that locate reflective events and then perform the tedious calculations required to determine which are echoes and which are not.¹² Typically, such echo-location software marks suspect events with a small “e” in the event table, rather than attempting to modify the waveform by erasing the reflection.

Although echoes are sometimes called *ghosts*, such terminology can be confusing because the word ghost can also mean something

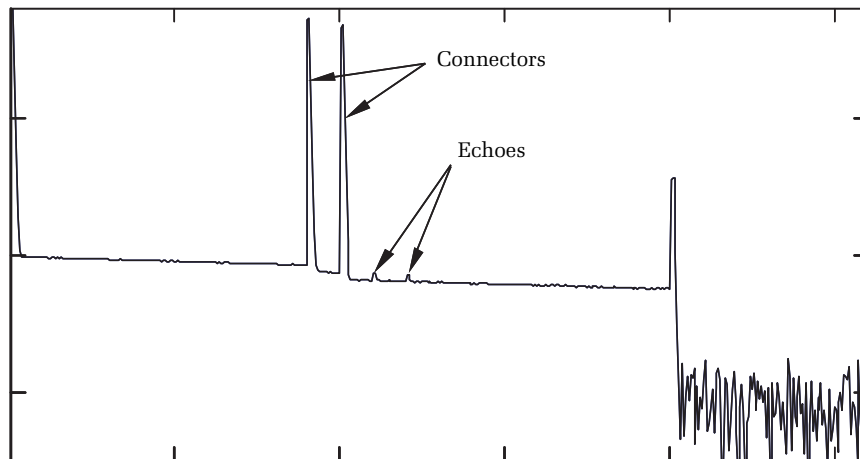


Figure 3.10. Two connectors spaced 200 meters apart. Light reflecting off these connectors results in a pair of echoes 200 meters after the last connector and spaced 200 meters apart. Observe that there is no loss associated with the echoes. The pair of connectors and the front panel each had -20 dB return loss. In this waveform, the pulse width is 20 meters, the fiber is single-mode, and the wavelength is 1310 nm.

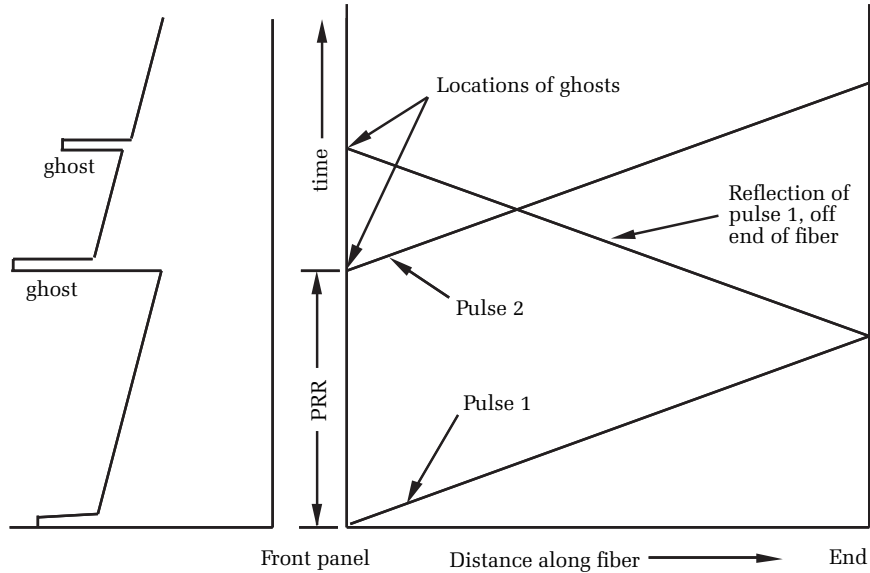


Figure 3.11. How ghosts can appear in an OTDR waveform. If the OTDR initiates a second acquisition (Pulse 2) before the end reflection from the first acquisition returns to the OTDR, then the reflective end of the fiber appears near the front of the waveform as a bogus event. Changing the OTDR's distance range (pulse-repetition rate, or PRR) eliminates the ghost. Changing the PRR does not eliminate echoes.

altogether different than the echo phenomenon we have just discussed. Ghosts are similar to echoes in appearance on the OTDR trace, but they occur for fundamentally different reasons. Echoes originate from components on the fiber-optic link, such as connectors, mechanical splices, and unterminated ends. Since they arise from the fiber-optic link, echoes are independent of the acquisition parameters used by the OTDR. Consequently, changing the acquisition parameters cannot move an echo.* Unlike echoes, ghosts arise from improperly selected acquisition parameters, so they can (and should) be avoided by selecting the proper pulse-repetition rate (which is a function of the distance range). Some manufacturers incorrectly specify that they have echo detection, when they actually are referring to algorithms for ghost elimination. Algorithms for ghost elimination automatically set the pulse-repetition

*Increasing the pulse width, however, raises the backscatter level and may (under some circumstances) cover an echo that would otherwise be visible with a shorter pulse. The echo is not moved. It is simply masked over by the higher backscatter level.

rate low enough to avoid ghosts. Ghost avoidance should be considered a requirement for properly designed OTDRs.

Figure 3.11 illustrates how ghosts can appear when the pulse-repetition rate is set too high. If the pulse-repetition rate is high, the reflection from the end of the fiber can return shortly after a second pulse is launched and a second acquisition is initiated. When this happens, the reflection from the end of the fiber overlaps backscatter near the front of the OTDR trace and appears as a reflective event. To eliminate ghosting, the pulse-repetition rate must be decreased. This is equivalent to increasing the OTDR's distance range. To avoid ghosting, some OTDRs automatically increase the distance range when large pulse widths (corresponding to large dynamic range) are selected by the OTDR operator. If an event moves or disappears when the range is changed, then the event is a ghost and not an echo.

3.10 Other types of OTDR configurations

The standard OTDR (see figure 3.1) is the configuration most often used by OTDR manufacturers who sell their instruments to telecommunications companies. This configuration provides the best balance of resolution, dead zone, dynamic range, and cost. Other configurations and methodologies are also in use or have been proposed. Some of these designs emphasize dynamic range, while others emphasize high resolution. Some are designed to test specific systems, such as those containing erbium-doped fiber-optic amplifiers, or EDFAs. Although this book is oriented mainly toward the design and operational methodologies of the standard OTDR configuration, we conclude this chapter with a brief description of some of these other design platforms.

3.10.1 Standard OTDR with an EDFA

OTDRs never seem to have enough dynamic range and resolution. As we shall see throughout this book, a standard OTDR's dynamic range becomes worse as the dead zone gets better. The reason for this is that the power of the Rayleigh backscatter is a function of the volume of fiber filled by the pulse and thus of the pulse length. Two-point resolution, on the other hand, is inversely proportional to the pulse length, so it gets better as the pulse gets shorter.

Two ways to improve the OTDR's dynamic range are to increase the output power of the laser and to increase the receiver sensitivity (while keeping the noise low). You can address each of these problems by using a fiber amplifier. Optical-fiber amplifiers use lengths of doped single-

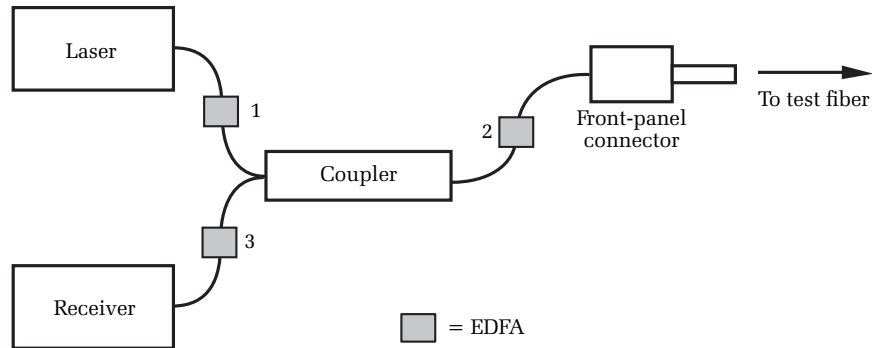


Figure 3.12. Possible locations for an EDFA in a standard OTDR.

mode optical fiber as their gain medium.* These devices are called erbium-doped fiber-optic amplifiers, or EDFAs, and they operate at roughly 1550 nm.† In operation, the doped fiber is energized by a pump laser‡ that excites ions in the fiber to a metastable state. Signal radiation from the OTDR's probe laser stimulates these excited states, which emit photons of the same wavelength and phase as those of the probe beam. This gain mechanism results in many photons being emitted for each signal photon that passes through the amplifier. Optical amplifiers are capable of extraordinary improvements in optical gain, but they are also a source of noise, so they must be used carefully. Just the same, the use of optical amplifiers in OTDRs presents the possibility of extraordinary dynamic range, with very good two-point resolution.

There are three places in a standard OTDR where the optical amplifier might be placed (see figure 3.12). For instance, you might wish simply to increase the power of the launch pulses. To do this, you could place an EDFA just after the laser (before the coupler). In this configuration, the EDFA should be optimized as a power amplifier. Placing the EDFA after the coupler results in amplification of both the outgoing pulse and the backscatter radiation. Placing the EDFA in the return leg (just before the optical receiver) results in amplification of only the backscatter signal.

*The dopant is usually erbium when operating near 1550 nm. A full discussion of fiber amplifiers is well outside the scope of this book. Refer to the Suggested reading at the end of this chapter.

†Most optical amplifiers operate at 1550 nm, but work is also progressing on semiconductor optical amplifiers that operate in the 1310-nm window.

‡The pump laser is coupled into the erbium-doped fiber with an optical coupler.

Each of these locations involves specific design goals and engineering trade-offs. For example, position 1 requires a power amplifier, yet EDFAs are best suited as low-gain amplifiers. High-power laser output brings problems associated with laser safety and nonlinear effects in the fiber. Placing the EDFA in position 2 requires an EDFA that operates effectively as both a low-gain amplifier and a high-gain amplifier. In position 3, the EDFA can saturate the receiver with spontaneous emissions and also with the light from the lasers used to pump the amplifier.* To prevent saturation, the OTDR must use efficient narrow-band optical filters and a narrow-frequency laser source, but these can cause problems with coherent standing waves and must be carefully considered in the design details.

Although EDFAs offer dramatic improvements in dynamic range even with small pulse widths, their principal disadvantage is cost. Along with the doped single-mode fiber, an EDFA consists of optical filters, a pump laser, and the necessary electronic circuitry to drive the pump. Because of these expensive components, EDFAs are still rather expensive, so they have been used only in a small number of full-featured mainframe OTDRs.

3.10.2 Coherent-detection OTDR

In chapter 2 we discussed the concept of coherence. We saw that when the coherence length is very short, optical-path lengths in an interferometer must be nearly identical, or interference fringes will not occur. A standard OTDR uses lasers that operate over a relatively wide range of wavelengths, so their coherence length is rather small (usually less than a millimeter).† If we make the coherence length long enough, however, and modify the receiver portion of the OTDR, we can arrange to have the backscattered light interfere with the source. When we do this correctly, we can improve the OTDR's dynamic range.

Figure 3.13 illustrates the block layout of a coherent OTDR. The coherent OTDR does not use laser pulses. Instead, it launches a frequency-chirped signal into the fiber. The optical source must be stable in phase and frequency and is typically a narrow-band laser with

*It can also do this in position 2. The EDFA spontaneously emits over the width of its gain curve, which is several tens of nanometers wide. Although the power of this spontaneous emission in a narrow spectral band is small compared with the amplified signal, the integrated spontaneous emission can be quite large.

†These lasers have spectra that are wide when compared with devices such as narrow-width lasers used in holography, but they are narrow compared to sources such as LEDs.

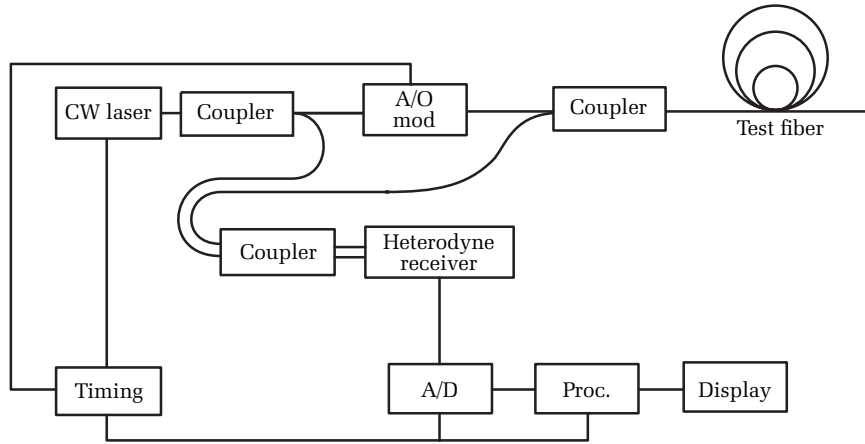


Figure 3.13. Layout of a coherent OTDR. Theoretically, coherent OTDRs have more dynamic range than standard OTDRs. In practice, however, they have some problems with polarization fading that have the same impact on measurements as reduced dynamic range. They also tend to be more expensive because of the extra optical components they require, such as the two extra couplers and the external modulator.

a feedback loop. To achieve frequency chirping,* the coherent OTDR uses an external Bragg cell. The Bragg cell changes the optical frequency of the laser beam and can either increase or decrease the wavelength by an amount equal to the electronic modulation frequency (usually a few hundred megahertz). In figure 3.13 you can see that part of the light from the narrow-band source is split off and connected through a coupler to a heterodyne receiver. The remaining portion of the continuous laser signal passes through the external modulator, where it is chirped and then launched into the test fiber. The scattered and reflected light from the test fiber is coupled into the heterodyne receiver, where it mixes with the light from the OTDR's laser.

Since the probe signal is chirped, the frequency of the mixing signal in the receiver changes with time and is correlated to the location on the fiber from which the light scattered. Improvement in dynamic range results because the mixing is coherent, so the strength of the mixing signal is proportional to the square of the electric field of the

*Frequency chirping means that the frequency (wavelength) of the light is changed rapidly as a function of time. In this example, the change is very small compared to the carrier frequency of the light. For example, the carrier frequency might be several terahertz, while the amount of chirp is only in the megahertz range.

source and scattered fields.* If the reference and scattered fields each have amplitude A , then the intensity of the constructive interference of these two fields is $4A^2$. In contrast, when two waves add incoherently, their amplitudes add in RMS fashion. If the reference and scattered fields each have amplitude A and they add incoherently, then the resulting irradiance is only $2A^2$. Another advantage results because the optical receiver now operates over a narrow frequency range (the bandwidth of the chirp signal). Since receiver noise increases with bandwidth, a narrow frequency range allows narrow-band filtering, which results in less receiver noise. These two effects combine to give the coherent OTDR a theoretical signal-to-noise advantage over the standard OTDR.

In spite of the theoretical advantage they enjoy, coherent OTDRs are not strong contenders as practical test instruments. There are several reasons for this. First, as you can see in figure 3.13, the coherent OTDR requires more expensive optical components. The narrow-band laser, for example, is considerably more expensive than the standard Fabry–Perot lasers used in conventional OTDRs. The coherent OTDR also requires an external modulator and two extra couplers that are not used in a standard OTDR.

Another problem with the coherent OTDR relates to a phenomenon called *polarization fading*. Two electromagnetic waves cannot interfere coherently unless they have the same state of polarization. We will see in chapter 10 that fibers can rotate the state of polarization of light propagating along their length. Consequently, the mixing signal in the heterodyne receiver can be modulated by the state of polarization of the light as it propagates along the fiber. The result of this polarization fading is that the OTDR waveform is noisy. This noise is not necessarily random (that is, it repeats from one acquisition to the next and cannot be averaged away), but it still has the effect of making small events on the fiber difficult to identify and measure. Although polarization fading can be reduced, the solutions to polarization fading add to the instrument's complexity and cost.

3.10.3 Correlation OTDR

One of the things that limit the dynamic range in a conventional OTDR is that only one pulse may be in the fiber at one time. Correlation OTDRs attempt to improve the dynamic range by using a long coded sequence of

*This is because the mixing signal is a photocurrent that is proportional to intensity, which is proportional to the square of the electric field.

pulses so that more of the fiber is filled. They avoid problems of reduced two-point resolution by using a specially designed code such that the autocorrelation of the coded sequence is an impulse function.

Correlation OTDRs have been marketed commercially, but they have not been a major success. The primary reason is that they work best on long fibers but not as well as conventional OTDRs on shorter fibers. On long fibers, correlation OTDRs can provide significant improvements in dynamic range. Most customers, however, need the combined capability of an OTDR that can test long fibers as well as short ones. Unlike the previous two examples, correlation OTDRs use the same types of low-cost optical components found in conventional OTDRs. Figure 3.14 illustrates a high-level schematic drawing of a correlation OTDR.

3.10.4 Short-coherence-length coherent OTDRs (multimode)

All the OTDRs we have examined thus far have been designed primarily for testing lengths of fiber that you might find in either telecommunications or local-area networks (LANs). None of these devices could be used, for example, to test an optical connector or integrated optical waveguide by looking inside the device to see where a crack or failure occurred.

Evaluating integrated optical devices requires a unique type of OTDR that is based on interferometric testing with a low-coherence source (see figure 3.15). In this OTDR, called an *optical low-coherence reflectometer* (OLCR), the device under test is placed in one arm of an interferometer, and a moving mirror is placed in the other arm of the interferometer. In the example shown in figure 3.15, the two arms of

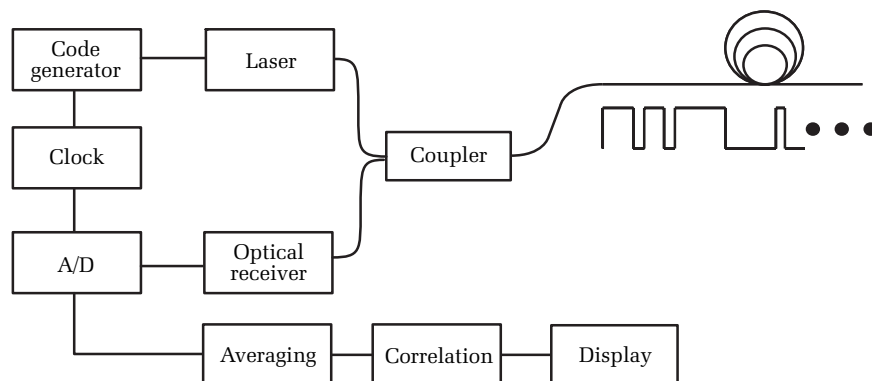


Figure 3.14. Schematic drawing of a correlation OTDR.

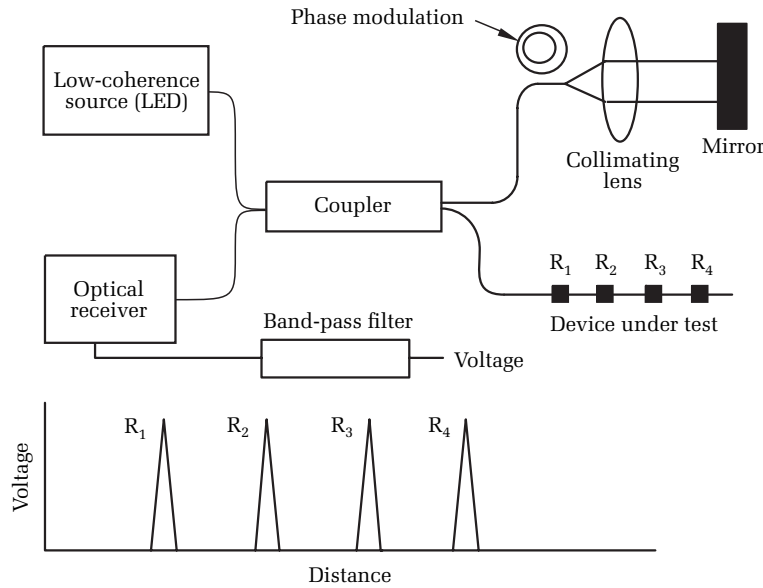


Figure 3.15. Low-coherence reflectometer. This device uses a continuous-wave (not pulsed) low-coherence source, such as an LED. Because the coherence length is so short, coherent mixing occurs only between light scattered from the test device that is the same optical distance from the coupler as the mirror in the reference arm. Scanning the reference mirror results in a modulated signal that is representative of the amount of light reflected from different locations along the test device.

the interferometer are formed from the two output legs of an optical coupler.

Notice that the light source is an LED, so it has very low coherence (the coherence length is measured in microns). Because of this, the only coherent interference that takes place is between the reference arm and a specific point in the test arm that is the same optical distance from the coupler as the mirror. Reflected light from all other places along the test arm adds incoherently with the light from the reference arm and constitutes a simple DC signal. If the mirror in the reference arm is moved, the received optical signal is modulated. This modulation results from coherent interference between the light in the reference arm and light reflected from points in the test arm that are the same distance from the coupler as the moving mirror.

Since the coherence length of the light source is very short, the distance resolution for this type of OTDR can be as little as a few tens

of microns. This makes it possible to test inside optical components such as pigtailed lasers, detectors, and connectors. Usually the receiver sensitivity is insufficient to resolve backscatter, but the high resolution of reflective events can be a powerful diagnostic tool.

3.10.5 Photon-counting OTDRs

When testing over typical lengths involving fibers, the standard OTDR design serves very well. But when testing over very short distances, as when testing the internal characteristics of optical components, the standard OTDR is unsatisfactory. For example, suppose you are testing an optical isolator and you know the total reflection is too high but are unsure which component within the isolator is causing the problem. An isolator is an optical component with many tiny parts inside, and the total length of the isolator is only a few centimeters. Inside, the distances between surfaces may be only a millimeter or so. Clearly, with pulse widths measured in meters, the standard OTDR has no hope of diagnosing which of the internal components may have a defective reflective surface. The photon-counting OTDR resolves this problem (see figure 3.16) with an instrument that is designed to address short-distance applications.

A limiting factor for the standard OTDR configuration is the sensitivity of the detector, which is typically an APD. An APD is a solid-state detector that produces many carriers for each photon that impinges on its surface. A typical gain might be roughly 100, meaning that for each photon that reaches the detector, 100 charge carriers are produced

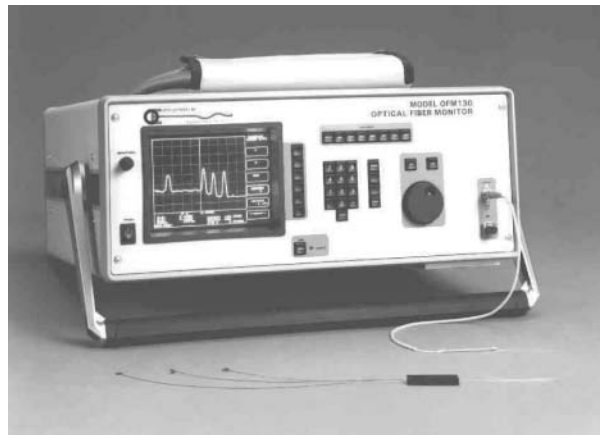


Figure 3.16. Photon-counting OTDR used in high-resolution applications. [Credit: Tempo Opto-electronics.]

in the APD. When the APD is operated like this, the current in the APD is proportional to the flux of photons.

When operated as a photon-counting detector, the bias voltage across the APD is increased to the point that an individual photon creates such an avalanche of charge carriers that just one photon can be detected. This is sometimes called the *Geiger mode*. In this mode a single photon triggers the APD, releasing all its energy, and the gain may reach a level of several thousand.

In the Geiger mode the sensitivity is so great that a single photon can dump all the energy stored in the APD. This has the advantage of greatly increasing the sensitivity, but it also means that the current through the APD is no longer proportional to the photon flux. In essence, the APD becomes a digital device, in which it registers a current pulse for each photon.

When using the APD in this digital mode, it is possible to measure very short distances if the supporting electronic circuitry is fast enough. In such a design the laser pulse is made so short that, on average, each pulse results in less than one photon coming back to the APD from any given reflective event in the optical component. The waveform then becomes a histogram showing the relative number of photons that are reflected after a given amount of time.

This is a significant difference. In the standard OTDR configuration, the output varies continuously as a function of input, and averaging serves only to lower the amount of noise that we see in the waveform. But in the photon-counting configuration, the output is a statistical one, in which the waveform becomes a time-correlated histogram. In the photon-counting configuration, the dead zone of the APD no longer applies because each pulse produces, on average, less than one photon, and each photon produces at most only one detection event. As such, photon-counting techniques allow the use of subpicosecond pulses and resolution that can be smaller than 1 mm. Because of this, when testing optical components (as in the case of a manufacturer that is testing an optical circulator, connector, coupler, etc.), the photon-counting OTDR is the preferred solution.

3.11 Summary

We end this chapter by noting the wide variety of OTDRs that have been built and tested by commercial companies and research institutions worldwide. In this last section we examined a few, but not all of the

possibilities. Time and space do not allow us to give more than passing acknowledgment of these various configurations, many of which are truly unique and inventive.

Of all the designs that have been suggested, by far the most popular is the standard configuration, shown in figure 3.1. Its strengths are found in its simple and inexpensive optical design and in the fact that it adequately satisfies the needs of the vast majority of OTDR users. In the future, as technology and operational requirements change, the standard OTDR may lose its place as the preferred embodiment, but for the present, its position seems secure. We devote the remainder of this book to discussions about the finer details associated with the standard OTDR's operating specifications, how to use it for precise measurements, and how to make some surprising measurements of optical-fiber parameters that you may not think possible with a standard OTDR.

Suggested reading

- Saleh, B. E. A., and Teich, M. C., *Fundamentals of Photonics* (New York: Wiley, 1991).
- Melle, S., and MacGregor, A., "How to choose avalanche photodiodes," *Laser Focus World* (October 1995).
- Dereniak, E. L., and Crowe, D. G., *Optical Radiation Detectors* (New York: Wiley, 1984).
- Hentschel, C., *Fiber Optics Handbook* (Germany: Hewlett Packard, 1988).
- Miller, S. E., and Kaminow, I. P., *Optical Fiber Telecommunications II* (San Diego: Academic Press, 1988).
- Bjarklev, A., *Optical Fiber Amplifiers: Design and System Applications* (Norwood, MA: Artech House, 1993).
- Yeh, C., *Applied Photonics* (San Diego: Academic Press, 1994).
- Milonni, P. W., and Eberly, J. H., *Lasers* (New York: Wiley, 1988).
- Barnoski, M. K., and Jenson, S. M., "Fiber waveguides: A novel technique for investigating attenuation characteristics," *Applied Optics*, Vol. 14 (1976), p. 2112.
- Personick, S. D., "Photon probe—an optical-fiber time-domain reflectometer," *Bell System Technical Journal*, Vol. 56 (1977), pp. 355–366.
- Brinkmeyer, E., "Backscattering in single-mode fibers," *Electronics Letters*, Vol. 16, No. 9 (April 1980).
- Okada, K., Hashimoto, K., Shibata, T., and Nagaky, Y., "Optical cable fault location using correlation technique," *Electronics Letters*, Vol. 16, (1980), p. 629.
- Healey, P., "Optical orthogonal pulse compression codes by hopping," *Electronics Letters*, Vol. 17 (1981), p. 970.

- Zaboli, M., and Bassi, P., "High-spatial-resolution OTDR attenuation measurement by a correlation technique," *Applied Optics*, Vol. 22 (1983), p. 3680.
- Nazarathy, M., Newton, S. A., Giffard, R. P., Moberly, D. S., Sischka, F., Trutna, W. R., Jr., and Foster, S., "Real-time long-range complementary correlation optical time-domain reflectometer," *Lightwave Technology*, LT-7, 24 (1989).
- Sumida, M., "OTDR performance enhancement using a quaternary FSK modulated probe and coherent detection," *IEEE Photonics Technology Letters*, Vol. 7 (1995), p. 336.
- MacDonald, R. I., "Frequency-domain optical reflectometer," *Applied Optics*, Vol. 20 (1981), p. 1840.
- Eickhoff, W., and Ulirch, R., "Optical frequency-domain reflectometry in single-mode fibers," *Applied Physics Letters*, Vol. 39 (1981), p. 693.
- Dolfi, D. W., Nazarathy, M., and Newton, S. A., "5-mm-resolution optical-frequency domain reflectometry using a coded phase-reversal modulator," *Optical Letters*, Vol. 13 (1988), p. 678.
- Tsuji, K., Shimizu, K., Horiguchi, Tsuneo, and Koyamada, Y., "Coherent optical frequency domain reflectometry for a long single-mode optical fiber using coherent lightwave source and an external phase modulator," *IEEE Photonics Technology Letters*, Vol. 7 (1995), p. 804.
- Youngquist, R. C., Carr, S., and Davies, D. E. N., "Optical coherence-domain reflectometry: a new optical evaluation technique," *Optical Letters*, Vol. 12 (1987), p. 158.
- Danielson, B. L., and Whittenberg, C. D., "Guided-wave reflectometry with micrometer resolution," *Applied Optics*, Vol. 26 (1987), p. 1836.
- Takada, K., Himeno, A., and Yukimatsu, K., "High sensitivity and submillimeter resolution optical time-domain reflectometry based on low-coherence interference," *Lightwave Technology*, LT-10 (1992), p. 1998.
- Koyamada, Y., Nakamoto, H., Ohta, N., "High-performance coherent OTDR enhanced with erbium-doped fiber amplifiers," *Journal of Optical Communications*, Vol. 13, No. 4 (1992), pp. 127–133.
- Seikai, S., Fukuoka, T., and Tohi, T., "Application of an Er³⁺-doped fiber amplifier to an OTDR operating at 1.6 μm ," *Electronics Letters*, Vol. 30, No. 15 (1994).

Problems

1. True or false: Echoes can be eliminated by changing the OTDR's range.
2. True or false: Ghosts result from reflective connectors and high dynamic range.
3. True or false: Multimode OTDRs have an inherent advantage in dynamic range.
4. True or false: Single-mode fibers have smaller numerical apertures than multimode fibers.

5. True or false: Rayleigh backscattering is the primary source of loss in optical fibers, and the phenomenon that makes OTDR able to measure the loss of splices and connectors.
6. True or false: Connectors are reflective.
7. True or false: Fusion splices are usually reflective.
8. True or false: OTDRs convert the vertical scale to decibels by taking the base-10 logarithm and multiplying by 5, instead of 10, because the light passes both directions through the fiber.
9. True or false: OTDRs convert the horizontal scale to distance by multiplying the time base by the group velocity in fiber and dividing by 2 (to account for the two-way trip through the fiber).
10. True or false: OTDR receivers use PIN detectors for maximum gain because PIN detectors have gain greater than 1, while APDs have gain less than 1.

¹ Personick, S. D., "Photon probe—an optical-fiber time-domain reflectometer," *Bell System Technical Journal*, Vol. 56 (1977), pp. 355–366.

² Neumann, E. G., Analysis of the Backscattering Method for Testing Optical Fiber Cables, *AEU*, Vol. 34, No. 4 (1980), pp. 157–160.

³ Ibid.

⁴ Ibid.

⁵ Nakazawa, M., "Rayleigh backscattering theory for single-mode optical fibers," *Journal of the Optics Society of America*, Vol. 73, No. 9 (Sept. 1983).

⁶ Brinkmeyer, E., "Backscattering in single-mode fibers," *Electronics Letters*, Vol. 16, No. 9, (April 1980).

⁷ Scheerer, C., "TDR pulse power limit in on-line monitoring of optical fibers owing to stimulated Raman scattering," *Electronics Letters*, Vol. 32, No. 7 (1996).

⁸ *Corning Engineering Handbook*, October 1994.

⁹ NEC part number NDL1202, detecting area diameter 240 μm . NEC catalog of *Optical Semiconductor Devices*, May 1995.

¹⁰ NEC part numbers NDL5171P, NDL5171P1, NDL5171P2, detecting area diameter 100 μm . NEC catalog of *Optical Semiconductor Devices*, May 1995.

¹¹ NEC part numbers NDL5561P, NDL5561P1, NDL5561P2, detecting area diameter of 80 μm . NEC catalog of *Optical Semiconductor Devices*, May 1995.

¹² Anderson, D. R., Method and apparatus for identifying echoes detected by an optical time-domain reflectometer, U.S. patent 5,373,356.

Chapter 4

Performance characteristics of OTDRs

4.0 Introduction

Thus far we have reviewed the history of OTDRs and examined their evolution in terms of performance and feature set. We have looked at basic fiber optics and fundamentals of OTDRs. Now we shift our focus to a more specific examination of OTDR characteristics and capabilities.

This chapter deals with the specific performance characteristics of OTDRs and lays important groundwork for coming chapters, where we discuss these issues in greater detail. Specifications are important to almost everyone. For automotive engineers, specifications are couched in terms of horsepower, engine size, torque, speed, and at least a hundred other esoteric terms. For a lighting engineer the important specifications might be brightness, number of lumens, and color saturation. The world of OTDR design has its own unique set of specifications that attempt to summarize the performance of a given OTDR and help make comparisons between different instruments easier. Some of these terms might sound familiar, but you will see that they often have to be slightly modified to suit the specific needs of fiber-optic technicians.

In this chapter we introduce and review the concepts of *dynamic range*, *resolution*, *speed*, *linearity*, and *accuracy*. In most cases, these specifications must be clearly understood and defined to be of practical use when making comparisons between different instruments. Dynamic range is a good example of this since it has several common definitions. In this chapter we attempt to clarify some of the more commonly used OTDR specification parameters. For additional information, we refer the reader to Danielson's article.¹ After reading this chapter you will be better prepared to address the myriad specifications that are used concerning OTDRs.

4.1 Figures of merit

As we write this book there are about a dozen OTDR manufacturers, each producing one or more types of instruments. Altogether this makes roughly 20 different OTDRs, each having different size, style, cost, and performance characteristics. Not surprisingly, the utility, functionality, and effectiveness of each of these OTDRs in testing fibers vary from model to model. This large array of contenders makes selection and

use of an OTDR for a particular application a daunting task, especially since available literature on various OTDR models is not written around standard performance characteristics. Instead, a small number of historical performance parameters have emerged over time, and these, together with price and features, form the basis for OTDR promotion by suppliers and selection by end users.

The historical performance parameters, although now traditional in use, are somewhat confusing because they are not always well defined. A related problem is the natural tendency for OTDR manufacturers to promote characteristics in which they excel while avoiding reference to other specifications in which their instruments perform poorly. From the buyer's point of view, these neglected specifications often make a tremendous difference in actual testing applications. One intent of this chapter is to organize the wide range of available OTDR specifications and help you understand which of them may be significant for your particular application. Being aware of these specifications and their utility better prepares you to concentrate on those of most significance to you.

Besides the historical specifications, there are a number of lesser-known specifications that are often valuable in the selection process. Unfortunately, many OTDR manufacturers do not specify their instrument's performance regarding some of these. This is unfortunate, since there are a large number of alternative performance parameters that are generally not reviewed by end users in their selection processes. These alternate performance characteristics can help to define the suitability of an OTDR style for a particular application. In the early formative days of OTDR, Bellcore made a tremendous contribution toward reducing confusion in this regard, by defining performance standards that speak to the utility of an OTDR rather than to abstract characteristics.* In this chapter we examine both the traditional and alternative performance characteristics and provide useful methods by which the end user can evaluate prospective OTDRs.

We refer to any performance characteristic or feature as a *figure of merit* in our discussion of OTDR utility. This term collectively refers to performance parameters, costs, features, environmental characteristics, and human interface properties.

*Bellcore comprised a group with Bell Communications Research and was involved in the late 1980s with establishing standards for the regional Bell operating companies for performance standards for OTDRs. Bellcore has since been purchased by SAIC and renamed Telcordia. Since most of the work on OTDR standards was conducted under the auspices of Bellcore, we have used their historical name.

4.2 Historical figures of merit

In the past when normal single-mode and multimode fibers were being developed for telecommunications, their increasing performance levels demanded ever better methods for measuring light-transmission quality. The OTDR was developed in parallel with fiber. Ever-decreasing fiber loss and ever-increasing transmission system power and sensitivity have led to the use of longer and longer fibers for communications systems. Thus, the OTDR has been required to “see” or “shoot” ever-increasing lengths of fiber. However, reflective events and nonreflective losses within the fiber sometimes appear relatively close together. The instrument has been required to identify these closely spaced events as well. These measurement requirements have led to a continual evolution of OTDR performance, both in terms of the instrument’s ability to probe long fibers *and* to isolate closely spaced events within the fiber.

The requirement of the OTDR to probe long fibers demands that the instrument use high-powered laser sources to offset the attenuation loss that a pulse of light experiences while traveling the full length of a fiber. The returned signal travels the entire distance of the fiber length as well, so when it reaches the OTDR receiver there may be only nanowatts of power remaining. This requires the OTDR’s receiver to be extremely sensitive, with a very low noise floor.

Typically, the largest signal the OTDR experiences is the reflection from the front-panel connector or some other reflective event (such as an unterminated end) that is not too far away. The smallest signal the OTDR can measure is the random noise in its receiving and amplifying circuitry, commonly referred to as the instrument’s *noise floor*. In the log domain, the difference between the largest signal measurable by the OTDR and the OTDR’s noise floor can be expressed as a decibel amount (dB). This value is called the *dynamic range* (DR) of the OTDR.

Because of the historical importance of dynamic range, and because it indicates “how far the OTDR can shoot,” the DR has become the OTDR’s single most important figure of merit. The statement “Dynamic range is everything” is a popular selling point for some suppliers. Indeed, this dictum goes far toward describing how competitive a particular instrument can be. Modern long-range single-mode OTDRs have dynamic ranges in the area of 42–45 dB; multimode instruments have a dynamic range of about 25 dB. The dynamic range of commercial instruments is ever on the increase and has roughly doubled since 1986. This represents a 10,000-fold increase in the range over which the instrument can measure optical-power levels.

A second important figure of merit is the ability of the OTDR to resolve closely spaced events in the fiber. This relates to the instrument's time resolution, which is a source of great controversy and misunderstanding in the industry. The OTDR has an *event resolution*, or *event dead zone* (EDZ), that determines its ability to identify two discrete reflective events separated by a short distance. In single-mode OTDRs, this value can be as low as about 1 meter. For multimode instruments, the shortest EDZ is about 20 cm. The amount of event dead zone you require depends on your testing application. If you are testing inside a central office in which you have short patch cords, you may find 1-meter EDZ is barely sufficient. On the other hand, if you are installing fiber and are interested only in qualifying splices that are many kilometers apart, then EDZ may be unimportant to you.

A third parameter used to specify OTDR performance is the *attenuation dead zone* (ADZ), or *loss-measurement dead zone* (LMDZ). In some applications, OTDRs analyze optical fibers that contain discrete reflective events at various locations. If the optical return loss of the events is large enough (–20 to –30 dB, for example) the amount of peak power returning to the OTDR is appreciable compared to the level of power from Rayleigh scattering. Thus, the OTDR receiver detects a large amount of power momentarily, and then the power drops as much as 40 dB. When the large pulse, or “big bang,” is received by the OTDR, the optical detector and preamplifier can become temporarily saturated. It can take as much as a microsecond (100 meters in distance, as viewed on the OTDR's display) for the detector to recover fully from this pulse. Even without saturation, the amplifier is still bandwidth limited, so the received signal cannot return immediately to the backscatter level. As if saturation and bandwidth limitations were insufficient, a spurious signal (detector tail) due to slow currents in the detector is also sometimes present. When any of these effects (saturation, bandwidth limitations, or tail) is present in significant quantities, no useful information can be obtained from the OTDR signal due to distortion. In addition, some OTDR receivers experience nonlinear behaviors following large pulses. These recovery problems are manifested in the preamplifier portion of the OTDR receiver. The distance over which the normal OTDR signal is distorted due to saturation, bandwidth effects, or detector tail is the LMDZ, or ADZ, of the instrument.

While dynamic range has continually increased in the past 10 years, instrument resolution has improved relatively little. The industry has long awaited a breakthrough in LMDZ for normal single-mode

measurements. Ideally, the LMDZ should be no larger than the EDZ for measuring fibers containing closely spaced reflective events, such as in telephone central offices and in passive optical network (PON) applications providing fiber to the home (FTTH), where optical splitters of up to 128 splits are used. Optical splitters will be at various locations at differing distances (up to 20 km). These problems represent an unsolved technological barrier, and there are few indications it will be surmounted in the immediate future.

4.3 Detailed figures of merit

We devote this section to detailed discussions of the figures of merit for OTDR performance. While many figures of merit exist, the most common (and often most misunderstood) include the following:

- Dynamic range:
 - Reflective dynamic range
 - Scattering dynamic range
- Measurement range
- Event resolution
- Loss-measurement resolution
- Return-loss range
- Linearity
- Data resolution
- Clock accuracy
- Cursor resolution
- Refractive-index uncertainty
- Measurement speed
- Interleaving noise
- Data-processing speed
- Display speed
- Event-detection accuracy

We treat some of these topics only briefly. To other topics, we devote considerable discussion. Dynamic range, for example, is arguably one of the most important specifications for an OTDR. Since it is often given high priority by OTDR users and manufacturers alike, we discuss at length the concept of dynamic range and the interrelatedness of the several different definitions. In similar fashion, we discuss event resolution and loss-measurement resolution in detail (we also revisit the topic in later chapters).

4.3.1 Reflective dynamic range

Reflective dynamic range is not a term that is commonly used to specify OTDRs. It refers to the ratio (in decibels, 5 log) of the power reflected from a given reflection near the OTDR's front-panel connector to the power in the OTDR's system noise. Reflective dynamic range is not a useful specification for determining the range over which the OTDR can make splice-loss measurements. It is useful, however, for determining the range over which the OTDR can make reflectivity measurements. Some OTDRs have saturation problems with high reflectance, so knowing the OTDR's reflective dynamic range can help you determine if the instrument you are considering is able to make the reflectivity measurements that concern you. If you mostly deal with fusion splices, then reflectivity dynamic range is of little concern. However, if you install fiber-optic systems that are sensitive to reflections, you may want to consider OTDRs with a high reflective dynamic range. Such instruments are useful since you need to test reflective events to be sure their reflectivity is below desired thresholds (we discuss this in more detail in chapter 7).

Figure 4.1 shows how to measure the reflective dynamic range.

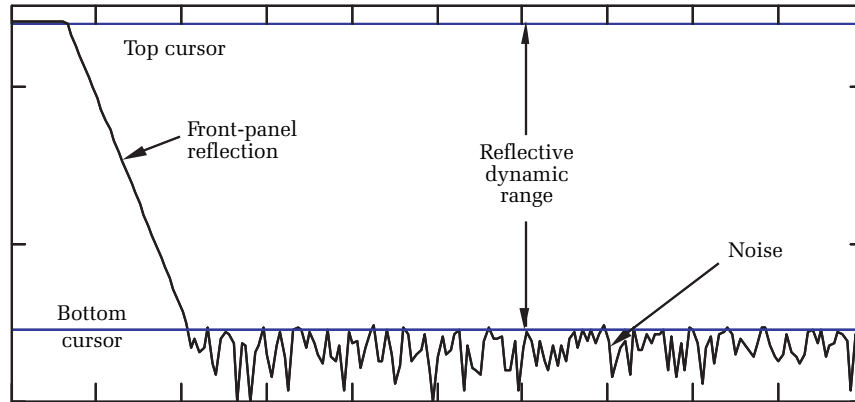


Figure 4.1. Measuring an OTDR's reflective dynamic range. Disconnect the front-panel connector and acquire a waveform. Place one cursor on top of the reflection and one at the noise floor. Measure the vertical separation between the cursors, as indicated by the OTDR's vertical scale. This is the reflective dynamic range.

1. Select the pulse width and averaging time at which you want to measure the reflective dynamic range. Be sure to select a range that is consistent with the lengths of the fibers you plan to test.*
2. Disconnect any test fibers from the OTDR and acquire a waveform.†
3. Place one cursor on top of the displayed reflection and the other at the noise floor.‡
4. Measure the vertical height between the two cursors, as displayed by the OTDR. This is the reflective dynamic range.§

4.3.2 Scattering dynamic range

Scattering dynamic range is what you typically think of when associating dynamic range with an OTDR. It is the ratio (in decibels, 5 log) between the backscatter signal at the OTDR's front-panel connector and the instrument's noise level. To measure it, follow this simple procedure.

1. Connect a fiber to the OTDR. The fiber should be about the same length as fibers you anticipate testing, and the OTDR's test range should be slightly longer. Be sure you have a good and clean connection, or you will underestimate the dynamic range.
2. Select the pulse width and averaging you plan to use or at which you wish to measure the dynamic range.
3. Acquire a waveform.

*Selecting a range that is shorter than the fibers you normally test results in more effective averaging during a given test time and an artificially low noise floor. Selecting a range that is longer than the fibers you normally test results in less effective averaging and an artificially high noise floor. Select a range that is as long as but not much longer than the longest fiber you expect to test.

†If the OTDR has an APC connector, attach a short jumper whose opposite end is either a flat cleave or a flat polish. In any event, be sure the cleave or polished connector is clean and free of moisture or dirt (these can change the event's reflectivity).

‡In the following sections we describe how to locate the noise floor accurately according to several definitions used throughout the industry.

§Strictly speaking, this is the reflective dynamic range for a -14-dB reflection (due to the unterminated connector). For other reflectivities, the reflective dynamic range may change, depending on the OTDR's linearity and saturation levels.

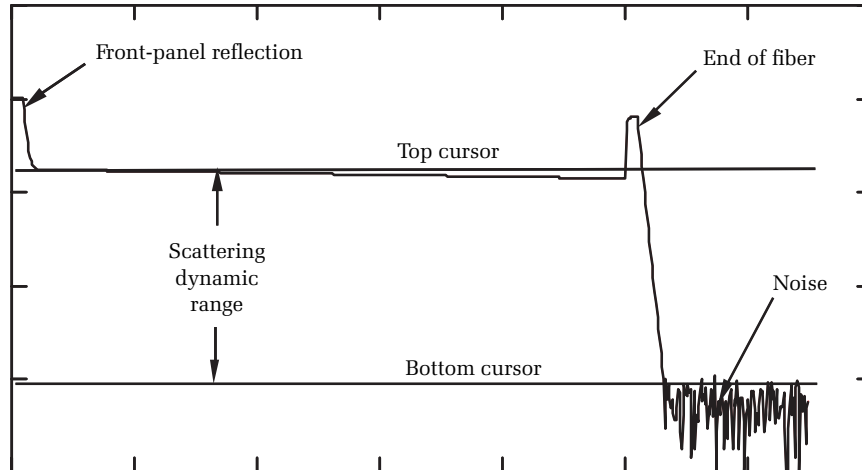


Figure 4.2. Measuring the scattering dynamic range. Acquire the waveform using a test fiber of typical length. Use a pulse width and averaging time that are typical for your testing applications. Acquire the waveform. Place one cursor at the extrapolated front-panel backscatter level. Place a second cursor at the noise floor. The scattering dynamic range is the vertical separation between the two cursors, as indicated by the OTDR's vertical scale.

4. Extrapolate the backscatter level to the beginning of the front-panel reflection, and place the top cursor at the intercept (see figure 4.2).
5. Place the bottom cursor on the noise floor (we discuss how to define the noise floor later in this chapter). The scattering dynamic range is the vertical separation between the two cursors, as viewed on the OTDR's vertical scale.

There are some anomalous features in OTDR waveforms that can alter this method of measuring dynamic range. Offset errors are among the most significant. OTDRs use analog-to-digital converters (ADCs) to change the analog signal from the optical receiver into a digital signal that can be processed and displayed. The ADC has an offset, however, and this must be removed before the data are displayed. Because OTDRs show a logged display, errors in removing the offset result in a waveform that rolls up or down when the backscatter signature approaches the noise floor (see figure 4.3). When roll-off is present, it effectively limits the OTDR's ability to make measurements near the fiber's end. It is an effective source of noise (though not random) that adds to the noise floor. To reflect this type of problem properly in the measured dynamic

range, place the bottom cursor at the point where the waveform deviates from linearity. We discuss problems associated with offset errors in considerably more detail later in this chapter.

Offset errors that result in roll-off show clearly only in long fibers that extend near the noise floor. On shorter fibers, too much roll-off actually gives the false impression of increased dynamic range rather than reduced performance. Roll-off associated with offset errors illustrates a good reason to test dynamic range using a long fiber. Often, problems that occur near the noise floor do not show up on short lengths of fiber. Additionally, it is easy to select a short range with a short fiber inadvertently. With short fibers, however, the OTDR can use a smaller pulse-repetition rate (PRR) and effectively average more in a given amount of time. Thus, the measured dynamic range on short fibers is sometimes higher than it is on longer fibers.* Because of these problems you should make every effort to test the dynamic range of your instrument on fibers of roughly the same length as those you intend to measure in the field.

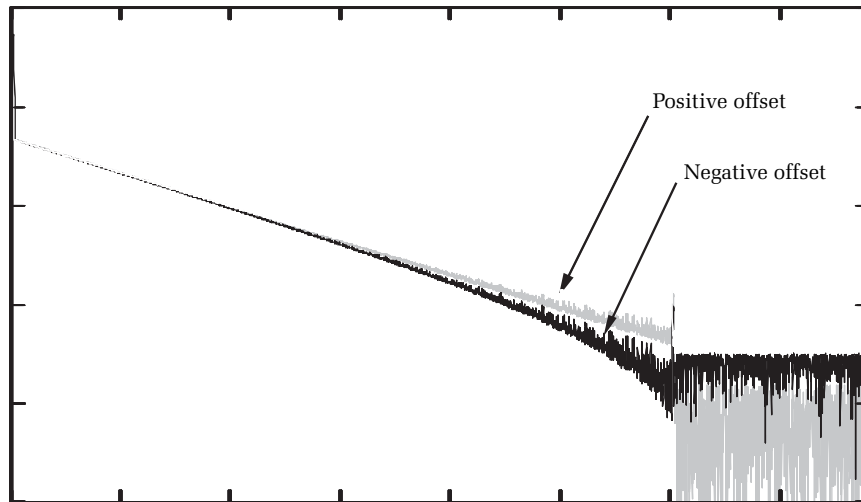


Figure 4.3. Examples of offset error. If insufficient offset is removed, the waveform rolls up near the fiber's end. If too much offset is removed, the waveform rolls down. In either case, offset errors make events (especially nonreflective ones) difficult to see and constitute an effective source of noise.

*This is true because the amount of averaging in performance tests is typically set by the test time (which is the parameter of interest) and not by the actual number of averages.

In discussing reflective and scattering dynamic range we have described the methods used with manual OTDRs. Many OTDRs have automatic modes that select their pulse widths and averaging times based on the length of the fiber being tested and on other factors. In OTDRs that select the acquisition parameters, it is often difficult to establish the dynamic range because you no longer have control (or even knowledge) of the acquisition parameters. A more pragmatic test is needed for automatic modes. This test determines the OTDR's measurement range. We discuss measurement range later in this chapter.

To help appreciate the wide range of signals an OTDR must measure, let's consider a simple example. Imagine for a moment that we wish to design an OTDR. We select the best laser available, a modern strained-layer multi-quantum-well device (SL-MQW laser) having a peak power of about 200 mW at 1310 nm. We couple this laser to the fiber under test using a 50/50 fused tapered-fiber coupler and interpose a robust FC/PC connector whose forward loss is 0.5 dB and whose reflectivity is -40 dB. We present the returning signal to an avalanche photodiode (APD) whose conversion is 0.8 A/W with an internal gain of 40. Let's look at the *reflective* signal loss budget for this system (see table 4.1).

Performance parameter	Value	Units
Laser power	23	dBm
Outgoing coupler loss	3	dB
Connector reflectivity	-40	dB
Incoming coupler loss	3	dB
Net power	5	μ W
Convert using 0.8 A/W	4	μ W
Photocurrent after gain of APD	160	μ W

Table 4.1. Reflective signal loss budget for typical OTDR.

The instrument noise floor is defined essentially by the shot noise of the dark current in the detector, which is about $1 \text{ pA}/\sqrt{\text{Hz}}$. For measurements using 10-ns pulses, a preamplifier bandwidth of about 50 MHz is required. Thus, the instrument noise floor is about 7 nA. Therefore, the instrument will have a dynamic range (without averaging) for reflections of*

$$\text{DR} = 10 \log(160\mu\text{a}/7\text{nA}) = 43.6 \text{ dB}$$

*Assuming the reflections do not saturate the optical receiver or exceed the capacity of the ADC.

Since OTDRs deal in the 5-log domain, the OTDR's dynamic range for one-way reflective measurements is one-half this value, or about 21.8 dB.

This is the instantaneous dynamic range for a single pulse. Assuming random noise, we can improve the noise floor by acquiring many waveforms and averaging. Commercial OTDRs do this routinely. When you average random noise, the variance reduces inversely with the number of averages, and the standard deviation (which is the basis for OTDR dynamic-range calculations) reduces as the inverse root of the number of averages. If the repetition rate is 1 kHz and the averaging takes place for an interval of about 3 minutes, the OTDR accumulates 200,000 averages.* This improves the dynamic range by

$$5 \log (\sqrt{200,000}) \approx 13.3 \text{ dB}$$

So the fictitious single-mode OTDR we have invented achieves about 35 dB of reflective dynamic range, corresponding to a signal range of over 10 million to 1.

Our previous example was based on the maximum signal produced by a -40-dB reflection. Some modern OTDRs, having logarithmic preamplifiers, can measure front-panel signals from a 4% reflection (-14 dB) without saturation. Such OTDRs develop more than 48 dB of reflective dynamic range, or a signal range of about 4 billion to 1. In this sense, the OTDR is unique in its ability to measure a tremendous range of signals yet support an electrical bandwidth from DC to nearly 1 GHz.

In chapter 2 we learned that microscopic discontinuities in the optical fiber result in the scattering of small amounts of light. Most of this scattered light does not couple to the waveguide, but a small fraction does and travels back toward the OTDR.^{2,3,4,5,6} From equation [3.5] we can calculate the power in this backscattered light for a laser pulse of arbitrary width. Using equations [3.5] and [3.6] we see that, for typical single-mode optical fibers, the power in the backscattered light is approximately -80 dB relative to the launch pulse at 1310 nm, for a 1-ns pulse of light. Suppose we test using a 10-ns (1-m) pulse. The scattering level is

$$-80 + 10 \cdot \log (10/1) = -70 \text{ dB}$$

*The pulse-repetition rate is fixed by the fiber length. The rate must be sufficiently low that each laser pulse has time to travel to the end of the fiber and back again before the next pulse is fired. Having a pulse-repetition rate that is too high results in a phenomenon called *ghosting*. Refer to chapter 3 for a discussion of ghosting. A 1-kHz rate corresponds to a fiber that is about 100 km long.

Now, in our previous example the reflection was -40 dB, so the scattering level for a 1-m pulse starts 30 dB below the reflection. Since the reflection peak power is $160 \mu\text{A}$, the scattering level is 1000 times lower, or 160 nA . The scattering dynamic range can now be calculated from the reflective dynamic range as

$$\begin{aligned} \text{DR (scattering)} &= \text{DR (reflective)} - 30/2 \text{ dB} \\ &= 35 \text{ dB} - 15 \text{ dB} = 20 \text{ dB} \end{aligned}$$

This is the scattering dynamic range of our hypothetical OTDR using a 10-ns (1-m) pulse and 3 minutes of averaging. The dynamic ranges for other pulses may be calculated by using equation [3.7].* Recall that the dynamic range increases as the pulse width increases. If the amount of averaging is constant, then the increase in dynamic range for a given increase in pulse width is

$$\text{DR}_2 = \text{DR}_1 + 5 \log \left(\frac{W_2}{W_1} \right) \quad [4.1]$$

In equation [4.1], DR_2 is the dynamic range at the second pulse width (W_2) and DR_1 is the dynamic range at the first pulse width (W_1). In our example, a 10- μs pulse has a dynamic range of

$$\text{DR} (10 \mu\text{s}) = 20 \text{ dB} + 5 \log(10 \mu\text{s}/10 \text{ ns}) = 20 \text{ dB} + 15 \text{ dB} = 35 \text{ dB}$$

We have assumed in this last calculation that the OTDR's bandwidth remains at 50 MHz even for the 10- μs pulse. With such a wide pulse, however, this is unnecessary and reduces the instrument's dynamic range by raising the noise floor. With a 10- μs pulse, a bandwidth of 1 MHz is more likely. With this bandwidth the noise floor falls from 7 nA to about 1 nA. Therefore, lowering the system bandwidth lowers the noise floor and increases the dynamic range by about 4 dB. This gives the OTDR in our example a scattering dynamic range of a little over 39 dB.

Notice that to get this dynamic range approaching 40 dB, the OTDR pulse width must be increased and the system bandwidth decreased. Both of these affect the instrument's dead zone, which we discuss later in this chapter and in chapter 7. We encounter this trade-off frequently. Dead zone and dynamic range are almost always obtained at the expense of each other.

*This equation does not consider changes to dynamic ranges that result from changes in the OTDR's system bandwidth when the pulse width is modified.

When high dynamic range is obtained by virtue of a low-noise front end, it is always a performance advantage. In such instruments the same SNR can be obtained with a shorter pulse width, resulting in better all-around measurement capability. Additionally, most OTDRs have a mode called *real time* in which the OTDR trace is updated quickly (typically faster than one update per second). In real-time mode the OTDR can be used to monitor a fusion splice as it is being made, to perform an acceptance test on a reel of cable (see figure 4.4), or to monitor and verify the loss during alignment. As with other modes of operation, high intrinsic dynamic range resulting from a low-noise front end allows more effective use of the OTDR in real-time mode.

4.3.3 Derivation of the noise floor

In our discussion so far, we have treated the noise floor as if it were an easily measured quantity with a precise definition. Unfortunately, this is not the case. In this section we show that the noise floor is defined differently by various OTDR manufacturers and that this lack of uniform definition can result in confusion. We show that these different definitions are all related, however. If you understand *how* different OTDR manufacturers define the noise floor, you can make corrections to their various specifications so that all are based on a common definition and are thus directly comparable.

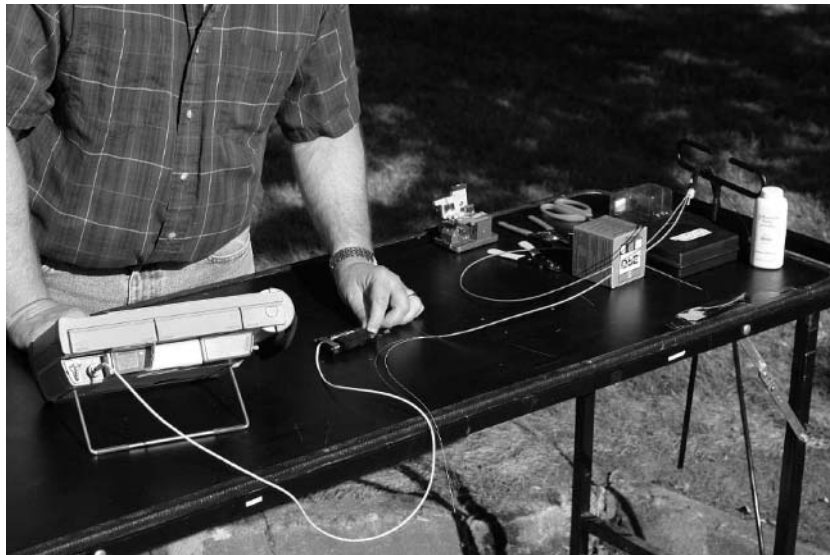


Figure 4.4. Fiber-optic technician performing acceptance test of cable. [Credit: The Light Brigade.]

One definition of the noise floor is the *noise equivalent power*. Assuming a Gaussian noise distribution, the noise equivalent power equals the RMS or standard deviation of the noise distribution. For many practical purposes the noise in the OTDR's receiver can be modeled as a Gaussian, or normal, distribution. The equation for a continuous Gaussian distribution is

$$G(x, \mu, \sigma) = \frac{1}{\sigma\sqrt{2\pi}} \exp\left(-\frac{1}{2} \left(\frac{x - \mu}{\sigma}\right)^2\right) \quad [4.2]$$

In equation [4.2], σ is the distribution's standard deviation and μ is the distribution's mean. Recall that the variance of a distribution is the sum of the squared differences from the mean, multiplied by the probability (the function's value). The RMS is the square root of the variance. For continuous probability functions this becomes an integral, and for a Gaussian distribution the RMS level equals σ :

$$\text{RMS} = \int_{-\infty}^{\infty} (t - \mu)^2 G(t, \mu, \sigma) dt = \sigma \quad [4.3]$$

For the normal distribution, roughly 68% of the noise lies within the RMS limit:

$$\int_{\mu - \sigma}^{\mu + \sigma} G(t, \mu, \sigma) dt \approx 0.68 \quad [4.4]$$

Equation [4.3] applies to the linear OTDR data, but the waveforms you are most likely to obtain will be logged. In the linear domain the waveform noise is randomly arranged around zero with a Gaussian distribution. The standard deviation of data in this linear format may be calculated from the following equation:

$$\sigma_{\text{noise}} = \frac{1}{N} \sum (w_i - \bar{w})^2 \quad [4.5]$$

In equation [4.5], N is the number of waveform data points, w_i are the waveform data, and \bar{w} is the mean of the waveform data.

If you have a computer and can read the OTDR waveform, you can calculate the RMS noise (assuming the OTDR has no offset error). Equations [4.3] and [4.5] apply for linear data with a normal (Gaussian) two-sided distribution. The way the OTDR data are logged, however, changes the noise distribution, so it is inappropriate to apply these equations as they are written. Fortunately, it is still possible to

calculate the RMS noise if we make certain assumptions about the noise distribution and how the data are logged.

When an OTDR logs its waveform data, it must deal with the negative numbers for those parts of the waveform past the end of the fiber, where there is no signal.* The logarithms of negative numbers are complex, so some arbitrary rule must be employed since only real numbers are shown in the waveform display. This arbitrary rule invariably distorts the Gaussian distribution, making a correction necessary to equation [4.3]. A common rule for logging the data is

$$w_{\log_i} = \begin{cases} 5 \log(w_i) & \text{if } w_i > 0 \\ 0 & \text{otherwise} \end{cases} \quad [4.6]$$

Assuming the logging procedure of equation [4.6], if we unlog the data we have a Gaussian distribution that is single-sided, and superimposed on the distribution is a delta function at $w = 1$ that has a height of 0.5. The mean of this unlogged distribution is[†]

$$\mu_{\text{unlog}} = \int_0^{\infty} \frac{1}{\sigma\sqrt{2\pi}} \exp\left(-\frac{1}{2}\left(\frac{x}{\sigma}\right)^2\right) x dx + \frac{1}{2} \quad [4.7]$$

In equation [4.7], μ_{unlog} is the mean of the waveform data *after* they have been logged according to equation [4.6] and then unlogged. The RMS noise of the waveform *before it is logged* is σ .

Solving equation [4.7] we find the RMS value of the unlogged linear waveform data is a function of the mean of the logged data. The expression is

$$\sigma = \sqrt{2\pi} \left(\mu_{\text{unlog}} - \frac{1}{2} \right) \quad [4.8]$$

Using equation [4.8] you can calculate the RMS noise of the unlogged data, and from this you can calculate the dynamic range. The method is as follows:

*Negative numbers result from random noise. This random noise is as likely to be positive as negative. Consequently, when the backscatter signal is zero (as it is past the fiber's end), the received signal consists only of noise and fluctuates over positive and negative numbers.

[†]This is strictly true only if there is no waveform-offset error (the mean equals zero). We discuss waveform-offset errors and the problems they create for dynamic-range estimations later in this chapter.

1. Obtain logged waveform data taken on a relatively short fiber. Be sure the OTDR's range is set such that several hundred data points exist in the noise well past the end of the fiber.
2. Select a section of the waveform that is beyond the end of the fiber and beyond the impulse response of the detector and receiver amplifier.
3. Calculate the mean of the waveform data.
4. Using the mean calculated in step 3, calculate the RMS noise (of the unlogged data) using equation [4.8].
5. Determine the logged value of the waveform backscatter near the OTDR's front-panel connector. Calculate the linear value of the waveform near the front panel from the equation

$$w_{\text{lin}} = 10^{w_{\text{log}}/5}$$

6. Determine the dynamic range from the equation

$$\text{DR} = 5 \log (w_{\text{lin}}/\sigma)$$

This procedure, culminating in step 6, gives what is called the RMS dynamic range. The procedure assumes the logging operation described by equation [4.6]. It also assumes Gaussian noise and no offset errors.

The RMS noise-floor definition may have come about historically because the original OTDR designers were oscilloscope or amplifier designers first. It turns out that the RMS, or $\text{SNR} = 1$, definition, while useful for comparing OTDRs, is rather useless for defining the actual performance of an OTDR when probing fibers with significant loss. Indeed, if $\text{SNR} = 1$, the peak-to-peak noise fluctuations are larger than the signal itself, and very little useful information is available. In addition, the RMS level is difficult to locate when observing the OTDR waveform. Because of these problems, the noise floor for OTDRs has evolved toward more practical definitions.

Equation [4.8] allows ready calculation of the RMS noise floor if you have a computer and access to the numeric waveform data. Except for the few experts who carry about signal analysis tools in their heads, most of us cannot easily look at a noisy signal and identify the RMS noise level. This is particularly true of OTDR signals, whose noise fluctuations are represented on a logarithmic scale. It is, however, quite possible to count noise peaks that appear above a certain level. Suppose, for example, we display 500 data points on the OTDR screen, identify the highest 10 points, and place a line such that those 10 points lie above

the line.* In this process, we have isolated 2% of the noise above the line and 98% of the noise below the line. We can call this the *98% noise level*. For a uniform Gaussian distribution of noise, this 98% noise level occurs at approximately 2.05 standard deviations:

$$\int_{-\infty}^{\mu+2.05\cdot\sigma} G(x, \mu, \sigma)dx = \frac{1}{2} + \int_{\mu}^{\mu+2.05\cdot\sigma} G(x, \mu, \sigma)dx \approx 0.98 \quad [4.9]$$

Comparing the 98% noise level with the $\text{SNR} = 1$ definition, we see that $5 \log(2.05) \approx 1.56$. This means an OTDR's dynamic range specified according to the 98% rule will show about 1.56 dB less dynamic range than one specified according to the RMS level.

Equation [4.9] is based on the assumption that the OTDR logs the linear data according to equation [4.6]. This is not necessarily the case, however. For example, the OTDR might log the data according to the rule

$$w_{\log_i} = \begin{cases} 5 \log(w_i) & \text{if } w_i > 0 \\ 5 \log(-w_i) & \text{if } w_i < 0 \\ 0 & \text{otherwise} \end{cases} \quad [4.10]$$

Strictly speaking, equation [4.10] is as valid as equation [4.6], yet they give different results. Suppose we apply our 98% rule on data that have been logged according to equation [4.10]. In this case, the RMS level lies about 1.8 dB below our line, since

$$2 \int_0^{\mu+2.33\sigma} G(t, \mu, \sigma)dt \approx 0.98$$

$$5 \log(2.33) \approx 1.8$$

Bellcore defined the noise floor according to the 98% rule under the assumption that the OTDR logs the data according to equation [4.6].[†] Using Bellcore's definition, you determine the noise floor from the following equation:

$$\text{floor} = \frac{1}{N} \sum_i P_i + 2.33 \left[\frac{1}{N} \sum_i P_i^2 - \left[\frac{1}{N} \sum_i P_i \right]^2 \right]^{0.5} \quad [4.11]$$

*These data points must lie beyond the end of the fiber and beyond the end of the OTDR's response to the end reflection.

[†]Bellcore *Technical Advisory*, TA-TSY-000196 (1988).

In equation [4.11], P_i are the unlogged data and $floor$ is the noise-floor level in the linear domain. On the OTDR's log display, the difference between the noise floor defined by Bellcore (equation [4.11]) and the RMS level agrees approximately with equation [4.9]. That is

$$5 \log (floor/\sigma) \approx 1.50$$

Suppose that two OTDRs have exactly the same noise floors and backscatter levels but that OTDR A specifies its dynamic range to the $SNR = 1$ level and OTDR B specifies its dynamic range to the 98% noise level. OTDR A appears (on the specification sheets) to have about 1.5 dB more dynamic range than OTDR B. This is an important point that you should be aware of whenever comparing specifications for dynamic range. Not only must you be certain that the specifications apply at the same pulse width and averaging times (making corrections using equation [3.7] as necessary), but you must also verify that all specifications use the same definition of dynamic range.

If some OTDRs specify their dynamic ranges at the $SNR = 1$ point, and others specify dynamic ranges at the 98% point, you must compensate some of the specifications so they all apply to the same definition. For example, you may decide to standardize your definition for dynamic range by using Bellcore's 98% rule. You then subtract 1.5 dB from the dynamic-range specifications of those OTDRs that use the $SNR = 1$ definition and normalize to common pulse width and averaging settings.* Table 4.2 demonstrates the complete procedure using another example.

The 98% noise level is convenient because it is relatively easy to place a cursor such that 98% of the random noise lies below it. It may be tempting to try an even more convenient method that requires the operator to count even fewer data points. For example, you might decide to place the cursor such that all the noise lies below it. This is called the *peak noise* level, or *3-sigma* noise level. It is simply the level of three standard deviations of the Gaussian distribution. The decibel difference between the peak-level dynamic range and the RMS dynamic range is $5 \log(3) \approx 2.4$.

The authors personally do not approve of this definition because a single noise spike, which statistically can rise above the 3-sigma level, easily affects the measured dynamic range. This makes the 3-sigma test

*Notice that we assume that OTDR manufacturers all treat negative numbers by assigning their logarithms to 0.

OTDR	Specified DR	Pulse width for specified DR	Averaging time for specified DR	Normalized DR
A	35dB SNR = 1	400 m	3 min	30.0
B	32 dB 98% point	300 m	3 min	29.2
C	30 dB SNR = 1	100 m	1.5 min	28.6

Table 4.2. Comparing dynamic range between OTDRs that use different definitions. Column 1 identifies the OTDR manufacturer. Column 2 shows their published dynamic-range specifications and how they define dynamic range. Column 3 shows the pulse widths at which the dynamic ranges are specified. Column 4 shows the averaging times for which the dynamic ranges are specified. Column 5 shows the normalized dynamic ranges in which the specifications have been converted to the predicted performance at a pulse width of 100 m, an averaging time of 2 minutes, and a definition of dynamic range at the 98% noise level.

less accurate and more prone to statistical variations. Several other definitions of noise floor have been proposed and appear in the literature. The interested reader is encouraged to examine these alternative definitions.⁷ The 98% point seems to be the most practical definition since it is relatively straightforward and can easily be performed using most OTDRs. The two most common ways of specifying dynamic range use the 98% noise floor and the RMS noise floor.

4.3.4 Dynamic-range margin

Accurate evaluation of fiber events requires good signal-to-noise ratio at the point of measurement. This means that some dynamic-range headroom, or *margin*, is required at the far end of the fiber beyond the last event you need to measure. In chapter 5 we discuss this quantitatively and show that the required dynamic-range margin depends on the event's loss, the required accuracy of the measurement, the pulse width, and the number of data points used in the measurement algorithm.

As an example, suppose you want to measure a 0.1-dB fusion splice on an OTDR waveform that was acquired with a 100-meter pulse and 10-meter sample spacing. Suppose your measurement algorithm uses 50 points on each side of the event to make a linear regression loss measurement. To make the measurement with ± 0.01 -dB accuracy, you need 10 dB of dynamic-range margin. To test this event at the end of

a fiber having a 28-dB loss requires an OTDR with 38 dB of dynamic range.*

Figure 4.5 illustrates the principle of dynamic-range margin. This figure shows an OTDR trace of a test fiber composed of five segments that are each 30 km long. The fiber's total length is 150 km. The fiber loss is 0.2 dB/km, so the fiber loss of each segment is 6 dB. Each of the segments is connected to its neighbor by low-reflectance mechanical splices each having a nominal loss of 0.1 dB. The OTDR has a 37.5-dB dynamic range to the 98% level. The last splice is 120 km away, where the total link loss is 24.4 dB. To measure this event accurately, the OTDR must have about 32 dB of dynamic range. To check for loss due to fiber bends or other problems, however, the OTDR must have more dynamic range than this. With a 37.5-dB initial dynamic range, there is still sufficient margin to test a 0.1-dB event at the end of the fiber, 150 km away. This example clearly shows that good long-haul fiber-measurement accuracy can only be achieved with high-dynamic-range OTDRs.⁸

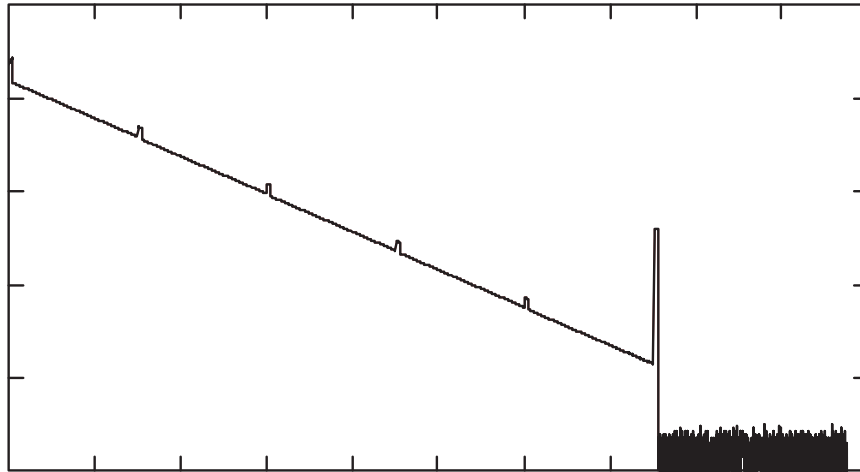


Figure 4.5. Measurement of 150-km test fiber using a high-dynamic-range OTDR. Observe the dynamic-range margin required to make accurate splice-loss measurements near the fiber's end.

*This calculation is based on equation [6.11], which uses a 2-sigma definition for dynamic range (roughly equivalent to the 98% noise definition) and assumes that the loss-measurement accuracy is at the 2-sigma confidence level (probability is 95% that the true loss differs from the measured loss by less than the calculated measurement uncertainty).

4.3.5 Usable dynamic range

Closely associated with OTDR margin is the concept of *usable dynamic range*. This can be defined as the range over which measurements can be made with accuracy exceeding a certain value. As we mentioned earlier, the instrument cannot necessarily make useful measurements over the entire dynamic range. As the signals approach the noise floor, the SNR decreases. This increases the uncertainty of fiber-loss and splice-loss measurements. As the waveform approaches the noise floor, it gets noisier and measurement accuracy degrades. Beyond a certain limit, this waveform noise makes the accuracy of distance and loss measurements essentially useless. When the peak-to-peak noise becomes approximately equivalent to the size of the loss to be measured, the limit of detectability has been reached.* The range of signals above this limit is known as the *usable dynamic range* of the instrument. It is common to define the usable DR limit relative to a 0.2-dB loss. We can approximate the difference in decibels between the usable DR limit and the RMS noise floor. When the peak-to-peak noise is 0.2 dB, we have

$$0.2 \text{ dB} = 5 \log [(S + N)/(S - N)]$$

where S = signal and N = peak noise. Solving this equation for S/N , we get

$$S/N \approx 6.68 \text{ dB}$$

Thus, the usable DR limit is about 7 dB above the 98% noise floor.

In this example, if the instrument dynamic range is 37.5 dB and you need reasonably accurate measurements of a 0.2-dB splice, then a 7-dB margin is required. The usable dynamic range is therefore $37.5 - 7.0 = 30.5$ dB. If the average fiber loss is 0.20 dB/km, the usable dynamic range implies a measurement distance of no more than 150 km. Increasing instrument dynamic range expands the distance-measurement range. At 1310 nm, an increase of 1 dB in dynamic range provides approximately 3 km of additional distance range. At 1550 nm, 1 dB provides about 5 km of additional range. This example should enable the OTDR user to determine the usefulness of the instrument dynamic range for a particular application and whether a performance improvement is required.

*This is a useful approximation, but it should be used mainly as a rule of thumb. Advanced filtering and smoothing algorithms, along with sophisticated digital signal-processing techniques, can locate and accurately measure events when the peak-to-peak noise level exceeds the splice loss.

4.3.6 Measurement range

As OTDRs have evolved, they have become easier to use and require less specialized knowledge to achieve accurate measurements. Key to this achievement has been the relatively recent development of software algorithms that acquire and analyze the OTDR waveform. With these algorithms the OTDR operator is freed of the cumbersome duty of waveform interpretation. This makes testing far more accurate and much faster than equivalent manual operations.

Because of the simplicity they offer, automatic algorithms can complicate the process of trying to measure specific hardware parameters, such as dynamic range. When you connect the OTDR to a test fiber, for example, the automatic mode selects its pulse width (and, sometimes, averaging) to analyze the fiber it is testing. If the fiber is short, the OTDR selects a short pulse. Longer pulses are used on longer fibers.

For automatic modes, the performance of the software algorithms becomes as important as the performance of the acquisition hardware. If the algorithms select the wrong acquisition parameters (such as the wrong pulse or gain settings), the test accuracy can be compromised. To test OTDRs with automatic algorithms, Bellcore developed the concept of measurement range. Whereas dynamic range is a measure of the system signal-to-noise ratio, measurement range is a practical test that determines the maximum distance to a predefined event at which the OTDR can still detect and measure the event with a predefined accuracy.

Measurement range is somewhat arbitrarily defined as the maximum distance (in decibels) to a nonreflective event of a 0.5-dB loss at which the event can be located at least three times out of four acquisitions. The loss-measurement accuracy must be within 0.1 dB. Although the parameters of the event are somewhat arbitrary, they serve as a useful baseline for comparing the performance of different OTDRs.

The test for measurement range is more practical than that for dynamic range, because it evaluates the combined performance of the OTDR's hardware and event-marking software. Dynamic range is a specific hardware parameter that, by implication, relates to performance. Measurement range, as a system parameter, has direct implications for practical applications. However, the test for measurement range typically takes longer to perform, and the test fixture is more complicated.

Because some OTDRs have measurement ranges over 100 km, there may be a temptation to use shorter test fibers and to incorporate

variable attenuators near the front end. This should be avoided, since the optical attenuator is an unlikely component in a real fiber-optic system. It also introduces excessive loss near the OTDR that can lead to spurious results that are inconsistent with real-world applications. Similarly, avoid fiber circulators, because they frequently have excess noise (refer to chapter 12).

To determine measurement range it is best to use a long fiber with a series of fusion splices at regular intervals (every 10 km, for example). The measurement range can be determined simply as the link loss to the furthest splice the OTDR reliably locates and measures. Although more difficult to build, such a test fixture is worth the effort for anyone seriously interested in testing the performance of OTDRs.

4.3.7 How offset errors affect dynamic-range and measurement-range calculations

Before ending our discussion of dynamic range and measurement range, we need to revisit and expand upon some issues that can affect the measurement of these performance parameters. The normal data acquired by an OTDR consist of an exponentially decaying signal punctuated with discrete events. Because of the wide range of signal values they deal with, OTDRs display the logarithm of the OTDR signal, with the vertical scale marked in decibels. This will linearize the trace and make small events visible over the entire range of the display, instead of just near the beginning of the trace (see figure 4.6).

As light travels along the optical fiber, a fixed percentage is lost after transit through a fixed length of fiber. This results in optical signals decaying exponentially. When you take the logarithm of an exponentially decaying signal, the result is a linear trace, as shown by equation [4.12].

$$5 \log(\exp(-\alpha x)) = \frac{-5\alpha}{\ln(10)} x \quad [4.12]$$

Ideally, this is what happens in the OTDR's trace, and the result (for a bare fiber with no events) is a waveform trace that is a simple straight line whose slope is given by equation [4.12]. In the real world, however, things are not quite so simple. The nature of the OTDR acquisition circuitry is such that an offset voltage is added to the optical signal from the fiber under test. This offset signal is substantial, sometimes equaling 10–20% or more of the peak signal level. When a constant offset is added to an exponentially decaying term and then logged, the resulting signal

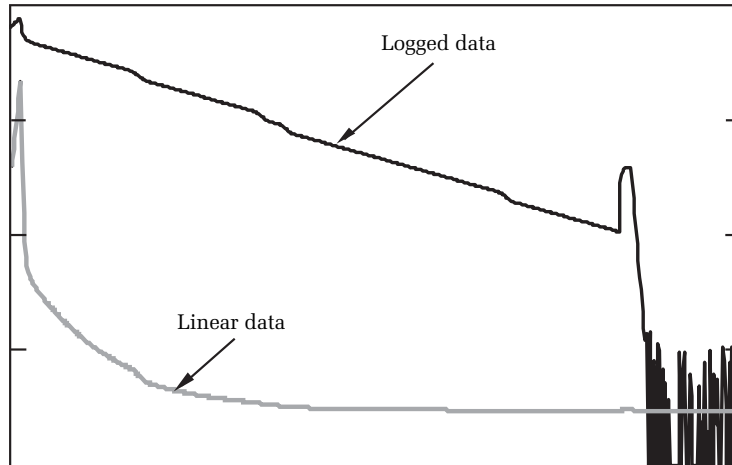


Figure 4.6. Comparison of logged and linear OTDR data. Events are easier to see in the logged data because steps in the waveform are a function of the ratios of amplitudes. The logged data also show the backscatter signature as a linear trace, because the linear data are a decaying exponential.

is nonlinear. You can see this by taking the first few terms of the Taylor's expansion of an exponential with constant offset:

$$5 \log(\exp(-\alpha \cdot x) + a) \approx \frac{5}{\ln(10)} \left[\ln(1+a) - \frac{\alpha}{(1+a)} x + \frac{1}{2} \left(\frac{\alpha^2}{(1+a)} - \frac{\alpha^2}{(1+a)^2} \right) x^2 \right] \\ + \frac{5}{\ln(10)} \left[\frac{1}{6} \left(\frac{\alpha^3}{(1+a)^2} - \frac{\alpha^3}{(1+a)} + \frac{2a\alpha^3}{(1+a)^3} \right) x^3 \right]$$

Without offset, the logged exponential is a linear curve with slope dependent on the attenuation factor. When offset is present, the logged expression is an infinite polynomial. Instead of being linear, the logged data show curvature. The amount of curvature increases as the amount of offset increases relative to the signal level. Later we show how this waveform curvature results in estimation errors of an OTDR's dynamic range and in loss-measurement errors that reduce the OTDR's measurement range.

If the initial offset were simply left in the OTDR waveform, the trace would be seriously distorted. To linearize the waveform properly, the OTDR designer must remove the offset. Ideally all the offset is

removed. But sometimes in practice residual offset may remain; other times too much offset is subtracted.

When an OTDR has residual offset or when too much offset is subtracted, the nonlinear shape of the waveform results in measurement errors. It also results in errors in estimating the OTDR's dynamic range. Positive offset results in underestimation of the dynamic range, while negative offset results in overestimation of the dynamic range. Offset does not affect the OTDR's true dynamic range; it affects only the estimate of dynamic range we make from examination of the waveform using, for example, the 98% noise rule. Offset, however, does limit the OTDR's measurement range. This is because measurement range is a function of loss-measurement accuracy, and offset results in measurement errors.

Figure 4.7 illustrates two waveforms. One was acquired with positive offset and the other with negative offset.* Observe that the

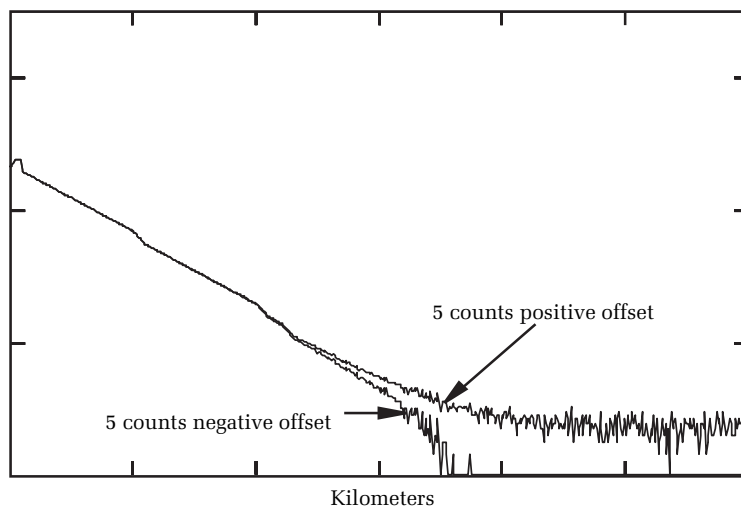


Figure 4.7. Waveforms with positive and negative offset. Positive offset makes the waveform bend upward near the end and negative offset makes the waveform bend downward. Although the noise for both waveforms is exactly the same, the dynamic range determined from the Bellcore method (backscatter to 98% noise) varies considerably with offset. Negative offset gives artificially high readings, and positive offset gives artificially low readings.

*With positive offset, the constant a in the preceding equation is positive, and with negative offset the value of a is negative.

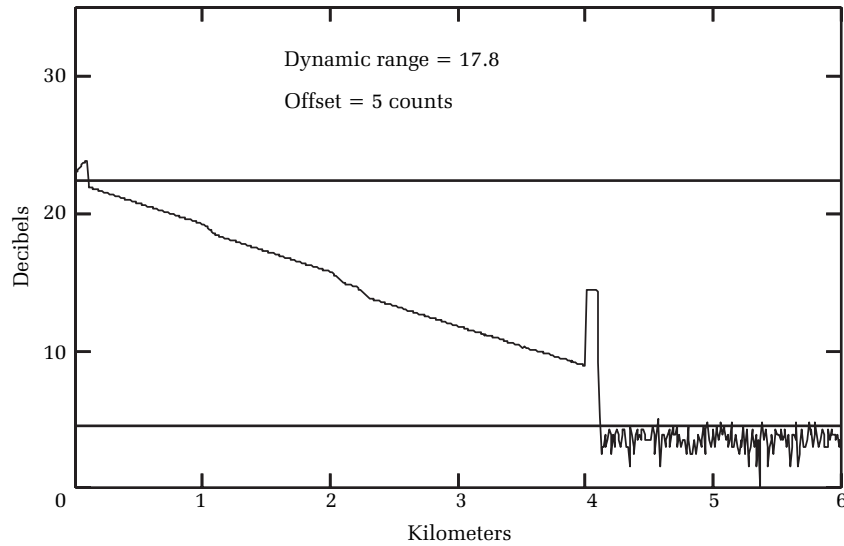


Figure 4.8. Waveform from a multimode OTDR with five counts of offset error. Notice that the noise floor is raised. Measuring from the top of the noise floor (98% noise level) to the backscatter level at the front panel, we determine a dynamic range of 17.8 dB.*

waveform with positive offset curves upward and the one with negative offset curves downward. This curvature is most noticeable near the noise floor, but actually extends throughout the waveform (though it is quantitatively insignificant when sufficiently far above the noise floor).

To see how offset affects measurement-range estimations, consider figures 4.8 through 4.11. Figure 4.8 shows a multimode OTDR waveform with five counts of positive offset error.[†] Since the fiber is short, you do not notice the waveform nonlinearity (you would if the fiber were longer and extended into the noise, as in figure 4.7). Figure 4.9 shows the same waveform with no offset error. When the dynamic range is measured from the backscatter level (near the front panel) to the top of the noise, the waveform with five counts of offset error shows 17.8 dB of dynamic

*In measuring the backscatter level at the front panel, we extrapolate the backscatter signature to the point $x = 0$.

[†]The waveform in this OTDR was encoded with 16-bit words. The offset is specified in counts of the least significant bit. In this case the offset corresponds to five parts out of 65,536.

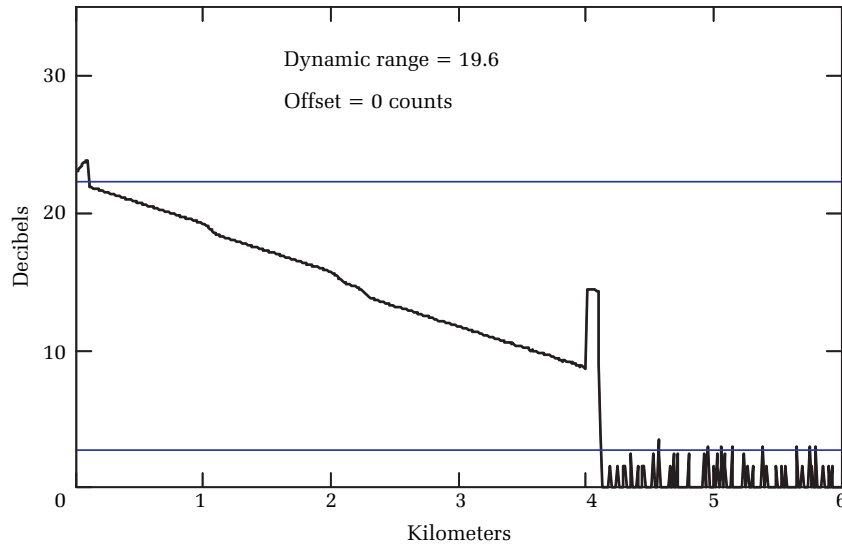


Figure 4.9. Waveform from a multimode OTDR with zero counts of offset. Measuring from the top of the noise (98% noise level) to the backscatter level at the front panel, we determine a dynamic range of 19.6 dB. This is 1.8 dB more than we measured on the same waveform with five counts of positive offset.

range. The OTDR without offset shows a dynamic range of 19.6 dB, a difference of 1.8 dB.*

Figure 4.10 shows the same waveform again, this time with two counts of negative offset error. With two counts of negative offset, the measured dynamic range increases to 20.9 dB. When the negative offset decreases to five negative counts (figure 4.11), the measured dynamic range increases again, this time to 22.3 dB. The difference in dynamic range between five counts of positive offset and five counts of negative offset is thus 4.5 dB, even though the actual signal levels and RMS noise in all four figures are exactly the same.

The important thing to observe in figures 4.8 through 4.11 is that the true dynamic range is exactly the same in all four waveforms. Dynamic range is the ratio of the signal level to the noise level, and all four waveforms have equal RMS noise levels and equal backscatter levels. Consequently, the dynamic range of the waveform in figure 4.8

*This difference depends on the number of bits in a word, the amount of noise, and the amount of offset. With more averaging (and less noise) the difference would be greater.

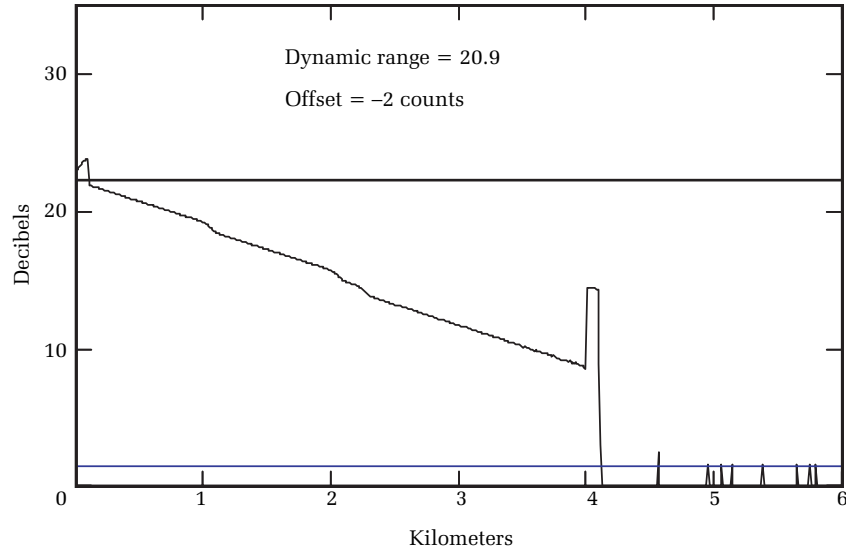


Figure 4.10. Waveform of multimode OTDR with two counts of negative offset. Measuring from the top of the noise (98% noise level) to the backscatter level at the front panel, we determine a dynamic range of 20.9 dB. This is 3.1 dB more than we measured on the same waveform with five counts of positive offset.

is exactly the same as the dynamic range of the waveform in figure 4.11. The dynamic ranges determined by measuring the distances from the tops of the noise to the backscatter levels, however, differ dramatically. Even though figure 4.11 seems to show a lower noise floor, the amount of system noise present is exactly the same as in figure 4.8.* The system noise is equal, although the measured dynamic range is 4.5 dB higher in figure 4.10 than in figure 4.8.

Estimation errors resulting from offset illustrate a serious problem with the traditional method of determining dynamic range. In this traditional method, dynamic range is estimated by measuring the distance from the top of the noise to the backscatter level. Figure 4.11 shows that a negative offset makes the dynamic range look considerably better than it really is. However, figure 4.7 shows that negative offset (when seen on a sufficiently long fiber) actually has more curvature near the noise floor than a waveform with positive offset. Furthermore, since the offset is negative, it pulls down and hides real events located near the

*This was verified by observing the peak-to-peak noise near the end of the fiber in all four waveforms. The peak-to-peak noise is the same.

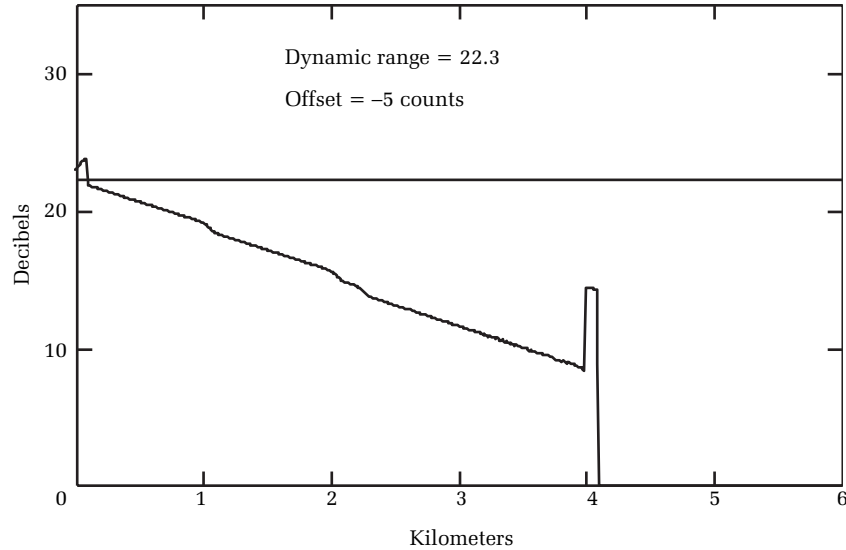


Figure 4.11. Waveform of multimode OTDR with five counts of negative offset. Measuring from the top of the noise (which is now below the horizontal axis) to the backscatter level at the front panel, we determine a dynamic range of 22.3 dB. This is 4.5 dB more than we measured on the same waveform with five counts of positive offset.

fiber's end. Thus, the traditional method of estimating dynamic range can lead to the selection of an inferior product when that product has negative offset.

With short fibers it is very difficult to determine the existence of offset, especially if the offset is small and the noise is high or the offset is negative. This is a good reason for testing the OTDR on fibers sufficiently long to extend into the noise floor. Since offset causes curvature, it is a performance parameter that should be specified and measured. Long fibers make this possible. When offset occurs, you should measure the dynamic range from the backscatter level to the point where the waveform departs from linearity, or the effective dynamic range, as shown in figure 4.12. This method gives a more practical measure of the range over which an OTDR may be used to make accurate measurements. Furthermore, as figure 4.12 shows, it correctly penalizes OTDRs if they have either positive or negative offsets.

Since offset results in waveform curvature, it is natural to examine the possible effects this curvature might have on loss-measurement accuracy. Consider first an OTDR without offset errors. If S_1 is the

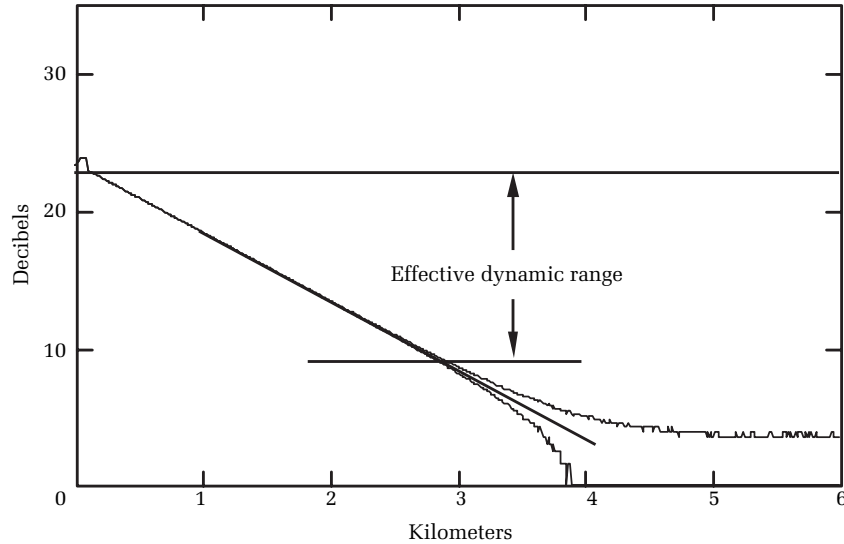


Figure 4.12. The effective dynamic range is determined by testing the OTDR on a fiber that is sufficiently long to reach the noise floor. Waveforms with positive or negative offset deviate from linearity before they reach the noise floor. Measure the dynamic range between the backscatter level at the front panel and the point where the waveforms deviate from linearity (by a predetermined amount). Using this method you can determine the correct dynamic range for OTDRs without offset, and you can adjust properly the dynamic-range estimate for OTDRs that have either positive or negative offset.

backscatter level before a splice (linear domain) and S_2 is the backscatter level after the splice, then the true splice loss is

$$L_t = 5 \log (S_1/S_2) \quad [4.13]$$

Now suppose we add some offset, f . With offset, the signal level before the event is $S_1 + f$ and the signal level after the event is $S_2 + f$. Accordingly, the measured splice loss is

$$L_m = 5 \log ((S_1 + f)/(S_2 + f)) \quad [4.14]$$

If the signal level just before the splice is h dB above the offset level (as seen on the OTDR's vertical scale), then

$$h = 5 \log ((S_1 + f)/f) \quad [4.15]$$

Taking the difference between the measured splice loss (equation [4.14]) and the true splice loss (equation [4.13]), we find the loss-

measurement error as a function of h (the height of the event above the offset level) is given by*

$$E(h, L) = 5 \log \left(\frac{1 + (10^{h/5} - 1)}{(10^{h/5} - 1) \cdot 10^{-L/5} + 1} \right) - L_t \quad [4.16]$$

From equation [4.16] we see that the loss-measurement error is a function of the loss of the event and its height above the offset level. For practical estimations, equation [4.16] may be approximated by the simple formula

$$E(h, L) \approx -L \cdot \exp(-h \cdot 0.44) \quad [4.17]$$

Figure 4.13 illustrates the magnitude of loss-measurement error due to offset. The zigzag plot shows numerical results from equation [4.16],

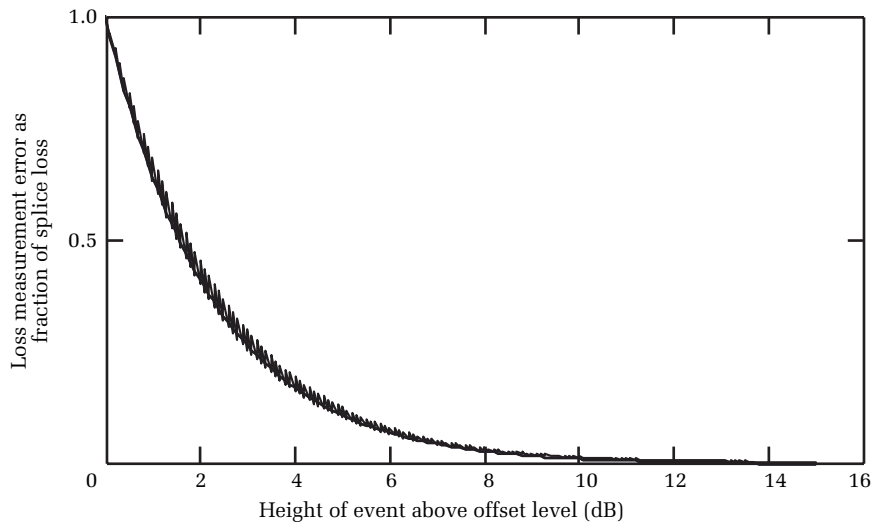


Figure 4.13. Magnitude of loss-measurement errors caused by offset.[†]

The vertical scale shows the loss-measurement error divided by the total splice loss, and the horizontal scale shows the height of the event above the offset level. If the offset level is zero, then h is infinity and the measurement error is zero. According to equation [4.16] the function has a weak dependence on the amount of splice loss (shown by the modulated zigzag curve). Equation [4.17], which is an approximation, shows no dependence on the amount of splice loss. The solution to equation [4.17], somewhat difficult to see, is the solid curve through the zigzag line.

*Equations [4.16] and [4.17] are for positive offset only.

[†]This plot shows the magnitude of the error. When the offset is positive, the measured loss is less than the true loss. Thus, for positive offset, the error is negative.

and the solid line (through the zigzag curve and somewhat difficult to see) shows numerical results from equation [4.17]. From figure 4.13 you see that when an event is roughly 3.66 dB above the offset level, the loss-measurement error equals one-fifth of the loss. Measurement range is commonly defined as the distance (in decibels) between the OTDR and a 0.5-dB event, when the event is at the threshold of being reliably found and measured to within 0.1-dB accuracy. Since offset affects loss-measurement accuracy, it is clear it also directly affects an OTDR's measurement range.*

Exactly how offset errors affect measurement range is somewhat complicated. Loss-measurement error results from offset, but it also results from waveform noise. The measurement range is reached when the total contribution of measurement error from offset and noise equals 0.1 dB on a 0.5-dB event. The noise-induced loss-measurement error is[†]

$$\text{Loss}_{\text{error}} = 3.071 \cdot 10^{-0.2\delta} \cdot \sqrt{\frac{\Delta x}{L} \left(1 + \frac{3(W+L)^2}{L^2 + 2\Delta x^2} \right)} \quad [4.18]$$

In equation [4.18], δ is the distance of the event above the noise floor, W is the displayed pulse width, L is the length over which the linear regression is performed in the splice-loss measurement, and Δx is the sample spacing.[‡] Table 4.3 illustrates the degradation that offset errors can have on measurement range. As you can see, when offset errors are comparable in magnitude to the 2-sigma noise, they lessen the measurement range by only about 1 dB or less. When the 2-sigma noise is much less than the offset, the measurement-range penalty increases and can exceed 2 dB.

In summary, offset is often difficult to see on short fibers. It is best observed and quantified on longer waveforms that extend to the OTDR's noise floor. By testing a long fiber you can estimate the OTDR's effective dynamic range by observing the point where the waveform curves up or down. Offset errors result in several negative effects, among which are:

*Waveform noise also limits the OTDR's measurement range, and offset errors may not be the primary limiter, though they will always limit measurement range given sufficiently low noise.

[†]This is the loss-measurement error, due to waveform noise, at the 2-sigma (95%) confidence level. We derive this equation in chapter 6.

[‡]The noise floor is defined here as an imaginary line that lies above 98% of the noise.

2-sigma noise level (dB)	Offset level (dB)	Measurement-range penalty with offset (dB)
3	3.5	0.89
2	3.5	1.27
1	3.5	1.75
5	5.0	0.73
4	5.0	1.05
3	5.0	1.50
2	5.0	2.03
1	5.0	2.69

Table 4.3. Measurement-range penalty from offset. Column 1 shows the vertical scale reading of the 2-sigma noise level without offset. Column 2 shows the vertical scale reading of the offset level when offset is present. Column 3 shows the measurement-range penalty incurred by the offset. Given two identical OTDRs, with equivalent noise levels, the measurement range of the OTDR without offset exceeds the measurement range of the OTDR with offset by the amount shown in column 3. [These calculations assume a 100-meter pulse, 300-meter linear regressions, 10-meter sample spacing, and 0.5-dB fusion splice. Measurement range is defined as the distance to the point where the loss-measurement error equals 0.1 dB.]

1. Gross errors in estimating the OTDR's dynamic range
2. Loss-measurement errors
3. Reduction in the OTDR's measurement range
4. Errors in link-loss measurements and observations of fiber linearity

4.3.8 Event resolution

Earlier in this chapter we introduced the concept of event dead zone (EDZ). We defined the EDZ as the ability to identify two discrete reflective events separated by a short distance. Now we explore this in more detail. Consider a single reflective event appearing on an OTDR waveform, as shown in figure 4.14.

This component could be a mechanical connector or splice, for example. Although the OTDR emits a rectangular pulse, the shape of the reflected pulse is somewhat rounded due to the limited bandwidth of the OTDR preamplifier or digital filtering system.* Thus, the falling

*This is nominally true, especially for longer pulses, although shorter pulses (less than 20 meters) may sometimes be rounded due to bandwidth limitations in the laser and its drive circuitry.

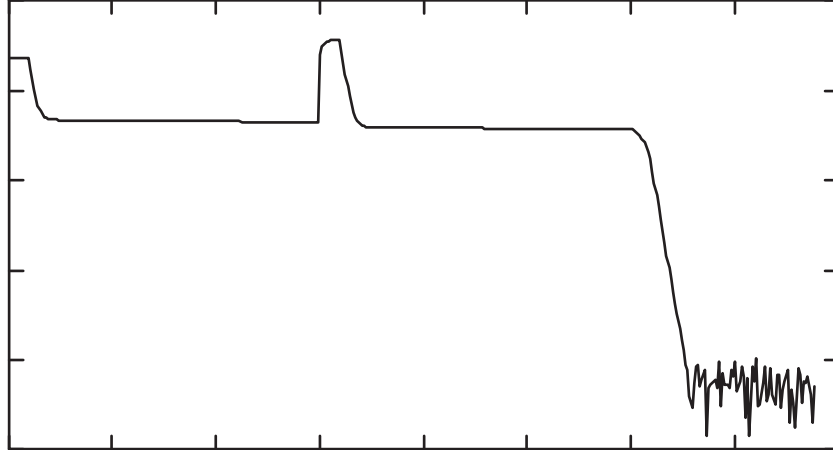


Figure 4.14. A single reflective event. Notice that the event is rounded at the top on the rising edge, falls linearly at first, and then falls more gradually on the trailing edge as the signal response from the reflection blends in again with the normal backscatter signature. Rounding of the pulse arises from many complicated effects, including the system bandwidth, and is responsible (along with the pulse width) for the event and loss-measurement dead zone.

edge of the pulse drops uniformly and gradually at a predictable rate. In fact, it is possible to estimate the rate at which the pulse falls if we know the OTDR's effective system bandwidth. Alternatively, if we measure the rate at which the pulse falls, we can calculate the system bandwidth.

If we model the OTDR's system response as a single-pole amplifier, the normalized rising edge of the pulse is given by*

$$5 \log (1 - e^{-t/\tau}) \quad [4.19]$$

where t is the time constant of the resistive-capacitive (RC) network in the single-pole model. The rate at which the pulse falls is given by

$$5 \log (e^{-t/\tau}) \approx -2.171 \cdot t/\tau \quad [4.20]$$

From elementary circuit theory we have $t_r = 2pt$, where t_r is the rise time of the RC network and $t_r = 0.35/b$, where b is the system bandwidth. Furthermore, the system falls 5 dB in one rise time, by definition. Therefore, to determine the system bandwidth, we first

*In the approximate analysis that follows, we ignore the effects of backscatter, which constitute a DC signal added to the reflection.

identify the distance (time) required for the pulse to fall 5 dB and use the fact that the bandwidth is 0.35 divided by this amount of time. Time can be converted to distance on the OTDR by using the approximate relationship, 10 ns = 1 meter.

As an example of this technique, suppose we measure the decay rate of the pulse and find that it falls 5 dB in a distance of 35 meters. This distance is equivalent to 350 ns. Therefore, 350 ns is the rise time of the system and the bandwidth is equal to $0.35/350 \text{ ns} = 1 \text{ MHz}$. If the OTDR is equipped with a two-point slope-calculation function that reads in dB/km, then this slope can be converted directly to a bandwidth by the relationship*

$$\beta = m/134 \quad [4.21]$$

In equation [4.21], β is the system bandwidth (in MHz) and m is the slope of the linear portion of the trailing edge of the reflection in dB/km.

Clearly, because the system has limited bandwidth, the fall time of the pulse is not infinitely fast. Thus, if we have two reflective events closely spaced, there is a critical separation such that the signal from the first event does not fall significantly before the signal from the second event becomes appreciable. When two reflections are spaced closer than this limit, they become essentially indistinguishable. We define this limit as the EDZ of the system. It is equal to the distance between the leading edge of a reflection and the point on the falling edge where the signal level drops 3 dB below the top of the reflection.[†] This definition is illustrated in figure 4.15. The EDZ is defined in terms of how a human operator would identify two closely spaced events. However, some modern OTDRs with sophisticated event-detection algorithms are able automatically to detect events whose spacing is smaller than the event dead zone as we have defined it here.

4.3.9 Loss-measurement resolution

In section 4.2 we discussed the notion of loss-measurement dead zone (LMDZ). We described briefly the phenomena that limit the OTDR's ability to identify and measure events closely following large reflective

*To use this equation, measure the slope of the falling edge near the top of the pulse, where the slope is roughly linear. As the pulse response comes nearer the backscatter level, it becomes nonlinear as it blends with the backscatter signal. Avoid this region when measuring the slope used in equation [4.21].

[†]This definition, obviously, makes sense only if the reflection extends more than 3 dB above the backscatter level.

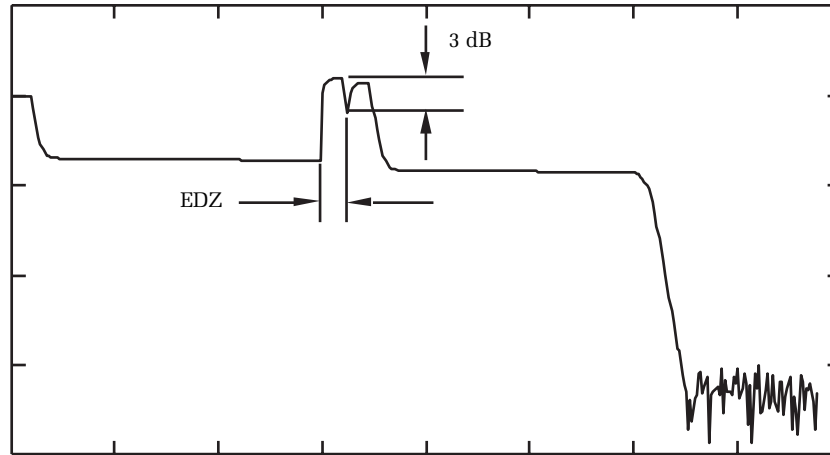


Figure 4.15. Illustration of the event dead zone for reflective events. The event dead zone is the distance from the leading edge of the first reflection to the point past the reflection where the signal level has dropped by 3 dB.

events: detector tail, preamplifier recovery, and saturation. We use the term *loss-measurement resolution* (LMR) to describe the performance of the OTDR in this respect. In the past, an ad hoc criterion, illustrated in figure 4.16, has been used to evaluate this performance. It can be described in the following way: When an OTDR is used to measure a fiber having a large reflective event, the fiber waveform may be distorted in the region immediately following the reflective event. The loss-measurement dead zone is the distance from the onset of the reflection to the point where the OTDR's waveform has recovered to within 0.5 dB of its undisturbed level.

In former times, the losses of fusion splices and mechanical connectors were relatively large, sometimes as large as 1 dB or more. Given such losses, it made sense to define the LMDZ as the point where the waveform had recovered within 0.5 dB of the backscatter. Modern fusion splices have considerably lower loss. Typically the losses of fusion splices and mechanical connectors are less than 0.5 dB, and they are often less than 0.1 dB, which meets the TIA/EIA 758 "customer-owned outside plant" standard, which specifies a .1-dB averaged splice value. Thus, another loss-measurement dead zone is sometimes used that is based on the recovery of the waveform to within 0.1 dB of the scattering level. This definition, of course, leads to longer recovery distances than

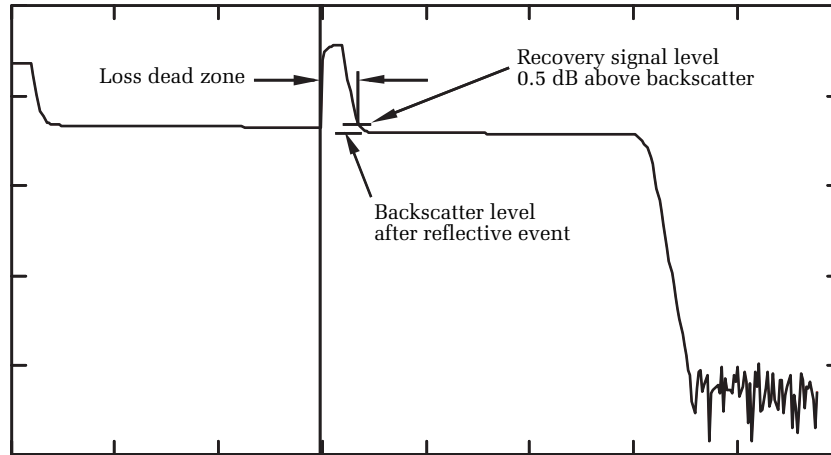


Figure 4.16. Traditional definition of loss-measurement dead zone. The traditional measure of LMDZ is the distance from the reflection's leading edge to the point past the reflection where the waveform has fallen to within 0.5 dB of the normal backscatter level. LMDZ depends on the characteristics of the OTDR's optical receiver, system bandwidth, thermal characteristics, and a host of secondary effects.

the 0.5-dB definition, but it provides a more realistic measure of the true loss-measurement dead zone.

4.3.10 Return loss

When reflective events are present in a fiber system, they can lead to bit errors at receivers used in digital systems and increased carrier-to-noise ratio (CNR) in analog systems. The errors are produced by two mechanisms. In the first case, the reflective event returns a certain amount of power to the transmitter. This feedback at the transmitter laser effectively reduces the modulation bandwidth of the laser and thereby leads to bit errors. In the second mechanism, multiple reflections within the fiber system can lead to bits or "1s" superimposed on the "0s" of the bit sequence. This *intersymbol interference* is also a form of bit error. In both cases, reflections produce unwanted errors, and the best ways to reduce the errors are by either reducing the reflections or eliminating them altogether. The amount of light reflected by an event has been historically known as the *return loss* of the event and is commonly specified as optical return loss (ORL). This is a strange and unfortunate terminology (the term *reflectivity* is more descriptive). But again, history is the driving force behind the usage. Return loss is defined as -10 times

the logarithm of the reflected power divided by the power incident just before the reflection:

$$R_L \equiv -10 \log \left(\frac{P_r}{P_i} \right) \quad [4.22]$$

The actual value of an event's return loss tells little about the severity of the effect of reflected power on the system performance. To determine this, other factors must be taken into account along with the return loss. For example, the distance of the event from the transmitter, the presence of other reflections, the bit rate, and the transmitter power are other useful factors in this evaluation. It is a fairly complex problem to do the evaluation exactly for every fiber. Therefore, the system designer may use basic rules to simplify the problem. For example, the designer may require that there be no reflections with return loss less than 40 dB in the system. In that case, it is necessary to evaluate the return loss of each event in the fiber system.

OTDRs are useful instruments for identifying and measuring reflections. There is an established methodology for calculating return loss based on the OTDR pulse width and the height of the reflection above scattering. This technique, based on work done by Bellcore, is widely used in modern OTDRs. We discuss this technique in detail in chapter 6. Essentially, the method involves measuring the height of the reflection above the Rayleigh backscatter and using this information along with the OTDR's pulse width and the fiber's backscatter coefficient to calculate the return loss.

Another useful measurement is the *total reflection return loss* of the fiber system. This is obtained by integrating the individual reflected powers of all events together with the fiber scattering. All reflected power is adjusted for the known loss encountered in returning to the receiver, also measured by the OTDR. Normally, OTDRs have selectable settings for measuring either discrete (event) return loss or total (integrated) return loss. The accuracy of OTDR return-loss measurements is normally about 2 dB, which is usually adequate for system analysis and assurance testing.

4.3.11 Linearity

In many instances, it is necessary to measure the linearity of a fiber waveform. Applications requiring extremely linear OTDR measurements include fiber manufacture, cable manufacture, cable installation,

and contamination testing. The objective of such measurements is to determine that the fiber's loss per unit length is constant and within predetermined limits. OTDRs are ideally suited for these types of measurements, provided the linearity of the OTDR exceeds that of the fiber.

Nonlinearity of the OTDR waveform is specified as a fraction of error (in decibels) per decibel of signal change, over a given signal range (also specified in decibels). For most applications it is very difficult for the OTDR user to verify the instrument's linearity. It is important in such cases to purchase the OTDR from a manufacturer who has invested in the equipment and techniques required to certify the OTDR's performance to the required level of accuracy.

Modern electronic circuits can be designed with a small-signal linearity of about 1%. In the log domain, this amounts to about 0.02 dB in 1 dB of signal change. Normally, single-mode fibers have nonlinearities that do not exceed this amount. Thus, measuring linearity is problematic, because when a small nonlinearity is observed in the OTDR's waveform, it is usually not known whether it is the fiber itself or the OTDR that is producing the nonlinearity.

Nonlinearities in OTDRs are frequently caused by thermal effects in the discrete elements of the OTDR preamplifier. As we have already seen, nonlinearity is also caused by offset errors. First-generation OTDRs sometimes exhibited significant nonlinear effects due not only to preamplifier thermal effects but also due to ADC bit errors and nonlinearities due to unstable APD dark currents. Designers have developed ways of reducing the nonlinear effects due to thermal effects in the preamplifier. These advances have resulted in some modern OTDRs designed for extreme linearity, which achieve better than 0.02 dB/dB linearity over the entire scattering signal range. However, with improved linearity, it becomes increasingly more difficult to measure and calibrate the OTDR performance.⁹

4.3.12 Data resolution

Recall from chapter 3 that an OTDR is basically a multichannel analyzer. A laser pulse is launched into the fiber under test, and light that is scattered and reflected from the fiber returns to the OTDR, where it is sampled at uniform intervals in the time domain. At each sampling interval, the incoming signal is integrated during a sample window and a voltage is generated corresponding to the intensity of the optical power returned at that moment. A "bucket," or channel, is created

and a count value corresponding to the voltage is “dumped” into the bucket. Subsequent acquisitions repeat this process, continuing to add and store the count values in sequential time buckets. At the end of the acquisition process, the counts in each bucket are divided by the total number of acquisitions. Because of this multichannel nature of the signal processing, the information in the time domain is discrete, or granular (discontinuous). This granularity represents the maximum resolution in the time domain.*

The interval between sample points, expressed in distance, is known as the *data density*. It is usually given as a whole number, such as “10 meters” or “25 cm.” Although a true density would be the number of sample points per unit distance, the usage of the term has developed this way over time, and it has become an accepted way of specifying the sample resolution.† Of course, the higher the density, the better the resolution. Data density is normally limited by the acquisition range selected and the available on-board memory reserved for storing waveform points.

When OTDRs were first introduced, they were designed to acquire one distance point for every emitted laser pulse. This was a very inefficient sampling method, leading to extremely long acquisition times to acquire waveforms with high dynamic range. Modern high-speed acquisition systems allow multiple samples per acquisition, at a rate of 10 MHz or more. The sampling rate of 10 MHz corresponds to 100 ns in the time domain, or 10 meters (as seen on the OTDR’s waveform display). Thus, when the high-speed sampler is running continuously, one sample can be acquired for each 10 meters of fiber. This is sufficient sample spacing for long fibers, such as 50 km. However, for shorter fibers and narrow pulse widths, this sample spacing is inadequate.

To improve sample spacing, a technique known as *interleaving* is sometimes used. In the process of interleaving, a waveform is acquired with the maximum density of the sampling system, say, 10-meter sample spacing. In a subsequent acquisition, the laser pulse is fired, but the acquisition system is delayed a small amount before the sampler is allowed to trigger. This shifts the sampling sequence by an amount equal to the time delay. A second set of waveform points is acquired relative

*This is generally true, although sophisticated pattern-matching algorithms in some OTDRs manage to locate the positions of some events, such as fusion splices, with accuracy that is better than the sample spacing in the OTDR waveform.

†In this book we generally avoid the term *data density* in favor of the more descriptive term *sample spacing*.

to the first but shifted by the amount of the delay. A third acquisition is then started, and again delayed by twice the initial delay. This generates a third set of waveform points, which are stored relative to the first by twice the time delay. This process is continued until a complete set of waveform points is obtained, whose sample spacing is equal to that required for the overall settings of pulse width and range. In principle, this process could be continued without limit, with the only constraint being the time required to complete the overall acquisition.

So we need to ask, “What is the best sample spacing to use for a given pulse width and range?” Unfortunately, there is no set of rules that can be used to answer this question exactly. We have found from experience that we can use a fairly simple set of rules for estimating the sample spacing, based on what a reflective pulse looks like when the waveform is fully expanded on the display. We have found that about four or five data points per pulse width result in a fairly clean displayed pulse and fiber waveform. Additionally, a well-designed, automatic event-detection system responds optimally when at least four waveform points per pulse are used.

4.3.13 Clock accuracy

The time-domain analysis of the OTDR is coordinated by means of an on-board digital oscillator circuit, or *clock*. OTDR clocks normally operate in the 40-MHz frequency range. The best OTDR clocks have an accuracy specification of about 0.001%. This means that if a fiber 100 km in length is tested, the uncertainty of the distance measurement can be no better than $0.001\% \cdot 100 \text{ km} = 1 \text{ meter}$. This type of accuracy is more than sufficient for general-purpose OTDR tests involving long-haul single-mode fibers.

Sometimes OTDR manufacturers specify distance accuracy as if it were determined only by the sample spacing and clock accuracy. This leads to distance-measurement specifications that are considerably more optimistic than is practically possible. In chapters 5 and 6 we discuss distance-measurement accuracy in greater detail. In these chapters we show that interpretive errors and waveform noise are the dominant sources of distance-measurement error and that typically they exceed the generally insignificant errors caused by the clock frequency and even the sample spacing.*

*Interpretive errors relate to how the OTDR operator or event-marking algorithms interpret the waveform in the process of determining the location of an event.

4.3.14 Cursor resolution

Of paramount importance is the resolution with which the OTDR can display a fiber waveform. High-performance OTDRs use high-resolution CRT- or LCD-type displays, with many hundreds of pixels in the horizontal direction. Individual pixel size determines the maximum resolution with which the OTDR can display data. For example, suppose you acquire a waveform of a fiber that is 100 km long. If the display has 500 pixels in the horizontal direction, then each pixel represents a distance of 200 meters. Thus, although the OTDR clock may be capable of resolving down to 10 m in the fiber, the display resolves only 200 m when the entire 100-km waveform is displayed at once. We call this limitation the *cursor resolution* of the OTDR display. Clearly, the cursor resolution depends not only on the type of display used but also on the amount of fiber waveform shown on the display at any given time.

Display resolution affects not only the distance resolution, but the loss resolution as well. Suppose an OTDR has 40 dB of vertical scale range and 500 pixels in the vertical direction. Each pixel is the equivalent of about 0.1 dB. In this situation, a 0.05-dB event could easily go unnoticed since it is smaller than the display resolution. This highlights an important aspect of the OTDR's display. Remember that although display size often is given preferential treatment by OTDR users, pixel resolution is equally important.

To improve the display's ability to show the waveform data accurately, most OTDRs include a "zoom" mode. In the "zoom-on" mode, a portion of the entire acquisition range is expanded to fill the entire horizontal axis of the display. In properly designed OTDRs, continued expansion within the horizontal direction enables the OTDR user to resolve the maximum data density.

4.3.15 Refractive-index uncertainty

In chapter 2 we introduced the concept of a group refractive index for an optical fiber. In simple terms, the group refractive index is the speed of light in a vacuum divided by the speed of propagation of a light pulse guided by the optical-fiber core. It is reasonable, therefore, that we can determine the group refractive index of the fiber if we know (1) the length of the fiber and (2) the time required for a laser pulse to propagate the length of the fiber.

Let us imagine an experiment in which we measure the group refractive index of an optical fiber. Here are the steps we would use in doing this determination:

1. Measure the length of the fiber, L , using a mechanical method, such as spooling the fiber through a spindle that digitally counts off distance.
2. Inject a pulse of light into one end of the fiber using a high-speed laser.
3. Measure the time, t , required for the pulse to propagate through the fiber using a digital counter-timer.
4. Divide the length of the fiber by the propagation time to obtain the group velocity, v_g , of the fiber: $v_g = L/t$.
5. Divide the speed of light in a vacuum, c , by the group velocity, v_g : $n_g = c/v_g$.

This turns out to be a relatively simple experiment to perform and gives excellent results for the group index, n_g . Using this method, it is possible to measure the group index to a precision of about 1 in 10,000.

An OTDR can be used to measure the group index if the fiber's true length is already known. To measure the group index, simply connect the OTDR to the fiber and acquire a waveform. Measure the fiber's length on the OTDR display, and adjust the OTDR's group index setting until the measured length on the OTDR waveform equals the known length of the fiber.* This same technique is also used to adjust the OTDR's index of refraction to match the cable sheath length using the sequential markings on the cable.

For most applications the true length of the fiber is not known, so the group index cannot be measured by using the fiber's length. In most cases, however, the fiber's group index is specified by the fiber manufacturer. The OTDR operator normally enters this value into the OTDR and then uses the OTDR to measure the fiber's length. Thus, the OTDR operator must rely on the fiber manufacturer to give an accurate value for the refractive index. Other OTDR measurements that depend on length, such as loss per kilometer, are then limited in accuracy by the accuracy of the refractive index.

The refractive-index uncertainty is responsible for a large part of the OTDR's distance-measurement uncertainty. As an illustration of this, consider a fiber whose length is 50 km. Suppose we measure this fiber using a 100-meter pulse and a sample spacing of 10 meters. If we expand the horizontal display to maximum zoom, we can resolve each

*This technique is limited by the accuracy imposed by the sample spacing, unless the end of the fiber coincides with a sample point.

of these 10-meter data points, so our cursor resolution is 10 meters also. As we mentioned earlier, the internal clock has a precision of about 1 in 10^5 . This provides an uncertainty in the clock resolution of 50,000 meters $\cdot 10^{-5} = 0.5$ meters. Finally, our refractive index is about 1.456, with an uncertainty in the last digit of ± 1 . This is a refractive-index uncertainty of $0.001/1.456 = 0.00069$. To obtain the uncertainty in the fiber length due to the refractive-index uncertainty, we multiply $0.00069 \cdot 50,000 \text{ m} = 34 \text{ m}$. Thus, the total distance uncertainty is

$$\text{Distance uncertainty} = \sqrt{10^2 + 0.5^2 + 34^2} = 35.4 \text{ meters}$$

In an actual OTDR measurement, the distance uncertainty due to refractive-index uncertainty can be as much as 10 times the uncertainty due to clock and sample-spacing errors. This is a significant point that is not well appreciated in the industry. We discuss other aspects of distance-measurement uncertainty in more detail in chapters 5 and 7.

4.3.16 Speed of measurement

One of the most important figures of merit for OTDR performance is how quickly the instrument gets the job done. Speed of measurements is critical for applications such as installation of large-fiber-count cables, restoration of trunk lines and high-capacity distribution lines, and quickly locating faults in fibers providing critical services for CATV, telecommunications, and data communications lines. The speed of measurement of an OTDR depends on many factors, some of which involve esoteric design issues. Here we describe the four hardware parameters that most significantly affect measurement speed.* These are fiber length, interleaving, data-processing speed, and display speed.

4.3.16.1 Fiber length

To measure a fiber, the OTDR injects a pulse in the fiber and waits for the light to travel the fiber's length and back again to the OTDR. If the length of the fiber is L , the time required to travel the distance down the fiber and back is $2L/v_g$, where v_g is the group velocity of light in the fiber. If a fiber has a length of 100 km and if the refractive index is 1.456, then the time required for a pulse to travel the length and return is

$$T(100 \text{ km}) = 100,000 \text{ m} \cdot 2 \cdot (1.456/3 \cdot 10^8 \text{ m/s}) \approx 1 \text{ ms}$$

*Event-marking algorithms also affect measurement efficiency in a very significant way. Chapter 11 discusses some of the different event-marking algorithms and how their peculiar designs affect measurement speed. Here, however, we discuss only the specific hardware specifications that affect measurement speed.

Now suppose we set the OTDR to perform 32,768 averages. The total time required by this entire acquisition is about 32 seconds ($32,768 \cdot 0.001$ s). This simple physical limitation of the speed of light sets the ultimate limit on how fast the OTDR can acquire data. If we wish to speed up the total acquisition time, we must improve other aspects of the OTDR performance, such as dynamic range per individual acquisition (which reduces the need for so much averaging) and data-processing speed (which reduces some of the overhead time).

This calculation points to an important fact. When measuring dynamic range, it is important to do so using a fiber that is sufficiently long to carry the fiber backscatter signal into the noise floor. Offset errors and nonlinearity are two reasons to do this. Now we see that acquisition time is a third. More averages result in higher dynamic range. To determine properly the dynamic range achievable within a given amount of time on a long fiber, you must test on a long fiber. Testing on a short fiber allows the OTDR to acquire more averages and to present an artificially high dynamic range.

4.3.16.2 Interleaving

In section 4.3.12 we described how interleaving improves data resolution. When interleaving is performed, individual acquisitions are combined to increase the data density. In this technique, each set of data representing an individual acquisition sequence requires an equivalent amount of time to obtain. The total acquisition time is proportional to the total amount of interleaved acquisition sequences. This acquisition-time *penalty* has the effect of increasing the time required to attain a certain signal-to-noise ratio. Another way of saying this is that a particular averaging time in an interleaved system results in a lower dynamic range than in a system with no interleaving.

4.3.16.3 Data-processing speed

Modern OTDRs contain one or more internal processors (computers) that control functions such as acquisition, operating system, display, and I/O functions. Besides the time required for the signals to travel the fiber, time is required to process and display the data. In a typical OTDR acquisition system, an acquisition processor controls the laser triggering and the analog-to-digital conversion timing. Digital data are transferred to high-speed memory, where it can be additionally averaged. Sometimes the data are then transferred to low-speed memory, where they are digitally filtered and mathematically analyzed. Some examples

of mathematical analysis include conversion of the data to a logarithmic scale, automatic event detection, and waveform splicing.

All of these operations in the sequence from A/D conversion to data display require processing time. Even the transfer of data from high-speed memory to low-speed memory requires a significant amount of time. Processing times following A/D conversion are sometimes called *overhead*, since they can be equivalent amounts of time regardless of the selected averaging time. Overhead has a larger impact with short averaging times than with longer averaging times, since it represents a larger fraction of the total acquisition time. It benefits the overall speed of the OTDR to incorporate extremely fast processors and processing algorithms to reduce overhead. However, these faster techniques usually imply greater cost, so there are always trade-offs.

4.3.16.4 Display speed

Original designs for commercial OTDRs used sequential acquisitions (one time-domain data sample per laser pulse) to produce fiber waveforms. In those days, to represent the waveform on the display (a CRT) was as simple as sampling the charge on an integrating capacitor and transferring the voltage to the vertical amplifier of the CRT. In modern OTDR designs, high-speed sampling is performed and the data are first averaged, converted to log domain, digitally filtered, and finally transferred to the display driver.

The driver is a set of software instructions that form the interface between the digital data and the display “controller.” The controller is a hardware device that has all the electronic controls necessary to activate and control the vertical and horizontal points, or “pixels,” that actually represent the data on the display (CRT or LCD). To display the fiber waveform rapidly, both the controller and the driver software must be optimized for efficiency. Display technology is rapidly changing and is driven largely by the personal computer market. Considerable progress has been made in the past few years on the quality, contrast, resolution, and speed of displays, and we expect OTDR designers and end users to benefit greatly from future display-technology improvements.

4.3.17 Event-detection accuracy

Modern OTDRs incorporate mathematical algorithms for automatically analyzing an OTDR waveform to identify the locations of events and evaluate their individual characteristics. This *post processing* analysis is essentially the last step in data processing before the waveform is

displayed to the operator. In recent times, automatic event detection has become so important that it rivals the performance of the OTDR hardware in its amazing ability to improve fiber measurements.

Here, we simply mention the fact that event-marking algorithms play heavily in any evaluation of an OTDR's accuracy and measurement capabilities. We have deferred a full discussion of the limitations and measurement accuracy of event-marking algorithms to chapters 5, 6, and 9.

4.4 Standards

Historically, OTDR performance was driven primarily by the combined requirements of resolution and signal-to-noise ratios. Little attention was given to establishing standards for OTDR measurements. Perhaps one reason for this is that in the first few years of deployment, optical fibers were relatively “forgiving,” in the sense that even the most poorly performing fibers would do a good job of transmitting signals. In the past few years, however, increasing demands have been placed on fiber performance. To ensure increasing levels of fiber performance, system designers and installers have begun to require ever-increasing levels of OTDR performance. To establish ground rules for OTDR performance measurement and to level the field for OTDR selection, some standards have been established for OTDR testing and performance checks. We devote this section to a discussion of these standards.

In 1988, a group at Bell Communications Research (Bellcore) set out to establish the first standards on OTDR performance. Under sponsorship by several regional Bell operating companies (RBOCs), this team, led by John Peters, called for input from both the OTDR user community and OTDR suppliers. In the late 1980s, they brought forth a groundbreaking document that set the stage and the first ground rules for OTDR performance evaluation. This document, first released as Bellcore TA-TSY-000196 and later released as Bellcore GR-196-CORE, accomplished three notable results: (1) It provided excellent rules for OTDR evaluation, (2) it established a firm basis from which OTDR manufacturers can improve their designs, and (3) it supplied extremely useful information to the industry on how OTDRs are expected to perform in actual measurement situations.¹⁰ Among the attributes that the document covered are: performance characteristics, environmental standards, and ruggedness conditions.

Bellcore defined measurement range in terms of the ability of an OTDR to detect a certain-size event loss in the presence of a certain

signal-to-noise ratio. In the Bellcore definition, a small loss is placed between two sections of fiber. The OTDR is connected to the first section of fiber. The instrument is required successfully to detect and measure the event at least three times out of four acquisitions. If the OTDR meets this condition, the first fiber length is increased and the test is conducted again. This process continues until the OTDR is no longer able to locate and measure the event. The total loss from the OTDR front panel to the event is called the *measurement range*.

Experience has shown that measurement range is often a more useful performance parameter than dynamic range. Dynamic range alone does not guarantee that the OTDR can successfully identify and evaluate events in the fiber. The reason for this is that both hardware performance and software performance combine to provide overall instrument sensitivity and good measurement range. As time progresses, hardware and software improvements will continue and software algorithms will become increasingly important for detection sensitivity. As the community of OTDR users realizes the utility of measurement range, we expect that measurement range will replace dynamic range as the single most important OTDR performance parameter.

Automatic event-detection accuracy expresses the ability of the OTDR automatically to identify and evaluate events with a low degree of uncertainty and a high degree of repeatability. The Bellcore specification for measurement range encompasses the concept of detection accuracy. Some OTDRs provide values for event-loss uncertainty and location uncertainty. Again, as the OTDR user community becomes familiar with the concept of measurement range, we expect that OTDR users will demand that the instrument provide accuracy values along with event information.

4.5 Summary

Most of this chapter discusses what is arguably the single most important specification for OTDRs: dynamic range. Dynamic range is also perhaps one of the most misunderstood specifications. We described two types of dynamic range: reflective and scattering. When measuring reflectivity, you need an OTDR with high reflective dynamic range. When measuring splice loss over long lengths of fiber, you need an OTDR with high scattering dynamic range. Scattering dynamic range, the specification most people are familiar with, has several definitions. Bellcore defined scattering dynamic range based on a noise floor that lies above roughly 98% of the OTDR's system noise. Some OTDR manufacturers specify

the dynamic range based on a noise floor equal to the RMS noise. These definitions are related to each other through a simple constant offset, provided the noise is Gaussian and there is no offset error.

Offset errors are frequently overlooked in OTDR specifications, even though they potentially can significantly affect the instrument's performance and give false indications of dynamic range. Offset errors result in nonlinearity near the noise floor and generally cannot be observed unless you are testing a long fiber that extends into the noise floor. Too much positive offset results in underestimating the dynamic range but is less likely to delete events from the waveform. Too much negative offset results in overestimating the dynamic range and is more likely to delete events from the waveform.

Dead zone is the region after a reflective event where only limited measurements may be performed. *Event dead zone* is the minimum distance after a reflective event before the presence of another reflective event can be detected. *Loss dead zone* is the minimum distance after a reflective event before the loss of another event can be measured.

After dynamic range and dead zone we reviewed a plethora of minor specifications. These are not individually as significant as dynamic range and dead zone, but collectively they can make an important difference between different OTDRs.

Suggested reading

Hentschel, C., *Fiber Optics Handbook*, 2nd edition (Germany: Hewlett-Packard, 1988).

Jones, Jr., W. B., *Introduction to Optical Fiber Communications Systems* (New York: Holt, Rinehart, and Winston, 1988).

Senior, J. M., *Optical Fiber Communications Principles and Practice* (London: Prentice-Hall, 1985).

Neumann, E. G., *Single-Mode Fibers* (Heidelberg: Springer-Verlag, 1988).

Problems

1. Name two types of dynamic range.
2. If an OTDR uses the 98% noise floor definition, is the dynamic range specification greater or smaller than if they used the RMS noise floor definition?
3. True or false: Positive offset errors make the dynamic range look artificially large.
4. Which is typically a larger source of error for distance measurements, uncertainty in the IR setting or errors in the OTDR's clock?

5. True or false: Reflections cause problems in fiber-optic systems because they can result in intersymbol interference.
6. True or false: Linearity is the decibel error in an OTDR.
7. True or false: Loss-measurement dead zone is determined by the distance after a reflective event before the waveform recovers to within a defined distance from the backscatter.
8. True or false: OTDRs use a log scale on the vertical axis to make the waveform look less noisy.
9. True or false: Measurement range is usually larger than dynamic range.
10. True or false: Useful range is smaller than dynamic range, typically by about 7 dB.

¹ Danielson, B., "Optical time-domain reflectometer specifications and performance testing," *Applied Optics*, Vol. 24, No. 15 (1985), pp. 2313–2322.

² Brinkmeyer, E., "Analysis of the backscattering method for single-mode optical fibers," *Journal of the Optical Society of America*, Vol. 70, No. 8 (August 1980), pp. 1010–1012.

³ Neumann, E. G., "Analysis of the backscattering method for testing optical fiber cables," *AEU*, Vol. 34, No. 4 (1980), pp. 157–160.

⁴ Brinkmeyer, E., "Backscattering in single-mode fibers," *Electronics Letters*, Vol. 16, No. 9 (April 1980), pp. 329–330.

⁵ Nakazawa, M., "Rayleigh backscattering theory for single-mode optical fibers," *Journal of the Optical Society of America*, Vol. 73, No. 9 (September 1983), pp. 1175–1180.

⁶ Hartog, A. H., and Gold, M. P., "On the theory of backscattering in single-mode optical fibers," *Journal of Lightwave Technology* Vol. LT-2, No. 2 (April 1984), pp. 76–82.

⁷ Hettich, A., "Kriterien zur Beurteilung von Rückstreuemeßgeräten," Vol. 43, No. 5 (1990), pp. 386–392.

⁸ Bell, F., and Cook, R. A., "Testing long-haul fiber and cable," *Lightwave* (March 1994), pp. 38, 40, 44.

⁹ Möller, W., Hube, K., and Hünerhoff, D., "Uncertainty of OTDR loss scale calibration using a fiber standard," *Journal of Optical Communications*, Vol. 15 (1994), pp. 20–28.

¹⁰ "Generic requirements for optical time-domain reflectometer (OTDR) type equipment," *Bell Communications Research* (Bellcore), GR-196-CORE, Issue 1 (September 1995).

Chapter 5

Measuring nonreflective events

5.0 Introduction

Events on OTDR waveforms can be broadly categorized as either reflective or nonreflective. Nonreflective events involve only attenuation of the Rayleigh backscatter and no reflection. In this chapter we discuss the types of events that result in a nonreflective waveform signature and describe the techniques used to measure the event's loss and location.

This chapter also devotes special attention to the effects of waveform noise on OTDR measurement accuracy. We develop some equations you can use to estimate the distance-measurement uncertainty when you know the event's loss, the location above the noise floor, and the algorithm used to measure the event.* We show that waveform noise often limits the OTDR's distance-measurement accuracy and that dynamic-range specifications alone do not adequately reflect the true range over which an OTDR may be used. We show that waveform noise can easily result in measurement errors that may be larger than some calibration errors.

We end the chapter by reviewing some of the calibration issues that might affect the measurement accuracy of nonreflective events, and we describe some mathematical techniques for estimating the resulting errors.

Much of this chapter is devoted to understanding the limitations of, and ways to improve, measurement accuracy. The intent of this discussion is to provide the OTDR user with the analytical tools for estimating the measurement uncertainty. We hope that by our discussing measurement uncertainty in such detail, you will come to appreciate that measurement accuracy in OTDRs is a very complicated parameter.

5.1 Sources of nonreflective events

We saw in chapter 2 that optical fibers are typically joined using mechanical splices, connectors, or fusion splices. Mechanical splices and connectors physically align and restrain the fibers, usually by

*Distance-measurement accuracy is different for nonreflective events than for reflective events. We reserve chapters 7 and 8 for discussion of measurement errors for reflective events. Loss-measurement uncertainty is similar for both types of events and is discussed in detail in the next chapter.

aligning them with V-grooves or capillary tubes in ferrules. Mechanical splices restrain the fibers using locking cams or epoxy. Connectors align the fiber by restraining a ferrule in which the fibers are bonded with epoxy. Except when epoxy is used, mechanical splices can often be adjusted or replaced. Connectors, of course, are designed for many mating and demating cycles. Fusion splices, on the other hand, are formed by aligning the fibers and then fusing them with a hot electric arc. Once the fibers are fused, they essentially become one fiber, with a small localized loss in the area of the splice due to optical and/or mechanical tolerances.

Reflection occurs whenever light encounters a mismatch in the index of refraction of the material through which it is traveling.* In connectors, for example, there are always microscopic air gaps between the ends of the connector ferrules. Because of these gaps, the light goes from the fiber (index approximately 1.5) to air (index approximately 1) and back to fiber. Because of this rapid change in index, some of the light is reflected. This is true even for so-called physical-contact (PC) connectors. Similarly, in mechanical splices there are also microscopic gaps, between the fibers most of which are caused by slightly angled cleaves. Designers sometimes attempt to reduce the sizes of these reflections by using index-matching gels or epoxy. This reduces the amount of reflected light. But since the index match is never perfect, there is always some residual reflection (although in some cases the residual reflection might be very small).

Modern optical fibers are built to exacting standards of quality. Because of this effort to manufacture a high-quality product, when two optical fibers are fused together the light sees virtually no change in the index of refraction across the splice. As the OTDR's laser pulses travel along the fiber, they are gradually attenuated by Rayleigh scattering. When they encounter a fusion splice, they see essentially no change in the index of refraction, so there is no discernible reflection. With most splices, however, there are slight core mismatches, misalignments, or bending, so some of the pulse's light is lost as it crosses the splice and is dissipated in the cladding. The backscatter radiation after the pulse passes through the splice is also attenuated by the splice's slight imperfections. This means there is more power in the Rayleigh backscatter before the splice than after the splice. The result is that,

*In chapter 7 we discuss in detail some of the things that can cause an event to be reflective.

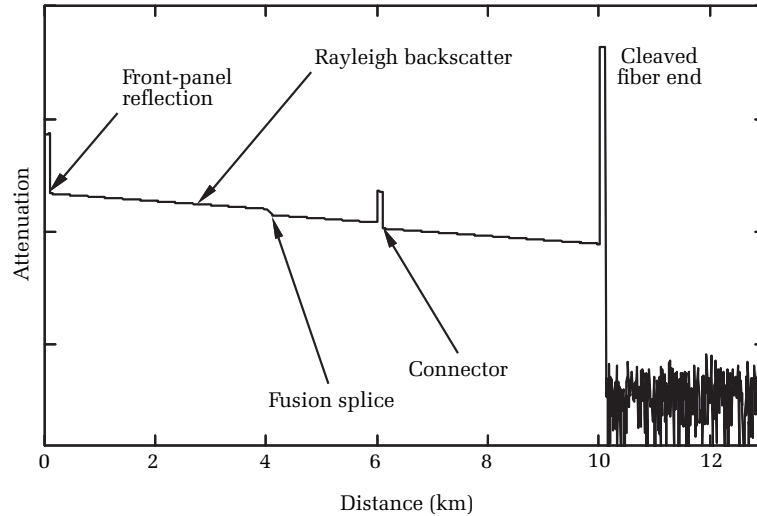


Figure 5.1. Comparison of the OTDR traces for reflective and nonreflective events. The fusion splice is nonreflective, so the OTDR trace across the fusion splices exhibits only a drop in the strength of the Rayleigh backscatter signal. Both connectors (the one at the front panel and the one immediately after the fusion splice) exhibit reflection, as demonstrated by the spike on the OTDR's waveform. The cleaved fiber end is more reflective than the connectors, so the height of its reflection is greater.

when viewing the signature of a fusion splice on an OTDR, you simply see a drop in the Rayleigh backscatter signal but no reflected spike (see figure 5.1).

Recall from chapter 2 that, like a fusion splice, a bend (macro bend) or localized pinch or stress (micro bend) in an optical fiber also results in optical attenuation. Macrobending and microbending losses result when light is coupled out of the waveguide and lost in the cladding. The geometry of either a micro- or macro bend is such that it reflects virtually no light, so a bend or stress, like a fusion splice, appears on the OTDR display as a simple drop in the backscatter without a reflective spike. With very few exceptions, when you see a drop in the Rayleigh backscatter but no reflection, the event is a fusion splice, micro bend, or a macro bend (we discuss bends further in chapter 7).*

*The least-squares approximation method is the most accurate manual method. Automatic event-marking algorithms, however, sometimes use methods that are more accurate. These methods are not generally applicable to manual measurements because they are too mathematically intensive.

5.2 Cursor placement for manual loss and distance measurements

For manual measurements, the most accurate way to measure the loss of a fusion splice is to use the least-squares approximation, or LSA method.* As the name implies, the LSA method involves the use of linear curve fitting. To measure a splice's loss manually using the LSA method, the OTDR requires vertically adjustable horizontal cursors with variable slopes. To make the loss measurement, place one cursor along the Rayleigh backscatter just before the event and the other cursor along the backscatter just after the event. Position these cursors so they are a best linear fit to the waveform data, as shown in figure 5.2. The splice's loss is the vertical separation between the two cursors (measured at the midpoint of the event).

The location of a nonreflective event is typically more difficult to measure than the location of a reflective event. Reflective events usually have sharp leading edges that may rise several decibels over a distance

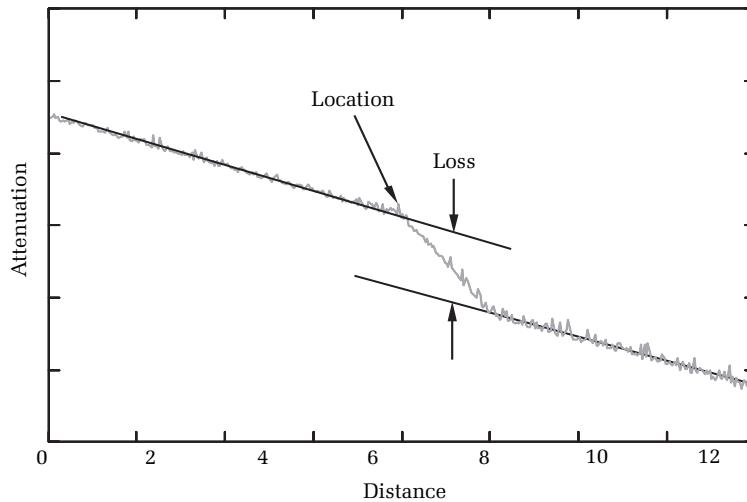


Figure 5.2. Measuring the loss and location of a nonreflective event. The event's location is the leading edge where the Rayleigh backscatter first starts to fall off faster than the normal fiber slope. The event's loss is determined by the vertical separation of two cursors (at the center of the event) when the cursors are fitted to the Rayleigh backscatter before and after the event.

*We show in chapter 7 that the *loss* of a reflective event is more difficult to measure than the loss of a nonreflective event.

of one or two sample points. This reflective edge is usually easy to locate, even when the waveform is noisy. A nonreflective event, on the other hand, shows only a drop one pulse width wide in the Rayleigh backscatter. The vertical drop equals the event loss plus the normal fiber loss over one pulse width. Since most fusion splices have losses of a few tenths of a decibels or less, the drop in backscatter is much less than the rise you typically see in the leading edge of a reflective event. Furthermore, with a nonreflective event, the drop in Rayleigh backscatter is spread over the width of the laser pulse, whereas the leading edge of a reflective event typically rises within a fraction of a pulse width. This makes the leading edge of the nonreflective event even less pronounced and easily obscured by waveform noise.

The location of the nonreflective event is the point where the waveform first starts to deviate from the linear Rayleigh backscatter of the OTDR waveform (see figure 5.2). The following procedure is a reliable algorithm for locating the leading edge of a nonreflective event manually.

1. Fit a cursor to the backscatter region before the event. Try to use a region of backscatter that is at least one pulse width wide.
2. Find the first point that lies below the cursor and is followed by a succession of points (all of which are also below the cursor) that are at least as wide as half a pulse width.
3. If the noise level is not significant compared to the loss of the splice, mark the point found in step 2 as the location of the splice. If the peak-to-peak noise is greater than (or equal to) the splice loss, then mark the location of the event one sample before the point in step 2.

Step three in this algorithm is necessary because the algorithm tends to be biased forward when the waveform noise is large compared to the splice loss. A common (though incorrect) trick is to fit one of the cursors to the backscatter before the event and the other cursor to the linear section of the event itself and then to mark the event's location as the point where the two cursors cross. Although this technique is frequently more repeatable than simply finding the event's leading edge, it has an offset error because the nonreflective event is not composed of linear segments. Since the offset error is a function of the pulse width, event loss, and bandwidth, correcting the offset error is usually too difficult for manual calculations.

Most OTDRs are capable of performing linear curve fitting automatically, although many OTDRs do not have rotatable cursors that allow the user to fit lines manually to the Rayleigh backscatter before and after the event. When making automatic measurements, the OTDR automatically selects a group of points before and after the event for use in the LSA computation. Many automatic LSA algorithms fail to use step 3, so their distance measurements sometimes have offset biases when measuring events found in noisy data. Ideally, the OTDR should provide a means for measuring nonreflective events automatically as well as allowing manual measurements using rotatable cursors.

5.3 Distance-measurement errors of nonreflective events

In this section we discuss some of the most significant sources of distance-measurement errors for nonreflective events. Frequently, when people consider the measurement error of an OTDR, they pay considerable attention to calibration errors, such as those associated with the instrument's time base, the setting of the index of refraction, or offset errors. Often overlooked are measurement errors caused by waveform noise. This is unfortunate because waveform noise is frequently the dominant source of measurement error. In this section we discuss waveform noise in great detail and examine how it can introduce measurement errors. We also look at some specific measurement algorithms and derive equations that allow you (in some circumstances) to estimate the amount of distance-measurement error that results from the waveform noise. We also examine calibration issues and the extent to which they affect distance-measurement accuracy.

5.3.1 Distance-measurement errors caused by waveform noise

All measurements, from those performed with a simple measuring stick to sophisticated techniques involving coherent mixing of laser radiation, involve some degree of measurement uncertainty. Sometimes this measurement uncertainty results from calibration errors, such as errors in the OTDR's time base or incorrectly entering the fiber's index of refraction. Sometimes overlooked, but frequently very important, are statistical errors that result from random fluctuations in the waveform. Often the measurement uncertainty caused by waveform noise is unknown, crudely estimated, or simply guessed. In this and subsequent sections we develop some of the mathematical techniques and equations for estimating the distance-measurement uncertainty that results from waveform noise. We show that this uncertainty is a function of the

OTDR's noise floor, the location of the event, the sample spacing, and the measurement algorithm employed by the instrument. A similar analysis of loss-measurement uncertainty follows in chapter 6.

Imagine a yellow tape measure that is 10 meters long, with black lines precisely marked along its length every centimeter. Imagine that these lines are drawn by a machine using a very sharp tool, so they are very thin, say, 0.5 mm. As the machine proceeds down the tape, the tool that draws the lines becomes flattened and the lines become wider. Further along, the lines not only are wider, but also have softer edges with increasingly low contrast.* After 1 meter, the lines have broadened from 0.5 millimeter to 1 millimeter. After 2 meters the lines have broadened to 2 millimeters wide. At 5 meters the lines are 5 millimeters wide, and their fuzzy edges are beginning to overlap. At 10 meters the lines totally overlap, and the tape is solid black.

The scale accuracy of our imaginary ruling machine is virtually perfect. However, the changing widths of the lines and their fuzzy edges result in measurement accuracy that continually degrades as you move farther down the tape. Near the beginning of the tape the measurement accuracy is roughly 1 mm. Near the middle of the tape the measurement accuracy is probably no better than 1 cm. At its end, the tape measure cannot be used for any distance measurements at all.

This example of a tape measure with gradually increasing line widths and degrading edge contrast is loosely analogous to the gradual distance-measurement error you encounter using an OTDR. As we see later, there are a number of systemic contributions to an OTDR's distance-measurement accuracy. These include time-base errors and errors introduced by variations in the OTDR's wavelength. These systemic errors are usually small, however, and do not significantly contribute to the OTDR's overall distance-measurement accuracy. In our analogy of the tape measure, these systemic errors correspond to the calibration accuracy of the ruling machine that marks the tape. Sample spacing is, of course, a fundamental limit and corresponds in our analogy to the distance between ruling marks. Frequently, however, the greatest impediment to distance-measurement accuracy is noise on the OTDR's waveform. Waveform noise corresponds in our analogy to the fuzzy edges and increasing width of the ruling lines on our tape.

*Imagine a felt-tipped pen that starts out sharp and then gets flatter and possibly bent over with frayed edges.

Analogies are good for developing an intuitive feel for a particular phenomenon, but we must be careful about taking them too far. In this section we derive some quantitative relationships between waveform noise and distance-measurement accuracy that should help you estimate the amount of error you can expect for some typical measurements. It is important to realize that an OTDR's distance-measurement accuracy is complicated and cannot be specified by a simple number or two. An OTDR's distance-measurement accuracy depends on the type of event being measured, the algorithms the OTDR uses, the size of the event, and how far the event is from the noise floor.

Measuring the position of a nonreflective event is one of the most difficult measurements made with an OTDR. This is because nonreflective splices are typically low-loss fusion splices, and these events have very subtle edges that are difficult to discern. Studies performed by one of the authors (Anderson) regarding the human interpretation of OTDR waveforms show that many operators measure the positions of nonreflective events using the simple algorithm in section 5.2, except for step 3. This algorithm is an example of a linear predictor, and it is a relatively good algorithm for finding the position of a nonreflective event.* The measurement uncertainty of this algorithm is not too difficult to model. To begin, let's examine the probability that any given point beyond the true position of the fusion splice satisfies the qualifications for being chosen as the splice's position. To qualify as the position of the nonreflective event, the n th point and all succeeding points (for about one pulse width) must lie below the mean. The probability that this will occur is

$$P_n = \prod_n^{\left(n + \frac{W}{\Delta x}\right)} \int_{-\infty}^{\Delta L} \frac{1}{\sigma_{\text{dB}} \cdot \sqrt{2\pi}} \exp\left(-\frac{1}{2} \left(\frac{x}{\sigma_{\text{dB}}}\right)^2\right) dx \quad [5.1]$$

In equation [5.1], σ_{dB} is the standard deviation (measured in decibels) of the local noise in the OTDR's waveform around the best linear fit. The OTDR's pulse width (as measured on the OTDR display) is W , and ΔL is the vertical distance (measured in decibels) of the point in question from the linear predictor (without noise).[†] In words, the probability that the

*Automatic event-marking algorithms have much more powerful algorithms, but these are generally too complicated for human operators.

[†]We assume in this derivation that the linear predictor is found by using enough points that its slope and offset are known with sufficient accuracy that the linear predictor's uncertainty does not affect the calculations.

n th data point qualifies is equal to the probability that the n th point and all succeeding points (for one pulse width) lie below the linear predictor. For points within one pulse width after the leading edge of the event, an approximation for ΔL is $(l/W) \cdot \Delta x \cdot n$, where l is the event's loss.*

To be chosen as the location of the event, the n th point must also be the first one to meet the qualifications. This probability is

$$P_c = \prod_{i=0}^{i=n-1} (1 - P_i) P_n \quad [5.2]$$

In a given waveform, none of the points near the leading edge of the fusion splice has 100% probability of being chosen by the linear predictor algorithm. One of the points has the highest probability, but others may still have a significant chance of being chosen. For any given set of circumstances, we can calculate $P_{c,n}$ for all points and then determine the mean sample point that will be chosen (over many independent measurements) as the event's location. The value of this mean data point is given by the following equation:

$$M = \sum_n n \cdot P_{c,n} \quad [5.3]$$

We can also calculate the standard deviation, or average measurement error, using the equation

$$S = \sum_n P_{c,n} (n - M)^2 \quad [5.4]$$

Equations [5.3] and [5.4] provide the significant statistical information about the measurement uncertainty associated with the linear predictor described in section 5.2. When we measure the location of a nonreflective event using the linear predictor algorithm, about 95% of the measurements lie within two standard deviations of the mean sample point given by equation [5.3].

Evaluating equations [5.3] and [5.4] requires more computing power than is found in most handheld calculators. Figure 5.3 illustrates a numerical solution for a typical case. Superimposed on the numerical solution are the test results from actual OTDR operators.† Observe

*This approximation assumes the splice signature is composed of linear segments. This is not true, but it is an adequate approximation for our present calculations.

†These test results were obtained by D. R. Anderson during investigative experiments in human interpretation of OTDR waveforms conducted at Tektronix.

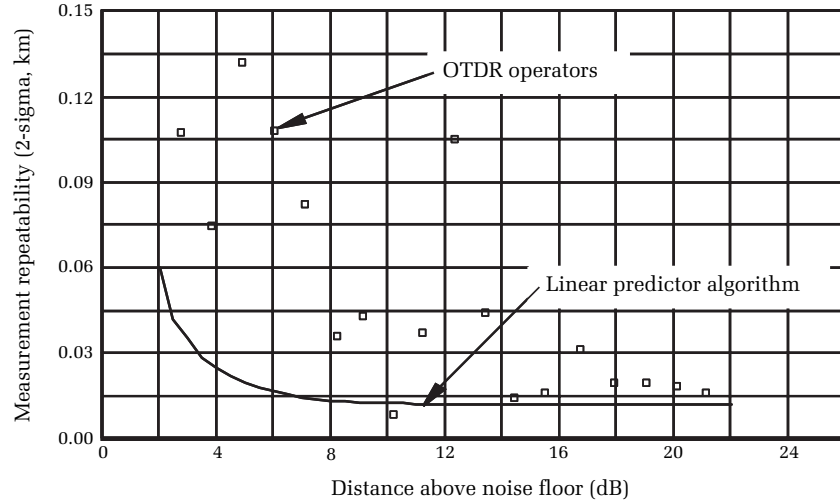


Figure 5.3. Performance comparison between the linear predictor (described in section 5.2) and the averaged performance of six OTDR operators. The events nominally had a loss of 0.5 dB and were measured with a 100-meter pulse and 5-meter sample spacing.

that the operators have the same general trend as the linear predictor algorithm but generally do not perform quite as well. This is easily explained in terms of the operator's technique. The computer in the OTDR executes the algorithm exactly, using precise numerical values for each point in the waveform. The operators, on the other hand, must select the optimum window size, place cursors using visual cues, and make their determinations largely based on qualitative evaluations of the waveforms.* Consequently, the operators are less likely to execute the algorithm exactly, and this increases their measurement uncertainty.

Figure 5.4 shows how the distance-measurement uncertainty of the linear predictor algorithm changes as the sample spacing changes. Observe that the baseline variation at high signal-to-noise ratios varies in direct proportion to the sample spacing. Thus, a reduction in the sample spacing by a factor of 10 (for example) reduces the variance at high SNR. At low SNR, the advantage of high sample density becomes less significant, although high-density sampling maintains its advantage over nearly the full dynamic range.

*Placing a window around the event permits the operator to expand its apparent size. This is usually performed using the zoom function. This function allows events to be viewed with greater magnification and clarity.

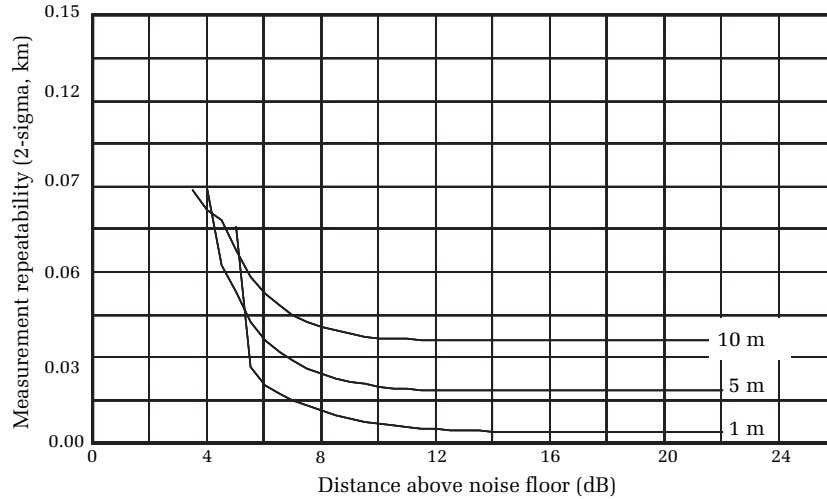


Figure 5.4. How distance-measurement repeatability of nonreflective events changes with sample spacing. The lowest curve corresponds to a sample spacing of 1 meter, and the highest curve corresponds to a sample spacing of 10 meters. The pulse width for all three curves was 100 meters, and the splice loss was 0.2 dB.

Observe that for each sample spacing the variation is relatively constant until a threshold is reached, whereupon the measurement variation begins to increase. With higher-density sampling, this threshold occurs at higher SNR. For example, in figure 5.4, when the event is roughly 14 dB above the noise floor, sampling at 1 meter begins to degrade. In contrast, with sampling at 10-meter intervals, the measurement repeatability does not begin to degrade until the event is about 11 dB above the noise floor.*

Figure 5.5 shows the effect of distance-measurement repeatability on pulse width. Observe that for a given dynamic range, the measurement repeatability is better for short pulses than it is for longer pulses. Of course, the OTDR's dynamic range also depends on pulse width, and reducing the pulse width reduces the dynamic range. We have, therefore, competing objectives. On the one hand, reducing the pulse width improves the measurement repeatability by making the

*This does not mean that 10-meter samples give better repeatability at 11 dB above the noise floor; in fact they do not. Observe that the advantage of the 1-meter sampling density over the 10-meter sampling density is less at 11 dB above the noise floor than it is at 14 dB above the noise floor.

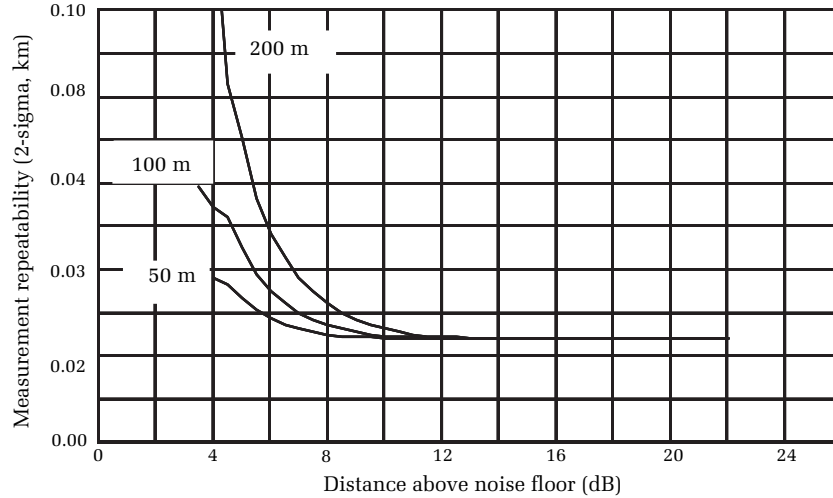


Figure 5.5. How distance-measurement repeatability of nonreflective events changes with pulse width. The sample spacing in all cases was 10 meters, and the event loss was 0.2 dB. For a given SNR, longer pulses result in less distance-measurement repeatability. However, longer pulses also result in higher dynamic range, so the net effect of increasing the pulse width may not always be obvious.

step slope of the event region more noticeable. On the other hand, reducing the pulse width reduces the measurement repeatability because it reduces the OTDR's dynamic range. Choosing the optimum pulse width, therefore, becomes rather difficult because it involves calculations that balance algorithm performance, noise, and dynamic range.^{1*} For manual measurements this balance is achieved imperfectly through the operator's intuition and training. In chapter 10 we discuss some advanced algorithms that perform this optimization of acquisition parameters automatically and adjust them for the individual events along the fiber.

*A paper given by D. R. Anderson at the NFOEC '96 conference shows that a key figure of merit for distance-measurement repeatability is independent of pulse width for constant averaging. Specifically, the ratio of the average slope in the nonreflective event to the local noise is pulse-width independent. This assumes the noise floor does not change with pulse width (an assumption that is frequently violated because OTDRs often change system bandwidth when changing pulse width). Consequently, distance-measurement repeatability may be independent of pulse width, though a detailed understanding of the OTDR's system architecture is required to make this determination.

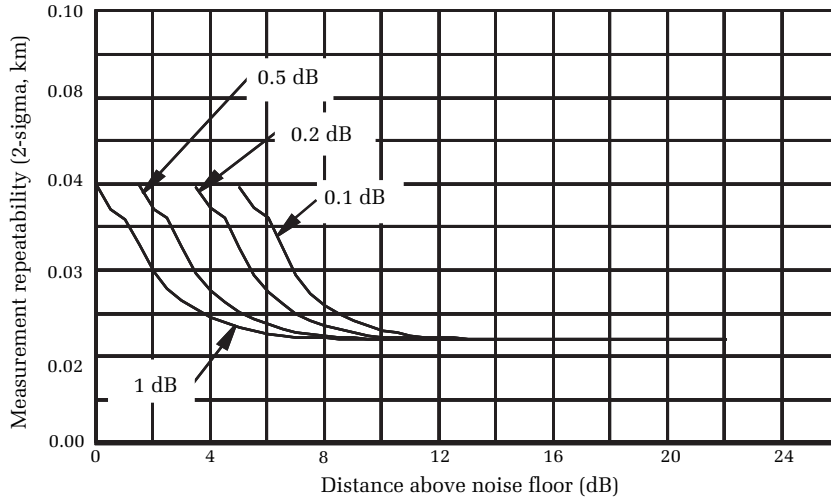


Figure 5.6. How distance-measurement repeatability depends on the nonreflective event's loss when using the linear predictor algorithm given in section 5.2. Distance-measurement repeatability generally improves as the event loss increases. For all events, the pulse width was 100 meters and the sample spacing was 10 meters.

Figure 5.6 shows how loss affects the distance-measurement repeatability. Small events are not only more difficult to detect, they are also more difficult to measure. Larger events are easier to detect, and their distance-measurement repeatability is better.

In examining the data in figures 5.3 through 5.6, you must be cautious about drawing unwarranted conclusions about the event-marking software in commercial OTDRs or even about the uncertainty of manual measurements. These figures are illustrative only and apply strictly to the simple linear predictor algorithm described in section 5.2. General conclusions, however, are valid. The distance-measurement accuracy improves as the sample spacing decreases, as the pulse width decreases (assuming constant SNR), and as the event loss increases.

By now the complexity involved in trying to specify the distance-measurement accuracy of an OTDR should be evident. When examining OTDR data sheets, too often we find a simple specification for distance-measurement accuracy. In the best of cases these specifications apply only to the optimal accuracy attainable under ideal conditions, with the instrument's smallest sample spacing. In the worst cases, it might simply indicate the instrument's sample spacing alone or time-base accuracy.

From the previous discussion, it is obvious that time-base errors and sample spacing account for a small amount of the instrument's distance-measurement error and are insufficient for determining the instrument's true measurement accuracy. Optimally, the OTDR should calculate and display in its event table the measurement uncertainties in both loss and distance. This takes the burden off the OTDR operator and indicates that the manufacturer has satisfactorily dealt with the fact that measurement uncertainty is a very complicated issue.

In figures 5.4, 5.5, and 5.6 we see that the distance-measurement error remains relatively constant as an event gets closer to the noise, until a certain threshold is reached. Upon reaching this threshold, the measurement error increases dramatically as the event continues to get closer to the noise floor. For example, in figure 5.6 we see that the threshold for a 0.1-dB event is roughly 10.5 dB. If the event is more than 10.5 dB above the noise floor, then the distance-measurement error is essentially constant. Below this threshold, however, the measurement error increases rapidly, doubling by the time the event is 6 dB above the noise floor. This threshold occurs approximately when the change in loss over a distance of one sample equals the standard deviation of the local waveform noise. This happens approximately when

$$\sigma_{\text{dB}} = \frac{\Delta x}{W} L \quad [5.5]$$

In equation [5.5], Δx is the spacing between sample points, W is the displayed pulse width, and L is the event's loss. The standard deviation of the local noise is a function of the distance of the event from the noise floor, δ .^{*} In chapter 6 we derive an expression for δ (see equation [6.10]). For now, we can simply say that when we substitute the equation for δ into equation [5.5] we have

$$\delta_{\text{critical}} \approx -2.2 \ln \left(0.92 \cdot \frac{\Delta x}{W} L \right) \quad [5.6]$$

According to equation [5.6], the critical distance to the noise floor for a 0.1-dB fusion splice acquired using a 100-meter pulse and 10-meter sample spacing is 10.3 dB. This is consistent with our observations of figure 5.6. For fusion splices of 0.2 dB, 0.5 dB, and 1 dB, the critical distances to the noise floor are 8.8 dB, 6.8 dB, and 5.2 dB, respectively. Comparing these results with figure 5.6 we see again that equation [5.6]

^{*}Here we define the noise floor as being the 2-sigma level.

gives a reasonably accurate prediction of the critical distance to the noise floor for the linear prediction algorithm described in section 5.2.

Since this linear prediction algorithm represents an approximate limit to the repeatability of OTDR operators, equation [5.6] serves as a useful estimator of the usable dynamic range for a given set of measurement conditions. For example, suppose Company XYZ is installing a fiber-optic link and that they want to measure the distance to a fusion splice that has 0.1-dB loss (nominally). Furthermore, they want to measure the splice with 2-meter sample density and a 50-meter pulse. According to equation [5.6], the useful dynamic range for these measurements is about 12 dB less than the OTDR's specified dynamic range for a 50-meter pulse.*

5.3.2 Distance-measurement errors caused by filtering

Low-pass filtering is a frequently used technique for increasing an OTDR's dynamic range, and it may be implemented in either the analog or digital domain.† Although filtering can be effective at reducing the noise on the waveform, it can also introduce serious distance-

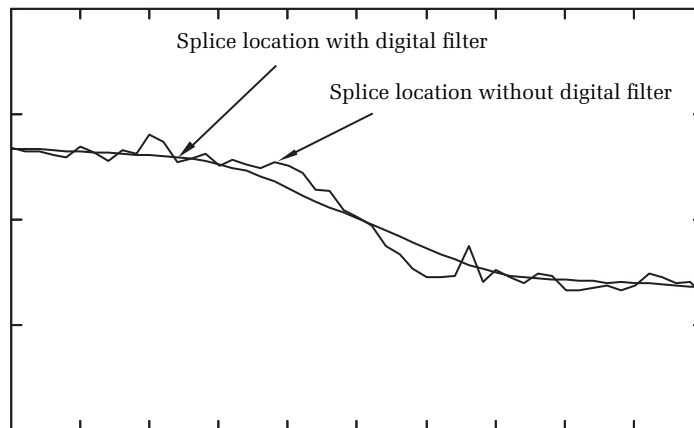


Figure 5.7. Distance-offset error introduced by digital filtering. The noisy waveform shows the area around a fusion splice. The smooth waveform shows the area after digital filtering. The digital filter replaced each sample point with the average value of its 18 closest neighbors. In applying the filter, the noise characteristics and dynamic range are greatly improved, but an obvious distance error is introduced.

*This assumes, of course, that the instrument's specified dynamic range is based on a noise floor at the 2-sigma noise level (see chapter 4).

†Low-pass filtering is used in many other applications besides OTDRs.

measurement errors when applied improperly. For example, figure 5.7 illustrates a nonreflective event acquired with high bandwidth and the resulting distance-measurement error from a digital filter.

Since receiver noise increases with bandwidth, the waveform in figure 5.7 shows noticeable noise. Overlaid in figure 5.7 is the waveform after digital filtering. For this example, the digital filter was a simple mean filter that replaced the value of each data point with the average value of the nine samples before the point and the nine samples after it.* Although this filtering technique leaves the center of the event unchanged, the leading edge (which is used to locate the event) moves backward by nine sample points. This introduces a considerable error.

The example in figure 5.7 shows how digital filtering might introduce measurement errors, but these errors can also be introduced by analog filtering. To see how analog filtering introduces distance-measurement errors, let's begin by approximating reflections (in the linear time domain) as rectangular pulses. The result is a frequency-domain response that is[†]

$$H_r(f) = H \cdot D \frac{\sin(\pi f D)}{\pi f D} \quad [5.7]$$

In equation [5.7], H is the amplitude of the reflection and D is the width. From equation [5.7] we see that the response decays at a rate of

$$1/\pi f \quad [5.8]$$

Next, we approximate a nonreflective fusion splice as the convolution of the excitation pulse and the step loss that occurs across the event. In the time domain this is represented by

$$h_{nr}(t) = g(t) \cdot \text{step}(t) \quad [5.9]$$

In equation [5.9], $g(t)$ is the excitation pulse whose transform is given by equation [5.7] and $\text{step}(t)$ is the step loss across the event. The transform of equation [5.9] is

$$H_{nr}(f) = \frac{H \cdot D}{2j} \cdot \frac{\sin(\pi f D)}{(\pi f)^2 D} + \frac{H \cdot D}{2} \delta(f) \quad [5.10]$$

*This is a convolution filter, which is equivalent to a low-pass frequency-domain filter.

†This analysis was provided by William Trent of Tektronix, Inc.

It can be shown from equation [5.10] that the response decays at a rate of $1/(\pi f)^2 D$, which causes most of the energy in the return signal of a nonreflective event to be concentrated at low frequencies.

Common OTDR receivers typically have a transfer function that can be approximated by a three-pole Bessel filter. This type of filter provides reasonable noise reduction and a good transient response for reflections. For this filter, the delay for nonreflective events is²

$$\text{Delay}_{nr} = \frac{1.75}{2\pi f_c} s \quad [5.11]$$

In equation [5.11], f_c is the receiver's 3-dB cut-off bandwidth. That high-frequency delay affects reflective events can be derived from the group delay characteristics of the filter, but it is easier to use the filter's step-response information. If a somewhat arbitrary point of 10% of the pulse amplitude is picked as the start of the reflection, the delay for reflective events will be

$$\text{Delay}_r = \frac{0.8}{2\pi f_c} s \quad [5.12]$$

For receivers with relatively low bandwidth (<1 MHz), the predicted event delay can be significant, as shown in table 5.1.

Bandwidth (MHz)	Delay for reflective events (m)	Delay for nonreflective events (m)
2	6	14
1	13	28
0.4	32	70
0.2	64	139

Table 5.1. Theoretical delay for reflective events compared with nonreflective events for various bandwidths.

From table 5.1 you can see that errors resulting from bandwidth effects can have a significant impact on the distance-measurement accuracy of an OTDR. Although the data in table 5.1 were obtained from equations derived from simple assumptions, the errors predicted are roughly consistent with errors found in some commercial OTDRs. Table 5.2 shows the actual distance-measurement variations found on a commercially available mainframe OTDR produced by a respected

manufacturer. Observe that the average distance measured to nonreflective events changed by over 100 meters when the bandwidth was changed from 0.5 to 1.5 MHz.*

Event	Distance, test 1 (km)	Distance, test 2 (km)	Distance, test 3 (km)
1 NR	2.1541	2.0659 (-0.088)	2.0475 (-0.107)
2 NR	27.1429	27.0814 (-0.062)	27.0733 (-0.069)
3 NR	37.1795	37.1208 (-0.059)	37.0762 (-0.103)
4 NR	Not found	47.0725	47.0587 (-0.014)
5 R	48.0458	48.0412 (-0.005)	48.0443 (-0.005)
6 NR	Not found	54.8637	55.1498 (0.286)
7 R	56.0602	56.0587 (-0.002)	56.0624 (0.002)

Table 5.2. Comparison of the average distances measured with a commercially available OTDR's event-marking software using different bandwidths. Test 1 was conducted using a bandwidth of 0.5 MHz and a 10-microsecond pulse. Test 2 was conducted with a bandwidth of 0.5 MHz and a 3-microsecond pulse. Test 3 was conducted with a 1-microsecond pulse and 1.5-MHz bandwidth. The numbers in parentheses show the variance with respect to test 1, except when the software failed to find the event, in which case they show the variance with respect to test 2. This OTDR shows distance-measurement variability that depends on both bandwidth and pulse width.

The key point to remember is this: If you suspect that an OTDR's filtering is introducing distance-measurement errors, check its accuracy by measuring the distance to a given nonreflective event at multiple bandwidths. Do this by either engaging and disengaging the filtering option (sometimes called the dynamic-range mode) or by changing the pulse width. Alternatively, you can measure the distance to the reflective end of a fiber and then splice another fiber to the end. If the OTDR is properly designed, the distance to the reflective end of the fiber will be the same as the distance to the newly made fusion splice.

5.3.3 Other contributions to distance-measurement errors

In section 5.3.1 we examined the distance-measurement error caused by noise, pulse width, and the event's loss. In most applications, errors due

*This change in bandwidth was accomplished by acquiring the waveform in resolution mode (high-bandwidth filter) and then in dynamic-range mode (low-bandwidth filter).

to these effects dominate your distance-measurement error. There are other causes as well, however, and we examine a few of them here.

As we saw in chapter 3, OTDRs measure the time it takes for a signal to return to the instrument. Then the instrument calculates the distance by dividing the time in half, multiplying by the speed of light in a vacuum, and dividing by the fiber's group index using the equation $d = (c/2n)t$. From this equation we see that if the manufacturer programs the wrong value for the speed of light into the OTDR, the distance measurement will have an error. Equivalently, if the OTDR's time base has a significant error, then the distance measurement will also be in error. Time bases, however, are typically very accurate, often better than 0.001%. In this case, the maximum distance-measurement error resulting from time-base errors, for a 20-kilometer fiber, is less than 20 centimeters. Compared with the possible errors caused by waveform noise, sample density, waveform interpretation, and filtering, the error due to time-base calibration is typically inconsequential.

Since the OTDR uses the fiber's group index to calculate the distance to an event, errors in setting the group index contribute directly to distance-measurement errors. Unlike time-base errors, however, setting the wrong group index is purely an operator error. The OTDR cannot and does not set its own group index. You can find the group index by setting the index arbitrarily and then measuring the distance to the reflective end of a fiber of known length. Then, you adjust the OTDR's group index (sometimes called the IR, for "index of refraction") until the measured length shown on the OTDR equals the known length of the fiber. You can see that the process of calibrating the group index is subject to interpretive errors as well as sampling errors. You can mitigate this to a certain extent by using a well-cleaved fiber end. This gives a strong reflection at the end of the OTDR trace that is easier to locate accurately than a weak reflection or a fusion splice. To reduce the effects of sample spacing, cut the fiber back slightly.* Cut the fiber back slowly (cutting off only small lengths each time) and measure the amount of fiber removed. Continue cutting the fiber until you see the reflection move in by one sample point; then stop. The end of the fiber is now located on a sample point (to within the accuracy of the variations in your cutbacks). Subtract the amount of fiber cut from the known length,

*Make sure you cleave the fiber each time you cut it so that the end reflection stays consistently strong.

and set the OTDR's group index so the measured length is the same as this known length.*

The so-called time-of-flight method is another way to measure the group index of the fiber. Figure 5.8 shows the equipment required to perform this test. Using the time-of-flight method, you measure the time required for the OTDR's pulse to travel a known distance through fiber. From this, you can calculate the group index by taking the known length of the test fiber (determined by some means other than an OTDR), dividing by the measured time, and dividing this velocity into the speed of light. For example, suppose the test fiber is 101.235 kilometers long and that the time required for the light to pass through the test fiber is 500 microseconds. The group velocity in the fiber is then 202,470,000 meters per second. Dividing this into 299,792,458 meters per second (the speed of light in a vacuum), we have a group index of 1.4807.

Equivalently, the time-of-flight method may be used to verify the OTDR's built-in value for the speed of light, its time base, and the way it mathematically uses the index of refraction. To do this, set the index on the OTDR to any value. Next measure the distance to the end of the fiber using the OTDR. Now measure the transit time of the pulses using the equipment shown in figure 5.8. Calculate the length of the test fiber by dividing 299,792,458 m/s by the OTDR's displayed index of refraction

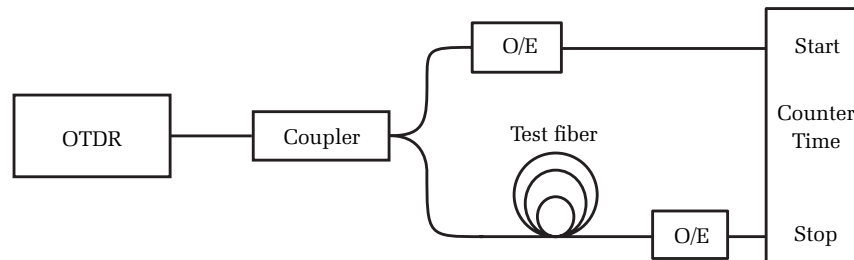


Figure 5.8. Equipment and setup used to verify the OTDR by the time-of-flight method. A zero reference is obtained by measuring the time differential between start and stop with the test fiber removed. It may be necessary to add a small length of fiber to the “Stop” path to ensure the stop pulse arrives after the start pulse. With the time delay known when the test fiber is out, replace the test fiber and measure the time delay again. This is the time delay for the test fiber, of known length, and allows the group velocity of the fiber to be calculated directly.

*This method of measuring the group index works well as long as there is not a calibration error in the location of the OTDR's zero point. The zero-point calibration error is sometimes called an offset error, not to be confused with waveform offset described in section 4.3.7.

and multiplying by the measured transit time. Compare this distance to the distance measured by the OTDR. These two distances should agree to within one sample spacing. If not, there may be a problem with the OTDR's time base, its stored value for the speed of light in a vacuum, or how it calculates distance from time and index data.*

The foregoing procedure determines the correct group index for the reference fiber of known length. If you use this group index for another fiber, however, you must expect some distance-measurement error because no two fibers have exactly the same group index. Suppose, for example, that you set your group index to 1.4780 using a reference fiber with a precisely known length. Now suppose you measure the length of another fiber that has (unknown to you) an index that is actually 1.4781. If you measure 50 kilometers of this fiber using 1.4780 as the index of refraction, the error due to the difference in the group index is approximately $-(\Delta n/n)d$, or about 3.4 meters.

Cabling errors are related to group-index errors. Cable manufacturers do not provide the index of refraction setting to match the optical cable, but pass through to the end user the fiber manufacturer's specifications. There is a great amount of difference when measuring a single fiber on a spool versus inside an optical cable. Consequently, the physical length of the fiber is different from the physical length of the cable. OTDRs, however, measure only the physical length of the fiber.†

The three major causes of inaccurate cable measurements are:

1. Fiber lay inside a loose tube buffer (see figure 5.9). The fiber length is actually longer than the buffer tube itself. This allows the cable and buffer tube to expand and contract with temperature without stressing the internal fiber.

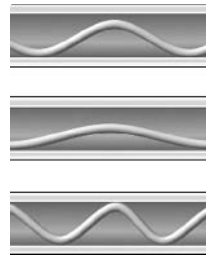


Figure 5.9. Optical fiber inside a loose buffer tube. [Credit: The Light Brigade.]

*Of course it is also possible that the equipment used to measure the time of flight is in error. So be careful to use only very accurate equipment, and be sure it is calibrated and in good repair.

†Actually, OTDRs measure the time required for light to travel to a given point on the fiber and then to return to the OTDR. This time is converted to a physical length, as we have just seen, by using the fiber's group velocity at the OTDR's wavelength.

2. Buffer tube's length. Buffer tubes do not lay lengthwise down an optical cable but spiral instead in one direction and periodically will reverse. This extra length of buffer tube versus the cable jacket (sheath) length adds an additional variation in the fiber versus cable length.
3. Inner and outer rows of buffer (see figure 5.10). When fiber counts within the cable exceed 72 fibers (six tubes with 12 fibers each), there is a high chance that the cable design is one provided in multiple rows of buffer tubes in both inner and outer positions. The inner row has less wrapping and total length, whereas the outer row must have larger wraps. Therefore, the external fibers must be longer than those in the internal rows. This requires extreme detailing on records. The inner layer fibers will be shorter and therefore use a different I.R. adjustment.

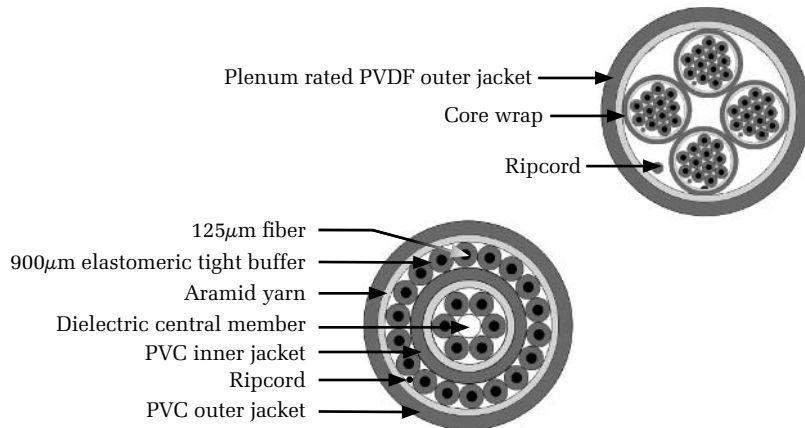


Figure 5.10. Example of inner and outer buffer tubes that would have different fiber lengths when measured with an OTDR.

By testing the cable with an OTDR, the user has the option to change the factory I.R. settings to those that will match the cable jacket's sequential markings. These recordings should be noted in any maintenance and restoration plans for more accurate locates.

You cannot assume that the distance to an event as measured by the OTDR is the same as the physical distance to the event as measured along the length of the cable. To make the latter measurement, you must know the cabling factor, or the ratio of the length of cable to the length of fiber inside it. To do this, you can calibrate the OTDR by using an equivalent cable group index of refraction as long as the cable has only

one row of buffer tubes. If there are two rows, then the process would be determined for each row. Determine the equivalent cable group index the same way you would determine the fiber index, except use a cable of precisely known length, as opposed to a fiber. Adjust the index of refraction until the OTDR measurement agrees with the physical length of the cable. This is the effective cable index. The cable group index typically has larger uncertainties associated with it because the cabling factor is not controlled as precisely as the fiber's group index. Some manufacturers mark the physical length of the cable along the outside, which makes it easier to measure the effective cable group index as well as to build an accurate map of the fiber plant (see figure 5.11).



Figure 5.11. Cable length marked on outside, in meters. [Credit: The Light Brigade.]

Another source of distance-measurement error becomes apparent when you compare the measurements of two different OTDRs. Not all OTDRs operate at exactly the same wavelength. Typically, OTDRs specify their testing wavelengths to tolerances of anywhere from ± 15 to ± 30 nm.³ Thus, it is possible for two OTDRs to have wavelengths that differ by up to 60 nm. The fiber's index of refraction changes with wavelength, however, so an index that is correct for one OTDR may not be correct for another. Wavelength errors are usually not very significant, especially when testing fibers near the zero-dispersion wavelength. At wavelengths far from the zero-dispersion point, the maximum error due to variations in wavelength can be several meters or more. For example, suppose you test 50 kilometers of standard fiber using an OTDR with a 1520-nm laser. Then you test the same fiber with a second OTDR having a wavelength of 1580 nm. Typical ITU-T G.652 non-dispersion-shifted fiber has a dispersion of roughly 17 ps/km-nm at 1550 nm. For a 50-km fiber, this corresponds to a difference of 120 ns.* Using a conversion

*The light must travel to the end of the fiber and back, for a 100-km roundtrip distance.

factor of roughly 10 ns per meter, we see this corresponds to an error of about 10 meters.

Yet another source of distance-measurement error results from offset errors. When an OTDR measures the distance to an event, it does so by assuming the start of the fiber is at a particular location, usually the instrument's front panel. If the start of the fiber is not at the front panel (due to a jumper, for example), then the distance-measurement error is directly affected. Similarly, if the OTDR's internal calibration mistakenly places the OTDR's front panel either before or after its true location, distance-measurement errors result. Errors caused by filtering can sometimes appear to be offset errors. For example, suppose the OTDR determines the zero point by locating the rising edge of the front panel's reflection. If this is the case, then the OTDR's distance error to some other reflective event due to filtering is small. This is because both the front panel and the reflective event have roughly the same measurement error, so the errors cancel when you take the difference between them. The distance error to nonreflective events, however, is large because filters typically shift nonreflective events differently than they do reflective events. Since the reflective and nonreflective events have different errors, they do not cancel when you take the difference between them. The distance-measurement error caused by filtering is constant for nonreflective events, irrespective of their distance from the OTDR. This gives the error the appearance of being caused by front-panel calibration offset, when it is really caused by filtering.

All the secondary errors we have discussed can be important when measuring distances to either reflective or nonreflective events. For reflective events, however, these secondary effects usually constitute a greater fraction of the total error than they do for nonreflective events. For nonreflective events, the dominant sources of distance-measurement error are noise, the interpretive algorithms, and filtering effects (if they exist). As we shall see in chapter 11, various event-marking algorithms can have significant differences in their distance-measurement accuracy and repeatability. For nonreflective events, perhaps the best way to ensure accurate and repeatable distance measurements is to pick an OTDR with the most advanced algorithms.

5.4 Summary

In this chapter we have seen that distance measurements of nonreflective events are more complex than many operators might expect. Distance-measurement errors depend on such things as the local waveform noise,

offset errors, time-base errors, errors in setting the index of refraction, and interpretive errors.

Estimating distance-measurement error is probably beyond the desires and capabilities of most OTDR operators. Even if an operator wanted to calculate the measurement uncertainty, the details of event-marking algorithms are proprietary and are unknown to him or her. This makes it almost impossible for the operator to calculate the expected errors in the instrument's measurements. The only practical way for the operator to know the measurement uncertainty is for the OTDR to calculate it specifically for each event. We summarize the various contributors to distance-measurement error, in roughly increasing order of importance:

- Waveform interpretation and algorithms
- Waveform noise
- Improperly designed smoothing filter
- Sample spacing
- Cabling structure factors
- Wrong setting for the index-of-refraction
- Wavelength differences between different OTDRs
- Time-base errors

Chapter 6 discusses the issues related to loss-measurement accuracy. These issues generally apply equally well to both reflective and nonreflective events.

Suggested reading

Bulmer, M. G., *Principles of Statistics* (New York: Dover, 1979).

Croxton, F. E., *Elementary Statistics* (New York: Dover, 1953).

Generic Requirements for Optical Time-Domain Reflectometer (OTDR) Type Equipment, GR-196-CORE (Bellcore, 1995).

Calibration of Optical Time-Domain Reflectometers, IEC TC86 (1994).

Shinn, G., "Practical OTDR cable measurements," *Test & Measurement World* (October 1987).

Danielson, B. L., "Optical time-domain reflectometer specifications and performance testing," *Applied Optics*, Vol. 24, No. 15 (1985).

Problems

1. True or false: Reflective events are caused by things like fusion splices and bends.
2. True or false: Nonreflective events show up as a drop in the fiber backscatter.
3. True or false: The biggest source of distance-measurement error in OTDRs is the time base.
4. True or false: In tests of repeatability, human operators are more consistent than a properly designed numerical algorithm.
5. True or false: When measuring the distance to a nonreflective event, the error remains relatively constant until the noise reaches a threshold, and when the noise exceeds this threshold the error increases dramatically.
6. True or false: If the amount of noise is kept constant, the distance-measurement error is less for larger pulses than for smaller pulses.
7. True or false: All fibers have the same group index of refraction.
8. True or false: Filters can reduce the noise in a waveform and also move events.
9. True or false: OTDRs can differ in their distance measurements because they have lasers of slightly different wavelengths.
10. True or false: The distance along the fibers inside a cable is the same as the distance along the cable.

¹ Anderson, D. R., "Multi-acquisition algorithms for fully optimized analysis of OTDR waveforms," *NFOEC Conference*, Session 15, 1996.

² Zverev, A. I., *Handbook of Filter Synthesis* (New York: Wiley, 1967).

³ *Generic Requirements for Optical Time-Domain Reflectometer (OTDR) Type Equipment*, GR-196-CORE (Bellcore, 1995).

Chapter 6

Loss-measurement error

6.0 Introduction

In the previous chapter we discussed how to measure the distance and loss of nonreflective events. We introduced the concept of measurement error and showed that distance-measurement error results from a combination of waveform noise and calibration errors.

This chapter is devoted exclusively to discussion of the sources of loss-measurement errors. We reserve discussions about loss-measurement error for this chapter because these are largely universal in nature, being mostly the same for both reflective and nonreflective events.

Like distance-measurement errors, loss-measurement errors are also highly dependent on noise, measurement algorithms, calibration, and methodology. In this chapter we show how to estimate the amount of loss-measurement error as a function of the local waveform noise and of LSA parameters. We also show that certain methodological errors that result from splicing dissimilar fibers can be eliminated by measuring the loss from both ends of the fiber and then averaging.* In the next chapter we discuss specific issues of measurement accuracy as they apply to reflective events.

6.1 Loss-measurement errors caused by waveform noise

As with any instrument, an OTDR's measurement accuracy is ultimately limited by noise. Consider figure 6.1, for example. Here we see a portion of the sampled OTDR waveform around a nonreflective event. Because of noise, the Rayleigh backscatter trace before and after the event is undulating, with peaks and valleys. These peaks and valleys result primarily from noise in the OTDR's receiver and are fundamentally random in nature.† Understanding the data points in the waveform to be random variables, we immediately see that the slope and offset of the linear fit to the waveform are also random variables. Since these linear fits are used in the loss-measurement algorithms, we see that the loss measurement itself is a random variable as well.

*This technique applies only to measurements on single-mode fibers.

†This is strictly true only for well-designed OTDRs that do not have synchronous system noise.

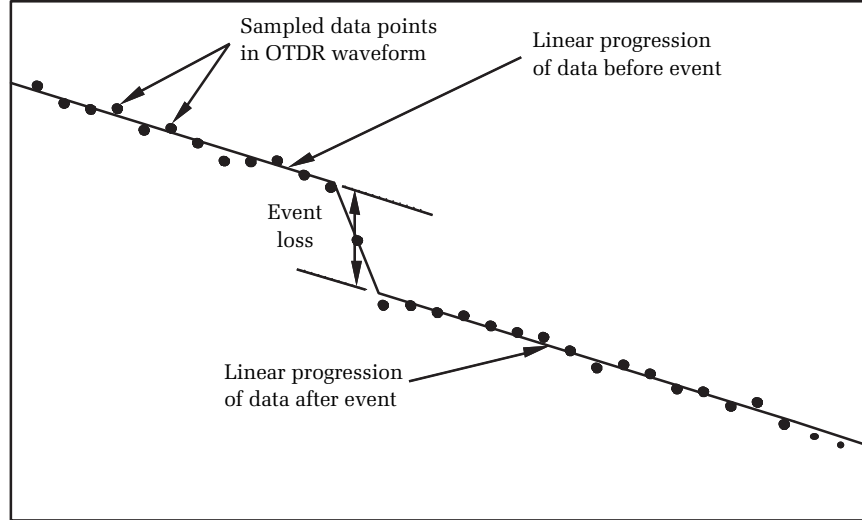


Figure 6.1. Various parts of the OTDR waveform around a nonreflective event. Note how the sampled data points contain noise. The linear regressions minimize the impact of the noise, but random errors still occur when estimating the event's loss.

To evaluate the loss-measurement uncertainty of the linear regression method, we must calculate the variability in the slope and the y -axis intercept of the least-squares fit lines. To do this, we begin by writing the equations for the slope and y -axis intercept of the linear regression of a set of n data points:¹

$$y = a + b \cdot x \quad [6.1]$$

$$b = \frac{\sum_i x_i y_i - N \cdot \bar{x} \cdot \bar{y}}{\sum_i x_i^2 - N \cdot \bar{x}^2} \quad [6.2]$$

$$a = \bar{y} - b \cdot \bar{x} \quad [6.3]$$

We define the y -axis so it passes through the center of the event. The linear regression extends from $-W/2$ to $-W/2 - L$ on the left of the event, and from $W/2$ to $W/2 + L$ on the right. Here, W is the pulse width (as seen on the OTDR display) and L is the length of the linear regression (assumed to be the same on each side of the event). We also assume the sampled data points are evenly distributed along the horizontal axis (this

is true for virtually all OTDRs) and the sample spacing is Δx . Under these assumptions, \bar{x}^2 is $[(W + L)/2]^2$. We have, for the measured loss of the event, $\text{Loss} = a_1 - a_r$, where a_1 is the y -intercept for the left-hand linear fit and a_r is the y -intercept for the right-hand linear fit. Next we assume the loss is sufficiently small that the standard deviation of the waveform noise on the right side of the event is essentially the same as that on the left side of the event.* In this case, $V(a_1) = V(a_r) = V(a)$, where $V(a)$ denotes the variance of the y -intercept. Thus, the variance of the splice loss is

$$V(\text{Loss}) = 2V(a) \quad [6.4]$$

The variance of the y -intercept is

$$V(a) = V(\bar{y} - b \cdot \bar{x}) = V(\bar{y}) + \bar{x}^2 V(b) \quad [6.5]$$

We define the variance of the waveform noise as σ_{dB}^2 . Substituting this into equation [6.5], and using the expression for the variance of a linear slope, we have²

$$V(a) = \frac{\sigma_{\text{dB}}^2}{N} + \sigma_{\text{dB}}^2 \cdot \frac{\bar{x}^2}{\sum (x_i - \bar{x})^2} = \sigma_{\text{dB}}^2 \left(\frac{1}{N} + \frac{\bar{x}^2}{\sum (x_i - \bar{x})^2} \right) \quad [6.6]$$

N is simply the length of the linear regression, L , divided by the sample spacing. Making this substitution, and simplifying, we write the variance of the loss as

$$V(\text{Loss}) = \frac{2\sigma_{\text{dB}}^2 \Delta x}{L} \cdot \left(1 + \frac{3(W + L)^2}{(L^2 + 2\Delta x^2)} \right) \quad [6.7]$$

Equation [6.7] expresses the loss-measurement variance as a function of the standard deviation of the localized waveform noise. To finish our derivation, we need to express this standard deviation as a function of some readily obtainable parameter. A good choice for such a parameter is the height (along the OTDR's vertical scale) from the event to the OTDR's noise floor. Using the convention from chapter 4,

*Since the Rayleigh scattering on the right side of the event is closer to the noise floor, the peak-to-peak noise on the log display is higher there than on the left side of the event. As long as the loss is not too great, the difference is relatively small. This is true only because we are working in the log domain. In the linear domain, of course, the noise level is constant.

we approximate the noise floor as twice the noise standard deviation.* The height from the event to the noise floor, which we call δ , is easily measured on most OTDRs. The standard deviation of the local waveform noise is

$$\sigma_{\text{dB}} = \sqrt{\frac{1}{N} \left[\sum_i \left[\left(5 \log(w_i + n_i) \right) - 5 \log(w_i) \right]^2 \right]} \quad [6.8]$$

In equation [6.8], w_i represents the linear waveform data and n_i the linear noise that is added to the linear waveform data by the OTDR's acquisition circuitry and optical receiver. By taking the first two terms of the Taylor's expansion of the logarithms and simplifying, we have

$$\sigma_{\text{dB}}^2 = \frac{1}{N} \left[\sum_i \frac{n_i^2}{w_i^2} \cdot \left[\frac{5}{\ln(10)} \right]^2 \right] \quad [6.9]$$

By definition, $\delta = 5 \log(w/2\sigma_n)$ where σ_n is the standard deviation of the linear noise. Substituting this definition of δ into equation [6.9], simplifying, and evaluating to three significant digits, we have

$$\sigma_{\text{dB}} = 1.09 \cdot 10^{-0.2\delta} \quad [6.10]$$

Substituting equation [6.10] into equation [6.7] and expressing the loss uncertainty as twice the loss-measurement standard deviation, we have

$$\text{Loss}_{\text{uncertainty}} = 3.071 \cdot 10^{-0.2\delta} \cdot \sqrt{\frac{\Delta x}{L} \left(1 + \frac{3(W+L)^2}{(L^2 + 2\Delta x^2)} \right)} \quad [6.11]$$

Equation [6.11] gives the 2-sigma loss-measurement uncertainty as a function of δ , W , L , and Δx . Here, δ is the height in decibels, as seen on the OTDR display, from the event to the noise floor (as defined by Bellcore; see chapter 4). The pulse width, as viewed on the OTDR display, is W , and L is the length of the linear regression. The distance between sample points in the OTDR's waveform is Δx . Remember also that equation [6.11] assumes the splice loss is sufficiently small that the waveform noise is essentially the same on both sides of the event. It also

*There are many ways of describing an OTDR's noise floor. We discuss several of them in chapter 4. Here, we describe the noise floor as twice the standard deviation of the waveform noise.

assumes the fiber slope is the same on both sides of the event and that the length of the linear fit is the same on both sides of the event.

As an example, suppose an event is 5 dB above the noise floor, the OTDR's pulse width is 500 meters, the sample spacing is 10 meters, and the linear fits on each side of the event are 1 km long. Using equation [6.11], we see that the 2-sigma loss-measurement uncertainty is 0.09 dB. If the event were 3 dB from the noise floor, the measurement uncertainty would be 0.21 dB; if the event were 7 dB from the noise floor, the uncertainty would be 0.03 dB. At the noise floor, the event uncertainty is about 1 dB.

In figure 6.2 we have plotted a few values from equation [6.11]. Notice that loss-measurement uncertainty, like distance-measurement uncertainty, remains relatively low and constant until the event falls below a certain threshold. When the event falls below the threshold, the loss-measurement uncertainty rises very quickly. The threshold depends on the number of waveform points used in the linear regression. As the number of points increases, the threshold drops. In other words, as the number of waveform points increases, the loss-measurement uncertainty decreases, and the usable range over which the OTDR can make accurate loss measurements also increases. Of course events (such

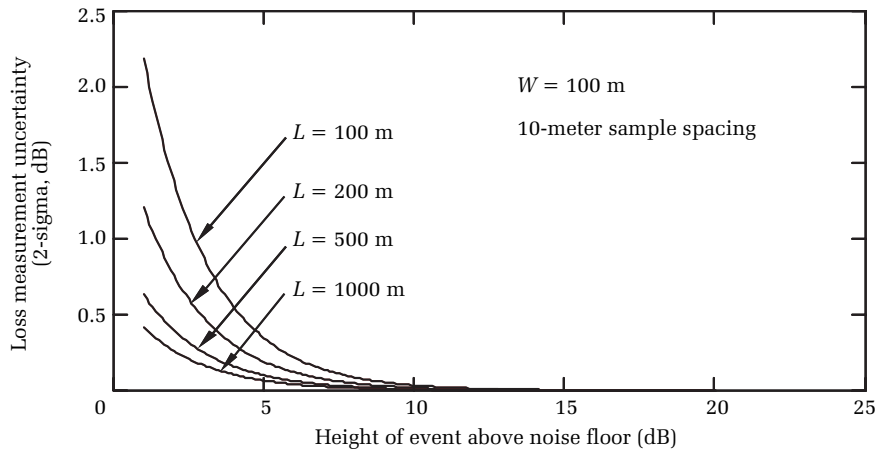


Figure 6.2. Loss-measurement uncertainty as a function of the event's height above the noise floor. Notice that the measurement uncertainty has a threshold. Above the threshold the measurement uncertainty is relatively stable and very good. Below the threshold, the measurement uncertainty changes rapidly and quickly degrades. Observe also that the measurement uncertainty improves as L (the length of the linear regression) increases.

as fusion splices) must be farther apart than the distances used in the linear regression, so once again we see a trade-off between measurement uncertainty, dead zone, and distance between events.

Manufacturers typically specify the OTDR's dynamic range as the height from the backscatter level near the OTDR's front panel to the noise floor. From the analysis we have just completed, however, you can see that the usable measurement range of the OTDR is considerably less. If you are measuring splices with small loss and you want less than 0.1 dB loss-measurement uncertainty, then the usable measurement range is several decibels less than the specified dynamic range. If you know the pulse width, sample spacing, and the distance between events, then you can use equation [6.11] to determine roughly the difference between the OTDR's measurement range and dynamic range for your particular application.*

Although you can calculate the loss-measurement uncertainty by using equation [6.11] and a calculator, it is far more convenient if the OTDR performs this calculation. When examining an OTDR's features, check to see that it calculates and displays the uncertainties for both the loss measurement and the distance measurement.

Before closing this section on loss-measurement uncertainty, consider again the threshold nature of the loss-uncertainty curve in figure 6.2. Notice that there is little advantage in having the event much farther above the noise floor than the threshold, because this does little to improve the loss-measurement uncertainty. Reviewing figures 5.3 through 5.6, we see a similar situation for the distance-measurement uncertainty. There is little advantage in having more dynamic range than what is sufficient to position a given event above the threshold. There are, however, disadvantages in having an event too far above the noise floor, because dynamic range is never free. It always exacts a toll in terms of acquisition time, dead zone, and cost.

Since dynamic range comes at a cost, it is disadvantageous to have more of it at a given event than is required to bring the event above the local threshold for loss- and distance-measurement uncertainty. This is an extremely important point because it shows the weakness of standard acquisition systems. Standard systems acquire data by testing with just one pulse width. Often many events on the fiber are more than 25 dB above the noise floor. This is an extreme waste of dynamic range, since

*Be careful to correct for any differences between how the OTDR manufacturer defines the noise floor and how we defined it in the derivation of equation [6.11].

events located so far above the noise floor have little better distance- and loss-measurement uncertainty than events located 10 dB lower. This means the events could have been acquired using shorter pulse widths, improving two-event resolution. In chapter 10 we describe software algorithms that control the OTDR's acquisition parameters and automatically change the pulse width and averaging for each event in the waveform. These intelligent algorithms optimize the acquisition parameters so that each event is acquired closer to the threshold regions shown in figures 5.3 through 5.6 and figure 6.2. The algorithms then display a composite waveform consisting of sections acquired with different pulse widths.

6.2 Loss-measurement errors due to mismatch of single-mode fibers

OTDRs measure loss by comparing the strength of the Rayleigh scattering on each side of the fusion splice. OTDR loss measurements, therefore, are based on the assumption that the scattering characteristics and the capture ratios of the two fibers are identical. This is never the case. There are always at least minute differences between the fibers. Because of this, each loss measurement has some degree of uncertainty arising from the fact that the splice joins different types of fibers.

Figure 6.3 is a schematic representation of an OTDR's laser pulse traveling down an optical fiber. The horizontal axis represents distance along the fiber, and the vertical axis represents the time since the leading edge of the pulse passed through the OTDR's front-panel connector. The broad horizontal line extending from $L - D$ to L represents the pulse at some arbitrary time t_1 .^{*} All light paths follow world lines with either positive or negative slopes of n_g/c , where n_g is the fiber group index and c is the speed of light in a vacuum. World lines with positive slopes move away from the OTDR; world lines with negative slopes move toward it. Notice that the distance and time scales in figure 6.3 have been chosen such that the angle between the world lines and either axis is 45° .

When the OTDR launches a laser pulse into the fiber, the backscatter signature at a given point on the OTDR display is the integrated sum of backscatter from different locations along the optical fiber. Refer again to figure 6.3. Suppose after traveling a distance L (corresponding to time t_1), a portion of the light in the leading edge of the pulse is scattered back toward the OTDR. (Actually, light is continually scattered from the pulse.

^{*} D is the pulse width on the fiber (twice the displayed pulse width).

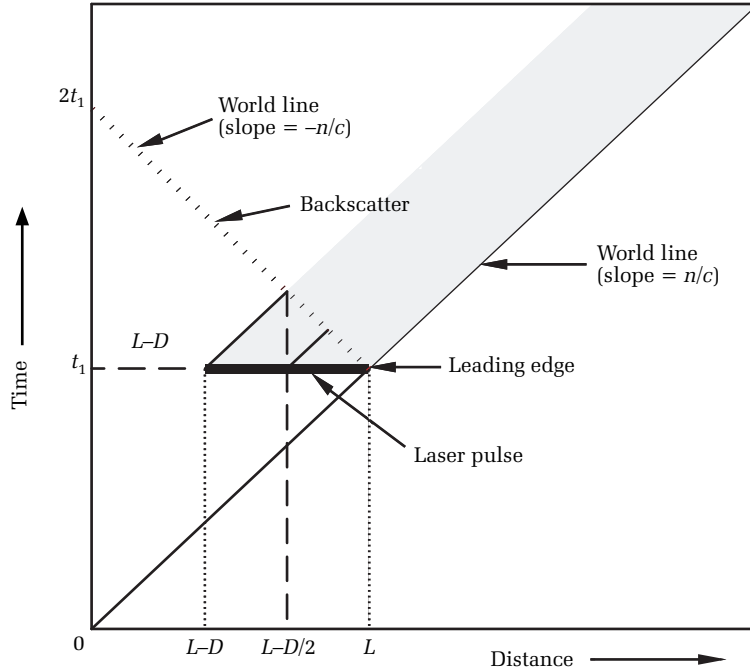


Figure 6.3. Schematic depiction of a laser pulse traveling down an optical fiber. The backscatter arriving at time $2t_1$ is scattered from points on the fiber between $L - D/2$ and L .

In this example, we do not intend to suggest any special significance about the time t_1 . The example is illustrative only; we are considering one possible time out of a continuum.) Accordingly, it arrives at the OTDR after time $2t_1$. Scattered light from the trailing edge also arrives at time $2t_1$. This light, however, scatters from a distance $L - D/2$, where D is the pulse width on the fiber. Similarly, backscattered light from any arbitrary portion of the pulse, $L - x$, arrives at the OTDR at time $2t_1$ when the backscatter originates from a point $L - x/2$ on the fiber.

The differential scattering from an infinitesimally short section of fiber is^{3,4}

$$dp(x) \propto k \cdot P(x)dx \tag{6.12}$$

where $k = \alpha_s S$. In equation [6.12], S is the fraction of the light scattered by the fiber element dx at the scattering point x , which is scattered backward toward the OTDR and captured by the fiber. The scattering coefficient (1/km) is α_s , and $P(x)$ is the instantaneous power of the pulse, over the differential pulse width dx , at the scattering point.

If we assume the OTDR uses pulses that are temporally square (a good assumption in most cases), then we have the following proportionality for the total backscattered power received at the OTDR at time $2t_1$ (corresponding to a displayed distance of L):

$$p(L) \propto k \cdot P_0 \int_0^D \exp\left(-2\alpha\left(L - \frac{x}{2}\right)\right) dx = \frac{\alpha_s S \cdot P_0}{\alpha} \cdot \exp(-2\alpha L) [\exp(2\alpha W) - 1] \quad [6.13]$$

In equation [6.13], W is the pulse width displayed by the OTDR and α is the attenuation coefficient (1/km) of the optical fiber. Note that W is half as wide as the actual pulse width D and that α is roughly equal to the scattering coefficient α_s for good-quality single-mode fiber.*

In chapter 3 we saw that the capture ratio, S , depends on the specific fiber parameters. For single-mode fiber, the scattering coefficient is nearly constant over a relatively large range of the normalized frequency. If the normalized frequency, V , is in the range $1.5 < V < 2.4$, then the capture ratio is given approximately as (see also equation [3.6])^{5,6,7,8}

$$S \approx \frac{1}{4.55} \left(\frac{\text{NA}}{n}\right)^2 \quad [6.14]$$

In equation [6.14], NA is the fiber's numerical aperture and n is the core index.

Substituting equation [6.14] into equation [6.13], we have (for square pulses)

$$p(L) \propto \left(\frac{\text{NA}}{n}\right)^2 \cdot \frac{1}{4.55} \cdot \frac{\alpha_s}{\alpha} \cdot P_0 \exp(-2\alpha L) [\exp(2\alpha W) - 1] \quad [6.15]$$

In equation [6.15], L is the distance from the OTDR to the point of measurement (the splice location, if we are measuring the backscatter just before the splice). The average power of the optical pulse as it leaves the OTDR is P_0 , and W is the OTDR's displayed pulse width. The fiber's scattering coefficient (1/km) is α_s , the fiber's attenuation coefficient (1/km) is α , NA is the fiber's numerical aperture, and n is the refractive index of the fiber's core.

*This is a point of confusion for some readers. The actual length of the pulse on the fiber is twice the displayed pulse width as seen on the OTDR's waveform. This is because the OTDR's time base is divided by 2 to account for the fact that the light must travel twice the length of the fiber in the time shown on the OTDR display corresponding to the fiber's length (refer also to chapter 3).

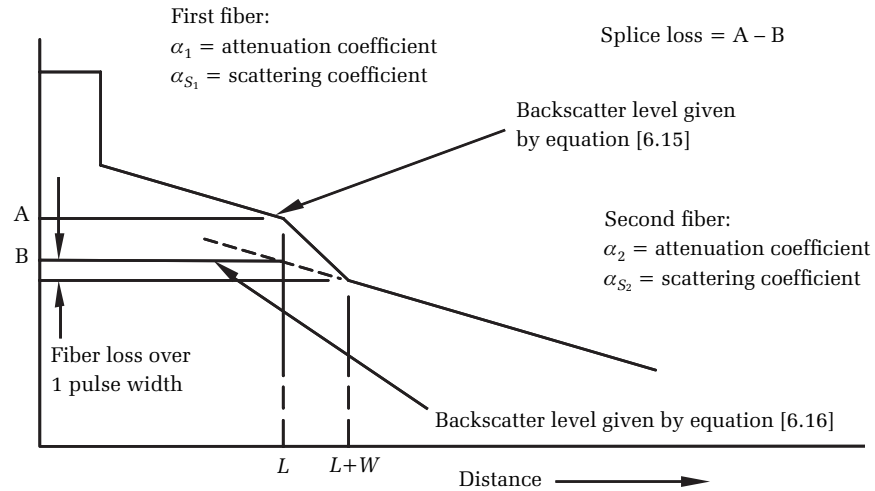


Figure 6.4. Proper measurement of nonreflective splice loss with fiber slope removed.

As we have seen, an OTDR measures splice loss by comparing the backscatter just before the splice to the backscatter about one pulse after the splice and then subtracting the expected fiber attenuation between the two measurement points, as shown in figure 6.4.* After removing the expected fiber loss, the strength of the backscatter in the second fiber, just after the splice, is

$$p(L) \propto \left(\frac{1}{L_f}\right)^2 \left(\frac{NA_2}{n_2}\right)^2 \cdot \frac{1}{4.55} \cdot \frac{\alpha_{s_2}}{\alpha_2} \cdot P_0 \exp(-2\alpha_1 L) [\exp(2\alpha_2 \cdot W) - 1] \quad [6.16]$$

In equation [6.16], L_f is the fractional loss of the splice (defined as the ratio of the optical power before the splice to the optical power after the splice).[†] The fractional loss is squared because light that is scattered back to the OTDR from the second fiber must pass through the splice twice. It is important to note that, unlike multimode fiber, the true loss in single-mode fiber is bidirectional.^{9,10}

Recall from chapter 3 that OTDRs calculate loss as 5 times the log of the ratio of the backscatter just before the splice to the backscatter just after the splice. A factor of 5 is used instead of 10 because all the

*Subtracting the fiber loss is done automatically when you fit the cursors to the backscatter and measure the loss as the vertical separation of the cursors at the middle of the event.

[†]Note that in equation [6.16], n_2 is the core index of the second fiber, not a cladding index.

light that reaches the OTDR must travel through the intervening fiber and events twice, once going in each direction. Consequently, the loss of a splice as measured by the OTDR (after removing expected fiber loss between the measurement points) is

$$L_{m_{1,2}} = 5 \log \left(\frac{\left(\frac{\text{NA}_1}{n_1} \right)^2 \cdot \frac{1}{4.55} \cdot \frac{\alpha_{S_1}}{\alpha_1} \cdot P_0 \exp(-2\alpha_1 L) [\exp(2\alpha_1 W) - 1]}{\left(\frac{1}{L_f} \right)^2 \left(\frac{\text{NA}_2}{n_2} \right)^2 \cdot \frac{1}{4.55} \cdot \frac{\alpha_{S_2}}{\alpha_2} \cdot P_0 \exp(-2\alpha_1 L) [\exp(2\alpha_2 W) - 1]} \right) \quad [6.17]$$

$$L_{m_{1,2}} = 5 \log(f_{p_1}) - 5 \log(f_{p_2}) + 10 \log(L_f) + 5 \log(\exp(2\alpha_1 W) - 1) - 5 \log(\exp(2\alpha_2 W) - 1) \quad [6.18]$$

In equation [6.18], f_{p_1} and f_{p_2} represent constants that are determined by the design parameters of fibers 1 and 2, respectively. If we measure the splice loss from the other end of the fiber, we have the same equation as [6.18], but with the indices interchanged:

$$L_{m_{2,1}} = 5 \log(f_{p_2}) - 5 \log(f_{p_1}) + 10 \log(L_f) + 5 \log(\exp(2\alpha_2 W) - 1) - 5 \log(\exp(2\alpha_1 W) - 1) \quad [6.19]$$

Equations [6.18] and [6.19] show that the true loss of the splice equals the measured loss whenever the fiber parameters on each side of the splice are equal. However, when different types of fiber are spliced together, these fiber parameters are usually not exactly equal. When this happens, the measured splice loss and the true splice loss are different. Even in such cases we can still determine the true splice loss by measuring the splice from both ends of the fiber and then averaging:*

$$\frac{L_{m_{1,2}} + L_{m_{2,1}}}{2} = \frac{10 \log(L_f) + 10 \log(L_f)}{2} = 10 \log(L_f) \equiv L \quad [6.20]$$

Thus we see that the two-way average of the OTDR's loss measurements equals 10 times the base-10 logarithm of the fractional splice loss, which by definition is the true splice loss in dB.

*Note, however, that this is strictly true only if we use the same OTDR pulse width for both measurements.

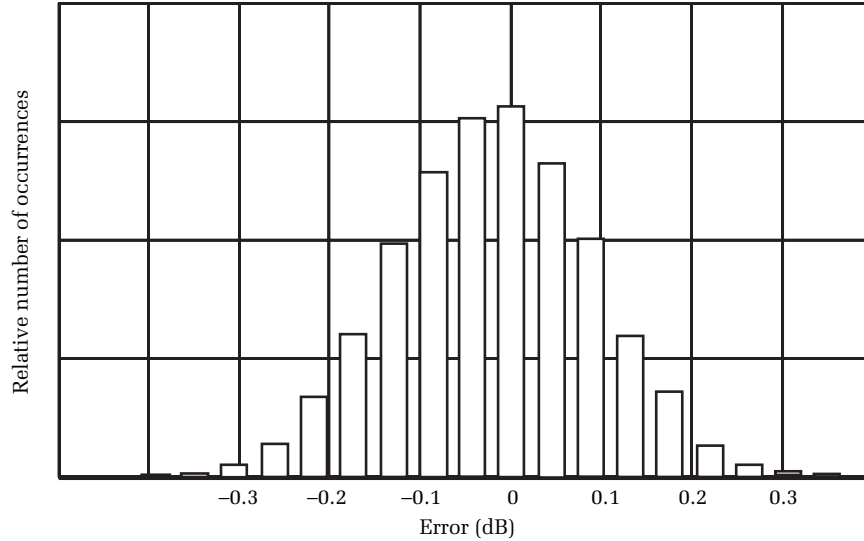


Figure 6.5. Histogram of the loss-measurement error resulting from a single-ended OTDR measurement of a fusion splice between two fibers. In this Monte Carlo analysis, we assumed the fiber numerical aperture to be 0.13 with a 1-sigma variation of 0.0023 (1.769%). This is roughly consistent with normal variations in the numerical aperture of single-mode fibers of the same type from the same manufacturer.

Figure 6.5 is a histogram illustrating the kinds of errors that fiber mismatch can cause, even when splicing two fibers of the same type from the same manufacturer. Errors of more than 0.1 dB are not uncommon or unexpected. This represents a significant source of error. For splices with loss specifications less than about 0.2 or 0.3 dB, it is generally necessary to measure from both ends of the fiber and to average according to equation [6.20]. Otherwise, errors caused by possible mismatch in the fiber parameters may be excessive.

6.3 Loss-measurement errors on multimode fiber

Splice loss in multimode fibers, unlike single-mode fibers, is not bidirectional. Consider, for example, a piece of 50/125- μm multimode fiber spliced to a piece of 62.5/125- μm fiber.* There is very little splice loss with the transmitter attached to the 50/125- μm fiber and considerably

*The first number is the core diameter in microns, and the second number is the cladding diameter, in microns. Thus, 50/125- μm multimode fiber has a core diameter of 50 μm and a cladding diameter of 125 μm .

more loss with it attached to the 62.5/125- μm fiber. Table 6.1 shows that the diameter and numerical aperture of the 50/125- μm fiber are both less than those of the 62.5/125- μm fiber. Consequently, when launching light from the 50- μm fiber into the 62.5- μm fiber, it is easy to couple light from all the modes. Upon reversing the situation, however, you find there are modes in the 62.5- μm fiber that do not couple into the 50- μm fiber. Some modes do not couple because they are spatially too large to match the modes in the smaller fiber. Others fail to couple because their angular divergence is too large, because the 62.5- μm fiber has a larger numerical aperture (NA) than the 50- μm fiber.

Manufacturer	Size (microns)	Index of refraction		Attenuation (dB/km)		Max distance (m)	
		850	1300	850	1300	850	1300
<i>Laser enhanced multimode fibers</i>							
Alcatel Glight 6931	62.5/125	1.497	1.492	≤ 2.9	≤ 0.8	—	—
Avaya							
LazrSPEED 150	50/125	1.483	1.478	≤ 3.5	≤ 1.5	600	600
LazrSPEED 300	50/125	1.483	1.478	≤ 3.5	≤ 1.5	600	600
OptiSPEED Plus	62.5/125	1.496	1.491	≤ 3.5	≤ 1.5	300	300
Corning							
Infinicor 600	50/125	1.490	1.486	≤ 2.5	≤ 0.8	600	600
Infinicor 300	62.5/125	1.496	1.487	≤ 3.0	≤ 0.7	300	550
Infinicor 2000	50/125	1.490	1.486	≤ 2.5	≤ 0.8	600	2000
Infinicor 1000	62/125	1.496	1.487	≤ 3.0	≤ 0.7	500	1000
Draka/Plasma							
Max-Cap	50/125	1.482	1.477	≤ 2.5	≤ 0.7	600	1000
Hi-Cap	62.5/125	1.496	1.491	≤ 3.0	≤ 0.7	500	1000
FiberCore							
GigaGrade 750	50/125	1.483	1.478	≤ 2.8	≤ 1.0	750	2000
GigaGrade 400	62.5/125	1.497	1.493	≤ 3.2	≤ 1.0	400	1000
OFS							
Lazrwave 150	50/125	1.484	1.497	≤ 2.4	≤ 0.7	750	550
Lazrwave 300	50/125	1.484	1.497	≤ 2.4	≤ 0.7	1000	550
Gigaguide 50	50/125	1.483	1.479	≤ 2.4	≤ 0.7	600	600
Gigaguide XL	50/125	1.483	1.479	≤ 2.4	≤ 0.7	600	2000
Gigaguide 62.5	62.5/125	1.496	1.491	≤ 2.9	≤ 0.7	400	550
Gigaguide XL	62.5/125	1.496	1.491	≤ 2.9	≤ 0.7	500	1000

Table 6.1. Physical and optical properties of common multimode optical fibers. Fiber sizes are in microns, and they state the diameter of the core/cladding.

It would be nice if there were a simple formula that allowed you to calculate the insertion loss between different multimode fibers.

Unfortunately, there is not.* Part of the complexity of this problem arises from the fact that the loss depends on the modal distribution.¹¹ We saw in chapter 2 that multimode fibers have hundreds of modes. The modal distribution refers to the relative amount of optical power in these modes. Typically, all the modes carry some of the optical power, with the central (lower-order) modes carrying more than the outer (higher-order) ones (see figure 6.6) This need not always be the case, however. It is possible to overexcite either the higher-order or the lower-order modes, depending on the type of transmitter used, and the type and placement of events such as connectors and splices. To see how this might affect the loss of the splice, let's return to our example of the 50/125- μm fiber with a numerical aperture (NA) of .20 being spliced to the 62.5/125- μm fiber with an NA of .275.

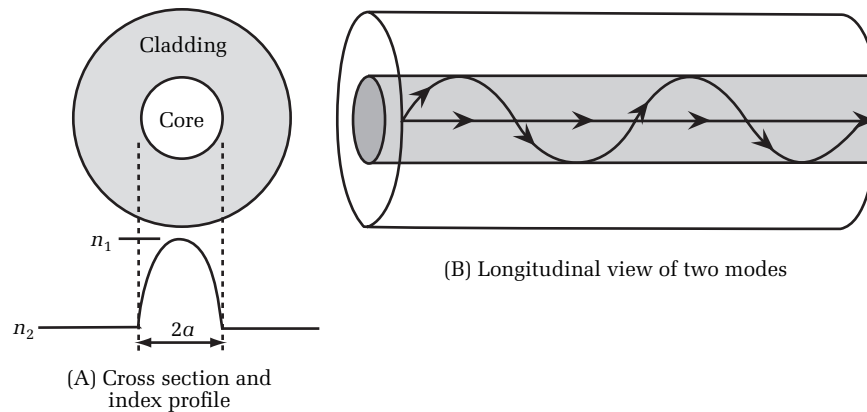


Figure 6.6. Higher- and lower-order modes in a multimode fiber core.
[Credit: The Light Brigade.]

It is possible to launch light into 62.5- μm multimode fiber with a single-mode laser such that only the fiber's lowest-order modes are excited. This is because the focused spot of the single-mode laser can be made small and not too divergent. In this condition it overlaps well with the low-order modes but poorly with the higher-order ones. With the low-order modes excited, most of the energy travels through the fiber's

*There are some approximations. One is to take the ratio of the square of the product of the numerical aperture and the core diameter. This approximates the loss when coupling from a fiber with a larger NA and diameter into one with a smaller NA and diameter. This is only a *rough approximation*, however, because it does not take into account the mode distribution in either fiber. With an equilibrium mode-field distribution, loss estimation with this method is typically accurate to within 0.5 or 1.0 dB.

central core. If you were to magnify the end of this fiber and image it, you would see an illuminated area that is smaller than the 62.5- μm fiber core. Depending on how far the light traveled and on exactly how you coupled it to the fiber, it is possible that the illuminated area of the core would be less than 50 μm . When this is the case, the light can couple efficiently from the 62.5- μm fiber to the 50- μm core without much, if any, loss. In this example the splice loss is low. New local-area network (LAN) standards, such as the IEEE 802.3 Gigabit Ethernet standard and the ANSI Fibre Channel interfaces operating at data rates in excess of 1 Gb/s, have VCSEL lasers as light sources and use both 50/125 and 62.5/125 multimode fibers for signal transmission.

Lower-speed LAN protocols operating up to 622 Mb/s with multimode fiber use the cost-effective LED as the common light source. Now suppose you use an LED instead of a single-mode laser. LEDs emit light from a relatively large area, so they cannot be collimated well or focused to tight spots. When coupling to a multimode fiber, the illumination pattern from an LED can fill both the high-order and the low-order modes. The highest-order modes are the most weakly guided, so these modes are usually stripped off rather quickly. Let's assume the 62.5/125- μm fiber is relatively short, so the high-order modes are still excessively populated when the light gets to the splice between the 62.5- and 50- μm fibers. If this is the case, the light distribution at the splice is much larger than the core of the 50- μm fiber. Furthermore, the divergence of the light from the higher-order modes in the 62.5- μm fiber exceeds the .20 numerical aperture of the 50- μm fiber. Consequently, the splice's loss looks relatively high.

Suppose we locate the 50- μm fiber a long distance from the point where the LED injects light into the 62.5- μm fiber. As the light travels along the fiber, it encounters inevitable bends, pinch points, additional connectors, etc. These events remove light from the higher-order modes more efficiently than they do from the low-order modes. At the beginning of the fiber, attenuation (dB/km) is higher than it is after the light travels farther away.* As the light travels down the fiber, the higher-order modes lose more power than the lower-order ones, so the mode distribution also becomes more heavily weighted toward the center.¹²

*Had the light been injected with a single-mode laser so that the higher-order modes were not excited, this would not be the case. In fact (depending on what other components are along the fiber) it is possible that light from the low-order modes might scatter into the higher-order modes. If this happens, the loss per kilometer starts out low and then increases.

When the light encounters the 50- μm fiber, there is still some loss, but not as much as when the splice was near the end of the fiber with the overfilled illumination pattern.

In most multimode fibers, the modal distribution eventually settles out into what is loosely called the *equilibrium mode distribution*. This term is somewhat flexible, but generally it implies a distribution with the lower-order modes being brighter than the higher-order modes. Once the light reaches its equilibrium mode distribution, the distribution remains unchanged with distance unless the light encounters a discontinuity (such as a splice or connector). Splices and connectors can help the fiber reach equilibrium faster when the higher-order modes are overpopulated or the lower-order modes are underpopulated. They can also disturb a distribution that is already in equilibrium. If this happens, the system requires additional fiber length to regain the equilibrium distribution.

This adds another level of complexity to the problem of making accurate splice-loss measurements on multimode fiber. It is possible for the presence of one splice to affect the loss of another. For example, suppose we have an underfilled launch condition,* followed a short distance later by a marginal splice. Since the mode distribution is weighted toward the fiber's core, the splice loss might not be too high. Next we cut the fiber between the splice and the source and introduce another splice between them. Suppose this splice is marginal in just the right way to up-convert the low-order modes into higher-order ones that are now lost at the second splice. This makes the second splice look as if its loss has increased, when in reality the splice has not changed at all.† Instead, the splice's loss appeared to change because the mode-field distribution changed.

This is an important point for multimode testing. The mode-field distribution is one of the most important factors affecting the losses of connectors and splices. However, the modal distribution is a function of the installed plant and cannot be controlled by the OTDR design engineer. Thus, conditions in the installed plant can change loss measurements, making the OTDR look inconsistent while the real culprit is outside the OTDR. The best the OTDR engineer can do is to design the instrument so the mode distribution at the OTDR's front panel is roughly equivalent to the equilibrium mode distribution. OTDR operators, on the other

*This can also be a restricted launch condition for use in systems using laser light sources including Gigabit Ethernet and Fibre Channel.

†That is, the physical relationship between the two fibers connected by the splice has not changed.

hand, should be aware that there is no “true” loss on multimode fiber. The loss measured by the OTDR may not agree exactly with what you experience with the fiber and data-transmission equipment because the OTDR and the data-transmission equipment may have different modal distributions.

As we have just seen, it is not possible to achieve perfect correlation in multimode loss measurements. Even so, the OTDR designer can do some things to reduce the problem’s impact. One of the most important things the designer can do is to achieve an equilibrium mode distribution at the front panel. This can be difficult because of the laser light sources used by most OTDRs. Although the source may not be a single-mode laser, it is still possible that it will underfill the fiber. Our experience has shown that fused couplers are not effective at converting energy in the low-order modes into higher-order modes. Connectors, splices, and fiber twists are also inefficient.* Consequently, the OTDR designer should not rely on just the fused coupler and front-panel connector to achieve the equilibrium mode distribution. We have found that an effective mode scrambler is obtained by going from graded-index fiber to step index and back to graded index (using fibers of the same core diameter). Unfortunately, these types of scramblers also have high loss.

Loss on multimode fibers depends on the mode-field distribution. The mode-field distribution, in turn, depends on the locations and types of other events as well as on the launch conditions from the light source. There is another difference between splice (or connector) loss on multimode compared with single-mode fiber. With single-mode fibers, splice loss depends on the wavelength of light (see chapter 2). If there is no stress or bending, the loss of a fusion splice at 1550 nm is less than it is at 1310 nm. If there is bending or stress, however, the loss at 1550 nm may greatly exceed that at 1310 nm. In contrast to single-mode fibers, multimode fibers show very little sensitivity to wavelength, even if there is micro- or macrobending. Fiber loss (dB/km) still depends on wavelength. This is because Rayleigh scattering is a major contribution

*Bending the fiber is an effective way of removing light from the higher-order modes, but it is a poor method of trying to up-convert energy from low- to high-order modes. The reason is quite simple: The higher-order modes are more sensitive to bending loss. Thus, if you bend the fiber enough to couple light out of the lower-order modes (in an attempt to put the energy into the higher-order ones), you already have enough fiber bending to remove immediately any light that you might put into those higher-order modes. Devices that bend the fiber are sometimes incorrectly referred to as *mode scramblers*. These devices are more accurately referred to as *mode strippers*, since they primarily remove energy from the higher-order modes.

to the fiber attenuation, and Rayleigh scattering is inversely proportional to the fourth power of the wavelength. Event loss, however, depends primarily on the modal distribution, and it is essentially independent of wavelength.

6.4 Bending loss and stress loss in single-mode fibers

Under ordinary conditions, optical fibers do not exhibit undue loss when microbends or macrobends occur. We saw in chapter 2 that the exception to this rule occurs when the bending radius becomes too small. When this happens, light from the guided modes can be coupled to cladding modes and lost. For single-mode fibers, this critical-bend radius is a strong function of the wavelength (see figure 2.16). At 1310 nm the minimum bend radius might be as small as 1.5 cm, while at 1550 nm it might be 2.5 cm or more. When optical fiber is built into a cable, cable strength members prevent the fiber from being bent too sharply. In splice trays, however, or other areas where the buffered fiber is exposed, it may be possible to bend the fibers enough to cause noticeable loss.

When a fiber is bent or stressed enough to cause loss, on the OTDR display the loss appears similar to the nonreflective fusion splices shown in figures 5.1 and 5.2. There is no noticeable reflection associated with the event, and it can easily be confused with a fusion splice. Using a dual-wavelength OTDR, it is relatively simple to determine if the event's loss is due to macro- and microbends when testing single-mode fiber. To

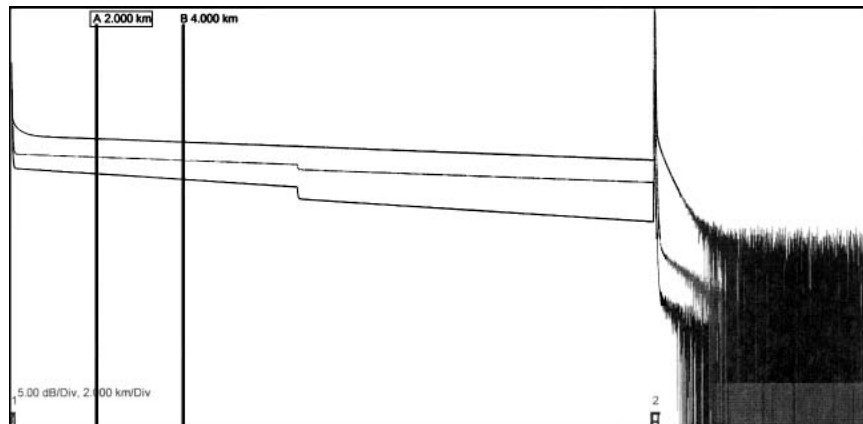


Figure 6.7. Three wavelengths—1310 nm, 1550 nm, and 1625 nm—overlaid on an OTDR screen with macro- and microbends. [Credit: The Light Brigade.]

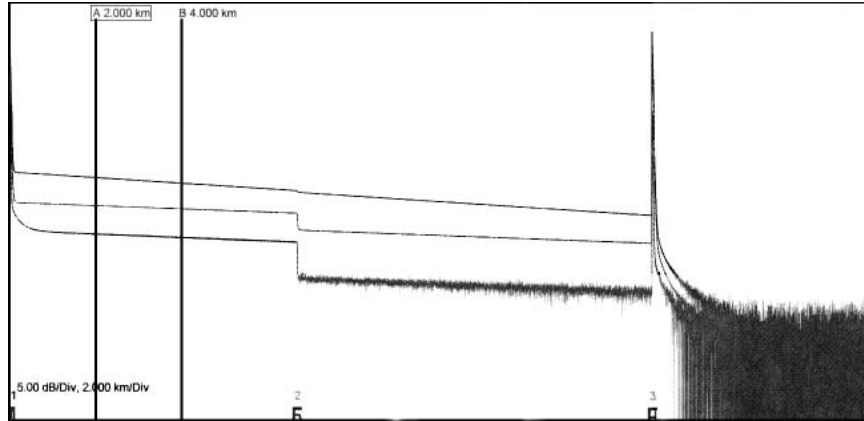


Figure 6.8. Three wavelengths—1310 nm, 1550 nm, and 1625 nm—overlaid on an OTDR screen without macro- and microbends. [Credit: The Light Brigade.]

do this requires a dual-wavelength OTDR that operates at both 1310 nm and 1550 or 1625 nm.

The trick behind identifying macro- and microbends is that both of these affect single-mode fiber and are sensitive to wavelength (see figure 6.7). With fiber splices, ordinarily the loss at 1550 or 1625 nm is slightly less than it is at 1310 nm (see figure 6.8). (We describe the reasons for this quantitatively in section 6.5. For now, it is sufficient to know that a fusion splice without bending has slightly less loss at longer wavelengths than at shorter wavelengths.) If the loss is caused by a fiber bend, the loss is greater at longer wavelengths, such as 1550 or 1625 nm, than it is at 1310 nm. This suggests a simple test that determines the extent to which fiber bending is contributing to an event's loss. Test the fiber at both 1310 nm and a longer wavelength, such as 1550 or 1625 nm, and compare the two loss measurements. If the loss is slightly less at, for example, 1550 nm than it is at 1310 nm, the event is a fusion splice and bending is inconsequential.* If the event's loss is slightly greater at 1550 nm than at 1310 nm, the fiber has a small amount of fiber bending. If the event's loss is much larger at 1550 nm than it is at 1310 nm, the fiber is bent significantly.†

*The technique works equally well with reflective events, such as connectors and mechanical splices.

†The next section deals more quantitatively with this technique.

6.5 Wavelength-dependent loss in fusion splices and connectors between single-mode fibers

In chapter 2 we saw that when you splice two fibers together, the resulting loss comes from lateral misalignment, fiber bending, or the intrinsic mismatch between the fibers. Two of these causes (lateral misalignment and bending) depend on wavelength. The third cause (intrinsic mismatch) is essentially independent of wavelength.

When there is negligible bending, the splice loss at 1550 nm is less than it is at 1310 nm because the mode-field diameter (MFD) of the fiber is larger at 1550 nm. Splice loss, in decibels, as a function of lateral misalignment is (see also figure 2.14)^{13,14}

$$\text{Loss} = 10 \log \left(\exp \left(\frac{-x^2}{\omega_0^2} \right) \right) \quad [6.21]$$

In equation [6.21], x is the lateral offset and ω is the fiber's mode-field diameter (at the point where the power density falls to $1/e^2$ times the peak power density). From equation [6.21] you can see that, for a given value of x , a larger value of ω_0 results in a smaller value for the loss.

Simplifying, equation [6.21] becomes

$$\text{Loss} = \frac{-10}{\ln(10)} \frac{x^2}{\omega_0^2} \quad [6.22]$$

When the wavelength changes, the fiber's MFD increases or decreases. The difference in loss for two different mode-field diameters (assuming the lateral misalignment does not change) is

$$\begin{aligned} \Delta \text{Loss} &\equiv L_1 - L_2 = \frac{-10 \cdot x^2}{\ln(10)} \left[\frac{1}{\omega_1^2} - \frac{1}{\omega_2^2} \right] \\ \Delta \text{Loss} &= \text{Loss}_1 \left(1 - \left(\frac{\omega_1}{\omega_2} \right)^2 \right) \end{aligned} \quad [6.23]$$

Substituting equation [2.22] into equation [2.28] and assuming the numerical aperture is wavelength invariant (a reasonably good assumption), we see the quantity $(1 - (\omega_1/\omega_2)^2)$ is very nearly a linear function. If ω_1 is 1.310 μm , then we can write the approximation as

$$(1 - (\omega_1/\omega_2)^2) \approx -0.9918 + 0.7559 \cdot \lambda_2 \quad [6.24]$$

In equation [6.24], the wavelengths must be in microns. Substituting equation [6.24] into equation [6.23] and rearranging, we have

$$\Delta\text{Loss} = \text{Loss}_{1310} - \text{Loss}_{\lambda_2} = \text{Loss}_{1310} (0.7559\lambda_2 - 0.9918) \quad [6.25]$$

Solving equation [6.25] for the loss at λ_2 we have:

$$\text{Loss}_{\lambda_2} = \text{Loss}_{1310} (1.9918 - 0.7559\lambda_2) \quad [6.26]$$

In equation [6.26], Loss_{1310} is the loss at $1.310 \mu\text{m}$, and λ_2 is the second wavelength (this wavelength must be in microns). For example, suppose the splice loss at $1.310 \mu\text{m}$ is 0.3 dB and that we want to know the splice loss at $1.550 \mu\text{m}$. From equation [6.26] we see the expected loss at $1.550 \mu\text{m}$ is 0.25 dB .

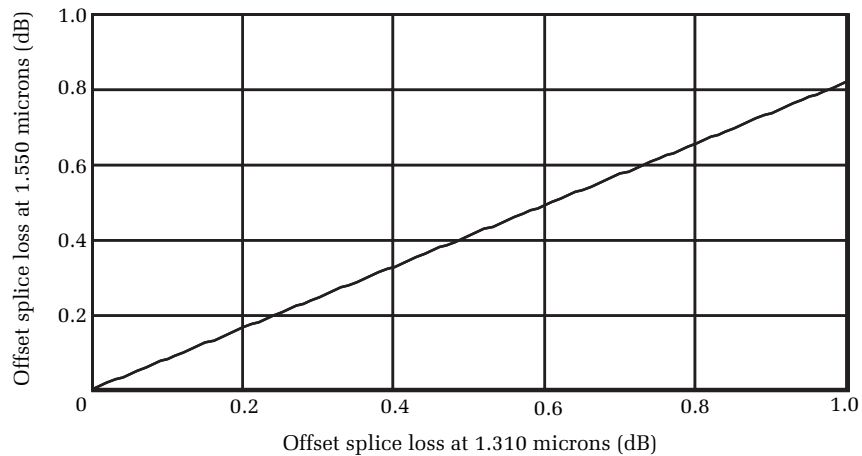


Figure 6.9. Offset splice loss at $1.550 \mu\text{m}$ as a function of the offset splice loss at $1.310 \mu\text{m}$. The loss at $1.550 \mu\text{m}$ is less than it is at $1.310 \mu\text{m}$ because the modal distribution is larger at $1.550 \mu\text{m}$ than it is at $1.310 \mu\text{m}$.

Figure 6.9 is a plot of the offset splice loss at $1.550 \mu\text{m}$ as a function of the offset splice loss at $1.310 \mu\text{m}$ according to equation [6.26]. Equation [6.26] can serve as a useful diagnostic tool. If the loss at $1.550 \mu\text{m}$ is less than it is at $1.310 \mu\text{m}$, and by roughly the amount given by equation [6.26], then bending loss is insignificant. On the other hand, if the loss at $1.550 \mu\text{m}$ is greater than at $1.310 \mu\text{m}$, then most of the loss at $1.550 \mu\text{m}$ is due to bending, not misalignment of the cores.

6.6 Intrinsic loss in single-mode fusion splices

Whenever a fiber-optic technician splices two optical fibers together, there is some optical loss. This optical loss may be broadly defined as caused by intrinsic or extrinsic effects. Extrinsic splice loss results from external factors, such as lateral misalignment, fiber bending, and contamination. Intrinsic splice loss results when the two fibers being joined have different mode-field diameters or numerical apertures. All optical fibers also have tolerances that will vary. Short of replacing the fibers being spliced together, there is little the optical technician can do to improve the intrinsic splice loss.

As splice-loss specifications become lower, the possible impact of intrinsic mismatch between fibers becomes more significant. When extrinsic effects result in excessive loss, the splice technician can improve the splice loss by repairing and cleaning the splicing equipment. When intrinsic effects result in excessive loss, however, the only option available is to replace one or both of the fibers. When a fusion splice or connector exceeds its specified loss, therefore, it is important to understand the cause in order to take the correct action. Usually excess loss is caused by extrinsic effects, but occasionally intrinsic effects can be significant. If the splicing technician is unaware of intrinsic effects, much time can be wasted trying to improve a splice that cannot be made any better.

First, let's examine the possible magnitude of the problem. Suppose that we splice two fibers together and that they have slightly different mode-field diameters. For fibers with unequal mode-field diameters, the intrinsic splice loss is^{15,16}

$$\text{Loss}_{MFD} = -10 \log \left(\frac{4\omega_1^2 \omega_2^2}{(\omega_1^2 + \omega_2^2)^2} \right) \quad [6.27]$$

In equation [6.27], ω_1 and ω_2 represent the radii of the fundamental modes in the two fibers at the $1/e^2$ point.

The fundamental mode of single-mode fiber is approximately Gaussian, so the numerical aperture and mode-field diameter are approximately related by a constant:*

*For Gaussian beams, the beam divergence is inversely proportional to the diameter of the beam's waist. Our assumption breaks down somewhat since the mode distribution in single-mode fiber is only approximately Gaussian (see chapter 2).

$$\begin{aligned} \text{MFD}_1 &= 2\omega_1 = \frac{K}{\text{NA}_1} \\ \text{MFD}_2 &= 2\omega_2 = \frac{K}{\text{NA}_2} \end{aligned} \quad [6.28]$$

Substituting equation [6.28] into equation [6.27] and rearranging, we have

$$L_{\text{NA}} = -10 \log \left(\frac{4 \cdot R}{(1 + R)^2} \right) \quad [6.29]$$

In equation [6.29], $R = (\text{NA}_1/\text{NA}_2)^2$. As an example, consider a typical single-mode fiber with a mode-field diameter of $10.5 \pm 1.0 \mu\text{m}$ at 1550 nm. We assume this specification is at the 2-sigma confidence level. From this assumption, we can perform a Monte Carlo analysis to investigate the expected magnitude of the intrinsic loss when splicing together random pieces of this type of fiber. Figure 6.10 is a histogram generated from such a Monte Carlo analysis using equation [6.29], figure 6.11 illustrates the cumulative probability.¹⁷

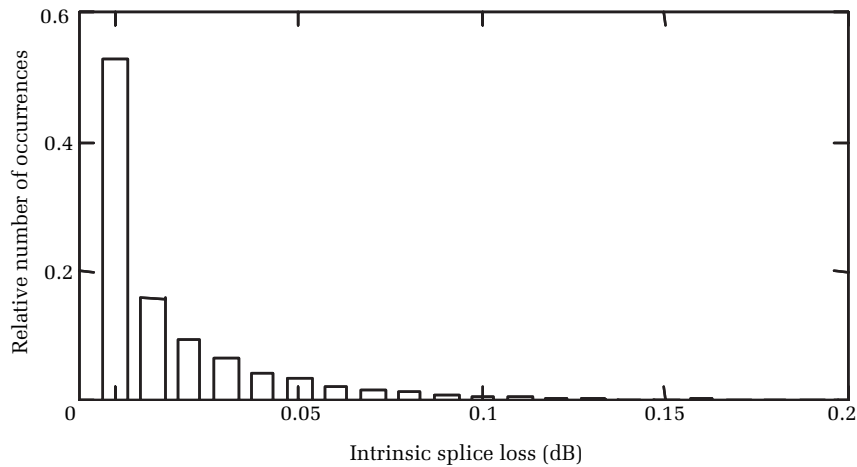


Figure 6.10. A Monte Carlo histogram of the intrinsic splice loss between two randomly selected pieces of single-mode fiber, each having a nominal mode-field diameter of $10.5 \mu\text{m}$, where the standard deviation of the numerical aperture was 4.76%. The x-axis shows the splice loss, and the y-axis shows the expected number of splices (normalized) that, statistically speaking, can be expected to be in that range.

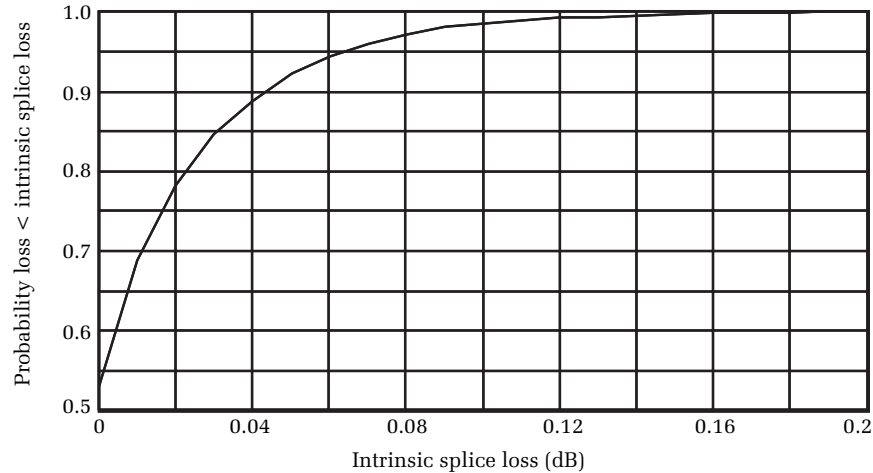


Figure 6.11. Probability that the intrinsic splice loss will be less than the value shown along the x-axis. For example, there is a 95% probability that the intrinsic splice loss between two randomly selected SMF-28 fibers will be less than 0.07 dB. Notice that about 2.5 splices out of 100 will have intrinsic splice loss that exceeds 0.10 dB.

Usually the intrinsic loss is insignificant, being only a few hundredths of a decibel. About 2% or 3% of the time, however, the intrinsic loss can be high enough that it might approach that of the splice-loss specification. In this respect, the problem can be especially insidious. Since the intrinsic loss is usually low, the splicing technician may not suspect the problem, so when high intrinsic loss does occur it is unexpected and goes undiagnosed. Of course, if you inadvertently try to splice dissimilar fibers together, such as dispersion-shifted fiber to non-dispersion-shifted fiber (see figure 6.12), the intrinsic loss can be very high, many times more than 0.5 dB. In such cases, it is important to know that the splice loss is intrinsic.

Wavelength	Manuf. A A-B PAS	Manuf. A B-A PAS	Manuf. B A-B PAS	Manuf. B B-A PAS	Manuf. C A-B PAS	Manuf. C B-A PAS	Manuf. D A-B PAS	Manuf. D B-A PAS
1310	.87	-.72	.96	-.79	1.14	-.80	1.12	-.69
1550	.60	-.47	.70	-.59	.80	-.60	.88	-.48
1625	.48	-.38	.58	-.49	.68	-.54	.77	-.41

Figure 6.12. Mismatched single-mode fibers with losses from A-B and B-A direction using different fusion splicers. [Credit: The Light Brigade.]

As equation [6.29] shows, the intrinsic loss is a function of the ratio of the square of the numerical apertures of the fibers. Usually, however, the OTDR operator has no prior knowledge (beyond the manufacturer's specifications) of the numerical apertures. Fortunately, it is possible to use OTDR measurements from both ends of the fiber-optic link to determine the ratio of the numerical apertures.

When you splice two fibers that have different mode-field diameters, R is a function of the bidirectional losses measured with an OTDR. The square of the ratio of the numerical apertures is¹⁸

$$R = 10^{\left(\frac{F_1 - F_2}{5}\right)} \cdot \frac{\alpha_{S_2}}{\alpha_{S_1}} \quad [6.30]$$

where F_1 is the relative backscatter parameter for fiber 1, F_2 is the relative backscatter coefficient for fiber 2, α_{S_1} is the scattering attenuation factor for fiber 1, and α_{S_2} is the scattering attenuation factor for fiber 2.* The scattering attenuation factors are approximately equal to the fiber slopes in good-quality telecommunications-grade optical fiber.

The difference between the relative backscatter parameters is¹⁹

$$F_1 - F_2 = L_{m_{1,2}} - L \quad [6.31]$$

where $L_{m_{1,2}}$ is the OTDR-measured loss when connected to fiber 1 and L is the true splice loss.

According to equation [6.30], the true splice loss is just the average of the loss measured from each end of the fiber-optic link. So we have

$$F_1 - F_2 = \left(\frac{2L_{m_{1,2}} - (L_{m_{1,2}} + L_{m_{2,1}})}{2} \right) = \frac{L_{m_{1,2}} - L_{m_{2,1}}}{2} \quad [6.32]$$

Substituting equation [6.32] into equation [6.29], we have

$$L_{NA} = -10 \log \left(\frac{4 \cdot R}{(1 + R)^2} \right)$$

*This is the attenuation due only to Rayleigh scattering. It does not include attenuation from absorption. In high-quality modern telecommunications fiber, attenuation loss mostly results from Rayleigh scattering.

where

$$R = 10^{\left(\frac{L_{m_{1,2}} - L_{m_{2,1}}}{10} \right)} \cdot \frac{\alpha_{S_2}}{\alpha_{S_1}} \quad [6.33]$$

Equation [6.33] thus allows us to calculate the intrinsic splice loss without prior knowledge about the fiber's numerical aperture. All the information required is contained in the two-way measurements that are already standard for many fiber-optic installations.

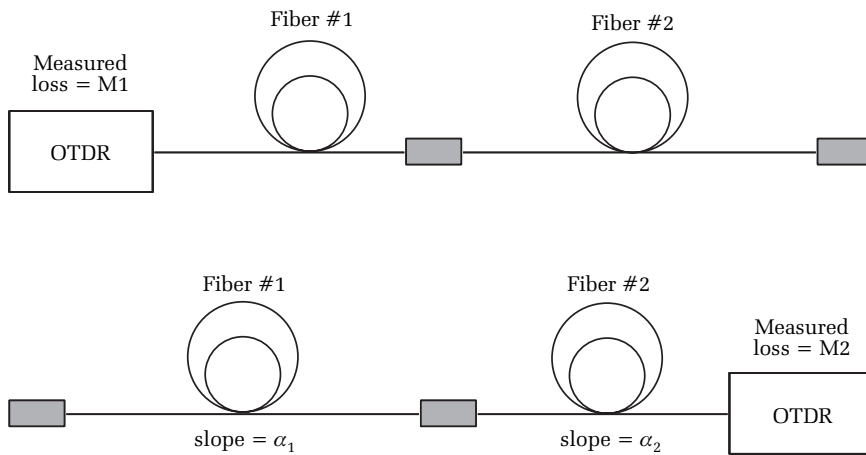


Figure 6.13. Algorithm for finding the intrinsic loss of a splice between two single-mode optical fibers.

The following steps summarize the algorithm for measuring intrinsic loss of a splice (see also figure 6.13).

1. Measure the splice loss from one end of the optical link. Call this M1.
2. Measure the attenuation coefficient, or fiber slope, before the splice. Call this α_1 .
3. Measure the attenuation coefficient, or fiber slope, after the splice. Call this α_2 .
4. Measure the splice loss from the other end of the optical link. Call this M2.
5. Calculate the ratio R from equation [6.34].
6. Substitute the results of equation [6.34] into equation [6.35]. The result of equation [6.35] is the intrinsic splice loss in decibels.

$$R = 10^{\left(\frac{M1-M2}{10}\right)} \cdot \frac{\alpha_2}{\alpha_1} \quad [6.34]$$

$$\text{Loss}_{\text{intrinsic}} = -10 \log(4R/(1 + R)^2) \quad [6.35]$$

6.7 Summary

In this chapter we have shown that loss-measurement error depends on such things as the local waveform noise, mismatch between fibers (single-mode fibers), modal distribution (multimode fibers), and linearity in the OTDR's receiver.

As we saw with distance-measurement error, estimating loss-measurement error is probably not feasible for the OTDR operator. Proprietary event-marking algorithms make it almost impossible for the operator to calculate the expected loss-measurement errors in the instrument's measurements. The only practical way for the operator to know the loss-measurement uncertainty is for the OTDR to calculate it specifically for each event. The various contributors to measurement error are summarized here, in roughly increasing order of importance:

- Mismatched fibers (for single-ended measurements only)
- Waveform noise
- OTDR calibration and nonlinearity

We also saw that the loss of a fusion splice depends on wavelength. Longer wavelengths tend to have less loss at a given splice, in the absence of bending, than shorter wavelengths. This leads to a simple way to see if a splice has significant bending, by testing the splice at a longer wavelength and then at a shorter wavelength. For example, you might test at 1310 nm and at 1550 nm. Or you might test at 1550 nm and at 1625 nm. If the loss is slightly greater at the shorter wavelength than at the longer wavelength, there is essentially no bending loss. If the loss is greater at the longer wavelength than at the shorter wavelength, bending loss is significant.

Finally, we saw that single-mode fibers have intrinsic splice loss due to mismatches in their mode-field diameters. Usually, loss due to mismatched fibers is small, but sometimes it can be 0.5 dB or greater. If you test the optical fiber from both ends, you can use the test data to estimate the intrinsic splice loss and ratio of the numerical apertures of the two fibers. This can be useful information if you have very tight specifications on splice loss.

Suggested reading

Bjerkan, L., "Optical splice loss predictions from one-way OTDR measurements based on a probability model," *Journal of Lightwave Technology*, Vol. 7, No. 3 (1989).

Kashima, N., *Passive Optical Components for Optical Fiber Transmission* (Norwood, MA: Artech House, 1995).

Evers, G., "Calculation and measurement of mode transition matrices for different mode attenuation and differential mode delay characterization of optical fibers," *Optical Engineering*, Vol. 27, No. 2 (1988).

Kiang, Y. C., and Klieber, T. E., "Macrobending effects on fiber numerical aperture," *Journal of Lightwave Technology*, LT-5, No. 5 (1987).

Miller, C. M., Mettler, S. C., and White, I. A., *Optical Fiber Splices and Connectors, Theory and Methods* (New York: Marcel Dekker, 1986).

Caviglia, F., and Cselt, P. R. C., "Noise error in OTDR splice loss measurement," *NIST Technical Digest Symposium on Optical Fiber Measurements* (1994).

Warder, J., Li, M., Townley-Smith, P., and Saravanos, C., "Effects of fiber parameter mismatch on uni-directional OTDR splice loss measurement," *NIST Technical Digest Symposium on Optical Fiber Measurements* (1994).

Tanji, H., and Ito, S., "Practical improved splice loss estimation for single-mode optical fibers," *NIST Technical Digest Symposium on Optical Fiber Measurements* (1994).

Howare, R. M., Hullett, J. L., and Jerrery, R. D., "Range and accuracy in backscatter measurements," *Optical and Quantum Electronics*, Vol. 18, No. 4 (1986).

Brininstool, M. R., "Integrated OTDR/throughput loss measurement system for environmental testing of cabled optical fibers," *Proceedings of SPIE, Short-Haul and Long-Haul Measurements and Applications III*, Vol. 559, San Diego (1985).

Problems

1. True or false: Best-in-class OTDRs have no waveform noise.
2. True or false: Waveform noise results in loss-measurement errors.
3. True or false: The noise on an OTDR waveform is the same for all events.
4. True or false: The loss seen on an OTDR's screen is the same as the true loss, even when the fibers being spliced are dissimilar.
5. True or false: Intrinsic loss in a splice can be reduced by more careful splicing.

6. True or false: The true loss on a splice in multimode fibers can be determined by measuring the splice from opposite ends of the fiber and averaging the results.
7. True or false: The true loss on a splice in single-mode fibers can be determined by measuring the splice from opposite ends of the fiber and averaging the results.
8. True or false: The loss of splices and connectors in multimode systems depends on how the light is distributed among the fiber's different modes.
9. True or false: It is possible to determine the relative numerical apertures of single-mode fibers that are spliced together by using an OTDR.
10. True or false: If a splice has greater loss at longer wavelengths, then the splice may actually be a bend or there may be excessive bending at the splice point.

¹ Bulmer, M. G., *Principles of Statistics* (New York: Dover, 1979) p. 212.

² *Ibid.*, p. 214.

³ Personick, S. D., "Photon probe—An optical-fiber time-domain reflectometer," *Bell Systems Technical Journal*, Vol. 56 (1977), pp. 355–366.

⁴ Neumann, E. G., "Analysis of the backscattering method for testing optical fiber cables," *AEU*, Vol. 34, Mp/4 (1980), pp. 157–160.

⁵ *Ibid.*

⁶ *Ibid.*

⁷ Nakazawa, M., "Rayleigh backscattering theory for single-mode optical fibers," *Journal of the Optical Society of America*, Vol. 73, No. 9 (Sept. 1983).

⁸ Brinkmeyer, E., "Backscattering in single-mode fibers," *Electronics Letters*, Vol. 16, No. 9 (April 1980).

⁹ Nemoto, S., and Makimoto, T., "Analysis of splice loss in single-mode fibers using a Gaussian field approximation," *Optical Quantum Electronics*, Vol. 11 (1979), p. 447.

¹⁰ Miller, Stewart E., and Kaminow, Ivan P., *Optical Fiber Telecommunications II* (San Diego: Academic Press, 1988).

¹¹ Eriksrud, M., Michelson, A. R., Aamlid, S., and Espe, B. "Mode dependence on splice loss in graded-index optical fibers," *IEEE Journal of Quantum Electronics*, Vol. QE-19 (1983), pp.788–791.

¹² Evers, G., "Calculation and measurement of mode transition matrices for different mode attenuation and differential mode delay characterization of optical fibers," *Optical Engineering*, Vol. 27, No. 2 (1988).

¹³ Marcuse, D., "Loss analysis of single-mode fiber splices," *Bell Systems Technical Journal*, Vol. 56 (1977), pp. 703–717.

¹⁴ Nemoto, S., and Makimoto, T., "Analysis of splice loss in single-mode fibers using a Gaussian field approximation," *Optical Quantum Electronics*, Vol. 11 (1979), p. 447.

¹⁵ Marcuse, D., "Loss analysis of single-mode fiber splices," *Bell Systems Technical Journal*, Vol. 56 (1977), pp. 703–717.

¹⁶ Nemoto, S., and Makimoto, T., "Analysis of splice loss in single-mode fibers using a Gaussian field approximation," *Optical Quantum Electronics*, Vol. 11 (1979), p. 447.

¹⁷ These theoretical calculations agree well with experimental data from Corning, as reported by Birrell, B., and Cooper, S., "Practical guidelines for mass mechanical splicing," *Fiberoptic Product News* (April 1995), pp. 27–30.

¹⁸ Anderson, D. R., "Making true splice loss measurements with OTDRs from one end of the fiber," *NFOEC 95*.

¹⁹ *Ibid.*

Chapter 7

Measuring reflective events

7.0 Introduction

In this chapter we describe reflective events, discuss the types of fiber-optic components that cause them, and cover how to measure reflections using an OTDR. We begin with a general discussion of the problems reflections might cause in a fiber-optic communications system. We then describe the ways reflections arise, and we present some equations that describe the amount of reflection you can expect from cleaved fiber ends, mechanical splices, and connectors (see figure 7.1).

Following this introductory background, we show how to measure the distance to and loss of a reflective event. You will see that the method of measuring the loss of a reflective event is nearly the same as it is for a nonreflective event. The equations for loss-measurement uncertainty that we derived in chapter 6 also apply here. You will also see that distance-measurement accuracy is different for reflective events than it is for nonreflective events. We provide a simple algorithm for finding the location of a reflective event and describe its uncertainty.

A reflection is defined by its distance, loss, and reflectivity. In this chapter we discuss how to measure the reflectivity of an event using an OTDR. Reflectivity measurements require special calibration procedures for the measurements to be accurate to better than a few decibels. In this chapter we thoroughly discuss techniques for calibrating reflectivity measurements, and we provide calibration procedures for setting the backscatter coefficient. We also discuss some of the problems (besides calibration) that lead to errors in reflectivity measurements.

We end the chapter with a discussion of integrated return loss. A mathematical treatment shows how to calculate the return loss measured by a continuous-wave reflectometer (CWR) and how to make similar measurements by integrating the energy under an OTDR's waveform and using the proper normalizing factor.

7.1 Background

Anyone who has ever been in a room with poor acoustic qualities understands how annoying echoes can be. Echoes are a source of confusion. Engineers of all types work to minimize them in systems ranging from telecommunications to interior design. Echoes arise

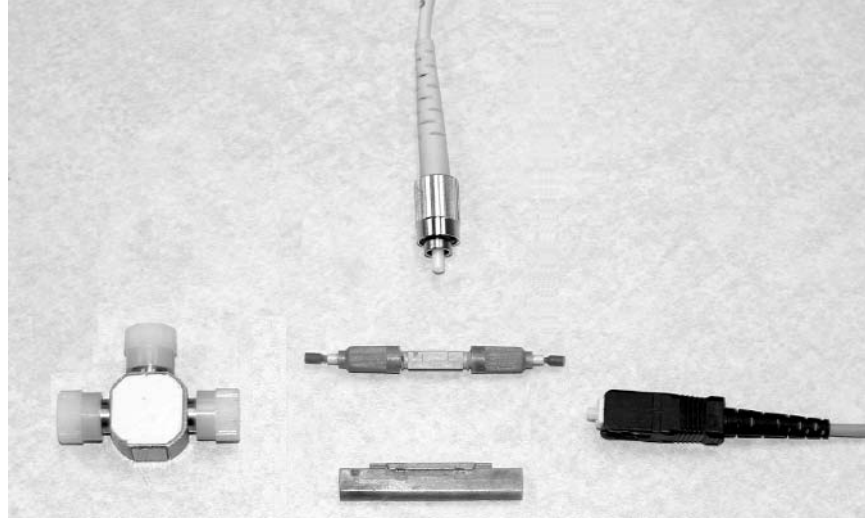


Figure 7.1. Unterminated optical fibers, plugs, mechanical splices, and lensed devices are all reflective. [Credit: The Light Brigade.]

whenever mechanisms exist to reflect waves that carry information. Not surprisingly then, reflective components are a prime concern for engineers who design fiber-optic communications systems.

One way that reflections degrade fiber-optic communications systems is by causing echoes that interfere with the received signal. Because they result from reflections, echoes follow a path to the receiver that is longer than the path followed by the primary data stream. The echoes are delayed. Because of this, echoes are usually uncorrelated with the primary data stream and constitute a source of noise. This is the familiar effect you hear in a large, empty room with smooth, high-density walls. In this setting, acoustic echoes are very noticeable. In such surroundings, you hear the transmitted signal (another person across the room speaking, for example) as well as an attenuated and delayed, or echoed, copy of the signal.

In fiber-optic communications, the effects of echoes reach beyond simply interfering with the received signal. Fiber-optic communications systems often use transmitters, such as distributed-feedback (DFB) lasers, that are sensitive to feedback from reflections. When such a transmitter is exposed to reflections, its amplitude and frequency may be modulated. When this happens, the quality of the transmitted signal becomes degraded and the bit-error rate increases. To use our analogy

of a person speaking, it would be as if the echoes, when fed back to the speaker, interfered with the person's speech.

Because of these effects, fiber installers frequently need to verify that the reflectivities of various components in the system are below predetermined thresholds. To accomplish this, technicians have access to two important tools: the continuous-wave reflectometer (CWR) and the OTDR. Figure 7.2 illustrates the principal parts of a CWR. The CWR and OTDR are very similar in some respects and very different in others. Like an OTDR, the CWR has a light source (typically a laser) connected to one of the input ports of a 3-dB coupler. The other input port is connected to an optical detector (typically an APD). One of the coupler's output legs is connected to the CWR's front panel, and the other output leg is terminated with a very low reflection. The test fiber is connected to the CWR's front panel. When the CWR's laser is turned on, the coupler directs the light through the front-panel connector and into the fiber being tested.* When the light encounters reflective components along the fiber, part of the light is reflected back to the CWR, where

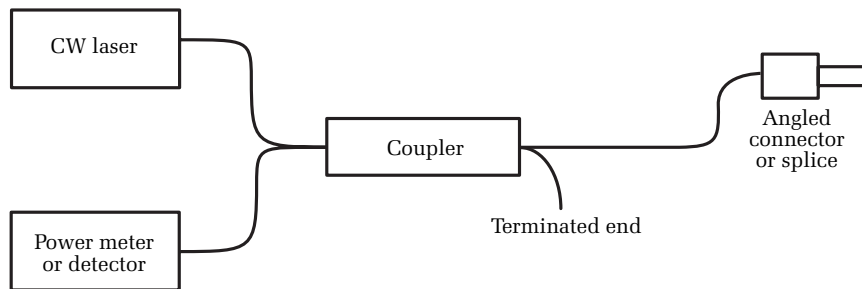


Figure 7.2. A typical continuous-wave reflectometer (CWR). You can purchase a commercial instrument or build your own from discrete instrumental building blocks. It is important that the instrument's front-panel connector has very low reflectivity to eliminate reflections that would otherwise contaminate the CWR measurements. Angled connectors, discussed later in this chapter, are typically required to achieve the necessary reduction in front-panel reflection. Alternatively, you may want to use a pigtail adapter with the CWR and splice it to the fiber being tested. Reducing instrumental back-reflections is also the reason for terminating the fourth leg of the coupler and using a coupler with ultralow reflection.

*Unlike the OTDR, the CWR laser is not pulsed. It operates in what is called the *continuous-wave*, or *CW, mode*.

the instrument's optical detector senses it. When properly calibrated, therefore, the CWR can readily determine what percentage of the light is reflected and scattered by the fiber under test.

The CWR is essentially an OTDR with zero bandwidth. Unlike the CWR, the OTDR is capable of measuring the individual reflectivities of the components distributed along the fiber as well as the total light reflected and scattered from a fiber-optic link. The CWR is useful for determining whether the total link meets a predetermined specification for total reflectivity. If the link fails, however, the CWR cannot determine which component caused the fault. The OTDR, being a time-based instrument, can resolve the locations and reflectivities of the components along the fiber. Using an OTDR, therefore, can tell you not only whether the link is meeting specifications, but also which component is the likely cause of a failure.

7.2 Causes of reflections

When light traveling through a dielectric medium encounters a discontinuity in the index of refraction, a portion of the light transmits through the discontinuity and a portion is reflected. Discontinuities in fiber-optic systems typically occur at connectors, mechanical splices, and cut, or cleaved, fiber ends. For connectors and mechanical splices the manufacturer's specifications will commonly use the term optical return loss (ORL) when stating their values.

For a perpendicularly cleaved fiber, the reflection from the end is

$$R = \left(\frac{n_t - n_i}{n_t + n_i} \right)^2 \quad [7.1]$$

In equation [7.1], n_t is the index of the medium into which the light transmits and n_i is the index of the fiber. For air, the index is approximately 1.000; for single-mode optical fibers the index is about 1.468. The reflection from a square fiber cleave is about 3.6%, or -14.4 dB.

7.2.1 Reflections from angled cleaves

If the end of the fiber is not cleaved squarely, then equation [7.1] no longer gives the power in the reflected light that is coupled back into the fiber. This is because the fiber is sensitive to the angular divergence of the light coupling into its core (see figure 2.16). For small cleave angles, the total reflected power is still about 3.6%. Because of the angled cleave,

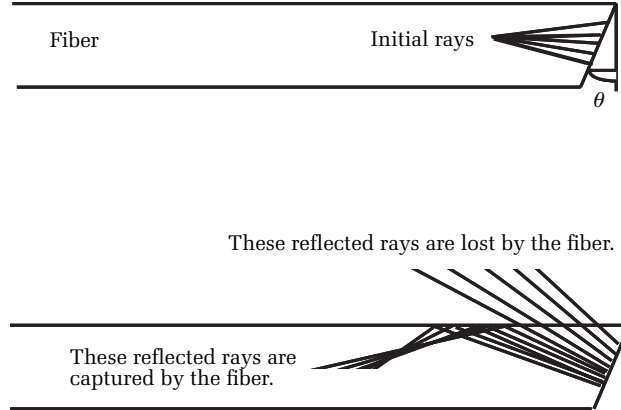


Figure 7.3. Loss of reflected light from angled cleave. When the fiber is cleaved at an angle, some of the light is reflected outside the fiber's numerical aperture. This light is coupled into cladding modes and lost. If the cleave angle is sufficiently large, essentially all of the reflected light is lost and the fiber's core captures none of the reflected light.

however, some of the reflected light has an angular divergence that is outside the fiber's numerical aperture, and it is not coupled into the waveguide. Instead, this light is coupled into cladding modes, where it is lost (see figure 7.3).

If the end of the fiber is cleaved so that it is θ° from a 90° cleave, then the reflected light is angularly misaligned by twice this amount relative to the fiber's core.* From figure 2.16 and equation [7.1], the total amount of reflected light (for single-mode fibers) coupled into the fiber core (in decibels) from an angled cleave is

$$R = -10 \log \left[\left(\frac{n_2 - 1}{n_2 + 1} \right)^2 \exp \left[- \left(\frac{2\theta\pi n_1 \omega_0}{\lambda} \right)^2 \right] \right] \quad [7.2]$$

In equation [7.2], n_1 is the fiber's cladding index, θ is the angle of the cleave (from normal, in radians; see figure 7.3), ω_0 is the mode-field radius at the $1/e^2$ irradiance point, and λ is the wavelength. Equation [7.2] assumes the cleaved fiber is in air.

*Think of a light beam reflecting off a mirror. If the mirror is perpendicular to the light beam, the beam bounces back on itself. If you rotate the mirror by 5° , the reflected light beam rotates by 10° . Rotate the mirror 45° , and the reflected light beam is 90° relative to the initial beam.

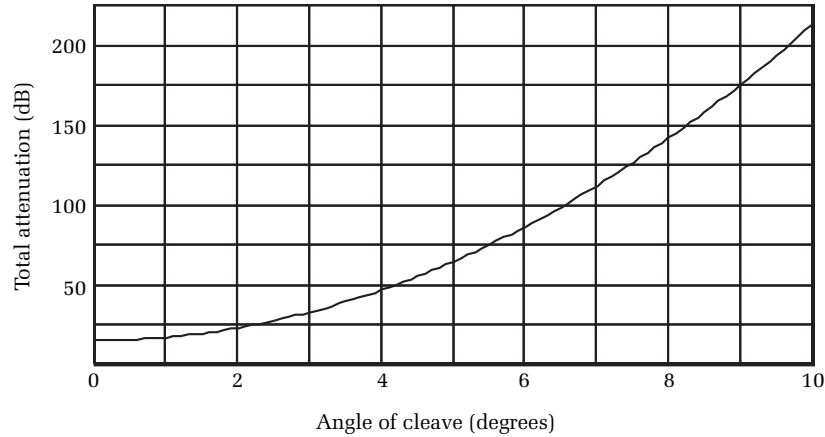


Figure 7.4. Total theoretical attenuation of reflection from a cleaved fiber as a function of the cleave angle (see figure 7.3 and equation [7.2]).

For example, suppose the fiber's index is 1.468, the wavelength is $1.310 \mu\text{m}$, the mode-field radius is $5.5 \mu\text{m}$, and the polished angle at the fiber's end is 5° . Then the total reflection coupled back into the fiber is attenuated by about 64 dB relative to the power of the incident light. Cleaving the fiber at an angle of 7° reduces the total coupled reflection more than 100 dB below the incident signal. Figure 7.4 illustrates the attenuation of the reflection as a function of the cleave angle.*

7.2.2 Reflections from connectors

Many designs exist for optical connectors (see figure 7.5). In chapter 2 we reviewed a few of them. Most of these designs are variants of the ferrule-in-sleeve construction. In the ferrule-in-sleeve design, the fibers are first placed in ceramic ferrules and secured, usually with epoxy. Then the ends of the ferrules, along with the embedded fibers, are polished. The connection is made via inserting two polished ferrules into opposite ends of a sleeve, which will axially align them. With the ferrules axially aligned, the fibers embedded in them are also aligned. Additionally, there is a mechanical mechanism that tightly holds the ferrules in the sleeve and keeps their polished ends pressed against each other.

*This theoretical calculation assumes a perfect polish. Polishing defects cause light to scatter into the core and coupling that would otherwise have been lost in the cladding. Thus, with polishing, defects may place a lower limit on how far the coupled reflection may be reduced.

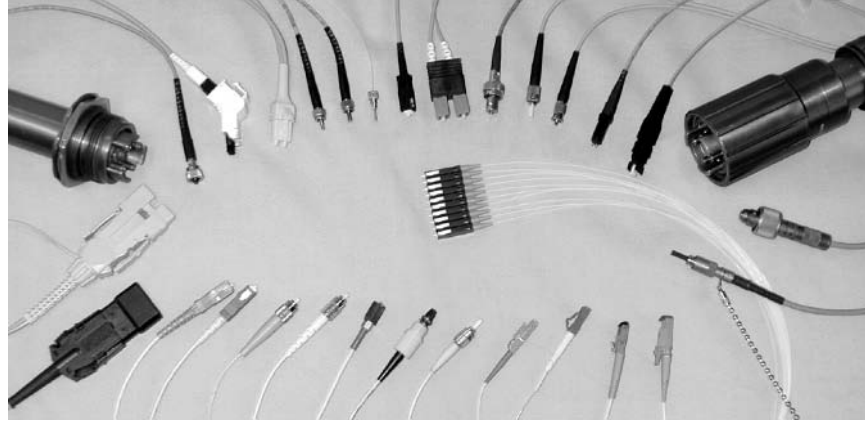


Figure 7.5. A variety of fiber-optic connector styles. [Credit: The Light Brigade.]

Light traveling through a fiber-optic connector must pass from one fiber to the next. Since polished surfaces and mechanical tolerances are never perfect, residual air gaps always exist in these connectors and result in the reflection of some of the light. The reflections from connectors are usually much smaller than the 3.6% reflection from a square cleave because modern fiber connectors are specifically designed for reduced reflection. One way to do this is to design the connectors so the residual air gap that inevitably exists between the fibers in the ferrules is minimized. When properly cleaned and undamaged, these physical-contact (PC) connectors typically have ORL values below -40 dB. When dirty or damaged, however, their reflectivity can increase substantially.

To see why connectors have low reflectivity when their ferrules touch, let's look a little closer at what causes reflections within a fiber-optic connector. When the ferrules in a connector are separated, they form a weak Fabry–Perot resonator, with each ferrule surface reflecting roughly 3.6% of the light. Since light is an electromagnetic phenomenon, the reflections from each ferrule add coherently. Sometimes these reflections add constructively, or in phase. When this happens, the connector's total reflectivity is high. Other times the reflections from the two ferrules add destructively, or out of phase. In these cases, the total reflection from the connector is very low. Usually, the reflections from the two polished ferrules add in some state between these two extremes (that is, the phase difference between the two reflections randomly varies between 0 and 2π radians). Because of this interference phenomenon,

a connector's reflectivity is sometimes sensitive to wavelength and environmental effects.

When the ferrules in a connector touch, the reflections interfere destructively and the connector's reflectivity is very low. The touching surfaces also minimize the connector's sensitivity to wavelength and environmental effects. To make sure the ferrules touch at the center (where the fibers are), PC connectors have a slight convex polish (see figure 7.6). It is important to keep the ferrules clean and in proper repair to ensure they stay in physical contact. Even small amounts of dirt or oily films can result in minuscule separations between the ferrules that result in reflections or increased insertion loss.* When kept in proper repair, PC connectors have low reflectivity.

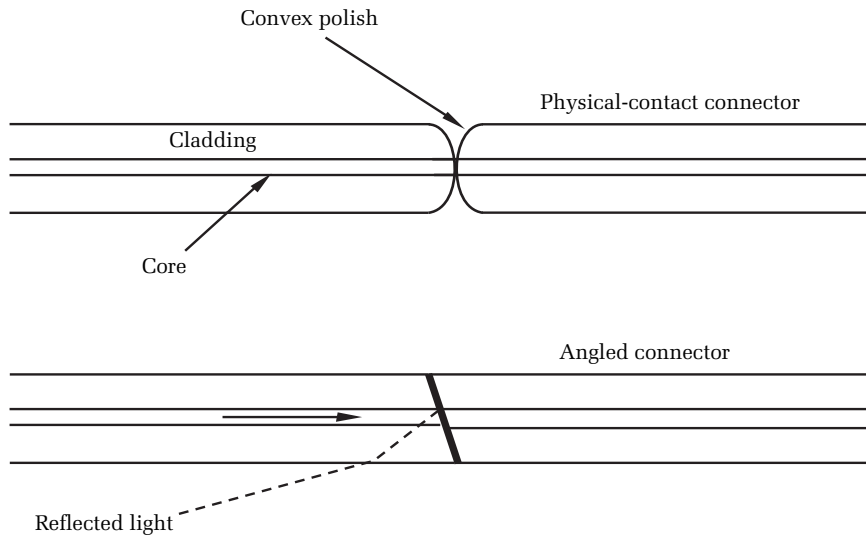


Figure 7.6. Physical-contact and angled connectors. Physical-contact connectors are designed to minimize the amount of reflection by bringing the fiber cores into intimate contact by means of a convex polish on the ferrules. Ideally, this method works very well. In practice, however, there is always some residual reflection because dimensional tolerances such as concentricity result in a very tiny gap. Angled connectors are designed to minimize the amount of reflected light that is coupled back into the fiber's core. The angle deflects the reflection outside the core's numerical aperture and into the cladding, where the light is harmlessly dissipated and lost.

*Minimum reflectivity occurs when there is no separation between the ferrules. Maximum reflectivity occurs when the ferrules are 0.25 wavelengths apart.

As we noted previously, if the faces of the ferrules are slightly separated, the reflections can sometimes add constructively, resulting in large reflections. In some cases the total reflection may be much larger than 3.6%. These large reflections are only part of the problem you may experience when the ferrules do not touch. With the ferrules separated, the connector is also more sensitive to environmental effects and changes in wavelength. This is because environmental effects may perturb the system, resulting in slight changes in the gap. Even if the gap changes by fractions of a micron, the resulting change in reflectivity can be significant. The total reflectivity for the connector (discounting coupling loss due to damage or misalignment in the connector) is

$$R = \frac{\cos\left(4\pi \frac{x}{\lambda}\right) - 1}{\cos\left(4\pi \frac{x}{\lambda}\right) + \frac{-n^4 - 6n^2 - 1}{(n-1)^2(n+1)^2}} \quad [7.3]$$

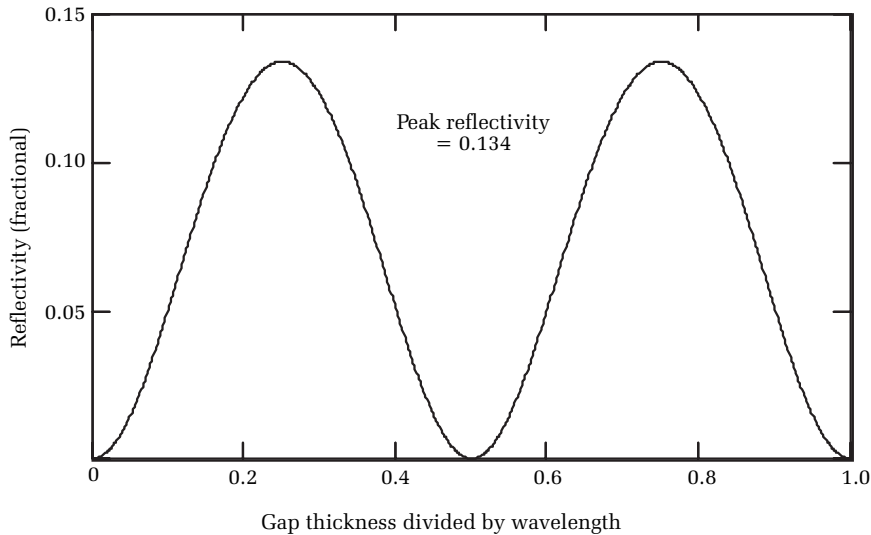


Figure 7.7. Reflectivity of a fiber-optic connector as a function of gap thickness. The reflectivity varies sinusoidally. With zero gap, the reflectivity is zero. When the gap is $\lambda/4$, the reflectivity is maximum. When the gap is $\lambda/2$, the reflectivity returns again to zero. In this figure, the fiber index was 1.468 and the gap was filled with air. The maximum reflectivity is 0.134 (−8.7 dB).

In equation [7.3], n is the index of the fiber, λ is the wavelength of light, and x is the physical gap between the two connector ends. Equation [7.3] assumes that the gap between the fibers is filled with air ($n = 1$) and that both fibers have the same index. The reflectivity given by equation [7.3] ranges from 0.134 (-8.7 dB), when the gap is $1/4\lambda$, to 0.000 ($-\infty$ dB), when the gap is totally closed. The amount of reflectivity varies sinusoidally, as shown in figure 7.7.

Another way to reduce the reflectivity of connectors is deliberately to grind and polish the ends of the ferrules at an angle. With the ferrules polished at an angle, the reflected light fails to couple to the waveguide and so is lost to cladding modes according to equation [7.2]. If the mating ferrule is polished at the same angle, then the fiber cores can still be aligned and the total connector loss kept within reasonable bounds* (see figure 7.6).^{1,2}

Table 7.1 summarizes the reflectivity of several typical components that might be found in a fiber-optic installation. Figure 7.8 illustrates how these components appear on an OTDR trace (single-mode fiber), using a 50-meter pulse at 1310 nm.

Component	Typical reflectivity (dB)
Cleave or flat polish, unconnected	-14
Multimode connectors	
Flat polish	-15 to -30
Single-mode connectors	
Premise (flat polish)	-26
Physical contact (PC)	-40
Superphysical contact (SPC)	-45
Ultrapysical contact (UPC)	-50 to -55
Angle polished	-60
Macro-/microbend	Nonreflective
Fusion splice	Nonreflective

Table 7.1. Reflectivities of some typical fiber-optic components.

*It is important to note the differences between angled and PC connectors. Angled connectors emphasize de-coupling reflections from the waveguide. PC connectors emphasize reducing the amount of reflection. Since reflected light contributes to connector loss, angled connectors typically have higher loss than PC connectors, although this is not a strict rule.

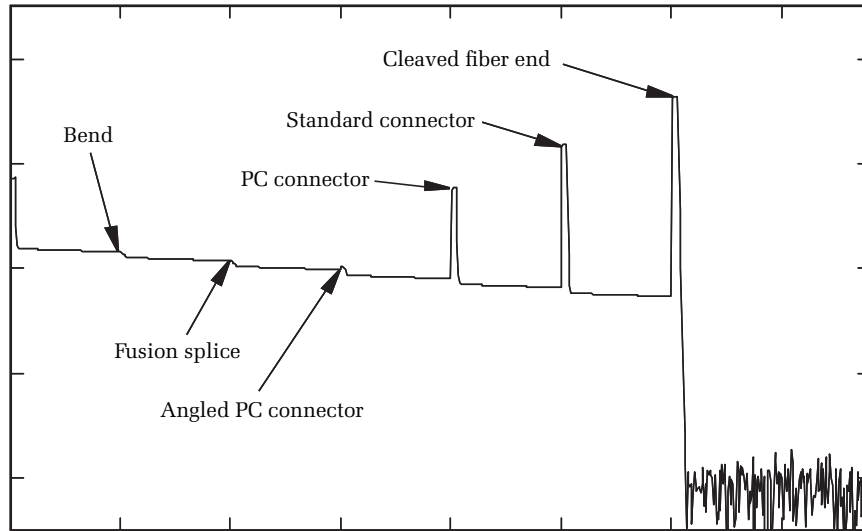


Figure 7.8. OTDR trace of some typical reflective components on single-mode fiber. The OTDR pulse width was 50 meters. Notice that the reflectivity of the angled PC connector is nearly as low as the bend and the fusion splice. With a 100-meter pulse, the reflection from the angled connector is almost indistinguishable in the OTDR trace.

The reflection from a broken fiber can be anywhere from 0% to 3.6%, depending on the nature of the break. In some cases the fiber may be broken almost as cleanly as if it were cleaved. More often, however, the break is jagged and angular, so the reflection does not couple efficiently back into the fiber. Other times, the broken fiber may be submerged in a fluid, such as water, which acts as an index-matching material and helps to reduce the amount of reflection. Frequently, a broken fiber end appears on an OTDR trace as an attenuated reflection.

In this section we have seen that reflections result from discontinuities in the optical fiber. These discontinuities occur in connectors and mechanical splices, where two fibers are joined in alignment but not fused together. Special connector designs help reduce the amount of reflection. The two most common methods are to polish the connectors at an angle (to decouple the reflection from the waveguide) and to polish the fibers with a convex surface so they touch. In the next section we describe the methods used to measure the locations, losses, and reflectivity of connectors and mechanical splices using an OTDR.

7.2.3 Reflection from mechanical splices

Mechanical splices are popular due to their simplicity and low cost when compared to the cost of a fusion splicer. Mechanical splices can be temporary or permanent, depending on the application, and all are somewhat reflective. ORL values must be considered before using mechanical splices in analog or high-speed digital applications.

The OTDR is used to measure both the insertion loss and the ORL of the mechanical splice. Like the fusion splice, the quality and attenuation value of the splice are dependent on the quality of the cleaving tool and the angle of the cleave. The better the cleave, the lower the splice loss. Splice losses of less than 0.1 dB are routinely achieved with mechanical splices when used with modern, tight-tolerance single-mode fibers.

A typical mechanical splice will use index-matching fluids (IMFs) or gels (IMGs) to minimize ORL from the mating surfaces of the two fibers being spliced. The closer the value of the index of refraction of the IMG to the fiber under test, the lower the measured ORL value will be. A typical index of refraction for the IMG is 1.46, which is close to the typical 1.46–1.48 values used in most single-mode fibers.

Index-matching gels and fluids are affected by temperature, with ORL values of 60 dB when used at room temperature, but can vary from 35 dB when used at temperature extremes of -40° to $+80^{\circ}\text{C}$. With



Figure 7.9. The OTDR trace of a mechanical splice is very similar to that of an APC (angled) fiber-optic connector. Both the APC and a mechanical splice with index-matching fluid or gel have ORL values of 50–60 dB.



Figure 7.10. Reusable Norland UVC splice for testing unterminated optical fibers. [Credit: The Light Brigade.]

an angled cleave, the splice performs at 55 dB or better across the temperature range.

Applications for mechanical splices vary with the type of users. Even though fusion splices are the dominant splice method due to their nonreflective splices, mechanical splices have become standard products for use in emergency restorations by telephone companies, utilities, and cable television operators due to their simplicity and low losses. These users still need to verify and achieve known ORL values, which must be maintained for the duration of the emergency restorations until the permanent restoration can occur using fusion splices.

Another common role of the mechanical splice is for use as a temporary connection between the OTDR's front-panel connection and the fiber and cable under test (see figure 7.9). Acceptance testing of an optical cable requires a splice that is simple to use and doesn't wear easily. The "UVC" splice (see figure 7.10), by Norland Products, provides for this need for the temporary connection during fiber acceptance testing between an OTDR and the fiber to be tested. It can be used with any fiber with an outside diameter of 125 μm .

7.3 Measuring reflective events using an OTDR

In section 7.1 we saw that OTDRs are ideally suited for measuring reflections because they operate in the time domain and can thus

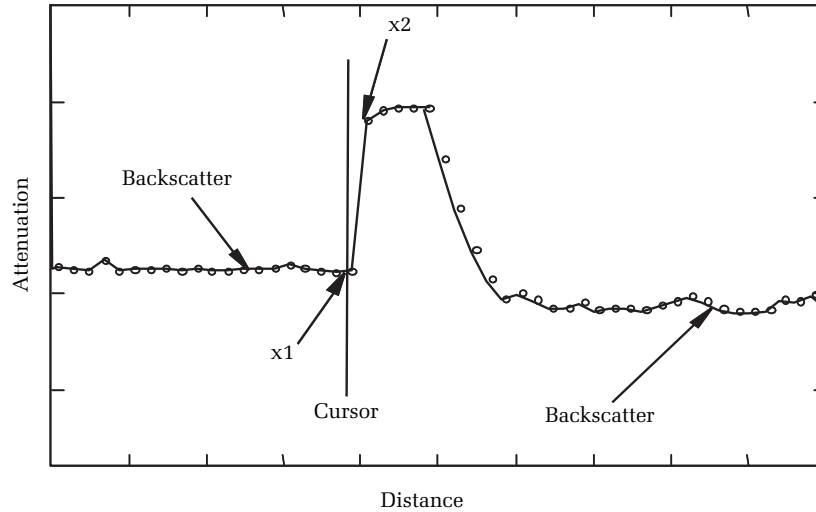


Figure 7.11. Locating the position of a reflective event in an OTDR's waveform. First, locate the position of sample point x_1 , which is the last sample point not on the event's rising edge. To this, add one-half of the sample spacing. This is the reflective event's position.

separately measure the individual reflections of components in the fiber-optic system. Figure 7.11 illustrates a reflective event as seen on an OTDR's display. Recall from chapters 3 and 5 that the sloping lines before and after the reflective event result from Rayleigh scattering, which is caused by microscopic imperfections in the fiber. The reflection in figure 7.11 is located near the OTDR's noise floor, and the undulations in the backscatter signal result from random noise. Discrete components (such as connectors and splices) typically reflect large amounts of light relative to Rayleigh scattering. Consequently, reflective events usually appear as spikes on the OTDR waveform.*

Cursor placement is important in determining the location and loss of a reflective event. Figure 7.11 shows the correct cursor placement for locating the event's position. The location accuracy of the event is limited primarily by noise and by the sample spacing in the OTDR's waveform. To locate the event, place the cursor on the last sample point

*Sometimes the reflection is barely discernible, depending on the type of reflection and the pulse width used. Recall from chapter 3 that the backscatter level depends on the pulse width. The reflection height, however, does not. An event with low reflectivity may, when acquired with a long pulse width, appear to have little reflection height above the backscatter level.

just before the waveform starts to rise up the reflective event (point x_1 in figure 7.11). The best estimate of the event's location is this distance plus one-half of the sample spacing.

Some OTDR operators and event-marking algorithms fail to add the one-half sample spacing to x_1 , biasing their measurement errors. To understand why this bias occurs, consider the following argument. The last sample point *not* on the reflection is x_1 . By definition, this sample point is *before* the reflection. The first sample point *after* the reflection's edge begins to rise is x_2 . The point x_2 is *after* the reflection. It is incorrect, therefore, to assign the reflection's position to either x_1 or x_2 . On average (over many measurements of different reflective events), the location of the reflection is midway between x_1 and x_2 .*

To measure the reflectivity of the event, place a horizontal cursor on top of the reflection, as shown in figure 7.12, and place another horizontal cursor on the backscatter just before the reflection. Measure

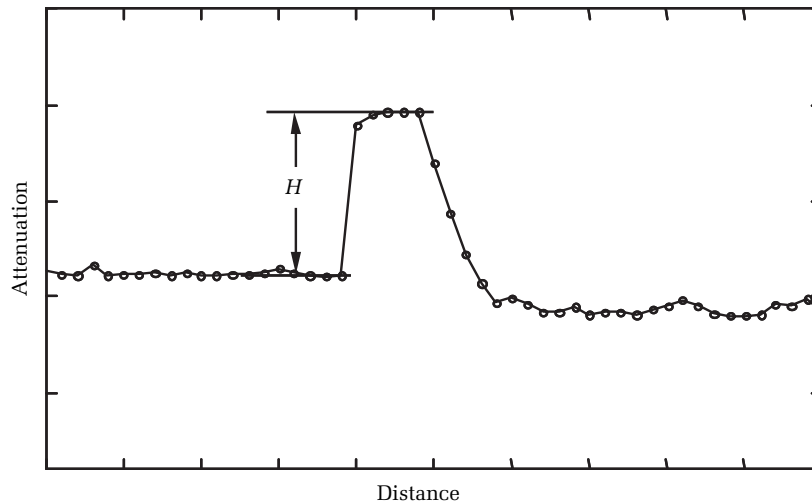


Figure 7.12. Measuring the height of a reflection for reflectivity measurements. Measure the distance (as indicated on the OTDR's vertical scale) in decibels from the highest point on the reflection to the backscatter level just before the event. Use this measurement as the value for H in equation [7.4] to determine the event's reflectivity.

*In describing this technique we are, of course, assuming that other sources of measurement error, such as bandwidth effects, are inconsequential. These sources of error sometimes dominate, so the technique of removing one-half of the sample bias becomes inconsequential.

the display height (in decibels) from the backscatter to the top of the reflection and use the following equation:³

$$R = B_{ns} + 10 \log ((10^{(H/5)} - 1)D) \quad [7.4]$$

In equation [7.4], H is the height of the top of the reflection above the backscatter, D is the OTDR's pulse width in nanoseconds, and B_{ns} is the backscatter level (in decibels, relative to the launch pulse power) of a 1-nanosecond pulse.* We refer to B_{ns} as the backscatter coefficient; later in this chapter we explain how to estimate or measure it.

Equation [7.4] is actually an approximation that assumes that the backscatter level scales linearly with pulse width and that the OTDR's bandwidth is essentially infinite.[†] For many measurements these assumptions are reasonably acceptable, but there may be times when you need a more exact formulation. We derive such a formulation in section 7.4.

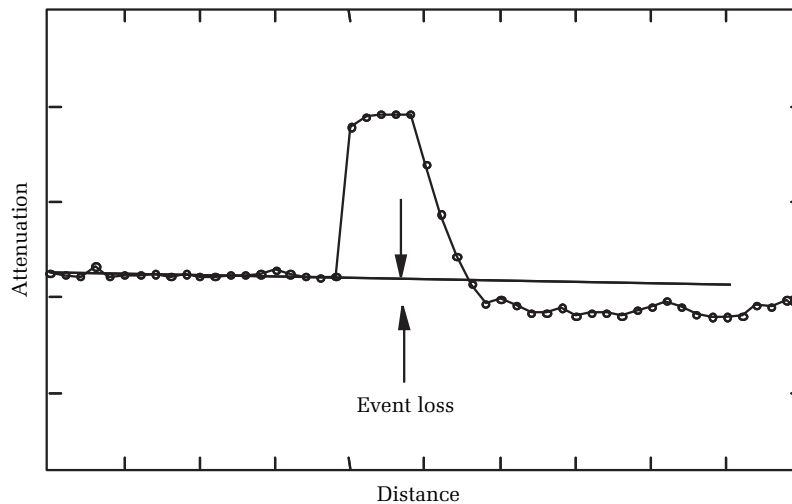


Figure 7.13. Proper cursor placement for making loss measurements of reflective events with OTDRs. Fit a cursor to the backscatter just before the event. Fit a second cursor to the backscatter just after the event, being careful to avoid fitting to the region of amplifier recovery. The event's loss is the vertical distance between the cursors, as measured on the OTDR's vertical scale.

* B_{ns} is a negative number.

[†]Backscatter scales linearly with pulse width if the OTDR pulses are all the same shape (usually square) and if the fiber's attenuation over a pulse width is negligible. Short pulses, however, are sometimes more rounded than are longer pulses, and with very long pulses the fiber's attenuation is sometimes not negligible.

Figure 7.13 shows the proper cursor placement for measuring the loss of a reflective event. Cursor placement for reflective events is similar to that for nonreflective events. Orient one adjustable horizontal cursor to fit the backscatter signature before the event, and then align the second cursor to fit the Rayleigh backscatter signature after the event. The event loss is then equal to the vertical spacing between the cursors at the center of the event.

In spite of their similarities, it is more difficult to measure the loss of reflective events than of nonreflective ones. The extra difficulty in measuring the loss of reflective events arises because it is not always obvious where the reflective event ends and the Rayleigh backscatter resumes. This makes it somewhat difficult to determine how to fit the second rotatable cursor to the waveform.

The difficulty in locating the Rayleigh backscatter signature after a reflective event results from the finite time response of the OTDR's amplifier. Observe in figure 7.13 that, because of the amplifier's finite bandwidth, the OTDR trace after a reflection does not return immediately to the backscatter level. Instead, the trace falls at a predictable rate determined primarily by the OTDR's bandwidth and characteristics of the APD. As the falling waveform approaches the level of Rayleigh backscatter, its rate of decrease slows and it gradually blends in with the normal Rayleigh backscatter signature. To measure the loss of the reflective event, it is important to fit the cursors to the part of the waveform corresponding to fiber backscatter and not to the region of amplifier recovery.

Not all OTDRs have cursors that can be aligned with the horizontal trace of the Rayleigh backscatter. When such cursors are not available, you may perform less accurate measurements* by simply measuring the discrete loss between two points.⁴ Whenever you do this, however, you must be careful to remove the fiber loss between the two points.[†] For example, suppose you measure the loss of an event by using the two-point loss between a point that is just before the event and a point that is 1.5 pulse widths after the event. If the pulse width is 200 meters and the fiber slope is 0.35 dB/km, then the fiber loss is 0.11 dB. If the two-point measurement is 0.5 dB (for example), then the event loss is $0.50 - 0.11 = 0.39$ dB.

*The horizontal cursors allow you to average the noise so that their measurement is more accurate. Point-loss measurements are more limited by the local waveform noise.

†This is done automatically with horizontal rotatable cursors, since their slope matches the fiber slope.

7.4 Effects that can reduce the accuracy of reflectivity measurements

Usually OTDRs make accurate reflectivity measurements. Like all instruments, however, their performance is greatly influenced by unique circumstances. In this section we review some of the things that can introduce errors into the OTDR's reflectivity measurements. We also suggest some techniques that can help obtain accurate results even in the face of such extenuating circumstances.

As we have seen, an OTDR measures the reflectivity of an event by measuring the height of the reflection above backscatter and using this with equation [7.4]. Implicit in the derivation of equation [7.4] is the assumption that the backscatter level changes linearly with the pulse width. As long as the fiber's attenuation over the pulse width is small and the different pulses are the same shape, this assumption is warranted. For longer pulse widths (on the order of a kilometer or more), the assumption begins to break down and, for optimum accuracy, we need to modify equation [7.4]. To do this we begin with the basic equation for coupled backscatter. For sufficiently short, square laser pulses,* the total backscatter coupled into single-mode fiber is (see also equations [3.5] and [3.6])^{5,6,7,8}

$$P_{bs} = \left(\frac{NA}{n_1} \right)^2 \cdot \frac{\alpha_s}{4.55} \cdot W \cdot P_0 \quad [7.5]$$

In equation [7.5], NA is the fiber's numerical aperture, n_1 is the core index of the fiber, α_s is the scattering coefficient (1/km), W is the OTDR's displayed pulse width (km), and P_0 is the power of the laser pulse at the point on the fiber where the Rayleigh scattering originates.^{†,‡}

We derive the equation for reflectivity by first expressing equation [7.5] in terms of differentials and as a function of scattering from some arbitrary location, x , along the fiber. Doing this, we have (assuming $\alpha \approx \alpha_s$)

$$dP_{bs} = \left(\frac{NA}{n} \right)^2 \cdot \frac{\alpha}{4.55} \cdot dx \cdot P_0 \cdot e^{-2 \cdot \alpha \cdot x} \quad [7.6]$$

*"Short" is relative to fiber attenuation. For most fibers, pulses less than a few hundred meters satisfy the requirements of this assumption.

†To convert the scattering coefficient from dB/km to 1/km, multiply the value in dB/km by $\ln(10)/10 \approx 0.23$.

‡The OTDR's displayed pulse width is actually half the true pulse width because the time base is divided by 2 in order to account for the two-way travel of OTDR light signals through the fiber.

Suppose a reflective event exists at some distance L . The optical received power from the Rayleigh backscatter at point L on the OTDR display is

$$P_{bs}(L) = \left(\frac{NA}{n}\right)^2 \cdot \frac{\alpha}{4.55} \cdot P_0 \int_{L-W}^L e^{-2 \cdot \alpha \cdot x} dx \quad [7.7]$$

Integrating equation [7.7] we have

$$P_{bs}(L) = \left(\frac{NA}{n}\right)^2 \cdot \frac{\alpha}{4.55} \cdot P_0 \left(\frac{\exp(-2\alpha(L-W)) - \exp(-2\alpha L)}{2\alpha} \right) \quad [7.8]$$

The received power from the reflection is

$$P_R(L) = P_0 \cdot 10^{-(R+2\alpha L)/10} \quad [7.9]$$

The height of the reflection above backscatter, as seen on the OTDR display, is

$$H = 5 \log \left(\frac{P_R(L) + P_{bs}(L)}{P_{bs}(L)} \right) \quad [7.10]$$

Substituting equations [7.8] and [7.9] into equation [7.10], solving for the event's reflectivity R , and simplifying, we have:

$$R = B_{ns} + 10 \log((10^{(H/5)} - 1) \cdot 10,000((\exp(2\alpha W) - 1)/2\alpha)) \quad [7.11]$$

In equation [7.11], H is the height of the top of the reflection above backscatter (see figure 7.11), α is the attenuation coefficient (1/km), B_{ns} is the backscatter level for a 1-ns pulse, and W is the pulse width (in kilometers) as seen on the OTDR display.

For small pulses, the fiber attenuation over the pulse width is small and equation [7.11] is approximately equal to equation [7.4]. For small pulse widths, there is little impact on the reflectivity measurement when using equation [7.4]. Even for longer pulses the effect is relatively minor, especially compared with other errors associated with calibrating the backscatter coefficient. For example, suppose W is 2 km, the fiber's attenuation coefficient is 0.35 dB/km (0.08/km), and the scattering coefficient is -80.5 dB. If H is 5 dB, then the reflectivity determined from equation [7.11] is -27.23 dB. The reflectivity determined from equation [7.4] is -27.95. So, even in the most extreme cases (most OTDRs have no pulse widths over 2 km), the difference between equations [7.11] and [7.4] is less than 1 dB.

Another potential cause of reflectivity error results from bandwidth limitations in the OTDR. Since an OTDR determines an event's reflectivity by measuring the reflection's height above the backscatter level, errors may result if the OTDR's receiver has insufficient bandwidth to reach the top of the reflection. When this happens, H is underestimated and the reported reflectivity is too small.

There are several approaches to solving bandwidth-related reflectivity errors, but perhaps the simplest is to calculate the reflectivity by integration. Some OTDRs allow the user to place distance cursors around an event. The instrument then calculates the total reflectivity between the cursors. In this procedure, the user places one vertical cursor just before the reflection and the second vertical cursor after the reflection at about the point where the waveform has returned to the Rayleigh backscatter level. By integrating over this region, the instrument accurately calculates the event's reflectivity, regardless of any limitations from bandwidth.*⁹

The method of integration works by measuring the total energy reflected by a component and normalizing this to the pulse width. In an ideal amplifier, energy is not lost when the bandwidth is too low to resolve a sharp pulse fully. Instead, the energy is simply distributed over a wider region of the waveform trace (this is why the pulse looks wider). By integrating under the broadened pulse, the OTDR measures the total energy in the reflection. Since the true pulse width is known, the OTDR can easily calculate how high the pulse would have been had it not been spread out by the amplifier's finite bandwidth. In this way the OTDR can calculate a correct reflection height, from which the true reflection follows from equation [7.4] or equation [7.11].

Another possible source of reflectivity error is undersampling. Virtually all OTDRs display a sampled version of the waveform. If the OTDR samples the waveform many times over the length of a pulse, there is little danger of measurement error from undersampling. On the other hand, if the OTDR samples only once for each pulse width, it may not sample at the top of the reflection. In such cases, the reflection height is reported incorrectly and the reflectivity measurement is in error.

When we integrated equation [7.7] to get equation [7.8], we assumed that the OTDR's laser pulses are square. If the laser pulses are not square, an error results in the reflectivity measurement unless

*This technique, however, does not compensate for saturation in the OTDR's receiver or amplifier circuits.

the OTDR takes into account the pulse distortion. Generally, the laser pulses from OTDRs are relatively square, and you do not need to be too concerned with this problem. With very short pulses, however, the shape of the laser pulse may deviate significantly from that of a square. This effectively reduces the pulse width and, if not corrected, can result in significant error in the reflectivity measurement.¹⁰ Errors associated with short pulse widths are further complicated because the OTDR's system bandwidth is sometimes less capable of reaching the top of the reflection than with longer pulses. Typically, there is little that an OTDR user can do to correct for errors caused by bandwidth and pulse shape. This emphasizes the importance of buying an OTDR designed with the proper internal calibration corrections that take these effects into account.

7.5 Calibrating the OTDR's backscatter coefficient

In the previous section we saw that bandwidth errors can affect the accuracy of reflectivity measurements and that you should use equation [7.11] instead of equation [7.4] if the fiber's attenuation is significant over the length of one pulse width. The largest and most common source of error in reflectivity measurements, however, relates to the OTDR's calibration. In this section we discuss some of these calibration issues and describe methods you can use to calibrate your instrument.

We saw in chapter 3 that the vertical scale on an OTDR shows relative power on a 5-log scale. Because the vertical scale is relative and uncalibrated, OTDRs cannot simply measure the reflectivity of events by noting their vertical scale readings.* To overcome this problem, OTDRs measure reflectivity by referencing the height of the reflection to the backscatter level, as we saw in figure 7.11. The fiber's backscatter trace provides a calibrated reference level, assuming the proper backscatter coefficient has been entered into the OTDR. Given the correct backscatter coefficient, the reflectivity is (see also equation [7.4])[†]

$$R = B_{ns} + 10 \log ((10^{(H/5)} - 1)D) \quad [7.12]$$

In equation [7.12], H is the height of the reflection above backscatter (as read on the OTDR's 5-log display), D is the OTDR's laser pulse width (in nanoseconds), and B_{ns} is the backscatter coefficient (expressed in

*The vertical scale needs to be linear, and OTDR manufacturers work hard to make this so. Reflectivity and loss measurements, however, are relative. Consequently, there is no absolute calibration of the OTDR's vertical scale.

[†]For simplicity, we assume the pulse width is short relative to the fiber attenuation, so we do not need to use equation [7.11].

decibels). If W is the OTDR's displayed pulse width in meters, then D (in nanoseconds) is

$$D \approx W \cdot 10 \quad [7.13]$$

For example, if you are using a 100-meter pulse, D is 1000 nanoseconds.

From equation [7.12] you can see that errors in either the backscatter coefficient, pulse width, or height above backscatter result in errors in the reported reflectivity. Most OTDRs come with preset default values for the backscatter coefficient, and in many cases these default values suffice to make reflectivity measurements that are accurate to within a few decibels. If you desire more accuracy than this, you must calibrate the backscatter coefficient of the test fiber.

7.5.1 Calculating the backscatter coefficient

One way to determine the backscatter coefficient is to calculate it from the fiber's material properties. To do this, the first fiber parameter you need to know is the Rayleigh scattering coefficient (see figure 7.14).^{*} By considering all the relevant physical parameters of the fiber (which, unfortunately, are usually unknown), you can determine the amount of Rayleigh scattering. Typically, however, you must determine the scattering coefficient experimentally. The Rayleigh scattering coefficient, or contribution to fiber loss, is given by the following equation:

$$\alpha_S = A \cdot \lambda^{-4} \quad [7.14]$$

Manufacturer	Index of refraction			PMD	Backscatter coefficient (dB)		
	1310	1510	1625		1310	1550	1625
Alcatel 6900 TeraLight (NZDS) 6910	1.464	1.4645 1.4692	1.469	$\leq 0.1\text{ps/km}$ $\leq 0.08\text{ps/km}$	-76.7 -77.5	-81.7 -80.5	-81.4
OFS Truewave (NZDS) Allwave (NZDS)	1.466 1.471 1.466	1.467 1.47 1.467	1.467 1.47 1.467	$\leq 0.1\text{ps/km}$ $\leq 0.06\text{ps/km}$ $\leq 0.08\text{ps/km}$	-49.6 -45.4 -49.6	-52.1 -49.8 -52.1	-53.1 -51.1 -53.1
Corning SMF-28 SMF-DS LEAF (NZDS) MetroCor (NZDS)	1.4677 1.4718	1.4682 1.4711 1.468 1.469	1.469	$\leq 0.1\text{ps/km}$ $\leq 0.04\text{ps/km}$ $\leq 0.1\text{ps/km}$	-77 -75 -75 -75	-82 -81 -81 -81	-82 -82 -82 -82

Figure 7.14. Backscatter coefficients for common single-mode fibers.

^{*}Do not confuse the Rayleigh scattering coefficient with the backscatter coefficient. The Rayleigh scattering coefficient is the loss per kilometer that results from Rayleigh scattering. The backscatter coefficient is the power of backscattered light from a 1-ns pulse (expressed in decibels).

In equation [7.14], λ is the wavelength and A is a constant that depends on the fiber and has units of $\text{dB} \cdot \mu\text{m}^4/\text{km}$.

In chapter 2 we saw that optical fibers transmit light by a process called *total internal reflection*. One consequence of total internal reflection is that light “rays” that are not sufficiently parallel to the axis of the fiber are lost and not transmitted by the fiber. Because backscatter radiation emits in all directions, most of it is lost (it is scattered outside the fiber’s numerical aperture) and is not transmitted back to the OTDR. Only the portion of the backscatter that is emitted within the fiber’s numerical aperture is captured. For sufficiently short square laser pulses, the total backscatter coupled into single-mode fiber is (see also equation [7.5])*

$$P_{bs} = \left(\frac{\text{NA}}{n_1} \right)^2 \cdot \frac{\alpha_s}{4.55} \cdot W \cdot P_0 \quad [7.15]$$

In equation [7.15], NA is the fiber’s numerical aperture, n_1 is the core index of the fiber, α_s is the Rayleigh scattering coefficient (1/km), W is the OTDR’s displayed pulse width (km), and P_0 is the power of the laser pulse at the point on the fiber where the Rayleigh scattering originates.[†]

Typical single-mode fibers have a numerical aperture of about 0.12, a core index of 1.468, and an attenuation coefficient of about 0.25 dB/km, or 0.0575/km (at 1550 nm). Let’s assume the attenuation coefficient is essentially equal to the Rayleigh scattering coefficient (a fairly good assumption for low-loss communications-grade fiber). Given this assumption, the backscattered light from an OTDR with a 100-meter pulse has 50.7 dB less power than the laser pulse at the point where the scattering occurs. If the OTDR could generate square pulses only 1 nanosecond long, then the displayed pulse would be 0.1 meter and the backscatter power about –80.7 dB.

By definition, the backscatter coefficient is the backscatter power, relative to the peak pulse power, for a 1-nanosecond pulse. Consequently, if you know the numerical aperture, index, and Rayleigh scattering coefficient of the fiber, you can calculate the backscatter coefficient by using equation [7.16].

*“Short” is relative to fiber attenuation. For most fibers, pulses less than a few hundred meters satisfy the requirements of this assumption.

[†]To convert the scattering coefficient from dB/km to 1/km, multiply the value in dB/km by 0.23.

$$B_{ns} \equiv 10 \log \left(\frac{P_{1ns}}{P_0} \right) = 10 \cdot \log \left(\left(\frac{NA}{n_1} \right)^2 \cdot \frac{\alpha_s}{4.55} \cdot 0.0001 \right) \quad [7.16]$$

The accuracy of the backscatter coefficient depends on the uncertainty of the fiber parameters, such as the numerical aperture. Typically, the numerical apertures of single-mode fibers are randomly distributed about the specified mean. For example, the mode-field diameter of a single-mode fiber may be specified at $10.5 \pm 1.00 \mu\text{m}$ at 1550 nm. For single-mode fiber, the mode-field diameter is approximately inversely proportional to the numerical aperture, so the NA, which is nominally 0.13, can really be as low as 0.118 and as high as 0.142.* From equation [7.16], we see that the backscatter coefficient is sensitive to numerical aperture, and that the difference in backscatter coefficient for these two numerical apertures is about 1.6 dB. The index of refraction, as well as the attenuation coefficient, also varies slightly from fiber to fiber, so these further widen the uncertainty in any calculation that is based solely on the manufacturer's data sheets.

Figure 7.15 illustrates the results of a Monte Carlo analysis showing the variability in backscatter coefficient for a typical type

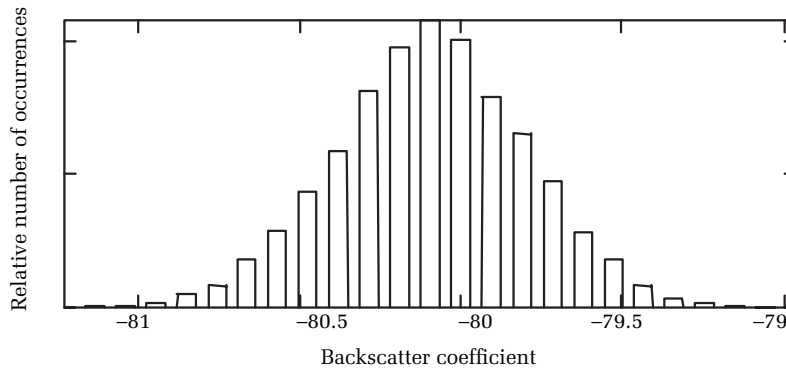


Figure 7.15. Normal variation in backscatter coefficient for a typical type of single-mode fiber, due to variations in fiber parameters. Assumed variations are: $NA = 0.13 \pm 2.69\%$; $\alpha_s = 0.25 \text{ dB/km} \pm 8.3\%$; fiber core index = $1.468 \pm 0.03\%$. These uncertainties are at the 1-sigma confidence level.

*For most single-mode fibers, the fundamental mode is nearly Gaussian. For Gaussian beams, the beam divergence in the far field (numerical aperture) is inversely proportional to the radius of the beam waist. See, for example, the chapter on Gaussian beams in *Fundamentals of Photonics* by B. E. Saleh and M. C. Teich, especially equation 3.1-20 on page 86.

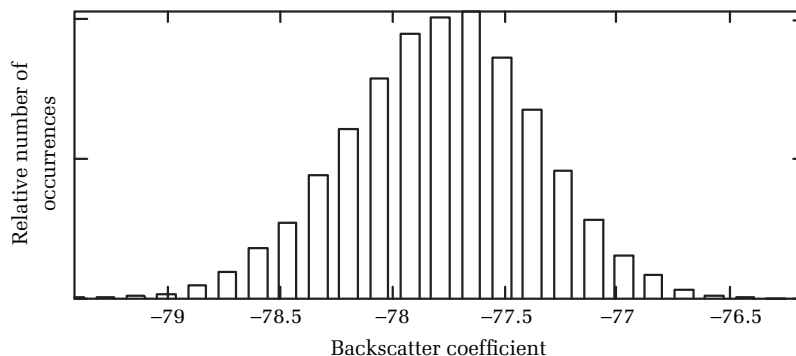


Figure 7.16. Normal variation in backscatter coefficient for typical dispersion-shifted fibers due to typical variations in fiber parameters. Assumed variations are: $NA = 0.17 \pm 4.01\%$; $\alpha_S = 0.25 \text{ dB/km} \pm 8.3\%$; fiber core index = $1.468 \pm 0.03\%$. These uncertainties are at the 1-sigma confidence level.

of single-mode fiber, using equation [7.16].* Figure 7.16 shows the results of a similar analysis for a typical type of dispersion-shifted fiber. These results show that the true backscatter may differ from the calculated value (using the nominal fiber parameters) by as much as 1.5 dB. Of course, if you measure the actual numerical aperture, Rayleigh scattering coefficient, and fiber index with sufficient accuracy, you can use equation [7.16] with less error than indicated by the histograms in figures 7.15 and 7.16.

7.5.2 Measuring the backscatter coefficient

When the uncertainties associated with equation [7.16] are unacceptable, you can measure the backscatter coefficient directly. We discuss three techniques for accomplishing this. Two of these techniques are best performed in the laboratory, but the third allows you to calibrate the backscatter coefficient by using a fiber of known coefficient and an OTDR. This third method can easily be performed in the field.

7.5.2.1 Measuring the backscatter coefficient with a calibrated reflector

At the beginning of this chapter we saw that reflections occur in fiber-optic networks whenever there is a change in the index of refraction. We

*Assuming that the specifications on Corning's data sheets applied to the 2-sigma certainty level.

also saw that a common example of a reflective event is a cleaved fiber end. From equation [7.1], when light is incident normally upon an index discontinuity, the fractional power in the reflected light is

$$R = \left(\frac{n_t - n_i}{n_t + n_i} \right)^2 \quad [7.17]$$

In equation [7.17], n_t is the index in the transmit region and n_i is the index in the incident region. As we saw at the beginning of this chapter, for typical single-mode communications-grade optical fiber, the effective index of refraction is about 1.468. The index of refraction for air is nearly 1.000, so the reflection at a square, cleaved fiber end is about 0.0360, or -14.4 dB.

Equation [7.17] is quite accurate in bulk optics even when the light is a few degrees from being perfectly perpendicular. As we have already seen, however, in fiber optics you must be careful to have nearly perfect cleaves; otherwise the reflectivity is less than predicted by equation [7.17] because the back-reflecting light does not couple efficiently into the fiber (see equation [7.2]).

Equation [7.17] suggests a relatively simple way to calibrate the backscatter coefficient in an OTDR. First, select a long fiber such that the backscatter trace is reasonably free of noise but the top of a -14.4-dB reflection at the end of the fiber is not in the saturated region of the OTDR's receiver.* Next, cleave the end of the fiber to within at least 0.5° of perpendicularity, and adjust the OTDR's backscatter coefficient until the OTDR measures the reflection at -14.4 dB. The backscatter coefficient that gives a -14.4-dB reading is the correct coefficient for that fiber.†

Preparing a cleave with the necessary perpendicularity may be somewhat difficult and might involve the use of an optics lab with a microscope for examining the cleave. This makes the cleave method somewhat impractical for field use, unless you use a precision fiber cleaver that gives consistently square cleaves (see figure 7.17). Alternatively, you can use a polished connector. If you do this, however,

*Alternatively, you may want to use an optical attenuator near the OTDR's front panel to attenuate the backscatter and reflection. If you do this, take care to have a sufficiently long fiber so the amplifier response from the front-panel reflection can drop all the way to the level of the attenuated backscatter well before the end reflection.

†We have assumed that the fiber's index of refraction is 1.468. This might not always be true. If the fiber's index of refraction is different from 1.468, apply equation [7.17] to calculate the true reflection and use that number instead of -14.4.

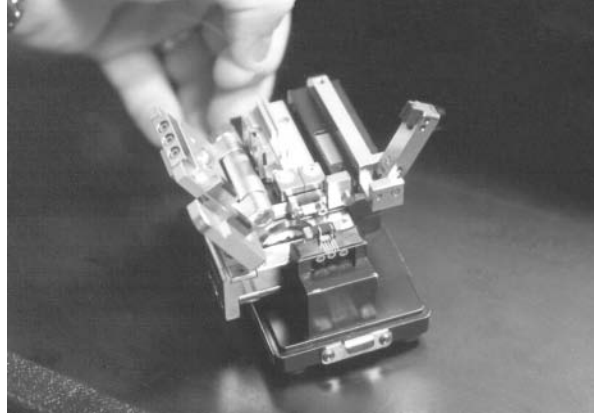


Figure 7.17. Precision cleaver for consistently square fiber cleaves. [Credit: The Light Brigade.]

be certain that the end is perpendicular and clean and that the polishing technique does not alter the fiber's index sufficiently to invalidate the results of equation [7.17].

You can also use this method with any calibrated reflection, not just a cleaved fiber end. A calibrated reflector can be expensive, however, so the cleaved fiber offers a relatively inexpensive alternative. On the other hand, some OTDRs may not fully resolve the large difference between backscatter and the top of a -14.4 -dB reflection.* If this is the case, a lower calibrated reflection can be useful. Whatever reflective event you use, the top of the reflection must not be in the OTDR's saturation region, must not be limited by the OTDR's bandwidth, and must not be wavelength sensitive. Wavelength sensitivity generally rules out using a mated connector because the endfaces of the connected fiber pair form a weak Fabry-Perot resonator whose reflectivity is strongly dependent on wavelength as shown in equation [7.3]. Connectors are also subject to environmental perturbations, so their reflectivity can easily change with time.

7.5.2.2 Measuring the backscatter coefficient using a CWR

Another experimental way to determine the backscatter coefficient is to measure it using a CWR (see figure 7.1). This device uses a continuous (nonpulsed) laser source to fill the test fiber with optical radiation. The power meter in the return leg measures the total reflected and

*If this is the case, the backscatter coefficient determined by this procedure is wrong.

scattered radiation. You can use the CWR to measure the backscatter coefficient of an optical fiber directly. Suppose, for the moment, that a CWR is connected to a 0.1-meter length of fiber whose opposite end is terminated so that it does not reflect any light back into the CWR. The fiber's backscatter coefficient is, by definition,

$$B_{ns} \equiv 10 \log(P_{1ns}/P_0) \quad [7.18]$$

In equation [7.18], P_{1ns} is the scattered power and P_0 is the incident power.

Making this measurement with only 0.1 meter of fiber is difficult because the scattered power is about 80 dB less than the incident power. This places extreme requirements on the receiver and the reflectivity of the other optical components, such as the CWR's front-panel connector and coupler. To make this method more practical, you can increase the signal level (the amount of backscattered radiation) by increasing the fiber's length. If we use a fiber that is L meters long, for example, the total backscattered power is

$$P_{bs} = 10^{\left(\frac{B_{ns}}{10}\right)} P_0 \sum_{i=0}^{i=N} \exp(-2\alpha \cdot \Delta x \cdot i) \quad [7.19]$$

In equation [7.19], Δx is 0.1 meter, N is the number of times Δx divides into L , α is the attenuation coefficient (1/km), and B_{ns} is the backscatter coefficient.

Rearranging equation [7.19], integrating, and simplifying, we can write the experimentally determined backscatter coefficient as

$$B_{ns} = 10 \log\left(\frac{2\alpha \cdot P_{bs} \cdot \Delta x}{P_0(1 - \exp(-2\alpha \cdot L))}\right) \quad [7.20]$$

In equation [7.20], P_{bs} is the total backscattered power and P_0 is the total power launched into the fiber.

If you are using a CWR made from discrete components, it is helpful first to use an OTDR to measure the test fiber's length, attenuation coefficient, and end-to-end loss. Then determine the launch power by measuring the transmitted loss from the end of the test fiber and correcting for the end-to-end loss that you measured with the OTDR. If you are using a calibrated commercial CWR, measure L and α with an OTDR and P_{bs}/P_0 with the CWR.

Observe from equation [7.20] that with a 10-km fiber (for example), the backscattered power increases from about -80.7 dB (for a 0.1-meter length of fiber) to about -33 dB. This is easily within the measurement range of most CWRs and handheld optical power meters. A fiber that is only 1 km long has a total return backscatter of -41 dB, so the backscatter coefficient of even relatively short fibers can be measured using the CWR and equation [7.20]. As a final note, to use the CWR method, you must completely terminate the reflection at the end of the fiber so that only Rayleigh backscatter is measured. Before measuring the backscatter power, use an OTDR to verify that there is no reflection at the end of the fiber. Do this by using the shortest possible pulse that still shows backscatter out to the end of the fiber. An effective way of terminating the end of the fiber is to break the end of the fiber and then wrap the last half-meter of fiber tightly around a pencil and immerse the fiber end in index-matching gel. Another important point is to null the CWR by measuring the scattered and reflected power that originates from the coupler and front-panel connector and subtracting these from the backscatter power measured from the test fiber.

7.5.2.3 Measuring the backscatter coefficient using an OTDR

Measuring the backscatter coefficient using a standard reflector or CWR requires care and must usually be done in a laboratory environment. However, if you calibrate the backscatter coefficient of one fiber properly, it is fairly simple to transfer that calibration to another fiber using a standard OTDR. To do this:

1. Carefully measure the backscatter coefficient of your standard fiber by using either a calibrated reflector or a CWR.
2. Connect the calibrated fiber to the fiber with unknown backscatter coefficient.
3. Connect them in any way (connector, fusion splice, mechanical splice, etc.), but the connection's loss must be stable.*
4. Connect your OTDR to the reference fiber and measure the connection's loss in decibels. Call this measured loss M1.
5. Move the OTDR to the other end of the unknown fiber and measure the splice loss again. Call this measurement M2.

*The amount of loss at the connection is not important as long as it does not exceed the OTDR's dynamic range.

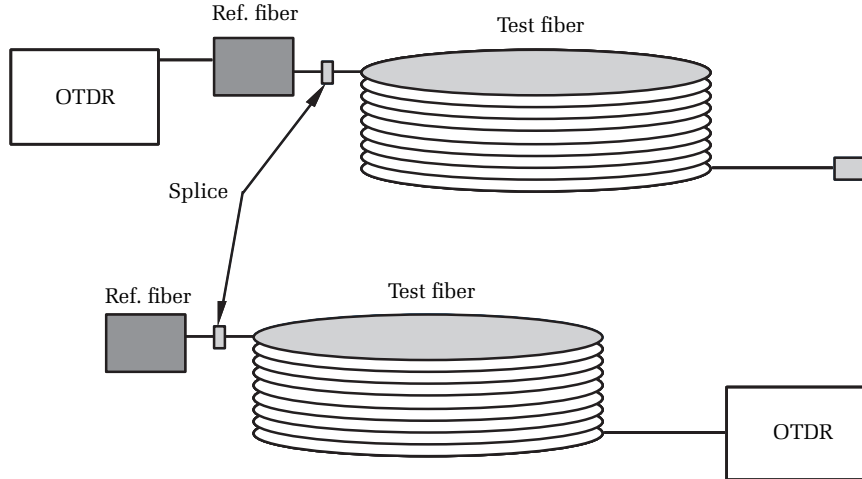


Figure 7.18. Determining the backscatter coefficient of an unknown fiber by measuring the loss between the unknown fiber and a reference fiber with an OTDR. First, with the OTDR connected to the reference fiber, measure the loss of the splice between the reference fiber and the test fiber. Call this measurement M1. Next, with the OTDR connected to the opposite end of the test fiber, measure the splice between the reference and test fiber again. Call this measurement M2. Be careful not to disturb the splice during this procedure. The backscatter coefficient of the test fiber, relative to the reference fiber, is then given by equation [7.21].

The backscatter coefficient for the unknown fiber is now (see figure 7.18):

$$B_{ns_unknown} = B_{ns_Ref} + M2 - M1 \quad [7.21]$$

Derivation of equation [7.21] is straightforward. With the OTDR attached to the reference fiber, the measured loss is*

$$M1 = 5 \log \left(\frac{P_0 \cdot 10^{\left(\frac{B_{ns_1}}{10}\right)}}{P_0 \cdot \frac{1}{L_f^2} \cdot 10^{\left(\frac{B_{ns_2}}{10}\right)}} \right) = 10 \log(L_f) + \frac{B_{ns_1}}{2} - \frac{B_{ns_2}}{2} \quad [7.22]$$

*This follows from equation [7.18], the definition of loss measurement with an OTDR, and the assumption that splice loss does not change with pulse width.

In equation [7.22], Lf is the true fractional loss of the splice. Similarly, with the OTDR attached to the test fiber, the measured loss is

$$M2 = 10 \log(Lf) + (B_{ns_2}/2) - (B_{ns_1}/2) \quad [7.23]$$

Taking the difference we have

$$M2 - M1 = B_{ns_2} - B_{ns_1} \quad [7.24]$$

from which equation [7.21] follows directly.

As an example of this method, we connected a standard piece of Corning SMF-28 single-mode fiber to a piece of Corning SMF dispersion-shifted fiber. With the OTDR attached to the SMF-28 fiber (our reference fiber), the measured loss was $M1 = -1.549$ dB.* With the OTDR attached to the dispersion-shifted fiber, the measured loss was $M2 = 2.745$ dB. Thus, from equation [7.21], the backscatter coefficient for the dispersion-shifted fiber is about 4.29 dB greater than it is for the non-dispersion-shifted fiber. If the non-dispersion-shifted fiber has a backscatter coefficient of -80.7 dB, then the backscatter coefficient of the dispersion-shifted fiber is -76.4 dB.

For the fibers used in this test, Corning specified the numerical aperture of its dispersion-shifted fiber at 0.17 ± 0.014 and the numerical aperture of its SMF-28 fiber at 0.13 ± 0.012 .† The measured attenuation coefficient of the dispersion-shifted fiber was 0.359 dB/km and for the non-dispersion-shifted fiber was 0.347 dB/km. If you consider only differences in attenuation coefficients and numerical apertures, equation [7.16] shows that the calculated backscatter coefficient for the dispersion-shifted fiber should be 0.96–4.00 dB greater than for the non-dispersion-shifted fiber. The actual measured value of 4.26 dB indicates that one or both of the fibers may be slightly out of specification.‡ From equation [7.16] you can see that the backscatter coefficient is very sensitive to the numerical aperture. For example, if the numerical aperture of the dispersion-shifted fiber were $0.17 + 0.019$ and that of the non-dispersion-shifted fiber were $0.13 - 0.014$, the calculated difference would agree with the measured difference. This illustrates the advantage

*The event appeared as a “gainer.” Hence, the loss reported is negative.

†Actually, Corning did not specify tolerances on the numerical aperture. We inferred these tolerances from those given for the mode-field diameter, which (for Gaussian modes) is inversely proportional to the beam divergence, or numerical aperture.

‡Recall that we assumed the mode distribution is Gaussian. This is not strictly true, so the difference may result from this assumption rather than the fiber being out of specification.

of making accurate measurements instead of relying on vendor data sheets and calculations.

7.6 Integrated return loss

We end this chapter with a slight digression. This chapter ostensibly deals with reflective events. The integrated return loss is the total reflected power, from discrete reflections as well as backscatter, that couples into the fiber and travels back to the OTDR. Integrated return loss is only partially related to the main subject of this chapter. However, the OTDR menu for event return loss is frequently coupled to the menu for integrated return-loss measurements. Furthermore, the compelling reasons for measuring event return loss usually apply for integrated return loss as well. In this chapter, therefore, it makes sense to include a discussion of integrated return loss, how to measure it with an OTDR, what the measurements mean, and techniques you can use to ensure accuracy in your results.

Suppose you want to measure the total reflected power that an optical transmission line directs back into an optical transmitter. You might use a CWR. Imagine, however, that when you test the optical fiber, the total reflected power exceeds your system specification. Although the CWR has detected a problem, you cannot easily diagnose it. To locate and solve the problem, you might use an OTDR. Since the OTDR is necessary to diagnose the problem and resolve it, you might wish to streamline your testing by bypassing the CWR altogether. This is only possible, however, if you can calculate the total reflected power using the OTDR waveform. Fortunately, many OTDRs do measure the total reflected power by calculating what is called the *integrated return loss*.

Figure 7.19 shows how to measure the integrated return loss using an OTDR.* First, decide over which region of the fiber you want to measure the optical return loss. Then place one cursor at the beginning of the section and the other cursor at the end. Be especially careful to place the first cursor on a region of waveform containing backscatter. If you are measuring the integrated return loss for the entire fiber, you must use a lead-in fiber, dead zone box, or an OTDR with internal fiber. This is necessary so that you have backscatter before the reflection at the beginning of the test fiber. If the end of the section of fiber you are testing has a reflection, place the second cursor slightly beyond the end of the reflection.

*This method is used by one particular manufacturer. Other manufacturers may implement the solution using a different human interface.

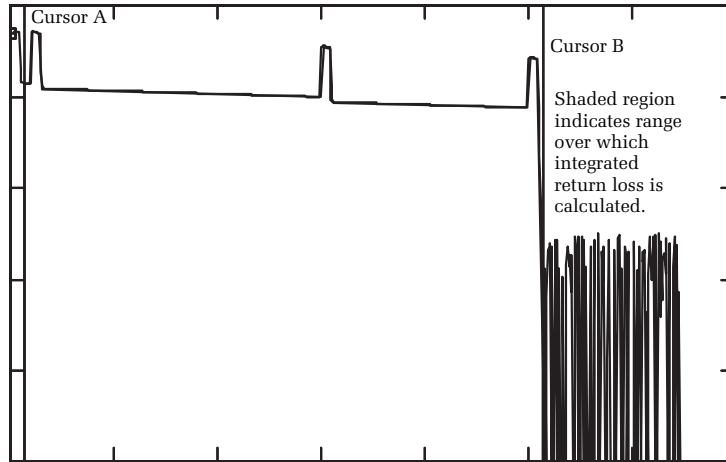


Figure 7.19. Measuring the total reflected and backscattered light using an OTDR. The OTDR integrates the total power between two cursors and multiplies by a normalizing factor. The resulting measurement is the return loss of the section bounded by the two cursors. The first cursor must be on backscatter, and the second cursor must lie beyond the end reflection. Measuring the total integrated return loss of the entire fiber requires either internal fiber in the OTDR or a sufficiently long jumper to obtain a clean backscatter signature before the test fiber.

Most OTDR manufacturers make it relatively easy to calculate integrated return loss. To do so, they employ algorithms designed to determine from the OTDR waveform what the optical return loss would be if a CWR were attached to the beginning of the selected fiber section. In some cases, it might be physically possible to make the equivalent measurement with a CWR (when measuring the integrated return loss of a single length of fiber, for example). Other times, if the section of interest lies somewhere within the test fiber, only the OTDR can make the desired integrated return-loss measurements.

The rest of this section describes how an OTDR calculates the integrated return loss from the acquired waveform. Understanding the derivation of the equations is not necessary to use the OTDR, but it may offer additional insights to the methodology and its possible limitations.

Suppose we wish to use a CWR to measure the total light scattered and reflected by a fiber that has N reflective events ($R_1, R_2, \dots R_N$) and is described by a cumulative splice loss function, $L_c(x)$. We modify equation [7.19], expressing the summation as an integral, obtaining

$$P_{bs} + P_R \equiv P_{bs} = 10^{\left(\frac{B_{ns}}{10}\right)} \frac{P_0}{\Delta x} \int_0^L L_C(v) \exp(-2\alpha v) dv + P_0 \sum_{i=1}^N L_C(v) \exp(-2\alpha x_i) R_i \quad [7.25]$$

In equation [7.25], Δx is 0.0001 km (corresponding to a 1-ns pulse and *not* the sample spacing) and P_0 is the pulse power injected into the fiber. Recall from equation [4.22] that optical return loss is defined as

$$R_L \equiv -10 \log\left(\frac{P_{bs}}{P_0}\right) \quad [7.26]$$

Substituting equation [7.25] into [7.26] and simplifying, we express the optical return loss, measured by the CWR, as

$$R_{L_{CWR}} \equiv -10 \log\left(\frac{10^{\left(\frac{B_{ns}}{10}\right)} \frac{P_0}{\Delta x} \int_0^L L_C(x) \exp(-2\alpha v) dv + \sum_{i=1}^N L_C(x) \exp(-2\alpha v) R_i}{P_0}\right) \quad [7.27]$$

Equation [7.27] expresses the optical return loss measured by a CWR. To measure the optical return loss with an OTDR, we need to perform calculations on the waveform that produce the quantity expressed in equation [7.27]. We begin by writing a simplified function describing the OTDR's waveform. From equation [3.4] we write the OTDR's backscatter signature as

$$P_{bs}(x) = P_0 \left(\frac{NA}{n_1}\right)^2 \frac{\alpha_s}{4.55} W(1 - W\alpha) \exp(-2\alpha x) L_C(x) \quad [7.28]$$

From equation [7.16] we have

$$\left(\frac{NA}{n_1}\right)^2 \frac{\alpha_s}{4.55} = \frac{10^{\left(\frac{B_{ns}}{10}\right)}}{\Delta x} \quad [7.29]$$

Remember, Δx in equation [7.29] is 0.0001 km and does *not* represent the OTDR's sample spacing. Substituting equation [7.29] into equation [7.28] and simplifying, we have

$$P_{bs}(x) = \frac{10^{\left(\frac{B_{ns}}{10}\right)}}{\Delta x} P_0 \cdot W(1 - W\alpha) \exp(-2\alpha x) L_C(x) \quad [7.30]$$

Next we construct the OTDR waveform resulting from reflective events. We assume in this construction that the OTDR's bandwidth is infinite (the pulses are perfectly square). Later, as this derivation continues, we integrate the waveform. In section 7.4 we showed that integration preserves the reflectivity measurements under bandwidth limitations, so the assumption of infinite bandwidth is not critical; it only makes the derivation a little simpler. Assuming square reflections, the OTDR waveform signature due to reflections is

$$R(x) = P_0 \sum_{i=1}^N S_p(x_i, W, R_i) \exp(-2\alpha x) L_C(x) \quad [7.31]$$

Here, we define the function $S_p(x_i, W, R_i)$ such that

$$S_p(x_i, W, R_i, x) = \begin{cases} R_i & \text{if } x_i < x < (x_i + W) \\ 0 & \text{otherwise} \end{cases} \quad [7.32]$$

The total waveform signature (in the linear domain) is the sum of the backscatter signature and the reflection signature:

$$w_A(x) = P_{bs}(x) + R(x) \quad [7.33]$$

Now observe what happens when we integrate the OTDR waveform and normalize by dividing by the pulse width:

$$\begin{aligned} \frac{1}{W} \int_0^L w_A(x) dx &= \frac{1}{W} \int_0^L P_{bs}(x) dx + \frac{1}{W} \int_0^L R(x) dx \\ &= 10^{\left(\frac{B_{ns}}{10}\right)} \frac{P_0}{\Delta x} (1 - W\alpha) \int_0^L \exp(-2\alpha x) L_C(x) dx \\ &\quad + P_0 \sum_{i=1}^N \exp(-2\alpha x) L_C(x) R_i \end{aligned} \quad [7.34]$$

Suppose we have a section of interest on the fiber for which we want to determine the optical return loss. The reference power, P_0 , is the power entering the section, and the optical return loss is defined by equation [7.26]. Equations [7.34] and [7.27] have obvious similarities. If we assume the fiber attenuation is small over a pulse width, then $(1 - W\alpha) \approx 1$. Making this assumption, we see that

$$\begin{aligned}
-10 \log \left(\frac{\frac{1}{W} \int_0^L w_A(x) dx}{P_0} \right) &= \text{ORL}_{OTDR} \\
-10 \log \left(\frac{10^{\left(\frac{B_{ns}}{10}\right)} L}{\Delta x} \int_0^L L_C(x) \exp(-2\alpha x) dx + \sum_{i=1}^N L_C(x) \exp(-2\alpha x) R_i \right) &= \text{ORL}_{CWR}
\end{aligned} \tag{7.35}$$

Equation [7.35] tells us we can calculate from an OTDR trace the same optical return loss measured by a CWR if we integrate the OTDR waveform, divide by the pulse width, and then divide by the incident optical power. For the OTDR, we calculate the reference power from the backscatter level at the beginning of the section (defined by the location of cursor a):

$$P_0 = \frac{P_{bs_a} \cdot \Delta x \cdot 10^{\left(\frac{-B_{ns}}{10}\right)}}{W(1 - \alpha W)} \tag{7.36}$$

Here, P_{bs_a} is the backscatter power (linear domain) measured by the OTDR at the location of cursor a (the start of the section of interest). Combining equation [7.36] with equation [7.35], we have (keeping the assumption $(1 - \alpha W) \approx 1$)

$$\text{ORL}_{CWR} = \text{ORL}_{OTDR} = -10 \log \left(\frac{\int_a^b w_A(x) dx}{P_{bs_a} \cdot \Delta x} 10^{\left(\frac{B_{ns}}{10}\right)} \right) \tag{7.37}$$

In equation [7.37], B_{ns} is the backscatter coefficient, Δx is 0.0001 km (*not* the sample spacing), P_{bs_a} is the linear backscatter level at the input of the section of interest, and $w_A(x)$ is the linear waveform data acquired by the OTDR.*

Before closing this section, we need to make a few points about how equation [7.37] is used. First, the algorithmic implementation of equation [7.37] requires that the first cursor be placed on backscatter. Since this cursor is used to calculate the input power to the section, it

*Note that we have treated the linear waveform data as a continuous function. In reality, it is sampled, so actual implementation of this equation uses sampled data points and summation to approximate the integral.

is critical that the cursor be located correctly and not, for example, on a reflection. If the end of the section of interest has a reflective event (such as the end of a cleaved fiber), the second cursor should be placed after the end of the reflection so that the integration includes the full reflected power from the end reflection.

Implementation of equation [7.37] sometimes yields counter-intuitive results. For example, suppose you measure the event return loss of a cleaved fiber at the end of a 50-km spool. The correct value is about 14 dB. Now suppose you measure the link return loss of the entire fiber (assume the wavelength is 1310 nm). Assuming fiber attenuation of about 0.35 dB/km and a nominal backscatter coefficient of -81 dB, the link return loss is about 21.5 dB. With return loss, the higher the number, the smaller the reflected power. How can the reflected power for the entire link be less than the reflected power from an event on the link?

The answer lies in the definition of the incident power. For the total link return loss, the algorithm uses the power input to the beginning of the link. In the calculation for total integrated return loss, the reflected power from the fiber's end is very small. This is because of the attenuation resulting from 100 kilometers of fiber attenuation (50 kilometers two ways). When measuring the event return loss, however, the calculations use the optical power incident upon the reflection. Consequently, for event return loss, the fiber attenuation between the OTDR and the event is not included.

Comparing event return loss with integrated link return loss can help you determine which events are most significant to the optical transmitter. Suppose, for example, that the integrated return loss includes a reflective event and that the integrated return loss is greater than that of the event. If this is the case, then the event's contribution to total reflected power at the source is small compared with backscatter and other sources.

7.7 Summary

We began this chapter with a discussion of the kinds of components that might cause reflections on a fiber-optic link. We saw that examples of reflective components include connectors, mechanical splices, and unterminated fiber ends. Cleaved fibers (when the cleave is very perpendicular) reflect about 4% of the incident light back into the waveguide. Cleaves with small angles (even a few degrees) still reflect about 4% of the light, but much of it is lost in the cladding because the light reflected by the angled cleave does not couple efficiently into

the fiber core. Angled cleaves or polishes are the fundamental basis behind very low-reflectivity connectors. In other types of connectors, manufacturers attempt to minimize the reflectivity by designing the ferrules so they touch.

In section 7.3 we described the proper cursor placement for measuring reflective events. Like nonreflective events, reflective events are described by their locations and losses. In addition, a reflective event is also described by its reflectivity. Reflectivity is the ratio of the reflected power of the light to the incident power. The location of a reflective event is usually easier to measure than it is for a nonreflective event because of the sharp rising edge. Loss is a little more difficult to measure for a reflective event because you must discriminate the point where Rayleigh backscatter resumes and the reflection's "tail" ends. Reflectivity is determined using an OTDR by measuring the height of the top of the reflection above backscatter.

In section 7.4 we examined effects that can lead to errors in reflectivity measurements. These errors include using the wrong backscatter coefficient and low bandwidth. The wrong backscatter coefficient results in errors because backscatter is the reference for reflection measurements. Any errors in the backscatter reference translate directly into errors in reflectivity measurements. Low receiver bandwidth can result in reflectivity errors when the waveform fails to reach the top of the reflection within the time limit of one pulse width.

Errors caused by bandwidth can be corrected by integrating under the smeared pulse and normalizing to one pulse width. Errors caused by using the wrong backscatter coefficient can be corrected by properly calibrating the backscatter coefficient. We described several ways to do this. They are: (1) to calculate the backscatter coefficient from the fiber's design data; (2) use a calibrated reflection; (3) use a continuous-wave reflectometer; and (4) use a calibrated fiber and an OTDR. Of all these methods, perhaps the easiest is to use a calibrated fiber and an OTDR.

We ended this chapter with a brief description of integrated loss. We described how to measure integrated loss with an OTDR and illustrated some procedures that will help you obtain accurate and consistent results. We also showed that the integrated return loss measured by an OTDR is equivalent to the return loss measured by the CWR when the algorithms are integrated properly. Unlike the OTDR, however, the CWR cannot measure the integrated return loss of a subsection of the fiber or measure the reflectivity of discrete events on the fiber.

Suggested reading

- Kashima, N., *Passive Optical Components for Optical Fiber Transmission* (Norwood, MA: Artech House, 1995).
- Miller, C. M., Mettler, S. C., and White, I. A., *Optical Fiber Splices and Connectors, Theory and Methods* (New York: Marcel Dekker, 1986).
- Das, S. K., Judy, A. F., Alameel, G. M., Jopson, R. M., and Adda, T. F., "Reflectance measurements in lightwave systems: a comparison of various techniques," *Technical Digest Symposium on Optical Fiber Measurements*, NIST Special Publication 748 (Boulder, CO: NIST, 1988), pp. 25–30.
- Kapron, F. P., Thomas, E. A., and Peters, J. W., "OTDR measurements of optical return loss," *Technical Digest Symposium on Optical Fiber Measurements*, NIST Special Publication 748 (Boulder, CO: NIST, 1988), pp. 35–39.
- Reitz, P. R., "Calibration and use of an optical time-domain reflectometer for measurements of reflectance (return loss) of optical fiber components," *Technical Digest Symposium on Optical Fiber Measurements*, NIST Special Publication 748 (Boulder, CO: NIST, 1988), pp. 31–34.
- So, V., Lamont, J., and Vella, P. J., "Fault-locating accuracy with an OTDR: reflective versus nonreflective faults," *IEEE Journal of Selective Area Communications*, V.SAC-4 (1986), pp. 737–740.
- Ducos, L., and Facq, P., "Windowing technique for accurate measurement of low reflectances by OTDR," *Technical Digest Symposium on Optical Fiber Measurements*, NIST Special Publication 864 (Boulder, CO: NIST, 1994).
- Moeyaert, V. E., Jaunart, E., and Blondel, M., "Comparison of return loss measurements in point-to-point and point-to-multipoint passive optical networks," *Conference on European Fiber Optic Communications and Networks* (1995).
- Ta, L., "Determine OTDR distance accuracy," *Test & Measurement World* (March 1996), pp. 13–16.

Problems

1. True or false: Reflective events are characterized by three parameters: loss, location, and reflectivity.
2. True or false: Reflective events are harder to locate than nonreflective events because their leading edge is not as sharp.
3. True or false: It's harder to measure the loss of a reflective event because one must make a subjective determination of when the waveform returns to the normal backscatter level.
4. True or false: Examples of reflective events include fusion splices and bends.
5. True or false: The vertical scale is absolute on OTDRs and used to determine reflectivity.

6. True or false: Different fiber manufacturers and types, such as standard single-mode fiber and dispersion-shifted fibers, have different backscatter coefficients.
7. True or false: If you characterize the backscatter coefficient of a reference fiber, you can use it and an OTDR to accurately measure the backscatter coefficient of other single-mode fibers.
8. True or false: Physical contact connectors have lower reflectivity than flat-polished connectors.
9. True or false: Angled connectors have low reflectivity because light does not reflect well off angled surfaces.
10. True or false: The reflectivity of connectors often depends upon the wavelength of the light.

¹ Suzuki, N., and Nagano, O., "Low-insertion loss and high return-loss optical connectors for use in analog video transmission," *International Conference on Integrated Optical Fiber Communication (IOOC)* (1983), pp. 30A3–5.

² Nagasawa, S., Yokoyama, Y., Ashiya, F., and Satake, T., "A high-performance single-mode multifiber connector using oblique and direct endface contact between multiple fibers arranged in a plastic ferrule," *IEEE Photonics Technology Letters*, Vol. 3 (1991), p. 937.

³ Kapron, F. P., Adams, B. P., Thomas, E. A., and Peters, J. W., "Fiber-optic reflection measurements using OCWR and OTDR techniques," *Journal of Lightwave Technology*, Vol. 7, No. 8 (August 1989).

⁴ Caviglia, F. C., Cselt, P. R., and Romoli, G. R., "Noise error in OTDR splice loss measurement," *Technical Digest Symposium on Optical Fiber Measurements*, NIST Special Publication 864 (1994).

⁵ Neumann, E. G., "Analysis of the backscattering method for testing optical fiber cables," *AEU*, Vol. 34, No. 4 (1980), pp.157–160.

⁶ Neumann, E. G., "Theory of the backscattering method for testing optical fiber cables," *Electronic Communications*, Vol. 34 (1980), pp.157–160.

⁷ Nakazawa, M., "Rayleigh backscattering theory for single-mode optical fibers," *Journal of the Optical Society of America*, Vol. 73, No. 9 (September 1983).

⁸ Brinkmeyer, E., "Backscattering in single-mode fibers," *Electronics Letters*, Vol. 6, No. 9 (April 1980).

⁹ Poudyal, V., Reith, L. A., and Vogel, E. M., "Accuracy of optical component reflectance measurements using an OTDR," *SPIE Proceedings*, Photonics East Conference (Oct. 25, 1995).

¹⁰ Ibid.

Chapter 8

Complications caused by reflective events

8.0 Introduction

Anyone who has driven a car at night is familiar with the momentary loss of vision that occurs when the driver of an approaching vehicle fails to dim the headlights. In a similar fashion (though for different reasons), an OTDR becomes momentarily “blinded” by bright reflections. When this happens, the OTDR is unable to make loss measurements until the effects of the reflection have died away. We saw in chapter 4 that this region after a reflection is called the *dead zone*.

In this chapter we examine some of the measurement problems associated with reflective events. First, we review the concept of dead zone and the problems it causes. We show that the dead zone of a reflective event is usually larger than the pulse width because of the recovery time required for the OTDR’s system to recover from the reflection’s relatively bright light. One of the primary contributing factors to the dead zone is the OTDR’s system bandwidth, and we give some simple equations for estimating the dead zone based on this bandwidth.

Since reflections are a primary concern to many installers, we end the chapter by describing some equations for estimating the significance of reflections in a fiber-optic network. We provide equations that allow you to estimate the relative importance of reflections, compared to backscatter, as a function of their locations along the fiber-optic line. We also briefly summarize other possible problems, such as coherent mixing of echoes, that can result in a high bit-error rate (BER) when excessive echoes due to reflections are present.

8.1 Reflections and the dead zone

The distance after a reflection and before an OTDR can make measurements depends on the type of measurement you want, the strength of the reflection, and the OTDR’s bandwidth. Recall from chapter 4 that OTDR manufacturers typically specify two types of dead zones, event dead zone and loss dead zone.

Event dead zone is the minimum distance after a reflection before the OTDR can “see” another reflection of the same height.* This distance is limited almost exclusively by the OTDR’s pulse width and bandwidth.

*There is a somewhat arbitrary requirement that the waveform signal drop 3 dB from the top of the first reflection before the possibility of seeing the second reflection.

The linear sloping region of an OTDR's waveform just after the end of the reflection (the part of the waveform where the signal first begins to fall) is related to the OTDR's bandwidth by the equation*

$$m = \beta \cdot 134 \quad [8.1]$$

In equation [8.1], m is the slope of the waveform near the top of the falling edge of the reflection (in dB/km) and β is the OTDR's system bandwidth in MHz.

Recall from chapter 4 that event dead zone is the distance after a reflection for the OTDR waveform to rise to the top of the reflection and drop 3 dB. For nonsaturated reflections, using equation [8.1], we have:

$$dz_{\text{event}} = W + \frac{1}{\beta \cdot 44.7} \quad [8.2]$$

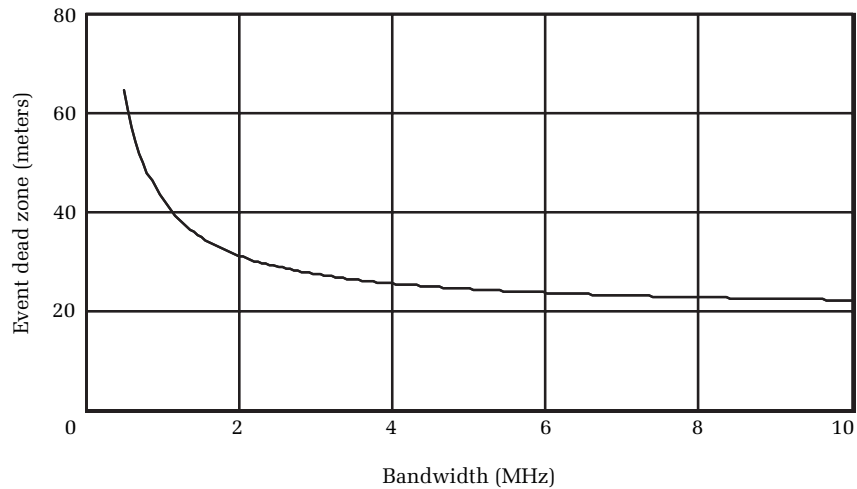


Figure 8.1. Event dead zone as a function of bandwidth. This figure plots equation [8.2] for the case of a 20-meter pulse. Observe that, for this pulse width, the dead zone is limited primarily by the pulse width for system bandwidths greater than about 10 MHz. Notice that for bandwidths less than about 2 MHz, the event dead zone is limited mostly by the bandwidth. The event loss was 0.2 dB, and the height of the reflection was 9.23 dB above backscatter.

*This equation applies only for OTDRs where the system response can be modeled as a simple single-pole amplifier. For the falling edge to be linear, it must be more than about 5 dB above backscatter. Consequently, this equation holds only for relatively large reflections. See chapter 4 for the derivation of this equation.

In equation [8.2], W is the displayed pulse width in kilometers. For example, suppose we have an OTDR with a 4-MHz bandwidth and a 20-meter pulse. Given these parameters we see that the event dead zone is 26 meters.* Figure 8.1 plots the event dead zone as a function of bandwidth for a 20-meter pulse width.

Loss dead zone is the distance from the leading edge of a reflective event to the point past the event where the waveform signature falls to within 0.5 dB of the normal Rayleigh backscatter signature. If another event, such as a fusion splice, is within the OTDR's loss dead zone, the OTDR is effectively unable to measure the individual losses of the two events and must instead measure only the total, or grouped loss, of the events.†

As with event dead zone, the loss dead zone is also a function of the OTDR's bandwidth. In addition, loss dead zone depends on the event's loss, reflectivity, and complicated thermal effects in the OTDR's optical receiver. Events with greater reflectivity have larger event dead zones, as do events with greater loss. Equation [8.3] illustrates the relationship between the loss dead zone, height of the reflection, bandwidth, and event loss. Figure 8.2 plots equation [8.3] (for a specific event loss, reflectivity, and pulse width) as a function of bandwidth.

$$dz_{\text{loss}} = W - \frac{100}{2\pi\beta} \left(\ln \left(\frac{10^{-0.2 \cdot L} (10^{0.1} - 1)}{10^{0.2 \cdot H} - 10^{-0.2 \cdot L}} \right) \right) \quad [8.3]$$

In equation [8.3], L is the optical loss of the event (in decibels), H is the height of the reflection above backscatter (in decibels, as read off the OTDR's vertical scale), W is the displayed pulse width (in meters), and β is the system bandwidth in megahertz.

Equations [8.2] and [8.3] represent lower limits to the dead zone of an OTDR whose system may be modeled as a simple single-pole amplifier. When other complicating factors are included, such as amplifier saturation and thermal effects, the effective dead zone may be

*Sample spacing also contributes. The dead zone cannot be less than the sample spacing.

†Depending on the type and size of an event, the OTDR may also be unable to see events that are near but outside the loss dead zone. Loss dead zone should be viewed as one way to compare the recovery characteristics of different OTDRs. The dead zone specification should not be viewed as a guarantee that (for example) a 0.1-dB fusion splice can be seen this close to a reflective event.

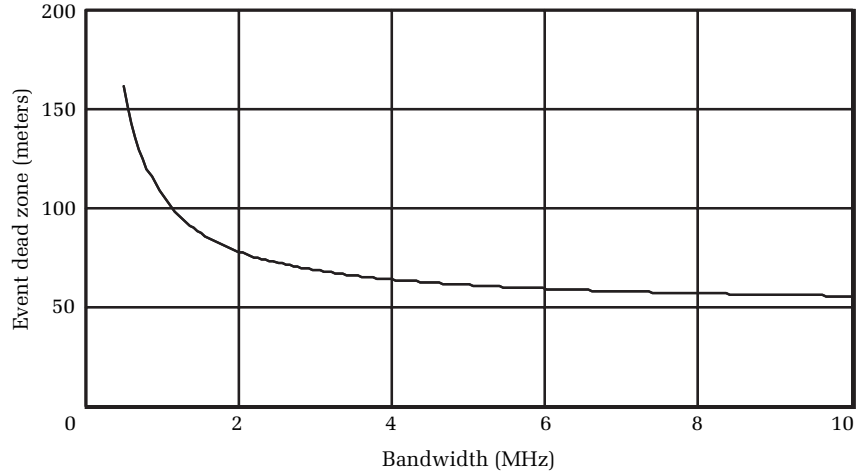


Figure 8.2. Loss dead zone as a function of bandwidth. This figure plots equation [8.3] for the case of a 20-meter pulse. As with event dead zone, we observe that, for this pulse width, the loss dead zone is limited primarily by the pulse width for receiver bandwidths greater than about 10 MHz. Notice that, for receiver bandwidths less than about 2 MHz, the loss dead zone is limited mostly by the bandwidth.

larger. Figure 8.3 shows an OTDR waveform acquired with a 20-meter pulse at 1310 nm, using an amplifier having 4-MHz bandwidth. The first two events are a pair of reflections separated by the event dead zone. The second two events are a reflection followed by a nonreflective event, separated roughly by the loss dead zone.

From equations [8.2] and [8.3] we see that the dead zone gets smaller as the bandwidth increases and as the pulse width decreases. As we have pointed out before, however, the OTDR's dynamic range gets larger as the bandwidth decreases and the pulse width increases.* Again we see that dynamic range and dead zone are in competition. By trying to improve one, you degrade the other.

8.2 Improving the dead zone by optical masking

We just saw that decreasing the system bandwidth, which increases the system dynamic range, also increases the OTDR's dead zone. One way of partially overcoming the conflict between dynamic range and dead zone is to use optical masking. Optical masking uses a fast optical switch in

*Lowering the bandwidth decreases the noise, and increasing the pulse width increases the backscatter signal.

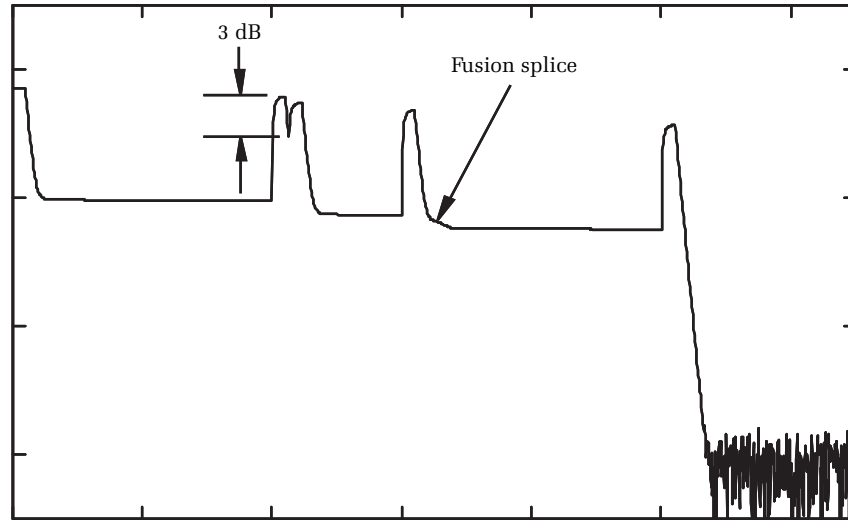


Figure 8.3. Event dead zone and loss dead zone. This OTDR waveform was acquired at 1310 nm using a 20-meter pulse and 1-meter sample spacing. The OTDR's bandwidth was 4 MHz. The first pair of events are two reflections, each with -40 dB reflectivity, separated by 26 meters. This is roughly the instrument's event dead zone (see figure 8.1). The second pair of events is a reflection (-40 dB reflectivity) followed 50 meters later by a fusion splice. This is roughly the instrument's loss dead zone (see figure 8.2). All four events have 0.5 dB loss. The front-panel reflection and end reflection both have -40 dB reflectivity.

the return leg of the OTDR (the leg with the receiver in it) to mask the bright light of reflections (see figure 3.4).^{1,2}

Optical masking was used more commonly in the past. Its use was restricted primarily to mainframe OTDRs, however, because of the extra cost and electrical power to operate the optical switches. Since then, advances in receivers and avalanche photodetectors (APDs) have dramatically closed the performance gap between OTDRs with and without optical masking. As a result, optical switching is found mostly in older mainframe OTDRs and rarely in modern instruments.

The switch used in optical masking is usually either an electro-optic or acousto-optic device. Generally, acousto-optic devices are preferred because they are less expensive, are less sensitive to polarization, and have lower optical loss. Polarization sensitivity can introduce noise on the waveform (we discuss this in more detail in chapter 13). This polarization noise cannot be averaged away, so it

effectively limits the OTDR's measurement dynamic range by making splice-loss measurements less accurate (and events more difficult to recognize). Although electro-optic switches are faster than acousto-optic switches, generally the difference is not significant for OTDRs used to test telecommunications fiber and does not warrant the extra cost and technical difficulties.

How optical masking is implemented varies somewhat from manufacturer to manufacturer. Typically, the operator defines the portion of the waveform to be masked by positioning cursors around the reflective event, as shown in figure 8.4. Some manufacturers allow masking for only a limited number of reflections. Others offer essentially unlimited masking with a selection of manual, semimanual, and fully automatic modes.

With manual masking, the operator must acquire two waveforms to make complete measurements on reflective events. In the first waveform the operator places the masks and measures the reflectivity. In the second waveform the operator engages the masking function and measures the

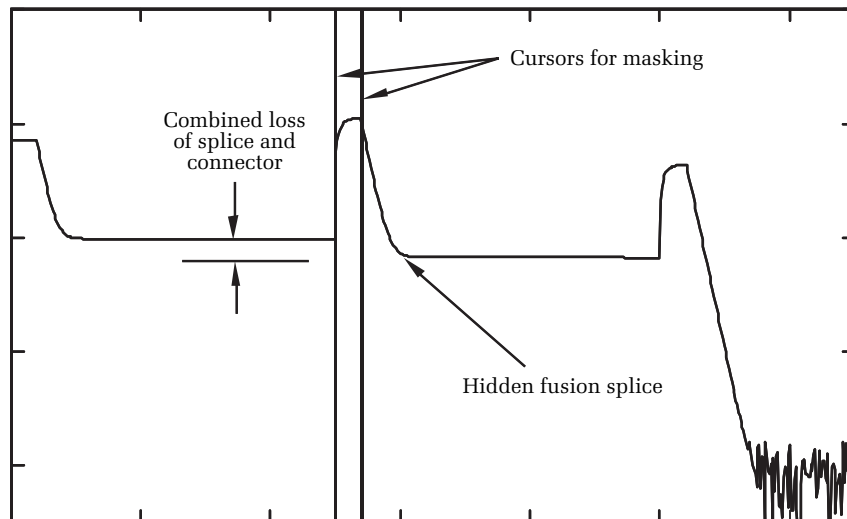


Figure 8.4. Placing cursors around a reflective event for masking. The reflective event in this case is followed closely by a nonreflective fusion splice. The fusion splice is close enough to the reflective event to be hidden by the amplifier's response to the bright reflection. This response, sometimes called tail, is the sloping region after the second cursor. Because of the reflection's tail, the loss of the reflection and the loss of the splice cannot be measured separately.

individual losses of the closely spaced events. The most advanced OTDRs find reflections and select the masking regions automatically. They still acquire two waveforms, but they do it automatically, so they are much faster and more accurate than OTDRs that require the operator to acquire two waveforms manually and place cursors around the masking regions.

Figure 8.4 shows what looks like an isolated reflective event in the middle of an otherwise featureless fiber. This first waveform is the one in which we place the markers that determine where the OTDR applies the masking function (shown by the locations of the two vertical cursors). When we acquire the second waveform, the mask turns on at the first cursor and turns off at the second. Figure 8.5 shows the second acquisition of the fiber with the masking function engaged. Observe that the region of the reflection is now below the backscatter level, due to the attenuation of the blocking switch. Also, observe that, with the masking function engaged, a fusion splice is visible that was previously hidden

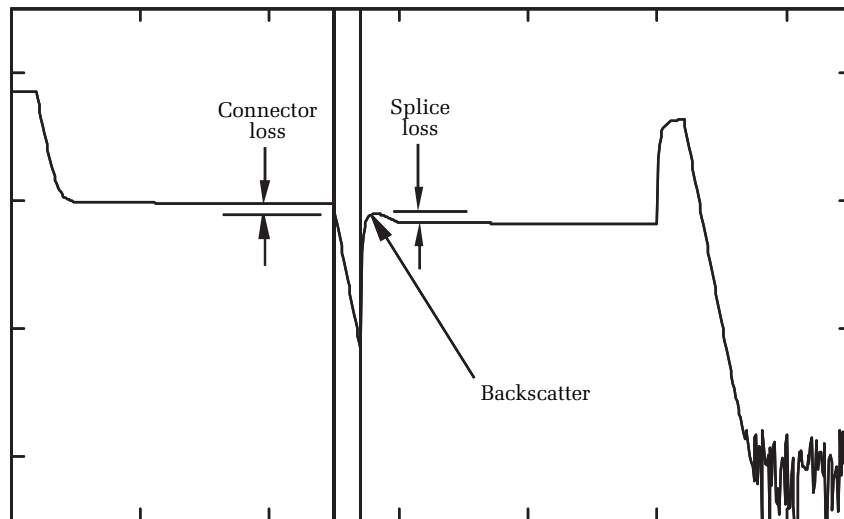


Figure 8.5. The waveform from figure 8.4 with the region around the reflection masked by an optical switch. Observe that the fusion splice that was hidden in the reflection's tail in figure 8.4 is now clearly visible. The large drop in the waveform, where the reflection appeared previously, results from the masking property of the optical switch. In advanced OTDRs the instrument would combine the waveforms shown in figures 8.4 and 8.5. In the composite waveform, both the reflection and the fusion splice would be visible.

by the reflective event (compare with figure 8.4). With the masking function, this fusion splice is now evident, and its loss is easily measured independent of the reflective event. The dead zone is still limited by the pulse width, but with optical masking it is much improved.

Figure 8.5 shows an obvious disadvantage of optical masking. With the reflection masked, you cannot make reflectivity measurements. This disadvantage is overcome in OTDRs that incorporate a fully automatic masking mode in which the OTDR acquires two waveforms, one without masking and one with masking (in this mode it also automatically selects the masking regions). The OTDR automatically combines the reflectivity data from the waveform without masking with the backscatter and loss data from the waveform with masking.³ The resulting composite

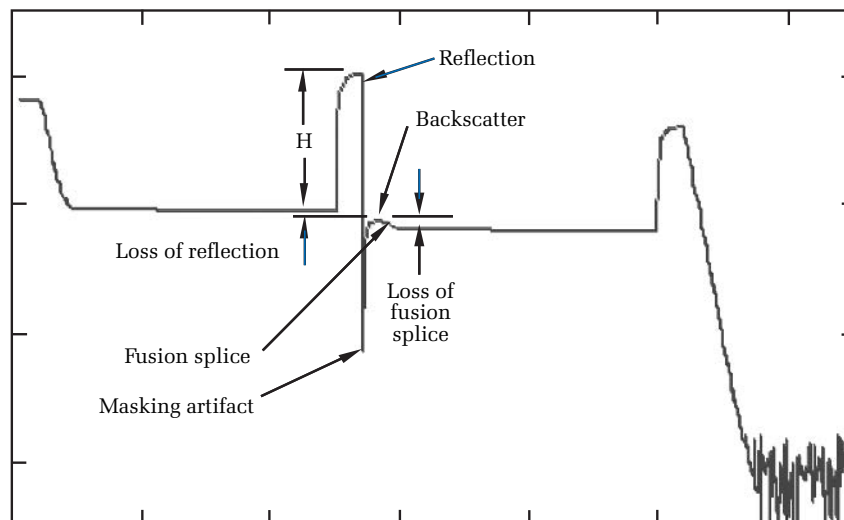


Figure 8.6. Composite masking waveform. This waveform consists of elements of the waveforms in figures 8.4 and 8.5, spliced together into one composite waveform. In the waveform of figure 8.4, you can measure the reflectivity of the reflective event and the insertion loss of the grouped (reflective and nonreflective) events. In the waveform of figure 8.5, you can measure the individual losses of the reflective and nonreflective events but not the reflectivity of the reflective event. In this waveform, however, you can measure the reflectivity of the reflection as well as the individual losses of the reflective and nonreflective events. Splicing the waveforms into a composite provides you with the maximum amount of information. It also simplifies your measurements and allows you to archive all measurement information by saving one waveform file.

waveform is calculated and displayed without requiring the operator to place cursors or manually acquire more than one waveform.

This automatic mode makes the masking operation (which sometimes can be intimidating because of its perceived complexity) almost transparent to the operator. The operator can then make accurate loss and return-loss measurements from one waveform. This feature provides the operator with all the inherent advantages of optical masking while freeing him or her from the technical details required to make optical masking work (see figure 8.6). It also reduces the requirements of the waveform archival structure, since only one composite waveform must be saved instead of two waveforms (one with masking and one without masking).

8.3 Impact of reflections on transmitters and receivers

In chapter 7 we described how reflections arise in fiber-optic systems and how to measure them using an OTDR. In this chapter we have examined some of the unique measurement challenges posed by reflections and shown how optical masking can help to reduce the dead zone. Now let's examine the possible impact that reflections might have on the transmitting and receiving elements of a fiber-optic network and look at some of the circumstances in which you might want to reduce their reflectivity.

High-speed fiber-optic transmission systems frequently use narrow-bandwidth distributed-feedback (DFB) lasers as transmitters. These lasers can be sensitive to light that the optical system reflects back into their lasing cavities.⁴ This reflected light can modulate the laser's power output and/or the laser's spectral frequency. Either of these effects is detrimental to the system's operation. Unwanted modulation of the laser's output power directly increases the system's bit-error rate (BER) for digital systems and carrier-to-noise ratio (CNR) levels for analog systems. Unwanted modulation of the laser's optical frequency can result in channel cross-talk in systems with wavelength-division multiplexing or increase chromatic dispersion, both of which also increase the bit-error rate.

There are a number of ways to reduce the effects of reflective events. One approach is to use low-reflectance connectors, such as PC connectors or angled connectors. Another approach is to replace your connectors with fusion splices. A third possibility is to use an optical isolator in front of your optical source. Optical isolators are similar to electrical diodes. They allow light to pass in one direction but attenuate

it strongly when it travels in the other direction. An optical isolator allows light from the laser to be launched into the optical fiber but prevents reflections and backscatter from the fiber from being coupled back into the laser.

In determining a reflection's significance, we might ask how the reflected power compares with the total power that is scattered by the fiber. Scattered power depends only on the wavelength of light and the physical properties of the fiber. If the light from a discrete reflection is small compared with the total backscattered light (the integrated sum of all the Rayleigh scattering along the fiber's length), then replacing the connector with a fusion splice may have little effect. In such cases, replacing the connector with a fusion splice may not help solve BER problems; if optical feedback is actually the problem, an optical isolator is required. On the other hand, if a reflection is the dominant source of optical feedback, then replacing or repairing the connector might help (if the total optical feedback is excessive). We need a way of comparing the total scattered power with the reflected power from a discrete component. Recall from equation [7.18] that the fiber's backscatter coefficient is defined as

$$B_{ns} = 10 \log \left(\frac{P_{1ns}}{P_0} \right) \text{ for 1-ns pulse} \quad [8.4]$$

In equation [8.4], P_{1ns} is the power of the Rayleigh backscatter for a 1-ns pulse and P_0 is the incident power of the laser pulse.

As we saw in equation [7.16], you can calculate a rough approximation for the backscatter coefficient if you know the fiber's numerical aperture, core index, and attenuation per unit length due to scattering. For single-mode fibers, the formula is

$$B_{ns} = 10 \log \left(\left(\frac{NA}{n_1} \right)^2 \cdot \frac{\alpha_s}{4.55} \cdot 0.0001 \right) \quad [8.5]$$

In equation [8.5], NA is the fiber's numerical aperture, n_1 is the fiber's core index, and α_s is the fiber's Rayleigh scattering coefficient (attenuation due to Rayleigh scattering, 1/km). For modern telecommunications-grade fiber, the scattering coefficient is approximately equal to the attenuation coefficient. The factor 0.0001 is the pulse width in kilometers of a 1-ns pulse, as seen on the OTDR display.

Rearranging equation [8.4], we see that if we connect a 0.1-meter section of fiber to a source, the total power reflected back to the source from Rayleigh scattering is*

$$P_{1ns} = P_0 \cdot 10^{\left(\frac{B_{ns}}{10}\right)} \quad [8.6]$$

Now, if the fiber length is shorter than 0.1 meter, we can write:

$$dP_{bs}(x) = 10^{\left(\frac{B_{ns}}{10}\right)} P(x) \frac{dx}{W} \quad [8.7]$$

In equation [8.7], $P(x)$ is the power of the optical pulse, W is 0.1 meter, dx is a differential length of fiber, and $dP_{bs}(x)$ is the differential amount of power scattered by the differential length of fiber at point x .

Now suppose we launch unmodulated laser light into the optical fiber. By integrating equation [8.7], we can calculate the total amount of light that is scattered back to the transmitter by the fiber:

$$P_{bs}(L) = \frac{10^{\left(\frac{B_{ns}}{10}\right)}}{0.1\text{m}} \int_0^L P(x) dx = \frac{10^{\left(\frac{B_{ns}}{10}\right)} P_0}{0.1\text{m}} \int_0^L \exp(-2\alpha \cdot x) dx \quad [8.8]$$

$$Q_{bs}(L) \equiv \frac{P_r(L)}{P_0} = \frac{10^{\left(\frac{B_{ns}}{10}\right)}}{2(0.1\text{m})\alpha} [1 - \exp(-2\alpha \cdot L)] \quad [8.9]$$

Equation [8.9] gives the ratio of the total backscatter power from a fiber of length L relative to the launch power. In equation [8.9], B_{ns} is the backscatter coefficient and α is the fiber's attenuation coefficient (1/km). Observe that our derivation of equation [8.9] assumes that the fiber is fully filled with light (the laser operates continuously). In digital transmission systems there are (on average) as many "on" bits as "off" bits, so the fiber (on average) is only half filled. You can still use equation [8.9] in such cases by setting P_0 equal to half of the optical power associated with the "on" bits.

*It is true that a 1-nanosecond pulse from an OTDR is actually 0.2 meters long. However, the total backscatter registered at the OTDR in a given instant originates from a length of fiber that is only 0.1 meter long. See figure 1 in *Making True Splice-Loss Measurements with OTDRs from One End of the Fiber*, D. R. Anderson, NFOEC '95 proceedings.

Now suppose there is a reflection at the end of the fiber. The power reflected by the reflection back to the transmitter is

$$R(L) = P_0 10^{\left(\frac{R}{10}\right)} \cdot \exp(-2\alpha \cdot L) \tag{8.10}$$

$$Q_R(L) \equiv \frac{R(L)}{P_0} = 10^{\left(\frac{R}{10}\right)} \cdot \exp(-2\alpha \cdot L) \tag{8.11}$$

In equation [8.11], R is the event's reflection in decibels. The ratio of the total power received from the reflection to the total power received from backscatter (in decibels) is

$$\Delta_{dB} = 10 \log \left[\frac{10^{(R/10)}}{\frac{10^{(B_{ns}/10)}}{2(0.1\text{ m})\alpha} (\exp(2\alpha L) - 1)} \right] \tag{8.12}$$

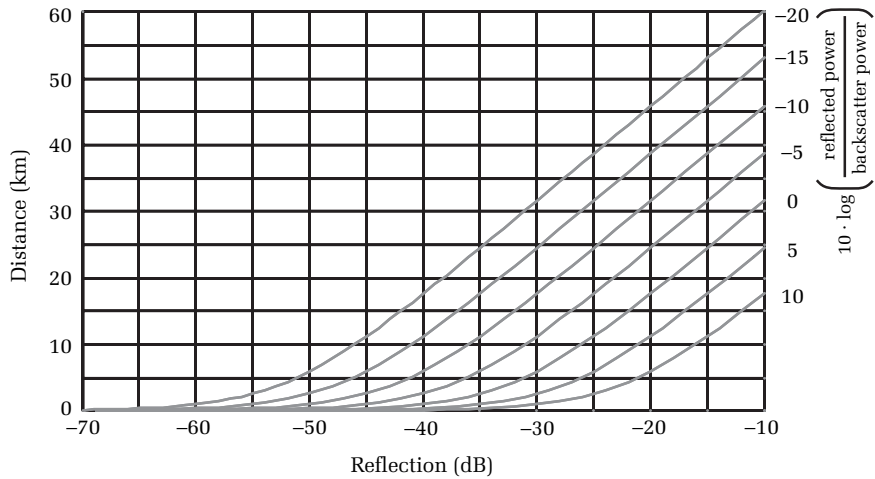


Figure 8.7. Relative power of reflection and backscatter at the laser transmitter. The right vertical axis shows the total backscatter relative to the total reflected power (in decibels). The horizontal axis shows the reflectivity of the reflective event at the fiber's end, and the left vertical axis shows the distance to the reflective event. For example, suppose the total reflected power is 10 dB lower than the total backscatter power, and suppose the reflectivity of the reflective event is -25 dB. Under these circumstances, the event is about 25 kilometers away. Note that the calculations used to generate this figure assume that the fiber is transmitting data.

Solving for the length, in terms of the other variables, we have

$$L = \frac{1}{2\alpha} \cdot \ln \left(1 + 2(0.1 \text{ m})\alpha \cdot 10^{\left(\frac{R - B_{rs} - \Delta_{dB}}{10} \right)} \right) \quad [8.13]$$

Solving for the reflectivity in terms of the other variables, we have

$$R = 10 \log \left(\frac{10^{\left(\frac{\Delta_{dB} + B_{rs}}{10} \right)}}{2(0.1 \text{ m})\alpha} (\exp(2\alpha L) - 1) \right) \quad [8.14]$$

Equations [8.12], [8.13], and [8.14], relate Δ_{dB} (the ratio of the reflected power to the backscattered power), L (the length of the fiber), and R_0 (the event's reflection) to each other. Given any two variables, these equations allow you to calculate the third. Figure 8.7 plots some of the results from equation [8.13]; figures 8.8 and 8.9 plot some of the

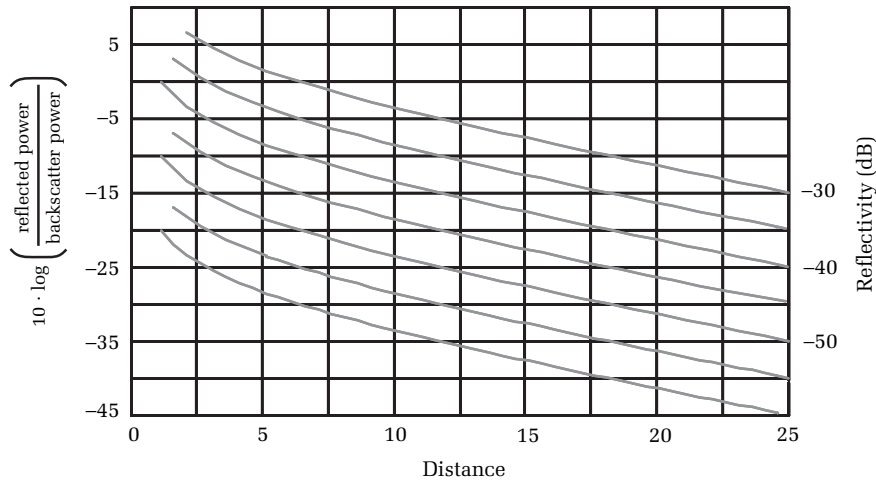


Figure 8.8. Variations of Δ_{dB} (the ratio of the reflected light to the backscattered light in decibels) with distance of the reflection from the transmitter. Each of the curves corresponds to a different reflection. The top curve is for a -30 dB reflection. It shows, for example, that the power in the reflected light is 15 dB lower than the total power from backscattered light if the reflection is about 24.5 km from the source.

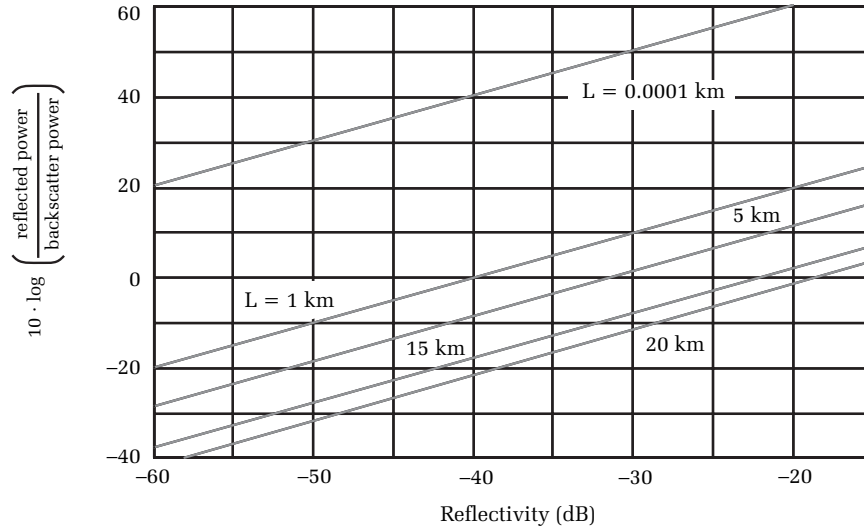


Figure 8.9. Variation of Δ_{dB} (the ratio of the reflected light to the backscattered light in decibels) with changes in the reflectivity of the end of the fiber. Each of the curves corresponds to a different length of fiber. The top curve is for a fiber that is only 0.1 m long. The curve second from the top is for a fiber that is 1 km long. The second curve shows, for example, that the power in the reflected light is 10 dB lower than the total power from backscattered light if the reflection is -50 dB.

results from equation [8.12]. Observe from these figures that it is not uncommon for the Rayleigh backscatter power to be greater than the reflected power. For example, we see from figure 8.7 that if a reflection is -35 dB and 5 km from the transmitter, the Rayleigh backscatter power is about 5 dB greater than the reflected power at the receiver.

In addition to interfering with laser transmitters, reflections can also introduce noise in the receiver. Any time a fiber-optic link has more than one reflective component, echoes between these components can interfere with the direct signal at the receiver. When the transmitter has a narrow bandwidth (as when using a DFB laser), coherent mixing of the echoes with the direct signal results in an increase in the receiver's noise floor. Noise from this coherent mixing is called *relative-intensity noise*, or RIN. The RIN increases as the reflectivity of the components in the telecommunications system increases, and it is most significant for systems with narrow-bandwidth transmitters. If the RIN is high enough, it can result in increased BER and system degradation.⁵

8.4 Dead zone box

Often, the connector of interest is the one that is connected to the OTDR via a patch cord or jumper. This is typically a connector located at the patch panel inside a central office or head end and may be one that is often connected and disconnected, which means it may be at a higher risk of being damaged or dirty. Typical OTDRs do not have a large amount of fiber inside the instrument's front panel, and so there is typically no backscatter trace before the front-panel connector. This makes it impossible to measure the loss of the connector that is attached to the OTDR. In addition, the OTDR may not have a low-reflectance connector, which means the dead zone after the reflection can be high and can mask other important events that are near the OTDR.

To solve this problem, some OTDR manufacturers put a small spool of fiber, roughly 50–100 meters, inside the OTDR. This allows the front-panel loss to be measured. If your OTDR does not have this feature, the alternative is to use what is called a *dead zone box* (see figure 8.10), a small box with a coiled length of fiber inside. Specific connector, polish, fiber type, length, and manufacturer can be specified when ordered. The TIA/EIA 455 FOTP's 59A and 61A recommend a length of fiber 20 times the pulse width of the OTDR, but give latitude to the buyer



Figure 8.10. Single-mode fiber-optic dead zone box. [Credit: The Light Brigade.]

because all OTDRs have differing optical characteristics. Attaching the dead zone box to the OTDR and then to the fiber under test allows the first connector on the fiber under test to show up hundreds of meters away from the OTDR. In this manner you can clearly see the backscatter trace on each side of the first connector and easily measure its loss and ORL values. Furthermore, you can configure the dead zone box with a type of connector that matches the system you are testing and that has as low reflectivity as possible, thus reducing the dead zone after the first connector and making it easier to measure close-in events.

To measure the far termination of an installed span, the user can use a second dead zone box or an optical terminator. A terminator is a modified plug (see figure 8.11) with the mating surface of the fiber polished to match the connector type and the polish, and it is used at the far-end location (e.g., FC/APC). The fiber at the rear of the “terminator” plug is dead-ended by the manufacturer so that no light is reflected. This modified plug will mate to the connection and allow reflective measurements to be taken at the glass-to-glass surface of the far-end connection. If a terminator or dead zone box isn’t used at the far-end termination, then the resulting reflection measurement of approximately 14 dB will be erroneous.

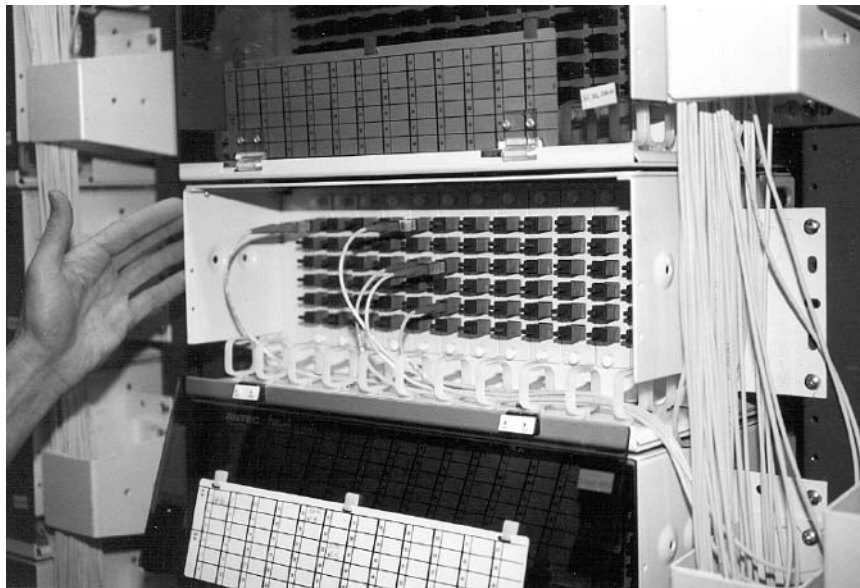


Figure 8.11. An SC/APC terminator being plugged into a fiber-optic patch panel. [Credit: The Light Brigade.]

8.5 Summary

In this chapter we have seen how the dead zone following a reflective event depends on the height of the reflection, the OTDR's bandwidth, and the event's loss. Increased bandwidth reduces the dead zone but also increases the system noise, thus reducing the instrument's dynamic range. In section 8.2 we examined optical masking and saw that it is an effective way to improve the OTDR's dead zone while maintaining high dynamic range.

We ended this chapter by discussing some of the ways that reflections can cause problems in fiber-optic systems. One way they cause problems is by interfering with the laser transmitter and causing power or frequency modulation. Another way they cause problems is by coherent mixing in the optical receiver. We provided some simple equations that allow you to estimate the relative significance of reflections and backscatter to the laser transmitter.

In chapters 5, 6, 7, and 8 we have dealt with traditional OTDR measurements. In the next few chapters we describe some of the less common measurements that an OTDR is also useful in making.

Suggested reading

Sasaki, S., Nakano, H., and Maeda, M., "Bit-error-rate characteristics with optical feedback in 1.5- μm DFB semiconductor lasers," *Proceedures of the European Conference on Optical Communications* (ECOC) (1986), pp. 482–486.

Gimlett, J. L., and Cheung, K., "Effects of phase-to-intensity-noise conversion by multiple reflections on gigabit/second DFB laser transmission systems," *Journal of Lightwave Technology*, Vol. 7, No. 6 (June 1989), pp. 888–895.

Problems

1. True or false: Increasing the pulse width increases the dead zone.
2. True or false: Reducing the bandwidth reduces the dead zone.
3. True or false: Adjusting the pulse width and bandwidth to reduce the dead zone also increases the dynamic range.
4. True or false: If a fusion splice is within the event-loss dead zone, the OTDR is guaranteed to see it.
5. True or false: The event dead zone is roughly how close two reflective events can be together and still be resolvable on the OTDR.
6. True or false: Optical switching was used primarily on older mainframe OTDRs, to improve the loss dead zone.

7. True or false: Reflective events can cause system problems if they reflect too much optical power back into the laser transmitters.
8. True or false: Even large reflections cannot cause echoes that are so big they cause noise at the receiver.
9. True or false: Dead zone boxes and optical terminators are used when testing optical spans for the measurement of the attenuation and reflection of optical connectors.

¹ Jones, M. D., "An acousto-optic coupler for optical time-domain reflectometry," *Tektronix Laboratories Technical Report No. ESL-EO04/87* (1987).

² Goll, J. H., "Compensation method to improve performance of OTDR with optical switch," *Tektronix Laboratories Technical Report No. ESL-EO.06/88* (1988).

³ Goll, J. H., Trent, W. A., Lane, R. I., Bell, F. G., and Marineau, M. D., *Signal Acquisition Method and Automatic Masking for an OTDR*, U.S. Patent 5,023,445 (1991).

⁴ Sasaki, S., Nakano, H., and Maeda, M., "Bit-error-rate characteristics with optical feedback in 1.5- μm DFB semiconductor lasers," *Procedures of the European Conference on Optical Communications (ECOC)* (1986), pp. 483–486.

⁵ Gimlett, J. L., and Cheung, N. K., "Effects of phase-to-intensity noise conversion by multiple reflections on gigabit-per-second DFB laser transmission systems," *Journal of Lightwave Technology*, Vol. 7, No. 6 (1989).

Chapter 9

Measuring the numerical aperture and mode-field diameter of single-mode fiber

9.0 Introduction

Recall from chapter 2 that light traveling along a single-mode optical fiber has a specific irradiance distribution orthogonal to the fiber's axis. This distribution is brightest near the fiber's core and decreases as a Gaussian function into the core-cladding boundary and beyond. In typical single-mode telecommunications fiber, the modal distribution extends well into the cladding, which carries about 20% of the optical power. By international convention, the mode-field diameter (MFD) is defined by the point of $1/e^2$ power density.¹ In typical single-mode telecommunications fibers, the MFD is about $10\ \mu\text{m}$.

For fiber manufacturers, mode-field diameter is a critical parameter. Failure to control the mode-field diameter properly results in high intrinsic splice loss (see section 6.6). Intrinsic loss is a nuisance for fiber-optic installers because it results from a mismatch between the fiber MFDs, so it cannot be reduced except by changing one or possibly both fibers.

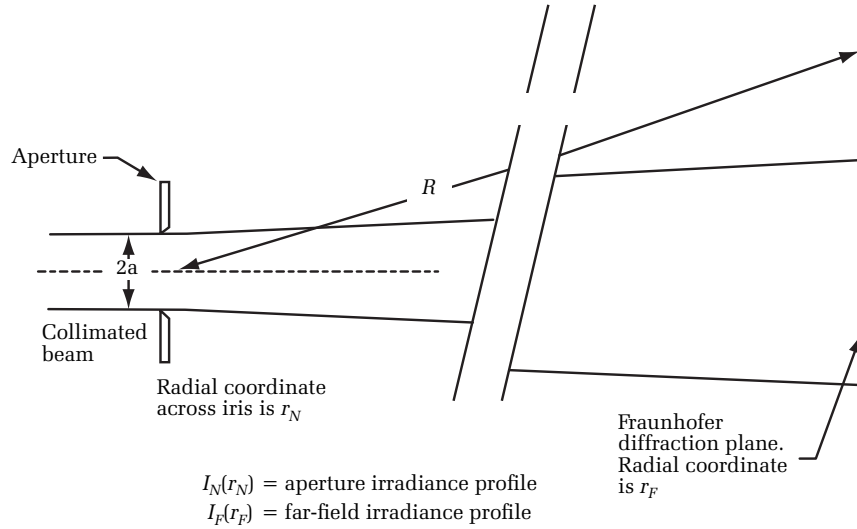
For some fiber installations with very-low-splice-loss specifications, intrinsic splice loss may be important to the overall power budget. To minimize this intrinsic splice loss, installers need to be sure that the MFDs of their fibers do not deviate excessively from each other. They can partially ensure this by buying fiber that is guaranteed to meet a certain specification. This, however, still leaves the installer dependent upon the fiber manufacturer. In some cases, if concern about intrinsic loss is significant enough, the installer may desire an inexpensive method of verifying the mode-field diameters of the fiber. One of the amazing things about the OTDR is that, given a properly calibrated reference fiber, it is capable of making useful field measurements of the fiber mode-field diameter.

Sometimes the cut-off wavelength is also important to know. Recall from chapter 2 that the cut-off wavelength is defined by the normalized frequency, V . When the normalized frequency is greater than 2.405, the fiber supports more than one mode. This has important consequences for bend-loss sensitivity, attenuation, and mode dispersion. Not only can OTDRs measure the numerical apertures of single-mode optical fibers, they can also measure the cut-off wavelengths.

9.1 The far-field scanning method of determining numerical aperture

There are several established procedures for measuring the numerical aperture of optical fiber. The purpose of this section is to give you a sense of the difficulty and involvement associated with some of these methods. Here, we will describe just one such method, the far-field scanning method.²

The far-field scanning method is based on Fourier optics. One of the truly remarkable aspects of optics is that the near-field and far-field distributions compose a Fourier transform pair.* Consequently,



$$I_F(r_F) = \left[2\pi \int_0^\infty \sqrt{I_N(r_N)} \cdot J_0 \left[\frac{2\pi}{\lambda R} r_N \cdot r_F \right] r_N dr_N \right]^2$$

$$I_N(r_N) = \left[\frac{2\pi}{(\lambda R)^2} \int_0^\infty \sqrt{I_F(r_F)} \cdot J_0 \left[\frac{2\pi}{\lambda R} r_N \cdot r_F \right] r_F dr_F \right]^2$$

Figure 9.1. Relationship between the irradiance distribution across an aperture and the irradiance distribution in the Fraunhofer diffraction plane. The irradiance distributions across the aperture and in the Fraunhofer diffraction plane are related through the two-dimensional Fourier transform.

*The far field is far from the diffracting aperture, in what is called the Fraunhofer diffraction region.

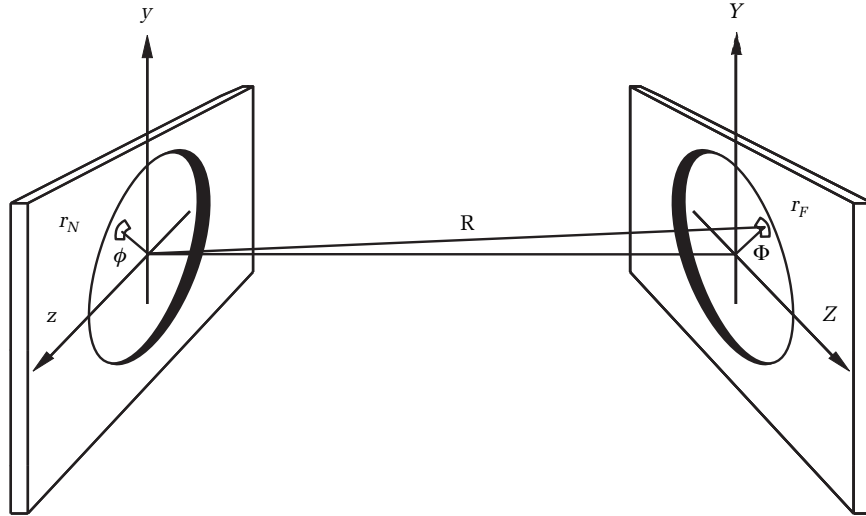


Figure 9.2. Geometry relating points in the source aperture and points in the Fraunhofer diffraction plane.

if you know the far-field distribution, you can calculate the near-field distribution. In practice, the optical fiber is cleaved and light from the fiber allowed to project on a plane with a scanning optical power meter (see figures 9.1 and 9.2).³ Light emanating from the fiber diffracts and forms an irradiance distribution at the plane. Generally, the shape of the aperture and the irradiance distribution are both arbitrary functions. For fibers, however, as well as many other applications, the aperture and irradiance distribution both have circular symmetry. The equation for the electric field in the Fraunhofer diffraction plane is⁴

$$E(Y, Z) = \int_{-\infty}^{\infty} \int_{-\infty}^{\infty} A(y, z) \exp\left(\frac{ik}{R}(Yy + Zz)\right) dy dz \quad [9.1]$$

In equation [9.1], (Y, Z) are coordinates in the image plane, (y, z) are coordinates in the aperture plane, and R is the distance from the aperture to the image plane. In the Fraunhofer limit, R is infinite. The amplitude function across the aperture is $A(y, z)$, k is $2\pi/\lambda$ and i is the square root of -1 .

Since we have assumed circular symmetry, equation [9.1] can be simplified to a single integral through the following substitutions (see figure 9.2):

$$\begin{aligned} z &= r_N \cos \phi \quad \text{and} \quad y = r_N \sin \phi \\ Z &= r_F \cos \Phi \quad \text{and} \quad Y = r_F \sin \Phi \\ dx \, dy &= d\theta \, r \, dr \end{aligned}$$

$$E(r_F) = \int_0^a A(r_N) \int_0^{2\pi} \exp\left(\frac{i \cdot k}{R} r_N r_F (\cos(\phi - \Phi))\right) d\phi \cdot r_N \, dr_N \quad [9.2]$$

Since $E(r_F)$ is circularly symmetric, the value for Φ is arbitrary, so we pick $\Phi = 0$. Furthermore, the zero-order Bessel function can be expressed as⁵

$$J_0(z) = \frac{1}{2\pi} \int_0^{2\pi} \exp(iz \cos \theta) d\theta$$

We note, from equation [9.2], that:

$$\int_0^{2\pi} \exp\left(\frac{i \cdot k}{R} r_N r_F \cos(\phi - \Phi)\right) d\phi = 2\pi \cdot J_0\left(\frac{k}{R} r_N r_F\right)$$

Thus, the expression for the far-field diffraction pattern is simply

$$E(r_F) = 2\pi \int_0^a A(r_N) J_0\left(\frac{k}{R} r_N r_F\right) \cdot r_N dr_N \quad [9.3]$$

Equation [9.3] is written in terms of the electric field at the aperture (the core of the fiber). Optical power meters, however, measure electrical photocurrent, which is proportional to the field squared. Therefore, to make the equations correspond to real measurements, we need to express equation [9.3] in terms of the more measurable quantity irradiance:*

$$I_F(r_F) = \left[2\pi \int_0^a \sqrt{I_N(r_N)} \cdot J_0\left[\frac{2\pi}{\lambda R} r_N \cdot r_F\right] r_N dr_N \right]^2 \quad [9.4]$$

In equation [9.4], $I_F(r_F)$ is the Fraunhofer (far-field) irradiance distribution and $I_N(r_N)$ is the irradiance distribution across the aperture (the near-field distribution).

*We assume that the phase across the mode distribution is constant.

The field distribution across the near field and the field distribution across the far field are a Hankel transform pair. Since we want to calculate the near-field distribution from the far-field distribution, we take the inverse transform of equation [9.4], obtaining

$$I_N(r_N) = \left[\frac{2\pi}{(\lambda R)^2} \int_0^\infty \sqrt{I_F(r_F)} \cdot J_0 \left[\frac{2\pi}{\lambda R} r_N \cdot r_F \right] r_F dr_F \right]^2 \quad [9.5]$$

Using equation [9.5], then, you can calculate the irradiance distribution of the fiber's mode by taking the Hankel transform of the far-field irradiance data.

In an experiment, we used the far-field scan method to determine the mode-field diameters of several fibers. The far-field scan used a three-axis slide that moved an optical power meter (with a small aperture over its detector) across the fiber's far-field irradiance distribution (see figure 9.3). Table 9.1 is a summary of the $1/e^2$ mode-field diameters for the four test fibers.

Fiber	Width at $1/e^2$ (microns)
1	9.149
2	8.934
3	8.716
4	6.179

Table 9.1. Mode-field diameters determined by the far-field scan method.

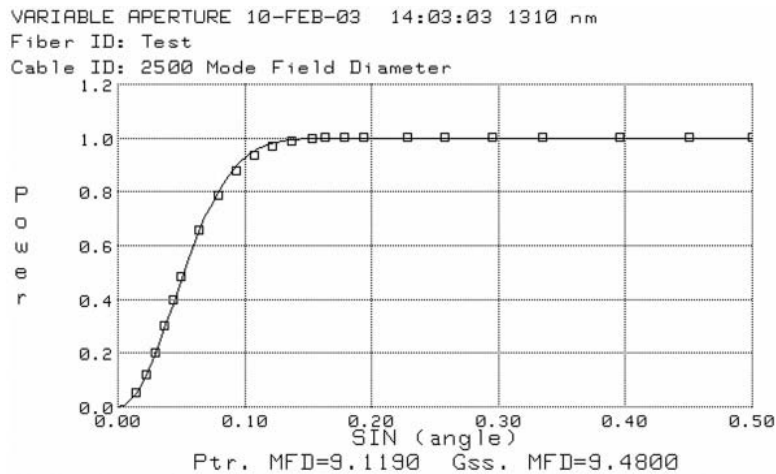


Figure 9.3. Far-field irradiance distribution from single-mode optical fiber at 1310 nm. [Credit: Photon Kinetics.]

9.2 Measuring the numerical aperture of a single-mode fiber using an OTDR

In chapter 6 we saw that the true loss of a splice between two single-mode fibers is⁶

$$L = L_{m_{1,2}} - F_1 + F_2 \quad [9.6]$$

In equation [9.6], $L_{m_{1,2}}$ is the measured loss (using an OTDR) of the splice between fibers 1 and 2 when the OTDR is connected to fiber 1. The relative fiber backscatter parameters for fibers 1 and 2 are F_1 and F_2 , respectively. The relative fiber parameter for a given fiber is

$$F = 5 \log \left(\left(\frac{\text{NA}}{n_1} \right)^2 \cdot \alpha_s \right) \quad [9.7]$$

In equation [9.7], NA is the fiber's numerical aperture, n_1 is the core index, and α_s is the scattering coefficient (1/km).

Inserting equation [9.7] into equation [9.6], we have³

$$L - L_{m_{1,2}} = 5 \log \left(\left(\frac{\text{NA}_2}{\text{NA}_1} \right)^2 \left(\frac{n_{a1}}{n_{b1}} \right)^2 \frac{\alpha_{s_2}}{\alpha_{s_1}} \right) \quad [9.8]$$

Standard (non-dispersion-shifted) single-mode fibers have simple step-index profiles. In these types of fibers, the core index is a function of the numerical aperture and the cladding index:

$$n_1^2 = \text{NA}^2 + n_2^2 \quad [9.9]$$

Substituting equation [9.9] into equation [9.8] and solving for the numerical aperture of the second fiber, we obtain*

$$\text{NA}_2 = n_2 \cdot \left[\left\{ \frac{\text{NA}_1^2 + n_2^2}{\text{NA}_1^2} \cdot \frac{\alpha_{s_2}}{\alpha_{s_1}} \cdot 10^{\left(\frac{L_{m_{1,2}} - L}{5} \right)} \right\} - 1 \right]^{-0.5} \quad [9.10]$$

Recall from chapter 6 that we can easily calculate the true loss of a fusion splice or connector by measuring the splice from both ends and

*In this equation, n_2 is the cladding index, which is assumed to be the same for both fibers.

averaging the two readings.* Substituting the expression for the true loss, in terms of the averaged bidirectional losses, into equation [9.10], we obtain

$$NA_2 = n_2 \cdot \left[\left\{ \frac{NA_1^2 + n_2^2}{NA_1^2} \cdot \frac{\alpha_{S_2}}{\alpha_{S_1}} \cdot 10^{\left(\frac{L_{m_{1,2}} - L_{m_{2,1}}}{10} \right)} \right\} - 1 \right]^{-0.5} \quad [9.11]$$

In equation [9.11], $L_{m_{2,1}}$ is the measured loss between fibers 1 and 2 when the OTDR is connected to fiber 2, and n_2 is the cladding index.

Recall from chapter 2 that optical fiber is manufactured by doping the center, or core region of pure optical silica, with impurities designed to raise the index of refraction. The boundary formed by doped and undoped regions of the glass defines the transition from core to cladding in the optical fiber. Since the cladding is undoped fused silica, we can approximate its index of refraction as⁷

$$n = \left[1 + \lambda^2 \left(\frac{0.6961663}{\lambda^2 - (0.0684043)^2} + \frac{0.4079426}{\lambda^2 - (0.1162414)^2} + \frac{0.874794}{\lambda^2 - (9.896161)^2} \right) \right]^{0.5} \quad [9.12]$$

In equation [9.12], λ is the wavelength in microns and n is the index of refraction. Using equation [9.12], we find the cladding index at 1310 nanometers is 1.4468 and at 1550 nanometers is 1.44402.

Equation [9.11] suggests a simple method for determining the numerical aperture of an unknown fiber if you have a length of calibrated reference fiber. To do this, connect the reference fiber to the unknown fiber using a splice or connector. Measure the connection loss between the two fibers from each end of the link, along with the scattering coefficients of the two fibers.† Using these data in equation [9.11] yields the numerical aperture of the unknown fiber.

We can use equation [9.11] to determine the fiber's spot size by assuming that the modal distribution is Gaussian. Although not strictly true, this is a good approximation. For Gaussian beams, the angular

*Obtaining the true loss by measuring from both ends and averaging is a well-established technique for OTDR measurements.

†For modern single-mode fiber, the attenuation coefficient measured by the OTDR is very nearly the same as the scattering coefficient.

divergence, wavelength of light, and mode-field radius are related by the equation

$$\theta_{1/e^2} = \lambda/(\pi \cdot \omega_0) \quad [9.13]$$

In equation [9.13], θ is the far-field angular divergence (in radians) defined by the $1/e^2$ irradiance point, λ is the wavelength of light, and ω_0 is the radius of the modal distribution.

Recall that the numerical aperture is the sine of the divergence and that for small angles of divergence $NA = \sin(\theta) \approx \theta$. Substituting this into equation [9.13] we have

$$NA_{1/e^2} = \lambda/(\pi \cdot \omega_0) \quad [9.14]$$

Equation [9.14] holds if we define the NA in terms of the angular divergence at the $1/e^2$ irradiance point. A more conventional definition, however, is to define the NA at the 5% irradiance point. This results in a somewhat larger value for the numerical aperture than given by equation [9.14].

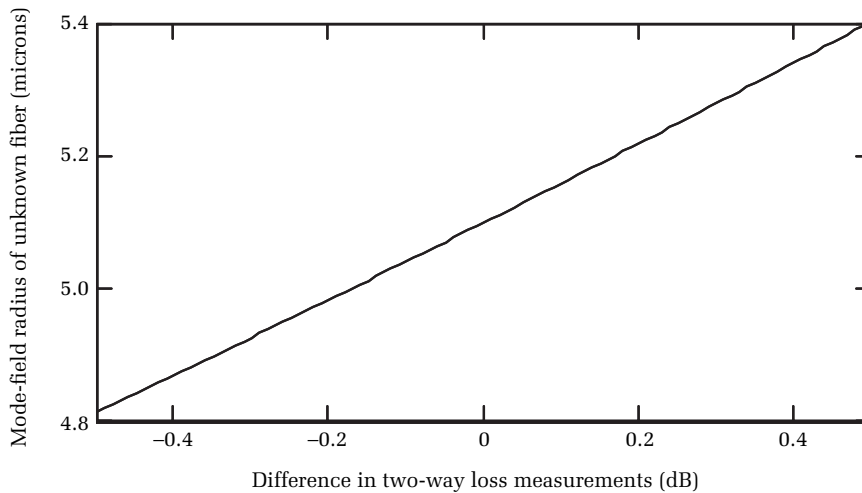


Figure 9.4. Mode-field radius of unknown fiber as function of $L_{m_{1,2}} - L_{m_{2,1}}$. Notice the variation is nearly linear, and the slope is approximately 0.6 microns per decibel. Assumptions in this example are: wavelength = 1.310 microns, core index = 1.5, scattering coefficient = 0.35 dB/km for both fibers, reference fiber mode-field radius is 5.1 microns.

Substituting equation [9.14] into equation [9.11], we have

$$\omega_2 = \frac{\lambda}{\pi \cdot n_2} \left[\left\{ \frac{\left(\frac{\lambda}{\pi \cdot \omega_{01}} \right)^2 + n_2^2 \alpha_{S_2} \cdot 10^{\left(\frac{L_{m1,2} - L_{m2,1}}{10} \right)}}{\left(\frac{\lambda}{\pi \cdot \omega_{02}} \right)^2 \alpha_{S_1}} \right\} - 1 \right]^{0.5} \quad [9.15]$$

Figure 9.4 is a plot of the dependence of the mode-field diameter of the unknown fiber, relative to the known fiber, as a function of the difference in the loss measurements of the splice. If the splice loss is smaller when measured from the end with the reference fiber, then $L_{m1,2} - L_{m2,1}$ is negative and the unknown fiber has a mode-field diameter that is smaller than that of the reference fiber. If the splice loss is greater when measured from the end with the reference fiber, then the unknown fiber has a mode-field diameter that is larger than that of the reference fiber. The difference in mode-field diameters is nearly linear, and for typical single-mode fibers the slope is about 0.6 micron per decibel difference in the loss measurements.

Fiber	MFD Far-field scan	MFD Equation 9.15
1	9.149	ref. fiber
2	8.934	8.745
3	8.716	8.870
4	6.179	5.715

Table 9.2. Comparison of mode-field diameters determined by the far-field scan method and equation [9.15].

Taking fiber 1 as our reference, we calculated the mode-field radius of the three fibers from table 9.1 using equation [9.15]. Table 9.2 summarizes the results from equation [9.15] and compares them with the answers obtained from the far-field scans.

9.3 Measuring the cut-off wavelength of a single-mode fiber using an OTDR

In this section we describe a method, reported in the literature, for determining the cut-off wavelength as a function of length along an optical fiber.^{8,9} This method is easily extended, through bidirectional

measurements, to measuring the cut-off wavelength of one fiber relative to another.

Consider a single fiber of length L . Suppose we acquire an OTDR waveform of this fiber from opposite ends. From one end the waveform signature is $S_1(z)$ and from the other end the waveform signature is $S_2(z)$. From these two functions we can define an imperfection function, $I(z)$:

$$I(z) = S_1(z) + S_2(L - z) \quad [9.16]$$

Now we define a modified imperfection function $I'(z)$:

$$I'(z) = I(z) - I(z_0) \quad [9.17]$$

In equation [9.17], the point z_0 is an arbitrary reference point on the fiber. This is the point to which the cut-off wavelength is referenced.

Having obtained the imperfection function and the modified imperfection function at one wavelength, we proceed to acquire OTDR waveforms at a second wavelength. From these second-wavelength waveforms we derive another set of imperfection and modified imperfection functions.* Taking the difference between the modified imperfection functions at the two wavelengths, we have

$$\Delta I(z) = I'(\lambda_2, z) - I'(\lambda_1, z) \quad [9.18]$$

A simple empirical expression developed by Marcuse relates the mode-field diameter of a single-mode, step-indexed fiber at a particular wavelength to the normalized frequency, V .¹⁰ Kowaliuk and Ferner showed how to rewrite the expression as a function of the wavelength, the fundamental mode cut-off wavelength, and the core radius. To eliminate the dependence on the mode-field radius, they evaluated the expression at two wavelengths. The ratio of the mode-field diameters, R , is thus

$$R \equiv \frac{\omega(\lambda_1)}{\omega(\lambda_2)} = \frac{0.65 + 0.434 \left(\frac{\lambda_1}{\lambda_c} \right)^{3/2} + 0.0149 \left(\frac{\lambda_1}{\lambda_c} \right)^6}{0.65 + 0.434 \left(\frac{\lambda_2}{\lambda_c} \right)^{3/2} + 0.0149 \left(\frac{\lambda_2}{\lambda_c} \right)^6} \quad [9.19]$$

*The first wavelength could be 1310 nm and the second wavelength 1550 nm. This is easy to do if you have a 1310/1550 dual-wavelength OTDR. For consistency, you should use the same pulse width and averaging for both wavelengths.

Kowaliuk and Ferner showed that the difference between the modified imperfection functions at two wavelengths is related to the ratio of the mode-field radius according to the expression

$$R(z) = R(z_0) \cdot 10^{(\Delta I(z)/20)} \quad [9.20]$$

To calculate the cut-off wavelength along the fiber, you must first determine the cut-off wavelength at the reference point and estimate $R(z_0)$ by using equation [9.20]. With $R(z_0)$ known, use equation [9.19] to determine $\lambda_c(z)$.*

Kowaliuk and Ferner showed that this technique for measuring cut-off wavelength is accurate to about ± 20 nm. The test is useful because of its speed, simplicity, and accuracy wherever you need to know the evolution of cut-off wavelength along the length of a fiber. The test is probably most applicable to fiber manufacturers, who must carefully control the fiber's numerical aperture, core diameter, and cut-off wavelength during the manufacturing process. Remember, this analysis is based on the assumption of a step-index fiber. It is inappropriate for some dispersion-shifted fibers and graded-index fibers.

9.4 Summary

Ordinarily we think of OTDRs as instruments for measuring the distances and losses of connectors and fusion splices on optical fiber. It might seem surprising, therefore, to see that OTDRs are also useful for making practical measurements of important fiber parameters such as numerical aperture, mode-field radius, and cut-off wavelength. These measurements are possible because the backscatter level depends on these fiber parameters. Rayleigh backscatter is the key to virtually all of the measurements made with OTDRs. In the absence of absorption from impurities, Rayleigh scattering is the dominant source of fiber loss. Fiber manufacturers work hard to minimize its effects. It seems ironic, therefore, that backscatter is also the mechanism that enables the most useful fiber-diagnostic tool to be of even more utility.

Suggested reading

O'Sullivan, M. S., and Lowe, R. S., "Interpretation of SM fiber OTDR signatures," *Proceedings of the SPIE, The International Society for Optical Engineering Optical Testing and Metrology*, Vol. 661 (1986).

*Equation [9.19] must be solved numerically.

Warder, J., and Saravanos, C., "Mode-field diameter and cut-off wavelength profile measurement using dual wavelength OTDR," *NIST Special Publication 7th Symposium on Optical Fiber Measurements*, No. 839 (Boulder, CO: NIST, 1992), pp. 15–17.

Marcuse, D., *Principles of Optical Fiber Measurement* (New York: Academic Press, 1981).

Chamberlain, G. E., Day, G. W., Franzen, D. L., Gallawa, R. L., Kim, E. M., and Young, M. "Optical-fiber characterization attenuation, frequency-domain bandwidth, and radiation patterns," *NBS Special Publication 637*, Vol. 2 (1983).

Problems

1. True or false: OTDRs can be used to measure the cut-off wavelength of fibers.
2. True or false: OTDRs can be used to measure the mode field diameter of optical fibers.
3. True or false: To measure the mode-field diameter of an optical fiber using an OTDR, you first need to characterize the OTDR's dynamic range and dead zone.

¹ *Mode-field Diameter Measurement of Single-Mode Optical Fibers (Near-Field Method)*, Electronic Industries Association (EIA), Fiber Optic Test Procedures (FOTP) 165.

² Hotate, K., *Applied Optics*, Vol. 18 (1979), p. 3265.

³ Kim, E. M., and Frazen, D. L., "Measurement of far-field radiation patterns from optical fibers," *NBS Special Publication 637*, Vol. 2 (1983).

⁴ Hecht, E., and Zajac, A., *Optics* (Reading, MA: Addison-Wesley, 1974), equation 11.61, p. 411.

⁵ Abramowitz, M., and Stegun, I. A., *Handbook of Mathematical Functions* (New York: Dover, 1972), equation 9.1.21.

⁶ Anderson, D. R., "Making true splice loss measurements with OTDRs from one end of the fiber," *National Fiber Optics Engineers Conference (NFOEC)*, Boston (1995), equation [21].

⁷ Gower, J., *Optical Communications Systems* (Englewood Cliffs, NJ: Prentice Hall, 1984), equation 2.2.32. (This equation was determined by Malitson of the National Bureau of Standards from data he fitted to a Sellmeier dispersion equation having three terms, two in the UV and one in the IR.)

⁸ Kowaliuk, K. W., and Ferner, J., "A technique to estimate the cut-off wavelength profile in single-mode fibers using a switchable dual wavelength OTDR," *Proceedings NIST '88 Symposium on Optical Fiber Measurements* (1988).

⁹ Wardner, J., and Saravanos, C. Costas, "Mode-field diameter and cut-off wavelength profile measurement using dual-wavelength OTDRs," *Proceedings NIST '92 Symposium on Optical Fiber Measurements* (1992).

¹⁰ Marcuse, D., "Loss analysis of single-mode fiber splices," *Bell System Technical Journal*, Vol. 56, No. 5 (1977), equation [8].

Chapter 10

Analyzing passive networks containing splitters and couplers

10.0 Introduction

Optical couplers, or splitters, are devices used to broadcast an optical signal from one fiber to many fibers. In the most general case, splitters are configured as M by N (see figure 10.1). In such devices, there are M input ports and N output ports. Optical signals on any of the input ports are branched to all the output ports.* If the splitter has only one input port it is called a 1-by- N splitter. Although construction techniques vary, one way to build a 1-by- N splitter is to combine a series of 1-by-2 splitters as shown in figure 10.2.

Theoretical		Component
1x2 = 3.0 dB (50/50)	50%	1x2 ≤ 3.6/3.6 dB (50/50)
1x4 = 6.0 dB	25%	1x2 ≤ 4.1/3.1 dB (45/55)
1x8 = 9.0 dB	10%	1x2 ≤ 4.7/2.7 dB (40/60)
1x16 = 12 dB	6.25%	1x2 ≤ 5.3/2.3 dB (35/65)
1x32 = 15 dB	3.125%	1x2 ≤ 6.0/1.9 dB (30/70)
		1x2 ≤ 6.8/1.5 dB (25/75)
		1x2 ≤ 7.9/1.2 dB (20/80)
		1x2 ≤ 9.3/0.9 dB (15/85)
		1x2 ≤ 11.3/0.6 dB (10/90)
		1x4 ≤ 7.0 dB
		1x8 ≤ 11.0 dB
		1x16 ≤ 14.3 dB
		1x32 ≤ 17.8 dB

Figure 10.1 Theoretical and manufacturer's component values for optical splitters.

Generally, if a splitter has N output ports, then the number of 1-by-2 splitters required to build the device is $N - 1$. For example, the splitter in figure 10.2 has eight output ports, so the number of 1-by-2 splitters required is $8 - 1 = 7$. For a balanced splitter (one in which the input optical signal is evenly distributed to all the output ports), each 1-by-2 splitter attenuates the signal in each of its two output legs by a factor of

*Optical splitters are also sometimes used to multiplex, or combine, several signals together and then broadcast all of them over the output ports. When used this way, different signals are applied to different input ports. Each signal at the input ports is broadcast to all the output ports (and attenuated accordingly). Consequently, the signals applied to the input side of the splitter are multiplexed together onto each of the output ports.

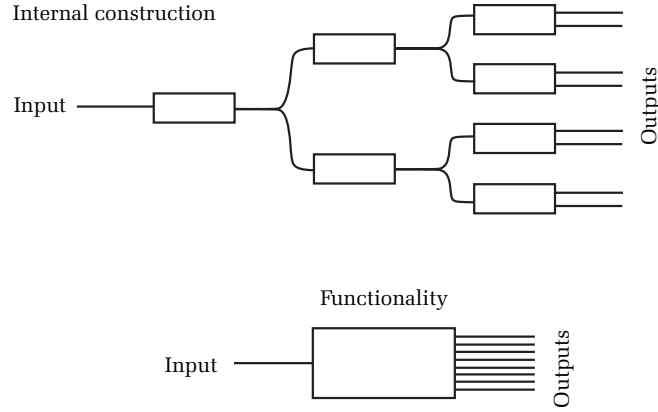


Figure 10.2. A 1-by-8 splitter constructed from seven 1-by-2 fused biconical taper (FBT) splitters. Externally, there is one input port and eight output ports. Optical signals on the input port are divided (and attenuated) among all the output ports.

1/2 plus excess loss. Ideally, the excess loss is zero; manufacturers try hard to achieve this goal. Typically, however, the excess loss is a few tenths of a decibel so the total loss is about 3.2 dB (or less) for each leg. Additional loss occurs because each pigtailed leg of the splitter must also be spliced or connectorized, depending on the application. For each split this would add one inbound and one outbound termination. The addition of two splices of 0.1 dB each would change this value to 3.4 dB. Using this number, the total loss, from the input port to any output port, of a balanced 1-by- N splitter is

$$3.4 \left(\frac{\ln(N)}{\ln(2)} \right) \text{dB}$$

As an example, for a 1-by-8 splitter, the attenuation at each output port is roughly 9.8 dB.

Perhaps the most common method of building a 1-by-2 coupler is to fuse two fibers together as shown in figure 10.3. These couplers, called *fused biconical taper* (FBT) couplers, are nonreflective, which makes them attractive for use in high-speed digital, CATV, and DWDM systems. In one manufacturing method, the fibers are held close together and held in tension while they are heated with a flame or electric arc. As the heat softens the fibers, they stretch and taper in the middle region near the flame. During this process the testing of the FBT occurs in real time by monitoring the input power and the output power levels of each

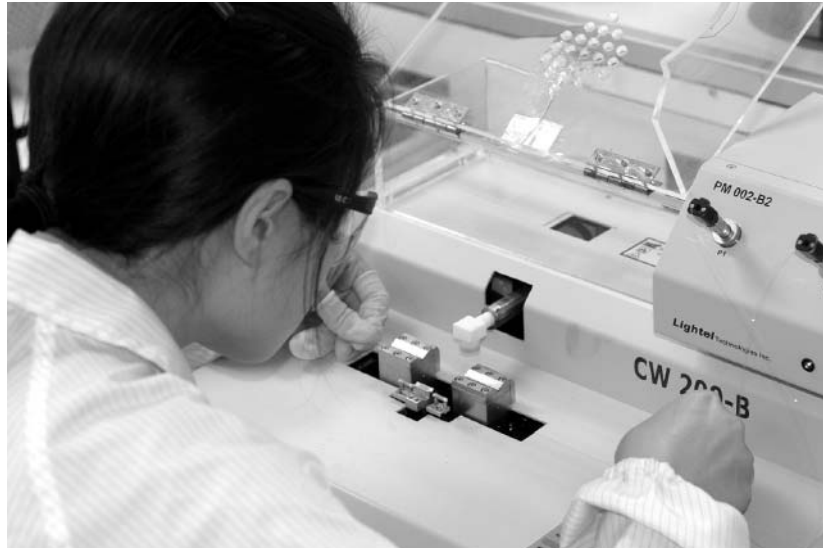


Figure 10.3. Fused biconical taper (FBT) fiber couplers are made by heating two fibers and drawing them together. The drawing process is controlled such that the claddings merge and their cores come close enough for light in the two fibers to couple. [Credit: The Light Brigade.]

leg of the splitter. Adjustments can be made in real time to achieve the designed split ratio. Continued heating causes the fibers to thin and the cores to come closer as the fibers fuse together. The center region of the coupler, where the fiber cores come close together, is called the *coupling region*. It is in the coupling region that optical energy is transferred between the two fibers.

Recall from chapter 2 that the fundamental mode in single-mode fibers extends into the cladding (see figure 2.13). When the cores of the two fibers are fused close together in the coupling region, the modes extend into the thin cladding region between the cores and overlap. When the modes from the two fibers overlap, they can exchange energy. In an analogous fashion, a mechanical system consisting of coupled springs can (when properly excited) result in energy transferring from one-half of the system to the other and then back again, in an endless exchange and reversal of energy flow. In similar fashion, when two fibers are brought close together, the light from one fiber can couple into the other. The amount of light that couples depends on the length of the coupling region, so by controlling the coupling region the design engineer can tailor the coupler's design specifications.^{1,2}

After the FBT coupler is fused, one of the two input legs is then snipped off and index matched so that no light is reflected off this fiber's end face. Because most couplers are wavelength-independent couplers (WICs), they will match attenuation specifications both at the 1310 and 1550 nm wavelengths and bidirectionally. This makes them ideal for testing with the OTDR's bidirectional transmission at the same wavelength and for applications including fiber to the home (FTTH), based on the ITU-T G.983 passive optical network (PON) standard, which uses 1550 nm downstream from the service provider and 1310 nm upstream from the home.

The internal details of how a coupler, or splitter, is built may vary from one manufacturer to another. The packaging styles are also different. Figure 10.4 illustrates splitters from different manufacturers. As you can see, the package styles vary significantly among the manufacturers, and some splitters with more output ports may actually be smaller than other splitters with fewer output ports. Often splitters come with their input and output ports unconnectorized, with the splitter connected into the network by fusion splices. Other times the splitter may come with connectors already attached.



Figure 10.4 Examples of commercially available splitters. Clockwise from top left: 1-by-2, 1-by-32, 1-by-4, and 1-by-8 splitter. [Credit: The Light Brigade.]

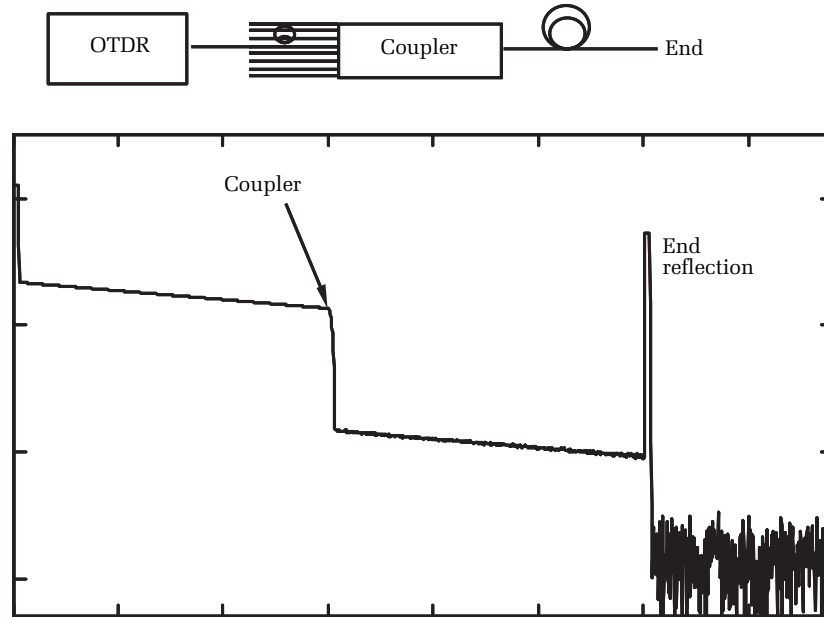


Figure 10.5. An OTDR waveform when the OTDR is attached to one of the output legs of a 1-by-8 coupler. The large loss at the coupler is approximately 10 dB. This large loss decreases the signal-to-noise ratio and makes it difficult to test events that are far beyond the coupler. The coupler in this figure was fusion spliced to the input and all the output fibers, so there is no reflection associated with it.

Splitters are used when broadcasting the signal from one fiber to several other fibers, as in CATV applications. Splitters may also be used to multiplex the optical signals from several fiber lines onto a single line. However they are used, splitters pose several problems to the OTDR operator. If the OTDR is connected to the N side of a 1-by- N splitter, then the waveform shows a large loss at the splitter (see figure 10.5). In our 1-by-8 splitter example, the loss is roughly 9.8 dB (assuming that the splitter is balanced and that the excess loss associated with each port is only 0.2 dB and an additional 0.2 dB for the two pigtail splices). This large loss limits the OTDR's ability to test far beyond the splitter because the loss represents an effective loss in the OTDR's dynamic range.

When connected to the input side of a 1-by- N splitter, the waveform shows a smaller drop than if the OTDRs were connected to one of the N output ports (5.1 dB in this example). The higher signal level results because the combined signatures of all the N fibers on the branching side

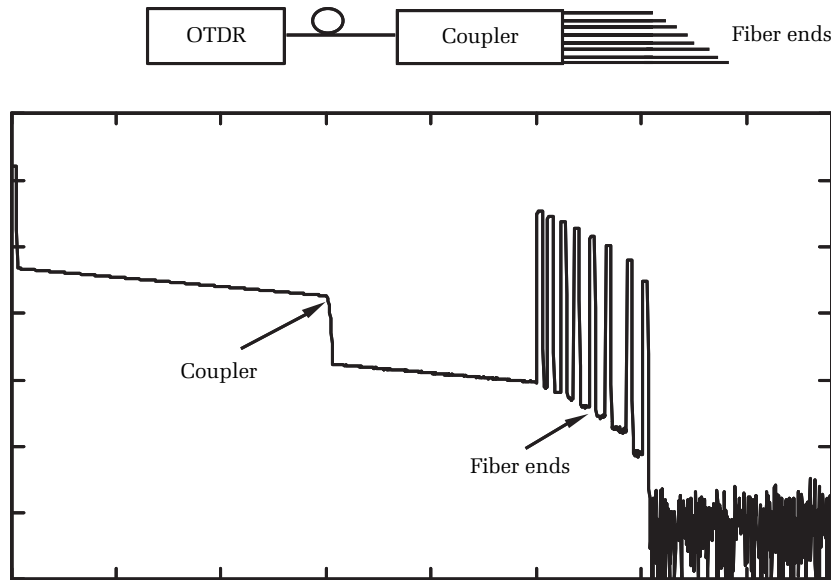


Figure 10.6. An OTDR waveform of a 1-by-8 splitter, tested with the OTDR at the input end. There is still a large loss at the splitter, though not as large as when testing from one of the eight fiber ends. The loss after the end of each fiber gradually increases until the loss after the end of the longest fiber. The backscatter signature after the splitter, and before the end of the first fiber, comes from all eight output fibers. The splitter in this figure was fusion spliced to the input and output fibers. The loss after the first reflective end is $5 \log(8/7)$. The loss after the second reflective end is $5 \log(7/6)$, etc.

of the splitter are superimposed (see figure 10.6). This superimposition makes it very difficult and sometimes impossible to associate events on the waveform with the specific lines on which the events occur. This is probably the most common problem faced by OTDR operators when dealing with splitters. If a Fresnel reflection shows at the splitter location, it is because one or more of the splitter pigtails are unterminated. During testing, the pigtails can be immersed in index-matching gel (IMG) to resolve this problem, or the legs can be terminated with optical terminators until future drop cables are spliced to the open leg.

10.1 Determining the locations of breaks in systems containing splitters

When you test a fiber-optic network from the input side of the splitter, the OTDR launches its laser pulse toward the N output ports. When

they reach the splitter, the OTDR's outward traveling pulses are divided among the output ports. These divided pulses travel along their respective fibers, scattering light back toward the splitter. This backscattered light from each of the output ports returns to the splitter, where it is combined onto the input line and returns to the OTDR. In the waveform on the OTDR display, the scattered light from all the output fibers superimpose into a single waveform. It is this superpositioning of the scattered light from the output lines that makes the OTDR signature ambiguous. Since the scattered light combines into a single composite waveform, it becomes very difficult to associate events on the output side of the splitter to the specific line that has the event.

Although it might seem impossible, under some conditions you can determine which output fiber has a specific event.³ To do this, the line you are testing must satisfy three conditions. First, any event you are trying to locate must have a sufficiently large loss so that it can be detected when added to the backscattered light from all the other output ports. Second, the output fibers must all be different lengths. Third, the fiber network must be properly documented at the time of installation (before any undocumented events occur).

Consider the example in figure 10.6. Here, each of the N fibers has a slightly different length from all the other fibers. In this example, the differences in the fiber lengths are about two pulse widths. With this configuration, and using the chosen pulse width, each of the fiber ends is individually visible. Now suppose that a break occurs in one of the N output fibers (see figure 10.7). Two things happen. First, the reflective end of the broken fiber disappears from the waveform (a new reflection may pop up at the break, depending on the nature of the break). Second, there is a drop in the backscatter signal at the location of the break. The drop in backscatter occurs because the backscatter contribution from the broken line disappears after the break. If the distance to the break is less than the distance to the end of the shortest output fiber, the loss of the break is about 0.3 dB.* Depending on the nature of the break, it may or may not be reflective. If the break occurs at a distance greater than the shortest output fiber, it may be obscured by the other reflective ends.

Figure 10.7 illustrates the case where the third fiber (numbering from the shortest) has a break. Observe that the reflective end from the third fiber is gone from the waveform and that the loss between the second and fourth fiber has increased. Observe, also, that there is

*The loss depends on the splitter. For a balanced 1-by-8 splitter, the loss is about 0.3 dB.

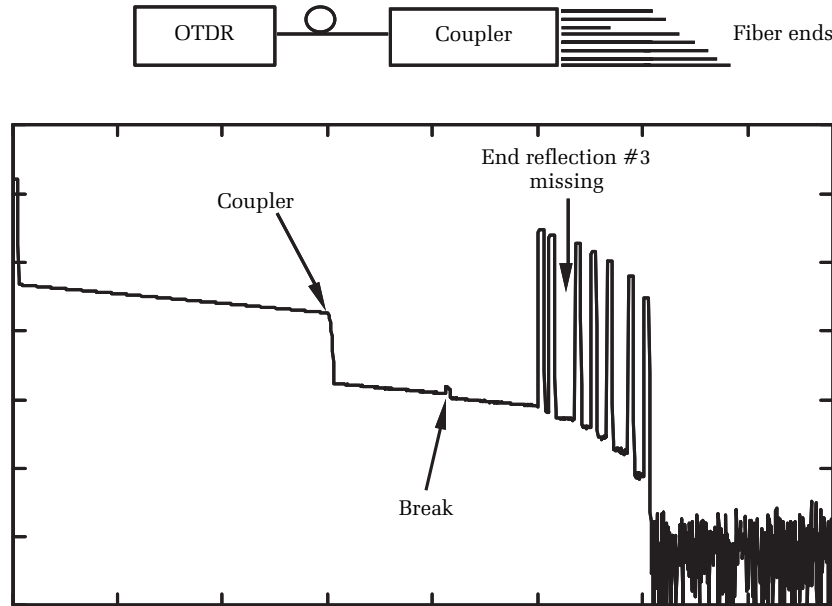


Figure 10.7. OTDR waveform when fiber number 3 is broken after the splitter. The new reflective event midway between the splitter and the end of fiber 1 shows where the break occurred. The missing reflection from fiber 3 shows that the break occurred on fiber 3. By comparing the waveform in figure 10.5 with the waveform in this figure, you can easily determine on which fiber the break occurred and its distance from the end of the input fiber.

a slightly reflective event between the fiber ends and the splitter. This reflective event locates the distance to the break, and the disappearance of the third reflection tells us the break occurred on fiber 3.

Things are not quite so simple if the fiber suffers a partial failure due, for example, to a bend instead of a break. The reason for this is the insensitivity in measuring the event's loss. This insensitivity results from the fact that the backscatter signature after the splitter arises from the combined signatures of (in our example) eight fibers. For instance, if one of the fibers breaks on a 1-by-8 splitter, then the backscatter level after the break drops by $5 \log(8/7)$, or 0.29 dB. Suppose, however, that instead of being broken, the fiber is only bent or stressed. In this example, the true event loss might be about 1 dB (a fractional loss of 0.21). Because of the backscatter contributions from the other fibers, the loss that we see on the OTDR screen is only $5 \log(8/(7 + 0.79))$, or 0.06 dB. If the bending

loss were only 0.5 dB, then the observed change in backscatter on the OTDR waveform would be only 0.03 dB.

Accurate measurements of these low losses are compounded by two things. First, the splitter's excess loss dramatically reduces the OTDR's dynamic range (by about 5 dB in our example). Second, resolving the different reflections from the output ends of the splitter typically requires a short pulse. Since short pulses reduce the OTDR's dynamic range, the problem of signal-to-noise ratio is further exacerbated.

Under certain circumstances, the end reflections can provide information about lower-loss events. Although the backscatter level drops by only a small amount relative to the event's true loss, the reflective end of the affected output fiber drops by the total amount of the event's loss. If the fiber breaks, the reflective end disappears altogether. If the fiber is bent, introducing a loss of 1 dB (for example), the reflection drops by 1 dB.

While it might be tempting to use this drop in the fiber's reflection to get a better estimate of the event's loss, you must be careful. The problem is that the reflective end may not have constant reflectivity. As we saw in chapter 7, the amount of reflection from a mated connector is very sensitive to the physical condition of the device. The reflectivity from the mated connector can easily change with temperature, humidity, or handling. Since these factors can never be ruled out, you are generally not justified in assuming the reflectivity of a mated connector has not changed (similar arguments hold for most mechanical splices as well).

The reflection from an unconnected polished fiber end or cleaved fiber end is relatively stable as long as it is not contaminated by dust, dirt, moisture, or skin oils from handling. Although this reflectivity is more stable than a connector's, you must still exercise caution in drawing conclusions based on a change of only a decibel or so in the reflectivity of even a cleaved fiber or polished connector end.

10.2 OTDR requirements for testing networks with splitters

To test networks containing splitters using the method described in section 10.1, all the splitter's output fibers must have different lengths. The differences in length must be sufficient to identify individually each of the reflective ends using a pulse width that is long enough to result in a clean backscatter waveform. Typically, the minimum difference in length between any adjoining output fibers must be about two pulse widths. The pulse width is determined by the amount of fiber you are testing and by the OTDR's dynamic range. You need to use a

sufficiently long pulse to have low-noise backscatter after the splitter but a sufficiently short pulse to resolve each reflective fiber end individually. From this, you can see that there is a somewhat complicated interplay between the OTDR's performance specifications, setup parameters, and the network configuration.

Complicating matters even more, we also saw that the displayed event loss is much smaller than the actual event loss. Unless the fiber is broken, the displayed event loss may be too small to detect, especially for splitters with large numbers of output fibers. For a splitter with N output fibers, the composite event loss when one of the fibers breaks is

$$L = 5 \log (N/(N - 1)) \quad [10.1]$$

For eight output fibers, a broken fiber appears as a 0.29-dB loss, for 16 fibers the displayed loss of a break is 0.14 dB, and for 32 fibers it is 0.07 dB. If the fiber is simply damaged (excessive bending, for example) and not broken, then the composite loss is even less. To determine where these faults occur, the OTDR must be able to locate these small events accurately. Clearly, the problem of fault location becomes more serious as the number of output ports on the splitter increases.

The dual requirements of high resolution and ability to measure low loss are very demanding. An OTDR's event resolution depends on the pulse width. The smaller the pulse width, the better the OTDR's event resolution will be. To measure low-loss events requires an OTDR with high dynamic range. Dynamic range, however, improves with increasing pulse width. Consequently, we are faced with two conflicting requirements. The best solution for this application is probably a high-performance OTDR coupled with detailed and accurate maps of the fiber plant. Documentation and waveform comparison are essential elements of this method. The OTDR must also work with software having mass-storage ability and the ability to display two waveforms simultaneously so they can easily be compared for any changes. Finally, since potentially small events need to be identified, the OTDR's event-marking algorithms must be capable of locating small events, especially in portions of the waveform where the noise level is high.

The FTTH/PON systems being installed (see figure 10.8) must be able to split the optical power to reach 32 users along with future expansions to 64 and 128 users. This equals 15 dB for 32 users and 21 dB for 128 users. This only accounts for the split losses and must still have enough dynamic range for the fiber, connectors, and splices. The fiber spans can be as long as 20 km and must also include the associated splices and



Figure 10.8. A fiber-to-the-home/PON installation in Wenatchee, Washington. [Credit: The Light Brigade.]

connections in the network. The challenge of measuring lengths and losses demonstrates the usefulness of the OTDR when the user can define its performance requirements. What is required in this case is an OTDR with enough dynamic range to overcome the loss from attenuation of the splitters, connectors, fibers, and splices while simultaneously testing with a sufficiently short pulse width to measure a 15-meter (50-foot) drop from the curb to the home at a distance of 20 km from the OTDR. This must be achieved while maintaining sample spacing consistent with testing closely spaced events, such as the splitter and the pigtail connection at the home.

Suggested reading

Takeda, K., and Koga, H., "Fault location in optical lines of passive double star networks by pattern matching of OTDR waveforms," *Electronics & Communications (Japan)*, Part 1, Vol. 77, No. 7 (1994).

Kashima, N., *Passive Optical Components for Optical Fiber Transmission* (Norwood, MA; Artech House, 1995).

Kapron, F. P., and Berardinelli, J. D., "OTDR measurements through optical splitters," *NIST Special Publication 839* (Boulder, CO; NIST, Sept. 1992).

Problems

1. True or false: When testing passive fiber-optic networks that have splitters, one of the most important diagnostic tools is an accurate OTDR trace of the system when it was working correctly.
2. True or false: If all of the fibers from the output of the splitter are exactly the same length, it's still possible to unambiguously determine the leg in which the fiber break occurs by using an OTDR.
3. True or false: If a break occurs in one of the output legs of the splitter, its signature on the OTDR trace is the same as a break in a single fiber.
4. True or false: The more legs on the splitter, the more difficult the diagnosis with an OTDR.
5. True or false: A 1-by- $2N$ splitter can be made by combining $2N-1$ splitters that are each 1-by-2.

¹ Kashima, N., *Passive Optical Components for Optical Fiber Transmission* (Norwood, MA: Artech House, 1995).

² Marcuse, D., "Coupled-mode theory of round optical fibers," *Bell System Technical Journal*, No. 52, pp. 817–842.

³ Jauvtis, H. I., "Locating fiber faults in FITL systems," *Fiberoptic Product News* (July, 1994).

Chapter 11

Automatic event-marking algorithms and calibration

11.0 Introduction

In chapters 5 through 9 we saw that measurement techniques for even simple types of events can sometimes be difficult. This is especially true when trying to estimate the measurement uncertainty or when including esoteric effects that occasionally affect accuracy. Accordingly, to help reduce the workload on the operator, improve measurement accuracy, and reduce test time, virtually all OTDR manufacturers now offer instruments that automatically evaluate the waveform as well as mark and measure the events.

In this chapter we describe some of the attributes that distinguish the types of automatic event-marking algorithms offered by OTDR manufacturers. We also describe some typical operating scenarios and look at the advantages and disadvantages offered by the various types of event-marking algorithms. We describe fully automatic, fully optimized algorithms that automatically set all acquisition parameters and scan the fiber with multiple pulse widths, averaging times, and gain settings. We examine the rules used by fully optimized algorithms to set the various acquisition parameters, and we show that these algorithms offer significant advantages for completeness, accuracy, repeatability, and archiving.

Later in this chapter we examine some of the infinite configurations of events with which measurement algorithms must deal. We show typical isolated and grouped events as well as examples of OTDR hardware characteristics that sometimes result in false, or bogus, events, and we examine the issues of measurement accuracy and repeatability.

11.1 Types of event markings

As we saw in chapter 1, the earliest OTDRs were laboratory experiments composed of oscilloscopes used in conjunction with discrete laser sources and receivers. The display was linear, not logarithmic, and distance had to be calculated by hand from the oscilloscope's time base. First-generation mainframe OTDRs incorporated all these functions into one box and added averaging capability, a log display, and a distance scale. These instruments typically had cursors that the operator could manipulate to measure the loss and distance of a particular event.

As mainframe OTDRs evolved, the initial emphasis was on the performance of the hardware. These OTDRs provided high-quality waveforms, but the operator still had to make virtually all the measurements. This began to change in the early 1990s with the arrival of automatic event marking. With automatic event marking, a computer in the OTDR evaluates the waveform, locates each event, and measures the distance, loss, and reflectivity for each event. The OTDR also generates an event table that shows the numbered events, their locations, losses, reflectivity values, and other appropriate information. Automatic event marking reduced the need for OTDR operators to be highly skilled in waveform interpretation. It also reduced measurement time, since manual waveform interpretation typically requires more time than automatic analysis.

Each OTDR manufacturer uses proprietary event-marking algorithms. These algorithms, along with the way they are implemented in the OTDR, have resulted in a mix of performance that varies considerably from one manufacturer to the next. Event-marking algorithms range from those requiring the operator to specify the acquisition settings to those that are totally automatic and control all instrument functions. Although not rigorously defined, event marking can be roughly organized into four types.

1. *Manual event marking.* In manual event marking, the OTDR operator selects the acquisition parameters, including the pulse width, range, averaging time, and possibly gain setting and bandwidth. Then the operator acquires the waveform and analyzes it. The OTDR does not perform any analysis functions. It does, however, provide the operator with cursors that can be manipulated, a digital readout that describes the distance to the cursors, the distance between the cursors, and the loss between the cursors.
2. *Semimanual event marking.* In semimanual event marking, the operator selects the acquisition parameters and acquires the waveform. Then the operator directs the OTDR to evaluate the waveform. The OTDR uses built-in algorithms that scan the fiber, locate the events, measure the events, and record these data in an event table.
3. *Semiautomatic event marking.* OTDR manufacturers sometimes promote this type of event marking as “one-button event marking,” although this is not strictly true. In semiautomatic event marking, the operator selects one of the parameters, such as the amount of averaging, and the OTDR automatically selects the rest of the

acquisition parameters, including pulse width and range. The OTDR automatically acquires the waveform, analyzes it, and prints the event table.

4. *Fully automatic, fully optimized event marking.* This is the most advanced event marking available. With fully optimized event marking, the OTDR automatically acquires waveforms using multiple pulse width, averaging, gain, and bandwidth settings. It does this to optimize the acquisition parameters at each event along the fiber. After acquiring several waveforms using multiple acquisition parameters, the instrument automatically evaluates each waveform and computes an event table. The OTDR also displays a composite waveform, made by splicing sections of the various acquired waveforms. This also allows the user to perform manual measurements if desired.

11.2 Functionality of different types of event markings

An example helps illustrate the advantages and disadvantages of the different types of event-marking options. Suppose a technician needs to characterize a fiber-optic link that is 50 kilometers long. Forty meters from the source end of the link (the end the technician tests from) is a connector that lies just inside the central office. Twelve kilometers from the central office is a vault with two splice closures, with 30 meters of slack cable between the two splices. Twenty-four kilometers from the central office is another splice vault with two splice closures, with 34 meters of slack cable between them. Thirty-eight kilometers from the central office is a third splice vault with two splice closures, with 25 meters of cable slack between them. The end of the fiber is 50 kilometers away. Let's examine how each of the four types of event marking would examine this fiber when testing at 1310 nm.

First, let's consider a manual measurement. If the operator knows the length of the fiber, then setting the range is relatively easy: Set it longer than the fiber and as short as otherwise possible. If the operator does not know the fiber's length, then a little experimentation may be required. For example, the operator might first pick a long range and relatively long pulse width. If the pulse width is not too long, the operator probably can see that there are splices at 12, 24, and 38 kilometers. In the interest of maximizing dynamic range, the operator might use a long pulse width that probably cannot resolve the connector at 40 meters, or the pairs of fusion splices at 12, 24, and 38 kilometers. Consequently, the operator's test data may result in improper documentation of the fiber link.

A skilled operator should recognize the possibility that multiple splices could be in the vaults or that a connector might be inside the central office. The skilled operator selects a smaller pulse width, increases the averaging (to maintain dynamic range), and acquires a second waveform. After acquiring at least two waveforms, the skilled operator has sufficient information to measure all the events except possibly the individual splices in the enclosure 38 kilometers away. Assuming an average time of 2 minutes to measure each event manually and assuming two acquisitions at 4 minutes each (including setup time), the manual measurements require 28 minutes.

Now consider a test using an OTDR with semimanual event marking. Since the operator must select the acquisition settings, this test could proceed like the manual test. As with the manual test, the operator may choose less-than-optimal settings for the first acquisition. Upon seeing the first waveform and analyzing its events, the operator decides a second acquisition is necessary. The advantage of the semimanual mode is the speed with which the OTDR can analyze the waveform. The operator using manual mode might spend 6 minutes to analyze the three events in the first waveform. In semimanual mode, he or she requires only about 1 minute for analysis, a savings of 5 minutes. Upon acquiring the second waveform, however, the operator probably has to make manual measurements of the closely spaced events. This is because most event-marking algorithms have difficulty making individual measurements of events that are spaced too close together. If this is the case, then the second acquisition and analysis takes about as much time as it did via manual mode (about 14 minutes). If the algorithms are very capable, they can measure the closely spaced events individually. In this scenario, analysis of the second acquisition requires only about 1 minute. Assuming the same amount of time to set the acquisition parameters and acquire the waveforms, in semimanual mode the total time for test and analysis is somewhere between 10 and 23 minutes.

Notice that the range of test times in semimanual mode results from questions about the algorithm's ability to measure all the events. If the algorithms are capable of measuring all the events, then test time is cut almost in half, compared with the manual test scenario. If the algorithms cannot find all the events, however, the incremental advantage of the semimanual mode is drastically reduced. For event-marking algorithms to provide a clear economic advantage, therefore, they must be sufficiently sophisticated to eliminate most of the need for any manual measurements.

Now consider a test with an OTDR using semiautomatic event marking. The operator first determines the averaging time. Suppose the operator selects 2 minutes. The operator pushes the START button, and the OTDR makes a quick scan of the fiber to locate the fiber's end. Then the algorithm selects a pulse width and range that allow sufficient dynamic range to make loss measurements near the fiber's end. In this case, the fiber is relatively long (50 kilometers), and at 1310 nm the fiber loss alone is 17.5 dB. To make accurate loss measurements the backscatter level needs to be about 6 dB above the noise floor, so the OTDR requires a total dynamic range of about 24 dB. To accomplish this in 2 minutes of averaging, the algorithm selects a 200-meter pulse. With the 200-meter pulse, the OTDR is unable to distinguish the connector at 40 meters or any of the secondary splices in the enclosures at 12, 24, and 38 km. Consequently, when the OTDR finishes its acquisition and analysis 3 minutes later, the operator has an event table that is missing four of the fiber's seven events.

If the operator is skilled, he or she may recognize the possibility that multiple splices are in the splice vaults, that macro- or microbends may be present in close proximity to the closure (see figure 11.1), and that multiple cross-connect panels and connectors may be present in

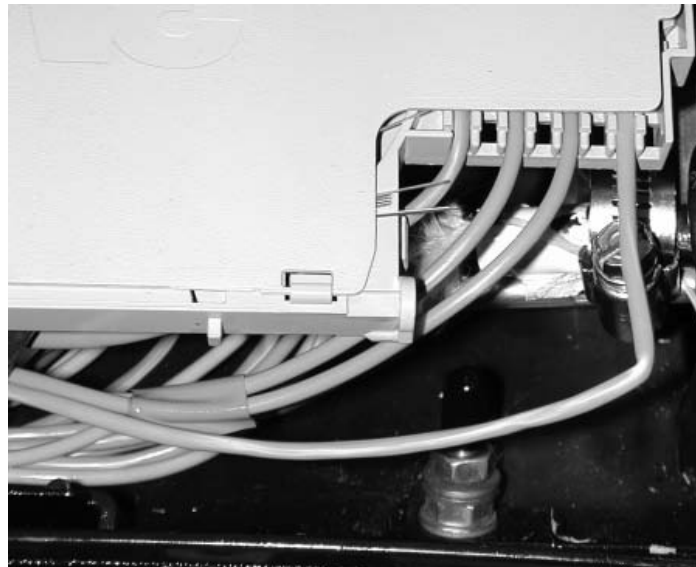


Figure 11.1. Example of macrobend inside a splice closure. [Credit: The Light Brigade.]

the central office. In this case, the operator needs to make at least one additional acquisition with manually selected acquisition parameters. Let's assume the first test takes 3 minutes for setup and semiautomatic analysis and that the second test takes 4 minutes to select the acquisition parameters manually and to evaluate the resulting waveform with the OTDR's algorithms. This gives a total test time with semiautomatic algorithms of 7 minutes. Note, however, that if the algorithms are not able to analyze the closely spaced events, then the operator must manually measure the second acquisition. In this scenario, the test time extends to about 21 minutes. Obviously, semiautomatic event analysis offers considerable advantages over manual acquisition and analysis, but there is still much inefficiency. Observe also that an OTDR with semiautomatic analysis must also have semimanual analysis or it is severely restricted, because semiautomatic algorithms cannot optimize the acquisition parameters over the full fiber.

The test scenario changes significantly when using fully automatic, fully optimized event marking. With fully optimized algorithms, the operator connects the test fiber to the fiber-optic line and presses START. Since the algorithms are fully automatic, there are no user-selectable settings except for wavelength and index of refraction. The OTDR automatically scans the fiber and partitions it into sections. Then the OTDR selects a *different* pulse width, averaging time, and gain setting for each of the sections. It selects these individual acquisition parameters to maximize dynamic range and resolution while minimizing testing time. For example, the first section on the fiber might be 20 kilometers long. For this section the OTDR might select 30 seconds of averaging time, low gain, and a 20-meter pulse. Using these acquisition parameters, the resulting waveform clearly shows the connector at 40 meters and the two fusion splices at 12 kilometers. The event-marking algorithms scan this section, isolate the three events, and enter them into the event table. Fully optimized algorithms typically perform well in detecting events that are closely spaced together. Using advanced algorithms, along with the short pulse in the first section, the fully optimized algorithms find the two splices at 12 kilometers and the jumper at 40 meters. The operator does need not make any additional manual measurements.

While the OTDR is analyzing the first waveform section, it begins acquiring the second section. For the second section, the OTDR might select high gain, a 40-meter pulse, and 1 minute of averaging time. The second section might extend from 20 to 35 kilometers. This time the waveform shows the fusion splices in the enclosure as being composed

of two events; but with insufficient backscatter between the events, the algorithm cannot measure them independently. Consequently, the algorithm reports two events but groups their loss.

The third section extends from 35 to 60 kilometers. For this section, the OTDR selects the 200-meter pulse, high gain, and 1.5 minutes of averaging. With the long pulse width, the OTDR is unable to distinguish two events in the last splice enclosure at all, so it simply reports a single splice and measures its loss. Thus, the total test time for the fully optimized algorithms is 3 minutes. At the end of those 3 minutes the fully optimized algorithms have reported six of the seven events. Although the algorithms did not separately measure the two splices at 24 kilometers, the composite waveform, which used a 40-meter pulse, allows the user to make a useful estimate without another acquisition.* This might take an additional 2 minutes. As with the other event-marking algorithms, the last pair of fusion splices probably cannot be individually resolved, so the total test time using fully optimized algorithms is less than 5 minutes.

For comparison, the manual test took 28 minutes and missed four out of seven events unless the operator was very skilled. The semimanual test took between 10 and 23 minutes and again missed four out of seven events unless the operator was very skilled. The semiautomatic test took between 7 and 21 minutes. Like the manual and semimanual tests, the semiautomatic mode required an experienced operator to locate and measure most of the events. The fully optimized measurements took less than 5 minutes and found six out of seven events. Although the fully optimized algorithms failed to measure the loss of the two events at 24 km individually, they provided the operator with a waveform that made the manual measurement possible without a second acquisition. Thus, the requirements for operator training are much lower with fully optimized algorithms.

This example illustrates the care you must take in evaluating algorithms in different OTDRs. Although the fully optimized instrument was much faster making a complete measurement of the fiber, the semimanual and semiautomatic OTDRs were faster for a given acquisition and analysis. The difference was that the fully optimized instrument acquired and analyzed three waveforms in 3 minutes while the semimanual instrument acquired and analyzed one waveform in 2.

*This is a very important advantage because skill level is not involved and extra acquisitions take time.

The 1-minute advantage held by the semimanual and semiautomatic instruments, however, is offset by the fact that their single acquisition and analysis failed to analyze the fiber completely. This necessitated the acquisition of a second waveform and manual follow-on measurement. After all the testing was done, the OTDR operator with the fully optimized instrument spent much less time testing the fiber than operators with semimanual or semiautomatic OTDRs.

Another advantage is the reduced requirements of documentation when using fully optimized instruments. With nonfully optimized instruments, several waveforms (with different pulse widths) may be required to document the fiber properly. With fully optimized instruments, the different acquisitions, each with a different pulse width, are automatically acquired and spliced into a single composite waveform. Only one file needs to be saved to archive fully the test results for each line.

11.3 Optimizing acquisition parameters

Throughout this book we have emphasized that distance- and loss-measurement accuracy depends a great deal on the pulse width that the OTDR uses. Shorter pulses are better for distance-measurement accuracy, provided a minimum dynamic range is available. This is because the change in waveform slope is more dramatic when it occurs over a shorter length. If the OTDR does not maintain a minimum dynamic range, however, the distance measurements are noise limited.

Longer pulse widths and longer averaging increase the dynamic range. Recall that the dynamic range varies as $5 \cdot \log(\text{pulse width})$ and $5 \cdot \log(\sqrt{\text{number of averages}})$. This means that longer pulses and more averaging time result in higher dynamic range. However, longer pulse widths and averaging time are disadvantageous in other ways. For example, longer pulse widths increase the OTDR's dead zone and make nonreflective splice location more difficult. Increasing the amount of averaging increases the test time and reduces the number of fibers that can be tested in a given amount of time, which affects efficiency and adds cost. Ideally, you would like to measure each event on the fiber with the minimum pulse width and minimum averaging required to just keep the noise-induced measurement uncertainty from being the dominant source of error. Table 11.1 shows how the various acquisition parameters affect OTDR performance.

For many fibers, testing with one set of acquisition parameters means compromising the measurements along much of the fiber. In

our example, we saw how the semiautomatic algorithms selected a pulse width that was too long to resolve separately most of the events along the fiber. This is because the semiautomatic algorithm was forced to pick one pulse width for analyzing the entire fiber. The 200-meter pulse might be appropriate for events near the end of the fiber, where a high signal-to-noise ratio is hard to obtain. However, it is certainly inappropriate for testing near the front of the fiber. Near the front of the fiber, the backscatter level is high and there is no need to test with a long pulse. With semiautomatic algorithms, however, you are forced to accept this compromise; otherwise the events at the end of the fiber would be indistinguishable. Experienced operators can (and often must) manually select different acquisition parameters. This is time consuming, requires a high degree of proficiency from the operators, and defeats the purpose of having automatic algorithms at all.

Performance parameter	Pulse width change for improvement	Averaging change for improvement
Dynamic range	Increase	Increase
Dead zone	Decrease	N/A
Test time	N/A	Decrease
Distance-measurement accuracy	Decrease	Increase
Loss-measurement accuracy	Decrease	Increase

Table 11.1. How an OTDR's performance parameters are affected by pulse width and averaging. The first column lists the OTDR's performance parameters. The second column shows how to change the pulse width to improve the performance parameter. The third column shows how to change the averaging to improve the performance parameter.

Using fully optimized algorithms, the instrument automatically optimizes the acquisition parameters for the best balance between pulse width, acquisition time, and dynamic range. When the instrument begins testing portions of the fiber that require more dynamic range, it increases the pulse width. Until that point is reached, however, the instrument properly uses shorter pulse widths to maximize two-point resolution. Additionally, near the front of the fiber there is no need to average for extended periods of time. As the test progresses along the fiber, however, dynamic range is more important, so the instrument automatically increases the amount of averaging time. The result of fully optimized testing is that the fiber is fully analyzed using optimally

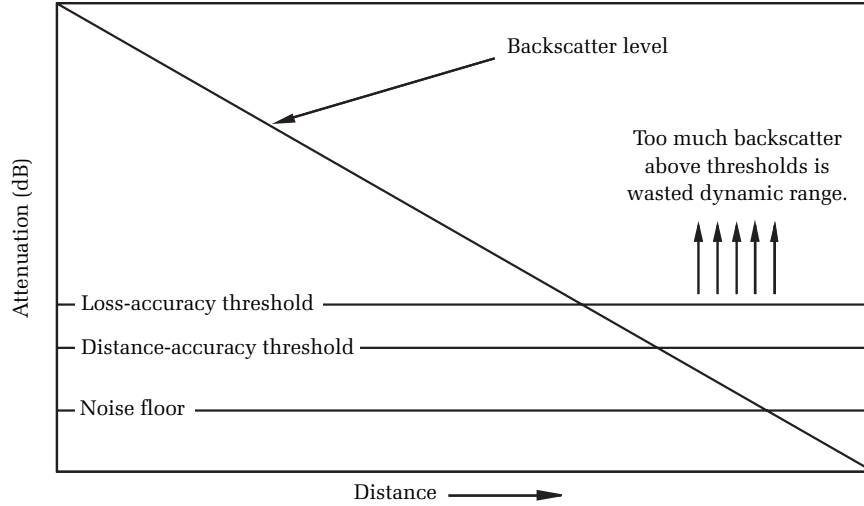


Figure 11.2. Acquisition parameters for semimanual and semiautomatic event-marking algorithms. Their single set of acquisition parameters provides optimization only near the fiber's end. Near events are high above the thresholds (described in chapters 5, 6, and 7), indicating wasted dynamic range, and insufficient two-point resolution.

selected acquisition parameters that change depending on the local requirements along the fiber.

Figures 11.2 and 11.3 show another way to visualize this optimization process. We have already seen in chapters 5, 6, and 7 that loss and distance measurements are characterized by thresholds. These thresholds are functions of the type of event being measured, the event's loss, and the pulse width used by the OTDR. Above the threshold, the measurement uncertainty is relatively constant. Below the threshold, the measurement uncertainty increases dramatically. We need to select our acquisition parameters so that events we want to measure remain above the threshold. On the other hand, we do not want the events to be too far above the thresholds. When the events are too far above the thresholds, then we have more dynamic range than we need, which unnecessarily worsens the dead zone.

With semimanual and semiautomatic event-marking algorithms, the user acquires only one waveform. The acquisition parameters must be chosen to keep events near the fiber's end above the thresholds (see

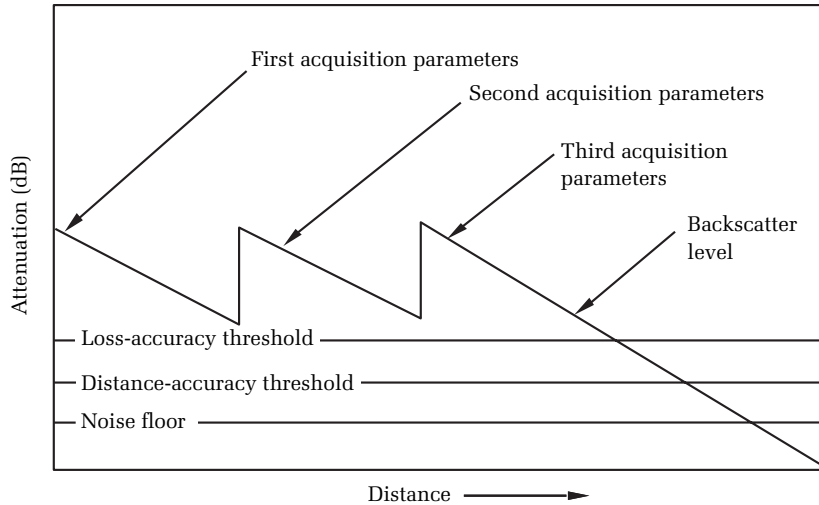


Figure 11.3. Acquisition parameters for fully optimized algorithms. The algorithms divide the waveform into sections and acquire a different waveform for each section. Each sectional waveform is acquired with acquisition parameters optimized for that section. This keeps more of the waveform near the thresholds and represents the most balanced approach to fiber analysis.

figure 11.2). Semimanual and semiautomatic event-marking algorithms optimize for events near the end of the fiber. This means the acquisition parameters near the front of the fiber are not optimized. With fully optimized algorithms, however, the instrument acquires several waveforms. This allows the OTDR to measure more of the events closer to (but not below) the thresholds, maintaining balance between dynamic range, dead zone, and test time.

To evaluate an OTDR's performance fully, it is essential to understand the capabilities and limitations of the instrument's event-marking software. In fact, the OTDR's event-marking capabilities can often make a significant difference between competing machines. The hardware components used in the OTDR are essentially commodity items. Lasers, APDs, couplers, WDMs, and connectors are widely available to all OTDR manufacturers. To achieve a performance advantage, therefore, OTDR manufacturers attempt to design the best acquisition systems (including receiver amplifiers) and the best event-marking software.

Event distance (km)	Event loss (dB)	OTDR 1 distance repeatability (m)	OTDR 2 distance repeatability (m)	OTDR 1 loss repeatability (dB)	OTDR 2 loss repeatability (dB)
2.028	-0.22	4.5	0.5	0.003	0.009
27.060	0.29	5.3	0.8	0.003	0.003
37.053	0.14	8.4	5.6	0.002	0.012
47.047	0.58	36.2	13.2	0.027	0.020
48.052	0.42	4.7	2.1	0.016	0.059
55.041	0.52	155	116	0.142	0.067
56.074	End	6.9	1.8	End	End

Table 11.2. Comparison between an OTDR using semiautomatic event-marking algorithms (OTDR 1) and an OTDR with fully optimized event marking (OTDR 2). OTDR 1 has more dynamic range than OTDR 2, but OTDR 2 has the best distance-measurement repeatability and nearly as good loss-measurement repeatability. This demonstrates the performance advantage that sophisticated event-marking algorithms can give an OTDR. (Repeatability is twice the standard deviation of the loss- or distance-measurements, taken over 10 tests of the fiber illustrated in figure 11.4.)

To appreciate the difference event-marking software can make, consider table 11.2, which compares the test results of an OTDR with fully optimized software against a more powerful OTDR using semiautomatic event marking. Figure 11.4 illustrates the test fiber.

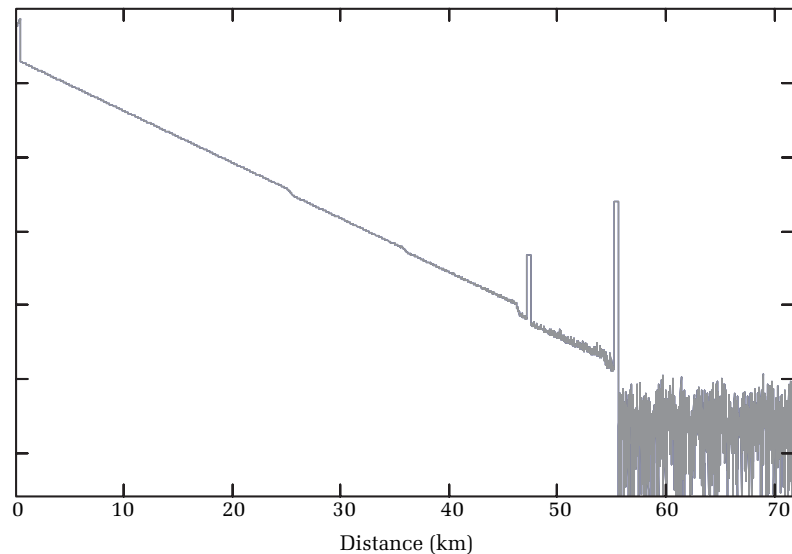


Figure 11.4. OTDR waveform of fiber used to compare fully optimized algorithms with semimanual and semiautomatic algorithms. Event locations and losses are described in table 11.2.

In table 11.2, OTDR 1 has 10 dB more dynamic range than OTDR 2. In spite of this, the event-marking software in OTDR 2 has better distance-measurement repeatability for every event and better loss-measurement repeatability for half of the events. The difference, in this case, is the event-marking software in OTDR 2.

Figures 11.5 and 11.6 compare the performance of OTDR 2, with fully optimized algorithms, against four other OTDRs with semiautomatic event marking. All four OTDRs had roughly the same dynamic range, but OTDR 2 had much better repeatability. The test fiber is similar to the one shown in figure 11.4. Notice that the fully optimized algorithms were the only ones that found all the events. They also had the most repeatable distance and loss measurements. This illustrates the advantage of algorithms that optimize the acquisition parameters for all events and not just those located near the end of the fiber.

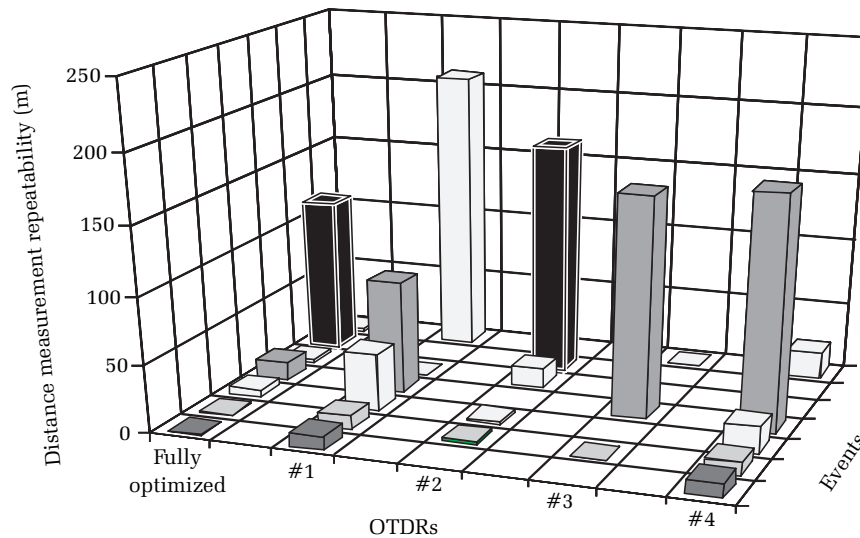


Figure 11.5. Comparison of distance-measurement repeatability. A mini-OTDR with fully optimized algorithms was compared with four other mini-OTDRs having only semiautomatic event analysis. Blank squares are missed events. The test fiber is similar to the one shown in figure 11.4. The fully optimized instrument was the only one that found all the events, and it consistently had the best distance-measurement repeatability (defined as twice the standard deviation over 10 measurements). Several of the mini-OTDRs that missed events had about 1 dB more dynamic range than the fully optimized instrument. Distance-measurement repeatability is twice the standard deviation of the distance measured for each event in 10 tests.

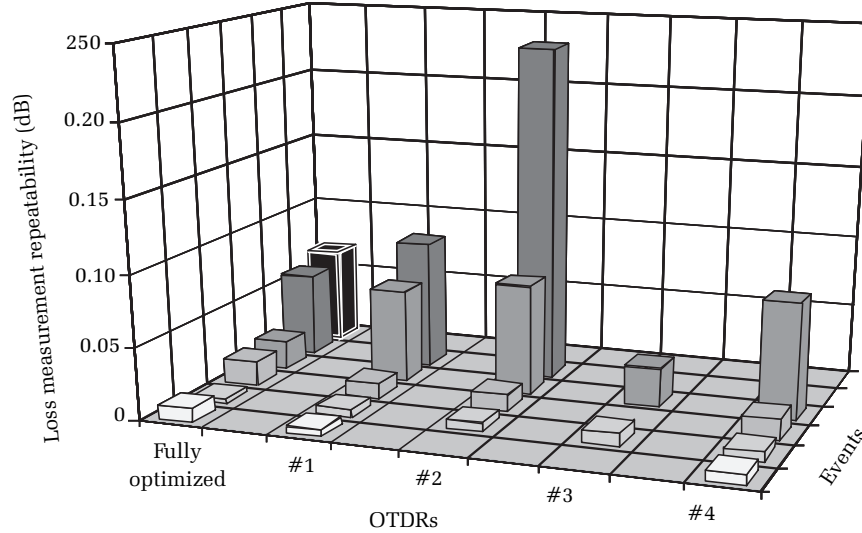


Figure 11.6. Comparison of loss-measurement repeatability. A mini-OTDR with fully optimized algorithms was compared with four other mini-OTDRs with semiautomatic event analysis. Blank squares are either missed or grouped events. The test fiber is similar to the one shown in figure 11.4. Loss-measurement repeatability is twice the standard deviation of the loss measured for each event in 10 tests.

Clearly, the ability of an OTDR to evaluate a fiber properly depends heavily on the types of algorithms used and how they optimize the acquisition parameters. On many fibers it is not possible to optimize the acquisition parameters for all the events using a single set of acquisition parameters. When testing these types of fibers, fully optimized algorithms present a clear advantage that can often compensate for a lack of raw dynamic range. It is important, therefore, to test the OTDR as a complete unit and not simply to compare hardware specifications. Designing test fibers and testing OTDRs with event-marking algorithms are the subjects of the following chapter.

11.4 Measuring individual events

Setting the proper acquisition parameters is the first step toward locating and measuring the events. As we have seen, fully optimized algorithms do this best. With the optimized acquisition parameters set, the next task for the event-marking algorithms is to locate and measure the individual events in the acquired waveform. This task is broken down into four subtasks.

1. Scan the acquisition and find all the regions that appear to have some sort of event or signature that is not pure fiber backscatter.
2. Determine which nonfiber regions actually contain events and which contain bogus data due to hardware anomalies, noise spikes, etc.
3. Evaluate the event regions (nonbogus regions that contain events). Determine their classifications (single event, grouped, reflective, nonreflective, etc.).
4. Scan the events with optimized tools. Determine the event locations, losses, etc. Measure the link loss, sectional loss, fiber loss, etc.

It is important to note that not all OTDRs perform all these subtasks, so the incidence of bogus-event reporting can change considerably from one manufacturer to another. There are five types of hardware anomalies that typically result in these bogus events: (1) offset errors; (2) ringing after reflective events; (3) dropouts; (4) synchronous noise; and (5) non-Gaussian noise.

When an OTDR acquires data, there is an offset associated with the amplifier and the analog-to-digital converter. This offset must be subtracted properly, or the waveform becomes nonlinear as it approaches the noise floor. If too much offset is subtracted, the waveform droops down; not subtracting enough offset causes the waveform to level off and become flat. Figure 11.7 illustrates a waveform with offset properly subtracted, along with a waveform with too much offset subtracted and one with too little offset subtracted.

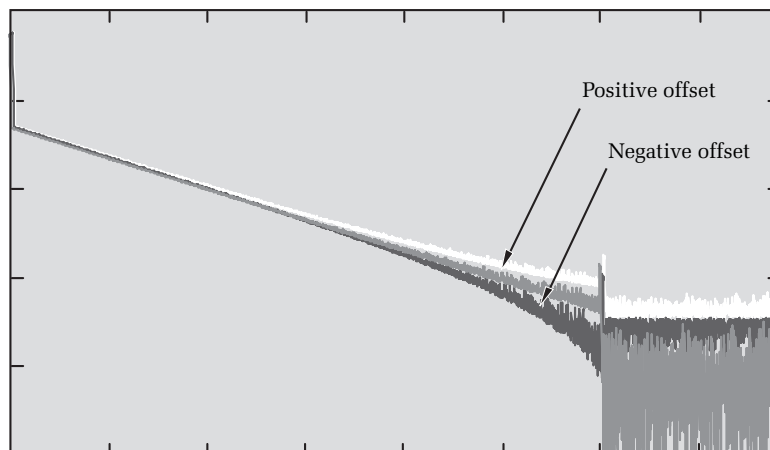


Figure 11.7. Effect on waveform appearance from improper offset removal.

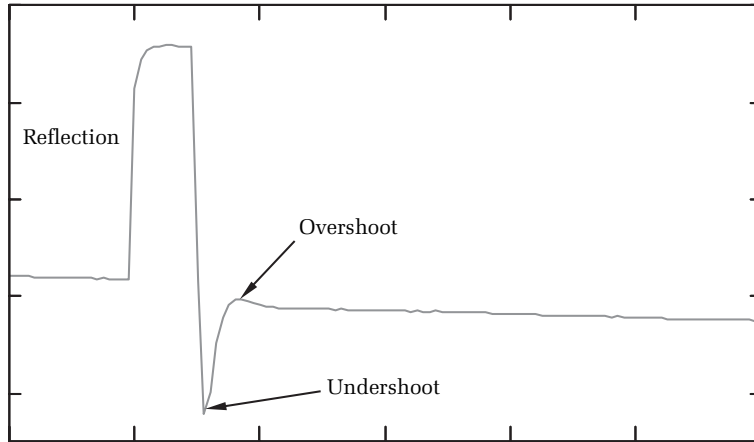


Figure 11.8. Ringing after a reflective event. The undershoot and overshoot can sometimes look like a fusion splice.

Another possible source of confusion for event-marking software is ringing after a reflective event (see figure 11.8). Ideally, the OTDR's receiver and amplifier should be critically damped. Sometimes, however, they can oscillate (or ring), especially with large reflections. When this happens, the waveform after the reflection dips below the backscatter level and then rises to meet it. To the event-marking algorithms, this ringing can appear to be a nonreflective event that is located just past the reflective event. This can be very difficult to discriminate because the

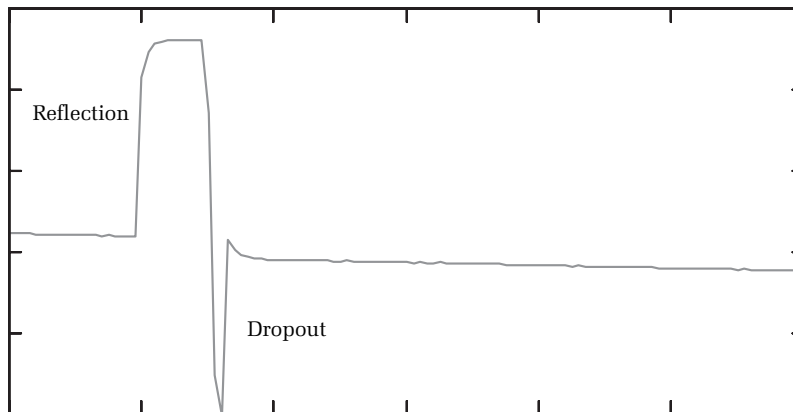


Figure 11.9. Dropout after a reflection. Similar in appearance to ringing, dropouts can also appear to the event-marking software as a reflective event or a nonreflective gainer.

spatial length of the ringing can be about the same as one pulse width and the depth can easily exceed the random noise. The event-marking algorithms should not simply ignore all such features near a reflection, because fusion splices commonly occur in proximity to reflective events.

Closely related to ringing are dropouts (see figure 11.9). This phenomenon can occur for a number of reasons, but the important issue for the designer of event-marking software is that dropouts can easily fool the OTDR. Depending on the depth and duration of the dropout, it can look like a reflection or a fusion splice. The challenge for event-marking software is to ignore these kinds of hardware anomalies while reporting each real event.

OTDRs are complicated instruments. They have high-speed data buses and other lines that emit pulsating electromagnetic radiation. This radiation is often synchronous with the waveform-acquisition circuitry. Without extreme care some of this emitted radiation can be coupled into the receiver, amplified, and appear on the waveform as synchronous noise. Synchronous noise can be especially difficult to deal with, for two reasons. First, because it is synchronous, averaging cannot reduce this type of noise. Thus, synchronous noise often establishes the instrument's minimum noise floor and its base dynamic range. Second, synchronous noise can easily have a periodicity that is similar to the pulse width. When this happens, the undulations caused by synchronous noise can appear, over a few pulse widths of waveform, to be an event (see figure 11.10).

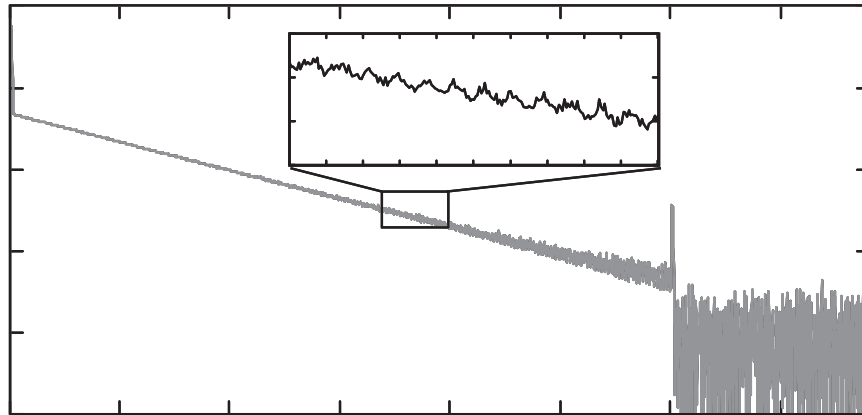


Figure 11.10. Waveform with synchronous noise. Observe that the synchronous noise has roughly the same spatial extent as the pulse width. This can confuse event-marking software and result in bogus events.

One form of synchronous noise is caused by some types of acquisition systems that use sampled interleaving. Sampling is a fundamental part of an OTDR's acquisition system. In a typical OTDR, the sampling circuitry might, for example, sample the waveform every 100 ns. Frequently you want variable sample spacing. For example, on a very long fiber you may want to sample at 10- or 20-meter intervals to prevent the total number of samples from becoming too large. Alternatively, on shorter fibers you may want to sample at 1- or 2-meter intervals to improve resolution. One way to accomplish this is to use a variable sampler. Another way is to use a fixed sampler (say, at 200 or 100 ns) and change the starting delay. The OTDR then acquires several waveforms with different delays and adds them together in an interleaved fashion to achieve a composite waveform. This simplifies the sampling circuitry, but can add synchronous interleaving noise if not done properly. Figure 11.11 shows a waveform with interleaving noise. Since it is synchronous and roughly the same width as a pulse, interleaving noise sometimes looks like real events.

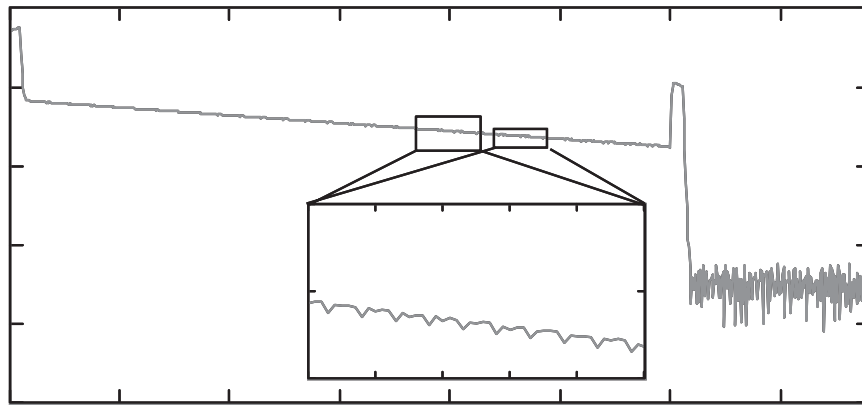


Figure 11.11. An OTDR waveform with interleaving noise.

Another source of noise results from the resolution limit in the length of the digital words used to encode the OTDR waveform. This noise sometimes appears near the noise floor of the OTDR, which results in a waveform with a blocky appearance. The blockiness occurs because of the discrete nature of the digital conversion process. If the digital words used to encode the waveform do not have sufficient resolution, then at small signal levels (such as those near the waveform's end) the waveform takes on a "digital" appearance. Insufficient resolution in the

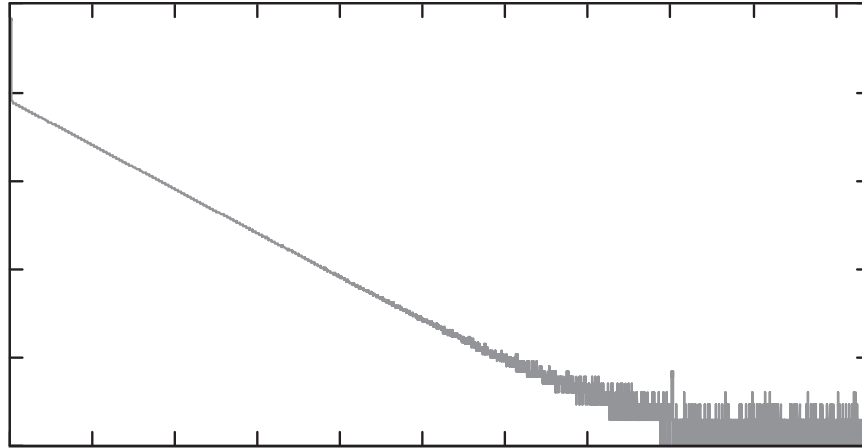


Figure 11.12. OTDR waveform with digitization noise. Digitization noise results from digital encoding of the OTDR waveform with insufficient digital resolution. This is evident in the blocky nature of the waveform near its end.

digital words can also limit the OTDR's dynamic range. Fortunately, this noise is usually easy to discern (see figure 11.12) and not much of a problem for event-marking algorithms.

The objective of the event-marking software is, of course, to find events. Generally, event-marking software is designed to err on the side of finding more bogus events and missing fewer real ones. To help compensate for bogus-event marking, the software usually allows the OTDR operator to scan through the events as they appear on the waveform and to delete them from the event list. To accomplish this task efficiently, the software should do two things:

1. Allow the operator to skip, or jump from one event to the next with a single button push. The OTDR should automatically center a magnified view of the event in the display window.
2. Allow the operator to delete an event from the event table with a single button push.

Giving the operator the option of deleting an event is important. Just the same, you do not want an OTDR that finds a plethora of bogus events. Deleting one or two bogus events might be tolerable, but deleting much more than this begins to affect the operator's efficiency. Furthermore, deleting events requires additional operator training and decision making. Since event-marking software is intended to reduce the operator's workload, bogus events are a hindrance to productivity.

Isolated events on an OTDR waveform come in two flavors: reflective and nonreflective. These two categories can be further divided into events with positive loss and events with negative loss (sometimes called *gainers*). Of course, the loss and reflectivity of these events are infinitely variable. When you begin to include grouped events, the number of possibilities becomes even greater. For example, you might have a nonreflective event just before a reflective one. You might have two closely spaced reflective events or two closely spaced nonreflective events. You might have a nonreflective event after a reflective event. When you consider all the combinations of event loss, reflectivity, and proximity, the number grows faster than a factorial.

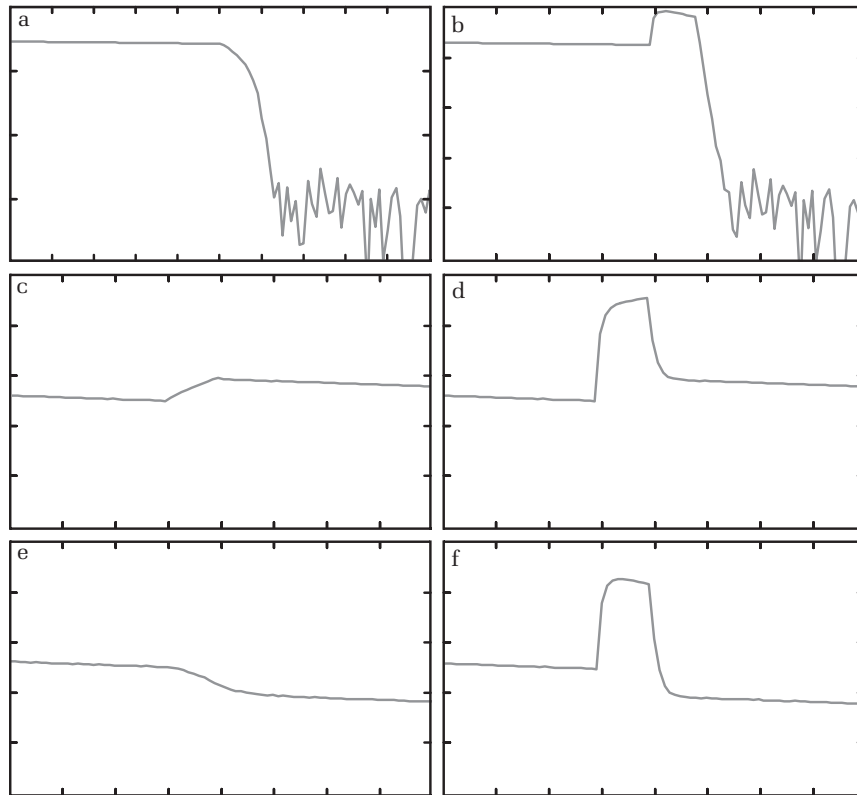


Figure 11.13. Types of isolated events: (a) Nonreflective fiber end, (b) reflective fiber end, (c) fusion splice with negative loss (gainer), (d) connector (reflective event) with negative loss (gainer), (e) fusion splice with positive loss, (f) connector (reflective event) with positive loss.

Figures 11.13 and 11.14 illustrate just some of the types of events you might encounter. Clearly, event-marking software cannot simply catalog different types of events and then report them by matching them to the catalog reference. The event-marking software must be adaptive. It must be able to examine the bogus events and reject them while properly identifying real events that come in an infinite number of sizes and configurations.

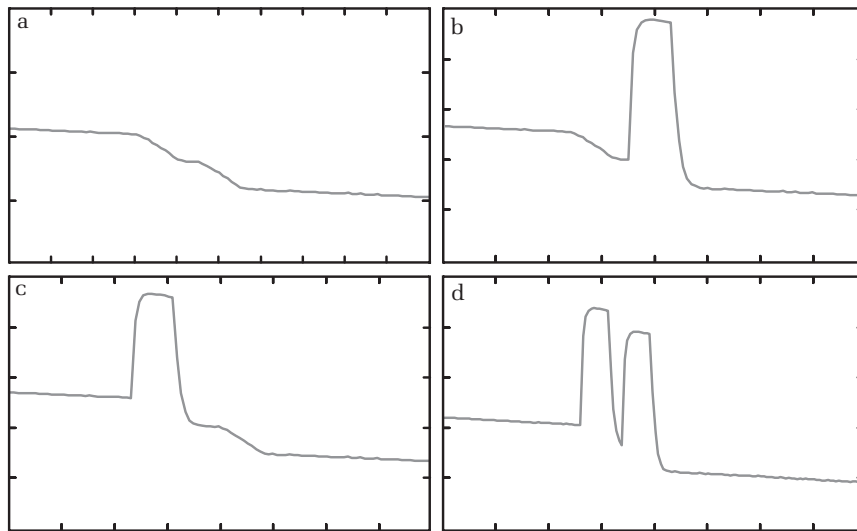


Figure 11.14. Types of grouped events: (a) pair of closely spaced fusion splices, (b) fusion splice preceding a reflective event by slightly more than one pulse width, (c) fusion splice about 1.5 pulse widths after a connector, (d) two reflective events about one pulse width apart.

Many types of event-marking software only locate isolated events with confidence. When the events are spaced too close together, these algorithms sometimes simply report a region of the fiber as a grouped event. They may also report the total group loss but not make satisfactory attempts to isolate the events and measure their losses separately. When you evaluate event-marking software, you need to pay close attention to how the algorithms deal with closely spaced events. Sometimes events are so close together they overlap. When this happens, their losses cannot be individually measured. Often events are close together but not overlapping. In these cases, the event-marking software should be able to resolve the individual events and measure their separate losses.

Some event-marking algorithms fail to measure such closely spaced events properly, and this can sometimes be a problem. When event-marking algorithms group events that should be measured individually, they require the operator to do extra work. Remember that the principal reason for using event-marking algorithms is to reduce training and workload for the operator. If the event-marking algorithms fail to find and measure events as they should or if they find too many bogus events, then they are failing in their primary objective to improve the operator's efficiency.

11.5 Testing event-marking software

The most important aspects of event-marking software are:

1. Distance-measurement accuracy.
2. Loss-measurement accuracy.
3. Ability to locate all events above a given loss threshold.
4. Minimum size of the event threshold.
5. Number of false, or bogus, events detected.
6. Ability to extend the instrument's measurement range by analyzing events near the noise floor.

11.5.1 Test-fiber calibration

Distance-measurement accuracy is very difficult to measure directly. The reason is the difficulty associated with the calibration of test fibers. To calibrate properly the distances to events on a test fiber, you must measure the distances using instruments other than OTDRs. A common mistake is to try to calibrate the distance using manual measurements and a high-performance OTDR. The fallacy in this approach, as we saw in chapters 5 and 6, is that manual measurements are relatively inaccurate, due to waveform noise and interpretation errors by the operator. Another common mistake is to try calibrating the distance using a high-performance OTDR and its event-marking algorithms. The problem with this approach is that the high-performance OTDR and its event-marking algorithm limit the calibration accuracy. As we saw in table 11.2, the OTDR and its event-marking algorithms may not be as accurate as the instruments being evaluated.*

*We make this statement on the assumption that accuracy can never be better than repeatability and that (in the case of the instruments in table 11.2) repeatability errors were dominant.

Typically, when assembling a test fiber, you splice or connect various spools of fiber of known lengths together into the desired configuration. To calibrate the test fiber properly, the length of each spool of fiber must be mechanically measured using precision spoolers that gauge the length of the spools to within a fraction of a meter. Additionally, you must determine the group index for each fiber using the time-of-flight method.*

The loss of each event must also be carefully calibrated using means other than an OTDR. One method is first to measure the insertion loss of each fiber spool using the cut-back method.[†] If the test fiber is to be used at more than one wavelength (1310 nm and 1550 nm, for example), then the insertion loss of each spool must be measured at both wavelengths.

After measuring the insertion loss of each spool, you can easily determine the losses of individual events as the test fiber is assembled. To do this, attach a light source to one end of the first spool in the test fiber. If you are calibrating the test spool for two wavelengths, multiplex two light sources to the first spool using a wavelength-division multiplexer (WDM) or coupler. It is essential not to disturb the coupling to the first spool once you begin the calibration process. Additionally, the light sources must be sufficiently stable so that when turned on, their output power is the same as before they were turned off (to within 0.005 dB).[‡] With the light source(s) attached to the first spool, perform the following procedure.

1. Measure the light power emanating from the opposite end of the first spool.[§]

*In this method, you measure the time required for a pulse of light to travel the length of a known piece of fiber. From this, you calculate the group velocity of the pulse. The group index is simply the speed of light (in a vacuum) divided by the group velocity of the pulse (see section 5.3.3).

[†]To use the cut-back method, couple light into the fiber at one end and apply a mode stripper by wrapping the fiber in loops to remove any cladding modes. Next, measure the optical power emanating from the far end of the fiber. Call this measurement M1. Cut the fiber just after the mode stripper and measure the light emanating from the fiber. Call this measurement M2. The insertion loss in decibels is $M2 - M1$ if the two measurements were made in decibels or decibel-meters. If M1 and M2 are made in linear units, such as megawatts, then the insertion loss in decibels is $10 \log (M2/M1)$.

[‡]One way to accomplish this is to use lasers with back-facet monitors and a feedback loop that holds the output power at a controlled, predetermined level.

[§]If you are calibrating at two wavelengths, turn off the first light source and turn on the second to measure the output power from spool 1 at both wavelengths.

2. Attach the second spool to the first using a fusion splice, mechanical splice, or connector.
3. Measure the power emanating from the end of the second spool.
4. Calculate the loss (in decibels) between the power out of spool 1 and the power out of spool 2 (this is 10 times the log of the ratio of the two powers).
5. Subtract the loss of spool 2 (at the appropriate wavelength) and you have the true insertion loss of the splice between spools 1 and 2.*
6. If you are calibrating the fiber at two wavelengths, turn off the first light source, turn on the second, and repeat the procedure.
7. Continue this procedure until you have assembled the entire test fiber and calibrated all the splices and connectors.

Having assembled the test fiber, you now have a fixture with events of known loss and at known distances. Furthermore, you have calibrated your test fiber using means other than OTDRs, and using equipment that is calibrated and traceable to measurement standards. The test fiber, however, still has some problems. Although the distance to each event is unlikely to change, the loss of each event is not necessarily stable. Fusion splices are the most stable, but bending within the splice protector (especially with single-mode fiber) can alter loss over time. Mechanical splices and connectors can easily change with time and temperature. If all the events are composed of connectors, the test fiber can be disassembled and the loss calibration can be repeated by reassembling the test fiber according to the previous procedure. If some of the events are made with fusion splices or permanent mechanical splices, the loss calibration cannot be repeated without tearing the test fixture apart and rebuilding. Thus, even after carefully calibrating the test fiber, the loss of each event cannot necessarily be guaranteed after a given amount of time.

11.5.2 Repeatability testing

The preceding discussion shows that calibrating an OTDR test fixture for distance and loss requires considerable care, effort, and cost. Fortunately, it is possible to screen for many typical problems associated with event-marking software without building a calibrated test fiber. You do not, for

*The uncertainty in this measurement results from uncertainty in measuring the loss of the spool, plus uncertainty in making the measurements in step 4. To keep the total uncertainty within reasonable bounds, each power measurement should be accurate to 0.005 dB or better.

instance, require a calibrated test fixture to measure an OTDR's distance- and loss-measurement repeatability. Since accuracy can never be better than repeatability, the repeatability test provides a good lower limit for assessing the instrument's calibration accuracy.* This is one reason the tests shown in figures 11.5 and 11.6 and in table 11.2 were repeatability tests.

To perform statistical testing on an OTDR, you need an appropriate test fiber with known approximate distances to and losses of events. In constructing your test fiber, you need to consider the types of events and their typical distances and separations. You may wish to build your test fiber with some sections spliced together and other sections connected with reflective components. By arranging these events strategically, you can test the instrument's event and loss dead zones. For statistical testing, you only need approximate distance and loss information for each event, and you can easily obtain this using a high-performance OTDR and manual measurements. For best accuracy, obtain these approximate values by measuring the test fiber multiple times and recording the average distance, reflectivity, and loss of each event.

Evaluate the OTDR by measuring the test fiber multiple times (ten is a good number). Each time you test the fiber, have the OTDR measure the distance, loss, and reflectivity of each event it finds. Standardize the test according to test time (if this is a controllable factor) and operating mode. It is best to test in the semiautomatic or fully optimized mode (if the OTDR has one), since this minimizes (for most OTDRs) the possibility of operator error. OTDRs are not necessarily compatible in all their features, so this may require some compromise. For example, an OTDR with fully optimized event marking makes all acquisition settings for the user, while an OTDR with manual or semimanual capability requires the user to make some of these settings. When comparing two such instruments, it is generally easier and more appropriate to set the acquisition parameters on the manual or semimanual instrument to coincide roughly with those of the fully optimized instrument. As an example, if the fully optimized instrument requires 1.5 minutes of test time, set the averaging time on the semiautomatic instrument so its acquisition-and-analysis time also takes about 1.5 minutes. (Note that this may give the semiautomatic instrument a slight advantage, since it must acquire only one waveform in 1.5 minutes, while the fully optimized instrument acquires several waveforms in the same amount

*The calibration accuracy may be worse than the repeatability, but it cannot be better.

of time. To balance this advantage and make a more realistic test, you should include some closely spaced events near the beginning of the test fiber.)

After measuring the test fiber, calculate the standard deviation of the distance measurements for each event. Calculate the standard deviation of the loss and reflectivity measurements for each event, the number of false events, and the number of times each event was missed. The loss and distance uncertainty, over ten tests, is approximately twice the standard deviation of the loss and distance measurements. Compiling this information can reveal a great deal about the relative performance characteristics of the event-marking software in different instruments.

If you are evaluating an OTDR with manual or semiautomatic event marking, compare the instrument's measurement repeatability when the pulse width or bandwidth is changed. This test reveals issues related to bandwidth or poor algorithm design. To perform this test, measure the distance to a nonreflective event several times with one bandwidth and pulse width setting, and calculate the mean distance.* Then change the bandwidth and/or pulse width to a different setting and perform the measurements again. Differences in distance greater than the statistical measurement repeatability might suggest calibration or algorithm errors.

Be especially aware of bogus events. These can cause confusion and increase testing time. In any case, the event-marking software should allow the OTDR operator to scan the waveform easily and remove any bogus events. Some event-marking software is especially prone to marking false events when the event threshold is set very low. To determine roughly how susceptible an OTDR is to false events, you might try testing a long length of fiber that has few events on it. If setting the loss threshold very low means many events get marked where none exist, the event-marking software is finding too many false events. Properly designed software should find no more than about one false event for every 8000 data points in an OTDR waveform. Before assigning an event to the bogus category, check it first. Your test fiber may have small nonreflective events due to bending where no fusion splices exist. Do not assume before checking that an unexpected event reported by the event-marking algorithms does not really exist.

*OTDRs typically do not have a bandwidth setting. This is typically performed in functions called *smoothing* or in *dynamic range* mode. To perform this test with confidence, you may need to contact the manufacturer of the OTDR to verify the conditions under which they apply bandwidth or digital filters.

11.5.3 Summary of testing event-marking software

Event-marking algorithms can be tested using a calibrated test fiber, but these are difficult to build and keep calibrated. A useful test that can be performed without careful calibration is the repeatability test. Here, you test an uncalibrated fiber with the OTDR ten times and then calculate the standard deviation of the measurements at each event. Twice the standard deviation is the measurement uncertainty. Small amounts of measurement uncertainty generally indicate more advanced algorithms and better instrument calibration. In chapter 12 we describe a special fixture that can provide useful information about dead zone. We also describe the reasons fiber circulators make poor test boxes for single-mode OTDRs but good test boxes for multimode OTDRs.

11.6 Event-marking features

With manual measurements, OTDR operators are limited to making loss, distance, reflectivity, fiber-slope, and link-loss measurements. Usually manual measurements include only loss and distance measurements. Even these limited measurements, if performed on enough events, take a great deal of time. With event-marking software, however, a wide range of measurements becomes possible. Here are some examples of measurements available with event-marking software.

- Loss of an event
- Distance to an event
- Identification of event type (reflective or nonreflective)
- Identification of echoes
- Fiber slope between events
- Link loss
- Reflectivity of individual events
- Total reflectivity or return loss of the fiber link
- Automatic two-way averaging for accurate splice-loss measurements
- Intrinsic splice loss
- Bending splice loss
- Offset splice loss
- Distance-measurement accuracy
- Loss-measurement accuracy
- Ability to add landmarks to trace, to identify specific physical locations

The list is daunting and could be longer. Obviously, event-marking software can inundate the user with information. Of course, we seldom want to eliminate data purposely. After all, you never know when you might need it. On the other hand, it is easy to become lost in a sea of information. One solution to this quandary is to use an OTDR that can print a customizable event table. This way you can have the OTDR display the relevant data, and if the types of data you want change, you can change the event table to list those data as well.

Most event-marking software packages measure and report loss, distance, reflectivity, and link loss. Some may also provide loss-measurement uncertainty and distance-measurement uncertainty. Fewer still are able to provide bidirectional averaging, intrinsic loss, bending loss, offset loss, and echo information.

We saw in chapters 5 and 6 that it is complicated to calculate loss- and distance-measurement uncertainties. Distance-measurement uncertainty, in particular, can change dramatically for different events, depending on their locations. Furthermore, it is nearly impossible to calculate the distance-measurement error without knowing how the event algorithms work. You could try to measure the distance-measurement accuracy, but we have already seen that this is very difficult to do because of the difficulty in properly calibrating the test fiber. Furthermore, the distance-measurement accuracy depends on the size of the event, the OTDR's pulse width, and the relative amount of noise. It is a practical impossibility to measure the distance-measurement accuracy of the OTDR for all possible events.

Because of these problems, it is important that the event-marking software tell the operator the calculated distance-measurement accuracy (as an option in the event table). This should be calculated specifically for each event and should include effects such as event loss, local noise, and pulse width. Simply printing the instrument's specifications is not acceptable. This is because specifications usually are based on time-base accuracy and sample spacing, which do not necessarily represent the distance-measurement error. Also, specifications generally apply to best-case scenarios, which seldom apply in the real world of optical fiber testing.

In chapter 3 we saw that echoes can represent a source of confusion and error for OTDR operators because the echoes look just like reflective events. Although trained operators can recognize echoes under some circumstances, this is difficult to do and even in simple

cases requires skill. Some OTDRs include algorithms that calculate the positions of echoes in OTDR waveforms. This can be a useful feature for event-marking software. Typically in OTDRs with this feature, events that are possible echoes are marked with a lower case “e” next to them in the event table. When asking about this feature, be sure to distinguish between algorithms that mark echoes and those that mark ghosts. Echoes result from reflective events on the fiber, and their locations cannot be modified by changing any of the OTDR’s setup parameters. Ghosts, on the other hand, result when the OTDR’s pulse-repetition rate (PRR) is too high. Most OTDRs have some provision for not letting the PRR get too high, and some manufacturers mistakenly refer to this as an echo-elimination feature.

Bidirectional loss measurements are the only way to measure accurately the loss of a splice on single-mode fiber. Consequently, it is very important that event-marking software can take two waveforms (one acquired from each end of the fiber) and automatically measure the average (true) loss for each event. As we saw in chapter 7, these bidirectional loss data also tell the intrinsic loss of the splice. Since these data are already available with bidirectional loss measurements, it is logical for the event-marking software to make the data also available to the operator. This is especially true if the intrinsic loss exceeds the operator’s setting for loss threshold. Doing this helps the operator avoid needlessly resplicing two fibers in a vain attempt to meet a splice-loss specification that is impossible to meet because of intrinsic splice loss.

Whenever installing fiber that carries information at 1550 or 1625 nm, a frequent concern is loss associated with fiber bends. Although relatively insensitive at 1310 nm, single-mode optical fiber exhibits significant loss at 1550 nm, and higher, if bent in a radius approaching 2.5 cm (see section 2.9). OTDRs with the ability to test at 1310 nm and 1550 nm are capable of measuring the relative amount of bending loss and misalignment loss in a fusion splice. They do this by comparing the loss at 1310 nm with the loss at 1550 nm. Although relatively straightforward to calculate, it is useful if the OTDR can make these measurements automatically. This can be accomplished also by OTDRs that are programmable by allowing the user to write a series of instructions (called *macros*) for the instrument to follow.

Systems sensitive to reflections require testing with an OTDR whose event table includes the reflectivity of individual events as well as integrated reflectivity over the full length of the fiber. Although continuous-wave reflectometers can measure the reflectivity of the

entire fiber link, they are inadequate for restoration and troubleshooting because they cannot resolve the reflectivities of individual events. OTDRs, on the other hand, when properly equipped, can measure the reflectivities of individual events as well as the reflectivity of the entire link. Link reflectivity is performed by integrating the normalized energy under the waveform. We saw in chapter 8 that the integration method is also useful for measuring the reflectivities of large reflections in waveforms acquired with medium bandwidth and narrow pulses. The ability to make integrated reflectivity measurements is an important one therefore and one you should make certain is in your OTDR.

In chapter 5 we saw that an OTDR's distance-measurement repeatability and accuracy depend strongly on the type of event-marking and event-measuring algorithms it uses. Figure 5.4 compares the theoretical distance-measurement error of a linear predictor algorithm with the average measurement errors of six OTDR operators. The event, in this case, was a 0.5-dB fusion splice at various distances above the noise floor. We saw that the theoretical performance of even the simple linear predictor exceeded that of the OTDR operators.

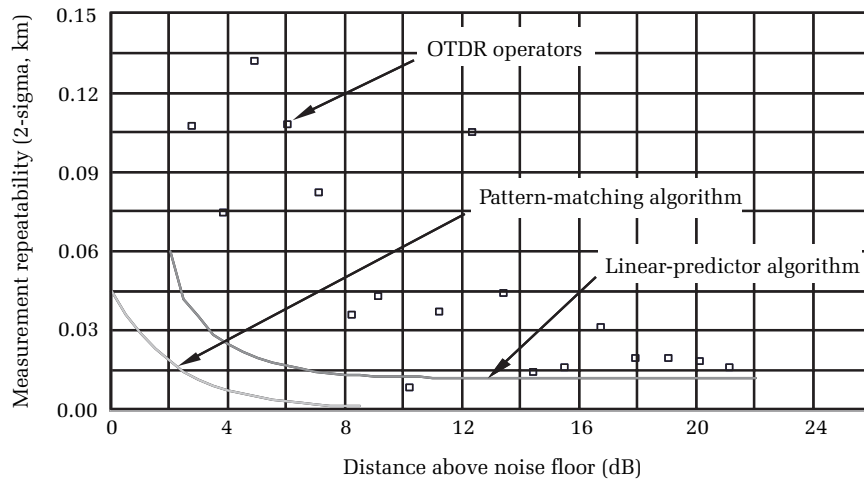


Figure 11.15. Distance-measurement repeatability of two algorithms compared with OTDR operators. The linear predictor algorithm is described in chapter 5. The pattern-matching algorithm fits a Z-shaped pattern to the nonreflective event. By moving the pattern and adjusting its loss, the computer minimizes the RMS difference between the pattern and the waveform. With this done, the event's location and loss are the same as those of the pattern.

Event-marking algorithms can clearly differentiate an OTDR's performance. The linear predictor we examined in chapter 5 is relatively simple and straightforward. Some OTDRs use event-marking algorithms that are far more advanced. One example is an event-marking algorithm that uses a method of matching a pattern to nonreflective events. This method allows the OTDR to locate the position of a nonreflective event with greater accuracy than the sample spacing. Figure 11.15 compares the measured performance of the OTDR operators against the theoretical performance of the pattern-matching algorithm and the linear predictor. You can see that the distance-measurement error of the pattern-matching algorithm clearly outperforms both of the other measurement techniques.

To emphasize the importance of event-marking algorithms, consider figures 11.5, 11.6, and table 11.2. The fully optimized algorithms in each of these tests also used advanced pattern-matching algorithms. The combination of pattern-matching algorithms and fully optimized algorithms largely contribute to this instrument's measurement repeatability.

11.7 Remote OTDRs for monitoring networks

One of the principal advantages of optical fiber is that it can carry so much information, or *traffic*. Because they carry so much traffic, high-speed fiber-optic networks represent a considerable amount of money, and each minute the network is down represents lost revenue. As a result, some portions of the network may be sufficiently critical, or carry enough traffic, to warrant automated periodic testing and fault analysis.

Remote OTDRs for monitoring networks typically consist of an OTDR, an optical switch, and specialized software and measurement algorithms. The software controls both the OTDR and the switch, connecting the OTDR to the fiber link that needs to be tested, running the test, and then analyzing the results (see figure 11.16).

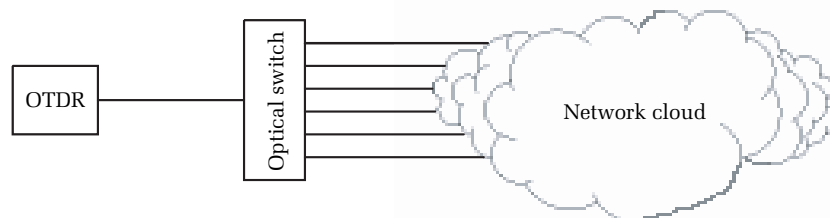


Figure 11.16. Remote OTDR system using an optical switch to periodically test various fibers in the optical network.

There are several technical issues with remote testing, and one of the most important is how to connect to the fiber and test it without interrupting traffic and without spoiling the OTDR's performance. For example, the OTDR could be connected to the fiber under test with a coupler. This is a simple solution, but it has several significant problems. First, the traffic on the fiber can interfere with the OTDR. In essence, the traffic looks to the OTDR like a noise source. Second, the OTDR pulses can interfere with data at the network receivers.

These problems can be solved by having the OTDR test at a wavelength different from the wavelength over which the system transmits data. For example, if the system is transmitting data at 1550 nm, the OTDR might be configured to operate at 1625 nm. Two other changes must also be made. First, the coupler is replaced with a wavelength-division multiplexer, or WDM. The WDM is designed so that it splits off and couples the OTDR wavelength while letting the wavelength for the system traffic travel straight through. This protects the OTDR from the noise caused by the system traffic. The second change is that the system receiver must be protected with filters that block the OTDR's pulses (see figure 11.17).

Ideally this configuration allows real-time, active testing using the OTDR on fibers that are actually carrying traffic. However, optical filters are not perfect, and so the problems with noise are not totally eliminated. The WDM, for example, will still leak a small amount of optical power from the system transmitters. And the system receivers

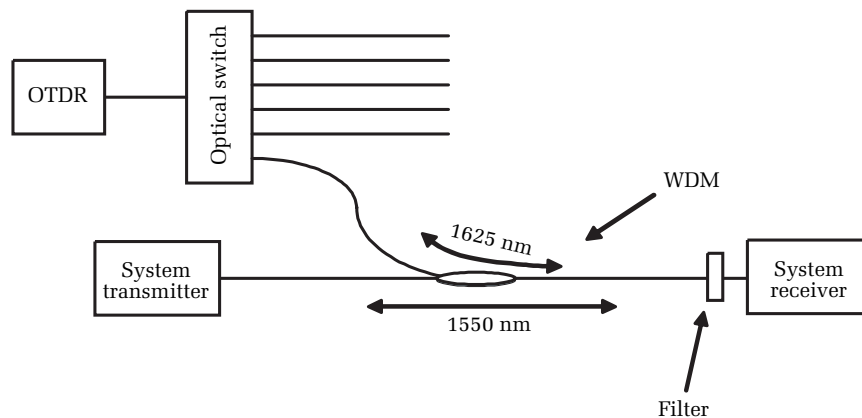


Figure 11.17. Remote OTDR testing on live optical fibers, using a WDM and optical filter to prevent the OTDR and system from interfering with each other.

will still see some of the light from the OTDR pulses, even though there is an optical filter in front of them that, ideally, blocks the OTDR's light. Consequently, the performance of the filters is essential to making sure the remote system works when used in this configuration.

In addition, the optical filters have some loss at the wavelengths they should pass. For example, the WDM will attenuate the light from the system transmitter that passes through it. Similarly, the filter in front of the system receiver will also attenuate the light at the system wavelength. So introducing the filters that allow real-time monitoring also increases the system loss and must be accounted for in the system design. Similarly, for the OTDR, the WDM reduces the dynamic range, and this must be taken into account as well.

As you can see, active testing on fibers that carry traffic requires careful design, and the OTDR must be treated as a network element (see figure 11.18). At the same time, however, the resulting OTDR tests are directly applicable to the health of the fiber being tested.

There is a simpler approach that doesn't require filters and doesn't reduce the OTDR's dynamic range or increase the loss on the fibers carrying network traffic. This approach involves testing dark fibers. *Dark fibers* are those fibers in a cable that don't actually carry traffic. That is, these are fibers that are not connected to transmitters or receivers in the

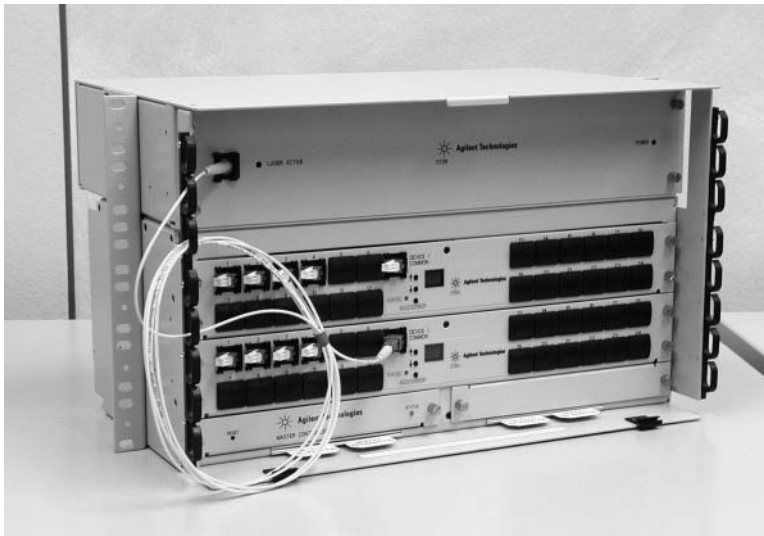


Figure 11.18. Rack-mount access fiber OTDR used for monitoring installed fiber optic networks. [Credit: Agilent Technologies.]

network. They are there for future network upgrades and enhancements, and these can be used to gauge the overall health of the optical cable.

If a cable has a dark fiber in it, then the OTDR can be connected to it. When testing in this configuration, one obviously makes the assumption that if the dark fiber in the cable is okay, then the rest of the fibers are also okay. This is probably a good assumption most of the time, but it may not be valid all the time. For example, if a backhoe digs up a cable, you would expect the dark fiber to break along with all the others. But it's possible, if the backhoe operator realizes what's going on in time, that he will halt before the cable actually breaks. In this scenario, it's possible for some fibers to be compromised without seriously damaging others.

On the other hand, testing with dark fiber does not require optical filters and does not result in any degradation of performance in either the network or the OTDR. So this approach offers significant advantages in terms of cost and complexity.

Whichever approach is taken (dark-fiber testing or active testing on fibers carrying traffic) there remains the problem of test management. Not only must the OTDR have stellar event-marking algorithms with few (if any) false-positive test results, the software management system must also be able to identify the physical location of any problems on a geographical map and then alert the proper personnel to fix the problem.

This means the remote testing system needs to be a total, embedded solution. It must have access to a detailed map of the network and must be able to correlate physical locations (such as highway intersections) with distance along the cable. Then, when a problem occurs, the network management system must be able to locate the problem and isolate it to a specific cable or fiber, detailing the type of problem (excess loss, too much reflection, etc.) while sounding the appropriate alarms and providing dispatch information.

Before ending this chapter, we should mention an additional advantage of remote testing and fiber management. Sometimes, in rare cases, a fiber splice can degrade with time. In other cases, some outside force may gradually apply stress to a cable, causing excess loss. Without the sort of periodic testing available in remote-testing systems, the network will continue to operate without anyone's knowing there is a problem, until some threshold (typically received power) is breached, upon which alarms will sound. At this point the system is probably already compromised or (worse) down. However, with remote systems

and periodic testing, gradual degradation in a fiber can be monitored and tracked. In this way, developing problems can be identified and maintenance scheduled in the least intrusive manner.

11.8 Summary

Event-marking algorithms are arguably the most complex aspect of modern OTDRs. They come in a wide range of styles and capabilities, and they are very difficult to evaluate and compare quantitatively. These algorithms range from the simple to the very complex. They are as simple as LSA calculations that assist manual loss measurements and as complex as fully automatic and fully optimized algorithms.

Event-marking algorithms must deal with a wide range of events. Furthermore, they must discriminate real events from hardware anomalies. Additionally, they must be able to locate and measure events that are very near the OTDR's noise floor, to maximize the OTDR's effective measurement range.

Event-marking algorithms can provide the OTDR user with a tremendous range of measured data. From link loss to reflectivity to loss-measurement uncertainty and distance-measurement uncertainty, event-marking algorithms can easily inundate the user with data. To help avoid data overload, the event-marking algorithms should acquire and measure as much as possible, but the OTDR should be designed to provide the user with the ability to select which measurement parameters to display.

Measurement uncertainty, especially, is an important parameter for some applications. When you return to measure a splice several months after installation, for example, you need to know if the splice loss has changed. Such change might portend the possibility of future failure. The event table from previous tests should include the loss-measurement uncertainty with which the initial measurements were made. Without this critical information, the OTDR operator can only guess the statistical significance of any difference in the measurements.

For example, suppose a splice is measured at installation and its loss is 0.10 ± 0.01 dB. Next, suppose that six months later it is measured again and the loss this time is 0.22 ± 0.02 dB. Knowing the measurement uncertainties, you can be reasonably confident that the splice has degraded by less than 0.17 dB and more than 0.13 dB. If, however, the first measurement was 0.10 ± 0.05 dB, and the second measurement was 0.20 ± 0.05 dB, you cannot be sure the event has changed at all. OTDRs

that calculate measurement uncertainty provide their operators with a powerful advantage compared to OTDRs that do not.

Event-marking algorithms are highly proprietary to the various OTDR manufacturers, and no standardized terminology exists for describing these algorithms. However, they can be broadly categorized as manual, semimanual, semiautomatic, or fully optimized. These descriptions generally proceed from the least automatic and least capable modes to the most automatic and most capable modes. The fully optimized algorithms set the standard for OTDR performance by optimizing acquisition parameters for each event.

In comparing OTDRs, pay close attention to the features each one offers in its event table, its measurement accuracy (where possible to evaluate), its repeatability, and its ease of use (single-button testing, as in the case of fully optimized algorithms, for example). Evaluating all these features can be a daunting task, especially if you are not intimately familiar with OTDRs. To help in this regard, be sure to select an OTDR manufacturer with depth of knowledge and experience and with technical support you can call upon when questions arise.

Future event-marking algorithms can be expected to perform even more OTDR operations and to supply even more information. The careful display of this information is important, or the operator can be overloaded with data. Future event-marking software may even incorporate elements of expert systems by monitoring the operator and making suggestions for test methodologies or for how to improve the performance of the test fiber. Given the advances we have seen since the first OTDRs were built, we can expect even more sophistication and intelligence from future generations of event-marking software.

Suggested reading

- Anderson, D. R., "Automatic event-marking software for OTDRs: how to make it work for you," *Outside Plant* (June 1993).
- Anderson, D. R., "A pattern-matching algorithm for remote systems that measures the distance and loss of fusion splices with high precision," *National Fiber Optics Engineers Conference* (NFOEC '94).
- Beller, J., "A high-performance signal-processing system for the HP 8146A optical time-domain reflectometer," *Hewlett-Packard Journal* (Feb. 1993).
- Lum, M., "Testing optical fiber with intelligent analysis in mini-OTDRs," *Tektronix Application Note* (1994).
- Anderson, D. R., "Multi-acquisition algorithms for fully optimized analysis of OTDR waveforms," *National Fiber Optics Engineers Conference* (NFOEC '96).

- Anderson, D. R., *Locating the Position of an Event in Acquired Digital Data at Subsample Spacing*, U.S. Patent 5,365,328.
- Liao, D. D., and Forber, A. E., *Method for Finding and Measuring Optical Features Using an Optical Time-Domain Reflectometer*, U.S. Patent 5,442,434.
- Parks, T. W., and Vandervort, A. L., *Method for Testing Optical Waveguide Fibers to Detect Reflection-Type Discontinuities*, U.S. Patent 5,450,191.
- Bell, F., "Picking the right OTDR," *Telephony*, Vol. 230, No. 10 (Mar. 4, 1996), pp. 30–33.
- Blanchard, P., Clin, R., and Ducos, L., "Improvement on nonreflective event locating accuracy with OTDR," *Electronics Letters*, Vol. 31, No. 23 (Nov. 9, 1995).
- Kowalski, A., Kuklinski, S., and Zakrzewski, A., "Automatic analysis of optical time domain reflectometer (OTDR) measurement results," *Proceedings of SPIE—The International Society for Optical Engineering Laser Technology IV*, Vol. 2202 (Sept. 26, 1994).
- Gu, X., and Sablatash, M., "Estimation and detection in OTDR using analyzing wavelets," *Proceedings of the IEEE-SP* (Oct. 25–28, 1994), pp. 353–356.
- Artiglia, M., "Cost 217 intercomparison of OTDR measurements on single-mode fibers," *NIST Special Publication 839* (Boulder, CO: NIST, Sept. 1992).

Problems

1. True or false: It is possible to optimize the acquisition for each event on a typical OTDR waveform.
2. True or false: For events located near the OTDR, it is okay to use shorter pulse widths because the fiber loss for those events is smaller and so longer pulse widths are unnecessary for dynamic range and shorter pulse widths give better two-event resolution.
3. True or false: For events located far away from the OTDR, it is okay to use less averaging because those events have more loss between them and the OTDR.
4. True or false: Event-marking algorithms are typically slower than human operators when it comes to measuring all the events in an OTDR trace.
5. True or false: Event-marking algorithms are based on industry-standard algorithms.
6. Which of the following items is not an example of a waveform anomaly that can lead to false events?
 - a. Digitization noise
 - b. Drop outs
 - c. Droop due to fiber bending
 - d. Synchronous noise

7. True or false: Fully calibrated test fixtures are difficult to build and must be calibrated using equipment other than OTDRs.
8. True or false: Practical test fixtures that allow repeatability measurements are comparatively easy to build.
9. True or false: The measurement error of an OTDR can be less than the repeatability.
10. True or false: Repeatability measurements require calibrated test fixtures.

Chapter 12

Test fixtures

12.0 Introduction

As we have seen, building calibrated fiber-optic test fixtures represents a challenge in itself. In this chapter we try to help you meet this challenge by describing some test fixtures and calibration procedures that you can use to evaluate an OTDR's performance. These fixtures are useful for measuring an OTDR's distance-measurement accuracy, dead zone, and bandwidth effects.

12.1 Dead zone fixture

Figure 12.1 illustrates a test fixture that allows you to evaluate the OTDR's response to an event that has fully adjustable loss and reflectivity.¹ The test fixture consists of a coupler, a variable attenuator, an adjustable loop loss, and two lengths of fiber. One of the output legs of the coupler is attached to the variable attenuator with a length of fiber, L1, after the attenuator. At the end of this fiber is a mirror. The mirror may be as simple as a cleaved fiber end or (for greater range) a ferrule with a reflective optical coating. The coupler's other output leg is attached to

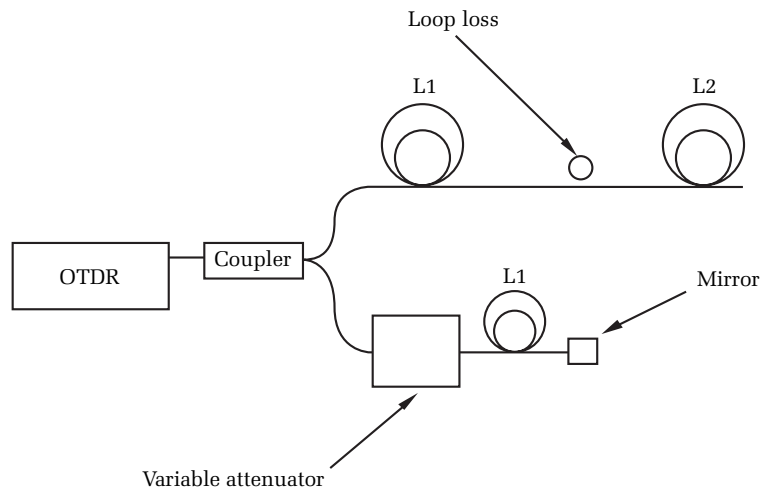


Figure 12.1. Test fixture with an event that has variable loss and reflectivity. The mirror and bend loss are exactly the same distance (L1) from the coupler.

the second length of fiber. Midway along this second length of fiber (at a distance $L1$) is an adjustable bend, so the distance from the coupler to the mirror is the same as the distance from the coupler to the bend.

To make a reflective event, reduce the loss of the variable attenuator and add some bending loss. To reduce the event's reflectance, increase the attenuator's loss. To increase the insertion loss of the event, reduce the bend radius. By controlling the amount of bending loss and the loss of the attenuator, you can easily design an event with almost any combination of loss and reflection. Part of the value in this particular test fixture is its ability to provide a stable, adjustable event for making careful measurements of the OTDR's dead zone under different conditions. It is also useful in evaluating an OTDR's measurement accuracy by verifying that the distance to an event (as reported by the OTDR) remains unchanged if the event is reflective or when the OTDR's bandwidth is changed.

Instead of using a bend to facilitate the event's loss, you can use an adjustable attenuator with very low reflection.* An adjustable attenuator may also be useful because bending loss is sometimes hard to achieve in multimode fiber, and bending loss is very sensitive to wavelength in single-mode fiber. This wavelength sensitivity with single-mode fibers is enough to cause loss-measurement differences between two different OTDRs because of the statistical difference in their operating wavelengths.

12.2 Fiber circulator

Another common test fixture is the fiber circulator. Under some circumstances, this fixture is very useful for testing distance-measurement accuracy and dynamic range. However, you must use the fiber circulator with care because it has some artificial features that make some measurements impossible or inappropriate.

The appeal in using a fiber circulator is its relative simplicity and low cost. When testing OTDRs, we frequently wish to determine the instrument's dynamic range, especially its ability to measure small events that are far away from the OTDR. To do this requires a test fixture consisting of long lengths of optical fiber. A fixture like this can be rather expensive, however, since high-dynamic-range OTDRs require well over 100 kilometers of fiber.

*Be sure to check the minimum insertion loss of the adjustable attenuator, because it may be too high for some testing you want to do.

Because of the cost and difficulty in building dedicated long-line test fixtures, it is tempting to consider using a fiber circulator like that shown in figure 12.2. The fiber circulator test fixture consists of a bidirectional coupler looped to a relatively short piece of test fiber. The test fiber may have splices or connectors in it. When the OTDR launches a pulse, the pulse passes through the coupler and is attenuated by about 3 dB. This is equivalent to a rather poor front-panel connection and consequently reduced dead zone.* After the pulse travels through the coupler, it continuously scatters light back to the OTDR as it circulates along the test fiber.

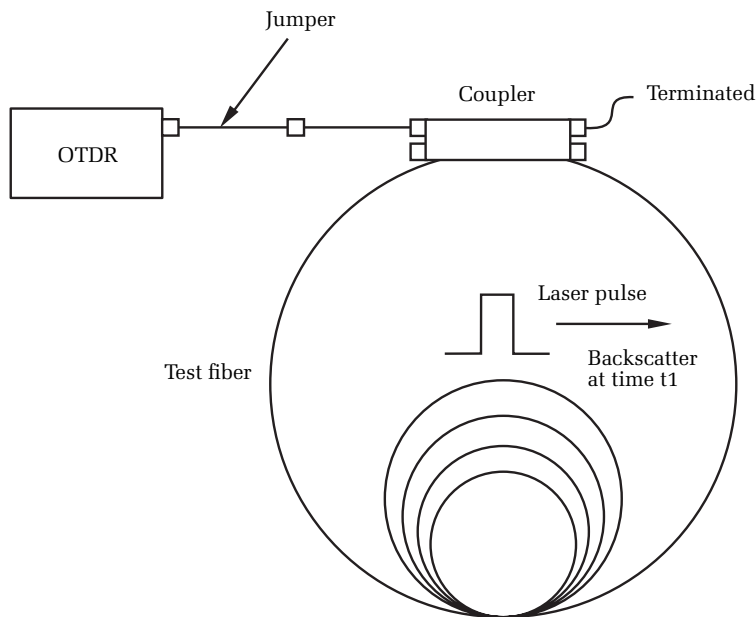


Figure 12.2. The laser pulse after time t_1 , when the pulse has traveled just slightly more than halfway through the test fiber.

Consider time t_1 , when the laser pulse, on its first circulation, has just passed the midpoint of the test fiber (see figure 12.2). At that point, just as at all points, it scatters light back toward the OTDR. Now consider time t_2 , when the laser pulse has just finished its first circulation and

*See chapter 8 for discussion of dead zone. Loss dead zone increases with event loss, so a poor front-panel connection increases the loss dead zone.

is beginning its second (see figure 12.3). At time t_2 , the pulse scatters light back toward the OTDR. The light scattered at time t_2 arrives at the coupler at the same time as the light scattered at time t_1 . Since the scattered light at times t_1 and t_2 came from the same laser pulse, they are coherent, and so they interfere with each other when they mix in the coupler. Notice, however, that the scattered light at t_1 and the scattered light at t_2 travel through different pieces of the test fiber. These sections of the test fiber are random general-phase plates that rotate the light's electric polarization vector.* The state of interference between the light from t_1 and from t_2 depends on the exact nature of the polarization coupling and the phase rotation of the different sections of the test fiber.

We can easily extend our reasoning to show that backscatter from each point on the fiber (after the pulse travels half the length of the test fiber) coherently mixes with the backscatter from other points on the fiber. The nature of the polarization coupling and phase rotation of the fiber sections is random. The relative orientation of the interfering field vectors changes randomly, resulting in an undulating waveform

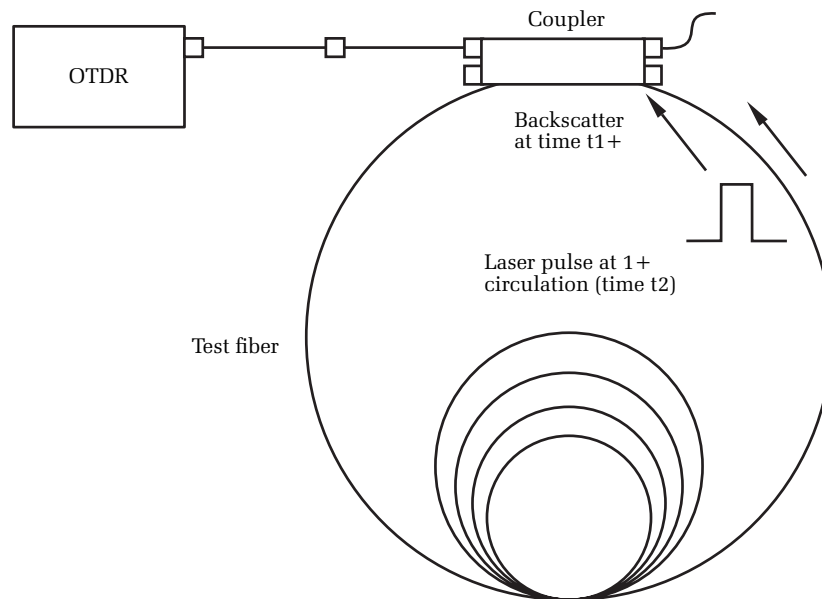


Figure 12.3. The laser pulse at time t_2 , just as the pulse has traveled slightly more than all the way around the test fiber.

*We discuss this in greater detail in chapter 13.

whose period of oscillation depends on (among other things) the fiber's polarization mode dispersion. Depending on the quality of the test fiber and the characteristics of the laser, this polarization noise can be rather significant, sometimes exceeding several tenths of a decibel's variation peak to peak. The period and modulation of the noise depend on the state of the fiber, the OTDR's pulse width, and the spectral width of the OTDR's laser source.

This noise from coherent mixing makes the circulator test fixture inappropriate for most evaluations involving single-mode OTDRs. This is because the coherent mixing noise represents a real waveform signal associated with the fiber that is non-Gaussian and cannot be averaged away. The noise represents an effective increase in the height of the noise floor (or, alternatively, an effective decrease in dynamic range). This noise signature is typically somewhat constant during the short time of an OTDR's acquisition, but it can easily change significantly from day to day because of the environmental sensitivity of polarization mode dispersion. Coherent mixing noise may have spatial-frequency components that are similar to those of the OTDR's laser pulse. Parts of the noise may be mistakenly identified by the OTDR's event-analysis software as a splice or connector. High-performance OTDRs typically find more of these events because of their more sensitive event-marking algorithms and lower event thresholds. These effects, combined with the day-to-day changes in the profile of the coherent mixing noise, make the fiber circulator a poor choice for evaluating an OTDR's performance.

Coherent mixing noise in a fiber circulator has short-term stability. This means that as long as the test fiber and jumpers are undisturbed, the signature of the coherent mixing noise remains unchanged, and cannot be reduced by averaging during the OTDR's acquisition. Moving the test fiber or test jumpers slightly, however, can change the profile of the coherent mixing noise. This suggests a simple way to reduce the noise. Simply make a loop in the jumper that connects the OTDR to the test fiber. Then, while the OTDR is acquiring its waveform, flip the loop (several hertz if possible) back and forth 180°. Although tedious, this method works relatively well if the test fiber has low polarization mode dispersion, if you flip the fiber fast enough through a sufficiently large angle, and for a sufficiently long waveform-averaging time. Of course, this method cannot be used for repeatable testing or comparison of OTDRs because of the uncertainty involved in manually scrambling the coherent mixing. You could not be certain, for example, that all OTDR operators will flip the fiber the same amount and in the same way.

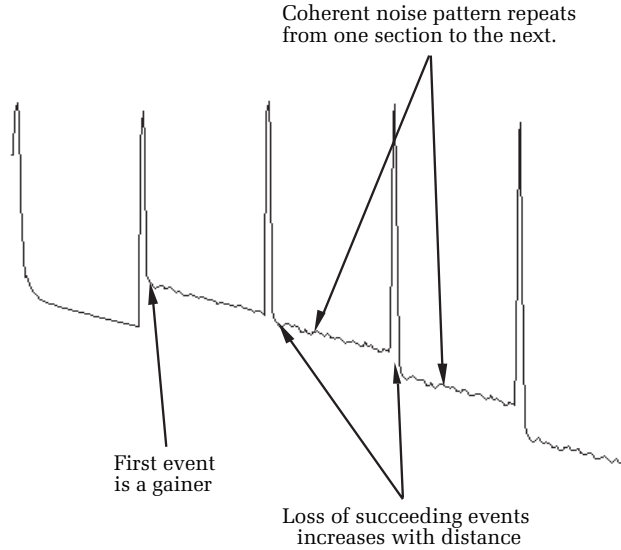


Figure 12.4. Waveform of a fiber circulator taken with a high-dynamic-range OTDR. Notice the distinguishing features: 1. The events are spaced equally apart. 2. The first event is a gainer, with a loss of about -1.5 dB. 3. Before the first event the waveform is very clean, since it only has normal system noise. 4. The loss of succeeding events increases with distance according to equation [12.4]. 5. The waveform noise increases dramatically after the first event because of noise associated with mixing in the coupler. 6. The mixing noise signature roughly repeats from section to section.

Figure 12.4 illustrates a waveform acquired with a high-dynamic-range OTDR on a fiber circulator. We can immediately identify several significant features of this waveform. First, it consists of a series of losses spaced apart by a distance of one-half the length of the test fiber. These losses are reflective if the coupler is connected to the test fiber with connectors, and they are nonreflective if it is connected with fusion splices.* The first part of the waveform is one-half the length of the fiber loop and does not have mixing noise, because this region of the fiber has no mixing in the coupler. The first event has negative loss (commonly called a *gainer*). You can understand why the first event is a gainer from the following argument. First, consider the backscatter level from just before the event. This backscatter comes only from the initial pulse and is attenuated by the loop attenuation:

*This assumes the connectors have some reflectance. Angled connectors, having very low reflectance, may result in a waveform without reflections.

$$P_{bs1} \propto L\alpha P_0 \quad [12.1]$$

where L is the length of the fiber loop, α is the fiber's attenuation (fraction per decibel), and P_0 is the average power of the laser pulse.

Figure 12.2 shows the laser pulse at time t_1 , just after the pulse has finished half its first circulation. Figure 12.3 shows the laser pulse at time t_2 , just after the pulse has finished its first circulation. The light scattered at time t_2 arrives at the coupler at the same time as the light scattered at time t_1 and interferes coherently with it. The backscatter signature from just after the first event comes from three sources. First, there is backscatter from the initial pulse after it has just passed the midpoint of the test fiber. This backscatter has the same strength as that in equation [12.1] minus the splitting loss of the coupler.* Second, there is backscatter from the pulse just after it completes the first loop and starts on the second circulation. The third source comes from the first pulse just as it starts the first circulation. This pulse scatters light back toward the OTDR. Part of this scattered light cross-couples through the coupler and shows up as the backscatter signature near the front panel of the OTDR. An equal part of the light couples into the test fiber and counterpropagates in the direction opposite to the OTDR pulse.† This counterrotating backscatter arrives at the coupler at the same time the laser pulse begins its second circulation. Thus, the total scattered light just after the first event is

$$P_{bs2} = L\alpha P_0 + L\alpha P_0 K + L\alpha P_0 K \quad [12.2]$$

where K is the coupling ratio of the coupler as the light traverses the circulator loop.

Taking five times the log of the ratio of equations [12.1] and [12.2], we find that the loss of the first event is

$$L_1 = -5 \log(1 + 2K) \quad [12.3]$$

If the splitter's ratio is 50/50, we see from equation [12.3] that the expected loss of the first event is -1.505 dB. This method can be used to measure the coupler ratio. For example, the loss of the first event in figure 12.3 is 1.474 dB. Solving equation [12.3] for the coupler ratio, we see that this circulator was built with a 0.486/0.514 coupler.

*Technically, this backscatter level is slightly less than in equation [12.1] because it is further attenuated by the fiber over one pulse width. However, for modern communications-grade optical fiber, the loss over one pulse width is not significant.

†Assuming a 50/50 coupler.

It is not too difficult to trace all the pulses and counterrotating backscatter that travel around the circulator ring. If we assume the OTDR detects only radiation that has been scattered once and that all detected radiation rotates clockwise, then we have the following formula for the expected loss* at the N th event (where $N \geq 2$):²

$$L_N = 5 \log \left[\frac{N \cdot K + N - 1}{K(N \cdot K + K + N)} \right] \quad [12.4]$$

Table 12.1 lists the expected losses for the first 10 events of the circulator in figure 12.3, which has a 0.486/0.514 coupler ratio. It also shows the measured losses of the first eight events from the OTDR waveform of the circulator. As you can see, the first event is a gainer, and succeeding events have increasingly greater loss. The expected loss approaches $5 \log(1/K)$ in the limit as the event number approaches infinity.

In summary, fiber circulators make poor test fixtures for single-mode fibers because of coherent mixing. They do, however, make excellent test fixtures for multimode OTDRs. Using a circulator with

Event number N	Expected loss ($K = 0.4856$, dB)	Measured loss (dB)	Difference between measured loss and expected loss (dB)
1	-1.474	-1.474	0.00
2	0.349	0.269	0.08
3	0.703	0.792	0.09
4	1.017	0.998	-0.02
5	1.325	1.117	-0.21
6	1.423	1.195	-0.23
7	1.528	1.25	-0.28
8	1.228	n/a	n/a
9	1.259	n/a	n/a
10	1.284	n/a	n/a

Table 12.1. Predicted loss for the first 10 events of a circulator built with a coupler having a split ratio of 0.486/0.514. The split ratio was chosen by solving equation [12.3] for K so that the measured loss of the first event agrees perfectly with its predicted value. Errors for the loss measurements are higher than normal because of the large amount of noise due to coherent mixing in the circulator.[†]

*We also assume the coupler has no excess loss.

[†]Beyond about the seventh event, the combination of coherent mixing noise and OTDR system noise resulted in too much loss-measurement error for meaningful comparison with the predicted values.

known events, it is possible to make a very “long” test fixture using a relatively short length of multimode fiber. They are also of some limited use in verifying the distance-measurement accuracy of single-mode OTDRs since they present a waveform with precisely spaced repetitive reflective events.*

12.3 External-source test fixture

A common problem with the test fixtures we have discussed in the previous sections is that each of them requires some degree of calibration of optical fiber. As we saw in section 11.5, calibrating events on optical fiber is a difficult task. The external source method avoids these problems by synthesizing an optical signal that is fed back into the OTDR. This synthesized optical signal is generated by external equipment that can be independently calibrated to traceable standards.^{3,4}

Figure 12.5 illustrates the setup used in the external source method. The OTDR is connected to an optical coupler and turned on. The operator initiates an acquisition. The OTDR’s laser pulses are transmitted out the front-panel connector and through the coupler, where they are split and

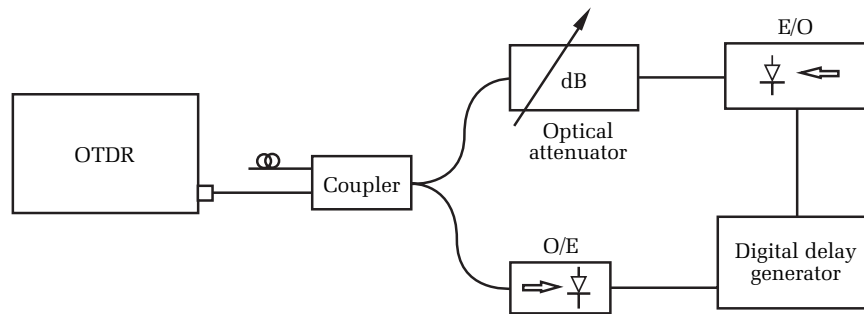


Figure 12.5. External feedback method. The OTDR launches its optical pulses into a coupler, where they are directed to an O/E converter. Signals from the O/E converter trigger the digital delay generator, which triggers (after a programmable delay) the E/O converter. The E/O converter transmits an optical signal (usually discrete pulses) into the variable optical attenuator and then to the coupler and back into the OTDR. The OTDR senses and displays an optical reflection rising out of the OTDR’s noise floor. This reflection, and known delay (from the digital delay generator), can be used to verify the accuracy of the OTDR’s time base.

*This assumes, of course, that the coupler is attached to the test fiber with reflective connectors or mechanical splices. If fusion splices are used, then the repetitive events are nonreflective. Due to the possibility of high polarization noise, these nonreflective events are difficult to locate accurately, and this makes a poor test fixture for evaluating distance-measurement accuracy.

directed to an optical-to-electrical (O/E) converter. The O/E converter senses the OTDR's laser pulses with an optical receiver and generates an electrical timing pulse that goes to the digital delay generator. After a preset time, the digital delay generator sends an electrical signal to an electrical-to-optical (E/O) generator. The E/O generates optical pulses using an LED or laser diode. These optical pulses pass through an optical attenuator, the optical coupler, and into the OTDR, where they are measured and displayed by the OTDR's optical receiver and display circuitry.

With this setup, what you see on the OTDR is a reflective event rising out of the OTDR's noise floor. By adjusting the digital delay generator you can move the position of the reflective event and test the OTDR's distance-measurement accuracy. A more sophisticated setup would include low-level light to simulate fiber backscatter, with discrete changes in light output to simulate events.

There are several issues related to the external source method that limit its utility. First, the external source method primarily tests the OTDR's time base.* Recall from chapter 5, however, that distance-measurement accuracy is determined mostly by noise and the event-detection algorithms.† The OTDR's time base is usually a small contributor. Consequently, the external source method is most valuable for identifying a broken OTDR. Unless it generates realistic waveforms with realistic events over the OTDR's range of noise and pulse widths, it cannot effectively be used to measure the distance- and loss-measurement accuracy of the OTDR when applied to real-world events.

12.4 Loss calibration with fiber standard

This method relies on an attenuator and calibrated fiber standard.⁵ Figure 12.6 illustrates the method. The OTDR is connected to an optical attenuator. The attenuator, in turn, is connected to a lead-in fiber and then to the fiber standard. The end-to-end loss and attenuation coefficient of the fiber standard are accurately calibrated using the cut-back method.⁶ The fiber standard should be a good piece of fiber with no point discontinuities and with very uniform slope.

*This is strictly true when the external source injects pulses of light into the OTDR. A more sophisticated external source, which injects variably attenuated light and simulates real events, may be used (if properly calibrated) to test event-marking algorithms if the resulting synthetic waveform is sufficiently realistic.

†Recall that the problem is more pronounced with nonreflective events than with reflective ones.

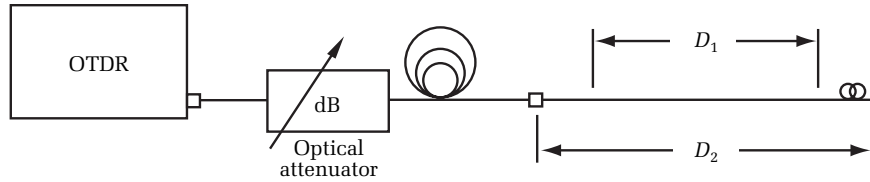


Figure 12.6. Fiber standard calibration setup. The optical attenuator need not be calibrated, because its only purpose is to move the waveform of the fiber standard up and down through the OTDR's vertical range. In this figure, the fiber standard is the section of length D_2 .

The intent of calibration tests with the fiber standard is to verify that a given loss appears constant and true over the OTDR's vertical range. To do this, set the optical attenuator to zero and acquire a waveform. Set two vertical cursors on the fiber standard. The first cursor should be far enough after the connector to avoid nonlinear regions associated with the OTDR's response to the reflective event (see figure 12.7). Place the second cursor near the end of the fiber standard.

Measure the fiber loss between the two cursors using a least-squares fit. It should not be a two-point measurement. Note the attenuator setting and loss between the cursors. Next, increase the loss of the adjustable attenuator. The increase is somewhat arbitrary and depends on the

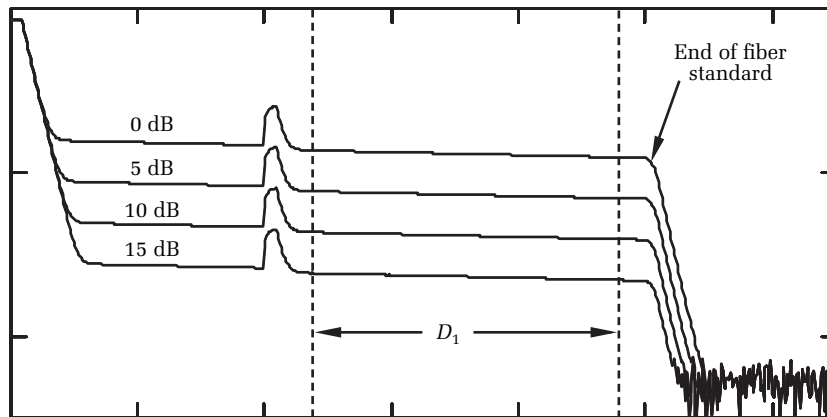


Figure 12.7. Verifying the linearity of the OTDR's vertical scale with a fiber standard. Each waveform is acquired with a different setting on the optical attenuator (see figure 12.5). The loss between the vertical cursors should remain constant. Variations in the loss between the cursors result from increasing noise in the optical waveform and nonlinearities in the OTDR's optical receiver and amplifier circuits.

granularity you want in your final test results. After adjusting the loss of the attenuator, acquire another waveform and again measure the loss between the cursors. Repeat this procedure for regular loss intervals.

The test results from this procedure consist of a table or plot of the loss between the cursors and the setting on the optical attenuator. With the waveform high above the noise floor you should see very little variation in the measured loss versus the attenuator loss. In other words, changes in attenuator loss should be accompanied by identical changes in loss measured by the OTDR. As the attenuator setting increases and the waveform lowers toward the noise floor, you should see more variation in the measured loss due to the increase in waveform noise.* Plotting the OTDR loss measurements against the attenuator loss measurements, you should see a straight line. Deviations from linearity suggest possible problems with the OTDR's vertical scale calibration that might result in loss-measurement inaccuracy.

12.5 Summary

For anyone involved in the calibration of OTDRs, test fixtures are certain to be a source of aggravation. They are difficult to calibrate, and test results on the fixtures are difficult to interpret. Much of this problem stems from the statistical nature of making measurements with OTDRs.

One approach is to design the test fixtures to measure strictly the hardware parameters of the OTDR. The external source method, for example, can accurately calibrate the time-base accuracy and horizontal scale of the OTDR. Similarly, the standard fiber provides verification of linearity in the OTDR's vertical scale. Thus, it is relatively straightforward to measure and verify the calibration of the OTDR's acquisition hardware.

The difficulty arises with the realization that the principal source of measurement error arises from waveform noise and interpretation and not from hardware calibration (see chapters 5, 6, and 7). It is common for waveform-interpretation errors to be many times larger than errors attributed to the OTDR's hardware calibration. While you can easily determine if the OTDR's vertical scale is linear and its horizontal scale is calibrated, you still do not know the loss- and distance-measurement accuracy when measuring real events. Hardware calibration satisfies metrology requirements but still leaves the OTDR user wondering about measurement accuracy.

*You can use the equations of chapter 6 to estimate the random variation in loss measurements as a function of height above the noise floor.

We described ways to build fixtures with known distances to events. The fiber circulator is one way to do this. Another way is to build a test fixture from fibers that are previously measured with calibrated, traceable means. Such fixtures allow true distance-measurement-accuracy measurements that include errors resulting both from hardware and event-marking algorithms. Loss measurements are more difficult. Although test fibers can be built with calibrated losses, it is difficult to check them periodically or to verify that the event loss has not changed.

Perhaps one of the simplest tests is to build a characterized but not necessarily calibrated test fiber and perform repeatability tests. Repeatability tests can quickly identify OTDRs with unstable hardware or poorly designed event-marking software. You must be careful, however, not to assume too quickly that good repeatability equates with good measurement accuracy. It is true that the measurement accuracy cannot be better than the repeatability, but it can be worse.

As an example, consider a comparison between two hypothetical OTDRs. One uses digital waveform enhancement to smooth the waveform, but it inadvertently moves the event from its true location (see section 5.3.2). Because of its waveform smoothing, the OTDR locates the event in exactly the same place with each measurement, thus showing outstanding measurement repeatability. The other OTDR does not use waveform enhancement, so its measurement repeatability is worse (a standard deviation of 20 meters, for example). Since it does not use waveform filtering, the second OTDR has a mean measurement error of zero, whereas the OTDR with waveform filtering has a mean error of 100 meters and a standard deviation of zero. In this case, the OTDR with the best repeatability is not the most accurate. This example illustrates that, while repeatability is an important factor, it does not always equate with measurement accuracy.

Suggested reading

Moeller, W., Hube, K., and Huenerhoff, D., "Uncertainty of OTDR loss scale calibration using a fiber standard," *Journal of Optical Communications*, Vol. 15, No. 1 (Jan. 1994), pp. 20–28.

IEC TC 86/WG4/SWG2, *Calibration of Optical Time-Domain Reflectometers* (1994).

Bellcore, *Generic Requirements for Optical Time Domain Reflectometer (OTDR) Type Equipment*, GR-196-CORE.

Problems

1. True or false: High-dynamic-range OTDRs need test fixtures with long test fibers for effective evaluation.
2. True or false: Test fixtures with recirculating loops are an inexpensive, practical, and effective alternative to long-fiber test fixtures for single-mode OTDRs.
3. True or false: Test fixtures with recirculating loops are an effective and cost-effective way of testing multimode OTDRs.
4. True or false: To verify that the loss of the OTDR is constant over the dynamic range, you first need to calibrate the loss of a reference fiber.
5. True or false: OTDRs with the best repeatability also have the lowest measurement error.

¹ Anderson, D. R., "Calibrated test fiber for optical time-domain reflectometers," *NIST Symposium on Optical Fiber Measurements* (Boulder, CO: NIST, 1996).

² Newton, S. A., Nazarathy, M., and Trutna, W. R., Jr., "Measured backscatter signature of a fiber recirculating delay line," *Applied Optics*, Vol. 25, No. 12 (1986), pp. 1879–1881.

³ Kamikawa, N., Nakagawa, A., Tanaka, G., and Yamada, Ken, *Optical Fiber Backscatter Signature Generator (OFBSG)*, U.S. Patent 4,952,057.

⁴ IEC TC 86/WG4/SWG2, *Calibration of Optical Time-Domain Reflectometers* (1994).

⁵ *Ibid.*

⁶ Marcuse, D., *Principles of Optical Fiber Measurement* (New York: Academic Press, 1981).

Chapter 13

Polarization mode dispersion

13.0 Introduction

When a very short pulse of light is launched into one end of a fiber, it typically emerges from the opposite end somewhat broadened.* *Dispersion* is the term we use for this pulse broadening; in single-mode fibers, the dominant cause is typically chromatic dispersion. However, in systems operating near the fiber's zero-dispersion point and using very narrow-line-width sources, the dominant source of pulse broadening can be differential group delay (DGD) due to birefringence in the optical fiber. After chromatic dispersion, DGD is the most likely effect limiting the transmission bandwidth of single-mode fiber, and it presents an inherent potential limitation in long-distance communications systems operating in the multigigabit range.¹

Suppose we conduct an experiment in which we measure the amount of time required for light in one polarized state to travel through the birefringent fiber. Then we rotate the polarization of the input light to the orthogonal state and measure the transit time again. Because of birefringence, the transit times are different (see figure 13.1). We call this difference the *differential group delay*, or DGD.² It is the DGD that results in pulse broadening.

Differential group delay results when two orthogonal polarized modes have different group velocities. To many people, the idea of a single-mode fiber implies that the fiber supports just one optical mode. In reality, the fiber supports two modes with orthogonal states of polarization. For a straight, optically perfect fiber with no perturbations along its length, these two modes are degenerate and have the same group velocities. In real fiber, however, there are always bends and twists, and the fiber core is never perfectly circular. These effects can break the degeneracy between the two orthogonal modes, so that one of them travels slightly faster than the other, resulting in DGD. In a fiber with DGD, after a sufficiently long distance the pulses separate slightly, resulting in pulse broadening. If the DGD is sufficiently large and the fiber length sufficiently long, the pulse broadening may significantly increase the bit-error rate (BER). For modest impact on the BER, the total dispersion should be less than about one-tenth of a bit period. Thus,

*An exception is transmission by solitons, although even solitons are subject to PMD.

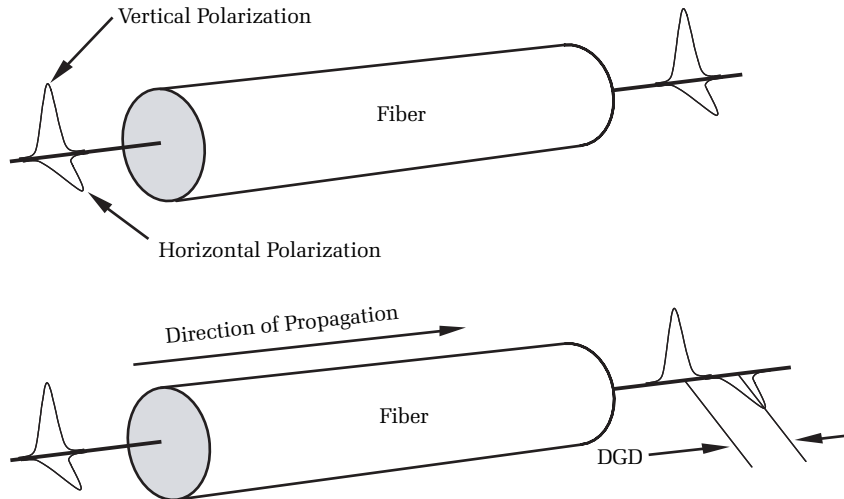


Figure 13.1. For a perfect fiber (top), the group velocities of the orthogonal polarization states are the same, so there is no pulse dispersion. Real fibers (bottom) always have some residual birefringence, resulting in slightly different group velocities for the orthogonal states. The difference in the arrival times of the pulses is the differential group delay, or DGD.

for a typical high-speed system operating at 10 gigabits per second, the maximum amount of total dispersion (chromatic and DGD) should be less than about 10 picoseconds.³

Unlike chromatic dispersion, DGD is nondeterministic. It randomly changes from day to day, in response to environmental and other effects. Another difference is that chromatic dispersion can be corrected by inserting special fiber or components (such as gratings) into the transmission line that compensate for the transmission fiber's chromatic dispersion. Since it is nondeterministic, this approach cannot be used with dispersion caused by birefringence, so DGD represents a fundamental limit to system bandwidth and is a special concern for systems that depend on the state of polarization. Because of its statistical nature, the DGD does not increase linearly with fiber length when the fiber is composed of concatenated sections spliced together. In sufficiently long fibers, the DGD increases with the square root of the fiber length, and we usually denote it in units of picoseconds per root kilometer.⁴

Since DGD depends on environmental effects, it changes with time. DGD also depends on stress-related causes that randomly reinforce

or cancel each other along the fiber's length. Consequently, the total differential group delay of a typical fiber effectively results from the combined effects of many randomly oriented sections of fiber. If a fiber is composed of many concatenated sections, then the DGD over a long time follows a Maxwellian probability distribution, and the expected differential group delay is⁵

$$\langle \tau \rangle = \sqrt{\frac{8}{3\pi} N \langle \Delta\tau \rangle}$$

$$\langle \Delta\tau \rangle = \sqrt{\langle \Delta\tau_1 \rangle^2 + \langle \Delta\tau_2 \rangle^2 + \dots + \langle \Delta\tau_N \rangle^2} \quad [13.1]$$

In equation [13.1], the terms under the radical represent the DGD for the various concatenated sections and N is the number of concatenated sections.

The causes for DGD may be subdivided into those that occur intrinsically and those that result from extrinsic factors. Intrinsic effects result from processes during the fiber's manufacture. For example, sometimes a fiber's core is slightly elliptical. When this happens, the waveguide solutions result in slightly different group velocities for the two polarization modes. Other times, the fiber may have some built-in asymmetric stress. These stresses cause the index for one polarized state to differ slightly from that for the other, resulting in DGD.

Extrinsic factors all result from stress. Stress may result from twisting or bending the fiber or from environmental effects like changes in temperature, thermal gradients, or vibration due to wind-blown aerial plant or fiber that is installed next to railroad lines. Twisting and bending occur in fibers resting against each other in fiber bundles when they are organized in splicing trays or when they are organized into cables. It is important to note that extrinsically induced stress can change with temperature and time. For example, Galtarossa et al. have shown that variations in the output state of polarization as large as 100% occurred when the temperature changed by about 10°C in 20 minutes.⁶ Furthermore, they showed that the effect was not reversible when the temperature returned to normal. Polarization changes resulting from more slowly changing temperature, of about 1°C/ hour, are reversible.

Because of its random nature, DGD is usually specified from a statistical basis. For long fibers, the parameter of interest is the average value of DGD over a long time, and this expected (mean) value is called

the *polarization mode dispersion*, or PMD. For fibers that exhibit a large degree of energy coupling between polarization modes, PMD scales with the square root of fiber length (whether or not it is made of different sections concatenated together) and, as mentioned previously, is often specified in picoseconds per root kilometer. In practical lengths of optical fiber, the differential group delay also varies randomly with wavelength. Theory predicts, and experiments confirm, that the statistical variation of DGD over many wavelengths in a short amount of time is equivalent to the statistical variation at a given wavelength over a long period of time. For this reason, PMD measurements are typically made by averaging the DGD over a relatively wide spectral range.⁷

13.1 Measurement techniques

There are many different methods for measuring PMD. Figure 13.2 shows a test procedure called the *fixed-analyzer method*. The optical output from a broadband light source, such as an LED, is coupled into

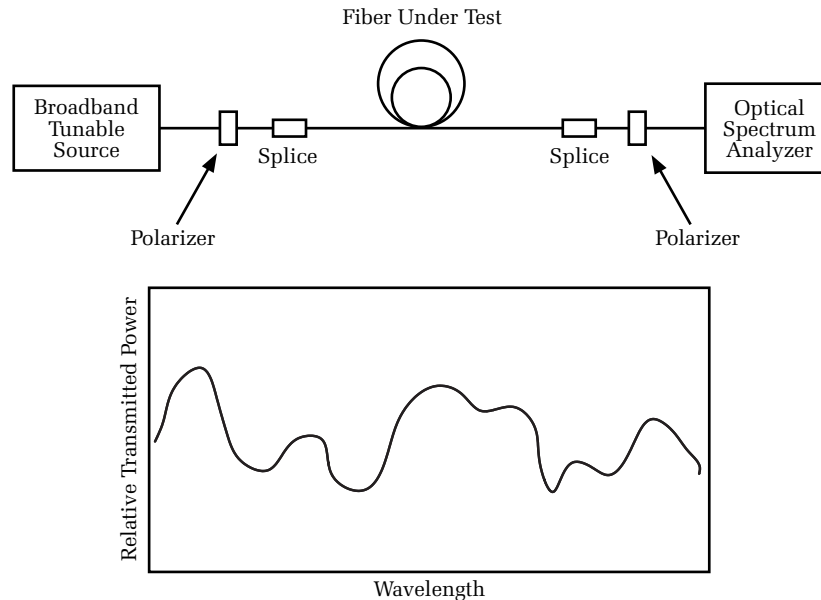


Figure 13.2. Fixed-analyzer method. A tunable broadband source transmits through a fixed-input polarizer and test fiber. At the output, the light passes through another polarizer, and the relative output power is measured as a function of wavelength by an optical spectrum analyzer. The relative PMD is then determined from the fluctuations in the signal over wavelength.

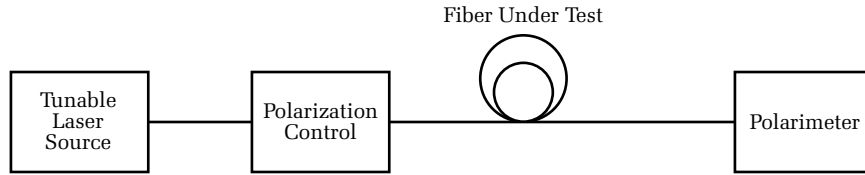


Figure 13.3. Method of measuring PMD using Jones matrices. The polarization control orients the input state of polarization at relative angles of 0° , 60° , and 120° . For each of these input states, the polarimeter determines the output state of polarization, and from this it calculates the Jones matrix. With the Jones matrix known at the two closely spaced wavelengths, the DGD is calculated using equation [13.2].

a fiber through a polarizer. The orientation of the polarizer is fixed, so the input state of polarization is constant for all wavelengths. As the light travels through the optical fiber, its state of polarization changes because of the fiber's DGD. The light exiting the fiber passes through another polarizer, which power modulated according to the output state of polarization. The optical spectrum analyzer scans the relative output over a given wavelength range, and the PMD is then a function of the number of maxima and minima and the scan range.

The relative PMD is then determined from the fluctuations in the signal over wavelength.

Figure 13.3 illustrates a test procedure developed by researchers at Hewlett-Packard.⁸ This procedure calculates the DGD by finding the Jones matrix of the fiber at different wavelengths. The tunable source transmits three precisely known input states of polarization through different polarizers at multiple wavelengths. The polarimeter measures the output states of polarization. From these data, the Jones matrix of the fiber is determined. Knowing the Jones matrix representation of the fiber at two closely spaced wavelengths allows you to determine the DGD from the following equation:*

$$\Delta\tau = \frac{1}{\Delta\omega} \cdot \arg\left(\frac{\lambda_{e1}}{\lambda_{e2}}\right) \quad [13.2]$$

In equation [13.2], $\Delta\omega$ is the difference in optical frequency between the two wavelengths at which the Jones matrix for the fiber is determined and λ_{e1} and λ_{e2} are the eigenvalues of the matrix $T_{\omega+\Delta\omega} \cdot T_{\omega}^{-1}$. Here, $T_{\omega+\Delta\omega}$

*The product of the differential group delay and the difference in optical frequencies must be less than pi for test fibers with polarization-independent loss.

and T_ω represent the Jones matrices of the fiber at optical frequencies $\omega + \Delta\omega$ and ω , respectively. Measuring the DGD over many different wavelengths and averaging them gives the PMD.

Both preceding methods of measuring PMD use relatively expensive equipment that is not easy to operate outside a laboratory environment. This may be a significant hindrance for installers who wish to measure PMD in the field. Here, the polarization OTDR (POTDR) (see figure 13.4) may offer a substantial advantage. Ordinarily, an OTDR manufacturer designs its instruments so that the receiver leg is insensitive to the state of polarization. If you place a polarizer in the output leg of the OTDR, however, the receiver leg becomes sensitive to the state of polarization. When this happens, the resulting periodicity in the waveform can be used to calculate the amount of PMD in the fiber.⁹

Figure 13.5 compares a typical OTDR waveform with one obtained from a POTDR. Observe that the noise on the typical OTDR waveform is rather small, and is due entirely to system noise in the OTDR. This system noise, being random and asynchronous with the waveform, averages down during the OTDR's acquisition. In the POTDR, the large noise signature results because the birefringent fiber is constantly changing the phase between the two orthogonal states of polarization. These phase changes, which occur randomly, result in a changing state of polarization when the light scatters back to the OTDR. The transmission efficiency of this randomly changing state of polarization thus changes from point to point along the waveform. This results in an undulating waveform whose spectral components contain the information to estimate the fiber's PMD.

The POTDR is limited to measuring the PMD of fibers with relatively low DGD. This is because fibers with high PMD exhibit POTDR waveforms with high spatial frequencies. The maximum spatial



Figure 13.4. Example of a platform OTDR with a polarization module.
[Credit: EXFO.]

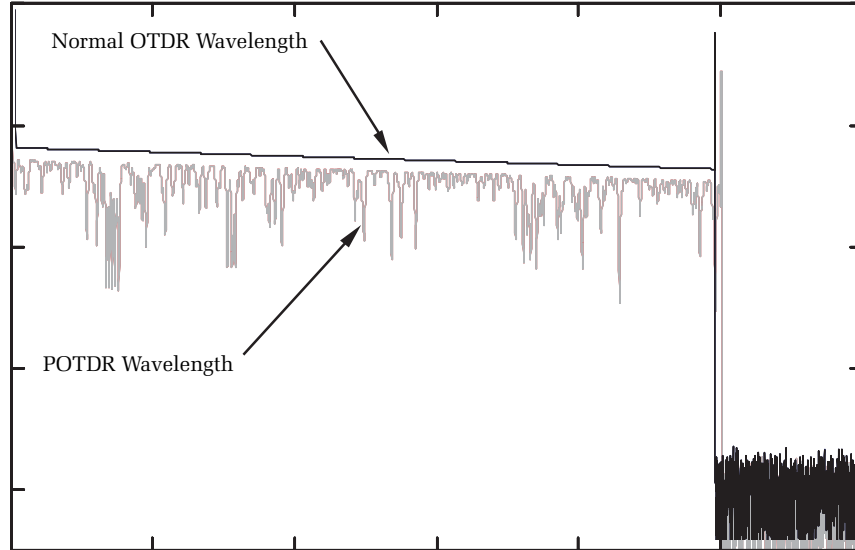


Figure 13.5. Waveforms from polarization OTDRs (POTDRs) exhibit high modulation. The modulation frequency of this PMD-induced waveform variation can estimate the total amount of PMD in the optical fiber.

frequency the POTDR can resolve, however, is limited by the OTDR's pulse width. Consequently, when testing fibers with high PMD you must use a short pulse, and this results in lower dynamic range. As the PMD becomes less significant, the POTDR's pulse width may be increased.

13.2 PMD model of optical fiber

Here we develop a model for a birefringent single-mode fiber. We develop this model by assuming the fiber is composed of many different sections that can each be modeled as separate phase plates. A different Jones matrix defines the polarization transmission characteristics of each section.¹⁰ For the general phase plate, the Jones matrix is*

$$T = \begin{bmatrix} \cos\left(\omega \cdot \frac{\tau}{2}\right) + i \cdot \sin\left(\omega \cdot \frac{\tau}{2}\right) \cos(2\theta) & i \cdot \sin\left(\omega \cdot \frac{\tau}{2}\right) \sin(2\theta) \\ i \cdot \sin\left(\omega \cdot \frac{\tau}{2}\right) \sin(2\theta) & \cos\left(\omega \cdot \frac{\tau}{2}\right) - i \cdot \sin\left(\omega \cdot \frac{\tau}{2}\right) \cos(2\theta) \end{bmatrix}$$

[13.3]

*We obtain equation [13.3] from $S(-\theta) \cdot G \cdot S(\theta)$, where $S(\theta)$ is the rotation matrix (equation (9) in the paper by R. Clark Jones) and $G(\theta)$ is the matrix for a general retardation plate whose axes are parallel to the x - and y -axes (equation (25) in the paper by Jones).

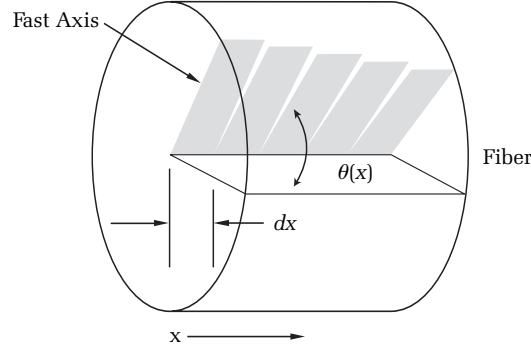


Figure 13.6. A length of fiber modeled as a series of arbitrary waveplates. Each differential waveplate is defined by its angle between the fast axis and the x -axis and its DGD. The state of output polarization is determined by the fiber's Jones matrix, which is the reverse product of the Jones matrices of the individual waveplates (see equation [13.5]).

In equation [13.3], ω is the optical frequency (in radians per second) and τ is the differential group delay between light polarized along the x -axis and light polarized along the y -axis. The angle between the phase plate's fast axis and the x -axis of the coordinate system is θ .

Now suppose we have two phase plates in series, with light passing through phase plate 1 and then through phase plate 2. Each phase plate has its differential group delay and orientation to the x -axis. We can model the combination of these two phase plates with a third Jones matrix that is simply the product of the individual matrices of the two phase plates

$$T_{\text{total}} = T_2 \cdot T_1 \quad [13.4]$$

Observe in equation [13.4] that the order of the matrix multiplication is reversed from the order in which the light passes through the phase plates.

Each of the n individual retardation plates that makes up the optical fiber is specified by its Jones matrix, and has a specific orientation relative to the x -axis and a specific DGD (see figure 13.6). By extension, if we have n general waveplates, with light passing through each of them serially, then the output state of polarization is determined by a Jones matrix that is

$$T_{\text{total}} = T_n \cdot T_{n-1} \cdot T_{n-1} \cdots T_3 \cdot T_2 \cdot T_1 \quad [13.5]$$

Now suppose that T_ω is the fiber's Jones matrix for the fiber at some optical frequency ω and that $T_{\omega+\Delta\omega}$ is the fiber's Jones matrix at a slightly different optical frequency. We can show that the differential group delay is ¹¹

$$\text{DGD} = \frac{1}{\Delta\omega} \cdot \arg\left(\frac{\lambda_{e1}}{\lambda_{e2}}\right) \quad [13.6]$$

In equation [13.6], λ_{e1} and λ_{e2} are the eigenvalues of the matrix $T_{\omega+\Delta\omega} \cdot T_\omega^{-1}$. To show this, we begin by writing the equation for the fiber's Jones matrix at optical frequency ω :

$$T_k = \begin{bmatrix} \cos\left(\omega \cdot \frac{\tau}{2}\right) + i \cdot \sin\left(\omega \cdot \frac{\tau}{2}\right) \cos(2\theta) & i \cdot \sin\left(\omega \cdot \frac{\tau}{2}\right) \sin(2\theta) \\ i \cdot \sin\left(\omega \cdot \frac{\tau}{2}\right) \sin(2\theta) & \cos\left(\omega \cdot \frac{\tau}{2}\right) - i \cdot \sin\left(\omega \cdot \frac{\tau}{2}\right) \cos(2\theta) \end{bmatrix} \quad [13.7]$$

The inverse of equation [13.7] is

$$T_k^{-1} = \begin{bmatrix} \cos\left(\omega \cdot \frac{\tau}{2}\right) - i \cdot \sin\left(\omega \cdot \frac{\tau}{2}\right) \cos(2\theta) & -i \cdot \sin\left(\omega \cdot \frac{\tau}{2}\right) \sin(2\theta) \\ -i \cdot \sin\left(\omega \cdot \frac{\tau}{2}\right) \sin(2\theta) & \cos\left(\omega \cdot \frac{\tau}{2}\right) + i \cdot \sin\left(\omega \cdot \frac{\tau}{2}\right) \cos(2\theta) \end{bmatrix} \quad [13.8]$$

Next we approximate $T_{\omega+\Delta\omega}$ in terms of the differentials of its components

$$T_{\omega+\Delta\omega} = \begin{bmatrix} a(\omega) & b(\omega) \\ c(\omega) & d(\omega) \end{bmatrix} \quad [13.9]$$

where

$$a(\omega) = \cos\left(\omega \cdot \frac{\tau}{2}\right) + i \cdot \sin\left(\omega \cdot \frac{\tau}{2}\right) \cos(2\theta) + \frac{d}{d\omega} \left(\cos\left(\omega \cdot \frac{\tau}{2}\right) + i \cdot \sin\left(\omega \cdot \frac{\tau}{2}\right) \cos(2\theta) \right) \Delta\omega$$

$$b(\omega) = c(\omega) = i \cdot \sin\left(\omega \cdot \frac{\tau}{2}\right) \sin(2\theta) + \frac{d}{d\omega} \left(i \cdot \sin\left(\omega \cdot \frac{\tau}{2}\right) \sin(2\theta) \right) \Delta\omega$$

$$d(\omega) = \cos\left(\omega \cdot \frac{\tau}{2}\right) - i \cdot \sin\left(\omega \cdot \frac{\tau}{2}\right) \cos(2\theta) + \frac{d}{d\omega} \left(\cos\left(\omega \cdot \frac{\tau}{2}\right) - i \cdot \sin\left(\omega \cdot \frac{\tau}{2}\right) \cos(2\theta) \right) \Delta\omega$$

Multiplying $T_{\omega+\Delta\omega} \cdot T_\omega^{-1}$ and simplifying, we have

$$T_{\omega+\Delta\omega} \cdot T_{\omega}^{-1} = \begin{bmatrix} \frac{i}{2} \Delta\omega \cdot \tau \cdot \cos(2\theta) + 1 & \frac{i}{2} \Delta\omega \cdot \tau \cdot \sin(2\theta) \\ \frac{i}{2} \Delta\omega \cdot \tau \cdot \sin(2\theta) & 1 - \frac{i}{2} \Delta\omega \cdot \tau \cdot \cos(2\theta) \end{bmatrix} \quad [13.10]$$

Next we solve for the eigenvalues of equation [13.10], obtaining

$$\begin{pmatrix} \lambda_{e1} \\ \lambda_{e2} \end{pmatrix} = \begin{bmatrix} 1 + \frac{i}{2} \Delta\omega \cdot \tau \\ 1 - \frac{i}{2} \Delta\omega \cdot \tau \end{bmatrix} \quad [13.11]$$

The argument of the ratio of these two eigenvalues is $2 \cdot a \tan(1/2 \Delta\omega \cdot \tau)$. In the limit, when the product $\Delta\omega \cdot \tau$ is small and the approximation $a \tan(\theta) \approx a\theta$ is acceptable, we have $2 \cdot a \tan(1/2 \Delta\omega \cdot \tau) \approx a\Delta\omega \cdot \tau$. Upon division by $\Delta\omega$ we are left with the DGD, or τ .

It is relatively straightforward to apply this analysis to Monte Carlo techniques to determine the statistical nature of PMD. To do this, we create a mathematical model of the fiber by randomly selecting the orientation and DGD for n sections of fiber and then calculating the Jones matrix for the fiber using equation [13.5]. Next we calculate the Jones matrix at a slightly different wavelength and then use equation [13.6] to determine the fiber's total DGD.

If we apply this technique to create thousands of synthetic fibers, calculating the DGD for each one, we find that the DGD changes and that the changes follow a Maxwellian distribution.^{12,13} For example, figure 13.7 shows the results of a Monte Carlo analysis based on 5000 fibers. In this analysis, each fiber was composed of 100 segments, each with a randomly chosen DGD and angular orientation.* The length of each section equaled the coupling length, which is the distance required for light injected into one polarized state to be equally distributed between the two polarized states. The modeling of this mode coupling was achieved by randomly selecting the orientation of the fast axis in each of the sections.[†] The smooth curve is that of a Maxwellian distribution, with a mean given by equation [13.1].

An important fact about PMD is that you need not measure thousands of fibers to determine the statistical nature of the distribution.

*The distribution of the differential group delays was Gaussian.

†The orientations were chosen randomly, with an even distribution between 0 and 2π radians.

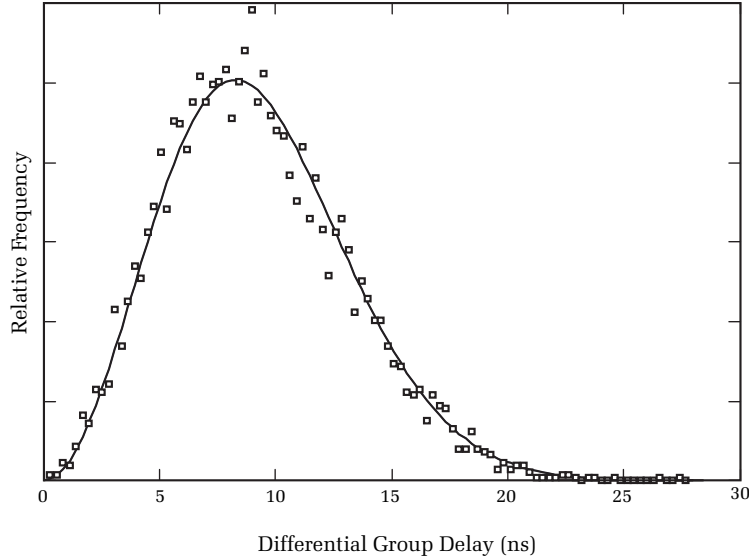


Figure 13.7. Monte Carlo analysis of PMD. This figure shows the relative frequency and differential group delay for 5000 simulated optical fibers composed of 100 segments each. The mean DGD of the segments was 1 ns, and the standard deviation was 0.1 ns. The fast-axis orientation of each segment was randomly selected between 0 and 2π radians. The solid line is a Maxwellian distribution determined from the mean DGD of the 5000 simulated fibers. The squares indicate the results of the Monte Carlo analysis.

Instead, you can measure the DGD on one fiber at one time but over many wavelengths to obtain the same information. For example, figure 13.8 illustrates the results of a Monte Carlo analysis in which the DGD of one fiber, composed of 200 sections, was calculated at 2000 wavelengths over a 10-nm spread. The mean DGD for each section was 1 ns, and the standard deviation was 0.1 ns. Observe that the mean DGD and standard deviation of the distribution are roughly the same as those in figure 13.7.

13.3 Mathematical model of a polarization OTDR

With a mathematical model of a fiber in place, we can now develop a mathematical model for synthesizing the waveform of a POTDR. To do this, we begin with the model of a fiber composed of n sections that we treat as individual waveplates with their associated Jones matrices. Next we assign a loss parameter to each section. This loss parameter is the amount of one-way loss between that section of the fiber and the

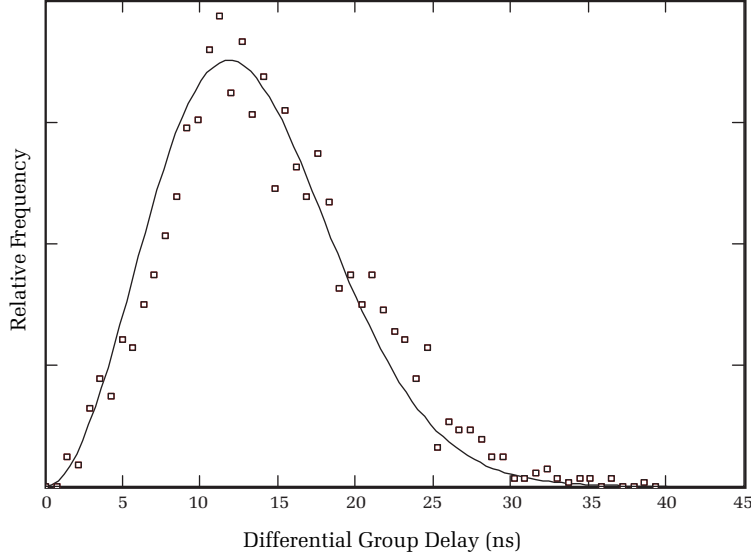


Figure 13.8. Monte Carlo analysis of PMD for one fiber at 2000 different wavelengths. The fiber had 200 sections, each with a randomly chosen DGD and orientation. The mean differential group delay of the segments was 1 ns, and the standard deviation of the segment DGDs was 0.1 ns.

end of the fiber to which the POTDR is connected. Ideally, these fiber sections are short compared with the OTDR's pulse width and the fiber's attenuation coefficient.

To model the POTDR, we first calculate the Jones matrix seen by any portion of the OTDR's pulse that travels out to a fiber section and then back to the OTDR. For example, suppose that we are calculating the Jones matrix of the fiber for light traveling from the OTDR to the p th section and then back to the OTDR. For the trip out to section p , the Jones matrix is

$$T_p = M_p M_{p-1} \dots M_2 M_1 \quad [13.12]$$

The electric vector at p is

$$\begin{pmatrix} E_{x,p} \\ E_{y,p} \end{pmatrix} = T_p \begin{pmatrix} E_{x,\text{in}} \\ E_{y,\text{in}} \end{pmatrix} \quad [13.13]$$

For the return trip, the light travels through the same fiber it passed through from the input to p . Consequently, the state of polarization when the light returns to the OTDR is¹⁴

$$\begin{pmatrix} E_{xout,p} \\ E_{yout,p} \end{pmatrix} = \begin{pmatrix} E_{x,p} & E_{y,p} \end{pmatrix} \cdot T_p \quad [13.14]$$

Recall from chapter 3 that OTDRs operate by launching laser pulses into a fiber and measuring the optical power of the scattered and reflected light as a function of time. Figure 13.9 is a schematic representation of a pulse traveling down an optical fiber. The horizontal axis represents distance along the fiber and the vertical axis represents the time since the leading edge of the pulse passed through the OTDR's front-panel connector. The broad, horizontal line extending from $L - D$ to L represents the pulse at some arbitrary time t_1 .

When the OTDR launches a laser pulse into the fiber, the backscatter signature at a given point on the OTDR display is actually the integrated sum of backscatter from different locations along the optical fiber. Refer again to figure 13.9. Suppose, after traveling a distance L (corresponding to time t_1), a portion of the light in the leading edge of the pulse is scattered back toward the OTDR. Accordingly, it arrives at the OTDR

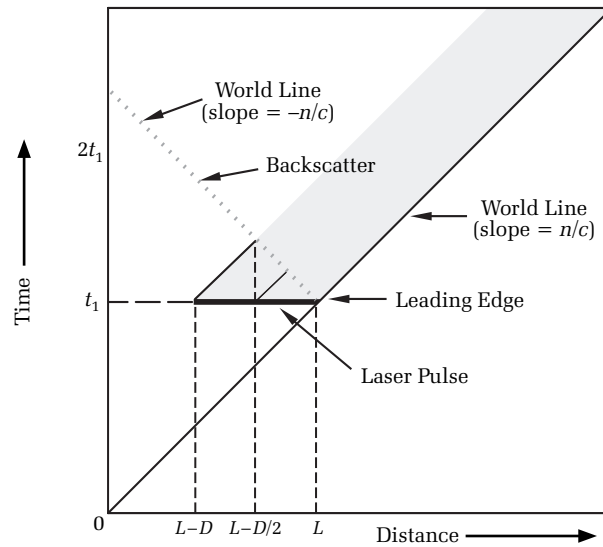


Figure 13.9. Schematic representation of an OTDR pulse traveling down an optical fiber. Observe that the light detected by the OTDR at any given time is scattered from a section of the fiber starting at $L - D/2$ and ending at L , where L is the length of the pulse on the fiber (L is twice the pulse width as seen on the OTDR screen).

after time $2t_1$. Scattered light from the trailing edge also arrives at time $2t_1$, if it scatters from a distance $L - D/2$, where D is the pulse width on the fiber. Similarly, backscattered light from any arbitrary portion of the pulse, $L - x$, will arrive at the OTDR at time $2t_1$, when the backscatter originates from a point $L - x/2$ on the fiber.

To build our synthetic POTDR waveform, we therefore sum the scattered light from sections over one-half the pulse width, multiplying the power received from Rayleigh scattering by the loss incurred at the polarizer due to the fiber's action as a general retardation plate. Suppose that dP_{bs_i} is the total backscatter from the i th section of the fiber in the absence of the polarizer. Furthermore, suppose that dp_{bs_i} is the fraction of that light (from the i th section) that is transmitted through the polarizer. Then we have

$$P_{bs_k} = \sum_{i=k-n}^k dP_{bs_i} dp_{bs_i} \quad [13.15]$$

From equation [13.15], $5 \log(P_{bs_k})$ is the signal level displayed by the OTDR at a distance of $k \cdot \Delta x$, where Δx is the OTDR's sample density and $n = D/2 \cdot \Delta x$, where D is the length of the pulse on the fiber.* We can calculate the value of dp_{bs_i} for each section of fiber by using the Jones matrix representation for a polarizer:

$$dp_{bs_i} = E_{x,i} \bar{E}_{x,i} + E_{y,i} \bar{E}_{y,i} \quad [13.16]$$

In equation [13.16]

$$\begin{pmatrix} E_{x,i} \\ E_{y,i} \end{pmatrix} = \begin{pmatrix} \cos^2(\theta) & \sin(\theta)\cos(\theta) \\ \sin(\theta)\cos(\theta) & \sin^2(\theta) \end{pmatrix} \begin{pmatrix} E_{xout,i} \\ E_{yout,i} \end{pmatrix} \quad [13.17]$$

In equation [13.17], the vector

$$\begin{pmatrix} E_{xout,i} \\ E_{yout,i} \end{pmatrix}$$

is derived from equation [13.14], and the matrix

$$\begin{pmatrix} \cos^2(\theta) & \sin(\theta)\cos(\theta) \\ \sin(\theta)\cos(\theta) & \sin^2(\theta) \end{pmatrix}$$

*We can sum the power from each section without regard to coherent effects because the coherence length of the lasers typically used in OTDRs is much smaller than the typical sectional length used in the mathematical fiber model.

is the Jones matrix representation for an infinite contrast polarizer with its main axis oriented at θ to the x-axis.

The method described here for synthesizing a POTDR waveform was used to generate the waveform seen in figure 13.5, and it gives reasonably good results compared to actual POTDR waveforms. The synthetic POTDR waveform is useful because it accurately models many features of the POTDR.

For example, the synthetic POTDR waveform shows that the POTDR is limited to testing fibers whose beat lengths are more than twice the pulse width.* When the pulse width becomes too large, it effectively averages out the polarization modulation on the waveform. Additionally, the analysis presented here applies only to OTDRs having infinitely narrow bandwidths. Typically, the OTDR's laser has a relatively broad bandwidth (several nanometers), and this also serves to reduce the modulation seen in the POTDR waveform. Because of optical bandwidth effects and limitations from pulse width, POTDRs generally cannot measure the PMD in highly birefringent fibers over long distances. This should not pose a serious problem, however, since most communications-grade fibers have very low PMD.

13.4 Summary

Polarization mode dispersion may set a bandwidth limit for high-bit-rate optical systems. The mechanism for polarization dispersion is birefringence, where the index of refraction for light depends upon its state of polarization. For most telecommunications applications, PMD does not pose a serious limit to bandwidth, unless the data rate exceeds OC-48 (roughly 2.5 Gb/s).

Several techniques exist for measuring PMD. Although reasonably accurate, these existing techniques are generally based on laboratory-quality instrumentation that is expensive and not readily usable in the field. Here, the POTDR may play a future role. The POTDR uses a polarizer to measure the evolving state of polarization as the laser pulse propagates along the fiber and, by various algorithmic operations on the waveform, estimates the amount of PMD. POTDRs have the potential advantage of being relatively low cost and field portable.

*The beat length is the physical length of fiber over which the electric field in the slow axis is delayed (relative to the electric field in the fast axis) by one wavelength.

Problems

1. True or false: DGD results from stress in optical fibers.
2. True or false: DGD can be compensated with a short section of fiber having negative DGD.
3. True or false: DGD is always the same in optical fibers.
4. True or false: Averaging the DGD over wavelength results in the same approximate answer as averaging over time.
5. True or false: A POTDR can test very high PMD over very long fiber.
6. True or false: PMD can cause excessive BER on systems operating at 10 gigabits per second and higher.

¹ Foschini, G. J., and Poole, C. D., "Statistical theory of polarization dispersion in single-mode fibers," *Journal of Lightwave Technology*, Vol. 9, No. 11 (November 1991).

² Ibid.

³ Heffner, B. L., and Hernday, P. R., "Measurement of polarization-mode dispersion," *Hewlett-Packard Journal* (February 1995).

⁴ Foschini, G. J., and Poole, C. D., "Statistical theory of polarization dispersion in single-mode fibers," *Journal of Lightwave Technology*, Vol. 9, No. 11 (November 1991).

⁵ Ibid.

⁶ Galtarossa, A., Someda, C. G., Matera, F., and Schiano, M., "Polarization mode dispersion in long single-mode-fiber links: a review," *Fiber and Integrated Optics*, Vol. 13, pp. 215–229.

⁷ Heffner, B. L., and Hernday, P. R., "Measurement of polarization-mode dispersion," *Hewlett-Packard Journal* (February 1995).

⁸ Heffner, B. L., "Automated measurement of polarization mode dispersion using Jones matrix Eigenanalysis," *IEEE Photonics Technology Letters*, Vol. 4, No. 9 (September 1992), pp. 1066–1069.

⁹ Vengsarkar, A. M., and Cohen, L. G., "Polarization optical time domain reflectometry for statistical evaluation of polarization mode dispersion," *Electronic Letters*, Vol. 29, No. 10 (May 1993), pp. 848–850.

¹⁰ Jones, R. Clark, "A new calculus for the treatment of optical systems," *Journal of the Optical Society of America*, Vol. 31 (July 1941), pp. 488–493.

¹¹ Heffner, B. L., "Automated measurement of polarization mode dispersion using Jones matrix Eigenanalysis," *IEEE Photonics Technology Letters*, Vol. 4, No. 9 (September 1992).

¹² Desbruslais, S. R., and Morkel, P. R., "Simulation of polarization mode dispersion and its effects in long-haul optically amplified lightwave systems," *The Institute of Electrical Engineers*, WC2ROBL, UK (1994).

¹³ Matera, F., and Someda, C. G., "Concatenation of polarization dispersion in single-mode fibers: a Monte-Carlo simulation," *European Transactions on Telecommunications and Related Technologies*, Vol. 3, No. 3 (1992), pp. 289–294.

¹⁴ Jones, R. Clark, "A new calculus for the treatment of optical systems," *Journal of the Optical Society of America*, Vol. 31 (July 1941), pp. 488–493.

Chapter 14

Dispersion in optical fibers

14.0 Introduction

In section 2.4, we introduced the concept of dispersion in optical fibers. In this chapter we expand on some of those ideas and show how an OTDR (in some circumstances) can be used to estimate a fiber's dispersion. In classical optics, *dispersion* refers to the phenomenon in which different wavelengths of light travel at different speeds within an optical dielectric, such as glass. Dispersion is also present in optical fibers, and its effect is to differentiate the speed of propagation of different wavelengths and different modes in the fiber.

In chapter 2 we saw that an optical fiber acts as a waveguide for light. In an optical waveguide the modes are not infinite plane waves. Instead, they are confined by the geometry of the waveguide, specifically the refractive index and radius of the core and cladding. Because of the modal characteristics of the waveguide and the dispersive characteristics of the glass it is made of, the speed of propagation in the waveguide depends on wavelength and the modal structure.* As various wavelengths propagate in the waveguide, the differential speeds introduce phase delays among the wavelengths. A waveguide in which the speed of propagation depends on wavelength is called a *dispersive* waveguide. To represent mathematically the propagation of the multifrequency wave, a quantity v_g is defined, which is the speed of propagation of the wave "group." Practically speaking, v_g is the speed at which information can be transmitted in the fiber. The phase velocity of the wave is v_p . When dispersion is present, v_p and v_g are not equal.

The dispersive effects of the waveguide are perhaps best understood by considering an amplitude-modulated (AM) analog signal transmitted in the fiber. Although this discussion refers to analog signals, similar reasoning applies to digital systems. An AM signal may be produced by first sinusoidally modulating the output of a high-speed laser diode at a carrier frequency ω_c . By mixing an information signal with the carrier, the amplitude of the resulting laser output varies with time, and it is said to be amplitude modulated. Typically, the information signal has a bandwidth or range of frequencies from 0 to ω_m . Modulation

*The speed of propagation also depends on the *frequency* of the light wave, since frequency and wavelength are inversely proportional.

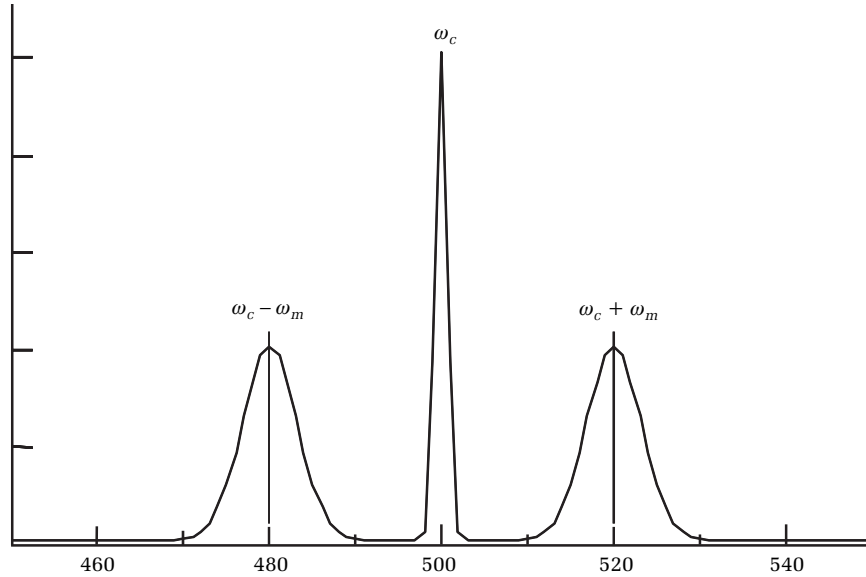


Figure 14.1. An amplitude-modulated signal contains two side bands of frequencies displaced from the carrier frequency by equivalent amounts. In this example, the carrier frequency is 500 MHz and the two side bands extend to 30 MHz on either side of the carrier.

of the center frequency produces sidebands. These sidebands cause the frequency range of the AM signal to extend from a minimum frequency $\omega_{\min} = \omega_c - \omega_m$ to a maximum signal $\omega_{\max} = \omega_c + \omega_m$, as shown in figure 14.1. When the optical signal is converted back to an electrical signal at the receiver, the envelope of frequencies is detected and demodulated to recover the information. In order for the signal to propagate without distortion, all frequencies in the band $2\omega_m = \omega_{\max} - \omega_{\min}$ must propagate with the same relative phase. That is, their phase velocities must be equal. However, due to the frequency dependence of the group velocity (dispersion), this is not possible. The extent to which certain frequencies are delayed more than others is called the *total dispersion* of the waveguide.

In a digital transmission system, information is carried by turning the laser diode on and off in a sequence to produce a binary code. As with analog modulation, digital modulation also generates frequency sidebands, so each pulse is made up of a range or band of optical frequencies. Due to dispersion, individual digital pulses become broadened as they propagate in the fiber. As adjacent pulses

broaden, they eventually overlap to the extent that individual pulses are indistinguishable by the transmission system's detection circuitry. This overlapping of adjacent pulses is known as *intersymbol interference*.

To avoid the effects of intersymbol interference, the distance between adjacent pulses must be much larger than the temporal broadening of individual pulses over a certain transmission length. This places a minimum limit on the distance between pulses and hence on the rate at which pulses can be transmitted in the fiber. Therefore, the bandwidth of a fiber transmission system is determined by the dispersive properties of the fiber as well as by its length and by the characteristics of the optical devices and modulation scheme.*

In this chapter we discuss the various types of fiber-optic dispersions and the extent to which they affect the performance of both single-mode and multimode systems.

14.1 Intermodal dispersion

In chapter 2 we introduced the concept of ray trajectories within multimode optical fibers. Since the number of modes in a multimode fiber can be large, there are many different rays of light moving in essentially different trajectories within the fiber. Because of these different trajectories, in a given amount of time some rays travel farther than others. Pulses that are made of rays following many different trajectories spread out. This type of pulse broadening is known as *intermodal dispersion* because it is related to the relative propagation velocities of different rays (different modes) within the fiber. Intermodal dispersion is also known as modal dispersion and differential mode delay (DMD). DMD limits the transmission distance a high-speed network such as Fibre Channel or Gigabit Ethernet can effectively transmit signals over multimode fibers. Intermodal dispersion cannot occur in single-mode fibers because these fibers have only one mode.† Intermodal dispersion is, however, the single most important dispersion mechanism in step-index multimode fibers, and we discuss it here in some detail.

As a simple derivation of intermodal dispersion, consider a multimode fiber transmission system that uses step-index fiber with a

*As we saw in chapter 13, polarization mode dispersion may combine with chromatic dispersion to limit the fiber's optical bandwidth.

†Recall from chapter 13 that this is not strictly true, since all fibers have some degree of birefringence, which breaks the degeneracy between the orthogonal modes of polarization.

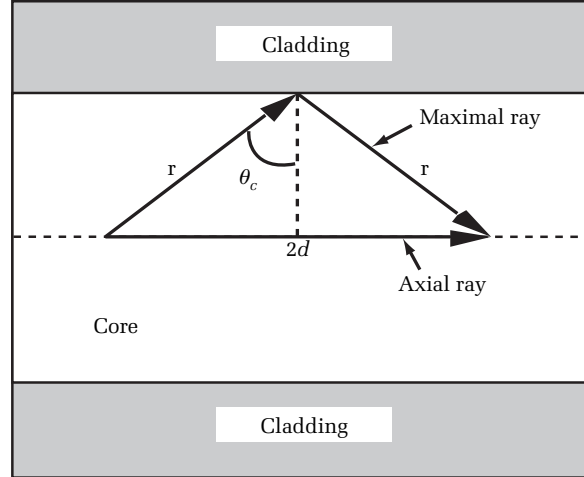


Figure 14.2. A longitudinal cross section from a step-index fiber. The cladding has a material index n_2 and the core has a material index n_1 . The axial ray travels a distance $2d$, and the maximal ray travels a distance $2r$ to arrive at the same point on the axis as the axial ray.

core index of n_1 and a cladding index of n_2 . Referring to figure 14.2, we see that within the fiber there are two extreme paths that a ray can travel. The faster trajectory is the one taken by a ray traveling directly along the axis of the fiber (axial ray). The slower trajectory is taken by a ray traveling at the critical angle for total internal reflection (maximal ray). The time taken by the axial ray to travel the distance $2d$ is $t_{\text{axis}} = 2d/v_1$, where v_1 is the velocity of propagation in the fiber's core. The time required for a maximal ray to travel the distance $2r$ and arrive at the effective distance $2d$ is $t_{\text{max}} = 2r/v_1$. The ratio of the maximal time to the axial time is $t_{\text{max}}/t_{\text{axis}} = r/d = 1/\sin(\theta_c) = n_1/n_2$. Over a certain propagation distance L , the total time delay between a maximal ray and an axial ray is

$$\Delta t = t_{\text{max}} - t_{\text{axis}} = t_{\text{axis}} \left(\frac{t_{\text{max}}}{t_{\text{axis}}} - 1 \right) = \left(\frac{L}{v_1} \right) \left(\frac{n_1}{n_2} - 1 \right) \quad [14.1]$$

The propagation speed v_1 in the fiber core is related to the core index n_1 by

$$v_1 = c/n_1 \quad [14.2]$$

From equation [2.3], the refractive index contrast (d) relates to the core and cladding indexes and the numerical aperture by the formula

$$d = (n_1 - n_2)/n_1 = \text{NA}^2/2n_1^2$$

Using this formula along with equation [14.2] in equation [14.1], we obtain an expression for the total time delay in terms of the core index and the difference between the refractive indexes of the core and the cladding:

$$\Delta t = \frac{Ln_1^2\delta}{cn_2} \quad [14.3]$$

Equation [14.3] represents the impulse response (broadening) to an input pulse of infinitesimally narrow width. For a pulse of finite width, the actual broadening is related to, but not equal to, the time delay. The half-power bandwidth resulting from this response is approximately¹

$$\omega_{3dB} \approx \frac{1}{\Delta t} \quad [14.4]$$

Equations [14.3] and [14.4] can be used to express this in terms of frequency:

$$f_{3dB} = \frac{1}{2\pi} \omega_{3dB} \approx \frac{1}{2\pi\Delta t} = \frac{cn_2}{2\pi Ln_1^2\delta} \quad [14.5]$$

As an example of the use of equation [14.5], consider a step-index multimode fiber having a numerical aperture of 0.275 and a core index of 1.456. Let us calculate the time delay over 1 km of fiber. The relative index difference is $d = 0.0178$, and the cladding index is $n_2 = 1.4298$. Equation [14.5] then gives $f_{3dB} = 1.8$ MHz.

Generally speaking, a precise relationship between the half-power bandwidth and the total dispersion depends upon the type of mathematical model used to describe individual pulses propagating in the fiber.^{2,3} The maximum data rate for pulse-coded modulation is about $f_{3dB} = 1/(4Dt)$. It is clear from this example that due to intermodal dispersion, also known as differential mode delay, step-index multimode fibers cannot be used for long-distance high-bit-rate transmission systems, but their use is limited to shorter distances and lower-frequency applications.

The dispersive properties of multimode fibers can be improved by changing the doping profile of the fiber core. Thus far we have assumed that the maximal ray and the axial ray travel at the same speed, as shown in figure 14.2. Since the maximal ray travels farther, however, it is reasonable to expect that if we could “speed up” the maximal ray,

the amount of time delay would be reduced. This can be accomplished by gradually reducing the material index of the core, from a maximum value at the axis to a minimum value at the core–cladding interface. In a fiber core whose profile is designed in this way, as a ray moves away from the axis, its velocity increases. This increase in speed offsets the increased distance the off-axis ray travels. Therefore, the overall time delay between an axial ray and an off-axis ray is reduced. Optical waveguides prepared in this way are known as *graded-index* fibers. In these multimode fiber types, the effects of intermodal dispersion are dramatically reduced.

In equation [14.3], we have taken a rather simplistic viewpoint that the time difference between the propagation time of an axial ray and of a maximal ray is entirely responsible for intermodal dispersion. While this may be a good approximation for multimode step-index fibers, intermodal dispersion in graded-index fibers requires a mathematical treatment whose complexity is beyond the scope of this book.

14.2 Intramodal dispersion

Dispersion can also occur within the same mode propagating in the fiber. This is called *intramodal dispersion* and sometimes *chromatic dispersion*, since it is always a wavelength-dependent phenomenon. There are primarily two types of intramodal dispersion: *material* and *waveguide*. We discuss each of these in turn.

14.2.1 Material dispersion

The mechanism of material dispersion is illustrated in figure 14.3. In this figure, the ordinate represents wavelength and the abscissa represents time. Recall from chapter 2 that all optical sources have a natural linewidth, or band of wavelengths. If the wavelength of the optical source (laser) were measured with an optical spectrum analyzer, we would see a band of wavelengths as shown in figure 14.3(a). This band of frequencies is generally known as the *wave group* in the material. Since the material index differs for the various wavelengths within the group, each of these wavelengths travels at a different speed in the material. When a laser pulse is introduced into a fiber, the pulse has a range of wavelengths, and each wavelength travels at a different speed in the fiber. Thus, after a certain distance, the pulse broadens in time because certain wavelengths lag behind others, as shown in figure 14.3(b). This broadening increases with distance, and as it does, adjacent pulses ultimately overlap, increasing the amount of intersymbol interference.

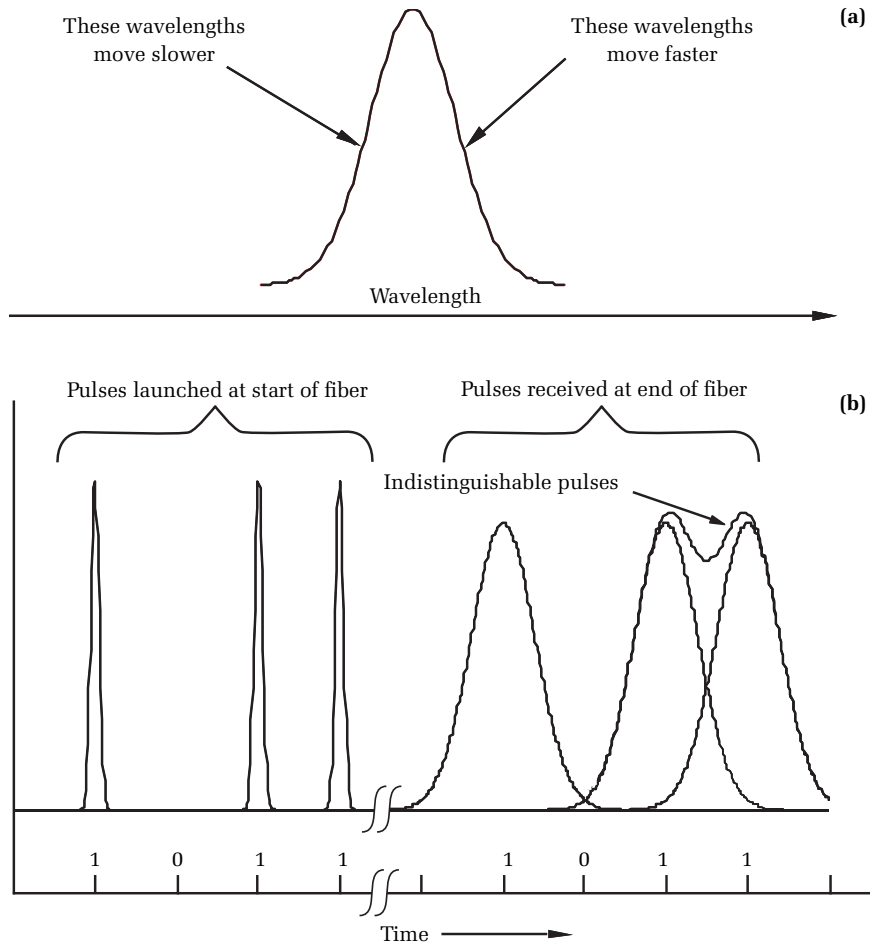


Figure 14.3. A band of wavelengths (a) move at different speeds within an optical fiber. This leads to (b) a broadening of the laser pulse as it propagates in the fiber.

In an optical waveguide, the time required for a wave envelope to propagate over a unit length is called the *group delay time*. This is simply the inverse of the group velocity in the material:

$$\tau_g = 1/v_g \quad [14.6]$$

From equation [14.2], this can be expressed as

$$\tau_g = n_g/c \quad [14.7]$$

where n_g is the group index of refraction.

The group index itself can be written in terms of the variation of the index with wavelength:

$$n_g = n_1 - \frac{\partial n_1}{\partial \lambda} \lambda \quad [14.8]$$

where n_1 is the material index of the fiber core.

Combining equations [14.7] and [14.8], the group delay time can be written as

$$\tau_g = \frac{1}{c} \left(n - \frac{\partial n}{\partial \lambda} \lambda \right) \quad [14.9]$$

The material dispersion parameter, D_m , is defined as the first-order wavelength variation of the wave group delay time:

$$D_m = \frac{\partial \tau_g}{\partial \lambda} \quad [14.10]$$

By substituting equation [14.9] into equation [14.10], the material dispersion parameter can be expressed in terms of the second-order wavelength variation of the material index:

$$D_m = -\frac{\lambda}{c} \frac{\partial^2 n}{\partial \lambda^2} \quad [14.11]$$

Material dispersion is a significant dispersion mechanism in both single-mode and multimode fibers. In silica glass the material dispersion parameter, D_m , is negative for wavelengths less than about 1310 nm and positive for wavelengths exceeding roughly 1310 nm. Group delay of the pulse occurs regardless of the sign of the dispersion parameter. Waveguides that exhibit only material dispersion normally have a certain wavelength at which the material dispersion is zero. Although the wavelength variation of the group delay is zero at this wavelength (equation [14.10]), the group velocity still depends on wavelength. Because of this, a slight distortion of the pulse occurs even at this wavelength.

14.2.2 Waveguide dispersion

We saw in chapter 2 that the spatial distribution of fiber modes depends on wavelength. Because the group velocity depends on the spatial distribution of the mode, the group velocity of the mode also depends on wavelength, even without material dispersion. This leads to a

mechanism known as *waveguide dispersion*; which is usually expressed in terms of the wavelength variation of the fiber-mode spot size, ω_0 :

$$D_\omega = \frac{\lambda}{2\pi^2 c \cdot n} \left[\frac{\partial}{\partial \lambda} \left(\frac{\lambda}{\omega_0^2} \right) \right] \quad [14.12]$$

In silica glass, the waveguide-dispersion parameter is a negative quantity.* Over most of the wavelength spectrum, waveguide dispersion is minimal, and material dispersion is the major contributor to chromatic dispersion (figure 14.4).

In some types of single-mode fibers, the core profile is changed deliberately to increase the contribution of waveguide dispersion and to move the wavelength at which the dispersion for the waveguide equals zero. The ITU-T G.653 dispersion-shifted fiber shifts the zero-dispersion point to about 1550 nm. For DWDM systems, zero dispersion can aggravate nonlinear effects, and so the ITU-T G.655 non-zero-dispersion-shifted fibers have a small but nonzero dispersion in the 1550-nm window. Still other fibers are designed so that the total dispersion is flattened over the wavelength of interest; these are called *dispersion-flattened fibers*.

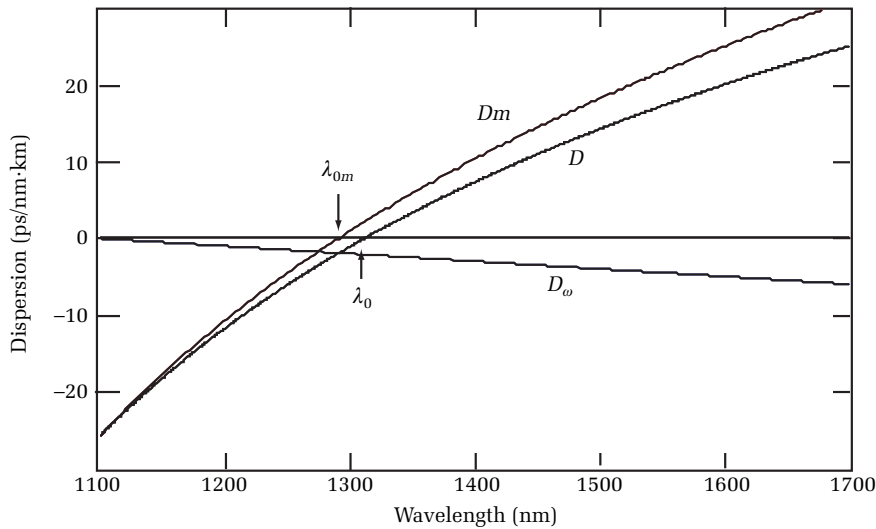


Figure 14.4. Over most of the wavelength region, material dispersion exceeds waveguide dispersion. The total chromatic dispersion parameter, D , is determined primarily by material dispersion.

*This is true for normal step-index fiber.

14.3 Dispersion reduction in optical fibers

The total dispersion in an optical fiber is the combination of both intermodal and intramodal dispersions. Both material dispersion and waveguide dispersion are types of chromatic dispersion and can be added linearly to obtain the total intramodal dispersion. Intermodal dispersion is independent of the wavelength of light. Hence, intermodal and intramodal dispersion are mutually independent and act independently to broaden optical pulses in fiber waveguides. Therefore, they must be added quadratically:^{4,5}

$$(\Delta t)^2 = (\Delta t_{\text{intermodal}})^2 + (\Delta t_{\text{intramodal}})^2 \quad [14.13]$$

where Δt is the total dispersion in the fiber.

For commercially available fibers, the amount of dispersion over a fiber's length can be estimated from the manufacturer's specifications. The chromatic dispersion of a fiber over a length L is obtained from the product of the total chromatic-dispersion parameter, D , the spectral width of the laser source, $d\lambda$, and the fiber length:

$$\Delta t_{\text{intramodal}} = D \cdot L \cdot \delta\lambda \quad [14.14]$$

As an example, Corning SMF-28 has a chromatic-dispersion constant of about 15 ps/(nm·km) at 1550 nm. When used with a laser source having a linewidth of $d\lambda = 0.1$ nm, over a length of 100 km, the total dispersion is

$$\Delta t_{\text{intramodal}} = (15 \text{ ps/nm}\cdot\text{km})(100 \text{ km})(0.1 \text{ nm}) = 150 \text{ ps}$$

If we keep this dispersion time less than one-quarter of the time between pulses, then the maximum bandwidth of the link is about 1 GHz when used with the 0.1-nm laser linewidth at 1550 nm. Sometimes the bandwidth property of a fiber is expressed in units of "speed" (km/s). This comes about by expressing a constant value of bandwidth times distance. For example, a single-mode fiber may have a bandwidth-distance product of 250 GHz·km.

To reduce dispersion in a single-mode optical fiber, sources with very narrow linewidths must be used. A modern multi-quantum-well distributed-feedback (DFB) laser typically has a half-power width of 0.1 nm. Along with narrow-linewidth sources, very short pulses should be used so that the distance between pulses can be minimized. Keep in mind, however, that reducing a pulse's width in the time domain increases its width in the frequency domain. For very narrow-linewidth lasers, reducing the pulse width can worsen the dispersion by increasing

the spectral linewidth. This is a fundamental property that results from the nature of the Fourier transform. Extremely narrow pulses have greater spectral widths due to a constant linewidth-pulsewidth product.⁶ Studies from 1995 suggest that this effect sets an ultimate bit-rate limit, for single-mode optical fibers, of about 100 Gb/s for fibers 100 km long and pulse widths of about 10 ps. For pulses of narrower width, the bit-rate penalty increases rapidly.⁷ In contrast, the *optical* bandwidth of single-mode fibers is about 25,000 GHz.

A third way to reduce dispersion is to minimize the dispersive effects of the fiber itself. From figure 14.4 you can see that for normal fiber there is a particular wavelength, λ_0 , for which the material dispersion and the waveguide dispersion have opposite sign and equal magnitude. Near this wavelength, the total chromatic dispersion is almost zero. For normal ITU-T G.652 single-mode fiber, this zero-dispersion point is about 1310 nm. Although ideal for this particular wavelength, figure 14.4 shows that the dispersion is significantly greater at longer wavelengths, such as 1550 nm.

Attenuation is lower at 1550 nm than at 1310 nm because Rayleigh scattering is inversely proportional to the fourth power of wavelength. Because of this, it is desirable to transmit at the higher wavelength in long-distance systems. However, with normal step-index fiber, larger dispersion at 1550 nm defeats attempts to transmit with high bit rates. To compensate for the increased dispersion at 1550 nm, systems use specially designed fibers known as *dispersion-shifted* and *dispersion-flattened* fibers. By manipulating the index profile of the fiber, the waveguide dispersion can be increased. Since the waveguide dispersion and the material dispersion are of opposite sign, the dispersion types can be made to cancel each other partially. These fiber types are designed either to shift the minimum dispersion point to higher wavelengths or to flatten the dispersion curve so that the fiber has reduced dispersion over a range of higher wavelength.

This technique effectively improves the dispersion characteristics at the expense of a slightly larger loss per kilometer. Modern fiber research is oriented toward optimizing all of these fiber properties. Using such fiber, modern 1550-nm systems may be optimized for minimum dispersive effects over distances of up to several hundred kilometers.

14.4 Measuring dispersion using an OTDR

It is possible to use an OTDR to measure dispersion under certain circumstances. One method is to measure the width of a launched

pulse as it propagates over a certain length of fiber. This places extreme performance requirements on the OTDR transmitter, receiver, and time-base resolution. If the OTDR's pulses are extremely narrow, its receiver bandwidth wide, and its time-base resolution high, then the OTDR can detect broadening of the pulse over a reasonable length of fiber.

Consider, then, an OTDR measurement of a 62.5/125-micron graded-index multimode fiber when used at 850 nm, which has the following dispersion characteristics:

Zero dispersion wavelength: $\lambda_0 = 1343$ nm

Zero dispersion slope = $S_0 = 0.097$ ps/(nm²km)

The chromatic dispersion is calculated from the formula

$$D(\lambda) = \frac{S_0}{4} \left(\lambda - \frac{\lambda_0^4}{\lambda^3} \right) \quad [14.15]$$

With the foregoing values,

$$D(850) = \frac{0.097}{4} \left(850 - \frac{1343^4}{850^3} \right) \text{ps}/(\text{nm} \cdot \text{km}) = -96 \text{ps}/(\text{nm} \cdot \text{km})$$

Laser sources used as transmitters for OTDRs typically have linewidths of about 10–40 nm. The dispersion is then about 1–4 ns per kilometer of fiber. To obtain the width of pulse D_L after dispersion, the initial width, D_0 , must be quadratically added to the pulse broadening caused by dispersion, Δt :⁸

$$D_L = \sqrt{(D_0)^2 + (\Delta t)^2} \quad [14.16]$$

If a pulse of 1 ns is emitted at $x = 0$ a fiber with chromatic dispersion of 1 nm per km, then after a distance of $x = 1$ km, the pulse has a width

$$D_L = \sqrt{(1 \text{ ns})^2 + (1 \text{ ns})^2} = 1.4 \text{ ns}$$

An OTDR emitting a 1-ns pulse with a receiver bandwidth of 1 GHz and a time-base resolution of 100 ps can easily detect this much pulse broadening.

As an example of dispersion measurement using an OTDR, we have used a high-performance multimode OTDR to probe a 2-km length of Corning LNF graded-index multimode fiber. The fiber in this example

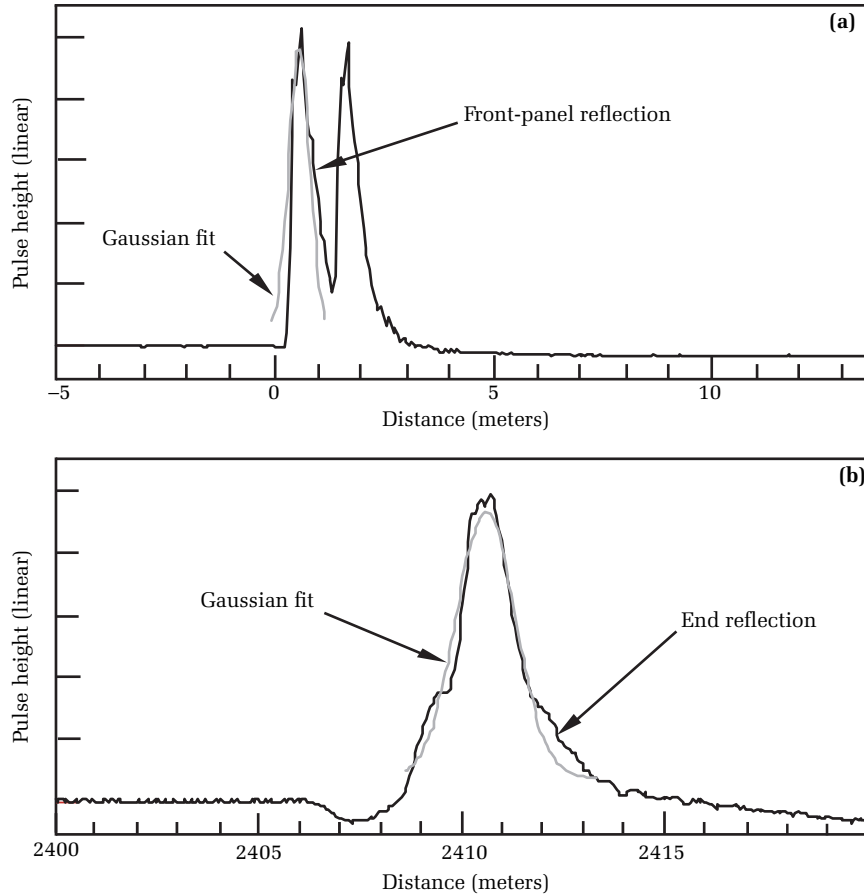


Figure 14.5. Measuring dispersion with an OTDR. In (a), the front-panel reflection appears as the first peak in the pair. Figure (b) is the pulse shape after being reflected from the end of a 2410-m spool of fiber. The reflected pulse is broadened by dispersion in the fiber. The amount of broadening can be used to estimate the fiber's total dispersion at the OTDR's wavelength.

has a diameter of 62.5 microns, a numerical aperture of 0.275, and a core axial index of $n_c = 1.4776$. We used the OTDR to inject a 1-ns pulse at 850 nm into the fiber, whose exact length was 2410 meters. Figure 14.5(a) shows the initial pulse as launched into the fiber. The first pulse of the pair represents a reflection from the connection between the OTDR front panel and a 1-m patch cord. The second pulse represents a reflection from the connection between the patch cord and the spool of fiber. By curve fitting the initial pulse to a Gaussian function, we obtain

an RMS width of $W_1 = 0.26$ m. Figure 14.5(b) shows the pulse after being reflected from the far end of the 2410-m spool of fiber. By curve fitting this pulse to a Gaussian function, we obtain an RMS width of $W_2 = 1.06$ m.

Using these data, we see that the pulse broadens by 0.80 meters; using the conversion factor $10 \text{ ns} = 1 \text{ m}$ for OTDR, we determine that the pulse width increases by 8 ns.* By inverting equation [14.16], we can determine the amount of pulse broadening due to dispersion as this pulse propagates over the length of the fiber:

$$\Delta t = \sqrt{D_L^2 - D_0^2} \quad [14.17]$$

Using the values $D_L = 10.6 \text{ ns}$ and $D_0 = 2.6 \text{ ns}$, we see that the total pulse broadening due to dispersion is 10.3 ns.

In this test, the spectral width of the OTDR laser was about 40 nm. From equation [14.15] we determine that the chromatic dispersion contribution is about $(4 \text{ ns/km}) \cdot (2.41 \text{ km}) = 9.6 \text{ ns}$, compared to the 10.3-ns total dispersion. Let's assume the remaining time delay is due to intermodal dispersion. With this assumption, from equation [14.13] we can calculate this contribution as 3.7 ns.

In a fiber of known length, chromatic dispersion can be approximated using an OTDR if the instrument is equipped with at least three laser sources. By measuring the time of flight for a separate pulse emitted by each of the lasers, the index of refraction for each wavelength can be evaluated. From this, the second derivative of the fiber core index can be obtained. Using these values, the chromatic dispersion can be determined from equation [14.11].

14.5 Measuring chromatic dispersion using multiple-wavelength OTDRs

Even though the OTDR produces test results that show the distance along a length of optical fiber, the actual measurements are made in the time domain. Only after measuring in the time domain is the conversion to distance performed, using the numerical aperture and the group index of refraction. Consequently, if the OTDR can operate at different wavelengths, it is possible to measure the chromatic dispersion directly. Conceptually, the measurement goes something like this:

*This conversion factor includes the time required for the pulse to travel down the fiber, reflect from the end of the fiber, and return to the OTDR.

1. Select one of the wavelengths, and measure the time required for the light to go down to the end of the fiber and back to the OTDR.
2. Repeat this for two other wavelengths.
3. Now make a plot. Along the horizontal axis, plot the wavelength; along the vertical axis, plot the delay.

Since you measure the delay at only a few wavelengths, this won't be much of a plot. But the science of fiber optics tells us something about the nature of the delay curve, so we can fit these three points to a type of curve that is representative of the delay found in common optical fibers (figure 14.6).

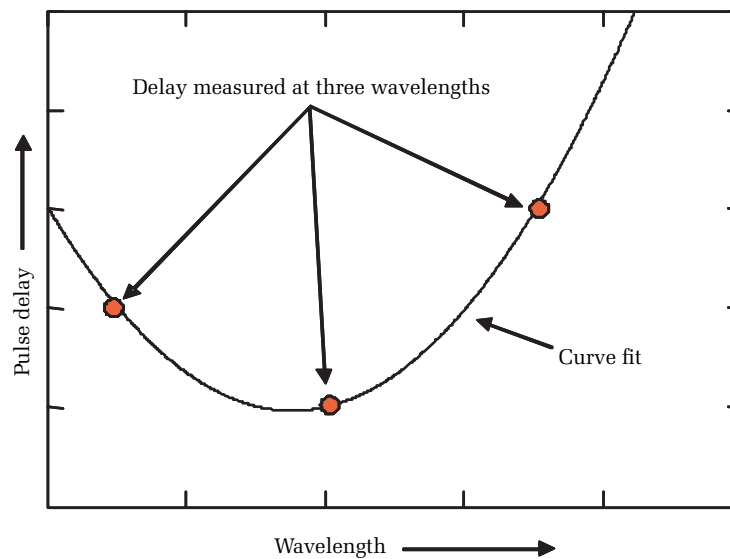


Figure 14.6. Relative delay measured at three distinct wavelengths and curve fit to data.

The result is a smooth curve showing the time delay as a function of wavelength. The time-delay data are not the dispersion. To find the fiber's chromatic dispersion, we must take the derivative of the curve that's fitted to the delay-vs.-wavelength data. It's the process of taking the derivative that makes curve fitting necessary, since derivatives are by nature noisy processes when applied to discrete data and since three points isn't nearly enough to arrive at a meaningful derivative using just the discrete measurements.

Several manufacturers offer OTDRs designed to measure chromatic dispersion in this way. Typical OTDR measurements determine the pulse

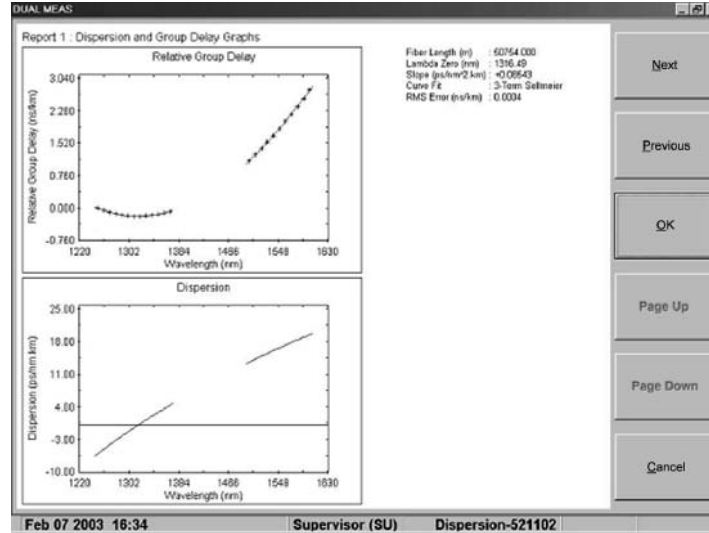


Figure 14.7. Screenshot from a commercial instrument used to measure chromatic dispersion. The top graph shows the relative group delay as a function of wavelength; the bottom graph shows the derivative, or the dispersion.

delay at only a few wavelengths, apply a curve fit to the pulse-delay measurements, and take the derivative of the curve fit to determine the dispersion. Other techniques use a tunable source at one end of the fiber and a receiver at the other end. These measurement techniques can measure the pulse delay at many more wavelengths (see figure 14.7).

The type of curve that is fitted to the data is different for each type of fiber (as described in FOTP-224). Consequently, before you can make an accurate measurement of the chromatic dispersion using this method, you need to know the type of fiber you are using. In addition, the instrument you are using must have stored in its memory the mathematical formula for that fiber. Because of this, if you are testing a link that has a mix of different types of fiber in it, this curve-fitting technique can lead to odd and possibly erroneous results.

The FOTP-224 standard also stipulates that most fibers, when tested over a wide wavelength range (which is the case with this technique), should be modeled by an equation with five unknowns. To solve such an equation unambiguously, the number of pulse-delay measurements must equal (or be greater than) the number of unknown terms in the equation. So this technique can have excessive errors if the OTDR does not test at enough wavelengths.

Another source of error in the OTDR method involves measuring the leading edge of the reflection that bounces off the far end of the fiber. For very long fibers, wide pulse widths are used to obtain adequate dynamic range. However, as we have already seen, when the OTDR tests long fibers, it uses wide pulse widths and the distance between sample points increases. This, in turn, directly affects the accuracy with which the distance (time delay) to the end of the fiber can be measured.

While these errors may be important, and even excessive in some instances, the OTDR method has one very important advantage: It allows testing from a single end of the fiber. The uncertainties of the measurement must be weighed against the need for speedy and convenient testing. If the requirements for test accuracy allow it, the OTDR method of determining chromatic dispersion can be a very convenient and cost-effective one.

14.6 Summary

Dispersion is an important factor limiting the rate of data transmission in fibers. We have provided a cursory description of the subject of dispersion. For a more detailed analysis of the various types of dispersion, refer to the Suggested reading listed at the end of this chapter. We also provide a partial list of the vast amount of information and several good texts and reviews.

Table 14.1 summarizes the relative importance of various optical-fiber dispersion effects we have discussed. Intramodal (chromatic) dispersion is present in both single-mode and multimode fibers. Chromatic dispersion is the most significant dispersion mechanism in single-mode fibers. Intramodal dispersion has two contributions: material and waveguide. Material dispersion is the primary type of intramodal dispersion; waveguide dispersion is less significant than material dispersion in both single-mode and multimode fibers.

Dispersion	Fiber type	
	Single mode	Multimode
Intramodal (chromatic)		
Material	Significant	Significant
Waveguide	Small	Very small
Intermodal	n/a	Significant

Table 14.1. Relative significance of the different types of dispersion to different types of fiber.

Over a large portion of the optical spectrum, waveguide and material dispersion have opposite signs. By suitable doping, waveguide dispersion can be increased in magnitude. When added to material dispersion, the total dispersion becomes reduced at wavelengths greater than the zero-dispersion wavelength. Fibers employing this type of compensation are known as dispersion-shifted and dispersion-flattened fibers. Intermodal dispersion occurs only in multimode fibers and presents a significant limitation to the transmission rate of multimode fibers.

OTDRs can be used to measure total dispersion in certain circumstances. In multimode fibers, where the dispersion is large, significant pulse spreading occurs over relatively short distances (about 1 km). Using a high-resolution OTDR, you can measure the width of the emitted pulse and the width of the pulse after it travels a distance of several hundred meters and reflects from the fiber's end. From the relative RMS pulse widths, the total dispersion can be evaluated. Assuming the spectral bandwidth of the OTDR source is known, you can then determine the fiber's total dispersion. Additionally, if either the chromatic dispersion or the intermodal dispersion is known, the other can be derived from the OTDR measurement.

Suggested reading

Gambling, W. A., Matsumura, H., and Ragdale, C. M., "Mode dispersion, material dispersion, and profile dispersion in graded-index single-mode fibers," *Microwaves, Optics, and Acoustics*, Vol. 3 (1979), pp. 239–246.

Gambling, W. A., Matsumura, H., and Ragdale, C. M., "Zero total dispersion in graded-index single-mode fibers," *Electronics Letters*, Vol. 15 (1979), pp. 474–476.

Garrett, I., and Todd, C. J., "Review: components and systems for long-wavelength monomode-fiber transmission," *Optical Quantum Electronics*, Vol. 14 (1982), pp. 95–143.

Gloge, D., Marcatali, E. A. J., Marcuse, D., and Personick, S. D., "Dispersion properties of fibers," *Optical Fiber Telecommunications*, Miller, S., and Chynoweth, A., editors (Orlando, FL: Academic Press, 1979).

Jeunhomme, L., "Single-mode fiber design for long haul transmission," *IEEE Trans. MTT*, Vol. 30 (1982), pp. 573–578, and *IEEE Journal of Quantum Electronics*, Vol. 18 (1982), pp. 727–732.

- Jeunhomme, L., *Single-mode Fiber Optics. Principles and Applications* (New York: Marcel Dekker, 1990).
- Jürgensen, K., “Dispersion-optimized optical single-mode glass fiber waveguides,” *Applied Optics*, Vol. 14 (1975), pp. 163–168.
- Marcuse, D., “Pulse distortion in single-mode fibers, part 1,” *Applied Optics*, Vol. 19 (1980), p. 1660.
- Marcuse, D., “Pulse distortion in single-mode fibers, part 2,” *Applied Optics*, Vol. 20 (1981), pp. 2969–2974.
- Marcuse, D., “Pulse distortion in single-mode fibers, part 3: Chirped pulses,” *Applied Optics*, Vol. 20 (1981), pp. 3573–3579.
- Marcuse, D., “Selected topics in the theory of telecommunications fibers,” *Optical Fiber Telecommunications II*, Miller, S., and Kaminow, I., editors (San Diego: Academic Press, 1988).
- Sugimura, A., Daikoku, K., Imoto, N., and Miya, T., “Wavelength dispersion characteristics of single-mode fibers in low-loss region,” *IEEE Journal of Quantum Electronics*, Vol. 16 (1980), pp. 215–225.

Problems

1. True or false: Under some circumstances, dispersion can be measured with a single-wavelength OTDR on multimode fibers.
2. True or false: Waveguide dispersion is not used to balance material dispersion in single-mode fibers.
3. True or false: The wavelength for zero dispersion is the same for all fibers.
4. True or false: Dispersion is what limits the information-carrying capacity of optical fibers.
5. True or false: One can have modal dispersion even when there is no chromatic dispersion.

¹ Jones, W. B., *Introduction to Optical Fiber Communications Systems* (New York: Holt, Rinehart and Winston, 1988).

² Olshansky, R., “Propagation in glass optical waveguides,” *Review of Modern Physics*, Vol. 51 (1979), pp. 341–367.

³ Gambling, W., Hartog, A. H., and Ragdale, C. M., “Optical fiber transmission lines,” *Radio Electronics Engineering Journal IERE*, Vol. 51 (1981), pp. 313–325.

⁴ Olshansky, R. and Keck, D. B., “Pulse broadening in graded-index optical fibers,” *Applied Optics*, Vol. 15 (1976), pp. 483–491.

⁵ Keck, D. B., *Optical fiber waveguides*, in *Fundamentals of optical fiber communications*, Barnowski, M. K., editor (Orlando, FL: Academic Press, 1981).

⁶ Sala, K. L., Kenney-Walace, G. A., and Hall, G. E., "CW autocorrelation measurements of picosecond laser pulses," *IEEE Journal of Quantum Electronics*, Vol. QE-16 (1980), pp. 990–996.

⁷ Kim, K. H., Lee, H. K., Park, S. Y., and Lee, E.-H., "Calculation of dispersion and nonlinear effect limited maximum TDM and FDM bit rates of transform-limited pulses in single-mode optical fibers," *IEEE Journal of Lightwave Technology*, Vol. 13 (1995), pp. 1597–1605.

⁸ Gowar, J., *Optical Communications Systems* (Englewood Cliffs, NJ: Prentice Hall, 1984).

Chapter 15

Considerations when selecting an OTDR

15.0 Introduction

We have spent most of this book discussing the specific, detailed performance of OTDRs and how to make both traditional and nontraditional measurements. Chapter 5 dealt with the measurement techniques and statistical errors associated with nonreflective events. Chapter 6 analyzed loss-measurement errors, and chapter 7 described the methods for measuring reflective events. In chapter 4 we discussed the specifications for an OTDR's dynamic range, dead zone, and other performance parameters. In this chapter we look at some of the aspects of OTDR design that are less directly related to the OTDR's usual array of performance specifications. Though these things can be of great importance to the OTDR operator, they often fall outside the detailed specifications. In this chapter we discuss, among other subjects, durability, the display, human interface, fiber-optic cleaning procedures, and safety.



Figure 15.1. Acceptance testing optical-power ground wire with an OTDR.
[Credit: The Light Brigade.]

15.1 Durability

Early OTDRs were laboratory instruments, but today's OTDR is the workhorse of fiber-optic installation, restoration, and maintenance crews (see figure 15.1). Today's OTDR is as likely to be used by a technician climbing a utility pole or a splicing technician underground as in an environmentally controlled room. Hazards to the OTDR include falling (shock), moisture (rain or even partial submersion), and shaking (bouncing in the back of a truck). We all try to take care of our tools, especially the expensive ones. Still, accidents happen, and purchasing a rugged OTDR that can survive rough environments can be very important.

The most important thing to remember when considering ruggedness is that it must be designed into the OTDR. Many of the features that make an OTDR durable in harsh environments are not visible from the outside. Cosmetic effects (such as rubber bumpers) can sometimes give the illusion of durability and ruggedness, but they may still leave delicate components and subsystems inside the OTDR vulnerable to shock. When discussing matters of ruggedness with the manufacturer's representative, it is prudent to request data documenting the testing cycles the manufacturer used to verify the instrument's ruggedness. These should include shake, shock, drop, humidity, and temperature testing (see figure 15.2) on a statistically significant number of instruments.¹



Figure 15.2. Temperature chamber for testing OTDRs. [Credit: The Light Brigade.]

Instrument suppliers should be willing to discuss the design steps that have been taken to ensure ruggedness. The most sensitive subsystem in most OTDRs is the display. Ask how the designers mounted the display and what steps the manufacturer has taken to ensure the display's survival if (for example) the instrument is ever dropped onto the floor. Generally, larger displays are more vulnerable. This is because large displays offer a larger area, so they are more likely to be hit if an object falls on the OTDR. Larger displays also require more mechanical support to prevent excessive flexing during the high deceleration that occurs if the instrument is dropped.

For best durability, the OTDR should also have a sealed front-panel display with membrane keys, softkeys, or some form of positive dust and moisture seal. This helps ensure that the OTDR does not easily become contaminated by dust and moisture; both of which can lead to component failure inside the instrument, while moisture can also affect instrument performance.

Another critical issue for design durability is how the mechanical design supports circuit boards inside the OTDR's case. If the designers mounted the circuit boards with inadequate support, the boards may shake loose, their mounting brackets might fail under shock, or they may flex, causing failure in critical components or internal to the board. When this happens, the boards can become dislodged inside the OTDR, touch, and short-circuit critical components. External padding can help reduce risk by cushioning the OTDR from shock. A padded carrying case, for example, not only helps protect the OTDR from shock, but it provides a handy way to keep accessories readily available.* For maximum utility, the OTDR should be fully functional inside the carrying case.

Disk drives are particularly sensitive to dirt and water. If you are working in extremely dirty environments, you may want to consider an OTDR that has internal memory and no floppy-disk drive. When configured this way, the OTDR can be sealed from the environment, virtually airtight and watertight. If you decide to purchase an OTDR that has only internal memory and no floppy-disk drive, be sure it has the right amount of memory for the particular application. The OTDR should have parallel or serial ports for uploading stored waveforms into your computer or downloading stored waveforms from the computer into the OTDR. The capability to upgrade the instrument's software by

*Rubber bumpers also reduce shock if the instrument is dropped, so they are not totally cosmetic.

downloading from a computer is a benefit that avoids the need to send the instrument to a service center for software upgrades. Educational organizations may also want to have access with a VGA output for presentation and staff development roles.

Even with the best care, the most durably designed OTDR may occasionally need repair. When this happens, the quality and performance of your manufacturer's service department are critical. Local service areas can be very helpful in such situations. This is especially true if you do not live in the same country where the OTDR was manufactured. In such cases, the local service center can dramatically improve response time by offering repair services on-site. Competent assistance over the phone from trained technicians, engineers, and scientists can be invaluable. If you can correct an apparent instrument failure by discussing the situation over the phone rather than returning the instrument to a service center, you save both time and money.

As a final and practical test, ask the salesperson to demonstrate the OTDR ruggedness by, for example, tossing it across the room. After all, if you are going to be using the instrument in the real world, chances are it will get this kind of treatment some time during its life. Admittedly, this test may not be definitive, but a salesperson's willingness to treat the OTDR this way (the way it might be treated in the real world) at least signifies faith in the level of engineering inside the instrument.

15.2 Display and controls

The most visible part of an OTDR is the display. The display shows the waveform, event table, setup parameters, and (on some models) softkeys for controlling the instrument and entering the setup parameters. The important parameters for the display are size, resolution, brightness, and contrast.

One of the most important things a display can do for the operator is to show a clear, crisp, high-resolution image of the waveform. To do this, the display must be large enough to see the waveform clearly and have enough resolution (pixels per inch) to show even small events adequately. Sometimes there is a tendency to focus on the display's size without addressing the importance of the display's resolution or the amount of the display actually dedicated to displaying the waveform. Figure 15.3 shows a high-resolution display with a waveform that has three events. Each of the events is clearly visible. Figure 15.4 shows a low-resolution display with a waveform having the same three events.

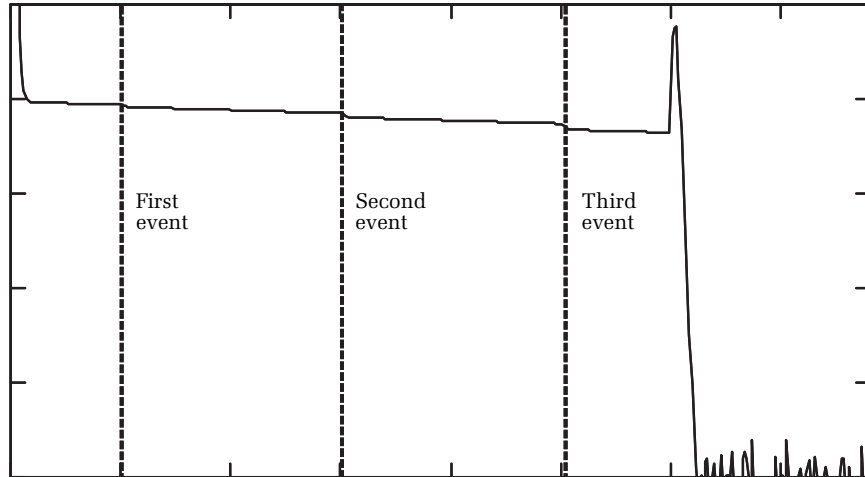


Figure 15.3. An OTDR waveform shown on a high-resolution display. Notice that all three events are visible in the unexpanded view.

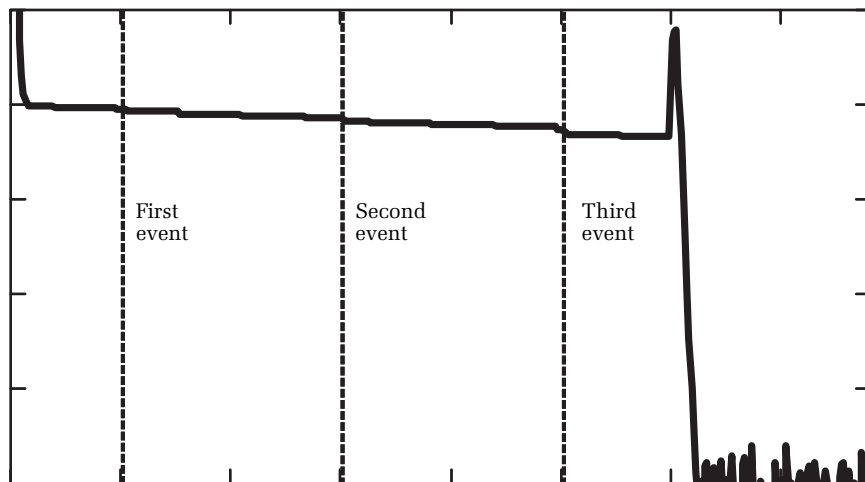


Figure 15.4. An OTDR waveform shown on a low-resolution display. This is the same fiber as shown in figure 15.3. Notice that the first two events are not visible because of the large pixel size. This shows how low-resolution displays may reduce event-detection accuracy. If the automatic event-marking software fails to find the first two events, they can easily remain undetected.

Both displays are the same size. Notice that the two smaller events are not visible in the low-resolution display.* If you expand around the two smaller events in the low-resolution display, you can see them. The problem is, if you cannot see them in the unexpanded view, you do not know where to expand the display to make them visible.

Of course, if the instrument has good event-marking software, the OTDR shows where the events are located, and then you can expand around them. If the event-marking software misses the event, however, the only alternate way of finding it is to scan the entire waveform in the expanded-view mode. This is tedious and wastes time. A high-resolution display, therefore, acts as a backup for detecting small events.

Many OTDRs allocate part of the display for softkeys and acquisition information. This is very useful, because it simplifies the human interface and makes the instrument more interactive. A possible problem occurs, however, when the design allocates too much space to nonwaveform information. The large screen loses much of its display advantage when softkeys and other such features squeeze the waveform into a small region. From the standpoint of event detection, the most important parameters are the size of the waveform (not just the display size) and the pixel size. Unfortunately, few OTDR manufacturers specify their displays in this way.

Color displays offer many advantages, but they also cost more. Still, in some instances the cost is justified by the extra functionality. Frequently the OTDR technician needs to compare two waveforms of the same fiber taken at different times. The purpose may be to check for changes in loss that have occurred since installation. On monochrome displays this can be difficult to see. To help separate the images, the OTDR manufacturer may display one waveform (the reference, for example) brighter than the other. With a color screen this waveform comparison is easier to visualize by displaying the two waveforms in different colors. Color cursors are also useful and enhance the information content of the display. The OTDR might, for instance, display the active cursor in one color and the inactive cursor in another color.

Display viewing is one of the most critical parameters for the liquid-crystal displays (LCDs) used in virtually all OTDRs. Information on LCDs is sometimes difficult to see in bright sunlight, or off angle.

*Discontinuities are visible in figure 15.4, but they are the same size as the “steps” in the display, and so are not readily recognizable as events.



Figure 15.5. A platform OTDR with a stylus. [Credit: Agilent Technologies.]

Contrast adjustment is important for these displays, and you should check viewing quality in several different types of illumination, from dim to glare to bright sunlight. Ambient temperature can affect the display contrast as well. This effect can be controlled if the instrument is designed to sense the temperature of the display and adjust the contrast bias accordingly. For viewing in dim conditions the display should have a backlight. Backlights reduce battery life, however, so be sure the backlight automatically turns off after an operator-selectable period of idle time. For users looking at mini-OTDRs used in field applications, including acceptance testing, the screen backlighting issue is critical to be able to see the screen. If the instrument will be in use for long periods, a second battery is suggested if access to AC power is unavailable.

Some OTDRs offer touch screens instead of conventional controls. While most touch screens are used manually, some instruments provide styluses for use (see figure 15.5). Whether touch screens work for you depends to some extent on personal preference. Touch screens can be difficult to operate when wearing gloves. Often you find your finger or hand covering the part of the screen you are trying to control. This can make control difficult, especially when trying to drag cursors across the display. Touch screen OTDRs usually have most or all of the controls on the display. This reduces the amount of room available for the

waveform and may limit resolution, even though the touch screen might be implemented with a large display. Since virtually all control of the instrument is achieved by touching the screen, there is the aesthetic problem of a screen that is perpetually smeared with fingerprints or scratches. On the positive side, touch screens offer a flexible human interface that is easily upgraded through software. Although not part of the display, finger pads are similar to touch screens and offer many of the same advantages and disadvantages.

15.3 Human interface

After the OTDR's display, the human interface is the most visible part of the OTDR—that part to which the operator has constant exposure. The human interface consists of the interaction between the operator and the display, control knobs, softkeys, and menus. It is the mechanism by which the operator controls the OTDR's operation. An effective human interface is one that is intuitive and easy to use, without requiring recourse to the user manual. A well-designed human interface results in fewer operator errors, more consistent and accurate testing, and less operator training. Simply put, it should be easy to learn, easy to use, and easy to remember. The human interface is, therefore, a critical component in the equation for testing efficiency and cost effectiveness.

When examining an OTDR's human interface, observe the menu structure. You should find it easy and natural to navigate through the menu structure without becoming lost. Observe the layout of the buttons and controls. An abundance of controls can be puzzling, but trying to place too much functionality into a small set of controls can be equally confusing. The best human interfaces are those that balance the need for single-function buttons and softkeys with the need to minimize the number of buttons and softkeys.

In today's computer-driven environment, the online help can be an important tool. Help screens should be informative and complete. Well-designed help screens offer real information and do not simply point out what is already obvious. For example, suppose you are selecting the pulse width and you are not sure how to continue or what the operational trade-offs are. In your quandary, you press the help button to see the significance of the pulse width selection button. A poorly designed help screen might simply read, "Selects the pulse width." This statement is, of course, obvious and of little help. A more useful statement might be, "Selects the pulse width. Selecting a longer pulse width increases dynamic range but also increases dead zone. Shorter pulse widths give

less dynamic range but have shorter dead zones. For long fibers, use a longer pulse; for shorter fibers, select a shorter pulse.” A well-designed online help function can be a useful training tool and can reduce testing errors by improving the operator’s testing efficiency.

Another important feature for a human interface is flexibility and programmability. OTDRs with configurable human interfaces allow you to custom-design aspects of your instrument. The event table, for instance, is part of the OTDR that the user should be able to customize fully. For example, you may want to customize your event table to show only distance, loss, and fiber slope while hiding reflectivity and link loss. Customizable power-up conditions, such as the acquisition parameters, are also essential.

15.4 Optical port

The front-panel connector of an OTDR consists of a precision ferrule secured inside a precision sleeve or adapter. When you test a fiber, you insert the ferrule of another plug (spliced to your test fiber) into the adapter sleeve of the OTDR. The adapter aligns the test fiber to the OTDR’s internal fiber. Because optical fibers are so small, the alignment tolerances are very demanding. If these alignment tolerances are not met (because of wear, dirt, or damage), the two fibers do not align properly, resulting in a large loss and/or high reflection. High loss at the front-panel connector directly impacts the OTDR’s dynamic range. This, in turn, results in a noisy waveform, poor measurement accuracy, and limited measurement range. High reflection at the front panel can mask close-in events. It is not surprising that when an OTDR exhibits signs of reduced dynamic range or poor resolution near the front panel, the problem is usually the result of contamination or damage to the front-panel connector.

Optical connectors are remarkably robust and are engineering marvels in their own right. These devices hold tolerances of fractions of a micron, and most of the time they properly align the fiber inside the OTDR to the test fiber. This facilitates an efficient launch of the OTDR’s laser pulses into the test fiber, resulting in maximum dynamic range. Connectors can, however, be easily contaminated or damaged. Damage usually results from inserting a dirty connector into the OTDR’s front-panel adapter. Because most connectors press the ferrule ends together, making a physical connection, particles of dirt on the end of a ferrule can easily fracture, pit, or scratch the fiber on the OTDR’s internal ferrule. Scratches, pits, and fractures result in poor coupling

efficiency into the test fiber. If you damage the internal ferrule or fiber, you cannot repair it without returning the OTDR to the manufacturer. This requires disassembling the instrument and repolishing or replacing the connector. To help prevent damage to the OTDR's internal fiber, it is essential to clean every connector before inserting it into the OTDR. While this may seem like a tedious task, it is important to resist the temptation to reinsert a connector you removed from the OTDR for "just a minute" without cleaning. Even microscopic bits of dust picked up from an otherwise clean desk can cause difficult-to-repair damage. The most important habit you should have when working with your OTDR is to properly clean every plug ferrule each time you connect it to the instrument.

Cleaning the connectors is not a difficult process and involves simple materials and tools. However, the techniques and the products used can affect the quality of the optical signal.

The most common technique for cleaning the connector involves the use of lint-free swabs designed for cleaning optical fibers. In the past, cotton swabs with a high-grade (95–99%), reagent-grade isopropyl alcohol (IPA) were used for connector cleaning. In recent years, though, IPA has been found to not adequately "lift" surface contaminants and simultaneously to leave a slim layer of surface residue that can both increase the loss and the reflection of the front-panel fiber-optic

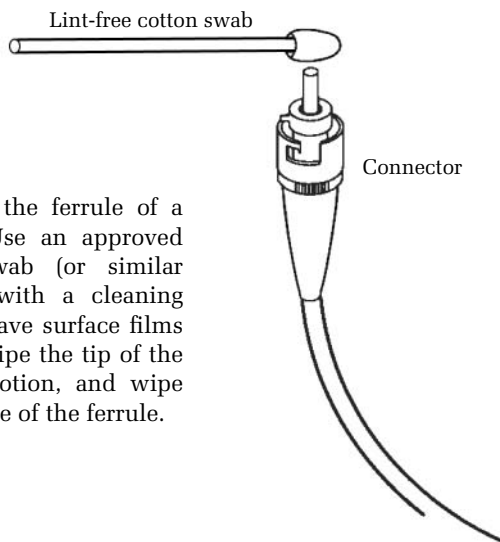


Figure 15.6. Cleaning the ferrule of a fiber-optic connector. Use an approved fiber-optic cleaning swab (or similar applicator) moistened with a cleaning solution that will not leave surface films on the fiber end face. Wipe the tip of the ferrule in a circular motion, and wipe around the circumference of the ferrule.

connector. IPA also absorbs water from the air, and water can react chemically to alter the surface chemistry of the fiber in the connector. The use of a principal hydrocarbon constituent such as isohexane does not absorb moisture as easily as IPA while leaving less surface residue.

When using this manual method, hold the connector with one hand and the approved swab with the other. Apply the cleaning solution to the swab, removing any excess, and then gently wipe the top of the ferrule and around its circumference, as shown in figure 15.6.* Follow this procedure once or twice, or more often if the connector has been heavily exposed to dirt. Examine the end of the connector by using an inspection scope with internal optical filters. You should see a smooth surface, without any blotchiness, residue, surface contaminants, or stained appearance. If contamination is still visible, repeat the cleaning process.†

Always clean the side of the ferrule *after* cleaning the fiber end. The side of the ferrule is not as subject to possible damage because it is not an optical surface (unlike the end, with its polished fiber). Also, the surface area of the ferrule's side is larger than that of the end, which reduces the significance of scratches. The ferrule's side is, however, one of the connector's precision surfaces. Due to the tight tolerances of fiber-optic components, contamination on the side of the ferrule can be pushed forward during each mating cycle. This eventually causes contamination of the fiber end face. Consequently, it is important to keep the ferrules clean and free from damage.

One of the potential problems when using swabs and alcohol is that the alcohol may be diluted or contaminated. IPA easily absorbs moisture from the air and can easily be diluted to 65% levels. If the alcohol has been contaminated, using it to clean the ferrule may leave an oily residue, and this oily residue can affect the connector's performance, especially its reflectivity (see figure 15.7). In such cases, cleaning with diluted or contaminated alcohol may actually make the connector worse, not better. One way for the solvent in any cleaning operation to become contaminated is to "double dip." Because of this, never insert a swab that

*You may also want to use compressed gas to blow off any significant particles of dirt before wiping the ferrule, especially if the ferrule is very dirty. Be careful to use an aerosol cleaner approved for fiber-optic connector cleaning.

†Some individuals also use sticky tape to clean the end of the fiber. We do not advocate this technique because some sticky tapes can leave residue that attracts dirt. Always be sure that any laser sources that may be connected to the fiber are turned off when cleaning the ferrule.

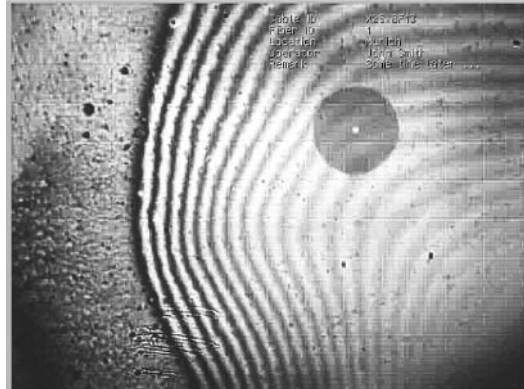


Figure 15.7. Oily residue left on the end of a connector ferrule after cleaning with contaminated solvent. [Credit: The Light Brigade.]

has been used for cleaning back into the reservoir holding the cleaning solvent.

Because you often don't have control over who uses cleaning solvents, it's often impossible to be certain that the solvent is not contaminated. To help solve this problem, several manufacturers now offer cassette-type cleaning solutions that involve pulling an encapsulated cleaning cloth or nonsticky tape through an opening where it is exposed and where the technician can draw the ferrule across it to clean the end (see figure 15.8). Such cleaning tapes are less susceptible to contamination and provide more consistently clean ferrules.

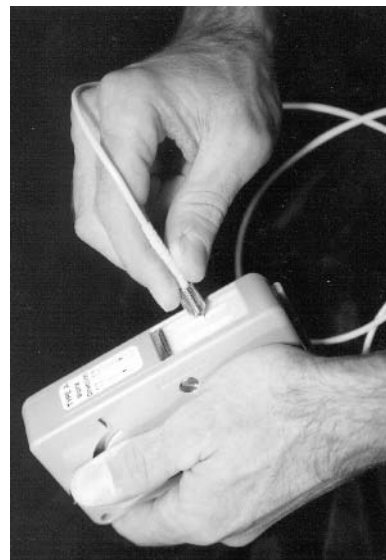


Figure 15.8. Using a cleaning-tape dispenser to clean the end of a connector's ferrule. [Credit: The Light Brigade.]



Figure 15.9. Bare fiber adaptor used at the end of a test jumper for accessing fibers. [Credit: The Light Brigade.]

After cleaning the ferrule, insert it into the front-panel connector right away. Do not set it on a table or other surface before inserting into the OTDR, due to the potential of contamination transfer. Do not put a plastic cap on it, set it aside, and then return later and insert it into the OTDR without cleaning it again. Plastic caps are good for preventing damage to the connector's ferrule, but they do not guarantee that microscopic dirt particles (the kind that can scratch the fiber in your OTDR) will not contaminate the ferrule's end. In fact, many dust caps are contaminated during the injection-molding manufacturing process and are a cause of contamination transfer to the ferrule's end face.

Consistent and careful cleaning of every connector that goes into your OTDR helps to extend its life and ensure that it is always in peak operating condition. Even so, accidents can happen. To add another layer of safety to your OTDR, we recommend that whenever possible you use a jumper that is left attached to the OTDR all the time. Rather than connect the test fibers to the OTDR directly, attach them to the test jumper (the jumper typically is only about 0.5 meters long). When the day's testing is completed, leave the jumper attached to the OTDR, and cover its connector with a protective cover. The same philosophy applies to the use of bare fiber adapters (BFAs) (see figure 15.9), which allow access to bare fiber ends during acceptance testing. Rather than plug the BFA

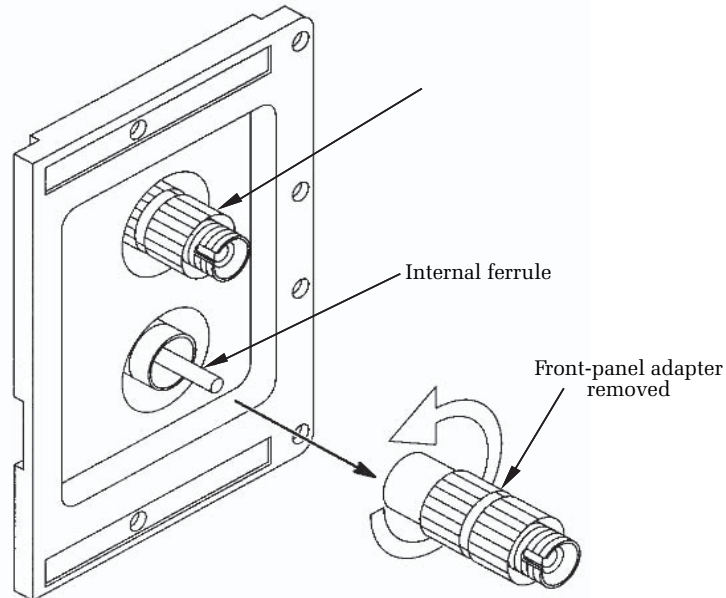


Figure 15.10. Removable, reconfigurable front-panel adapter. This feature allows you to clean the internal ferrule easily. A dirty internal ferrule can significantly reduce your OTDR's dynamic range, and it is the most common cause of poor OTDR performance. Without a removable front-panel adapter, you must send the OTDR back to the manufacturer or open the instrument's case and disassemble it. The removable, reconfigurable front-panel adapter also allows the type of connector that interfaces to your OTDR to be changed easily in the field.

directly into the OTDR's connector port, plug the BFA into the end of a test jumper. Remember that the acceptance testing of seven cable reels of 144 fibers each requires over 1000 fiber matings to the OTDR's internal connector. In this way, if damage occurs it is more likely to happen to the test jumper rather than the OTDR. Jumpers are much easier and less expensive to repair or replace than your OTDR.

Note: During acceptance testing, the operator also has the option of using mechanical splices instead of a BFA.

In spite of your best intentions, one thing you can be sure of is that eventually your OTDR's internal front-panel connector will get dirty. Even if you clean each connector, small bits of oil (especially from fingers) can remain on the ferrule. Contaminants exist in the air around us. These contaminants can find their way into the OTDR's front panel

and deposit themselves on the end of the internal connector. When you insert the ferrule, particles of material from the inside of the adapter can be scraped off, pushed into the adapter, and deposited on the end of the inside ferrule. These possibilities for contamination lead to one of the most important design features your OTDR can have: a removable adapter that allows quick and easy cleaning of the front-panel ferrule (see figure 15.10).

One purpose of the removable front-panel adapter is to allow easy cleaning of the internal ferrule. Another purpose is to allow easy field reconfiguration of the OTDR for different connector types. To meet these conditions, the front-panel adapter must be easy to remove without tools. Screwing the adapter off with fingers is preferable; using coins (as screwdrivers) is acceptable. Removing individual screws with a screwdriver while handling dangling fiber connectors is a situation to avoid.

Before cleaning the ferrule in the OTDR's front-panel connector, be sure you have cleaned the jumper or test fiber you are using and that the problem does not reside there. Every cleaning operation carries with it the risk of damage, so be sure that cleaning the internal OTDR ferrule is necessary before proceeding with the operation. After removing the front-panel adapter, clean the exposed ferrule just as you would any other connector. Also clean the adapter. To do this, blow through the barrel with compressed air, and then run a pipe cleaner (saturated with alcohol) through the barrel (see figure 15.11). Do this several times, and

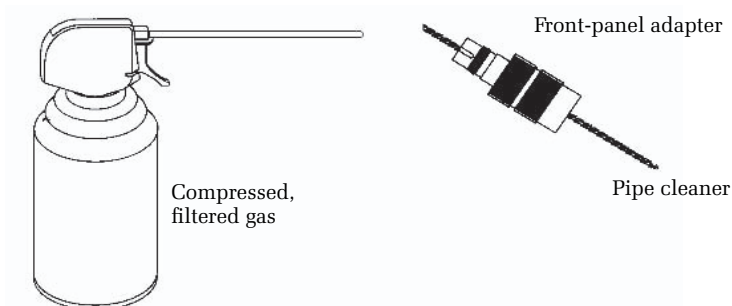


Figure 15.11. Cleaning the front-panel adapter. Blow through the adapter first with clean, compressed gas. Then moisten a pipe cleaner with isopropyl alcohol and run it through the adapter several times. Follow by blowing through the adapter again and visually inspecting to be sure no fibers from the pipe cleaner remain in the adapter. Repeat this procedure as necessary.

finish by blowing through the barrel one last time. After cleaning the ferrule and adapter, replace it as soon as possible to avoid any inadvertent damage or contamination to the internal ferrule. Follow this cleaning procedure each time you replace the adapter when reconfiguring for a new connector type.

15.5 Accessories, options, and features

The accessories and features you need for your OTDR depend mostly on how you intend to use it. Some accessories and features to consider include:

- Interchangeable front-panel connectors
- Battery charger
- DC cigarette-lighter cord
- Wide range of operating and charging voltages
- Carrying case (for durability and protection, storage of instrument and accessories) and items like spare fuses
- Easy-to-use user interface (UI) that includes a usable help menu
- Quick-reference card
- Keyboard
- Parallel and serial interfaces for direct download to PC, for remote operation, and printer option
- Printer
- Floppy-disk drive
- Memory card
- Solid-state internal memory
- Internal hard-disk drive
- VGA output
- Visible light sources, power meter, stable light sources
- Programming options
- Default options (default at startup, etc.)
- Optical return loss (ORL) measurement capability
- Factory support, warranty, and training
- Built-in functionality for acceptance testing, restoration, two-way loss measurements, etc.



Figure 15.12. Modular platform OTDR. [Credit: Agilent Technologies.]

- Dynamic range and resolution (for both reflective events and loss measurements) that support your testing requirements
- OSP software to map OTDR traces to GIS systems for as-built records
- Capable and effective real-time mode

When examining accessories, consider the OTDR's modular structure and the available optical modules offered by the manufacturer. For example, a fiber installer who works routinely with both single-mode and multimode fiber may want an OTDR that can hold two optical modules simultaneously (multimode and single-mode). Alternatively, you may choose an OTDR that holds only one module at a time, but one in which the optical modules can be quickly and easily exchanged. Modularity has the additional advantage of allowing easier field upgrades of the instrument's performance when new modules with enhanced features and performance become available from the manufacturer. Additionally, if a module fails, you can replace it and send the damaged part in for repair. This reduces downtime and helps improve testing efficiency. For optimum flexibility you may want to consider a manufacturer that provides modules besides OTDRs, such as

inspection microscopes and optical spectrum analyzers. Such modular platforms (see figure 15.12) result in a multifunction optical toolbox that can become the most important piece of equipment you use in maintaining your fiber-optic system.

Depending on your application, you may or may not want all of your accessories built into the OTDR. For example, suppose you need to document a fiber installation with printouts of the waveforms and event tables. One approach would be to print the waveforms and event tables in the field at the same time as you perform the testing. If this is your methodology, you might prefer an OTDR with a built-in printer. Another way would be to save the test data to internal memory, or on floppy disk, and then print it when you return to your office. If this is your methodology, you might prefer an OTDR with a separate printer that interfaces via serial or parallel port.

Power meters and light sources are two other instruments commonly used to test fiber-optic lines. Sometimes light sources and power meters are used to install the system, and an OTDR is used for qualification and documentation. Because they are often used together, some OTDR manufacturers offer light sources and power meters built into their instruments. For some applications, this may be beneficial. Other times, it may be cumbersome to carry the OTDR when all you need is a pocket-sized power meter or light source. In situations such as this, you might consider an OTDR with separate power meter and light source that fit into the OTDR's carrying case.

15.6 Safety

Virtually all OTDRs test optical fibers with high-powered optical pulses. It is natural, therefore, to consider issues of laser safety when using these instruments. Governmental agencies in the United States and Europe have developed strict guidelines for laser safety.^{2,3} Part of these guidelines is a system of classification for laser products, based upon their likelihood of causing serious personal injury, such as blindness. The safest category of laser is called Class I.* Class I laser systems are either inherently safe or totally enclosed systems. With very few

*Class I per 21 CFR 1040 is the FDA or CDRH classification (US). Class 1 per CEI/IEC 825-1: 1993 is the international classification. The American Standards Institute (ANSI) has released standard Z136.2-1997 to address the concerns of organizations and personnel involved with the use of optical systems. Also, you may want to consult *For the Safe Use of Optical Communications Systems Utilizing Laser Diode and LED Sources*, published by the Laser Institute of America, Orlando, FL, www.laserinstitute.org.

exceptions, commercially available OTDRs are Class I laser products.* Those OTDRs that are not Class I must carry the appropriate warning labels and safety interlocks. The OTDRs most likely to exceed Class I are instruments using Nd:YAG lasers or optical-fiber amplifiers. If you have specific concerns about the laser safety of your OTDR, you should contact the manufacturer.

OTDRs can emit pulses of laser light that have peak powers well in excess of 50 mW. For many laser sources, such power levels would rate the equipment much higher than Class I. OTDRs maintain their Class I status for three reasons. First, OTDRs usually operate in the near-infrared region. The shortest wavelength is usually 850 nm for multimode OTDRs and 1310 nm or 1550 nm for single-mode OTDRs. At these wavelengths, the eye's lens, vitreous humor, aqueous humor, and cornea (see figure 15.13) are considerably more absorbent than

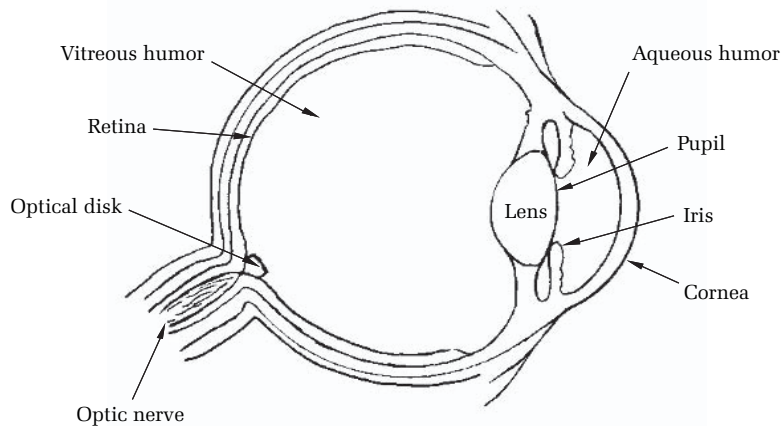


Figure 15.13. Cross-sectional illustration of the human eye. For light to reach the photosensitive receptors on the retina, it must first pass through the cornea, the aqueous humor, the lens, and the vitreous humor. At infrared wavelengths, absorption in these regions of the eye helps minimize the maximum irradiance at the retina. The light from optical fibers diverges. When held at normal viewing distances, the light from typical optical fibers overfills the iris. Light that is blocked by the iris does not reach the retina, so overfilling combines with attenuation to limit the irradiance of the focused spot in the eye.

*Increasingly, some OTDR manufacturers are offering their products with a CW mode (the laser is turned on continuously). In this mode, the instrument operates as a light source and not as an OTDR. When operating in CW mode, these instruments may exceed Class I specifications. See the manufacturer's instrument manual to determine the laser classification of your OTDR.

they are in visible light.^{*4} Because of this absorption, the light is highly attenuated when it reaches the retina. By nature, the eye concentrates light to a tightly focused distribution at the retina, while in the rest of the eye the energy distribution of the light is spread out, resulting in low peak irradiance. Consequently, attenuation in the bulky parts of the eye occurs where the irradiance is low, which helps protect the retina from excessive irradiance at the eye's focal point.

The second reason OTDR radiation is usually Class I is that the light from an OTDR is not collimated. Recall from chapter 2 (using the ray approximation) that optical fibers guide only light that diverges less than a critical angle defined by the fiber's numerical aperture. As the light from an OTDR emanates from the optical fiber, it diverges. When you hold an optical fiber at a normal viewing distance (about 21 cm), the light distribution from the fiber overfills your eye's iris. For example, a single-mode fiber diverges with a full angle of about 14°. At 21 cm, therefore, the irradiance distribution is roughly 5 cm in diameter. A fully adapted human eye, however, has an iris diameter of only about 7 mm, so the light distribution from the fiber greatly overfills the eye.[†] Because of the iris, only a fraction of the light from the fiber enters the eye, and this further attenuates the radiation reaching the retina.

The third reason OTDRs are inherently safe is they do not emit continuous radiation.[‡] OTDRs emit pulses of light that usually do not last more than 10 or 20 microseconds and that are often only a few hundred nanoseconds long. To accommodate the roundtrip time for the pulses to travel down the fiber and back, the duty cycle (time the laser is on, divided by the time the laser is off) is usually only a few percent or less. This means the laser's average power is often less than a milliwatt, although the maximum power might be many tens of milliwatts.

Absorption in the eye, divergence, and low duty cycle combine to make most OTDRs Class I instruments. Although they are classified as inherently safe, you should still avoid exposure to the light that is

*Absorbency at 850 nm is less than at the other wavelengths. Other considerations, such as very short pulse widths, help to make OTDRs operating at 850 nm safe.

†The overfill is not, however, proportional to the ratio of the areas of a 7-mm disk and a 50-mm spot. This is because the light distribution is roughly Gaussian, so it is more heavily weighted toward the center.

‡As noted earlier, some OTDRs do have a mode where the light source is left on continuously. In this mode, these OTDRs may exceed Class I levels for laser radiation. If you have any questions about the laser safety classification of your OTDR in any operating mode, you should contact the manufacturer.

emitted by the OTDR. Do not stare into the instrument's front-panel connector while the instrument is testing. Similarly, do not stare into the free end of a fiber that is connected to the OTDR while the instrument is testing. You are most likely to view the front-panel connector or a free fiber end when cleaning. To avoid unnecessary exposure, be sure the OTDR is not testing when you clean the front connector or any fibers connected to the OTDR. It is especially important to ensure that the OTDR is never operating when connected to a fiber that is being inspected with a microscope without an internal safety filter that meets your requirements.

15.7 Performing a fiber-acceptance test

Technicians who work with optical fibers in field applications must put all the lessons and knowledge together to hone their skills. OTDRs can be easy instruments to operate, but the knowledge of how they work and the fibers and components they test are what develops a technician from the apprentice to the journeyman level. The following sections apply to the most common tasks required of the technician working in premise and outside plant installations.

The purpose of the acceptance test is to make sure that the optical cable received matches both the optical and physical requirements of the order requisitioned. It is important that the operator know the criteria for the values such as length, fiber count, decibels-per-kilometer attenuation at the wavelengths applicable for their needs. This is normally 850 and 1300 nm for multimode applications and most commonly 1310 nm and 1550 nm for single-mode networks. For DWDM and long-haul trunk applications, where the 1550-nm window will be used, the 1550- and 1625-nm wavelengths are recommended for testing. The acceptance test also will include cable characteristics, including jacket, armoring, and construction. The acceptance test is also the best opportunity to adjust the fiber's index of refraction to match the sequential markings of the cable jacket prior to installation.

The OTDR operator must first organize a safe and effective work area for testing the cable. While most OTDR acceptance tests will take place at a receiving location, they are also performed in many diverse field environments. This should be considered for proper preparation. A table designed for fiber-optics work (see figure 15.14) is excellent for securing and organizing the optical cable, organizing tools, and providing a good, comfortable, and safe work surface for the operator and the OTDR.



Figure 15.14. A fiber-optic worktable used for acceptance testing. [Credit: The Light Brigade.]

15.7.1 Sequential steps of an acceptance test

1. Visually inspect the cable reel for shipping damage.
2. If cable documentation is attached to the reel, attach a copy of this information to the acceptance test form. There is traceability information on this report, along with optical test data (e.g., dispersion specifications), that should be forwarded to the engineering department.
3. Prepare the end of the cable for fiber access. On the acceptance test form, enter the sequential markings from both ends of the cable.
4. Organize the fibers based on industry-standard color code (TIA/EIA-598B).
5. Set up the OTDR for the tests to be performed.
6. Prepare and connect the pigtail and mechanical splices to the OTDR (see figure 15.15).
7. Strip and cleave fibers (organize 12 fibers at a time).
8. Insert fibers in proper sequence into the mechanical splice, and test.

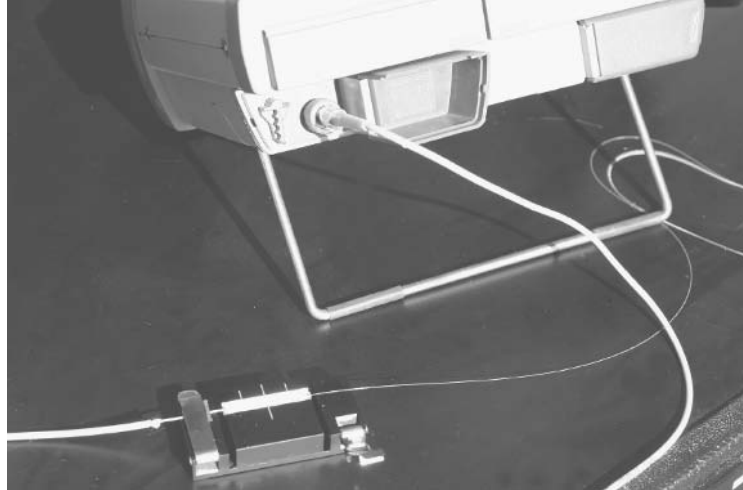


Figure 15.15. OTDR with pigtail and mechanical splices for testing optical fibers.

9. With the OTDR in real time, cleave the far end of the blue fiber and see if the Fresnel reflection changes (increases its height). If the reflection changes, this means the fiber is intact from end to end.
10. Place the B marker at this location, and increase the horizontal zoom for proper setting.
11. This distance measures from the front connector panel of the OTDR to the end of the cable. If using a test jumper, subtract the length of the test jumper. Many OTDRs have a function to subtract the length of any test jumpers or dead zone launch boxes used so that the extra length isn't added to the fiber under test.
12. Adjust the index of refraction to match the actual cable length. The best time to adjust for this number is during acceptance testing. This information should be forwarded to those in charge of maintenance and restoration. This will help tremendously in locating problems more accurately during restorations.
13. When measuring all the other fibers, make sure the end reflection is located at this same point (because all fibers should be the same length in the cable structure). If any fibers are not to this point, this would imply that the fiber is damaged or stressed within the cable structure and would require further investigation. One exception is if the cable structure is in two rows of buffer tubes, in which case all the outer rows will show a longer length than all the inner rows.

14. Check the requirements of the acceptance test: length, fiber count, cable structure, decibels per kilometer at each wavelength, sequential markings (footage or metric). These tasks will verify that the product being tested meets the order specifications.
15. Document fiber results (length and decibels per kilometer).
16. Check the optical performance tests (decibels per kilometer and length), and verify pass/fail criteria.
17. Trim each exposed fiber back 50% of the length after each test.
18. After all fibers have been tested, count your fiber traces (soft copy) or printouts (hard copy).
19. If the count of traces/printouts is accurate, cut back the remaining 50% of the exposed fiber length and properly reseal the cable ends.

15.8 Measuring the splice attenuation

During splicing, the need to identify the physical location of the optical splice, document the sequential numbers of the cable jackets, and document the optical attenuation of the splice is standard industry practice.

If the fiber has been pigtail spliced at the patch panel, the OTDR can be connected directly to the corresponding connector port. If the fiber has not yet terminated the process involved in the acceptance test, a mechanical splice or bare fiber adapter can be used to access the fiber to be tested.

Most organizations have established criteria for attenuation for an acceptable splice loss. If we use a common value of 0.1 dB/splice per the TIA/EIA 758 Customer Owned Outside Plant standard, we must make sure that the splice loss is equal to or less than the specified maximum value. Since all single-mode fibers have tolerances of the mode-field diameter of $\pm 0.5 \mu\text{m}$ and cladding of ± 1 micron, this means that measurements will also vary depending on the fibers and the direction of the tests. This means that we must understand the basics of how OTDRs work and the relationship to the measurements being performed. Fiber tolerances vary, which means all fibers being spliced together will have various loss measurements. This also means that the tests should be performed bidirectionally on each fiber for each splice. We also must test at both 1310 and 1550 nm for single-mode fibers and 850 and 1300 nm

for multimode fibers, because fiber attenuation is wavelength specific. If mechanical splices are used, then the additional task of measuring optical return loss is required.

The three main causes of incorrect splice-loss measurements are: (1) the pulse width is set incorrectly; (2) the number of averages is inadequate; and (3) the measurement technique is used improperly. Additional problems can include (4) fiber tolerances that create circumstances where high losses occur in one direction, creating a gain splice in the opposite direction; and (5) a bad launch from the connection or splice at the OTDR.

15.8.1 Corrective actions

1. If the pulse width is too low, the OTDR trace will be low on the screen approaching the noise floor. By increasing the pulse width, it is easier for the OTDR to analyze the backscatter levels both before and after the splice locations.
2. If the number (or time) of averages is inadequate, the trace will appear noisy. This makes it difficult to measure the amplitude variances in the two linear traces before and after the splice itself. By increasing the averages, the trace will be much smoother, and it will be easier for the instrument to take a repeatable and reproducible measurement.
3. OTDRs can measure performance of a splice using two-point or LSA techniques. The major difference is that two-point loss measures all the loss between the two markers (cursors). This distance is based on and limited by the pulse width of the laser itself. For example if the operator sets the OTDR to use a 100 meter pulse width (1/10 km) and the fiber has an attenuation specification of 0.4 dB/km, then the fiber will have 0.04-dB attenuation in the 100 meters of fiber between the two cursors. If the two-point loss is 0.12 dB, then the actual loss would be 0.08 and would pass. However, those looking at the test results would see the 0.12 dB, so the splice would be “out of spec.”

Measuring the same splice using the least-square approximation (LSA) technique only measures the amplitude (decibel) change between the two backscatter traces. For this reason it is recommended that the OTDR use the LSA technique whenever possible in measuring splice attenuation.

The only time that a two-point technique should be used to measure splice loss in a single-mode fiber is when measuring the closest splice in a span. In this circumstance, the pulse width may only be 10–50 meters in length and the fiber loss negligible. Two-point measurements are still valid for distance measurements to locate faults from a previous known location, such as in emergency restorations. Because spans are much shorter in multimode fibers, the pulse width of the OTDR is much smaller and the associated loss between the two points is negligible. Industry-specified splice-loss values for multimode fibers are also specified as 0.3 dB in the TIA/EIA 568 specification.

4. If the operator is measuring a splice loss in the A–B direction and the loss doesn't pass specification, the normal procedure is to resplice and retest. If this occurs, it is normal to resplice up to three times and, if the splice still doesn't meet the specification, to accept the last measurement and then test in the opposite (B–A) direction. If the splice tests as a gain in the opposite (B–A) direction, this is called a *gain splice*.
5. Because the OTDR must send and receive the laser's pulse, the quality of the connection at the OTDR's connector port, the patch cord used to access the network, and a temporary mechanical splice used in acceptance testing all affect the power level being transmitted, received, and measured. Always make sure that the correct type of connection and polish is used at the OTDR.

15.9 When should OTDR traces be taken?

When to test splices can create another problem that each organization needs to define. Options include:

1. Measure the splices while the splice crew is at the site. This is beneficial because if the splice doesn't meet specification, it can be respliced immediately. However, if the splice is good and during the final closing of the tray or splice closure the fiber or buffer tube is stressed, then the splice location will look bad during the final span measurements. This can be confirmed by performing dual-wavelength testing to isolate the fiber splice loss vs. stresses caused by micro- or macrobends.
2. The "splice now and OTDR test the span later" technique does save money, but it requires all "out-of-spec" fibers to be respliced and retested later, eventually increasing the cost of the splicing. Some

contractors and users prefer this technique and believe that, with good equipment, OTDRs, and experience, it is the best method.

3. Most current fusion splicers have an estimated loss function, which takes into account the basic fiber geometries to measure a splice. The only problems with this technique are that it isn't always accurate and it provides no trace information for later maintenance and overlay capabilities that the OTDR does provide.

15.10 Span measurements

When testing a fiber span after installation, the intention is to confirm and document all the applicable measurements for proof of performance and for future maintenance and restoration records. Span testing using the OTDR is basically a summary of all the tests performed as a completed system. It consists of many types of measurements and displays the entire fiber-optic physical plant under test.

15.10.1 What measurements are required?

Splice loss (decibels). Even though the splices have been individually tested, this test will also have all fiber-length and loss information on all segments.

Attenuation measurements of fiber segments (dB/km). Each segment will now be identified with distance and decibels-per-kilometer attenuation measurements.

ORL of reflective components (decibels). All connectors are reflective to some degree. The task now is to confirm the reflectance of each. Most OTDRs can identify the reflective loss if the instrument is configured and set up properly. To test both the front-end and far-end reflections requires specific products and matched connectors and polishes.

Testing the front connection. Due to the OTDR's pulse width, the first events are normally hidden in the trace (inside the dead zone). To be able to measure, we must then have a dead zone box, which would include 20 times the length of the shortest pulse of the OTDR's pulse width. If the shortest pulse width on the OTDR is 10 meters, then a dead zone box must have 200 meters of fiber internally stored.

Far-end connection. To measure the ORL of the far-end connection requires the use of a terminator. A terminator is a modified plug with the mating surface of the fiber polished to match the connector at the far-end location (e.g., FC/APC). The fiber at the other end of the plug is dead-ended by the manufacturer so that no light is reflected from the fiber's

end. This modified plug will mate to the connection and allow reflective measurements to be taken at the glass-to-glass surface of the far-end connection. If a terminator or dead zone box isn't used at the far-end termination, then the resulting reflection measurement of approximately 14 dB will be erroneous.

Optical splitters. Depending upon the application, optical splitters may be used in the span. If a 50/50 (3-dB) splitter is used, the OTDR will measure the loss through the splitter plus the adjacent pigtail splices (two in any path). If the split loss is equal, then the trace should drop 3 dB. Because the two equal "split" traces will overlay each other, the only way to distinguish between them is via their differing lengths and the resulting far-end reflections.

Accumulated loss. The OTDR can add the accumulated loss in an event table for easy review of components and system losses.

Dual-wavelength testing. Fiber attenuation is wavelength specific. Testing at both wavelengths allows for accurate loss measurements of all components. Dual wavelength testing will also identify any externally caused micro- and macrobends in the span. The ability to overlay dual-wavelength traces is critical in troubleshooting and recognizing faults. Saving OTDR measurements allows you to save waveform displays of the traces, details, and parameters of how and when the test was performed. This allows the user to recall and analyze trace information and to overlay traces for comparison and troubleshooting tasks.

Bidirectional testing. Since loss and event locations will vary from different directions, it is recommended that all spans be tested bidirectionally at both wavelengths. This will also resolve issues related to what appears to be out-of-spec splices that are actually gain splices. This will assist in emergency restorations when overlaying an older trace with a new trace from a specific location may be required.

Pass/fail analysis. Most organizations have fiber-optic criteria based on decibels per kilometer, ORL, and splice attenuation. Many OTDRs have a pass/fail capability that can be preset for quick identification of "out-of-spec" measurements.

15.11 Field technician's top-ten list

1. Easy-to-use setup screen
2. Personalized defaults for applications
3. Quick changes to real time from averaging, and from averaging to real time

4. Event table with applicable data on screen
5. Simple store, recall, and overlay capabilities
6. Dropdown menu with common fiber specifications for testing
7. Optical return loss (ORL) capability
8. Light weight and portability
9. Easy conversion from fiber index of refraction to match cable sheath length
10. Good screen display for brightness and signature resolution

15.12 Summary

OTDRs are without doubt the most versatile and useful tool for installing, repairing, maintaining, and documenting optical fiber for telecommunications networks. These tools have evolved from their somewhat humble beginnings to become sophisticated machines with built-in intelligence that allow technicians to perform tests in less time and with greater accuracy than ever before.

As they have evolved, OTDRs have acquired many advanced features. Foremost among these latest advances is the ability to perform waveform analysis and automatic event detection and measurement. In this chapter we have examined some of the practical features of OTDRs. From carrying case to replaceable modules to accessories and cleanable connectors, today's OTDRs provide test technicians with the latest in advanced capabilities.

It will be interesting to observe how OTDRs continue to evolve. We expect OTDRs to become even smaller and more powerful. We also expect much of the future improvement in OTDRs to be in the area of enhanced software capability. No matter what evolutionary path the OTDR follows, however, the well-informed and knowledgeable technician is always best prepared to meet the challenges of the future. Hopefully this book helps with this, the most demanding challenge of all.

Problems

1. True or false: When cleaning a jumper, before connecting it to the OTDR, it is okay to lay the cleaned connector on your worktable while doing other work.
2. True or false: One should never look at the end of an optical fiber that is connected to an OTDR while it is testing.

3. True or false: A well-designed OTDR has no need of a replaceable front-panel connector, because well-designed OTDR connectors never get dirty.
4. True or false: A fiber-optic jumper, left attached to the front panel, can help reduce wear on the OTDR's front-panel connector.
5. True or false: To test the front-end and far-end connectors for optical return loss, a dead zone box and optical terminator are recommended.

¹ Bellcore, *Generic Requirements for Optical Time Domain Reflectometer (OTDR) Type Equipment*, GR-196-CORE (1995).

² *Code of Federal Regulations*, Food and Drug, 21, Parts 800–1299.

³ International Standard, CEI IEC 825-1.

⁴ McKinlay, A. F., Harlen, F., and Whillock, M. J., *Hazards of Optical Radiation* (Bristol, CT; Adam Hilger, 1988).

Appendix A

Glossary of Terms

A

Absorption Optical absorption results when photons stimulate molecular resonances, changing the photons into heat energy.

Acceptance angle An angle that defines the acceptance cone for an optical fiber. Light within the cone can couple into the fiber and be guided. Light outside the cone may enter the fiber but is not guided. Consequently, outside light quickly decays and is not transmitted by the fiber.

Acquisition The act of obtaining a waveform on an OTDR.

Acquisition parameters The OTDR settings required to obtain and display a waveform. Not all of these may be user selectable. They include index of refraction (IR), wavelength, pulse width, range, and averaging time.

Aliasing An effect that introduces spurious signals (or attenuates real ones) when a repetitive signal is undersampled.

Amplitude modulation (AM) A method of adding information to an electronic signal in which the signal is varied by height to impose information on it. The information being carried causes the height of the sine wave (amplitude) to vary.

Aperture An opening that allows some light to enter while blocking the rest. A good example is the iris in the human eye.

Attenuation The loss of optical signal power. In applications involving fiber optics, attenuation is usually expressed in decibels (for discrete components such as splices) or in decibels per unit length (for fiber). Attenuation in fibers results from absorption and scattering. These in turn are caused by impurities in the fiber and the fiber's intrinsic material properties. Loss in discrete events results from bending, mode mismatch, or core misalignment. Since fiber loss is a function of fiber length, signal amplitude decreases as fiber length increases.

Automatic mode A test mode available with some OTDRs. In automatic mode, the OTDR selects its acquisition parameters, acquires the waveform, and analyzes the waveform for events.

Avalanche photodiode (APD) A solid-state device that converts photons to electrical current. High electric fields accelerate the charge carriers to a kinetic energy greater than the ionization energy. This allows them to create additional charge carriers, resulting in current amplification.

Averaging The amount of averaging (expressed in time or counts) performed by the OTDR in acquiring a waveform. Increased averaging reduces noise and improves dynamic range.

B

Backscatter The portion of Rayleigh scattering that couples into the optical fiber and travels in the opposite direction of the optical signal (see Rayleigh scattering). OTDRs measure the optical loss of an event by measuring the attenuation in the backscatter across the event.

Backscatter coefficient A measure of the amount of backscatter from a 1-ns pulse. Specifically, it is 10 times the base-10 logarithm of the ratio of the backscatter from a 1-ns pulse divided by the power in the pulse. The backscatter coefficient is used to calibrate reflectivity measurements made with the OTDR.

Bandwidth The capacity of an optical fiber to transmit information. It is also a measure of the speed with which an electrical system can respond to a changing input signal. The larger the bandwidth, the more information can be transmitted over the fiber in a given amount of time.

Bellcore A technical service provider that supports, among other things, efforts aimed at defining technical standards for the various regional Bell operating companies (RBOCs).

Bending loss The result of macrobends (curvature of fiber) or microbends (small distortions in the fiber) producing increased attenuation by coupling light energy from the fiber core to the cladding.

Birefringence Polarization-dependent index of refraction. Birefringence in optical fibers is caused by physical asymmetries and strain.

Bit-error rate (BER) The incidence of bit contamination in an information-carrying signal. A bit-error rate of 10^{-9} means that out of 10^9 bits, only one (on average) is wrong.

Bragg cell A piece of photorefractive fiber that is exposed to high-intensity ultraviolet interference patterns that will cause it to reflect a specific wavelength while being transparent to all other wavelengths.

Buffer A pliable, protective covering that surrounds a fiber's cladding. The buffer protects the cladding from nicks that might become cracks. It also helps prevent the fiber from being bent so tightly that it breaks.

Buffer coating A material with no optical function that covers and protects a fiber.

Buffer tube A secondary plastic coating either loosely or tightly adhered around the coating of an optical fiber to provide additional protection against damage. It can be either white, for cordage, or colored, in reference to the standard color code for multiple fiber-optic cable assemblies. Fabrication techniques include tight jacket or loose tube buffering as well as multiple buffer layers.

C

Cable A physical restraint that supplies strength and protection to one or more optical fibers within it.

Cabling factor The length of fiber in a cable divided by the length of the cable. The fiber is longer than the cable because it is wound as a spiral to avoid stresses applied to the cable. Consequently, the cabling factor is always a fractional number greater than 1.

Cathode-ray tube (CRT) A display device used on some older OTDRs.

Chromatic dispersion The group velocity of a laser pulse in fiber is a function of wavelength. A pulse composed of more than a single wavelength thus disperses (spreads out) as the different wavelengths travel along the fiber at different speeds. Chromatic dispersion is a measure of the spreading of the pulses due to spectral bandwidth of the source.

Cladding A layer of optically clear material, such as glass, that is fused to and surrounds the core of an optical fiber. To operate properly as a waveguide, the fiber's cladding must have a lower refractive index than the core. In glass fibers, the cladding is typically 125 microns in diameter.

Coarse wavelength-division multiplexing (CWDM) Applies to greater separation of wavelengths than DWDM. In the case of single-mode applications, CWDM defines 20-nm separation from 1470 to 1610 nm. With multimode fibers, the wavelengths are 778, 800, 825, and 850 nm. CWDM devices have a channel wavelength spacing less than 50 nm but greater than 1000 GHz (about 8 nm at 1550 nm and 5.7 nm at 1310 nm) and can cover several spectral bands.

Coherence The degree to which the phase and wavelength of a group of photons are correlated. When highly correlated, the light is very coherent; when not correlated, the light is incoherent.

Coherent-detection OTDR An OTDR that uses phase and amplitude information in the return optical signal to boost system dynamic range.

Collimating Photons from a normal light source, such as an incandescent light bulb, travel in all directions. In a collimated source, all photons travel in nearly the same direction. A collimated source produces a beam of light that remains constant with distance from the source, except for diffraction effects. [Note: Over large distances, diffraction effects can dramatically increase the beam's size.]

Connector Optical connectors are mechanical devices for aligning the cores of two fibers so that light can transmit from one to the other. Connectors are similar to mechanical splices, but they are designed to make connection and disconnection easier.

Continuous-wave (CW) reflectometer A device used to measure the total reflectance or return loss of an optical fiber, but not to distinguish the individual reflectances of distributed events.

Core The center of an optical fiber, where most of the light is carried. To operate properly as a waveguide, the fiber's core must have a larger index of refraction than the cladding.

Correlation OTDR An OTDR that uses coded pulse patterns to boost system dynamic range.

Coupler When used in one configuration, a device for splitting the optical signal from one fiber into two or more fibers. When used in an alternate configuration, this is a device for combining the optical signals from two or more fibers onto one fiber.

Critical angle An angle that defines the onset of total internal reflection.

Critical bend radius The radius at which further bending results in excessive loss.

Cut-back method A technique for measuring fiber attenuation or distortion by performing two transmission measurements. One is done at the output end of the full length of the fiber. The other is usually done within 1–3 m of the input end and accessed by “cutting back” the test fiber to determine the change in pre- and post-cut-back measurements.

Cut-off wavelength The wavelength that defines the boundary between single-mode and multimode operation of an optical fiber. At wavelengths shorter than the cut-off wavelength, the fiber is multimode. At longer wavelengths the fiber is single-mode.

CW Continuous wave or center wavelength.

CW reflectometer See Continuous-wave reflectometer.

D

Dead zone box Used for testing the front connection located within the dead zone of the OTDR. The TIA/EIA 455 standard recommends an internal length of up to 20 times the length of the shortest pulse of the OTDR's pulse width. If the shortest pulse width on the OTDR is 10 meters, then a dead zone box must have 200 meters of fiber internally stored. This allows the OTDR to measure both attenuation and ORL values. For optimum results, the connector should match the type and polish of the fiber under test.

Dead zone event (Sometimes called the two-point spatial resolution.) The minimum distance after a reflection before the OTDR can accurately measure the distance to a second reflection. Sometimes it is determined as the distance from the leading edge of the reflection to the point past the reflection where the OTDR signal drops at least 3 dB from the top of the reflection.

Dead zone loss The loss-measurement dead zone is intended to be the minimum distance after a reflective event before the OTDR can accurately measure the loss of a nonreflective event. Usually, however, it is not defined in conjunction with the OTDR's event-marking software. Typically, it is determined as the distance from the leading edge of the reflection to the point past the reflection where the OTDR signal returns to within 0.5 dB of the backscatter level. An alternate definition is the distance from the leading edge to the point where the OTDR signal returns to within 0.1 dB of the backscatter level.

Decibel (dB) A unit of measure comparing two power levels; defined as 10 times the base-10 logarithm of the ratio of two power levels. A gain or loss in

power is expressed in decibels. For example, a 3-dB loss is an approximate 50% decrease in power, a 2-dB loss is an approximate 37% decrease in power, and a 1-dB loss is an approximate 21% decrease in power.

Dense wavelength-division multiplexing (DWDM) Combining four or more wavelengths into an optical window (e.g., 1550 nm). DWDM devices have a channel spacing less than or equal to 1000 GHz and can cover one or more spectral bands.

Detector, optical A device that generates an electrical signal (typically an electrical current) when exposed to light. Common types are PIN and APD.

Differential group delay (DGD) The difference in transit times through an optical fiber for orthogonal polarization states.

Diffraction The spatial spreading of light when it encounters a physical object. Diffraction occurs when light passes through an aperture or next to a sharp edge.

Dispersion In bulk optics, relates to the change in phase velocity for a given change in wavelength. In optical waveguides, dispersion relates to the change in group velocity for a given change in wavelength. In optical fibers, dispersion is usually given in units of picoseconds per kilometer · nanometer. This refers to the number of picoseconds difference in transit time for two optical pulses whose wavelength difference is 1 nm, transmitted over 1 km of fiber. Sometimes dispersion refers to changes in group velocity from all sources, including polarization mode dispersion.

Dispersion-shifted fiber Fiber in which the zero-dispersion point is shifted, usually away from 1310 nm and toward 1550 nm. Also listed as ITU-T G.653.

Distributed-feedback (DFB) laser Uses specially designed optical devices or structures to reject all but one of the longitudinal modes that exist in a Fabry–Perot laser. Consequently, they have narrow spectral widths and are used (usually with external modulators) for transmitting data at high data rates. Because of their narrow spectral widths, they are also highly coherent and are used in coherent-detection systems.

Divergence The tendency for light to expand from a collimated state. Divergence results from diffraction and may also result from the action of optical elements.

Dropout When the OTDR waveform drops significantly below backscatter and then rises quickly to the backscatter level. This sometimes occurs after a reflection.

Dynamic range There are several definitions for dynamic range. Bellcore's definition is the displayed attenuation (in decibels) from the backscatter level at the front panel to an imaginary line that lies just above 98% of the noise. Another common definition is five times the base 10 logarithm of the ratio of the backscatter power at the front panel to the RMS noise power.

Dynamic range, end detection The maximum attenuation (in decibels) between the OTDR and an identifiable cleaved fiber end. This is much greater than the distance over which the OTDR can make splice-loss measurements.

E

Echo An optical signal that has reflected more than once before being sensed by the OTDR's optical receiver.

Erbium-doped fiber-optic amplifier (EDFA) A device similar to a laser fiber, but without optical feedback. It is used to amplify optical signals directly.

End-to-end loss The total loss, including events and fiber loss, between one end of a cable and the other end.

Equilibrium mode distribution The distribution of optical energy among the various modes in a multimode fiber, after transmission over a long fiber.

Event Any sudden change (that is statistically important relative to waveform noise) in the OTDR's backscatter signature. Events include discontinuities in the fiber's attenuation caused by, for example, fusion splices. They may also be upward spikes due to reflective components such as connectors. Events include breaks, bends, connectors, and fusion splices.

Event table A data table produced by automatic event-marking algorithms (sometimes modifiable with manual measurements). The table typically reports the distance, loss, and reflectivity of each event found in the auto mode. Some OTDRs also report measurement accuracy, link loss, fiber slope, etc.

Extrinsic splice loss Loss resulting from extrinsic factors, such as misalignment, reflection, and contamination (as opposed to mismatch between fiber types).

F

Fabry-Perot laser Composed of a suitably pumped laser medium between two mirrors that form a Fabry-Perot resonating cavity. Without wavelength-selective devices, such lasers support many longitudinal modes and typically have a total spectral width of a few nanometers.

Fabry-Perot resonator A cavity formed by two parallel reflecting mirrors. Light at a resonating frequency passes through the cavity, and light outside the resonant frequencies is blocked.

FAFO algorithms Fully automatic, fully optimized acquisition algorithms that optimize an acquisition by using multiple pulse widths, averaging, and bandwidth settings for different sections of the fiber.

Far-field distribution The electric field distribution in the Fraunhofer diffraction region.

Fault finder A simplified OTDR used to locate breaks in spans of fiber.

Fiber circulator A device that circulates OTDR pulses, generating a waveform of infinite length using a finite length of optical fiber. (Of course, the infinite length is not visible on the OTDR because of limited dynamic range.)

Fiber slope The attenuation coefficient of the fiber, usually expressed in decibels/kilometers. This is the slope of the line seen on an OTDR waveform, resulting from the Rayleigh backscatter of the fiber being tested.

Fraunhofer diffraction The diffraction pattern from an illuminated aperture in a plane that is a long distance away. To satisfy this condition, the distance to the diffraction plane must be large compared to the dimensions of the aperture and the wavelength of light.

Frequency chirping Changes in frequency. Standard OTDR lasers change their optical frequency slightly when they are pulsed, resulting in chirping. Chirping is deliberately initiated and used in some OTDR schemes.

Fresnel reflection Reflection resulting from a point discontinuity in a fiber's index of refraction. For example, a Fresnel reflection may be caused by the end of a cleaved fiber, an unterminated connector, a mated connector, or a mechanical splice. On an OTDR, Fresnel reflections appear as sharp, upward-pointing spikes.

Front-panel connector The connector used to attach an OTDR to a fiber being tested. Except for OTDRs with internal fibers, the front-panel connector is usually the first reflection at the beginning of the waveform.

Fusion splice A joint between two optical fibers, created by fusing the fibers at high temperature (usually within an arc of electrical current).

G

Gainer Caused by core mismatch, refers to an OTDR splice-loss signature showing splice loss in one direction and "gain" of the reflected signal in the opposite direction.

Germanium A crystalline semiconductor, typically doped with boron, gallium, and indium, that serves as a photoconductive detector capable of detection up to and beyond 100 μm . Commonly used in photodetectors and optical fibers.

Ghost A phenomenon that results from testing an optical fiber with a pulse repetition time (PRT) that is less than the time required to travel the length of the optical fiber and back. This means that events near the start of the fiber are folded into locations toward the fiber's end.

Graded-index (GI) fiber A fiber in which the core index is a function of the radial coordinate. Typically, the core index is highest on the fiber's axis and decreases according to a parabolic function toward the cladding.

Group delay time The difference in arrival times between two pulses that are launched simultaneously. The pulses may have different wavelengths or different polarizations. The group delay time is a measure of the fiber's dispersion.

Group index The ratio of the velocity of light in a vacuum to the group velocity of light in a waveguide. The index of refraction used by OTDRs is the group index of the optical fiber under test. The group index is characteristic of a particular fiber and can vary from fiber to fiber.

Group velocity The velocity with which a pulse of light travels through an optical material.

H

High-order mode A mode whose irradiance distribution generally lies farther from the center of a fiber. Consider a fiber that is single mode at a given wavelength. Reduce the wavelength. Below the cut-off wavelength, the fiber supports more than one mode. As the wavelength is further reduced, the fiber supports more and more modes. High-order modes are those that appear later on as the wavelength is reduced.

Hybrid fiber coax (HFC) A hybrid system using a fiber-optic backbone and coax cables for final distribution from the node to the customer.

I

Incident power The optical power before, or incident to, an event.

Index-matching fluid/gel Material whose index of refraction is almost equal to that of the fiber core. It is used to reduce Fresnel reflections in mechanical splices or cleave and crimp connectors.

Index of refraction (IR) Technically the group index of refraction, this is a common OTDR setting. See refractive index.

Infrared Light whose wavelength is outside the red end of the visible spectrum. OTDRs typically use infrared light in the range from 820 nm to 1600 nm.

InGaAs Indium gallium arsenide, the components of a crystalline semiconductor. Used in fiber-optic photodetectors.

Integrated return loss The total return loss from all optical components and fiber backscatter between two cursors on an OTDR waveform.

Interleaving A technique for reducing the sample spacing in an OTDR waveform. Several waveforms are acquired with a given sample spacing but slightly different delay times. Then the waveforms are meshed together (interleaved) to form a single composite waveform with smaller sample spacing.

Intermodal dispersion Dispersion in multimode fibers resulting from the different group velocities of the various modes (another name for multipath dispersion).

Internal reflection Ordinarily, when light travels from a material of high index to one of low index, some light is transmitted and some is reflected. If the light is incident at a sufficiently oblique angle, all the light is reflected, and none is transmitted. This is called internal reflection.

Intersymbol interference Interference between bits in a digital data stream resulting in an increased bit-error rate. Intersymbol interference may result from dispersion and/or reflections.

Intramodal dispersion Dispersion, such as chromatic dispersion, within a given mode.

Intrinsic splice loss Loss resulting from mismatch between fiber types, as opposed to mismatch in alignment.

Irradiance Optical-power density, expressed in watts per square meter, incident perpendicularly upon a surface.

Irradiance distribution A function describing the irradiance over a region of space.

L

Laser A source of coherent light generated by the stimulated emission of photons.

Light-emitting diode (LED) A solid-state device that emits light when an electrical current passes through it. Somewhat related to laser diodes, LEDs have wider spectral widths and are typically more divergent.

Linearity The amount of loss-measurement error for a given amount of loss, typically expressed in dB/dB. Given a perfect fiber, linearity may be imagined as deviations from a straight line in the Rayleigh backscatter when viewed on an OTDR. Linearity is related to the calibration of an OTDR's vertical scale.

Link loss The loss between the beginning and end of a link. The link may be the full length of the cable, or it may be a portion of the cable between two events.

Local-area network (LAN) An interconnected system of separate stations, usually computers, in one relatively small geographical location such as a building or complex.

Low-order mode A mode whose irradiance distribution generally lies closer to the center of a fiber. Consider a fiber that is single mode at a given wavelength. Reduce the wavelength. Below the cut-off wavelength, the fiber supports more than one mode. As the wavelength is further reduced, the fiber supports more and more modes. Low-order modes are those that first appear as the wavelength is reduced.

LSA loss measurements Least-squares approximation. A method of measuring the loss of an event. LSA measurements use linear regressions, applied to the backscatter before and after an event, to estimate the attenuation in the backscatter resulting from the event's loss.

M

Macrobend In an optical fiber, all macroscopic deviations of the axis from a straight line; distinguished from microbend.

Mainframe OTDR A term used to specify an AC OTDR with a larger (than a mini-OTDR) chassis. Mainframe OTDRs have CRT displays and internal printers, and are larger and heavier than most current OTDRs. They were the most common type used until the early 1990s. Mainframes could also be

provided with different laser and fiber modules as needed. See optical time-domain reflectometer.

Material dispersion Spreading of optical pulses composed of more than one wavelength due to the properties of the material from which the fiber is constructed. In optical fibers, dispersion is usually given in units of picoseconds per kilometer · nanometer. This refers to the number of picoseconds difference in transit time for two optical pulses whose wavelength difference is 1 nm, transmitted over 1 km of fiber.

Measurement accuracy The uncertainty in a loss, distance, or reflectivity measurement resulting from algorithm methodology, waveform noise, and instrument calibration.

Measurement range The maximum amount of attenuation between an OTDR and a 0.5-dB nonreflective event when the OTDR's event-marking software is just capable of finding the event at least three out of four times with a measurement accuracy of 0.1 dB.

Mechanical splice A method of connecting two optical fibers that involves mechanically joining or bonding together the two ends of the fibers.

Metropolitan-area network (MAN) An interconnected data-transmission system connecting users and LANs in a localized geographical area, such as a city.

Microbend Small imperfections in the core/cladding boundary. The larger the core, the less effect the imperfections will have. Also defined as pinching effects.

Micron A unit of length equal to one millionth (10^{-6}) of a meter. Light sources used in OTDRs typically have wavelengths between 0.82 and 1.6 microns. Single-mode fibers typically have core diameters of 9 microns and cladding diameters of 125 microns.

Mini-OTDR A term used as a comparison to the mainframe OTDR. The mini-OTDR emerged in the 1990s as a lightweight, low-cost version of the OTDR. Features include AC/DC power, LCD display, and various modules for specific fiber types and corresponding wavelengths. Usually without a printer, they can store traces on disk, memory card, or their internal hard disk. See optical time-domain reflectometer.

Mode Light transmission in an optical fiber is modeled as solutions to Maxwell's equations for electromagnetic radiation. These equations allow only discrete solutions, called modes. Physically, these modes exhibit themselves as distinct transverse irradiance patterns within the fiber core. Mechanical analogs of modes are the standing waves on a taut, vibrating piece of string.

Mode-field diameter The diameter of the irradiance distribution in a single-mode fiber, measured at the point where the irradiance falls to $1/e^2$ times the irradiance at the center of the core.

Mode-field distribution The irradiance distribution of a given mode as a function of radial and angular coordinates relative to the fiber's core.

Modulation Varying the amplitude or intensity of an information-carrying signal. Modulation contrast is a measure of the difference between high and low portions of the signal.

Monochromatic A light source that emits just one wavelength. In practice, all real light sources have finite bandwidth (emit light over a range of wavelengths). Many sources, such as lasers, may be considered essentially monochromatic for certain purposes.

Multimode fiber One of two fundamental types of fiber (multimode and single mode). A multimode fiber transmits multiple rays (or modes) of light. Multimode fiber cores are typically between 50 and 100 microns in diameter, which is much larger than the diameters of single-mode fibers.

Multipath dispersion Another name for intermodal dispersion. In multimode fibers the different modes travel at slightly different group velocities. Therefore, a pulse composed of many modes disperses (spreads out) as it travels along the fiber. This dispersion is called multipath dispersion.

N

Nanometer A unit of length equal to 10^{-9} meter (abbreviated as nm). The wavelengths of light sources used in OTDRs are often expressed in nanometers. For example, single-mode fibers typically operate at wavelengths of 1310 and 1550 nm.

Nanosecond A unit of time equal to 10^{-9} seconds (abbreviated as ns).

Near-field distribution The electric field distribution across an aperture.

Noise Random signals (usually electrical currents) unrelated to meaningful waveform data. White noise is uncorrelated to the OTDR's acquisition circuitry and covers a broad frequency range. Synchronous noise typically has a narrow spectral range and often repeats from one acquisition to the next.

Noise floor An imaginary line drawn on an OTDR display that lies above a given amount of the noise that exists past the end of the fiber being tested. Typically, the line is below 2% of the noise spikes (above 98%).

Normalized frequency See also V-parameter. The frequency used to describe the characteristics of a single-mode fiber. The spot diameter, cut-off wavelength, and modal characteristics are all functions of the V-parameter.

Numerical aperture The sine of twice the acceptance angle. The greater the numerical aperture, the greater the fiber's acceptance angle and the greater the divergence of light emanating from the fiber.

Nyquist rate Twice the frequency of the highest-frequency component in a bandwidth-limited signal. The Nyquist sampling theorem states that any bandwidth-limited signal may be perfectly reproduced if sampled at least twice the frequency of the signal's highest-frequency component. Sampling lower than the Nyquist rate results in aliasing.

O

Offset Constant-level (DC) noise either added to or subtracted from an OTDR's waveform. Offset errors affect an OTDR's linearity and measurement range. Offset may also result in errors estimating the dynamic range.

Optical circulator A multiport device that steers optical energy between specific ports.

Optical feedback Light that is fed back into an optical component. Sometimes the optical feedback is deliberate. Other times, optical feedback is a problem, such as when a reflection directs light back into a DFB laser.

Optical fiber A thin strand of ultrapure glass designed to transmit modulated light signals carrying voice, data, and video information.

Optical isolator A nonreciprocal device intended to suppress backward reflections along an optical-fiber transmission line while having minimum insertion loss in the forward direction.

Optical masking A technique used by some high-performance mainframe OTDRs to mitigate the effects of large reflections and improve dead zone without limiting other aspects of OTDR performance.

Optical return loss (ORL) The amount of light reflected from optical fibers and optical components. The fiber, connectors, or splices in an optical system can cause the reflection.

Optical time-domain reflectometer (OTDR) A versatile optical test instrument that measures the distances, losses, and reflectivities of events on optical fiber by testing from one end of the fiber. The optical time-domain reflectometer works by launching pulses of light into the fiber and processing the light that is scattered and reflected back to the OTDR. Typically, the OTDR displays a visual representation of the fiber as a waveform. Many OTDRs also analyze the waveform, locate and measure each of the events automatically, and report these data in an event table.

Outside plant (OSP) The portion of a communication network that exists mostly outdoors, but also between transmission sites. The OSP includes patch panels, closures, pedestals, the communications media (e.g., fiber, twisted pair, or coax), and the structure (aerial, underground, etc.) where the cable is installed and routed. The patch panels at each end are points of access for OSP testing but also points of separation of responsibilities for the transmission network.

P

Passive optical network (PON) A network made up of fiber-optic cabling and passive splitters and couplers that distribute an optical signal through a branched "tree" topology to connectors that terminate each fiber segment. Compared to other access technologies, PON eliminates much of the installation, maintenance, and management expenses needed to connect to customer premises. PON is a

point-to-multipoint system with one optical line terminal at the central office servicing up to 32 optical network terminals. The system is single-mode fiber with downstream traffic sent in the 1550-nm wavelength window and upstream traffic being sent in the 1310-nm wavelength window.

Pattern-matching algorithms Algorithms used to measure events by locating predefined patterns in the data. Pattern-matching algorithms can typically locate events to within less than the sample spacing of the OTDR.

Phase velocity The velocity with which wavefronts of constant phase travel through an optical material.

Photon The fundamental particle of light.

Picosecond A unit of time equal to 10^{-12} seconds (abbreviated as ps).

Pigtail Joining an optical fiber to a laser diode or photodiode.

Polarization mode dispersion (PMD) Dispersion resulting from the tendency of different states of polarization to propagate at different velocities. PMD is primarily an issue for single-mode fiber systems operating above several gigabits per second (roughly OC-48 and higher).

Positive-intrinsic-negative (PIN) diode A type of photodiode used to convert optical signals in a receiver.

POTDR An OTDR with polarization discrimination used to measure the polarization mode dispersion in an optical fiber.

Profile dispersion Dispersion resulting from the different wavelength dependencies of the refractive indexes of the core and the cladding. Typically, in single-mode fibers, profile dispersion is considered part of waveguide dispersion.

PRR Pulse-repetition rate, the inverse of the pulse-repetition time, or PRT.

PRT Pulse-repetition time. This is the time between an OTDR's pulses. PRT affects the OTDR's range and, when improperly set, may cause ghosting.

Pulse width The width of the laser pulse used by an OTDR. The actual width of the pulse (in time or distance) is twice the pulse width seen on the OTDR display. This is because the display's horizontal axis time base is divided by 2, since the light must travel down the fiber and back before being detected by the OTDR.

R

Range A common OTDR setting, also referred to as test range or maximum range. The range setting should be longer than the fiber, or ghosting may occur.

Rayleigh scattering Scattering caused by nonuniformities in an optical fiber that are very small relative to the wavelength of light. In optical fiber, Rayleigh scattering represents the fundamental limit to the attenuation coefficient. Rayleigh scattering is inversely proportional to the fourth power of the wavelength (see Backscatter).

Rayleigh scattering coefficient The attenuation of an optical fiber per unit length, typically expressed in decibels per kilometer, that is attributable directly to Rayleigh scattering. In high-quality single-mode fibers, the Rayleigh scattering coefficient and the attenuation coefficient are roughly the same.

RBOC Regional Bell operating company.

Reflectivity In decibels, reflectivity is 10 times the base-10 logarithm of the ratio of the reflected power divided by the incident power. In decibels, reflectivity is a negative number. The larger the reflectivity (the less negative it is) the more reflective the event is.

Refractive index The ratio of the velocity of light in a vacuum to the phase velocity of light in a given bulk material.

Return loss In decibels, return loss is -10 times the base-10 logarithm of the ratio of the reflected power divided by the incident power. In decibels, return loss is a positive number. The larger the return loss, the less reflective the event. See Optical return loss.

RIN Relative intensity noise. This is noise that results from coherent mixing of reflections at an optical receiver.

Ringling The tendency for some electrical circuits to oscillate when acted upon by a sudden change in electrical signal. Ringing on OTDRs exhibits itself as a damped sinusoidal signal, or dropout, after a reflection.

RMS noise floor One definition of an OTDR's noise floor. The RMS noise floor is defined as an imaginary line on the OTDR's display, equal to the RMS value of the noise.

Root-mean square (RMS) The standard deviation of a function or random variable. Often used to define the strength of a noise signal or the degree of uncertainty in noise-limited measurements.

S

Sample spacing The distance (as shown on an OTDR's display) between adjacent sample points in an OTDR's waveform. Sample spacing fundamentally limits distance-measurement accuracy for some event-marking algorithms.

Saturation A nonlinear effect occurring when an OTDR's receiver can no longer respond to high signal levels.

Scattered power The power scattered by the Rayleigh scattering process within the fiber.

Scattering coefficient The coefficient defining the bulk Rayleigh scattering. In this book, scattering coefficient is sometimes used synonymously with Rayleigh scattering coefficient, although (strictly speaking) the Rayleigh scattering coefficient refers only to that portion of the scattering that is captured by the fiber, and travels back toward the OTDR.

Signal-to-noise ratio (SNR) The ratio of the signal power to the noise-equivalent power. Often, the signal-to-noise ratio is expressed in decibels by taking 10 times the base-10 logarithm of the SNR.

Silicon detector Semiconductor that uses absorbed photon energy to stimulate carriers from one energy level to a higher one. The change in charge across the junction is monitored as a current in the external photodiode circuit. Silicon photodetectors are commonly used in multimode systems operating at 850 nm.

Single-mode fiber One of two general classes of optical fiber (the other being multimode). Single-mode fiber supports only one mode (loosely analogous to a single “ray”). Typical diameters for the cores of single-mode fibers are in the range from 6 to 10 microns.

Spectral bandwidth The range of wavelengths over which a source emits light. Spectral bandwidth is measured in terms of wavelength (nanometers, microns, etc.) or frequency (megahertz, hertz, etc.). Coherent sources have narrow spectral bandwidths.

Splice A joint between two pieces of optical fiber. The splice may be formed by fusing together the fibers or by joining them mechanically.

Splice loss Generally expressed in decibels, splice loss is a measure of the amount of light decoupled from a fiber as it passes through a splice. It is 10 times the base-10 logarithm of the ratio of the power incident to the splice divided by the power in the fiber after the splice.

Spot profile The irradiance distribution in a single-mode fiber.

Step-index fiber A fiber in which there is a sharp demarcation between the core index and the cladding index, and one in which the core and cladding indexes are independent of the radial coordinate. This is a common design for single-mode fibers.

Storage area network (SAN) A network that links host computers to storage servers and systems. The network protocols can include FC-AL, SSA, ATM, and Fast Ethernet. The storage technology can be a collection of servers on a network or a more complex and expensive host storage server, such as a midrange or mainframe computer.

T–V

Tail The recovery region after a reflective event before the waveform returns to normal Rayleigh backscatter. Tail results from system bandwidth and complicated effects within the OTDR’s optical receiver.

Terminator An optical plug with the fiber dead-ended so that there is no return loss. This could be made by breaking the end of the fiber and index matching it within the connector itself. Because they have to be measured for ORL, it is best to have several types, with the measurement value required.

Trace Another name for the waveform seen on an OTDR’s display, originating from oscilloscope CRT displays.

Two-point loss The loss, in decibels, between two points on an OTDR waveform. Two-point loss always includes fiber loss and sometimes includes splice loss (if a splice exists between the two points). Two-point loss is generally less accurate than LSA loss measurements because it is more sensitive to waveform noise.

Uniform mode distribution A distribution in multimode fibers where the amount of power carried by the various modes is equalized.

V-parameter The normalized frequency used to describe the characteristics of a single-mode fiber. The spot diameter, cut-off wavelength, and modal characteristics are all functions of the V-parameter.

W–Z

Waveform The graphic representation displayed by an OTDR indicating the characteristics (Rayleigh backscatter and other features) of an optical fiber.

Waveguide dispersion In single-mode fibers, the group index is a function of the core and cladding indexes and the mode profile. The mode profile, in turn, is a function of wavelength. Even without material dispersion, there is chromatic dispersion because of this wavelength dependence of the mode profile. Waveguide dispersion is chromatic dispersion that does not relate directly to the chromatic dispersion of the bulk material from which the fiber is manufactured.

Wavelength The distance between two consecutive points of equal phase on an electromagnetic wave. For visible light, the wavelength is roughly 0.5 microns. Light used in OTDRs typically has a wavelength of between 0.82 and 1.6 microns.

Wavelength-division multiplexing (WDM) Combining two or more wavelengths onto a single optical fiber. Typically, each wavelength carries a unique data stream. Wavelength-division demultiplexing occurs when the wavelengths are separated onto different fibers.

Wide-area network (WAN) An integrated data network linking metropolitan or local networks over common carrier facilities.

Zero-dispersion wavelength The wavelength where dispersion becomes zero.

Appendix B

Mathematical Glossary

α	<ul style="list-style-type: none"> • Attenuation coefficient (attenuation from all sources, expressed in 1/km or dB/km, depending on context) • Sometimes used as a dummy variable (explicitly stated in the text)
A	<ul style="list-style-type: none"> • Field amplitude • Power amplitude of reflections • The constant used in the equation for Rayleigh backscatter
$A(r)$	Mode-field or amplitude function
α_e	Electron ionization coefficient
α_h	Hole ionization coefficient in APD
a_l	Y-intercept for left-handed linear regression
a_r	Y-intercept for right-handed linear regression
α_S	Scattering coefficient (attenuation due to Rayleigh scattering, expressed in 1/km or dB/km, depending on context)
B	Fiber's bandwidth capacity
β	<ul style="list-style-type: none"> • Optical-fiber propagation constant • System bandwidth of an electrical circuit
B_{ns}	Backscatter coefficient, which is the backscatter level (in dB, relative to the launch pulse power) of a 1-ns pulse
\vec{B}	Magnetic induction vector
c	Speed of light
Δ	Refractive-index contrast
δ	<ul style="list-style-type: none"> • Distance of an event or point on waveform above the noise floor • Approximation for refractive-index contrast when contrast is small
D	<ul style="list-style-type: none"> • OTDR's pulse width on fiber • Chromatic-dispersion parameter
d	Distance
Δ'	Constant used to define the index profile of a parabolic fiber
Δ_{dB}	Ratio of the total power received from the reflection to the total power received from backscatter (in dB)
DGD	Differential group delay
D_λ	Wavelength dispersion
$\delta\lambda$	Source spectral bandwidth
D_m	Material dispersion
dP_{bs_i}	Total amount of backscatter from a differential element i
dp_{bs_i}	Total amount of backscatter from a differential element i that is transmitted through a polarizer

DR	Dynamic range
Δt	Time delay
$\delta(t)$	Impulse function
$\Delta\tau$	Differential group delay
\vec{D}	Electric displacement vector
Δx	Spacing between digitized sample points in OTDR waveform
D_ω	Waveguide dispersion
$\Delta\omega$	Difference in optical frequency between two wavelengths
$\langle\Delta\tau_1\rangle$	RMS differential group delay for individual fiber that forms a concatenated group
dz_{event}	Event dead zone
dz_{loss}	Loss dead zone
E	<ul style="list-style-type: none"> • Loss-measurement error • Electric field amplitude and phase across an aperture
\vec{E}	Electric field vector
$E_{x\text{in}}$	Electric amplitude component along x -axis at input to fiber
$E_{x\text{out},p}$	Electric amplitude component along x -axis at output of fiber
$E_{x,p}$	Electric amplitude component along x -axis at location p on fiber
$E_{y\text{in}}$	Electric amplitude component along y -axis at input to fiber
$E_{y\text{out},p}$	Electric amplitude component along y -axis at output of fiber
$E_{y,p}$	Electric amplitude component along y -axis at location p on fiber
f	<ul style="list-style-type: none"> • Offset error • Frequency
F	Relative fiber backscatter parameter
F_1	Relative backscatter parameter of fiber 1
F_2	Relative backscatter parameter of fiber 2
$f_{3\text{dB}}$	3-dB bandwidth (cycles/s)
f_c	Amplifier 3-dB cut-off frequency
f_{p1}	Fiber parameter constant, fiber 1
f_{p2}	Fiber parameter constant, fiber 2
$G(x,\mu,\sigma)$	Gaussian distribution as a function of mean (μ) and standard deviation (σ)
h	Signal level relative to offset (dB)
H	Height of reflection above backscatter level, as measured on OTDR display, in dB
\vec{H}	Magnetic field vector
I	Total amplified current in APD
i	<ul style="list-style-type: none"> • Square root of -1 • Index for random numbers

$I(z)$	Modified imperfection function
$Ia(r)$	Irradiance profile across aperture
$I_F(r_F)$	Fraunhofer (far-field) irradiance distribution
$I_N(r_N)$	Irradiance distribution across the aperture (the near-field distribution)
I_{op}	Photocurrent in APD
$I(z)$	Imperfection function
$J_0(r)$	Zero-order Bessel function
k	Propagation number
K	Coupler split ratio
$K_0(r)$	Modified Hankel function
k_α	Hole ionization constant divided by electron ionization constant (APD)
L	<ul style="list-style-type: none"> Length of fiber, distance along fiber, or length of linear regression when making loss measurements True event loss
λ_0	Zero-dispersion wavelength
λ_{e1}	First eigenvalue of Jones matrix used to estimate PMD
λ_{e2}	Second eigenvalue of Jones matrix used to estimate PMD
L_f	Fractional loss of event
L_m	Measured splice loss
$L_{m1,2}$	Measured splice loss between fibers 1 and 2 with the OTDR attached to fiber 1
$L_{m2,1}$	Measured splice loss between fibers 2 and 1 with the OTDR attached to fiber 2
$Loss_{MFD}$	Intrinsic loss resulting from mismatch in mode-field diameters (MFDs) of two fibers
LP_{11}	Fundamental mode
L_t	True splice loss
M	<ul style="list-style-type: none"> Number of modes in multimode fiber Mean data point chosen by the linear predictor as the location of a nonreflective event
m	Fiber slope (generally given in dB/km)
$M1$	Measured splice loss from one end of the fiber
$M2$	Measured splice loss from the other end of the fiber
M_e	APD multiplication factor
MFD	Mode-field diameter of fiber
M_p	Jones vector of the p th differential element of a fiber
n	Index of refraction
μ	Mean of random distribution

N	<ul style="list-style-type: none"> • Number of data points • Number of fibers, number of event, etc.
n_0	Axial core index of parabolic fiber
n_1	Core index of optical fiber
n_2	Cladding index of optical fiber
NA	Numerical aperture of optical fiber
n_{eff}	Effective index
n_g	Group index
n_i	<ul style="list-style-type: none"> • Index of initial medium in which light is traveling before encountering an interface between two materials • Random noise at the ith sample point in the OTDR waveform
n_t	Index of medium into which light transmits upon arriving at an interface between two materials
ORL_{CWR}	Optical return loss measured by a CWR
ORL_{OTDR}	Optical return loss measured by an OTDR, by integrating and normalizing between two cursors
$P(x)$	Laser power as function of distance along fiber
P_0	<ul style="list-style-type: none"> • Peak pulse power emanating from OTDR • Peak pulse power at point of scattering
$P_{1\text{ns}}$	Backscatter power from a 1-ns pulse
P_{bs}	Power scattered back toward an OTDR and captured by the optical fiber
P_i	<ul style="list-style-type: none"> • Unlogged digitized waveform data • Incident optical power
P_n	Probability that the n th data point will qualify as the location of a nonreflective event, using the linear predictor algorithm
P_r	Reflected optical power
P_R	Power received at OTDR from a reflection
q	Rayleigh backscatter capture constant
Q_{bs}	Ratio of the total backscatter power from a fiber of length L relative to the launch power
Q_R	Ratio of reflected power (from event at end of fiber) from a fiber of length L relative to the launch power
r	<ul style="list-style-type: none"> • Radial coordinate • Lateral offset • Length along a vector
R	<ul style="list-style-type: none"> • Reflectivity of event • Squared ratio of the numerical apertures of two fibers • Parameter used in estimating intrinsic splice loss • Distance from aperture to image plane • Ratio of mode-field radii
θ	Angular coordinate

θ_c	Angle with respect to normal, incident upon a cleaved fiber end at the critical angle
θ_i	Angle with respect to normal, incident upon an optical medium
R_L	Return loss
θ_t	Angle with respect to normal, upon transmission into an optical medium
S	<ul style="list-style-type: none"> • Backscatter factor • Standard deviation of the distance-measurement error of the linear predictor when measuring nonreflective events • Amount of light scattered back to the OTDR by a differential element
S_0	Zero-dispersion slope
S_1	Backscatter signal before splice
$S_1(z)$	Waveform signature from first end of the fiber
S_2	Backscatter signal after splice
$S_2(z)$	Waveform signature from second end of the fiber
S/N	Signal-to-noise ratio
$S(r)$	Spot irradiance profile
t	Time
T	Averaging time
\mathbf{T}	Jones vector
$\Delta t_{\text{intermodal}}$	Intermodal dispersion
$\Delta t_{\text{intramodal}}$	Intramodal dispersion
t_r	Rise time of electrical circuit
T_ω	Jones matrix at optical frequency
$T_{\omega+\Delta\omega}$	Jones matrix at optical frequency
u	Radial phaser parameter in the core
σ	Standard deviation of random distribution
σ_{dB}	Standard deviation of the waveform noise at a given distance above the noise floor
V	Normalized spatial frequency
v_g	Group velocity
v_p	Phase velocity
$V(x)$	Variance of random variable x
τ	<ul style="list-style-type: none"> • Delay or transit time • Time constant for an electrical circuit
W	OTDR's pulse width as seen on OTDR display ($D/2$)
w	Cladding delay parameter
τ	Differential group delay
\vec{w}	Mean value of digitized waveform data over an interval

w_d	Width of APD depletion layer
w_i	Digitized waveform data
x	<ul style="list-style-type: none">• Distance along fiber• Also used to denote lateral offset
\bar{x}	Mean of a random distribution of x -variables
ω	<ul style="list-style-type: none">• Angular frequency• Optical frequency
ω_0	Mode-field radius at the $1/e^2$ irradiance point
$\omega_{3\text{dB}}$	3-dB bandwidth (radians/s)
$\langle\tau\rangle$	RMS differential group delay for concatenated fibers
ω_c	Carrier frequency
ω_m	Modulation frequency
\bar{y}	Mean of a random distribution of y -variables
(Y,Z)	Coordinates in the Fraunhofer plane
(y,z)	Coordinates in the aperture plane

Appendix C

Answers to Problems

Chapter 2

1. Yes.
2. No.
3. Cut-off wavelength.
4. Rayleigh scattering.
5. Modal dispersion, waveguide dispersion, and chromatic dispersion.
Extra credit: polarization mode dispersion.
6. Graded-index profile.
7. True.
8. True.
9. False.
10. False.

Chapter 3

1. False.
2. False.
3. True.
4. True.
5. True.
6. True.
7. False.
8. True.
9. True.
10. False.

Chapter 4

1. Reflective and scattering.
2. Greater.
3. False.
4. Uncertainty in the IR setting.
5. True.

6. False. It is the error, in decibels, per 1-dB change in signal.
7. True.
8. False. The log scale makes the backscatter trace linear and increases the visible, useful display range.
9. False.
10. True.

Chapter 5

1. False.
2. True.
3. False.
4. False.
5. True.
6. False.
7. False.
8. True.
9. True.
10. False.

Chapter 6

1. False.
2. True.
3. False.
4. False.
5. False.
6. False.
7. True.
8. True.
9. True.
10. True.

Chapter 7

1. True.
2. False.
3. True.
4. False.
5. False. Reflectivity is measured relative to the Rayleigh backscatter level.
6. True.
7. True.
8. True.
9. False. The light reflects well off the angled surface but is coupled out of the optical fiber by the large reflection angle.
10. True.

Chapter 8

1. True.
2. False.
3. False.
4. False.
5. True.
6. True.
7. True.
8. False.
9. True.

Chapter 9

1. True.
2. True.
3. False.

Chapter 10

1. True.
2. False.
3. False.
4. True.
5. True.

Chapter 11

1. False.
2. True.
3. False.
4. False.
5. False.
6. C.
7. True.
8. True.
9. False.
10. False.

Chapter 12

1. True.
2. False.
3. True.
4. False.
5. True.

Chapter 13

1. True.
2. False.
3. False.
4. True.
5. False.
6. True.

Chapter 14

1. True.
2. False.
3. False.
4. True.
5. True.

Chapter 15

1. False.
2. True.
3. False.
4. True.
5. True.

A

- absorption, 20–23
- accessories/options of OTDRs, 394
- acquisition parameters, optimizing for
 - event marking, 292–299
- analog-to-digital converters, 110, 147
- analog filtering, 168
- angled cleaves, reflections from, 212–213
- angled connectors, 216, 257
- Agilent, 71, 385
- attenuation, 19–21
- attenuation coefficient, 227, 231, 232, 236, 239
- attenuation dead zone, 106, 249–253
- auto event-marking algorithms, 291
- avalanche photo detector (APD), 4, 7, 63, 65, 67, 84–86

B

- backscatter, 2, 3, 4, 10, 62–64, 69
- backscatter coefficient, 209, 224, 227
 - calculating, 230–233
 - calibrating, 229–230
 - measuring, 233–240
- bandwidth, system, 137
- beam splitter, 3
- Bellcore, 104, 119, 120, 124, 127, 140, 149
- bending, 48–51, 195–197, 199, 205
- Bessel filter, 169
- Bessel function, 270
- bit error rate (BER), 2, 29, 36, 55, 56, 249, 257, 262, 243
- Bragg cell, 94
- breaks, 284–289

C

- cabling errors, 173
- cable
 - installation, 140
 - manufacture, 125
- CATV, 146
- ceramic ferrules, 214
- chromatic dispersion, 28–35, 36, 343, 364, 367, 368, 369, 370, 372–375

- cladding, 16, 17, 18, 24, 26, 29, 30
- cleaved fiber ends, 209, 212,
 - reflections from, 212
- cleaver, 235
- clock accuracy, 107, 143
- coherence, 13, 52–55
- coherent-detection OTDR, 85, 93–95
- complications by reflective events, 249
- connectors, 2, 4, 9, 13, 42–48, 59, 61, 62, 63, 64, 69, 72, 81–82, 153–155, 192, 193, 194, 198–199, 209, 295, 301, 314, 331, 334
 - cleaning, 388–391
 - reflections from, 214–219
- considerations in selecting an OTDR, 379
- contamination testing, 141
- continuous-wave reflectometer (CWR), 1, 209, 211, 235, 246
- core, 16, 18, 24, 26, 27, 29, 30, 34, 35, 37
- Corning, 20
- correlation OTDR, 95–96
- couplers, optical, 279–288
- cursor placement
 - for nonreflective events, 156–158
 - for reflective events, 222–225
- cursor resolution, 107, 144
- cut-off wavelength, 36–42, 267
 - measuring, 275–277

D

- data density, 142
- data-processing speed, 146
- data resolution, 147
- dead zone, 66–67, 69, 81, 91, 106, 114, 135, 138–139, 151, 249, 250, 251, 252, 253, 263, 329
 - attenuation, 106
 - event, 106, 249–252
 - improve by masking, 252
 - loss measurement, 249, 251–252
 - test fixture, 329
- detector tail, 106, 138,
- differential group delay (DGD), 343–350, 352, 354
- diffraction, 14, 52

digital filtering, 167–168
 dispersion, 13, 16, 20, 24–35, 175, 343, 359
 chromatic, 28–35
 intermodal, 361–364
 intramodal, 364
 material, 364–367
 measuring using OTDR, 369–375
 multipath (modal), 24–28
 polarization mode, 343
 profile, 26–29, 34, 35
 reduction, 368–369
 and system bandwidth, 25
 zero-wavelength, 31
 waveguide, 31, 366–367
 dispersion-shifted fiber, 34, 35
 dispersive waveguide, 29, 30, 345
 display and controls of OTDRs, 381, 382–386
 display resolution, 282–283
 display speed, 107, 146, 148
 distance measurements, 156–158, 221–223
 distance-measurement error
 filtering, 167–170
 noise, 158–167
 distributed-feedback laser (DFB), 31, 210, 257, 262, 368
 drop-outs, 305, 306
 dual-wavelength OTDR, 65–66, 68–69
 durability of OTDRs, 379, 380–382
 dynamic range, 2, 6–7, 62, 65, 67, 68, 69, 70, 73, 74–78, 105, 107
 reflective, 108–109
 scattering, 109–115
 usable, 123
 dynamic range margin, 121

E

echoes, 87–91, 210, 317, 318–319
 eigenvalue, 347, 351–352
 equilibrium mode distribution, 194–195
 erbium-doped fiber-optic amplifier, 91–92
 event marking, 291–326
 features, 317–321
 individual events, 304–312
 optimizing acquisition parameters, 326
 testing, 312–317
 types of, 291–293

event
 complications by reflective, 249
 dead zone, 106, 135, 137–138, 151
 detection accuracy, 107, 148–149
 measuring individual, 294, 297, 304–312
 nonreflective, 153–176
 reflective, 209–246, 252–257
 resolution, 106, 107, 135–137
 return loss, 212, 240–245
 excitation pulse, 168
 Exfo, 348
 expert system, 8
 external-source test fixture, 337–338
 extrinsic splice loss, 200

F

Fabry–Perot laser, 8
 Fabry–Perot cavity, 215, 235
 far-field distribution, 269, 271
 far-field scanning method of
 determining numerical aperture, 268–271
 ferrule-in-sleeve, 214
 fiber attenuation, 19–23
 fiber circulator test fixture, 330–337
 fiber
 dispersion-shifted, 31, 34–35, 202, 233, 239
 graded-index, 26–28, 30, 195, 364, 370
 length, 4, 105, 113, 146–147
 manufacture, 140, 145
 mismatch, 185–190
 multimode, 73, 78–82
 non-dispersion-shifted, 34, 175, 202, 239
 single-mode, 1, 6–7, 10, 59, 73–74, 78–80
 step-index, 26–27, 31, 40, 56
 to the home, 288–289
 fiber optics, fundamentals, 13–58
 figures of merit, 103–107
 filtering
 analog, 168
 digital, 168
 low-pass, 167
 Fourier optics, 268
 Fourier transform, 268, 369
 Fraunhofer diffraction, 268–270

Fraunhofer limit, 269
 frequency-chirped, 93
 front-panel connector, 387–394
 fused coupler, 195
 fusion splice, 2, 4, 42–45, 47, 51, 56,
 153–155, 156, 253, 254, 307, 334

G

ghosts, 87–91, 319
 graded-index fiber, 26–28, 30, 195, 364, 370
 group delay time, 365, 366, 374
 group index, 171–175
 group velocity, 28, 29, 31, 32, 33

H

Hankel transform, 40, 271
 high-capacity distribution lines, 146
 human interface of OTDRs, 384, 386–387

I

index of refraction, 17, 22, 23, 28, 29, 32,
 33, 34, 36, 55, 145
 core, 258
 group, 171–173, 175
 integrated return loss, 240–245
 interleaving, 107, 142, 146, 147, 308
 intermodal dispersion, 361–364
 intersymbol interference, 139, 361, 364
 intramodal dispersion, 364
 intrinsic mismatch, 198, 200
 intrinsic splice loss, 200–205

J

Jones matrix, 347, 349–351, 354, 356, 357

K

Kao, Charles, 19
 Keck, Donald, 20

L

laser
 distributed-feedback (DFB), 31, 210,
 257, 262, 368
 Fabry–Perot, 8
 strained-layer multi-quantum-well, 8
 least-squares approximation, 155, 156
 lateral misalignment, 48, 198, 200
 light-emitting diode (LED), 54, 81, 97
 linear predictor, 160–162, 165

linear regression, 180–184
 linearity, 107, 111, 128, 131–132, 135,
 140–141
 loss, bending, 48–51, 196–197
 loss budget, 44
 loss calibration test fixture, 338–340
 loss dead zone, 249, 251–252
 loss, event return, 212, 240–245
 loss, intrinsic, 200–205
 loss, link return, integrated, 240–245
 loss-measurement dead zone, 249, 251–252
 loss-measurement resolution, 107, 137–139
 loss-measurement error, 179–208
 waveform noise, 179–185
 mismatch of single-mode fibers,
 185–190
 on multimode fiber, 190–196
 loss, return, 106–107, 139–140
 integrated, 240–245
 link, 245
 loss, splice
 extrinsic, 200
 intrinsic, 200–205
 loss, total reflection return, 140
 loss, wavelength-dependent, 198–199
 low-pass filtering, 167

M

mainframe OTDR, 67, 69–70
 masking, optical, 67–69, 252–257
 material dispersion, 364–366
 Mauer, Robert, 20
 Maxwell's equations, 37
 Maxwellian probability distribution, 345
 measurement range, 107, 112, 123, 124–125
 measurements, distance, 156–158, 221–223
 measurements, speed of, 107, 146
 measuring
 cut-off wavelength, 36–42, 267
 backscatter coefficient, 209, 224, 227
 using calibrated reflector, 233–235
 using CWR, 235–237
 using OTDR, 237–240
 dispersion using OTDR, 369–375
 individual events, 294, 297, 304–312
 numerical aperture, 267–278
 nonreflective events, 153–176
 polarization mode dispersion,
 346–349, 353–357
 reflective events, 209–246, 252–257

mechanical splices, 153, 154, 209, 210, 212, 219, 220–221, 314
 Michelson's interferometer, 52–54, 56
 mini OTDR, 64, 69–71
 mismatch, fiber, 185–190
 mode, 37–41
 mode dispersion, 24–27
 mode distribution, 41, 45
 mode-field diameter, 29, 42, 44, 47, 48, 51, 198, 200, 201, 203, 232, 239, 267–278
 mode-field distribution, 192, 194, 195
 multimode fiber, 73, 78–82
 loss-measurement errors, 190–196
 multipath dispersion, 24–28

N

near-field distribution, 269, 270, 271
 noise floor, 105, 108, 109, 110, 111, 112, 113, 114, 115–121, 295, 300, 301, 305, 307, 308, 320
 noise
 synchronous, 305, 307, 308
 non-dispersion-shifted fiber, 34, 175, 202, 239
 nonreflective events, 153–176
 cursor placement for manual measurements, 156–158
 distance-measurement errors of, 158
 sources of, 158–176
 numerical aperture, 23–24, 187, 190, 191, 192, 200–201, 203, 204, 258, 267–278

O

offset errors, 110, 111, 116–118, 125–135
 operating wavelength, differences
 between SM and MM OTDRs, 84–86
 optical attenuation, 17, 20, 22, 56
 optical couplers, 279–288
 optical isolator, 257–258
 optical masking, 67–69, 252–257
 optical port, 387–394
 optical power, 63, 64
 OTDR,
 accessories/options, 381, 394–396
 coherent detection, 85, 93–95
 considerations in selecting, 379–407
 correlation, 95–96
 design, 62–63
 display and controls of, 382–386

dual-wavelength, 65–66, 68–69
 durability of, 379, 380–382
 history of, 69–72
 human interface of, 384, 386–387
 multimode, 65, 66, 78–86
 operation, 59–100
 optical port of, 387–394
 performance standards, 104
 polarization, 348, 349, 353–357
 mainframe, 67, 69–70
 mini, 64, 69–71
 safety, 396–399
 short-coherence-length, 96–98
 single-mode, 65, 78–86
 waveform, 63–65

P

parameters, acquisition optimizing, 298–304
 pattern-matching algorithms, 321
 phase velocity, 28, 31–32
 physical-contact connectors, 154, 215–216, 218
 polarization fading, 94, 95
 polarization mode dispersion (PMD), 10, 343–357
 polarization OTDR, 348, 349, 353–357
 profile dispersion, 26–29, 34, 35
 pulse repetition rate, 111, 113
 pulse-width differences between SM and MM fibers, 83–84

R

radial irradiance distribution, 40–41
 Rayleigh backscatter, 63, 65, 72–74, 154, 155, 156–158, 251, 258, 262, 277
 Rayleigh scattering coefficient, 226, 227, 230, 231, 233
 reflections,
 causes of, 212–221
 from angled cleaves, 212–214
 from connectors, 214–219
 from mechanical splices, 220–221
 reflective events,
 complications caused by, 249–265
 and dead zone, 249–252
 measuring, 221–225
 reflective dynamic range, 107, 108–109
 reflectivity, 81–82, 108, 109, 112, 139, 212, 215, 216, 217

refractive index, *see index of refraction*
refractive-index uncertainty, 107, 144–146
relative intensity noise, 262
repeatability testing, 314–316
return loss, 106–107, 139–140
 event, 212, 240–245
 link, 245
ringing, 305–307

S

safety of OTDRs, 396–399
scattering, 19–23
scattering dynamic range, 109–115
scattering, Rayleigh, 63, 65, 72–74, 154,
 155, 156–158, 251, 258, 262, 277
Schultz, Peter, 20
selecting an OTDR, 379–407
short-coherence-length coherent OTDR,
 96–98
single-mode fiber, 1, 6–7, 10, 59, 73–74,
 78–80
Snell's law, 23–24
speed of measurements, 107, 146
splices,
 fusion, 2, 4, 42–45, 47, 51, 56,
 153–155, 156, 253, 254, 307
 mechanical, 153, 154, 209, 210, 212,
 219, 220–221, 314
splicers, 42–44
spot profile, 36–42
step-index fiber, 26–27, 31, 40, 56
strained-layer multi-quantum-well laser, 8
synchronous noise, 305, 307, 308
system bandwidth, 137

T

tail, detector, 106, 138
Tektronix OF150 OTDR, 5
Tempo, 98
test-fiber calibration, 312–314
test fixtures, 329–341
 dead zone, 329–330
 external source, 337–338
 fiber circulator, 330–337
 loss calibration, 338–340
testing event-marking software, 312–317
testing, repeatability, 314–316
total internal reflection, 13–19
time-base errors, 159, 165, 166, 171, 177
time-of-flight method, 172

traceable standard, 337
trunk lines, 146

U

usable dynamic range, 123

V

V-parameter, 36–42

W

wave group, 359, 364, 366
waveform, typical, 63
waveguide dispersion, 31, 366–367
wavelength, cut-off, 36–42, 267
wavelength-dependent loss, 198–199
wavelength-division-multiplexed
 systems, 1
wavelength-division multiplexer, 65, 322

Z

zero-dispersion point, 175, 343
zero-dispersion wavelength, 31, 56, 175